INSTITUTO
SUPERIOR
TÉCNICO

UNIVERSIDADE TÉCNICA DE LISBOA
INSTITUTO SUPERIOR TÉCNICO

Seismic Assessment of Existing Buildings Using Nonlinear Static Procedures (NSPs) - A New 3D Pushover Procedure

Carlos Augusto de Almeida e Fernandes Bhatt

Supervisor: Doctor Rita Bento, IST - Technical University of Lisbon

Co-Supervisor: Doctor Rui Pinho, University of Pavia, Italy

Thesis specifically prepared to obtain the PhD Degree in Civil Engineering

Draft

October 2011

Abstract

The good performance of Nonlinear Static Procedures (NSPs) on the seismic assessment of bridges and planar frames is nowadays generally recognized. However, the use of such methods in the case of real existing plan irregular structures has so far been studied by a limited number of authors. This fact limits the application of NSPs to assess current existing structures, the majority of which are irregular in plan. Existing studies on this topic usually focus on the evaluation of a single NSP. In order to obtain useful elements of comparison between different methodologies, the performance of four commonly employed nonlinear static procedures (CSM, N2, MPA and ACSM) is evaluated in this thesis. The appropriate variants of code-prescribed NSPs (CSM and N2) to be considered for subsequent evaluation were established as a preliminary study. An extension of CSM-FEMA440 to plan asymmetric buildings and a new 3D Pushover procedure are also proposed in this thesis. The case studies chosen are real existing reinforced concrete plan asymmetric buildings with different typologies. The accuracy of the NSPs is evaluated by comparison with nonlinear dynamic analyses for several levels of seismic intensity. The results obtained from the parametric studies showed that the Extended N2 method, the proposed Extended CSM-FEMA440 and the new 3D Pushover procedure exhibited the best performance on the analysed buildings, and seem to have potential to be incorporated in future seismic codes.

Keywords: earthquake engineering, nonlinear analysis, 3D Pushover analysis, nonlinear static procedures, nonlinear dynamic analysis, existing reinforced concrete buildings asymmetric in plan, torsion, performance based design, seismic assessment, seismic codes.

Resumo

O bom desempenho dos procedimentos estáticos não lineares (PENLs) na avaliação sísmica de pontes e pórticos planos é de um modo geral actualmente reconhecida. Contudo, a aplicação destes métodos no caso de edifícios existentes irregulares em planta foi apenas estudada por um número reduzido de autores. Este facto limita a aplicação de PENLs na avaliação de estruturas existentes, a maioria das quais irregulares em planta. Os estudos publicados sobre esta matéria concentram-se habitualmente na avaliação de apenas um PENL. Nesta tese, o desempenho de quarto procedimentos estáticos não lineares comummente utilizados (CSM, N2, MPA e ACSM) é avaliado, de forma a obter elementos de comparação úteis entre diferentes metodologias. As variantes adequadas dos PENLs recomendados em regulamentos sísmicos (CSM e N2) foram avaliadas num estudo preliminar. Nesta tese são também propostas a extensão do CSM-FEMA440 para edifícios irregulares em planta e uma nova Metodologia Pushover 3D para este tipo de estruturas. Os casos de estudo analisados são edifícios de betão armado existentes assimétricos em planta com diferentes tipologias. A precisão dos PENLs é avaliada através da comparação com análises dinâmicas não lineares para diferentes níveis de intensidade sísmica. Os resultados obtidos a partir dos estudos paramétricos desenvolvidos permitem concluir que a extensão do método N2 e do CSM-FEMA440 para edifícios irregulares em planta, bem como a nova Metodologia Pushover 3D são os métodos com melhor desempenho nos edifícios analisados, apresentando potencial para serem incluídos em futuros regulamentos sísmicos.

Palavras-chave: engenharia sísmica, análise não linear, análise Pushover 3D, procedimentos estáticos não lineares, análise dinâmica não linear, edifícios de betão armado existentes irregulares em planta, torção, dimensionamento baseado no desempenho, avaliação sísmica, regulamentos sísmicos.

Acknowledgments

I would like to deeply acknowledge Doctor Rita Bento, my supervisor, for all her dedication, motivation, commitment, amiability and scientific contribution in the guidance and supervision of the work developed in this thesis. The human qualities and friendship demonstrated by Dr. Bento through all these years have helped me to overcome with confidence all the obstacles and surpass with successfully negotiate the various stages of my career.

I would like to acknowledge Doctor Rui Pinho, my co-supervisor, for his kindness, friendship and valuable scientific contribution to the enrichment of the work herein presented. I acknowledge the opportunity of having spent two years of my PhD programme in the Eucentre and in Rose School at Pavia (Italy), allowing the development of my scientific knowledge in the seismic engineering field.

The author would like to acknowledge Professor Peter Fajfar (University of Ljubljana, Slovenia), Professor Anil Chopra (University of Berkeley, California, USA) and Professor Rakesh Goel (University of San Luis Obispo, California, USA) for their valuable contributions to the development of the work presented in this thesis.

I would like to acknowledge all my Professors from the Department of Civil Engineering and ICIST from Instituto Superior Técnico, namely the ones from the Structural Dynamics and Earthquake Engineering section.

A special thanks to Doctor Ihsan Bal for providing valuable data related to research work on the topic of this thesis.

The author would like to acknowledge the financial support of the Portuguese Foundation for Science and Technology (Ministry of Science and Technology of the Republic of Portugal) through the PhD scholarship SFRH/BD/28447/2006.

The work developed in this thesis was developed within the framework of the following projects, both funded by the Portuguese Foundation for Science and Technology: POCI/ECM/59306/2004 - Performance-based Seismic Design Procedures; PTDC/ECM/100299/2008 - Nonlinear Static Methods for Assessment/Design of 3D Irregular Structures.

I would like to specially acknowledge my mother, father, sister and brother who have supported me and encouraged me since the beginning with all their love and care. A special thanks to Ana for all her support full of love and tenderness.

To all my friends from Instituto Superior Técnico, Rose School, FEUP (Engineering Faculty from Oporto University) and Aveiro University, for their support and for the fruitful scientific discussions. A special thanks to my friends Eng. Miguel Branco,

Eng. Mário Arruda, Doctor Miguel Lopes, Doctor João Pacheco de Almeida, Doctor Ricardo Monteiro, Doctor Mário Marques, Eng. Alexandre Costa, Eng. António Correia, Eng. Helena Meireles, Eng. Romain Sousa and Eng. Pedro Ferreira.

List of Contents

List of symbols and abbreviations

Abbreviations:

NSP = Nonlinear Static Procedures
CSM = Capacity Spectrum Method
MPA = Modal Pushover Analysis
ACSM = Adaptive Capacity Spectrum Method
RSA = Response Spectrum Analysis
MDOF = Multi degree of freedom
SDOF = Single degree of freedom
MMP = Multi-Modal Pushover procedure
PRC = Pushover Results Combination
SRSS = square root of sum of squares
CQC = complete quadratic combination
UBPA = upper-bound pushover analysis
MMPA = modified version of MPA
ASP = Adaptive Spectra-based Pushover
AMC = Adaptive Modal Combination
IRSA = Incremental Response Spectrum Analysis
DAP = Displacement-based Adaptive Pushover
FTP = Force/Torque Pushover
RC = Reinforced concrete
ADRS = acceleration-displacement response Spectrum
PGA = peak ground acceleration
IDA = Incremental dynamic analysis
DM = Damage measure

IM = Intensity measure

DL = damage limitation

General symbols:

T = Period of the structure

T_B = First spectral characteristic period

T_C = Corner period between the short and medium period range

T_D = Third spectral characteristic period

Ω_x = Period ratio in the X direction

Ω_y = Period ratio in the Y direction

E = modulus of elasticity

f_c = compressive strength

η = damping correction factor used in the EC8 elastic response spectrum definition

S = soil factor used in the EC8 elastic response spectrum definition

β_0 = viscous damping

r = Ratio between the peak ground accelerations of the two components of a bi-directional ground motion record

M = Magnitude

R = distance

CM = Centre of mass

d = displacement

id = Interstorey drifts

cr = Chord rotations

d_r = design interstorey drift;

h = storey height;

ν = reduction factor, which takes into account the lower return period of the seismic action associated with the damage limitation requirement

Vsd = maximum shear value

Vrd = shear capacity

N2 method symbols:

S_e = Elastic acceleration spectrum

S_d = Elastic displacement spectrum

$\overline{F}$ = Vector of the lateral loads

$\overline{F_n}$ = Lateral load at roof level

Φ = Displacement pattern

Φ_n = Displacement at the centre of mass of the roof

M = Mass matrix

m_i = i-th storey mass

m_n = Storey mass at roof level

$\overline{F}_{uni}$ = Vector of the lateral loads with uniform distribution

F_b = MDOF base shear

d_n = Displacement at the centre of mass of the roof

U = displacement vector

$\ddot{U}$ = acceleration vector

R = internal forces vector

1 = unit vector

a = ground acceleration as a function of time

Γ = Transformation factor

m^* = SDOF system equivalent mass

d^* = SDOF system displacement

F^* = SDOF system base shear

T^* = Elastic period of the idealized bilinear SDOF system

F_y^* = Yield strength of the idealized bilinear SDOF system

d_y^* = Yield displacement of the idealized bilinear SDOF system

d_t^* = Target displacement

$S_e(T^*)$ = Elastic acceleration response spectrum at the period T^*

d_{et}^* = Target displacement of the structure with period T^* and unlimited elastic behaviour

q_u = Ratio between the acceleration in the structure with unlimited elastic behaviour $S_e(T^*)$ and in the structure with limited strength F_y^* / m^*

d_t = Target displacement of the MDOF system

MPA symbols:

w_n = Natural frequency of the n-th elastic mode of the building

ϕ_n = Mode of vibration of the n-th elastic mode of the building

V_{bn} = Building's base shear

u_{rn} = Building's roof displacement

s_n^* = Pushover force distribution

s_{ni}^{*} = Load vector at floor *i*

m_i = mass at the floor *i*

I_{pi} = polar moment of inertia at floor *i* about a vertical axis through the centre of mass

ϕ_{xni} = modal displacement component in the X direction of the mode *n* at floor *i*

ϕ_{yn_i} = modal displacement component in the Y direction of the mode *n* at floor *i*

$\phi_{\theta ni}$ = modal rotation component about a vertical axis of the mode *n* at floor *i*

u_{rg} = lateral roof displacement due to gravity loads

Γ = Transformation factor

F_{sn}/L_n - D_n = force-displacement relation for the *n*-th mode inelastic SDOF system

M_n^{*} = Effective modal mass

ϕ_{rn} = value of ϕ_n at the roof in the direction of the selected pushover curve

D_n = Peak deformation of the *n*-th mode inelastic SDOF system

β_n = Damping ratio of the *n*-th mode inelastic SDOF system

T_n = Elastic period of the *n*-th mode inelastic SDOF system

RHA = Response history analysis

u_{rn} = Peak roof displacement of the MDOF structure in the direction of the selected pushover curve associated with the *n*-th mode of the inelastic SDOF system

r_{n+g} = response due to the combination of $u_{rn} + u_{rg}$

CSM symbols:

PF_1 = modal participation factor for the first natural mode

α_1 = modal mass coefficient for the first natural mode

w_i / g = mass assigned to level *i*

ϕ_{i1} = amplitude of mode 1 at level *i*

N = Level N, the level which is the uppermost in the main portion of the structure

V = Base shear

W = building dead weight plus likely live loads

Δ_{roof} = roof displacement

S_a = spectral acceleration

S_d = spectral displacement

β_{eq} = equivalent viscous damping

β_{eff} = effective viscous damping

k = damping modification factor

β_1 = hysteretic damping represented as equivalent viscous damping

E_D = energy dissipated by damping

E_{So} = maximum strain energy

SR_A, SR_V = Spectral reduction factors (CSM-ATC40)

μ = ductility

β_0 = initial viscous damping

T_0 = fundamental period in the direction under consideration

T_{eff} = effective period

$B(\beta_{eff})$ = Spectral reduction factors (CSM-FEMA440)

M = Modification factor

MADRS = modified acceleration-displacement response spectrum

α = post-elastic stiffness

ACSM symbols:

$\Delta_{sys,k}$ = displacement of the equivalent SDOF system in the analysis step k

$S_{a-cap,k}$ = acceleration of the equivalent SDOF system in the analysis step k

$M_{sys,k}$ = effective mass of the equivalent SDOF system in the analysis step k

$V_{b,k}$ = base shear of the MDOF system in the analysis step k

m_i = mass associated with node i of the MDOF system

$\Delta_{i,k}$ = displacement of the node i of the MDOF system in the analysis step k

g = gravity acceleration

β_{eq} = equivalent viscous damping of the system

β_{eff} = effective viscous damping

β_0 = initial viscous damping

μ = is the ductility

α = is the ratio between the post-yield stiffness and the initial stiffness

k = is a measure of how well is the hysteresis instantaneous cycle of the structure represented by a parallelogram

T_{eff} = effective period

Shear strength:

$k = 1$ in regions of low ductility and 0 in regions of moderate and high ductility

$\lambda = 1$ for normal-weight aggregate concrete

N - axial compression force in pounds (zero for tension force)

V_n - total shear strength

V_C - shear strength due to the concrete

V_S - shear strength due to the transverse reinforcement

$f_c^{'}$ - design strength of the concrete

b_w - section width

d - section useful height

A_g - gross section

f_y - design strength of the transverse reinforcement steel

A_v - transverse reinforcement area

s - spacing of the transverse reinforcement

"Everything should be made as simple as possible, but not simpler."

(Albert Einstein)

1. Introduction

This section introduces the study developed in the thesis by contextualizing the selected topic within the civil engineering field with a particular focus on earthquake engineering research.

The main objectives of the thesis are outlined as well as the work developed in each chapter.

1.1 Foreword

Nonlinear Static Procedures (NSPs) can be integrated in a Performance Based Seismic Design philosophy. It is generally recognized that structures designed within these deformation-based criteria, using Performance-Based Design Procedures, are more likely to behave sensibly in seismic scenarios than the structures designed according to the classic force-based philosophy. It is also widely accepted that performance criteria can be better controlled by evaluating the deformations in the structure, both at global and component levels.

Nonlinear Static Procedures are deemed to be very practical tools to assess the nonlinear seismic performance of structures. On the other hand, nonlinear dynamic *time-history* analyses are very time-consuming, which is a relevant drawback in design offices, where the deadlines are restrictive.

The NSPs introduced in this context are a powerful tool for performance evaluation. Seismic design codes, like the FEMA273, FEMA356, FEMA440 and the ATC40, have recommended the use of this type of procedures. More recently, Eurocode 8 also incorporated the procedure as an evaluation technique.

Several scientific studies were developed demonstrating the good performance of some NSPs on the seismic assessment of relatively simple structures such as regular buildings capable of being analysed by planar frames and bridges, [1, 2, 3, for instance].

However, some issues still need to be clarified regarding the format with which the pushover analysis has to be performed, thus requiring further research and development. The positive outcome from recent research seems to indicate that it is certainly worthwhile to continue to pursue the further development and/or verification of NSPs taking a further step with the 3D Pushover problem, with the objective of arriving at an eventual introduction in seismic design codes and regulations of improved procedures capable of dealing with plan irregular structures.

1.2 Aims of the work

The employment of NSPs in the seismic assessment or design of structures has gained considerable popularity in recent years, backed by a large number of extensive verification studies that have demonstrated their relatively good accuracy in estimating the seismic response of regular structures (planar frames and bridges).

However, the extension of such use to the case of 3D irregular structures has been the object of only restricted scrutiny, which effectively ends up by limiting significantly the employment of NSPs to assess actual existing structures, the majority of which do tend to be non-regular [4, 5, 6, 7].

In addition, these few studies were typically concentrated on the application and verification of a single nonlinear static procedure only, rather than providing a comparative evaluation of the different available methodologies describing their relative accuracy and limitations.

In order to obtain useful elements of comparison between different methodologies, the performance of commonly employed nonlinear static procedures is evaluated in this work – Capacity Spectrum Method (CSM) with the features proposed in ATC40 and in FEMA440, original N2 presented in Eurocode 8, Extended N2 method to plan irregular structures, Modal Pushover Analysis (MPA) and Adaptive Capacity Spectrum Method (ACSM).

Comparison of the results obtained with nonlinear dynamic analysis, through the use of semi-artificial ground motions, enables the evaluation of the accuracy of the different NSPs.

NSP performance is evaluated by comparing the seismic response estimation of the analysed buildings in terms of lateral displacement profiles, top displacement ratios,

interstorey drifts, chord rotations, normalized top displacements and base shear. The performance of the procedures in evaluating the damage limitation according to the Eurocode 8 provisions is also verified.

Large-scale parametric studies were performed for several seismic intensities in order to evaluate NSP performance when the buildings go through different stages of structural inelasticity.

Furthermore, an extension of CSM-FEMA440 for plan asymmetric buildings is proposed. It combines the results of a pushover analysis performed according to the FEMA440 report recommendations and the results of a linear dynamic response spectrum analysis. The concept used for this proposal is based on the Extended N2 method proposed by Fajfar and his team [4, 8].

A new 3D Pushover procedure is also proposed in order to overcome the torsional problem in plan asymmetric buildings in a more accurate manner. It combines the most powerful features of some NSPs studied herein.

The case studies used in this work are three real existing reinforced concrete (RC) buildings asymmetric in plan. The buildings selected in this study are quite different namely in terms of height (number of storeys), plan configuration, material properties and reinforcement details. Additionally, the structural response specificities of the eight storey building, allow the assessment of the NSP performance in such particular cases.

This work has also the objective of contributing to the improvement of the most important seismic codes with respect to the nonlinear static analysis of plan irregular buildings. Therefore, a parametric study is developed, comparing the Extended N2 procedure with the original N2 proposed in Eurocode 8. The results obtained herein will corroborate the ones recently published by other authors contributing to the confirmation of this extended method as a potential procedure to be incorporated in the next version of Eurocode 8. The proposed Extended CSM-FEMA440 presents potential to be integrated in the next version of the ATC guideline. The new 3D Pushover procedure herein presented can also be integrated in seismic codes as a more refined method to assess plan irregular buildings.

The work that has been carried out over the recent years by leading researchers in the field is clearly producing promising results, which lend growing confidence to the employment of NSPs in the seismic assessment and design of irregular 3D structures. This work aims at contributing to the progress beyond the current state of the art, taking a further step in the 3D Pushover problem in order to reach more consolidated conclusions.

1.3 Thesis outline

A brief review of the content of each chapter will be presented as follows.

In chapter 1 an introduction of the thesis is presented, pointing out the main objectives of the work developed.

In chapter 2 the state of the art is reviewed. The seismic design philosophies and the seismic analyses procedures associated are presented. This chapter focuses on the evolution of the existing Nonlinear Static Procedures, describing their main features and innovations. In the last sub-section of the chapter the most popular and commonly used Nonlinear Static Procedures, which are analysed in this thesis, are duly described.

Chapter 3 presents the case studies used in this thesis and the modelling options assumed during the work developed.

In section 3.1 the analysed case studies are presented. Three real existing RC buildings were tested: the three storey SPEAR building irregular in plan representative of the construction in the Mediterranean region (mainly in Greece) in the 1970's and experimentally and numerically investigated in the SPEAR project (an European project within the 6^{th} framework), and two existing Turkish RC buildings with five and eight storeys.

In section 3.2 the options considered in the development of the 3D computer models of the analysed buildings are described. The dynamic properties of the case studies are also described. A comparison between the experimental results of the SPEAR building pseudo-dynamically tested in full scale at Elsa laboratory in Ispra, Italy, and the analytical results obtained with the 3D model is presented. Both results show good agreement, validating the modelling options considered in this work. It is important to note that the main objective of this study is to compare the potential of nonlinear static procedures and *time-history* analysis. Therefore, the models used in each type of analysis had the same properties in order to reach valid comparison results. The modelling options assumed seemed to be the best trade-off between efficiency and computation time of the analyses. Some simplifications were considered in the models in order not to increase the time taken by the analyses but keeping an acceptable level of accuracy. This accuracy was confirmed for the SPEAR building through the comparison between the numerical and experimental results.

Chapter 4 presents the accelerograms used in this work for each one of the analysed buildings, as well as the respective compatible and target response spectra. The analyses performed during the endeavour are also described.

In chapter 5, the pushover capacity curves obtained for each analysed building are presented and analysed. They are compared with the nonlinear dynamic analysis results obtained for increasing seismic intensities. Preliminary comments about the structural capacity of the buildings are outlined.

In chapter 6 the performance of CSM with the features proposed in ATC40 is compared with the CSM with the features presented in the FEMA440 report. The results are presented for all the analysed buildings and for a wide range of seismic intensities. The results are compared with the *time-history* results. Several measures are analysed such as: top displacement ratios, lateral displacement profiles, interstorey drifts and chord rotations, base shear index and normalized top displacements.

Chapter 7 presents a comparison between the performance of the original N2 method proposed in Eurocode 8 and of the Extended N2 method for plan asymmetric buildings proposed by Fajfar and his team. The results of the NSPs are compared with nonlinear dynamic analyses.

In chapter 8, the performance of the CSM-FEMA440, the Extended N2 method, the MPA and the ACSM on the seismic assessment of the analysed buildings is evaluated for increasing levels of intensity. Once again the results obtained are compared with the ones from *time-history* analysis. Eurocode 8 provisions in terms of damage limitations are verified for the NSPs under analysis. In this thesis, it is assumed that the structures are properly designed for shear, and therefore the collapse of the buildings is not due to brittle failures. In this section, the shear strength according to the specifications of ATC40 is verified for some elements in the three analysed buildings for the different seismic intensities tested.

In chapter 9 an extension of CSM-FEMA440 to plan asymmetric buildings is proposed. The good results of the method were presented for the analysed buildings for a wide range of seismic intensities and compared with the ones from nonlinear dynamic analyses.

In chapter 10 a new 3D pushover procedure for the seismic assessment of plan asymmetric buildings is proposed. This procedure is based on the most accurate and efficient features of some of the commonly used NSPs which were analysed in chapter 8. The good results obtained with the method for the seismic assessment of the analysed buildings are presented for several seismic intensities and they are compared with the nonlinear *time-history* analyses.

Finally, in chapter 11 conclusions of the work developed are drawn and future work is outlined.

2. State of the art

In the first section of this chapter the evolution of the nonlinear static procedures over time is presented. Starting from the first methods proposed to the recently advanced procedures, the state of the art overview is described.

In the second part of the chapter, the nonlinear static procedures used in this work are described in detail.

2.1 Seismic design philosophies

The seismic evaluation of structures has been generally based on a Force-Based design philosophy, where the structural elements are assessed in terms of stresses caused by the equivalent seismic forces. Therefore, the main concern within this design philosophy is to give strength to the structure rather than displacement capacity. Some procedures have been proposed in the past, such as the Response Spectrum Analysis (RSA) [9], which has been implemented in seismic codes all over the world and is still commonly used by the majority of structural design engineers. In this procedure, the structure is considered to have an elastic behaviour. The periods and the modes of vibration are calculated, and the response of the structure is computed through the application of a response spectrum. The forces in the elements are divided by a behaviour factor in order to take into account the nonlinearity of the materials. A complete description of the method can be found in [10].

More recently, Priestley [11] published a critical review on the drawbacks of this method. The main fallacies pointed out are the following:

1) A response spectrum is obtained from an accelerogram by running this record in several single degree of freedom (SDOF) systems with different periods of vibration. The value of the response spectrum corresponding to a certain period is obtained taking the maximum response of the SDOF with that period. As a consequence the duration effects of the dynamic response are ignored, which may not be valid in the case of plastic responses;

2) The response spectrum analysis uses the combination of modal responses, so the final response is a combination of the response associated with each mode of vibration. Thus, this principle leads to internal forces that do not respect the equilibrium;

3) The stiffness degradation is not taken into account. The method considers a mean value of this parameter which may produce wrong estimations of internal forces;

4) The design forces obtained from the modal combination are reduced using a behaviour factor, in order to take into account the ductility and overstrength of the structure. The use of a single value to reduce the internal forces seems to be a rough solution to represent the nonlinearity of the materials. In fact, the higher modes may not be controlled by the same level of ductility of the fundamental mode. Therefore, using the same force reduction factor in all modes may underestimate the higher mode effects in terms of internal forces;

Other authors have also been scrutinizing more drawbacks in the response spectrum analysis procedure. Gutierrez and Alpizar [12] mentioned that this procedure does not give any information about failure modes, required global ductility and corresponding inelastic deformation of structural elements. All these neglected features are very important to evaluate the seismic performance of the structure.

In recent years the need for changes in the existing seismic design methodology implemented in codes has been generally recognized. The structural engineering community has been creating a new generation of design and rehabilitation procedures based on a new philosophy of performance-based engineering concepts. It has become widely accepted that one should consider damage limitation as an explicit design consideration [13]. In fact, the damage and behaviour of the structures during an earthquake is mainly governed by the inelastic deformation capacity of the ductile members. Therefore, the seismic evaluation of structures should be based on the deformations induced by the earthquake, instead of the element stresses caused by the computed equivalent seismic forces, as happens in the Force-Based philosophy. In recent years, several attempts have been made to introduce displacement-based methodologies in seismic engineering practice. These methodologies can be divided into two main groups: displacement-based design methods for the design of new structures [14, 15], and displacement-based evaluation methods for the seismic performance assessment of pre-designed or existing structures.

Two key elements of a performance-based procedure are demand and capacity. The demand represents the effect of the earthquake ground motion (it can be defined by means of a response spectrum or an accelerogram). The capacity of a structure

represents its ability to resist the seismic demand. The performance depends on how the capacity is able to handle the demand. The structure must have the capacity to resist the demands of the earthquake such that its performance is compatible with the design objectives.

Within this context, nonlinear seismic analyses of structures are extremely important in order to correctly assess their seismic performance, Figure 2.1.

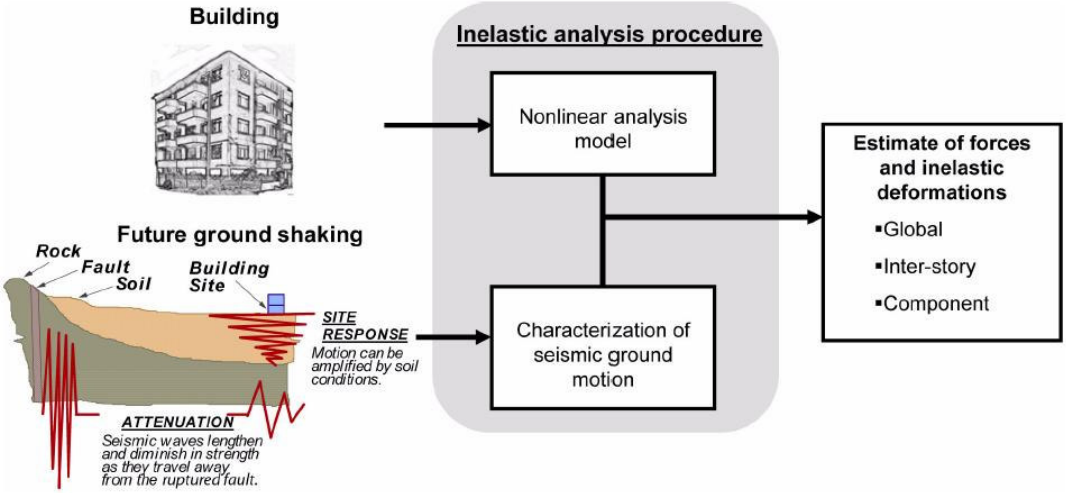

Figure 2.1 – Use of inelastic analysis procedures to estimate inelastic forces and deformations for given seismic ground motions and a nonlinear analysis model of the building [16].

2.2 Nonlinear dynamic *time-history* analysis

The nonlinear dynamic *time-history* analysis is widely accepted as being the most accurate method for the seismic assessment/design of structures. This method overcomes all the problems associated with the RSA previously mentioned. The properties of each structural element are properly modelled, including nonlinearities of the materials, with the analysis solution being computed through a numerical step-by-step integration of the equilibrium equation, Eq. 2.1, where M, C and K represent the mass, damping and stiffness matrixes, respectively, $\{a_r(t)\}$, $\{v_r(t)\}$ and $\{d_r(t)\}$ the relative acceleration, velocity and displacement vectors, respectively, and $\{a_g(t)\}$ the ground acceleration.

$$M \cdot \{a_r(t)\} + C \cdot \{v_r(t)\} + K \cdot \{d_r(t)\} = -M \cdot \{a_g(t)\} \qquad \textit{Eq. 2.1}$$

Therefore, it allows the assessment of the dynamic response of the structure over time, including local and global responses. This fact avoids the use of behaviour factors and their fallacious effects, since they may not account in a correct way for the

structural ductility. Despite the accurate results, the method presents important drawbacks which make its application in the majority of design offices almost impossible:

1) Step-by-step integration demands a considerable computational effort and is very time-consuming;

2) The dispersion of the results due to the nonlinear behaviour of the structures implies that it is necessary to consider a set of accelerograms and calculate the mean, median or maximum responses, in order to obtain reliable results. This implies more analyses for the structure under study, which is reflected in an increased time overhead;

3) There is a lack of knowledge in the common practice of engineers in terms of record selection to use in *time-history* analysis. The state of the art and the studies developed in this topic have not arrived at definitive conclusions;

4) Chopra [17] reports that the results obtained from a *time-history* analysis depend on the modelling options such as the hysteretic relationships of the materials;

5) The nonlinear effects can only be correctly reproduced by using sophisticated finite elements associated with lumped or distributed plasticity models. These elements should be able to correctly model specific dynamic properties such as stiffness and strength degradation and pinching. In order to obtain reliable results from the nonlinear dynamic analysis, the user should perfectly understand all these phenomena and introduce the correct input values in order to correctly describe them.

2.3 Nonlinear static procedures (NSPs)

It is generally accepted that nonlinear seismic analyses lead to more accurate results than RSA. In order to overcome the previously mentioned inherent difficulties of the *time-history* analysis and allow structural engineers to perform nonlinear seismic analysis in a practical but still accurate way, the so-called Nonlinear Static Procedures (NSP) have been recently developed.

The Nonlinear Static Procedure is based on a static nonlinear analysis called pushover analysis. In this procedure, a monotonic load (forces or displacements) representing the equivalent seismic action, with an invariant or adaptive pattern, is incrementally applied to the structure. This analysis should also include the gravity loads. The outcome of the pushover analysis is the so-called pushover curve (capacity curve), which represents the variation of the base shear (V) with respect to the roof displacement (D) in a selected controlled node, Figure 2.2. This curve gives important information about the global strength and deformation capacity of the structure under analysis.

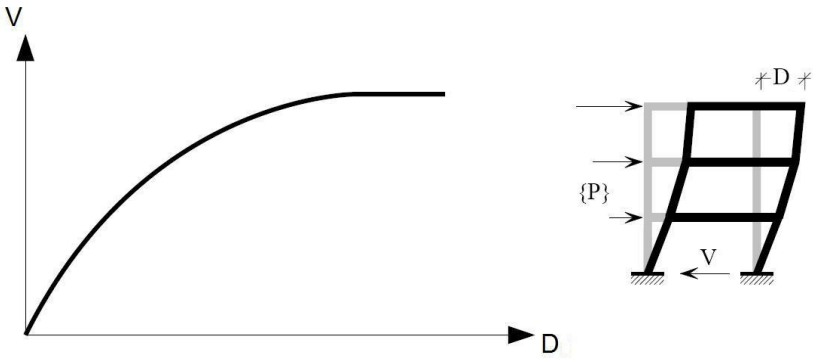

Figure 2.2 – Capacity curve of the MDOF system.

Afterwards, the pushover curve of the multi-degrees of freedom (MDOF) system is transformed into a pushover curve of an equivalent single degree of freedom (SDOF) system, Figure 2.3.

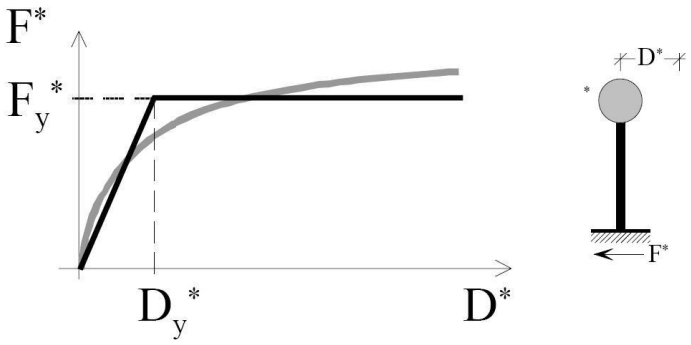

Figure 2.3 – Capacity curve of the equivalent SDOF system.

From this pushover curve it is possible to calculate the inelastic displacement of the equivalent SDOF – the so-called target displacement (D_t^*) – corresponding to the seismic action under study through the use of an inelastic or reduced spectrum, Figure 2.4.

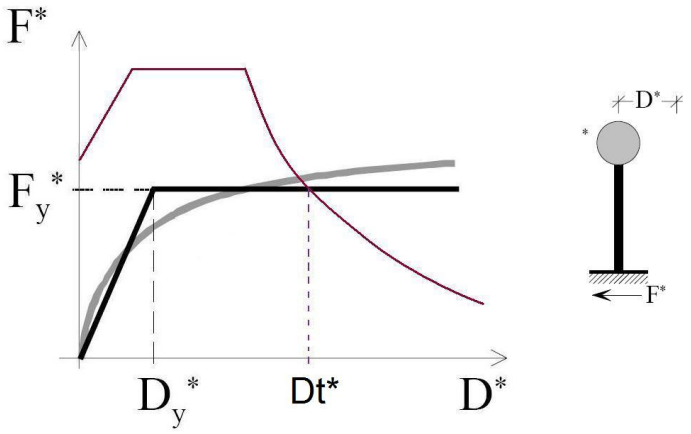

Figure 2.4 – Calculation of the SDOF target displacement.

The inelastic displacement of the controlled node (D_t) is obtained by making the correspondence of the target displacement of the SDOF system to the MDOF. In order to obtain the peak inelastic deformations of individual structural elements, such as interstorey drifts or chord rotations, one has to go back to the MDOF pushover curve step corresponding to the controlled node inelastic displacement previously calculated, and take the results in the desired elements, Figure 2.5. The specific features of each of the previously mentioned steps depend on the method used.

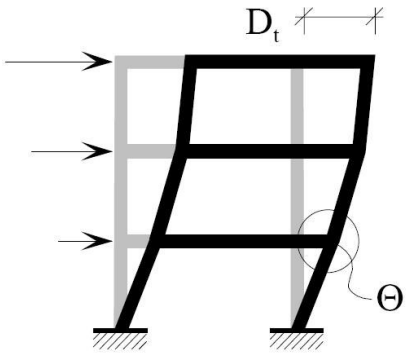

Figure 2.5 – MDOF results corresponding to the SDOF target displacement.

The nonlinear static procedures can be classified as displacement-based evaluation methods for the assessment and rehabilitation of existing structures. However, these methods can be applied together with displacement-based design methods for the seismic design of new structures. In fact, to perform a pushover analysis it is necessary to develop a nonlinear model of the structure, which includes the nonlinear formulation of the material relationships. In the case of reinforced concrete structures, the reinforcement in the elements must be correctly defined. Therefore, in new structures one should perform a preliminary design using displacement-based design methods, and afterwards check the acceptability criteria by using a nonlinear static procedure. If these criteria are not verified, a new design should be performed and a new verification should be done afterwards. This iterative process ends, when all the desired criteria are checked. The process described in this paragraph corresponds to the ideal seismic design procedure.

Despite the encouraging results obtained in several scientific studies, one should be aware that the NSPs have an intuitive basis instead of a pure mathematical basis [18].

The main advantages of the nonlinear static analysis when compared with the linear static and linear dynamic analysis are listed below:

1) The seismic assessment and design using nonlinear static analysis are performed based on the control of structural deformations;

2) The NSPs explicitly consider the nonlinear behaviour of the structure instead of using the behaviour factors applied to the linear analysis results. In fact, these factors are not accurately defined for all kinds of structures;

3) The nonlinear static analysis allows the definition of the capacity curve of the structure allowing the sequential identification of the structural elements that yield and collapse. This analysis identifies the structural damage distribution along the structure during the loading process, giving important information about the structural elements that first enter the inelastic regime which can turn out to be very useful when performing seismic strengthening of the structure;

4) The nonlinear static analysis is very useful within the performance based design and assessment philosophy, because it allows the consideration of different limit states and the performance check of the structure for the corresponding target displacements.

2.3.1 Pushover methods for 2D planar analysis

The use of nonlinear static procedures for the seismic assessment of planar frames and bridges has become very popular amongst the structural engineering community. The reason for their success lies in the possibility of gaining an important insight into the nonlinear seismic behaviour of structures in a simple and practical way. Their use is also supported by extensive scientific studies [1, 2, 19, 20] that validate their good performance in the seismic assessment of such relatively simple structures.

2.3.1.1 Conventional pushover methods

The nonlinear static procedures were officially introduced in design codes all over the world. They started to be implemented within the framework of performance-based seismic engineering ATC40 [21], FEMA237 [22] and FEMA356 [23]. Recently, the Japanese structural design code for buildings [24] has adopted the capacity spectrum method (CSM) [1, 19] of ATC40 as a seismic assessment tool. In Europe, the N2 method [2, 20] was implemented in Eurocode 8 [25].

The capacity spectrum method, first introduced by Freeman [19] and latter included in ATC40, and the N2 method created by Fajfar and his team [2] and included in Eurocode 8, rely on a pushover analysis using invariant load patterns (the load pattern does not change during the analysis, only the force intensity) to estimate deformation demands under seismic loads. The forces used in the pushover analysis are proportional to the first mode of vibration of the structure under analysis. The N2 method represents the seismic demand by an inelastic spectrum.

The FEMA440 report [16] presents several reasons to be cautious when using conventional force-based pushover methods to estimate the seismic demand in the entire deformation range:

1) These methods are not able to correctly reproduce the deformations when higher modes are important. This inaccuracy is also observed when the structure is highly pushed into its nonlinear post-yield range;
2) Force-based pushover methods cannot predict in a correct manner the local damage concentration which is responsible for the modal properties change;
3) They neglect sources of energy dissipation such as kinetic energy and viscous damping;
4) Three dimensional and cyclic earthquake loading effects cannot be easily taken into account by these methods.

It is generally recognized that these simplified procedures do not lead to adequate results in structures where the higher modes contribute to the response and the inelastic effects modify the distribution in height of inertia forces (e.g., Gupta and Kunnath [26], Kunnath and Kalkan [27], Kalkan and Kunnath [28], Goel and Chopra [29]).

2.3.1.2 Multi-mode pushover methods

In order to overcome some of the aforementioned drawbacks, several researchers have proposed new pushover procedures to account for higher mode effects, but keeping the invariant load patterns, the so-called Multi-Modal Inelastic Procedures. These new methods use the concept of modal combination:

a) some of them consider a single pushover analysis where the load vector takes into account the contribution of each elastic mode shape;

b) others consider a multi-run pushover analyses, using in each run a load vector that reflects the contribution of each elastic mode shape, and where the contribution of each mode is combined at the end.

These procedures aim to account for higher mode effects and use elastic modal combination rules, but using invariant load vectors. Paret et al. [30] first presented the Multi-Modal Pushover procedure (MMP). In this method, multiple pushover analyses are performed on the building using lateral load patterns proportional to mode shapes, leading to multiple modal pushover curves which are graphically plotted with the demand spectrum in order to calculate the seismic demand. However, the procedure does not specify how to combine the individual modal responses.

Latter, this procedure was refined by Moghadam and Tso [31]. In this improved version called Pushover Results Combination (PRC), the final response was calculated through a weighted sum of individual modal responses. The weights used in this equation were the modal participation factors.

The modal pushover analysis (MPA) of Chopra and Goel [3] is a more complete version of the multi-mode pushover analysis. This is a multi-run method, where several pushover curves are obtained from load patterns proportional to each mode of vibration. The final response is obtained combining the results corresponding to each pushover curve using an appropriate combination rule (e.g. SRSS - square root of sum of squares or CQC - complete quadratic combination). The MPA proposed by Chopra and Goel is the most famous multi-modal pushover with invariant loads.

The upper-bound pushover analysis (UBPA) procedure of Jan et al. [32] is another example of these new multi-modal methods. The procedure is based on a single pushover analysis with a single lateral force vector obtained as a combination of first mode and factored second mode shapes. The authors recommend using the envelope of the results obtained with a conventional pushover analysis with an inverted triangular force pattern and with the proposed procedure. In fact, the authors showed that the first one leads to good predictions in terms of drifts at lower stories while the proposed procedure leads to good estimations at the upper stories.

Later, Hernández-Montes et al. [33] have adapted the MPA technique into an Energy-based Pushover formulation. Recently, Chopra et al. [34] presented a modified version of MPA (MMPA) in which the inelastic response of the pushover analysis, using a load vector proportional to the first mode, is combined with the elastic contribution of higher modes. Kunnath has developed new lateral load configuration using factored modal combinations in order to represent the seismic demand in a more realistic manner [35]. All these methods led to improved estimations of interstorey drifts profiles when compared with conventional NSPs.

More recently in 2011, Fajfar and his team have proposed an extension of the N2 method to take the higher mode effects into account [36]. The original N2 method was developed for buildings where the response was controlled by the first mode of vibration. However, in medium and high rise buildings the higher mode effects can be very important to the structural response, mainly along the elevation of the building. This extended procedure considers that the structure remains in the elastic range when vibrating in higher modes. The seismic demand is determined by an envelope between the results of a pushover analysis, which does not include higher mode effects (e.g. the original N2 method), and the normalized responses of an elastic modal analysis, which includes higher mode effects. According to the authors, it was observed that the pushover analysis usually controls the response of the structure in the locations with the major plastic deformations while the elastic analysis controls the areas where the higher mode effects have more influence. The difference between this Extended N2 method and the MMPA previously described lies in the combination of the pushover analysis (representing the first mode influence) and the elastic modal analysis (representing the higher mode effects). The Extended N2 method calculates the seismic demand as the envelope of the pushover analysis and of the elastic modal analysis, while the MMPA combines the results of both pushover and elastic analysis using a SRSS or CQC combination rule. In [36] the authors compared the performance of the Extended N2 method with the MMPA, the MPA, the original N2 method (considering the first mode of vibration) and with the nonlinear *time-history* analysis, in medium and high-rise buildings, see Figure 2.6.

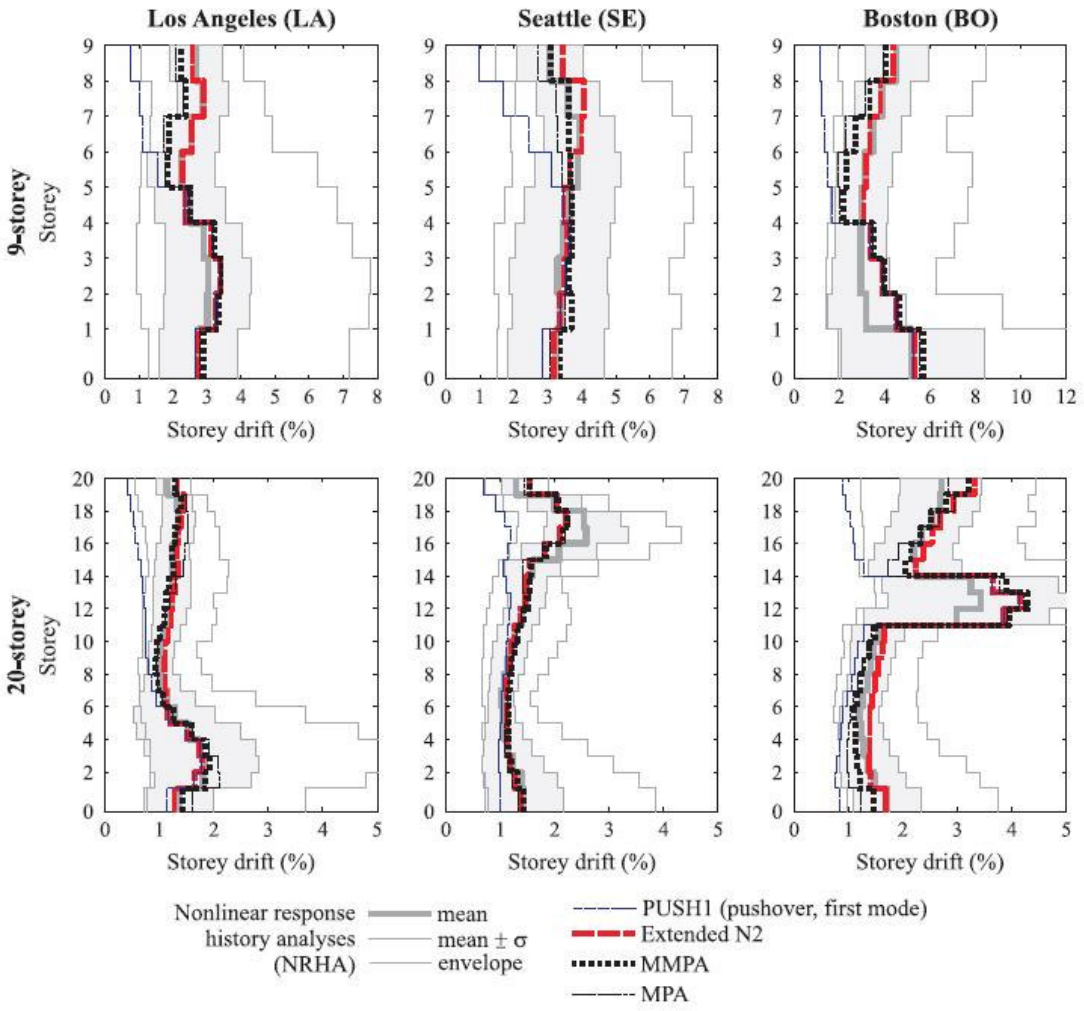

Figure 2.6 – Comparison between the Extended N2 method, MMPA, MPA, original N2 method and time-history analysis [36].

The results obtained show a significant influence of higher modes on interstorey drifts in the upper parts of the medium and high-rise test buildings. The authors concluded that the Extended N2 method usually led to slightly larger estimates than the MPA and MMPA, and they were generally conservative when compared with the mean values of the nonlinear dynamic analysis, see Figure 2.6. The accuracy of the evaluated NPSs decreased with an increasing height of the structures, increasing intensity of the ground motion and an increasing ratio between the spectral accelerations of the second and first mode periods. They also confirmed that the elastic analysis represents a conservative estimate of the response in the upper part of the buildings, while in the lower part the response is controlled by the pushover analysis. The authors end the work by saying that this Extended N2 method seems to be a good improvement of the original N2 method at least with respect to medium-rise buildings subjected to realistic intensities of ground motions.

2.3.1.3 Adaptive pushover methods

The previously described methods use invariant load patterns based on the initial elastic dynamic properties of the structure. However, they do not take into account damage accumulation, and consequently modification of the modal parameters. In fact, these two changes characterize the structural response for increasing loading levels. Krawinkler and Seneviratna [37] wrote that it is limiting to use fixed load patterns (whether first mode or multi-mode proportional) because a fixed distribution cannot reproduce the dynamic response over the entire deformation range. This fact motivated the development of a new class of pushover procedures called Adaptive Pushover methods. In these procedures the loading vector is updated at each analysis step in order to represent the progressive stiffness degradation of the structure during the inelastic range. They are also called Incremental Response Spectrum Analysis by some researchers [38] and they consider the effects of the higher modes and of the input frequency content.

Several adaptive procedures have been proposed by Bracci et al. [39], Sasaki et al. [40], Satyarno et al. [41], Matsumori et al. [42], Gupta and Kunnath [26], Kalkan and Kunnath [43], Requena and Ayala [44], Elnashai [45], Antoniou and Pinho [46] and Aydinoglu [38]. The procedures proposed by the last four are based on the same concepts, the difference is that Elnashai, Antoniou and Pinho implemented the procedure using fibre based elements. This fact allows a continuous load distribution update, instead of a discrete update.

The adaptive pushover method proposed by Bracci et al. [39] uses a lateral force distribution depending on the stiffness, and derived from incremental storey demands. Therefore, the method takes the higher mode effects into account, especially the development of mid-height storey mechanisms.

Matsumori et al. [42] presented a new modal combination rule for the procedures that used individual modal responses (storey forces or displacements). They proposed two new patterns of storey shear distributions which were computed from the sum and the difference of the first two modal storey shears.

Gupta and Kunnath [26] proposed an updated version of this procedure called Adaptive Spectra-based Pushover (ASP). In this method, a force pattern was used which was modified depending on the instantaneous dynamic properties of the system. The higher mode effects (considering the contribution of higher modes to the force pattern computation) and the ground motion characteristics are also taken into account. However, the combination of responses of individual modes at each load step does not respect the equilibrium of external forces and internal resistances, which is an important drawback of the proposed method.

More recently, Kalkan and Kunnath have proposed the Adaptive Modal Combination (AMC) procedure [43] in which the adaptive inertia force patterns applied to the structure are based on the mode shapes. The modal properties of the system are modified as the earthquake load carries on. The method incorporates the inherent

advantages of CSM and MPA. The MDOF to SDOF transformation is computed using an energy-based approach. The performance point is calculated intersecting the SDOF capacity curve with an inelastic response spectrum computed for a ductility level corresponding to the global system ductility. This procedure is repeated for each of the considered modes of vibration, and the final responses are obtained combining the peak modal responses using a SRSS or CQC combination.

Requena and Ayala [44] proposed two new approaches. One of them was an adaptive version of the force distribution proposed by Freeman et al. [47], where the lateral force applied in the pushover analysis was obtained combining the individual peak modal storey forces with the SRSS combination rule. The other one was an adaptive version of the force distribution proposed by Valles et al. [48].

Aydinoglu [38] presented the Incremental Response Spectrum Analysis (IRSA), which is an improved version of the adaptive spectra-based pushover (ASP) developed by Gupta and Kunnath [26]. The method considered a displacement vector instead of forces in the adaptive pushover analysis. It used an inelastic design spectrum instead of an elastic spectrum for the computation of intermodal scaling factors. The final responses were obtained combining the individual modal maximum results corresponding to the respective target displacement. The author also proposed the use of the equal displacement rule for the calculation of modal target displacements.

The adaptive procedures improved the response obtained with the pushover analysis, making its results closer to the nonlinear *time-history* analysis. The reasons for the better results are the following:

1) Use of spectrum scaling;
2) Consideration of higher modes contribution;
3) Change of the local resistance and modal properties due to the accumulated damage;
4) The methods update the loading vector using the eigenvalues solution from the nonlinear stiffness and mass matrix at each step.

It is recognized that these methods present a more refined and elaborate formulation than the previous generations of pushover analysis. However, the force-based adaptive pushover procedures do not bring much improvement when compared with the force-based invariant pushover procedures, especially in terms of deformation patterns estimation in buildings. In fact, both types of analysis cannot correctly predict this parameter [49, 50].

Kunnath [35] and López-Menjivar [51] showed that this poor performance is the result of the use of quadratic modal combination rules (SRSS, CQC) to compute the adaptive loading vector. In fact, using these rules one cannot reproduce the sign change in the applied loads, therefore the load vectors will be monotonically increased.

Antoniou and Pinho [46] have proposed the so-called Displacement-based Adaptive Pushover (DAP). In this method, the loading vector is updated at each step of the analysis based on the current dynamic characteristics of the structure. The loading vector is obtained by combining the contribution of the different modes of vibration in terms of displacements. The forces/shear are the result of the structural equilibrium with respect to the applied displacements. This method is able to reproduce the reversal of storey shear, even when using a quadratic combination. By applying displacements instead of forces, the method follows the recent seismic design/assessment trends of using displacements instead of forces. In fact, it is recognized that the structural damage induced by the seismic action is caused by the response deformations. The results obtained with the method, mainly in terms of deformation profiles, are more accurate than the ones obtained using previous pushover proposals [52]. Later, Casarotti and Pinho proposed the Adaptive Capacity Spectrum Method (ACSM) [53] to bridges. The method is based on the concepts of the Capacity Spectrum Method (CSM), in which the target displacement is obtained by intersecting the SDOF capacity curve with a reduced response spectrum. Instead of using an invariant force pattern, as happens in the original CSM, the ACSM uses the DAP methodology. This method was also tested on planar frames [54]. In both bridges and planar frames, the results obtained with the ACSM are quite accurate.

2.3.1.4 Target displacement calculation

Existing methods use different approaches for the target displacement calculation depending on how energy dissipation mechanisms are taken into account.

The first approach is based on equivalent linearization, in which the target displacement is computed intersecting the SDOF capacity curve with an overdamped elastic spectrum. This spectrum is obtained from the elastic spectrum by dividing it by a spectral reduction factor (e.g. Newmark and Hall [55], ATC40 [21], Ramirez et al. [56], Lin and Chang [57], Eurocode 8 [25], FEMA440 [16], Priestley et al. [15]). This factor can be a function of the equivalent viscous damping (e.g. Eurocode 8 [25], Ramirez et al. [56], Lin and Chang [57]). The equivalent viscous damping can be secant period based (e.g. Gulkan and Sozen [58], Kowalsky et al. [59], Grant et al. [60], Dwairi et al. [61], Priestly et al. [15]) or effective period based (e.g. Iwan [62], Kwan and Billington [63], Guyader and Iwan [64]).

The second approach consists of the use of an inelastic spectrum for the target displacement calculation (e.g. Newmark and Hall [55], Vidic et al. [65], Eurocode 8 [25]). The third one uses empirical displacement coefficients determined from statistical analysis to define displacement modification factors (e.g. Miranda [66], Chopra [17]).

The methods proposed in ATC40 [21], in FEMA356 [23] and in most of the previously mentioned methods, have several limitations.

In ATC40, the target displacement is obtained by equivalent linearization and in FEMA356 by using the displacement coefficient method. Other pushover procedures use an elastic spectrum with elastic modal periods, an inelastic spectrum such as the N2 method [20], or inelastic SDOF dynamic responses to approximate the target displacement such as the MPA [3].

Miranda and Akkar [67] showed that target displacements in short period structures obtained with ATC40 and FEMA356 are considerable different from each other, and significantly different from the *time-history* response. In order to overcome these limitations, the CSM and the displacement coefficient method were improved in the FEMA440 report [16]. These approximate methods as well as the ones that use the equal displacement rule may not be adequate for the period range of low to mid rise buildings in the case of near-fault records.

2.3.1.5 MDOF to SDOF transformation

The majority of the aforementioned procedures, e.g. the N2 method, the CSM and the MPA, consider the centre of mass of the roof as the control node to convert the MDOF system to the equivalent SDOF. However, this option is only meaningful for the first mode.

In these methods, the MDOF to SDOF conversion is made dividing the response of the centre of mass of the roof by a transformation factor. One of the major criticisms of this transformation procedure is the use of initial elastic properties to estimate the transformation factors, such as the modal participation factor. In fact, this is not theoretically consistent when the structure deforms inelastically.

Hernandez-Montes et al. [33] showed in 2004 that this procedure may lead to inadequate results, and to overcome this problem they proposed an energy-based representation of the capacity curve implemented in the MPA method. Although, this method considers two options which can lead to not so accurate results: the inelastic system features are obtained from the elastic modal properties; it uses an invariant load pattern, incapable of reproducing the structural yielding during the pushover analysis. The AMC procedure [43] overcomes the two drawbacks mentioned, by considering an adaptive force pushover proposed by Gupta and Kunnath [26] in 2000, and by transforming the MDOF system into the equivalent SDOF step by step through an energy based formulation.

In 2007, the ACSM [53] proposed by Casarotti and Pinho considers an MDOF to SDOF transformation based on the principle of Substitute Structure analogy which was also derived using the principle of the equal work developed. For this transformation, the method considers the contribution of all structural nodes considering the current deformed pattern.

2.3.2 Pushover methods for 3D plan asymmetric buildings

The use of Nonlinear Static Procedures (NSPs) for the seismic assessment of plan regular buildings and bridges is widespread nowadays. Their good performance in such cases is widely supported by the extensive number of scientific studies described in the previous pages. However, the applicability of NSPs on plan-irregular 3D buildings has so far been the object of a limited number of papers. This limitation leads to a minor use of these methods to assess current existing structures, the majority of which do tend to be irregular in plan. The most important issue that controls the structural response of this kind of structures is torsion. The aforementioned NSPs are not able to reproduce in a correct manner the torsional response of plan irregular buildings; therefore one should be cautious when using these methods to assess these structures.

In order to overcome the torsional problem in plan asymmetric buildings, some researchers have proposed new pushover approaches. In 1997 Kilar and Fajfar [68] have presented the use of a 3D model for the pushover analysis of plan irregular buildings. They used an invariant force pattern with an inverted triangular shape at the centre of mass of the floors. In this study the authors arrived at the conclusion that the torsional rotation was strongly dependent on the orthogonal structural elements.

In 1998 Faella and Kilar [69] tested different location in plan to apply the lateral forces of the pushover analysis of plan irregular buildings. Three eccentricities, measured from the centre of mass location, were applied. In this study, the target displacement was defined as the maximum response obtained from the nonlinear *time-history* analysis. The torsional rotation was always underestimated, even when the eccentricity was maximum.

In the same year, De Stefano and Rutenberg [70] considered in their study the interaction between walls and frames in a pushover analysis of 3D asymmetric multistorey wall-frame structures. They applied the pushover forces considering the design eccentricities prescribed in the Uniform Building Code [71]. The results obtained were generally close to the *time-history* except at the flexible edges where the pushover analysis overestimated the response.

In 2000, Azuhata et al. [72] included the torsional effects in the pushover analysis by introducing two factors to the analysis: the strength modification factor and deformation amplification factor, introduced originally by Ozaki et al. [73]. Despite leading to approximate results, the authors concluded that the method was conservative.

Moghadam and Tso [74] proposed in 2000 a 3D pushover procedure. In this method, the conventional pushover is performed independently in each resisting element using a planar analysis, and the target displacements are calculated considering the equal displacement rule. In fact, the target displacements of each resisting element (planar frames and walls) are calculated with an elastic response spectrum analysis of a 3D model of the building. However, it is generally recognized that the equal displacement

rule may lead to small inelastic displacements in the case of: near-fault ground motions; systems with low strength; soft soil conditions; hysteresis behaviour of the elements with considerable pinching or stiffness and strength degradation. Therefore, the use of this method may lead to not so accurate results.

In 2002 Ayala and Tavera [75] proposed a 3D pushover procedure where the load vector was applied simultaneously in the two directions at the centre of mass of each floor and it was constituted by forces and torques. This load vector also took into account the contribution of higher modes.

In the same year, Penelis and Kappos [76, 77] proposed a 3D pushover analysis. The load vector is applied at the centre of mass of the floors and it is constituted by lateral forces and torques. These components of the vector are defined as the ones necessary to produce the storey displacements and torsion profiles obtained from a multi-modal response spectrum analysis. This is a single run method with an invariant load vector. The equivalent SDOF capacity curve is obtained using the concept of Substitute Structure proposed by Gulkan and Sozen [58]. The results show that further studies are necessary to confirm the good performance of the method, namely for predicting local responses.

In 2004 Chopra and Goel [5] extended the application of the aforementioned Modal Pushover Analysis (MPA) to the case of plan asymmetric buildings. The method was based on multi-run pushover analysis, where the load vectors in each run are proportional to each 3D elastic mode of vibration of the structure. The load vectors are constituted by modal forces in the two translational directions and by torques. The total seismic response was obtained combining the response due to each modal load. Some drawbacks can however be mentioned for this method: since each run corresponding to each mode is run independently, the yielding in one mode is not reflected in the others and no interaction between modes in the nonlinear range is considered. A three dimensional modal pushover analysis of buildings subjected to two ground motions was also performed by Reyes and Chopra in 2011 [78]. In this work tall buildings were also evaluated.

Fajfar et al. [4, 8] proposed in 2005 an extended version of the N2 method for plan asymmetric buildings. In this proposal the pushover analysis of the 3D model is performed independently in each direction, the target displacement being calculated using the original N2 method procedure. In order to take torsional effects into account, the pushover results are amplified by torsional correction factors. These factors are computed through an elastic response spectrum analysis and a pushover analysis. No de-amplification of displacements due to torsion is considered by the method. In 2009 D'Ambrisi et al. [6] tested the Extended N2 method in an existing school, and in 2011 Koren and Kilar [79] tested the method in asymmetric base-isolated buildings.

In 2008, an International Workshop on Nonlinear Static Methods for Design/Assessment of 3D structures [80] took place in Lisbon, Portugal. Twelve famous researchers on the topic from different countries were invited. Names like Anil Chopra, Peter Fajfar, Helmut Krawinkler, Rakesh Goel, Stavros

Anagnostopoulos, Andreas Kappos, amongst others, contributed to the high quality of the presented papers, to the lively and fruitful discussions that followed and to the substantial and objective recommendations produced. At this international Workshop on 3D Pushover, several contributions were made and important results were outlined, which were compiled in the book [80]. The more relevant are described in the following:

- Kunnath examined one subset of issues related to the sensitivity of nonlinear material models, element formulations, analysis assumptions, etc, in seismic demand estimation in the inelastic range. It was clear that due attention and care should be paid to modelling issues (e.g. by means of accurately devised sensitivity studies) prior to the actual comparison between different seismic assessment methods.

- Goel presented a generalized pushover curve, defined as a relationship between the scaling factor that is applied to the "modal" force distribution during the pushover analysis versus displacement at any selected reference location. Since this generalized pushover curve does not explicitly need the base shear, it can be developed for three-dimensional structures for which modes excited during the earthquake ground motion may induce little or no base shear.

- Savoia proposed a new procedure, termed Force/Torque Pushover (FTP) analysis, to select storey force distributions for 3D pushover analysis of plan-irregular RC frame structures.

- Krawinkler demonstrated that pushover analysis is readily capable of accurately revealing P-Delta (or deterioration) structural sensitivity, when the latter contributes in a significant manner to seismic response. This needs, however, to be complemented with appropriately derived rules for computation of the target displacement, which should equally account for 2nd order effects and deterioration, something that seems not to be regularly recognized by analysts. Caution was also recommended in the use of the pushover analysis in an intensity range for which results may become collapse sensitive, given the uncertainty introduced by record-to-record variability, and the consequent effects on the results obtained.

- Moghadam calibrated, by means of an extensive parametric study considering 150 steel buildings, a modification factor that may be introduced within the scope of a Displacement Coefficient Method application to improve results prediction when the latter is applied to assess the seismic response of plan irregular structures.

- Kappos introduced an improved version of the MPA procedure for application to bridges. It seems to be a promising approach that yields more accurate results compared to the 'standard' pushover.

- Bento carried out a study that aimed at scrutinizing the effectiveness with which four commonly employed Nonlinear Static Procedures (CSM, N2, MPA, ACSM) are able to reproduce the actual dynamic response of the well known SPEAR building.

Other researchers have performed 3D pushover analysis on plan irregular buildings, such as: Fujii et al. [81], Yu et al. [82], Erduran and Ryan [7], Stefano and Pintucchi [83]. Despite the results obtained, definitive answers still need to be reached.

2.4 NSPs used in this work

The nonlinear static procedures evaluated in this study can be categorized into two major groups. The first group comprises the pioneering simplistic procedures, namely the Capacity Spectrum Method (CSM), introduced by Freeman and collaborators [1 and 19] and implemented in ATC40 guidelines [21], and equally innovative the N2 method, suggested by Fajfar and co-workers [2, 20] and included later in Eurocode 8 [25]. These procedures are similar in deriving the pushover/capacity curve – usually employing an invariant single load vector preferably proportional to the fundamental vibration mode shape – and differ in determining the performance point – the N2 method uses a constant ductility inelastic spectrum whilst the CSM utilizes an overdamped elastic spectrum to account for the hysteresis energy dissipation. Both methods were updated recently and thus two variants of each method were evaluated by a preliminary investigation. The first variants are the original versions represented here as N2 and CSM-ATC40. The second variants feature updated versions, namely the Extended N2, and CSM-FEMA440. The Extended N2 method [4, 8] incorporates the torsional effects due to plan-asymmetry through a correction factor which the original N2 procedure lacks. The CSM-FEMA440 variant, on the other hand, features an enhanced spectral scaling approach [16] compared to its original edition.

The second group comprises the improvement-intended procedures, whereby the capacity curve(s) is/are computed either by performing multiple pushover analyses using invariant/adaptive modal force vectors, such as the Modal Pushover Analysis [3, 5], or by single pushover analysis using adaptive displacement vector encompassing the effects of higher modes of vibration and progressive damage at each pushover step, such as the Adaptive Capacity Spectrum Method [53].

2.4.1 Original N2 method

The development of the N2 method started in the 1980s (Fajfar and Fishinger [2, 84]) at the University of Ljubljana. The N stands for nonlinear analysis and 2 for two mathematical models.

The basis of the method came from the Q-model proposed by Saiidi and Sozen [85], which was improved in 1996 by Fajfar and Gaspersic [86]. The N2 method was extended to bridges in 1997 [87]. In 1999, the N2 method was formulated in the acceleration-displacement format [88], which combines the advantages of the graphical representation of the capacity spectrum method developed by Freeman with the practicality of inelastic demand spectra. The method is actually a variant of the capacity spectrum method based on inelastic spectra.

The N2 method was included in Eurocode 8 [25] as the recommended nonlinear static procedure.

The steps of the original version of the N2 method are described herein.

Step 1: Data

A MDOF model of the building is developed including the nonlinear force-deformation relationships for structural elements under monotonic loadings, Figure 2.7a). An elastic acceleration response spectrum is also required corresponding to the seismic action under consideration, Figure 2.7b).

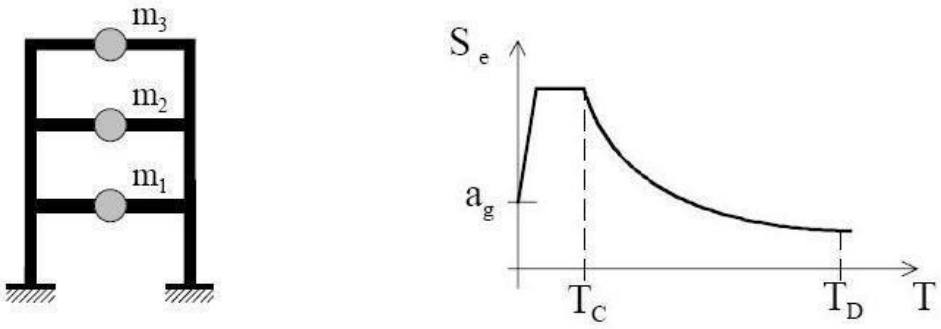

a) *b)*

Figure 2.7 – a) MDOF model of the building; b) elastic acceleration response spectrum [20].

Step 2: Seismic demand in AD (acceleration-displacement) format

The seismic demand is defined with a response spectrum in the format acceleration-displacement (ADRS). For SDOF, the displacement spectrum can be computed from the acceleration spectrum using Eq. 2.2.

$$S_d = \frac{T^2}{4\pi^2} S_e \qquad \textit{Eq. 2.2}$$

Where S_e and S_d are the values for the elastic acceleration and displacement spectrum, respectively, corresponding to the period T and a fixed viscous damping ratio. Examples of elastic acceleration and displacement response spectrum are plotted in Figure 2.8a). The same spectra are plotted together in the ADRS format in Figure 2.8b).

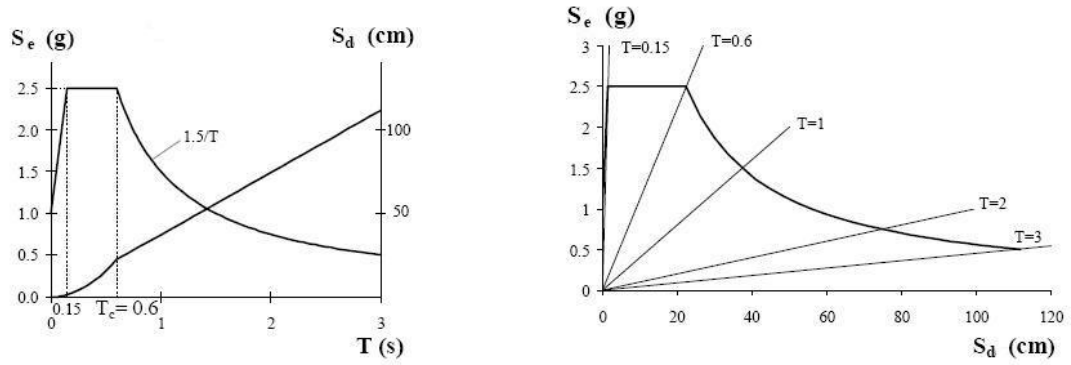

(a) *(b)*

Figure 2.8 - Elastic acceleration S_e and displacement S_d response spectrum for 5% damping normalized to 1.0g peak ground acceleration a) traditional format b) ADRS format [20].

Step 3: Pushover analysis

A pushover analysis is performed, applying to the structure a monotonically increasing pattern of lateral forces, Figure 2.9. These forces represent the inertial forces induced in the structure by the ground motion.

The N2 method uses a conventional non adaptive force based pushover. Any reasonable distribution of lateral loads can be used in the N2 method. According to Fajfar [20], the range of reasonable assumptions is relatively limited, and different assumptions lead to similar results. The Eurocode 8 recommends the use of at least two distributions: a first mode proportional load pattern and a uniform load pattern.

The vector of the lateral loads $\overline{F}$ used in the pushover analysis proportional to the first mode is determined as:

$$\overline{F} = pM\Phi \qquad \textit{Eq. 2.3}$$

The lateral force in the i-th level is proportional to the component Φ_i of the assumed displacement shape Φ, weighted by the storey mass m_i:

$$\overline{F_i} = pm_i\Phi_i \qquad \text{Eq. 2.4}$$

Note that the displacements are Φ normalized in such a way that $\Phi_n = 1$, where n is the control node, i.e. the centre of mass of the roof. Consequently $\overline{F_n} = pm_n$.

The determination of these lateral loads is justified by the following reasons:

1) The distribution of lateral forces would be equal to the distribution of effective earthquake forces if the assumed displacement shape was exact and constant during the ground motion;
2) The lateral load definition allows a transformation from the MDOF to the SDOF system and vice-versa based on pure mathematics and without approximations as happens in FEMA237.

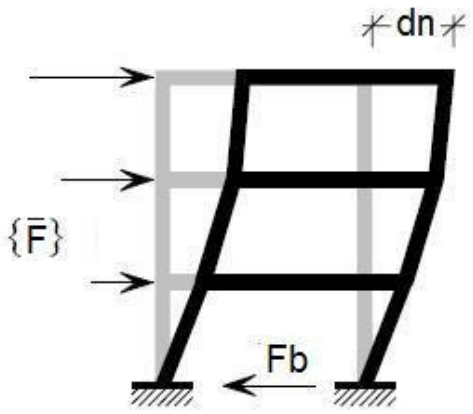

Figure 2.9 – Pushover analysis of the MDOF model.

The vector of the lateral loads $\overline{F}_{uni}$ used in the pushover analysis with a uniform distribution is determined as:

$$\overline{F}_{uni} = pM \qquad \text{Eq. 2.5}$$

$$\overline{F}_{uni\,i} = pm_i \qquad \text{Eq. 2.6}$$

From the pushover analysis one obtains the nonlinear force-displacement relationship of the MDOF system called a capacity curve. The N2 method prescribes that this curve should represent the base shear (F_b) and the displacement at the centre of mass of the roof (d_n).

Step 4: Equivalent SDOF system

At this stage of the procedure, the MDOF structure should be transformed into an equivalent SDOF system. The procedure to determine the SDOF features is described herein.

The definition of the transformation factor Γ is based on the equation of motion of a MDOF system. Considering only the degrees of freedom associated with the lateral translation in the direction under study:

$$M \cdot \ddot{U} + R = -M \cdot 1 \cdot a \qquad \textit{Eq. 2.7}$$

Where, U is the displacement vector, $\ddot{U}$ is the acceleration vector, M is a diagonal mass matrix, R is the internal forces vector, 1 is a unit vector and a is the ground acceleration as a function of time. For simplicity, the damping is considered in the response spectrum and not in equation Eq. 2.7.

The deformed pattern Φ is assumed to be constant during the structural response to the earthquake. This consideration is the most critical since the structurally deformed pattern changes in the nonlinear range. The displacement vector is then written as Eq. 2.8:

$$U = \Phi \cdot d_n \qquad \textit{Eq. 2.8}$$

Where d_n is the time dependent top displacement. The Φ is normalized in order to have its component at the top equal to 1.

From statics it follows that:

$$\overline{F} = R \qquad \textit{Eq. 2.9}$$

i.e., the internal forces R are equal to the statically applied external loads $\overline{F}$.

Introducing Eq. 2.3, Eq. 2.8 and Eq. 2.9 into Eq. 2.7 and multiplying the equation by Φ^T, it follows:

$$\Phi^T \cdot M \cdot \Phi \cdot \ddot{d}_n + \Phi^T \cdot M \cdot \Phi \cdot p = -\Phi^T \cdot M \cdot 1 \cdot a \qquad \textit{Eq. 2.10}$$

The equation of motion of the SDOF system can be written as:

$$m^* \cdot \ddot{d}^* + F^* = -m^* \cdot a \qquad \text{Eq. 2.11}$$

Where m^* is the equivalent mass of the SDOF system and it is calculated using Eq. 2.12.

$$m^* = \Phi^T \cdot M \cdot 1 = \sum m_i \Phi_i \qquad \text{Eq. 2.12}$$

The transformation of the MDOF to the SDOF system is made in the N2 method using Eq. 2.13 and Eq. 2.14, see Figure 2.10.

$$d^* = \frac{d_n}{\Gamma} \qquad \text{Eq. 2.13}$$

$$F^* = \frac{F_b}{\Gamma} \qquad \text{Eq. 2.14}$$

Where d^* and F^* are the displacement and base shear of the SDOF system. d_n and F_b are the top displacement and base shear of the MDOF system.

$$F_b = \sum \overline{F}_i = \Phi^T \cdot M \cdot 1 \cdot p = p \sum m_i \Phi_i = p \cdot m^* \qquad \text{Eq. 2.15}$$

The transformation factor Γ from the MDOF to the SDOF model and vice-versa is defined according Eq. 2.16.

$$\Gamma = \frac{\Phi^T \cdot M \cdot 1}{\Phi^T \cdot M \cdot \Phi} = \frac{\sum m_i \Phi_i}{\sum m_i \Phi_i^2} = \frac{m^*}{\sum m_i \Phi_i^2} = \frac{\sum \overline{F_i}}{\sum \left(\frac{\overline{F_i^2}}{m_i} \right)} \qquad \text{Eq. 2.16}$$

The transformation factor Γ is usually called the modal participation factor. Any reasonable shape of Φ can be assumed. Herein, the elastic first mode shape will be considered. As was mentioned before, the displacement shape Φ is normalized with respect to the centre of mass of the roof. Therefore, the value of Φ_n is equal to 1.0, where *n* denotes the roof level.

The SDOF capacity curve is defined by the displacement of the SDOF (d^*) and the base shear of this system (F^*). Since both displacement and base shear of the MDOF are divided by the same factor Γ, the force-displacement relationship has the same shape. Therefore, the initial stiffness of the SDOF system is the same as the one defined by the base shear-top displacement capacity curve of the MDOF system.

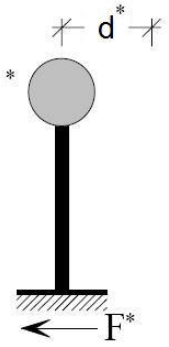

Figure 2.10 – Equivalent SDOF system.

Eurocode 8 prescribes a simplified elastic-perfectly plastic bilinear approximation of the SDOF capacity curve. Therefore, the post-yield stiffness of the bilinear approximation is equal to zero, as shown in Figure 2.11.

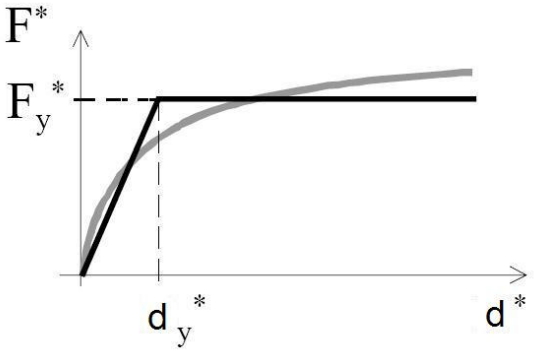

Figure 2.11 – SDOF capacity curve and its bilinearization.

The elastic period of the idealized bilinear SDOF system T^* is computed according to Eq. 2.17.

$$T^* = 2\pi\sqrt{\frac{m^* d_y^*}{F_y^*}} \qquad \textit{Eq. 2.17}$$

Where F_y^* and d_y^* are the yield strength and displacement respectively.

Step 5: Seismic demand for the equivalent SDOF system

The seismic demand of the equivalent SDOF system can be calculated using the graphical procedures illustrated in Figure 2.12 for short period structures and in Figure 2.13 for medium and long period structures. In these figures the ADRS spectrum and the bilinearized SDOF capacity curve are represented in the same graph.

The capacity curve of the SDOF in the acceleration-displacement (AD) format is obtained by dividing the forces in the force-displacement ($F^* - d^*$) curve by the equivalent mass m^*.

The target displacement of the structure with period T^* and unlimited elastic behaviour is given by:

$$d_{et}^* = S_e\left(T^*\right) \cdot \left[\frac{T^*}{2\pi}\right]^2 \qquad \textit{Eq. 2.18}$$

where $S_e\left(T^*\right)$ is the elastic acceleration response spectrum at the period T^*.

For the determination of the target displacement d_t^* for structures in the short-period range and for structures in the medium and long period ranges, different expressions should be used as indicated below. The corner period between the short and medium period range is T_C is the characteristic period of the ground motion, which is defined as the transition period between the constant acceleration section of the response spectrum (corresponding to the short period range) and the constant velocity segment of the response spectrum (corresponding to the medium period range).

a) For $T^* < T_C$ (short period range):

If $F_y^* / m^* \geq S_e\left(T^*\right)$ the response is elastic and thus

$$d_t^* = d_{et}^* \qquad \textit{Eq. 2.19}$$

If $F_y^* / m^* < S_e\left(T^*\right)$ the response is nonlinear and

$$d_t^* = \frac{d_{et}^*}{q_u}\left(1 + \left(q_u - 1\right) \cdot \frac{T_C}{T^*}\right) \geq d_{et}^* \qquad \textit{Eq. 2.20}$$

Where q_u is the ratio between the acceleration in the structure with unlimited elastic behaviour $S_e\left(T^*\right)$ and in the structure with limited strength F_y^* / m^*.

$$q_u = \frac{S_e\left(T^*\right) \cdot m^*}{F_y^*} \qquad \textit{Eq. 2.21}$$

b) For $T^* \geq T_C$ (medium and long period range):

$$d_t^* = d_{et}^* \qquad \textit{Eq. 2.22}$$

d_t^* need not exceed 3 d_{et}^*.

From Eq. 2.22 one can conclude that for the medium and long period range the equal displacement rule is applied. This means that the displacement of the inelastic system is the same as the corresponding elastic system for the same period.

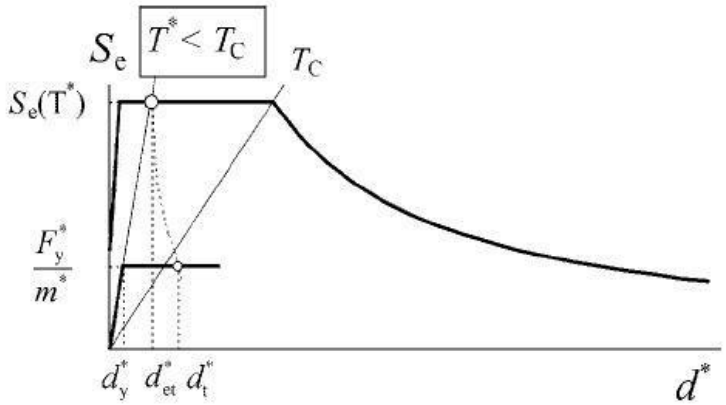

Figure 2.12 – Short period range [25].

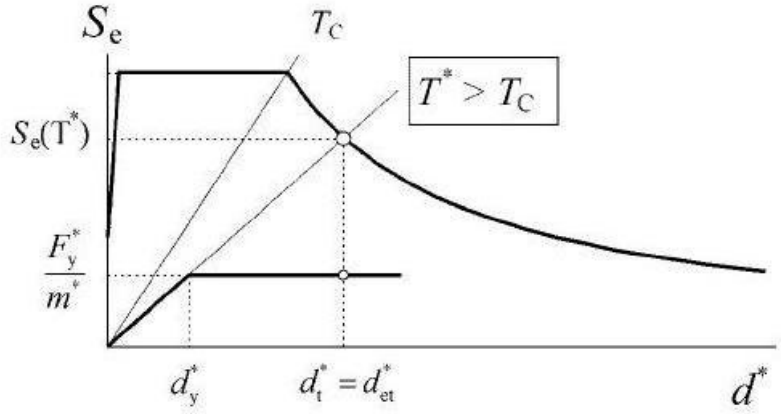

Figure 2.13 – Long period range [25].

The relation between different quantities can be visualized in Figure 2.12 and Figure 2.13. The figures are plotted in acceleration - displacement format. Period T^* is represented by the radial line from the origin of the coordinate system to the point in the elastic response spectrum defined by coordinates $d^* = S_e(T^*) \cdot (T^* / 2\pi)^2$ and $S_e(T^*)$.

Step 6: Global seismic demand for the MDOF model

The target displacement of the MDOF system d_t is calculated multiplying the target displacement of the SDOF obtained in step 5 by the transformation factor Γ, Eq. 2.23.

$$d_t = \Gamma \cdot d_t^* \qquad \textit{Eq. 2.23}$$

Step 7: Local seismic demand for the MDOF model

For determining the local seismic demand (e.g. interstorey drifts, chord rotations Θ), one should go back to the MDOF pushover curve (previously determined in step 3) to the analysis step corresponding to the seismic demand d_t (calculated in step 6), and take the distribution of deformations in the structure, Figure 2.14.

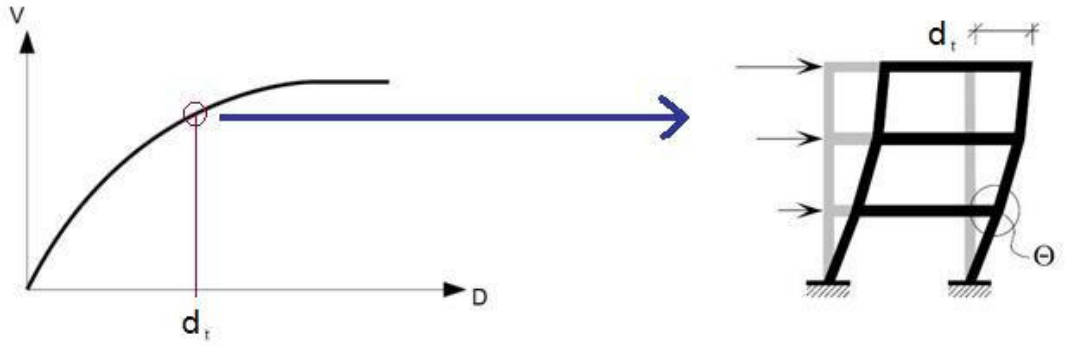

Figure 2.14 – Local seismic demands.

Step 8: Performance evaluation (damage analysis)

The performance evaluation is made by comparing the seismic demand determined in step 7 with the capacities for the relevant performance level.

Limitations of the method:

1) The N2 method was originally created for planar analysis of structures. The pushover analysis is performed with a constant force pattern proportional to the first mode of vibration. This assumption may lead to inaccurate results in structures where the higher mode effects are significant;

2) The force pattern in the pushover analysis is time-independent. By using such analysis, the method may not be able to capture the structural weaknesses created

when the dynamic characteristics of the structure change after the formation of the first plastic mechanism;

3) The equal displacement rule seems to be a good approach for structures on firm sites with the fundamental period in the medium or long period range with stable and full hysteretic loops. It leads to slightly conservative estimations of the mean inelastic displacement values. However, the equal displacement rule leads to small inelastic displacements in the case of near fault ground motions [89], hysteretic loops with significant pinching or significant stiffness and/or strength deterioration [22, 90], and for systems with low strength [91]. This rule leads to inaccurate results in soft soil conditions [92, 93];

4) The sensitivity of inelastic displacements to changes of structural parameters is greater in the short period range than in the medium and long ranges. Therefore, the estimations of inelastic displacements are less accurate in the short period range. The absolute values of displacements in this range are small, and in the majority of cases they do not control the design.

2.4.2 Extended N2 method

The original N2 method was developed for structures likely to be evaluated with planar analyses, such as bridges and plan symmetric buildings. However, the majority of the existing structures are plan asymmetric. The biggest problems related to this kind of structures are the torsional effects induced by the ground motion. Therefore, the original N2 method may lead to inaccurate results in such buildings since it is not prepared to capture the torsional motion. In this section, an extension of the N2 method proposed by Fajfar and his team [4, 8] is presented.

Plastic deformations are developed in elements as the structure goes into the inelastic range, changing the parameters that control the torsional structural response. The periods and period ratios change due to the change in stiffness of individual structural members and of the whole structure (which is different in different directions), therefore the influence of different modes of vibration may also change. The eccentricities also change during the inelastic regime. Due to all these specificities during the inelastic response, the effects observed in the elastic response may be modified.

Extensive parametric studies have been performed by Fajfar and his co-workers [4] in order to investigate the parameters that influence the inelastic torsional response of building structures. In this work, several conclusions were drawn for the structures analysed:

1) The inelastic torsional response is qualitatively similar to the elastic torsional response. Quantitatively, the torsional effects depend on the ductility demand, therefore on the ground motion intensity;

2) An upper bound of the torsional amplifications can be estimated with a linear dynamic response spectrum analysis;

3) The torsional effects decrease with the increase of plastic deformations. This trend is clear with the smaller amplification of displacements on the flexible side, see Figure 2.15. However, if the structure is subjected to small plastic deformations, characterized by ductility less than 2.0, the amplification at the flexible edge may be slightly higher than in the elastic structure;

4) The response at the stiff edge depends on the influence of different modes of vibration and on the ground motion in the transverse direction. This response depends on the structural and ground motion characteristics in both directions. It is difficult to make general conclusions about the response on the stiff side. De-amplification of displacements due to torsion on the stiff side decreases with increasing plastic deformations in elastic torsionally stiff structures. Sometimes, a transition from de-amplification to amplification can happen. In elastic torsionally flexible structures the amplification due to torsion decreases with increasing plastic deformations;

5) For large plastic deformations, the smaller torsional effects in the inelastic range when compared with the elastic range are usually illustrated by a flattening of the displacement envelopes in the horizontal plane, see Figure 2.15;

6) The dispersion of results is larger in the inelastic range than in the elastic regime.

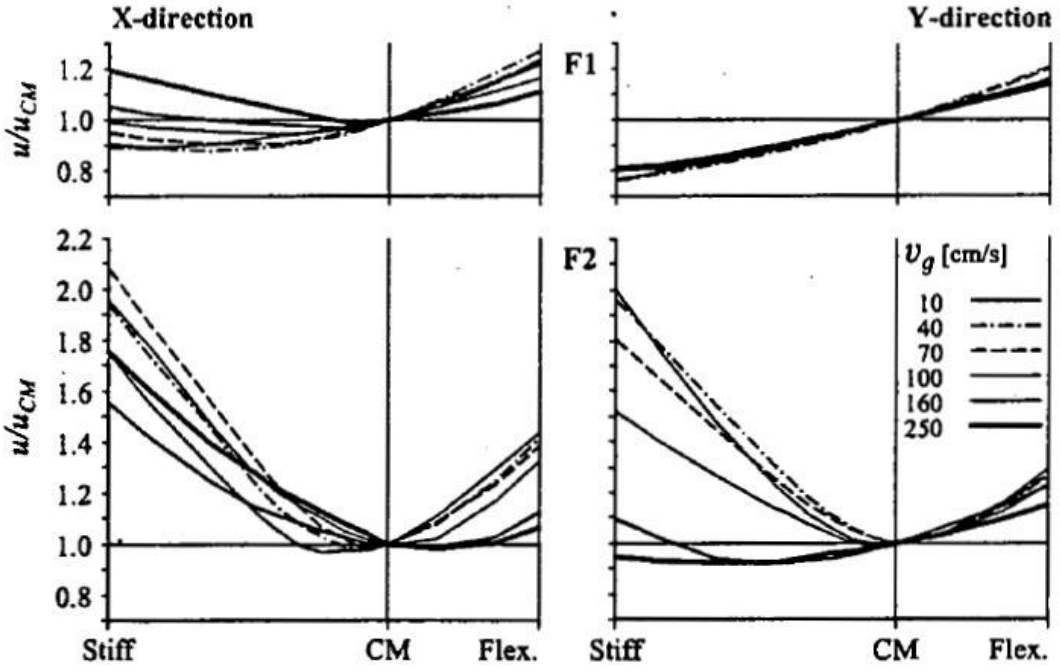

Figure 2.15 – Torsional effects for steel frame buildings named as F1 and F2, for different ground motion intensities [4].

Based on the results obtained, the following conclusions were taken. They are important for the development of simplified analysis methods and code guidelines:

1) A conservative estimation of the amplification of displacements due to torsion in the inelastic range can be determined by a dynamic elastic analysis;

2) Any reduction of displacements on the stiff side compared to the counterpart symmetric building, obtained from elastic analysis, will decrease or even disappear in the inelastic range.

These conclusions were used by Fajfar and his team [4, 8] to develop an extension of the N2 method to plan asymmetric building structures. The steps of the extended procedure are described in the following:

1) Develop a 3D mathematical model of the building and perform a pushover analysis. The loading is applied independently in two horizontal directions, in each direction with + and – sign. The load vectors used are the ones recommended in the original N2 method. Therefore, in each direction one should use two load distributions:

   a) one proportional to the mass and to the normalized modal displacement shape (the value in the CM of the roof is 1). In the 3D case, the modal shape Φ is constituted by two translational components and one rotational component, all three different from zero. In this method, as a simplification one should only consider the component in the direction under analysis:

$$\Phi^T = \left[\Phi_X^T, 0^T, 0^T\right] \qquad \textit{Eq. 2.24}$$

   For the X direction one should consider the first mode in which the dominant direction of motion is along the X direction. For the Y direction one should consider the first mode in which the dominant direction of motion is along Y.

   For example, the lateral force in the X direction at the *i-th* level is proportional to the component $\Phi_{X,i}$ of the assumed displacement shape Φ_X of the first mode Φ in which the dominant direction of motion is along X, weighted by the storey mass m_i:

$$\overline{F}_{X,i} = p \cdot m_i \cdot \Phi_{X,i} \qquad \textit{Eq. 2.25}$$

   b) and a uniform load distribution proportional to the mass, see Eq. 2.6.

   Therefore, 4 pushover analyses are performed in each direction;

2) Calculate the target displacement – displacement demand at the centre of mass of the roof – for each of two horizontal directions using the procedure proposed in the original N2 method, see section 2.4.1. In each direction, consider the larger value of the values obtained for the + and – sign;

3) Perform a linear modal analysis of the 3D model, independently for excitation in two horizontal directions. The results are combined using the SRSS rule;

4) Calculate the torsional correction factors to be applied to the pushover analyses results. The correction factors are computed dividing the normalized roof displacements obtained by elastic modal analysis by the ones obtained by pushover analysis. The normalized roof displacement is calculated dividing the roof displacement at a certain location by the roof displacement at the centre of mass. If the normalized roof displacement obtained by elastic modal analysis is smaller than 1.0, one should consider 1.0, i.e. no de-amplification due to torsion is taken into account. The correction factors are defined for each horizontal direction separately. They depend on the location in the plan;

5) The relevant quantities, such as deformations for the ductile elements, obtained by pushover analysis should be multiplied by the appropriate correction factors. For example, in a perimeter frame parallel to the Y axis, all quantities are multiplied with the correction factor determined with the pushover results obtained from loading in the Y direction and for the location of this frame.

As one can conclude from the previous steps, the Extended N2 method uses both nonlinear static pushover and elastic dynamic analysis. The displacement demand and its distribution along the height at the centre of mass of each storey are determined using the original N2 method. The amplification of displacements due to torsion is calculated by elastic dynamic analysis. The reduction of displacements due to torsion is not taken into account. The results obtained by Fajfar and his team show that this extended procedure leads to conservative estimations of the torsional response of plan asymmetric buildings. The inelastic torsion has a large randomness and uncertainty, leading to considerable dispersion of results. Therefore, the Extended N2 method should be tested in more buildings which are asymmetric in plan and with different configurations in order to reach consolidated conclusions about its applicability.

2.4.3 Modal Pushover Analysis (MPA)

As was previously mentioned, the modal pushover analysis (MPA) has been developed to include the contributions of all modes of vibration that have a significant influence on the seismic demands [3], being based on structural dynamics theory.

The MPA considers non adaptive force based pushover analyses based on modal proportional load patterns. It is a multi-run method, using in each run a different load pattern proportional to each mode of vibration of the structure. The final results are

obtained by combining the results computed from each pushover curve. Therefore, the method takes the higher mode effects into account.

The procedure was improved in terms of the calculation of P-Δ effects due to gravity loads and estimation of plastic hinge rotations [29]. It was also extended to compute member forces, and its accuracy has been evaluated for SAC buildings [29], height-wise regular generic frames [94] and irregular generic frames [95]. In 2003 an incremental response spectrum analysis procedure that considers multiple modes has been developed by Aydinoglu [38].

In 2004, the MPA was extended to plan asymmetric buildings by Chopra and Goel [5]. In this method, the seismic demand due to individual terms in the modal expansion of the effective earthquake forces is calculated by a pushover analysis using the inertia force distribution for each mode. In the case of plan asymmetric buildings, the load vector used in each mode includes two lateral forces and torque at each floor (stiff slab) level. The results obtained for the different modes considered are combined in the end using an appropriate combination rule in order to obtain an estimation of the total seismic demand for inelastic systems.

In this work, the extension of the MPA to plan asymmetric buildings was used. The steps of this procedure are described as follows:

1. Computation of the natural frequencies w_n, and modes of vibration ϕ_n, for elastic behaviour of the building.

2. For the *n*-th mode, develop the base shear-roof displacement V_{bn} - u_{rn} pushover curve by nonlinear static analysis of the building using the force distribution s_n^*, where s_{ni}^* is the load vector at floor *i*, see Eq. 2.26:

$$s_{ni}^* = \begin{Bmatrix} m_i \phi_{xni} \\ m_i \phi_{yni} \\ I_{pi} \phi_{\theta ni} \end{Bmatrix} \qquad \textit{Eq. 2.26}$$

Where,

m_i - is the mass at the floor *i*

I_{pi} - is the polar moment of inertia at floor *i* about a vertical axis through the centre of mass

ϕ_{xni} - is the modal displacement component in the X direction of the mode *n* at floor *i*

ϕ_{yn_i} - is the modal displacement component in the Y direction of the mode *n* at floor *i*

$\phi_{\theta ni}$ - is the modal rotation component about a vertical axis of the mode *n* at floor *i*

The modal expansion is represented in Figure 2.16.

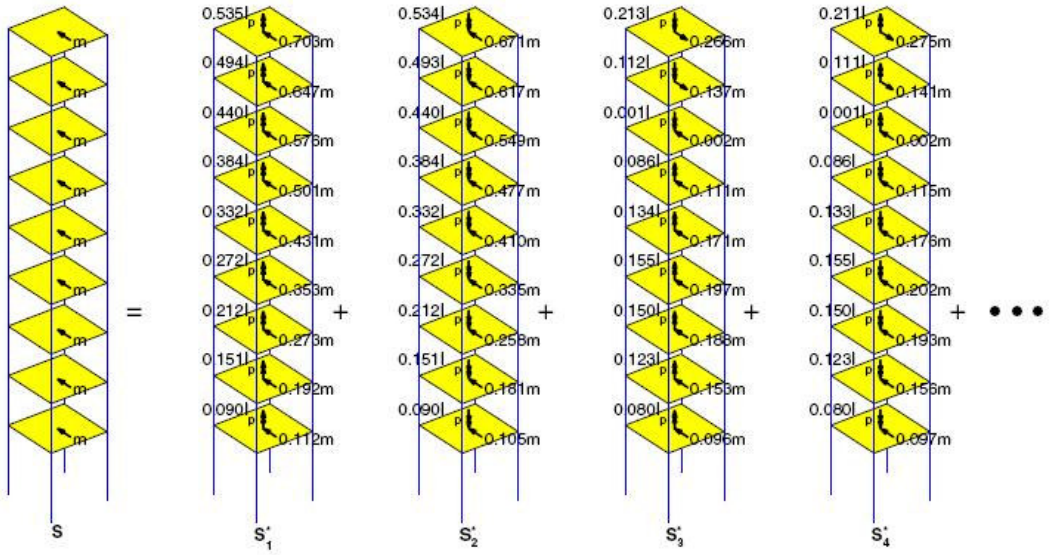

Figure 2.16 – Modal expansion for an asymmetric in plan building [5].

Two pushover curves are obtained corresponding to two lateral directions X and Y. The pushover curve in the dominant direction of motion of the mode should be chosen.

The gravity loads are applied before pushover analysis, the value of the lateral roof displacement due to gravity loads being u_{rg} .

3. Idealize the pushover curve as a bilinear curve.

4. The idealized V_{bn} - u_{rn} pushover curve should be converted to the force-displacement F_{sn}/L_n - D_n relation for the *n*-th mode inelastic SDOF system by using Eq. 2.27 and Eq. 2.28.

$$\frac{F_{sn}^{y}}{L_n} = \frac{V_{bn}^{y}}{M_n^{*}} \qquad \textit{Eq. 2.27}$$

$$D_n^{y} = \frac{u_{rn}^{y}}{\Gamma_n \cdot \phi_{rn}} \qquad \textit{Eq. 2.28}$$

In which $M_n^* = L_n \cdot \Gamma_n$ is the effective modal mass and ϕ_{rn} is the value of ϕ_n at the roof in the direction of the selected pushover curve. M_n^* and Γ_n correspond to the direction of ground motion under consideration (X or Y).

Both F_{sn}/L_n and D_n are related through:

$$\frac{F_{sn}^y}{L_n} = \omega_n^2 \cdot D_n^y \qquad \textit{Eq. 2.29}$$

5. Compute the peak deformation D_n of the *n*-th mode inelastic SDOF system which was defined by the force-deformation relationship in step 4 and damping ratio β_n. The elastic period of the system T_n can be calculated using Eq. 2.30:

$$T_n = 2\pi \cdot \left(\frac{L_n D_n^y}{F_{sn}^y} \right)^{1/2} \qquad \textit{Eq. 2.30}$$

   Knowing T_n and β_n of the SDOF system, one can calculate D_n using nonlinear response history analysis (RHA), inelastic design spectrum, or elastic design spectrum combined with empirical equations for the ratio of deformations of inelastic and elastic systems.

   In this work, D_n was computed using the inelastic spectrum of the N2 method, see section 2.4.1: Eq. 2.19, Eq. 2.20 and Eq. 2.22.

6. Calculate the peak roof displacement u_{rn} of the MDOF structure in the direction of the selected pushover curve associated with the *n*-th mode of the inelastic SDOF system using Eq. 2.31:

$$u_{rn} = \Gamma_n \cdot \phi_{rn} \cdot D_n \qquad \textit{Eq. 2.31}$$

7. Use the values of desired responses r_{n+g}, extracted from the pushover database (step 2). These values result from the combination of the effects of the gravity and lateral loads at roof displacement equal to $u_{rn} + u_{rg}$.

8. Steps 3-7 should be repeated for as many modes as required for sufficient accuracy.

9. Computation of the dynamic response due to the *n*-th mode $r_n = r_{n+g} - r_g$, where r_g is the contribution of gravity loads alone. In this work for the different analysed buildings it was concluded that the lateral response of the structure such as lateral displacement patterns, interstorey drifts, chord rotations, top displacement ratios, as well as the normalized top displacements, base shear and shear in columns, due to gravity loads only was negligible. Therefore r_g was practically zero.

10. Determine the total demand by combining gravity response and the peak modal responses using an appropriate combination rule.

2.4.4 Capacity Spectrum Method (CSM)

In 1975, Freeman and collaborators presented for the first time the innovative capacity spectrum method – the so-called CSM [19]. Since then, this method has gained considerable popularity amongst pushover users and the ATC40 guidelines [21] included it as the recommended nonlinear static procedure to be used. Later, the FEMA440 report [16] came out with an updated version of the method increasing the precision of its results.

The capacity spectrum method is a very practical tool in the evaluation and retrofit of existing concrete buildings. It provides a graphical representation of the global force-displacement capacity curve of the structure, comparing it with the response spectrum that represents the earthquake. The graphical representation allows a clear understanding of how a building responds to an earthquake.

The CSM was developed to represent the first mode response of a structure based on the idea that the fundamental mode of vibration is the predominant response of the structure. For buildings in which the higher mode effects can be important, the results obtained with the CSM may not be so accurate.

In this section the capacity spectrum method (CSM) is briefly described, emphasizing the differences between the CSM-ATC40 and the CSM-FEMA440 features.

Step 1: Data

A MDOF model of the building must be developed including the nonlinear force-deformation relationship, as happens in the original N2 method.

Step 2: Seismic demand in ADRS (acceleration-displacement response spectrum) format

Along the lines of what happens in the original N2 method, the seismic demand is defined with a response spectrum in the acceleration-displacement (ADRS) format. For a SDOF, the displacement spectrum can be computed using Eq. 2.2. See Figure 2.8.

Step 3: Pushover analysis

A conventional non-adaptive force based pushover analysis is performed, applying to the structure a monotonically increasing pattern of lateral forces. In CSM the lateral forces applied have a first mode proportional distribution, calculated in the same way as the N2 method, see Eq. 2.3 and Eq. 2.4.

From the pushover analysis one obtains the capacity curve that represents the base shear and the displacement at the centre of mass of the roof.

Step 4: Equivalent SDOF system

The structural capacity curve expressed in terms of roof displacement and base shear is then converted into a SDOF curve in terms of displacements and accelerations, which is called the capacity spectrum. The transformations are made using the following equations:

$$PF_1 = \left[\frac{\sum_{i=1}^{N} (w_i \phi_{i1}) / g}{\sum_{i=1}^{N} (w_i \phi_{i1}^2) / g} \right] \qquad \textit{Eq. 2.32}$$

$$\alpha_1 = \frac{\left[\sum_{i=1}^{N} (w_i \phi_{i1}) / g \right]^2}{\left[\sum_{i=1}^{N} w_i / g \right] \left[\sum_{i=1}^{N} (w_i \phi_{i1}^2) / g \right]} \qquad \textit{Eq. 2.33}$$

$$S_a = \frac{V / W}{\alpha_1} \qquad \textit{Eq. 2.34}$$

$$S_d = \frac{\Delta_{roof}}{PF_1 \phi_{roof,1}} \qquad \textit{Eq. 2.35}$$

Where,

PF_1 - modal participation factor for the first natural mode

α_1 - modal mass coefficient for the first natural mode

w_i / g - mass assigned to level i

ϕ_{i1} - amplitude of mode 1 at level i

N – Level N, the level which is the uppermost in the main portion of the structure

V - Base shear

W - building dead weight plus likely live loads

Δ_{roof} - roof displacement (V and the associated Δ_{roof} make up points on the capacity curve)

S_a - spectral acceleration

S_d - spectral displacement (S_a and the associated S_d make up points on the capacity spectrum)

Figure 2.17 shows that the participation factor and the modal mass coefficient vary according to the relative interstorey displacement over the height of the building. For example, for a linear distribution of interstorey displacement along the height of the building, $\alpha_1 \approx 0.8$ and $PF_1\phi_{roof,1} \approx 1.4$.

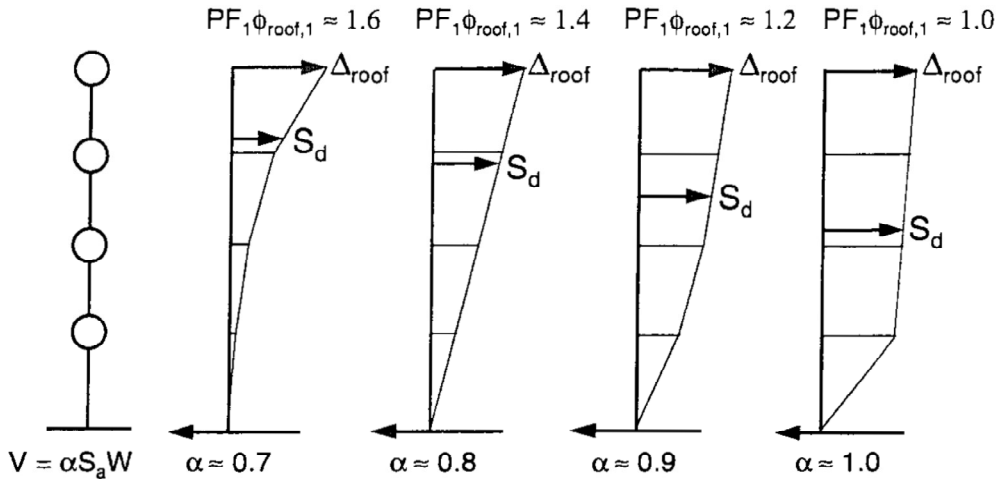

Figure 2.17 – Example modal participation factors and modal mass coefficients [21].

To convert the MDOF capacity curve into the SDOF capacity curve in the ADRS format (capacity spectrum), first it is necessary to calculate the modal participation factor PF_1 and the modal mass coefficient α_1 using Eq. 2.32 and Eq. 2.33. Afterwards, for each point of the MDOF capacity curve (Δ_{roof}, V) calculate the associated point (S_d, S_a) of the capacity spectrum according to Eq. 2.34 and Eq. 2.35.

As was mentioned, both CSM and N2 method consider a single control node for the SDOF characterization, usually the centre of mass of the roof. In the N2 method both displacements and the forces of the MDOF are divided by the same Gama factor that depends on the mass of each storey, the modal displacement at each floor normalized to the roof's centre of mass and of the equivalent mass, in order to obtain the SDOF curve force *vs.* displacement. The CSM (ATC40 and FEMA440) uses two different coefficients for the transformation of displacements and the accelerations, in order to calculate the SDOF curve in terms of acceleration vs. displacement. Note that, if one divides the SDOF forces in the N2 method by the equivalent mass (as defined by the method) in order to get the SDOF curve in the acceleration vs. displacement format, the equation of the SDOF accelerations will be the same as the one presented by ATC40 and FEMA440. The equations of the SDOF displacement transformation are the same as in Eurocode 8, ATC40 and in FEMA440.

Step 5: Calculation of the target displacement

The demand spectrum, with which the SDOF capacity curve will be intersected, must have an ADRS format (acceleration-displacement response spectrum). The calculation of the target displacement is an iterative process, where it is necessary to estimate a first trial performance point. For this purpose, there are several options one can use:

1) The first trial performance point can be estimated as the elastic response spectrum displacement corresponding to the elastic fundamental period. The response spectrum is defined for the viscous damping level considered (in buildings one usually considers 5%);

2) Consider a first trial equivalent damping value, for example 10%, and calculate the respective reduction factor. Multiply the elastic spectrum by this reduction factor and intersect the capacity curve with the reduced spectrum. The intersection corresponds to the first trial performance point.

The capacity curve is then bilinearized for this point, and a new effective damping can be computed and hence a new reduction factor can be applied. The new intersection between the capacity curve and the new reduced spectrum leads to a new performance point. If the target displacement calculated is within a tolerable range (for example within 5% of the displacement of the trial performance point), then the performance point can be obtained. Otherwise the iterative process continues until one finds convergence. Figure 2.18 represents the process schematically.

The difference between the ATC40 guidelines and the FEMA440 report lies in the estimation of damping and in the computation of the response spectrum's reduction factor.

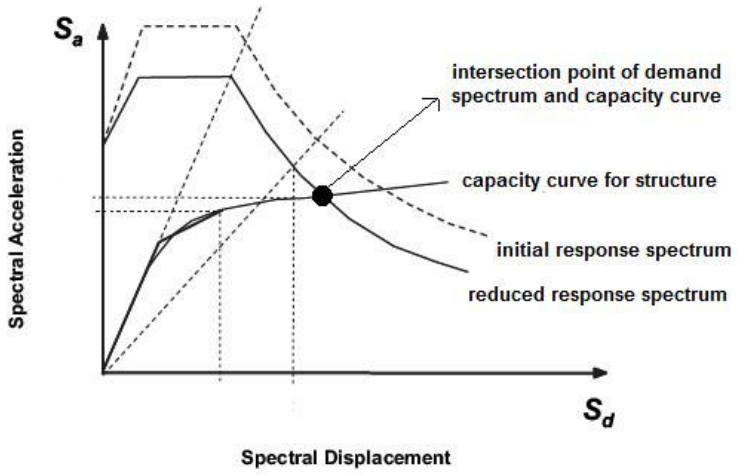

Figure 2.18 - General CSM procedure to compute the target displacement (modified from [5]).

Step 6: Determination of MDOF response parameters in correspondence to the Performance Point (converted from SDOF to MDOF)

At this stage of the procedure, one should go back to the MDOF pushover curve to the point corresponding to the value of the SDOF target displacement (calculated in the previous step) multiplied by the transformation factor. For this step, one should take the building's performance results, such as deformations, interstorey drifts and chord rotations.

The specificities of both guidelines, ATC40 and FEMA440 in computing the effective damping and the reduction factor are explained as follows.

2.4.4.1 CSM-ATC40

The Procedure A of the ATC40 guidelines to calculate the target displacement was used in this work. It was previously described in step 5 of the procedure.

Estimation of Damping and Reduction of the Response Spectrum

When a structure subjected to a ground motion enters the inelastic range the associated damping is a combination of a viscous damping and a hysteretic damping. Hysteretic damping is related to the area inside the loops that are formed when the earthquake force (base shear) is plotted against the structure displacement. This guideline defines an equivalent viscous damping to represent this combination and it can be calculated using Eq. 2.36.

This expression applied to existing reinforced concrete buildings, which are not typically ductile structure, overestimates realistic damping levels. To overcome this problem, ATC40 introduces the concept of effective viscous damping that can be obtained by multiplying the equivalent damping by a modification factor *k* (Eq. 2.37).

$$\beta_{eq} = \beta_1 + 5 \qquad \textit{Eq. 2.36}$$

$$\beta_{eff} = k\beta_1 + 5 \qquad \textit{Eq. 2.37}$$

Where,

β_{eq} - equivalent viscous damping

β_{eff} - effective viscous damping

k - damping modification factor

β_1 - hysteretic damping represented as equivalent viscous damping

5 – 5% viscous damping inherent in the structure (assumed to be constant)

The hysteretic damping represented as equivalent viscous damping can be calculated according to Chopra [10]:

$$\beta_1 = \frac{1}{4\pi} \cdot \frac{E_D}{E_{So}} \qquad \textit{Eq. 2.38}$$

Where,

E_D - energy dissipated by damping

E_{So} - maximum strain energy

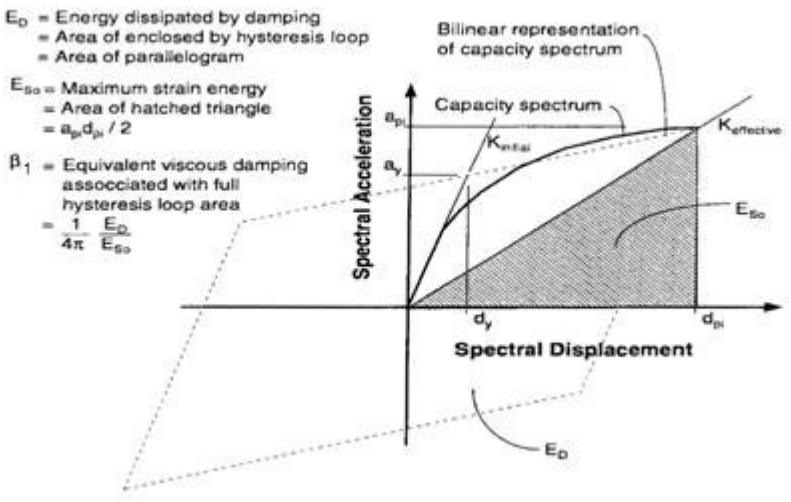

Figure 2.19 - Hysteresis parallelogram, modified from [21].

The physical meaning of both E_D and E_{So} is represented in Figure 2.19. E_D is the energy dissipated by the structure in a single cycle of motion, that is, the area enclosed by a single hysteresis loop. E_{So} is the maximum strain energy associated with that cycle of motion that is, the area of the hatched triangle.

Figure 2.20 shows the derivation of energy dissipated by damping.

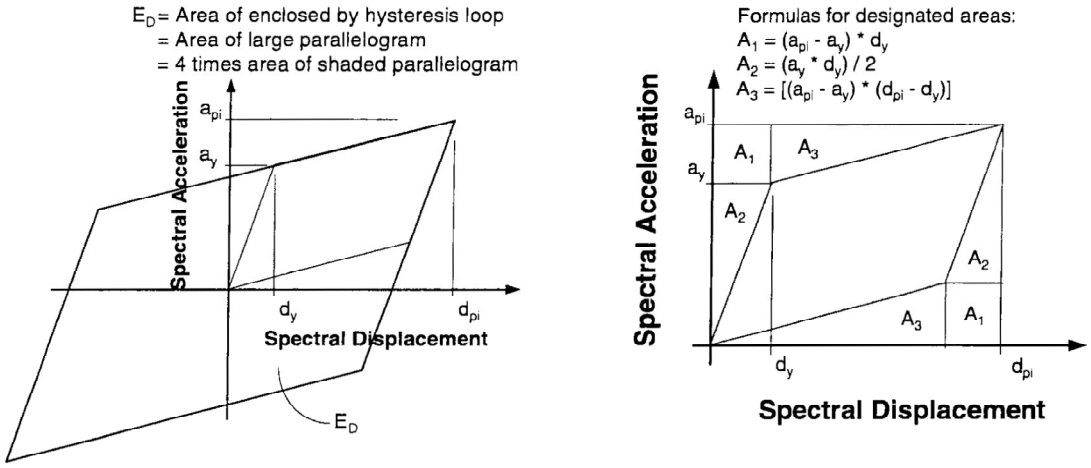

Figure 2.20 – Derivation of energy dissipated by damping, E_D [21].

Therefore, β_1 can be written as in Eq. 2.39:

$$\beta_1 = \frac{63.7(a_y d_{pi} - d_y a_{pi})}{a_{pi} d_{pi}} \qquad \textit{Eq. 2.39}$$

Where a_{pi} and d_{pi} correspond to a trial performance point, for instance the intersection between the capacity curve and the demand spectrum. The capacity curve should be bilinearized at this trial point, considering a post-yield stiffness. a_y and d_y correspond to this bilinear curve yielding point.

Hence, the effective damping can be written as Eq. 2.40.

$$\beta_{eff} = \frac{63.7k(a_y d_{pi} - d_y a_{pi})}{a_{pi} d_{pi}} + 5 \qquad \textit{Eq. 2.40}$$

The damping modification factor k measures the extent to which the actual building hysteresis is well represented by the parallelogram illustrated in Figure 2.19, either initially, or after degradation.

The *k*-factor depends on the structural behaviour of the building, which is related to the seismic resisting system quality and the duration of ground shaking. ATC40 defines three categories of structural behaviour. Type A represents stable, reasonably full hysteresis loops like in Figure 2.19; Type B represents a moderate reduction of area; Type C represents poor hysteretic behaviour with a significant reduction of loop area (severely pinched). In this work, Type B characterizes the structural behaviour of the buildings and it represents a moderate reduction in the area of the parallelogram.

Table 2.1 indicates the β_1 and *k* values corresponding to the structural behaviour type B.

Table 2.1 – Modification factor k.

Structural Behaviour Type	β_1 (percent)	*k*
Type B	≤ 25	0.67
	>25	$0.845-\frac{0.446(a_y d_{pi}-d_y a_{pi})}{a_{pi} d_{pi}}$

Numerical Derivation of Spectral Reduction

The spectral reduction factors are calculated as shown in Eq. 2.41 and Eq. 2.42.

$$SR_A=\frac{3.21-0.68\ln(\beta eff)}{2.12}=\frac{3.21-0.68\ln\left[\frac{63.7k(a_y d_{pi}-d_y a_{pi})}{a_{pi} d_{pi}}+5\right]}{2.12}\geq 0.44 \quad \textit{Eq. 2.41}$$

$$SR_V=\frac{2.31-0.41\ln(\beta eff)}{1.65}=\frac{2.31-0.41\ln\left[\frac{63.7k(a_y d_{pi}-d_y a_{pi})}{a_{pi} d_{pi}}+5\right]}{1.65}\geq 0.56 \quad \textit{Eq. 2.42}$$

One should multiply the response spectrum by these factors in order to reduce it.

2.4.4.2 CSM-FEMA440

In this endeavour the FEMA440's Procedure B – Intersection with MADRS (modified acceleration-displacement response spectrum) – is used to calculate the target displacement.

The formulas herein presented were calibrated from a large statistical study using SDOF oscillators with a variety of different inelastic hysteretic behaviour, including: bilinear hysteretic (BLH), stiffness- degrading (STDG), and strength-degrading, as shown in Figure 2.21. Parameters that have been optimized for all types of behaviour were also included.

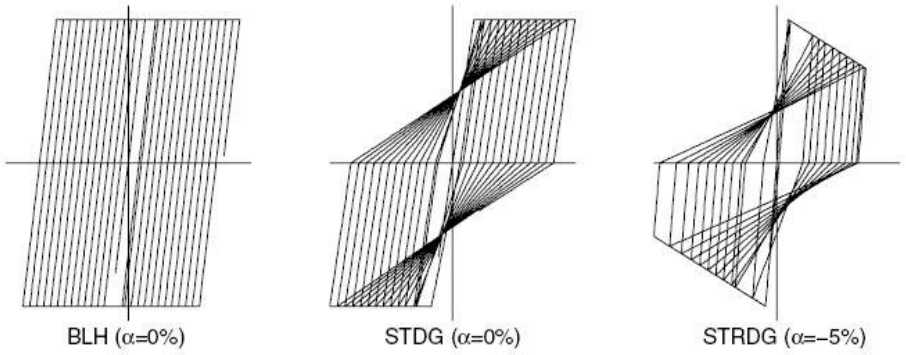

Figure 2.21 - Types of inelastic behaviour considered: BLH=Bilinear Hysteretic STDG=Stiffness Degrading, and STRDG=Strength Degrading [5].

Effective damping

The formulas herein presented apply to any capacity curve, independent of hysteretic model type or post-elastic stiffness value (α) used.

The effective damping is calculated using Eq. 2.43, Eq. 2.44 and Eq. 2.45 depending on the structure's level of ductility μ.

For $\mu < 4.0$: $$\beta_{eff} = 4.9(\mu-1)^2 - 1.1(\mu-1)^3 + \beta_0 \quad \textit{Eq. 2.43}$$

For $4.0 \leq \mu \leq 6.5$: $$\beta_{eff} = 14.0 + 0.32(\mu-1) + \beta_0 \quad \textit{Eq. 2.44}$$

For $\mu > 6.5$: $$\beta_{eff} = 19\left[\frac{0.64(\mu-1)-1}{[0.64(\mu-1)]^2}\right]\left(\frac{T_{eff}}{T_0}\right)^2 + \beta_0 \quad \textit{Eq. 2.45}$$

Where,

μ – ductility
β_0 – initial viscous damping (5% - concrete buildings)
T_0 – fundamental period in the direction under consideration
T_{eff} – effective period

The effective damping-ductility function defined by the equations previously mentioned is plotted in Figure 2.22. Note that the effective damping also depends on the initial viscous damping level β_0.

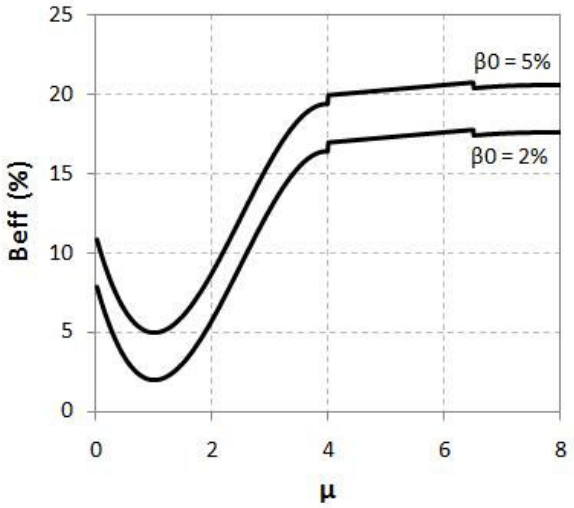

Figure 2.22 – Effective damping B_{eff} depending on the ductility level μ and viscous damping β_0.

Effective Period

Once again, the following equations apply to any capacity spectrum independent of hysteretic model type or post-elastic stiffness value. The effective period depends on the ductility level and is calculated using Eq. 2.46, Eq. 2.47 and Eq. 2.48.

For $\mu < 4.0$: $$T_{eff} = \left\{0.20(\mu-1)^2 - 0.038(\mu-1)^3 + 1\right\}T_0 \qquad \textit{Eq. 2.46}$$

For $4.0 \leq \mu \leq 6.5$: $$T_{eff} = \left[0.28 + 0.13(\mu-1) + 1\right]T_0 \qquad \textit{Eq. 2.47}$$

For $\mu > 6.5$: $$T_{eff} = \left\{0.89\left[\sqrt{\frac{(\mu-1)}{1+0.05(\mu-2)}} - 1\right] + 1\right\}T_0 \qquad \textit{Eq. 2.48}$$

The effective period also depends on the initial elastic fundamental period T_0. The effective period-ductility function defined by the equations previously mentioned is plotted in Figure 2.23 for several values of T_0.

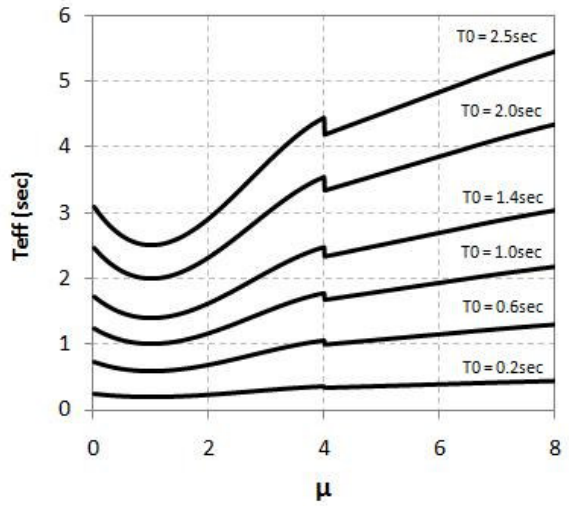

Figure 2.23 – Effective period T_{eff} depending on the ductility level μ for several values of T_0.

Spectral reduction factor for effective damping

The spectral reduction factor is a function of the effective damping and is called the damping coefficient, $B(\beta_{eff})$ and is calculated using Eq. 2.50. It is used to adjust spectral acceleration ordinates as shown in Eq. 2.49.

$$(S_a)_\beta = \frac{(S_a)_{5\%}}{B(\beta_{eff})} \qquad \textit{Eq. 2.49}$$

$$B(\beta_{eff}) = \frac{4}{5.6 - \ln \beta_{eff}(in\%)} \qquad \textit{Eq. 2.50}$$

The function relating the reduction factor B and the effective damping β_{eff} is plotted in Figure 2.24. It also depends on the initial viscous damping β_0.

Note that, the curve corresponding to a viscous damping $\beta_0 = 2\%$ starts at $B_{eff} = 2\%$, and the one corresponding to $\beta_0 = 5\%$ starts at $B_{eff} = 5\%$. From $B_{eff} = 5\%$ both curves coincide.

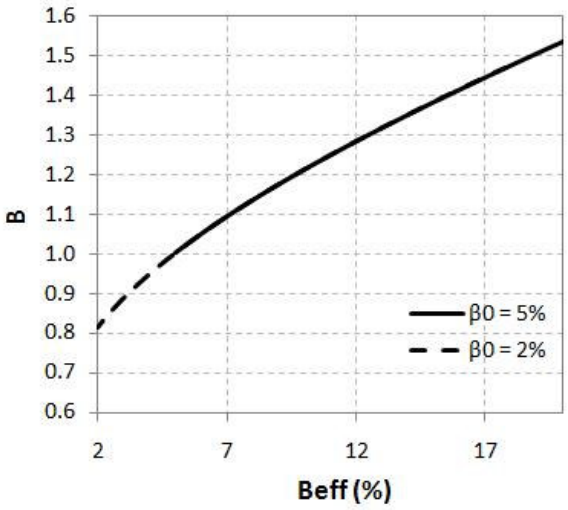

Figure 2.24 – Spectral reduction factor B depending on the effective damping level B_{eff} and viscous damping β_0.

Modificated acceleration-displacement response spectrum (MADRS)

After reducing the initial ADRS by using the $B(\beta_{eff})$ factor as described in Eq. 2.49, one should multiply the acceleration ordinates (i.e. not the displacement ordinates) of the new reduced ADRS by the modification factor, M. This factor is determined using the calculated effective period, T_{eff}, as shown in Eq. 2.51 and Eq. 2.52, in order to compute the modified acceleration-displacement response spectrum (MADRS).

$$M = \left(\frac{T_{eff}}{T_{\sec}}\right)^2 = \left(\frac{T_{eff}}{T_0}\right)^2 \left(\frac{T_0}{T_{\sec}}\right)^2 \qquad \textit{Eq. 2.51}$$

$$\frac{T_{\sec}}{T_0} = \sqrt{\frac{\mu}{1+\alpha(\mu-1)}} \qquad \textit{Eq. 2.52}$$

Where α is the post-elastic stiffness and μ the ductility, calculated as follows:

$$\alpha = \frac{\left(\frac{a_{pi}-a_y}{d_{pi}-d_y}\right)}{\left(\frac{a_y}{d_y}\right)} \qquad \textit{Eq. 2.53}$$

$$\mu = \frac{d_{pi}}{d_y} \qquad \textit{Eq. 2.54}$$

The function that relates the modification factor M and the ductility level μ is depicted in Figure 2.25.

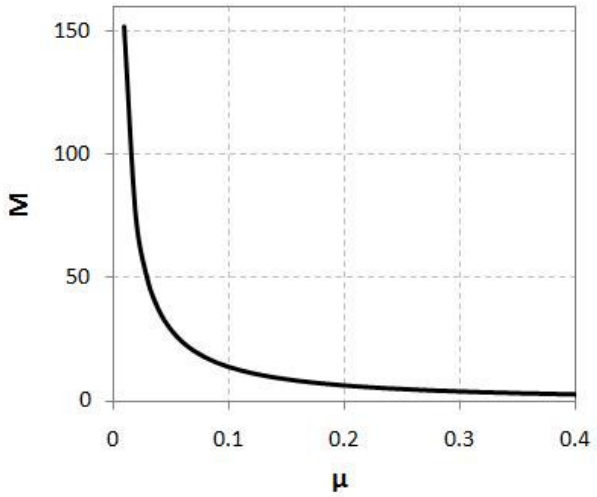

Figure 2.25 – Modification factor M depending on the ductility level μ.

The MADRS should be intersected with the capacity curve in an iterative procedure, in order to compute the performance point.

2.4.5 ACSM

The ACSM combines elements from the Direct Displacement Based Design [15] and the Capacity Spectrum Method (CSM) [1, 19]. The procedure is defined as a response spectrum-based approach, which uses an adaptive displacement pushover (DAP) [46] and employs the substitute structure methodology to model a SDOF inelastic system with equivalent elastic properties. The fact of considering an adaptive perspective justifies the method's nomenclature of the Adaptive Capacity Spectrum method (ACSM).

The steps of the procedure are described in detail as follows:

1: Develop a displacement adaptive pushover (DAP) analysis of the structure

The first step of the procedure consists in applying a DAP analysis to a nonlinear model of the MDOF structure.

The ACSM uses an adaptive displacement pushover, the so-called DAP [46]. This type of pushover is fully adaptive in the sense that it incrementally updates the lateral displacement pattern based on the modal properties of the structure at each analysis step. Therefore, it takes into account the stiffness degradation, period elongation and

the progressive structural damage. At each step, the eigenvalues and modes of vibration of the building are calculated considering the current structural stiffness state. The load pattern to be applied in the next step is obtained by making a combination of these different mode shapes. Therefore, the higher mode effects are taken into account. The spectral shape, that represents the contribution of each period and mode of vibration into the final displacement profile at each analysis step, for a given hazard, is considered through the use of spectral scaling. The steps of the DAP are duly described in [46].

2: Characterization of the 'equivalent SDOF adaptive capacity curve'

Instead of using a single control node like the other NSPs, the ACSM computes the equivalent SDOF structural displacement built on the current deformed pattern, which can turn out very useful in the 3D case.

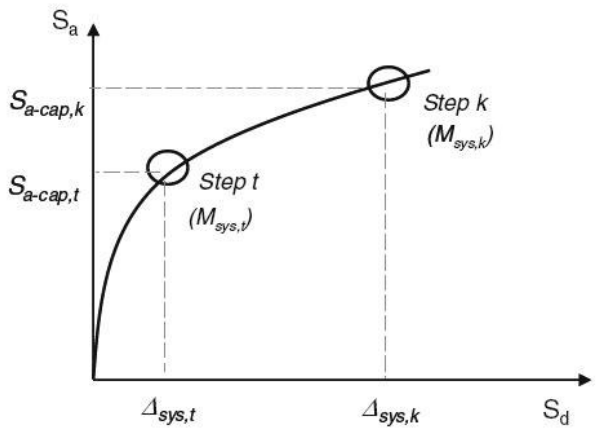

Figure 2.26 – Equivalent SDOF capacity curve [53].

The equivalent SDOF adaptive capacity curve is defined step-by-step, see Figure 2.26, calculating the equivalent system displacement $\Delta_{sys,k}$ and acceleration $S_{a-cap,k}$ based on the actual deformed shape at each analysis step *k*, using Eq. 2.55, Eq. 2.56 and Eq. 2.57.

$$\Delta_{sys,k} = \frac{\sum_i m_i \Delta_{i,k}^2}{\sum_i m_i \Delta_{i,k}} \qquad \textit{Eq. 2.55}$$

$$S_{a-cap,k} = \frac{V_{b,k}}{M_{sys,k}\, g} \qquad \textit{Eq. 2.56}$$

$$M_{sys,k} = \frac{\sum_i m_i \Delta_{i,k}}{\Delta_{sys,k}} \qquad \textit{Eq. 2.57}$$

Where,

$\Delta_{sys,k}$ - displacement of the equivalent SDOF system in the analysis step *k*

$S_{a-cap,k}$ - acceleration of the equivalent SDOF system in the analysis step *k*

$M_{sys,k}$ - effective mass of the equivalent SDOF system in the analysis step *k*

$V_{b,k}$ - base shear of the MDOF system in the analysis step *k,* obtained from the DAP analysis performed in point 1 of the procedure

m_i - mass associated with node *i* of the MDOF system

$\Delta_{i,k}$ - displacement of the node *i* of the MDOF system in the analysis step *k,* obtained from the DAP analysis performed in point 1 of the procedure

g - gravity acceleration

The $\Delta_{sys,k}$ and the $M_{sys,k}$ are obtained as the inverse of the modal participation factor and the modal mass. These measures are calculated step by step based on the current deformed pattern instead of being calculated based on invariant elastic or inelastic modal shape. Therefore, the $M_{sys,k}$ also varies at each step.

3: Application of the demand spectrum to the equivalent SDOF adaptive capacity curve

At this step of the procedure, the SDOF capacity curve is intersected with the demand spectrum in order to calculate the performance point (target displacement and inelastic acceleration), see Figure 2.27.

As happens in the capacity spectrum method (CSM), an iterative procedure is needed at this stage. The demand spectrum that is intersected with the capacity curve is reduced using a reduction factor that usually depends on the damping.

First, one should use an initial estimation of damping to compute the reduction factor. Afterwards, the demand spectrum reduced with the previously calculated reduction factor, is intersected with the SDOF capacity curve. This intersection corresponds to a first trial of the performance point. The next step consists in the bilinearization of the capacity curve at this trial performance point, and in the calculation of the associated damping. If this value is close to the first estimation of damping used, within a tolerable range such as 5%, then the performance point corresponds to the calculated

intersection. If not, one should use the new damping value to compute a new reduction factor, and the iterative procedure is repeated until one finds convergence.

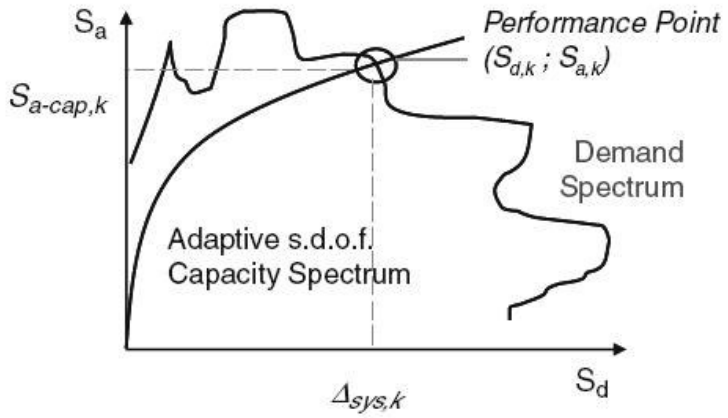

Figure 2.27 – Computation of the performance point [53].

There are several formulas for the reduction factor and damping calculation available in the literature [66, 96] that can be used in this step of the ACSM. In [54, 97] an extensive parametric study was performed, in which a large set of planar frame buildings were assed using the ACSM and the results compared with the *time-history*. Several reduction factors and damping formulas were tested in the ACSM in order to conclude which were the ones that lead to results closer to the nonlinear dynamic analyses.

The spectral reduction procedures available in the literature can be divided into two major groups. The first one is known as damping-based methods because the spectral reduction factors used are a function of the equivalent viscous damping. The second category is currently called ductility-based methods, because they directly depend on the displacement ductility of the system.

The first group of procedures is based on equivalent linearization in which the peak deformation demand is determined from the maximum displacement of an equivalent linear elastic system with lower stiffness (higher period of vibration) and with higher damping coefficient than those of the original system. This procedure is graphically illustrated in Figure 2.28a), in which the spectral reduction factor reduces both pseudo-spectral acceleration and spectral displacement equally resulting in a diagonal shift of the demand spectrum in the ADRS format.

The second approach computes the peak deformation demand by multiplying the maximum displacement of a linear elastic system with the same lateral stiffness and damping ratio of the inelastic system under analysis by the displacement modification factor based on the ductility of the inelastic system. This procedure is graphically illustrated in Figure 2.28b), in which the spectral reduction factor mainly reduces the pseudo-spectral acceleration and increases spectral displacements depending on the yield period of the system. Therefore, the demand spectrum shifts almost vertically in the ADRS format.

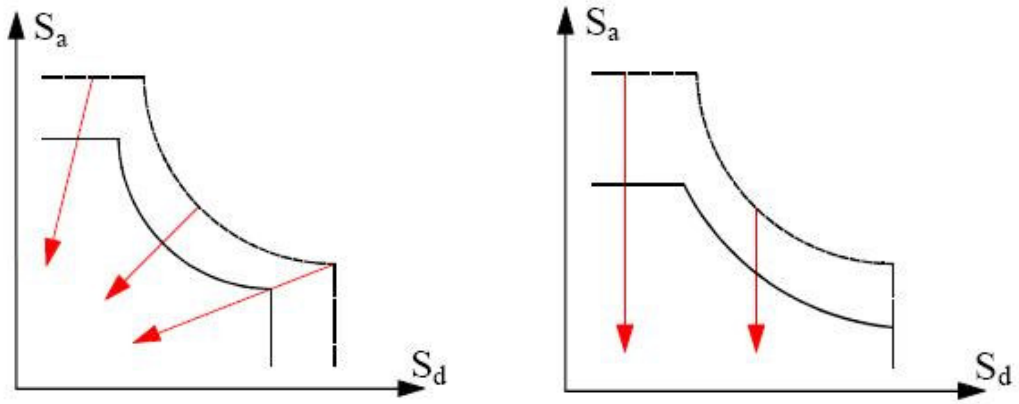

(a) *(b)*

Figure 2.28 – Spectral scaling procedures a) damping based; b) ductility based.

Reduction factors dependent on the damping:

For the computation of these factors it is necessary to first calculate the equivalent viscous damping of the system β_{eq}, which has a contribution of the viscous damping β_0 and a contribution of hysteretic dissipation.

The equivalent damping was calculated using different hysteretic models:

- ATC40 [21], developed from the bilinear model of Rosenblueth and Herrera [98]:

$$\beta_{eff-ATC40} = \beta_0 + k \cdot \frac{2}{\pi} \cdot \left[\frac{(1-\alpha)\cdot(\mu-1)}{\mu - \alpha \cdot \mu + \alpha \cdot \mu^2} \right] \qquad \textit{Eq. 2.58}$$

- Kowalsky [99], which uses the Takeda hysteretic model with post-yield hardening:

$$\beta_{eq-takKow} = \beta_0 + \frac{1}{\pi} \cdot \left[1 - \frac{(1-\alpha)}{\mu} - \alpha \cdot \sqrt{\mu} \right] \qquad \textit{Eq. 2.59}$$

- Gulkan and Sozen [58], developed from the Takeda hysteretic model without hardening:

$$\beta_{eq-takGulSoz} = \beta_0 + 0.2 \cdot \left[1 - \frac{1}{\sqrt{\mu}} \right] \qquad \textit{Eq. 2.60}$$

- Dwairi et al. [61] proposed a new secant period dependent damping ratio as shown in Eq. 2.61. In this work the C coefficient was used for concrete buildings (Eq. 2.62) and for steel buildings (Eq. 2.63) :

$$\beta_{eq-DwaKowNau} = \beta_0 + C \cdot \left[\frac{\mu - 1}{\pi \cdot \mu}\right] \qquad \textit{Eq. 2.61}$$

$$\begin{aligned} C = C_{TT} &= 0.5 + 0.4 \cdot (1 - T_{eff}) \qquad T_{eff} < 1s \\ C = C_{TT} &= 0.5 \qquad\qquad\qquad\qquad T_{eff} \geq 1s \end{aligned} \qquad \textit{Eq. 2.62}$$

$$\begin{aligned} C = C_{EP} &= 0.85 + 0.6 \cdot (1 - T_{eff}) \qquad T_{eff} < 1s \\ C = C_{EP} &= 0.85 \qquad\qquad\qquad\qquad T_{eff} \geq 1s \end{aligned} \qquad \textit{Eq. 2.63}$$

- Priestley proposed in 2007 [15] a similar damping relation Eq. 2.64 but with simplified effective period-independent coefficients. In this work the coefficients (Eq. 2.65) derived using the Takeda hysteresis rule (TF) for concrete wall buildings, using the Takeda thin model (TT) for concrete frame buildings, and the Ramberg-Osgood (RO) model for steel buildings were tested:

$$\beta_{eq-\mathrm{Pr}iestley} = \beta_0 + C \cdot \left[\frac{\mu - 1}{\pi \cdot \mu}\right] \qquad \textit{Eq. 2.64}$$

$$\begin{aligned} C &= C_{TF} = 0.565 \\ C &= C_{TT} = 0.444 \\ C &= C_{RO} = 0.577 \end{aligned} \qquad \textit{Eq. 2.65}$$

Where,

μ - is the ductility

α - is the ratio between the post-yield stiffness and the initial stiffness

k - is a measure of how well the hysteresis instantaneous cycle of the structure is represented by a parallelogram [21]

T_{eff} - is the effective period

The reduction factors, dependent on the equivalent damping, were calculated according to the following proposals:

- The combination of the formula recommended in EC8 [25] (Eq. 2.66) with the one proposed by Ramirez et al. [56] (Eq. 2.67), see Eq. 2.68.

$$B_{EC8} = \begin{cases} 1-(1-\eta)\dfrac{T}{T_b} & 0 \le T < T_b \\ \eta & T \ge T_b \end{cases}$$

Eq. 2.66

$$\eta = \sqrt{\frac{10}{5+100\cdot\beta_{eq}}} \ge 0.55$$

$$B_{Ram} = \begin{cases} 1-(1-B_{short})\dfrac{T}{T_b} & 0 \le T < T_b \\ B_{short} & T \ge T_b \end{cases}$$

Eq. 2.67

$$B_{EC8-Ram} = \begin{cases} B_{EC8} & 0 \le T < T_{dd} = T_d \dfrac{B_{Ramirez}}{B_{EC8}} \\ B_{Ram} & T \ge T_{dd} \end{cases}$$

Eq. 2.68

Where, B_{short} is function of β_{eq}, and T_b is the first spectral characteristic period, and T_d is the third spectral characteristic period.

- The formula proposed by Lin and Chang [57], see Eq. 2.69.

$$B_{Lin-Chang} = 1 - \frac{a\cdot T^{0.3}}{(T+1)^{0.65}}$$

Eq. 2.69

$$a = 1.303 + 0.436\cdot\ln(\beta_{eq})$$

- The formula proposed by Priestley et al. in 2007 [15] :

$$B_{Priestley} = \left(\frac{0.07}{0.02+\beta_{eq}}\right)^{0.5}$$

Eq. 2.70

Reduction factors dependent on the ductility:

Another approach is to reduce the demand spectrum defined for the level of viscous damping, using reduction factors that depend on the ductility of the system. The reduction factors dependent on the ductility were calculated using two proposals:

- Miranda [66]:

$$C_{Mir} = \left[1 + \left(\frac{1}{\mu} - 1\right) \cdot \exp\cdot\left(-12 \cdot T \cdot \mu^{-0.8}\right)\right]^{-1} \qquad \textit{Eq. 2.71}$$

- Vidic, Fajfar and Fishinger [65]:

$$C_{VidFajFish} = \begin{cases} \mu \cdot \left[1.35 \cdot (\mu - 1)^{0.95} \cdot \dfrac{T}{T_{c'}} + 1\right]^{-1} & T \le T_{c'} \\ \mu \cdot \left[1.35 \cdot (\mu - 1)^{0.95} + 1\right]^{-1} & T > T_{c'} \end{cases} \qquad \textit{Eq. 2.72}$$

$$T_{c'} = 0.75 \cdot \mu^{0.2} \cdot T_c \le T_c$$

The tested variants of the ACSM are summarized in Table 2.2.

Table 2.2 – Tested spectral scaling approaches.

ACSM variant	Damping-based		Ductility-based
	Damping	Reduction factor	
1	ATC40	EC8Ram	
2	ATC40	LinChang	
3	TakKow	EC8Ram	
4	TakKow	LinChang	
5	TakGS	EC8Ram	
6	TakGS	LinChang	
7	DawKowNau	EC8Ram	
8	DawKowNau	LinChang	
9	Priestley	Priestley	
10			Mir2000
11			VidFajFish

Figure 2.29 shows the ACSM's performance using different damping formulas and different reduction factors, in terms of bias of displacements of the planar frames analysed. More results are presented in [54, 97].

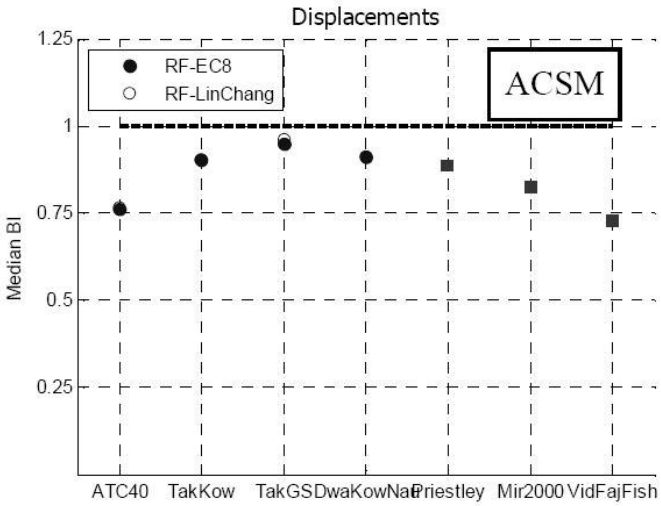

Figure 2.29 – Evaluation of the ACSM's performance using different damping formulas and different reduction factors [54].

From the obtained results it is clear that the damping dependent reduction factor proposed by Lin and Chang with the damping formulas proposed by Gulkan and Sozen were the ones that lead the ACSM to the best results (closer to the *time-history*) on the analysed structures.

Therefore, these reduction factor and damping formulas were used in this thesis in the ACSM procedure.

4: Determination of MDOF response parameters in correspondence to the Performance Point (conversion from SDOF to MDOF)

In order to calculate the MDOF response, one should go back to the pushover database to the step corresponding to the calculated performance point, see Figure 2.30. For this level, pick up the response of the structure in terms of displacement pattern, base shear, etc.

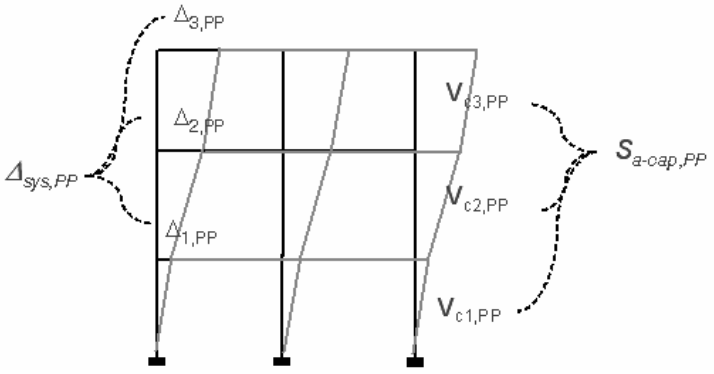

Figure 2.30 – SDOF to MDOF response conversion.

5: Check of acceptability criteria

At this stage, the demand in the elements calculated in the previous step, are checked against their capacity.

The ACSM procedure is schematically represented in Figure 2.31 [53].

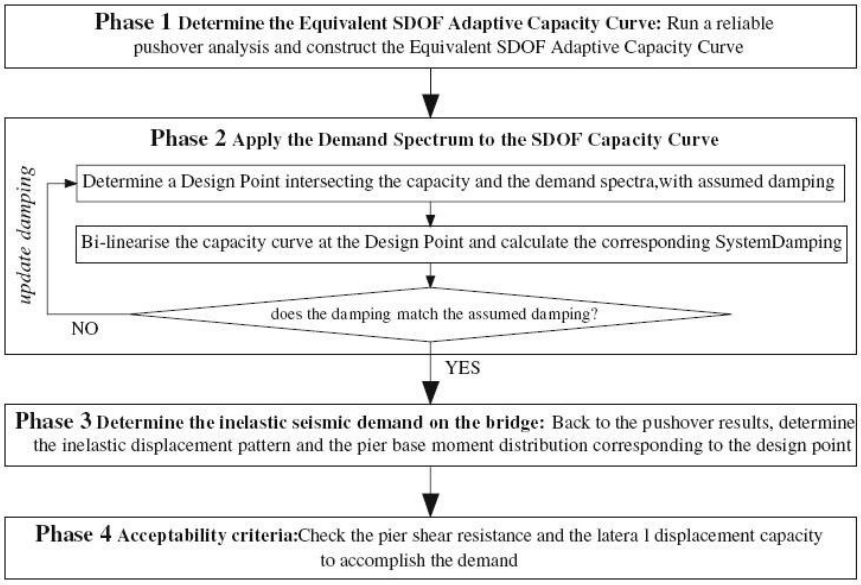

Figure 2.31 – ACSM flowchart [53].

2.4.6 Summary of studied NSPs

Table 2.3 shows a summary of the methods used in this work pointing out the main differences between the methods in each step of the nonlinear static procedure.

Table 2.3 – Summary of studied NSPs (modified from [100]).

	ACSM	CSM	N2	MPA
Pushover analysis type	Adaptive displacement-based	Conventional force-based		
Load pattern	Adaptive Displacements loading	1st mode proportional loading	1st mode proportional or uniform loading	All significant modes proportional loading
Capacity curve	Base shear vs. Displacement computed from all nodes	Base shear vs. Displacement of a reference/control node, usually recommended as the centre of mass of the roof		
Demand curve	Elastic viscous damping-based reduced spectrum		Inelastic ductility-based reduced spectrum	
Considered variants	One: - Preliminary study carried out in [54, 97]	Two: - ATC 40 - FEMA 440	Two: - Original N2 - Extended N2 method for plan asymmetric buildings	One: - MPA version for plan asymmetric buildings

3. Case studies and modelling features

The geometric properties of the case studies analysed are presented in the first part of the chapter.

In the second part, the modelling options assumed during the performed studies and the dynamic properties of the buildings are described.

A comparison between the experimental results of the SPEAR building pseudo-dynamically tested in ELSA laboratory at Ispra in full scale and the analytical results obtained with the 3D models is also presented.

3.1 Case studies

The case studies analysed in this work are real existing buildings asymmetric in plan: a three storey building, representing typical old constructions in Greece and in the Mediterranean region; a five storey and an eight storey buildings located in Turkey. The geographic locations of the case studies are represented in Figure 3.1.

Due to their plan irregularities, the buildings have to be analysed with 3D models.

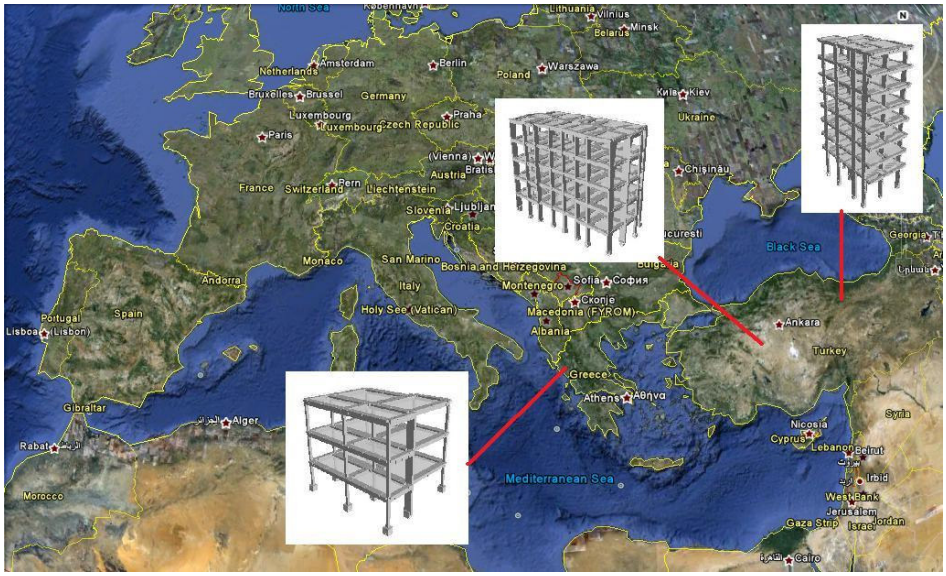

Figure 3.1 – Case studies location.

3.1.1Three storey building

The first case study to be analysed is the SPEAR building. It represents typical existing three-storey buildings in the Mediterranean region following Greece's concrete design code in force between 1954 and 1995. This structure was designed only for gravity loads based on the construction practice applied in the early 1970s that included the use of smooth rebars. It was tested in full-scale under pseudo-dynamic conditions, and subjected to bi-direction seismic loading, at JRC Ispra within the European SPEAR project framework. Plan and elevation views are shown in Figure 3.2, whilst further details on the structure and its pseudo-dynamic testing can be found in [101] and [102]. A 3D view of the building is presented in Figure 3.3.

The building is plan-asymmetric in both X and Y directions but it is regular in elevation (Figure 3.2).

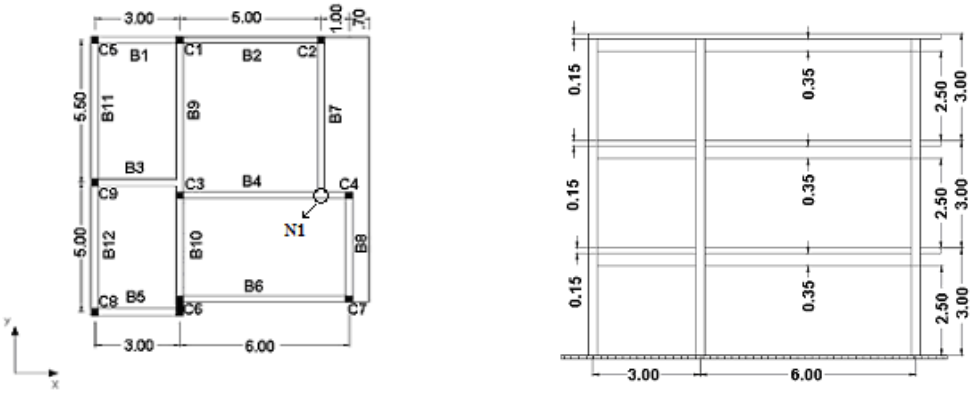

(a) *(b)*

Figure 3.2 - (a) Plan View (m), (b) Lateral View (m).

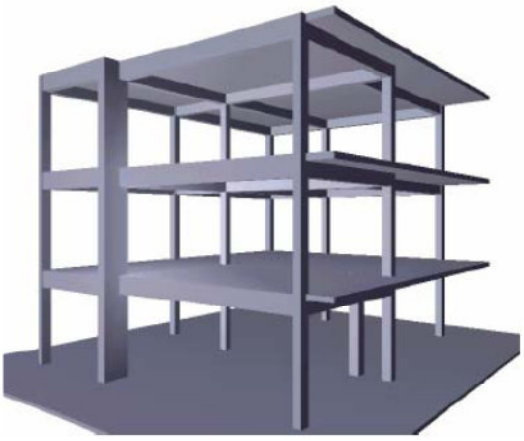

Figure 3.3 – SPEAR building 3D view.

Eight of the nine existing columns have a square cross-section of 250×250mm^2, Figure 3.4a). The column C6 has a rectangular section of 250×750mm^2, with the higher dimension oriented along the Y direction implying a "weak direction" along the X-axis (Figure 3.4a)). The column C6 and the presence of a balcony on the east side of the structure are the major causes for the in-plan irregularity, shifting the centre of mass (CM) away from the centre of stiffness (CR), which is very close to the central column (C3), thus causing the eccentricity to be larger in the Y direction. Column C2 is the flexible edge of the building and column C8 the stiff edge.

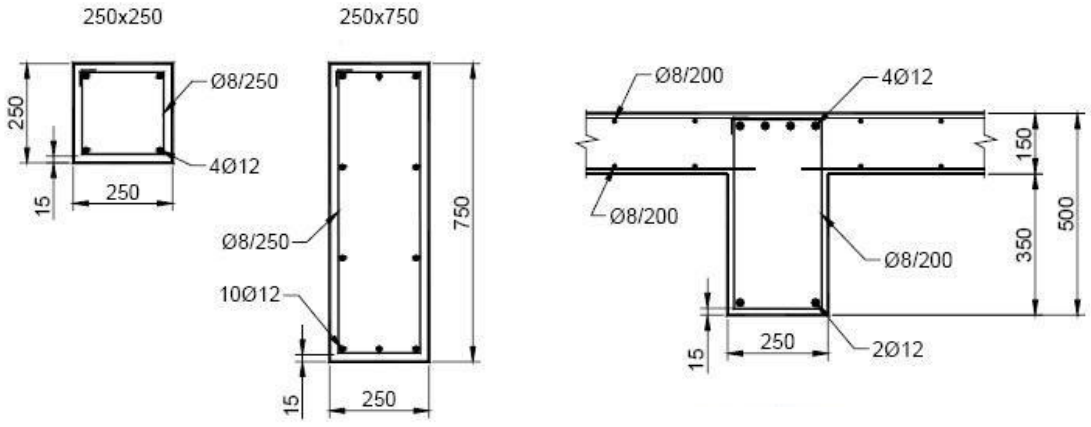

(a) *(b)*

Figure 3.4 - (a) Columns sections (mm), (b) Typical beam sections (mm).

The plan dimensions of the building are represented in Figure 3.2a).

The storey height is 3m, with 2.5m clear height of columns between the beams, Figure 3.2b). The slab was cast in place monolithically. It is 150mm thick and reinforced with 8mm bars with 200mm spacing.

The longitudinal reinforcement of the columns is characterized by 12mm plain bars, lap spliced over 400mm at each floor level, including the first level. Spliced bars have 180° hooks. Column stirrups are 8mm plain bars with 250mm spacing, closed with 90° hooks (see Figure 3.4a)). These stirrups do not continue into the joints.

In Figure 3.4b) and Figure 3.5 the typical beam longitudinal reinforcement is represented. It is characterized by two 12mm bars at the top, anchored with 180° hooks at the far end of the column. The beam reinforcement at the bottom is constituted by two 12mm bars anchored at the far end of the column with 180° hooks, and two other 12mm bars that are bent up towards the supports. The latter are anchored with downward bends into the joint core at exterior joints, and continue into the next span at interior joints. Additional longitudinal reinforcement, as well as bars of greater diameter (20mm) are used for some heavier loaded beams. Beam stirrups are 8mm bars with 200mm spacing, anchored with 90° hooks.

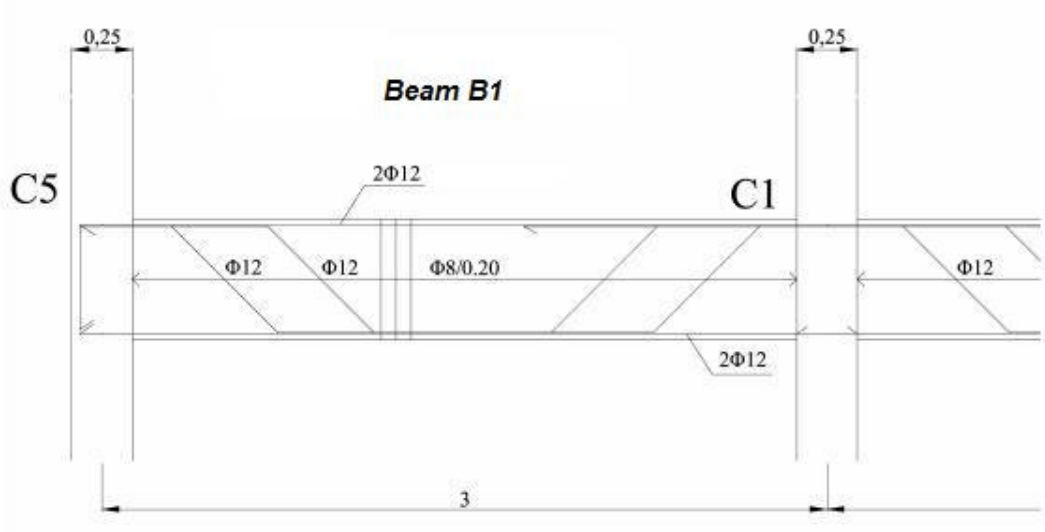

Figure 3.5 – Lateral view of a typical beam.

3.1.2 Five storey building

The second case study is a real Turkish reinforced concrete 5 storey building. It experienced the 1999 Golcuk earthquake without any damage. The building was designed according to the 1975 Seismic Code of Turkey.

The building is asymmetric in plan along the X axis, Figure 3.6, and all the floors have the same height, Figure 3.7. There are beams framing into beams leading to possible weak connections in the structure. There are also walls and elongated columns (wall-like columns), as presented in Figure 3.6.

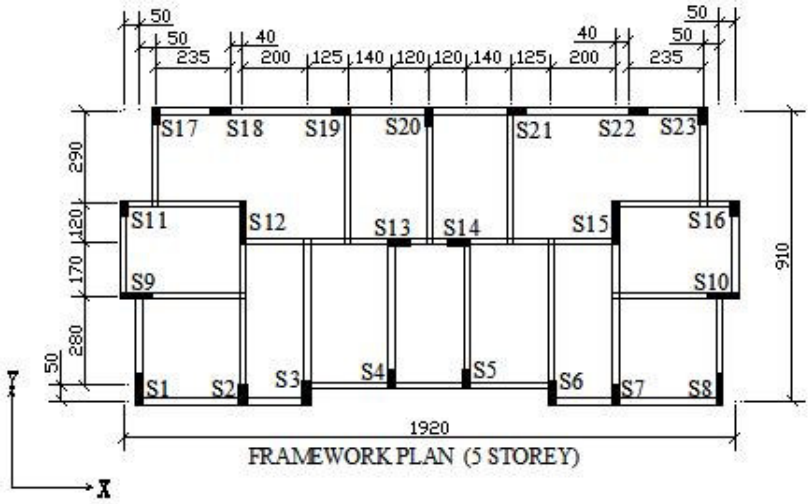

Figure 3.6 - Plan View (cm).

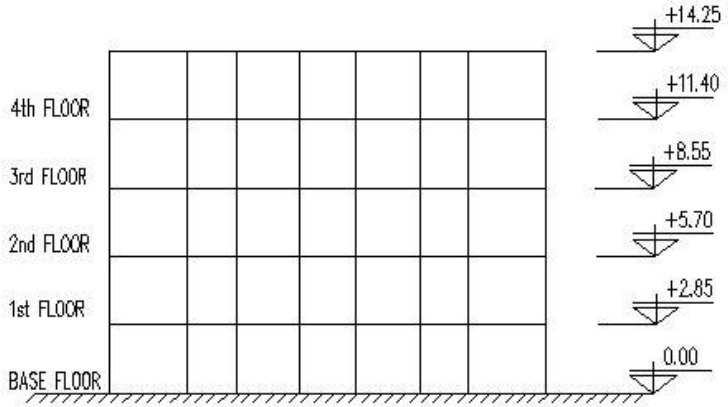

Figure 3.7 - Lateral View (m).

The column sections keep the same geometrical and reinforcement features along the height of the building. Column sections are represented in Figure 3.8. In columns the stirrups are ø8 with 20cm spacing, constant along the height.

The beam sections are mainly 0.20x0.50m^2 except the two located at the centre of the building that are 0.20x0.60m^2. The stirrups have 20cm spacing both for beams and columns. Typical beam sections are represented in Figure 3.9.

The slabs are 0.10m and 0.12m thick. For more details on the building's characteristics see [103].

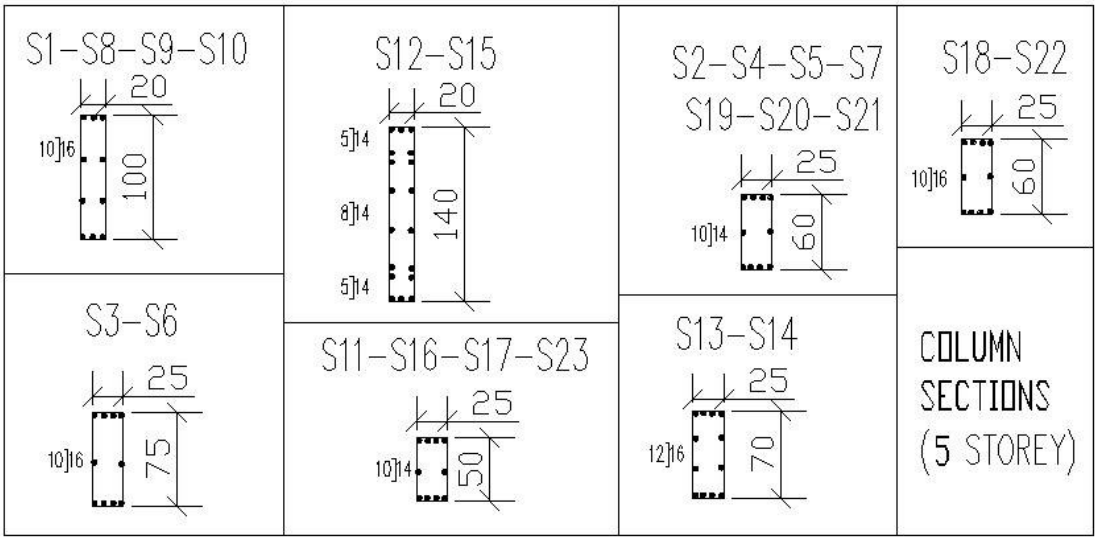

Figure 3.8 – Column sections (column dimensions in cm; reinforcement in mm).

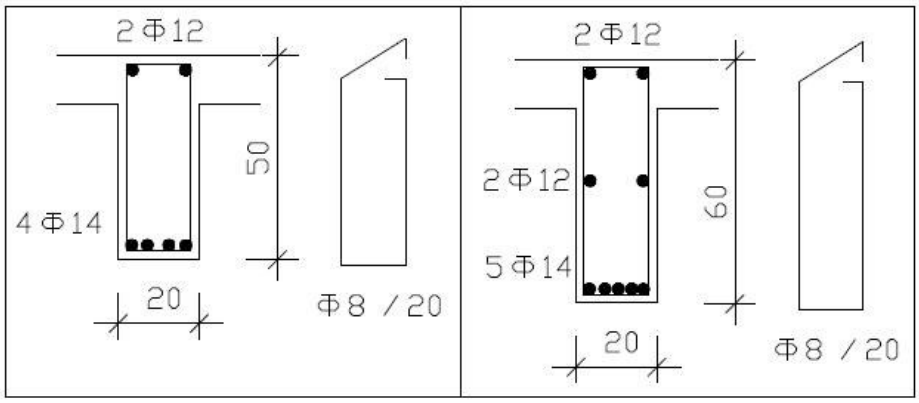

Figure 3.9 – Typical beam sections (beam dimensions and stirrup spacing in cm; reinforcement in mm).

3.1.3 Eight storey building

The third case study selected for this work is a real Turkish reinforced concrete 8 storey building. It is a plan-irregular structure since it is asymmetric along the X and Y axis, Figure 3.10a). The building was also designed according to the 1975 Seismic Code of Turkey.

The first storey height amounts to 5.00m and the other floors have the same 2.70m height, Figure 3.10b). There are beams framing into beams leading to possible weak connections in the structure. There are also walls and elongated columns (wall-like columns), as presented in Figure 3.10a), with the higher dimension always along the

Y direction. For this reason, the structure will be more stiff and resistant along the Y direction.

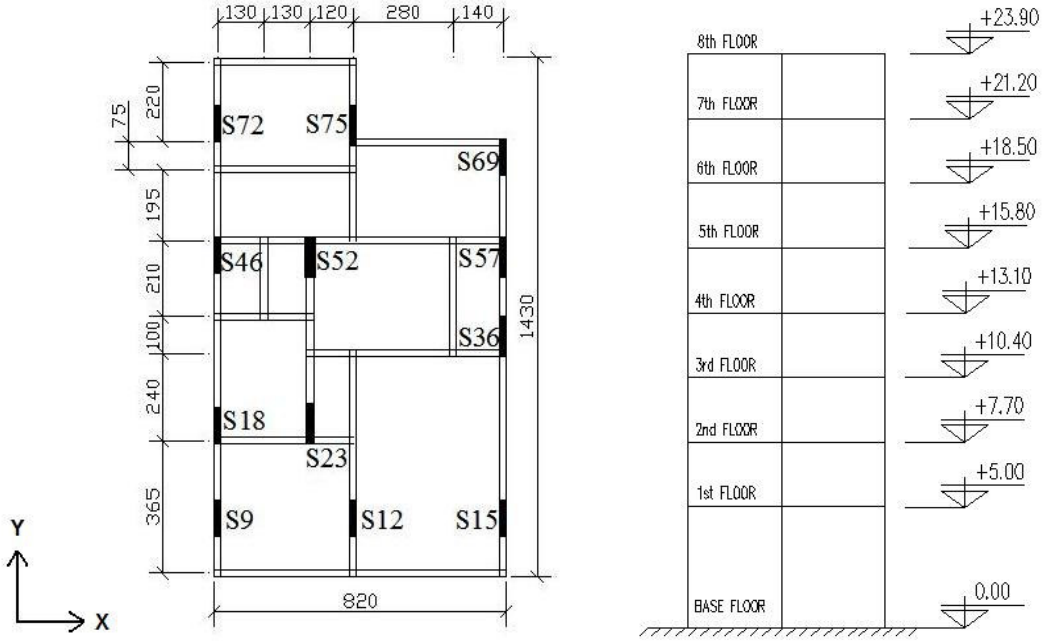

(a) *(b)*

Figure 3.10 - (a) Plan View (cm), (b) Lateral View (m).

The column sections and reinforcement are presented in Figure 3.11. They keep the same geometrical features along the height of the building, except column S52 that varies from 1.1x0.3m^2 (on the first floor) to 0.8x0.3m^2 (on the last floor). The height of this section is reduced by 0.1m every two storeys.

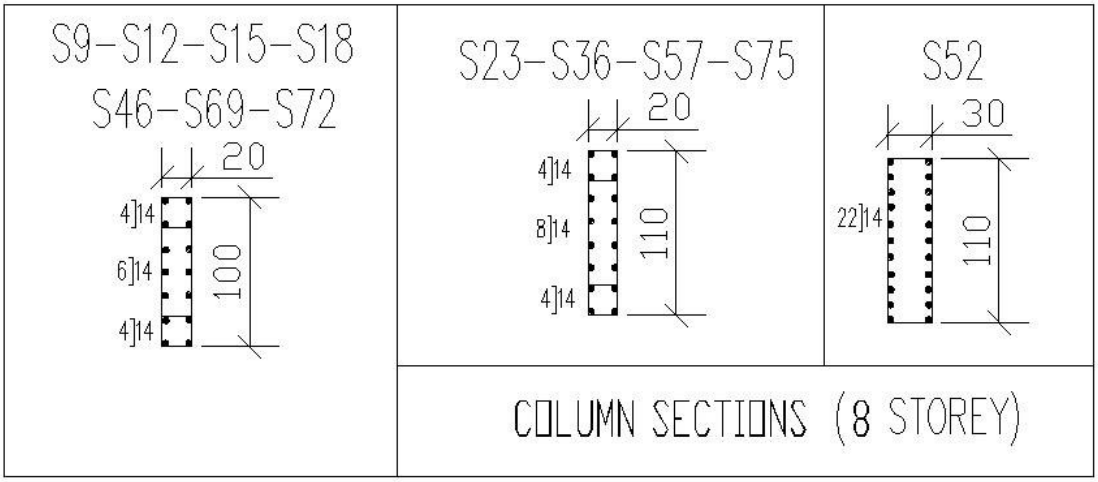

Figure 3.11 – Column sections (column dimensions in cm; reinforcement in mm).

Columns S9, S12, S15, S18, S46, S69 and S72 are 0.20x1.00m^2 and columns S23, S36, S57 and S75 are 0.20x1.10m^2, Figure 3.11.

In columns the stirrups are ø8 with 20cm spacing, constant along the height.

The beam sections are mainly 0.20x0.50m^2 except the two located at the centre of the building along the X direction that are 0.30x0.50m^2 and 0.25x0.50m^2 respectively. The slabs are 0.12m thick.

3.2 Modelling features

This section describes the modelling options used during the endeavour as well as the dynamic properties of the analysed buildings. Comparisons between experimental results obtained at the ELSA laboratory and analytical ones for the SPEAR building are presented at the end.

3.2.1 General modelling strategy

The 3D nonlinear models of the buildings under analysis in this work were developed using SeismoStruct [104], a fibre element based finite element software. It is capable of performing nonlinear static and nonlinear dynamic analysis, considering geometric nonlinearities, P-Δ effects, and material inelasticity. A distributed plasticity was assumed for the nonlinear modelling of the members, their inelasticity being modelled through the use of fibre element models.

The buildings were modelled by an assemblage of inter-connected frame elements using centreline dimensions and incorporating distributed material inelasticity through displacement based formulation along with geometric nonlinearity utilizing a corotational formulation.

Each element was discretized into four or five sub-elements with two integration Gauss points each, see Figure 3.12. Fiberized cross-sections – representing sectional details such as cover and core concrete and longitudinal reinforcements – were then defined at the respective integration points, whereby every fibre was assigned to an appropriate material constitutive relationship, as described below. The sectional stress-strain state of beam-column elements is obtained by integrating the nonlinear uniaxial stress-strain response of the individual fibres into which the section has been subdivided. Each section was defined with 300 fibres in the three storey building and with 100 fibres in the Turkish buildings. This option was taken because the models of the Turkish buildings were significantly heavier in terms of memory size than the three storey building model. Therefore, the SPEAR building model did not take such a long time to run (namely the nonlinear dynamic analysis) by considering each element characterized by 300 fibres. On the contrary, if one would adopt in the Turkish buildings, sections with 300 fibres, the models' running time would increase significantly and would make the large parametric study herein developed almost

unfeasible. The 100 section fibres used in equilibrium computations carried out at each of the element's integration sections seemed to be sufficient to guarantee an adequate reproduction of the stress-strain distribution across the element's cross-section. The sectional responses were obtained by integrating the material responses across a section using mid-point rule, whilst element-level responses were determined through a Gauss-Legendre integration scheme using section responses at integration points within the element. Further discussions can be found in [105]. The discretization of a typical reinforced concrete cross-section is represented in Figure 3.12.

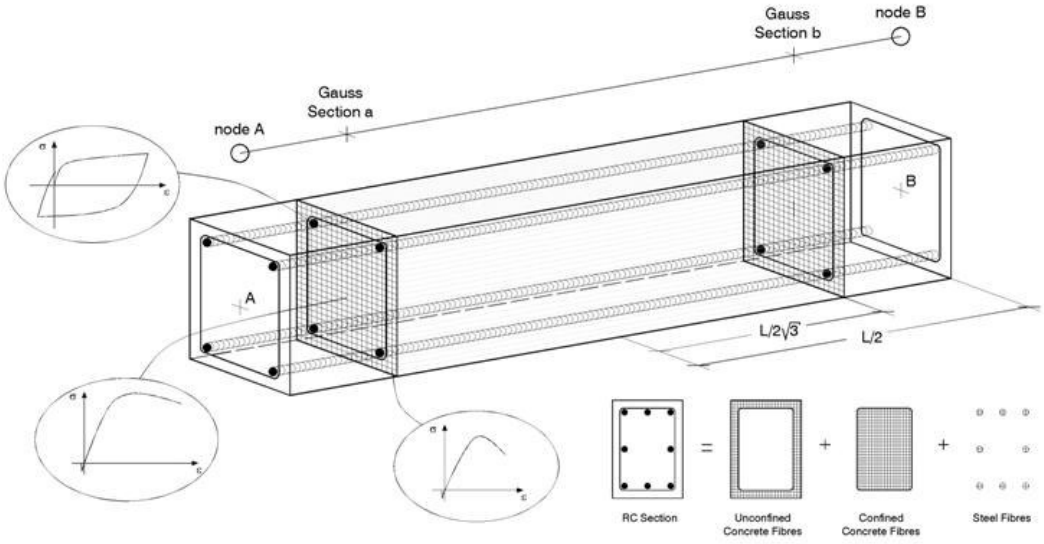

Figure 3.12 – Discretisation of a typical reinforced concrete cross-section [104].

The nonlinear modelling of a structure with distributed inelasticity is more precise than with a concentrated plasticity model. Besides that, the use of distributed inelasticity elements do not require the calibration of empirical response parameters as happens with the lumped-plasticity models. The advantages of using a fibre-based model instead of concentrated plasticity phenomenological models are: no requirement of a prior moment-curvature analysis of members; no need to introduce any hysteretic response of the element (as is implicitly defined by the material constitutive models); no need to define the plastic hinge length; direct modelling of axial load-bending moment interaction (both in terms of strength and stiffness); direct representation of biaxial loading, and interaction between flexural strength in orthogonal directions.

In order to keep the analytical models simple, the effect of beam-column joints, slippage and pullout of smooth reinforcing bars, etc., were not included in the model. Exclusion of these effects, as shown later, did not much affect on the accuracy of the results as verified from experimental data, but significantly reduced the analysis time which allowed the large parametric study required in the present work to be carried out.

The beams which have other beams being framed were subdivided so as to have a node at the beam being framed in order to respect the model kinematic compatibility. This type of modelling did not create any particular numerical issue.

In the three storey building, each structural member was subdivided into four elements. The material inelasticity usually develops at the edges of the members, so that their length is smaller, in order to more accurately model the formation of plastic hinges. The member subdivision type in terms of its total length, is 15%-35%-35%-15%, as represented in Figure 3.13.

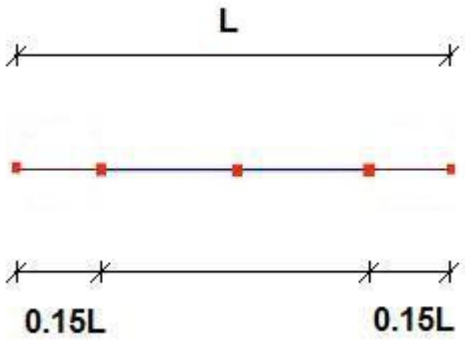

Figure 3.13 – 4 element subdivision.

In the five and eight storey building each element was subdivided into five elements. This option was taken in order to correctly model the reinforcement details along the elements of these buildings. The member subdivision type is described in Figure 3.14.

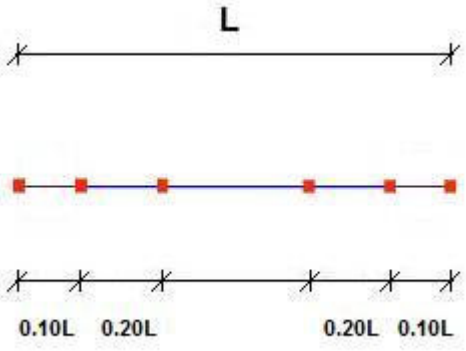

Figure 3.14 – 5 element subdivision.

The column-beam end connections were not modelled with rigid offsets, however, elongated columns were modelled as wall elements due to their larger dimension. In fact, these elongated columns were connected at each floor level to the adjacent beams with elastic elements with very high stiffness.

Figure 3.15 shows the 3D models of the case studies analysed in this work.

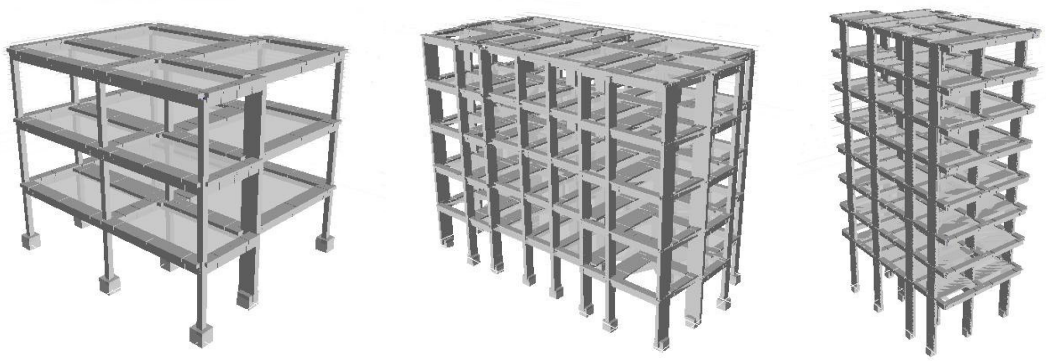

a) *b)* *c)*

Figure 3.15 – 3D models of the analysed buildings (a) three storey (b) five storey (c) eight storey.

3.2.2 Materials

The concrete was represented by a uniaxial model that follows the constitutive relationship proposed by Mander et al. [106] and the cyclic rules proposed by Martinez-Rueda and Elnashai [107].

A compressive strength of 25MPa was considered for the SPEAR building and 16.7MPa for the Turkish buildings.

The confinement factor is defined as the ratio between the confined and unconfined compressive stress of the concrete. It is used to scale up the stress-strain relationship.

The confinement effects provided by the lateral transverse reinforcement are taken into account by the rules proposed by Mander et al. [106] whereby constant confining pressure is assumed throughout the entire stress-strain range.

In the SPEAR building a confinement factor of 1.001 and in the Turkish buildings 1.2 was used.

In the SPEAR building the confinement factor was practically one because the building was designed only for gravity loads, leading to very small transverse reinforcement in the columns (ø8 with 25cm spacing), therefore the confinement effect is almost negligible.

The confined concrete constitutive model used in the SPEAR building is represented in Figure 3.16, and the one used in the Turkish buildings is in Figure 3.17.

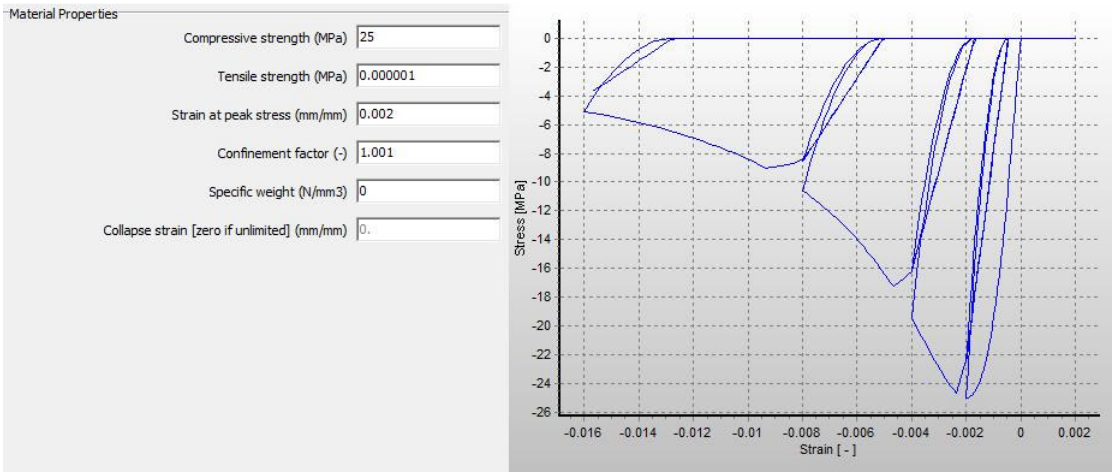

Figure 3.16 – SPEAR building: Confined concrete properties and constitutive model.

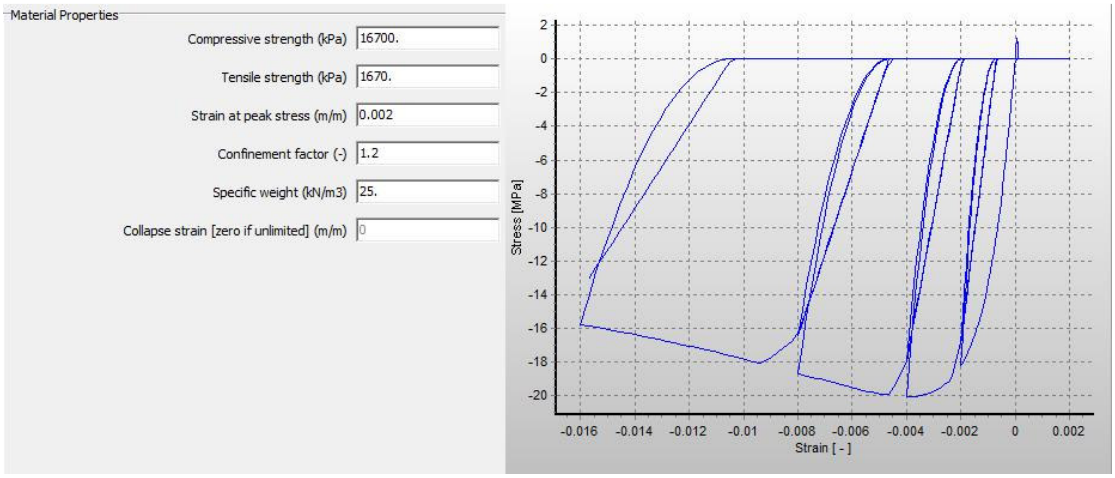

Figure 3.17 – Turkish buildings: Confined concrete properties and constitutive model.

The unconfined concrete constitutive model used in the cover thickness of the concrete sections is represented in Figure 3.18 for the SPEAR building and in Figure 3.19 for the Turkish buildings. The cover thickness of the concrete sections was considered to be 2.5cm in all the case studies. The confinement factor used for the unconfined concrete was 1.0.

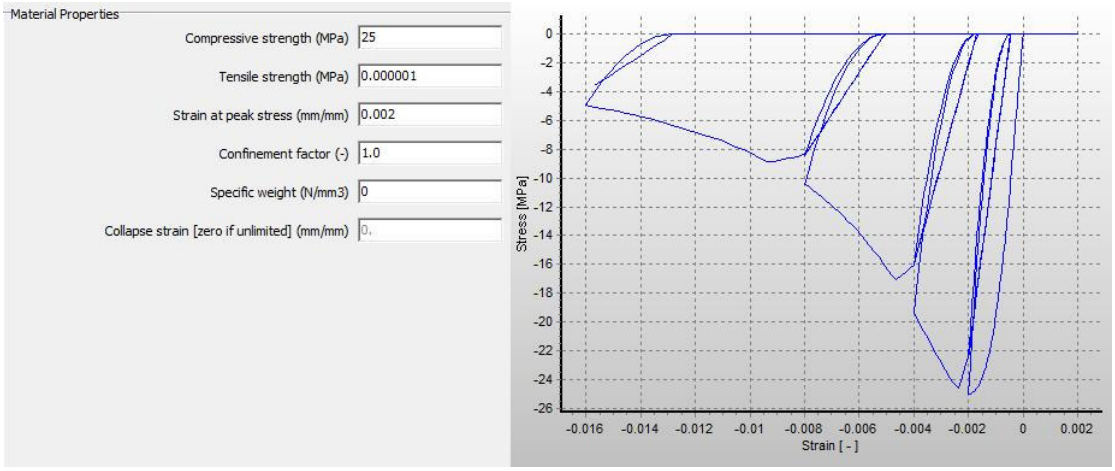

Figure 3.18 – SPEAR building: Unconfined concrete properties and constitutive model.

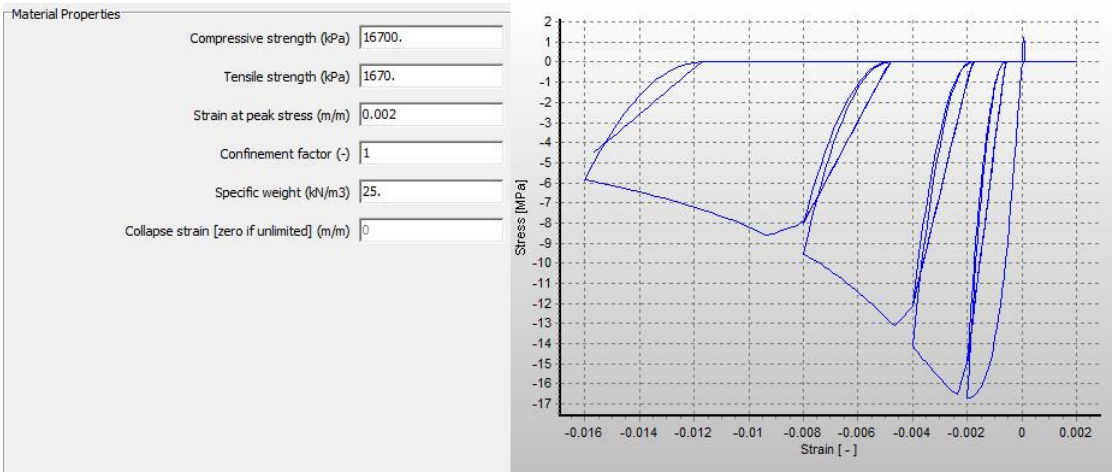

Figure 3.19 – Turkish buildings: Unconfined concrete properties and constitutive model.

The constitutive model used for the reinforcement steel was the one proposed by Menegotto and Pinto [108] coupled with the isotropic hardening rules proposed by Filippou et al. [109]. The average yield strength of 360MPa was assumed for the SPEAR building and 371MPa for the Turkish five and eight storey buildings.

The reinforcement steel properties and the constitutive model used in the SPEAR building is represented in Figure 3.20 and in the Turkish buildings in Figure 3.21.

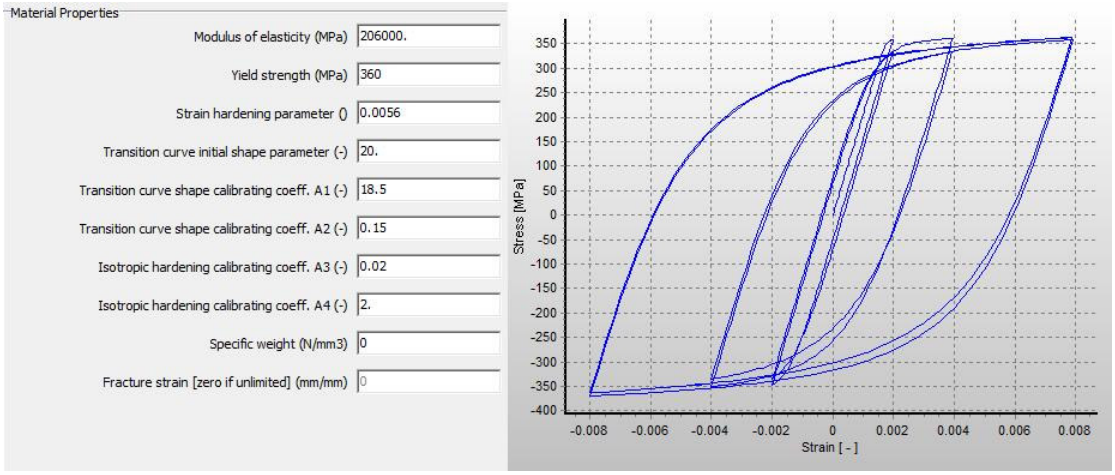

Figure 3.20 – SPEAR building: Reinforcement steel properties and constitutive model.

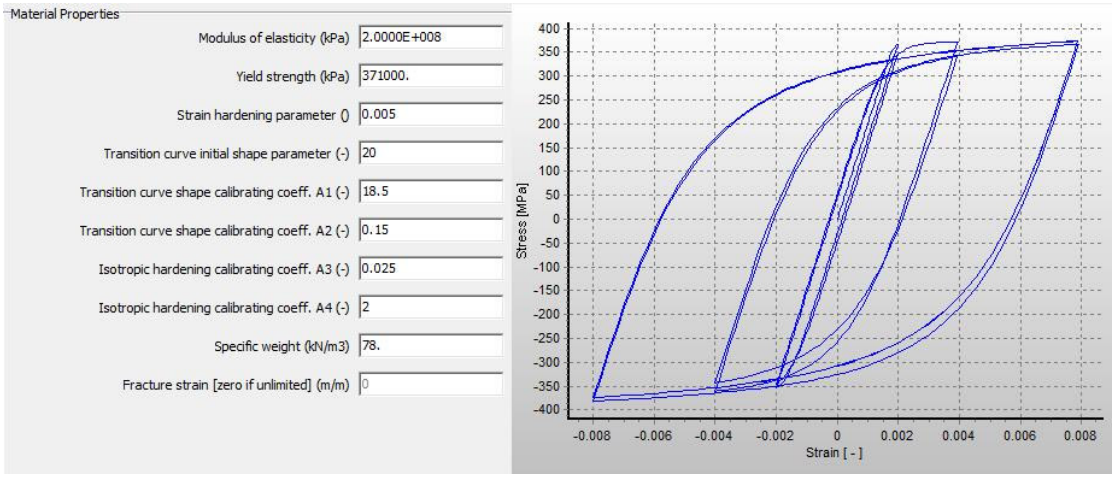

Figure 3.21 – Turkish buildings: Reinforcement steel properties and constitutive model.

Since there were no available data about the material properties of the Turkish five and eight storey buildings, the average values used were based on extensive laboratory tests on core samples collected from Istanbul and surroundings [110], where the buildings are located. These values represent the material properties of the existing building stock in the northern Marmara region.

3.2.3 Mass and loading

A lumped mass modelling strategy was adopted in the three storey building, in which masses were lumped at the nodal points according to the tributary area. In the five and eight storey building a distributed mass was considered along the beams calculated once again according to the respective tributary area.

Total translational masses in the three storey building amounted to 67.3ton each for the first two floors and 62.8ton for the roof. The centre of mass is located at X=4.53m and Y=5.29m. The sustained gravity loads were automatically computed by the software, using the defined masses.

In the five storey building, a mass of 263.41ton was considered at each storey except at the last storey where the mass was 150.14ton. The centre of mass is located at X=9.7m and Y=4.9m.

In the eight storey building a mass of 73ton was considered at the first storey, a mass of 56ton at the last storey and mass of 65ton at the other storeys. The centre of mass is located at X= 3.83m and Y=6.49m.

3.2.4 Damping

Hysteretic damping was already implicitly included in the nonlinear fibre model formulation of the inelastic frame elements.

In order to account for possible non-hysteretic sources of damping a tangent stiffness-proportional damping was used. For the SPEAR building a value of 2% was used, according to the experimental results at ISPRA, and for the Turkish buildings a 5% value was considered.

This non-hysteretic damping is due to phenomena like friction between structural and non-structural members, friction in opened concrete cracks, energy radiation through the foundation, etc, and it is mobilized during the dynamic response of the structure.

The scientific and engineering community does not have definitive answers concerning the type of viscous damping used to represent such energy dissipation. Priestley and Grant suggest that a tangent stiffness-proportional damping is the best option for common structures [111].

3.2.5 Diaphragm Modelling

The floor slabs of the buildings possess very high in-plane stiffness compared to the out-of-plane (flexural) one and thus can safely be modelled as a ‘rigid diaphragm’.

In the present work, such diaphragms were modelled by imposing kinematic constraints on the lateral displacements of all nodes at each floor so that they (nodal displacements) can be expressed by three rigid body motions of the respective floors, namely two horizontal translations and one rotation about the normal to the floor-

plane. This significantly reduces the number of dynamic degrees of freedom and hence increases the efficiency for large parametric studies.

To model the rigid diaphragm effect in the SPEAR building the Rigid Diaphragm with Lagrange multipliers modelling strategy was used. This option resulted from the calibration of the analytical model with the experimental results. Further details about the relative accuracy of other slab modelling approaches can be found elsewhere [112].

In the Turkish buildings the Lagrange multipliers option led to convergence problems when running nonlinear dynamic and nonlinear static analyses. Therefore, to model the rigid diaphragm effect of the slab in the Turkish buildings the option of Nodal Constraints with Penalty Functions was taken. The penalty function exponent used was 10^7.

Since the slab was not explicitly modelled, the effects of flexural stiffness of the slab were considered by assigning appropriate flange widths to the beams. The weight of the slab was applied lumped in the nodes, in the case of the SPEAR building, and distributed along the beams, in the case of the Turkish buildings, according to the respective tributary area.

3.2.6 Dynamic properties of the case studies

The modal properties of the three analysed buildings are presented herein. Table 3.1 shows the periods and the effective modal mass percentages in both X and Y directions (U_x and U_y), for the three case studies.

Table 3.1 – Periods and Effective Modal Mass Percentages.

	3 STOREY BUILDING			5 STOREY BUILDING			8 STOREY BUILDING		
Mode	Period (sec)	[Ux]	[Uy]	Period (sec)	[Ux]	[Uy]	Period (sec)	[Ux]	[Uy]
1	0.617	60.45%	7.83%	0.617	76.72%	0.00%	1.445	91.22%	0.00%
2	0.527	23.49%	42.99%	0.593	0.00%	77.94%	0.636	0.41%	1.81%
3	0.441	3.15%	31.59%	0.509	5.02%	0.00%	0.482	0.21%	79.21%
4	0.217	7.40%	0.77%	0.194	10.21%	0.00%	0.446	4.69%	1.87%
5	0.180	2.83%	3.91%	0.173	0.00%	12.29%	0.241	0.77%	0.00%
6	0.150	1.64%	0.00%	0.153	0.40%	0.00%	0.198	0.00%	0.20%

From Table 3.1, one can conclude that the three storey building has a fundamental mode of 0.617sec characterized by translation along the X direction, a second mode

of 0.527sec with torsional motion and a third mode of 0.441sec with translation along the Y direction. It is important to mention that in this case study, the translational modes are coupled with torsion. Figure 3.22 illustrates the first three modes of vibration of the SPEAR building.

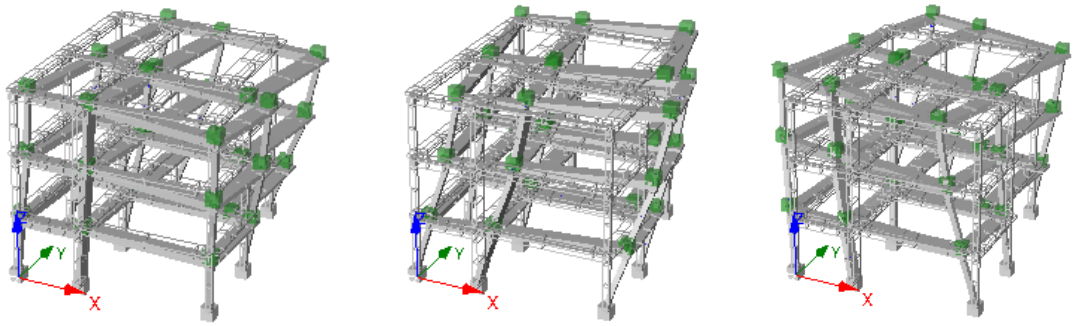

(a) *(b)* *(c)*

Figure 3.22 – Three storey building: a) first mode of vibration; b) second mode of vibration; c) third mode of vibration

The five storey building presents a first mode of 0.617sec with translation along the X direction, a second mode of 0.593sec with translation along the Y direction and a third mode of 0.509sec with torsional motion. In Figure 3.23 are plotted the first three modes of vibration of the five storey building.

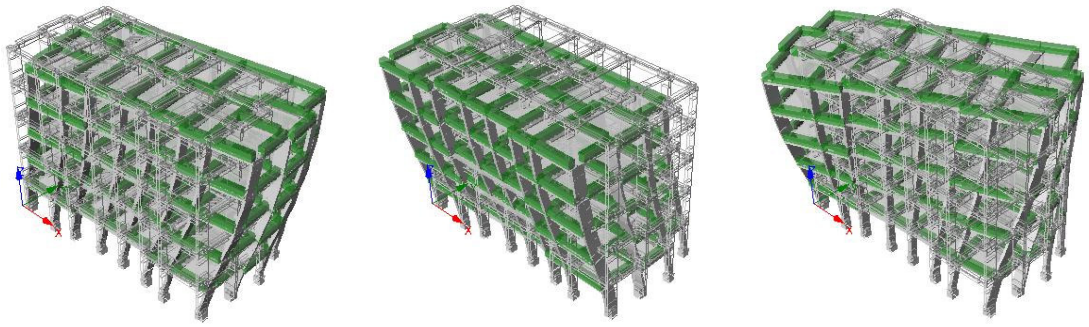

(a) *(b)* *(c)*

Figure 3.23 – Five storey building: a) first mode of vibration; b) second mode of vibration; c) third mode of vibration

Finally the eight storey building has a first mode of 1.445sec with translation along the X direction, a second mode of 0.636sec with torsional motion and a third mode of 0.482sec with translation along the Y direction (Figure 3.24).

(a) *(b)* *(c)*

Figure 3.24 – Eight storey building: a) first mode of vibration; b) second mode of vibration; c) third mode of vibration

The analysed buildings present torsional features due to their irregularities in-plan.

According to Fajfar [4] the period ratios of a structure have an important influence on its torsional behaviour. The period ratios Ω_x and Ω_y are defined as the uncoupled translational period divided by the uncoupled torsional period in the X and Y directions, respectively.

The influence of the predominantly torsional mode of vibration on the response in the direction considered when compared with the predominantly translational mode increases if the period ratio decreases.

Structures with period ratios larger than 1 are usually classified as torsionally stiff and structures with period ratios smaller than 1 as torsionally flexible. A structure can be torsionally stiff in one direction and torsionally flexible in the other.

Table 3.2 shows the period ratios Ωx and Ωy for the three buildings.

Table 3.2 – Period ratios.

	Ωx	Ωy
3 storey building	1.2	0.8
5 storey building	1.2	1.2
8 storey building	2.3	0.8

From Table 3.2 one can conclude that the three storey building is classified as torsionally stiff in the X direction and torsionally flexible in the Y direction. The five storey building is torsionally stiff in both X and Y directions. The eight storey building is torsionally stiff in the X direction and torsionally flexible in the Y direction.

3.2.7 Analysis options

In the nonlinear dynamic analysis the implicit integration Hilber-Hughes-Taylor algorithm [113] was used. The method's parameters values used in this work were: $\alpha = -0.1$, $\beta = 0.3025$ and $\gamma = 0.6$.

In this endeavour the Skyline solver (Cholesky decomposition, Cuthill-McKee nodes ordering algorithm, Skyline storage format) available in the software was used. This method tends to be more numerically stable than the Frontal solver introduced by Irons [114] featuring the automatic ordering algorithm proposed by Izzuddin [115], and also available in the software. For further details one should check for example [116, 117, 118, 119].

The integration time step Δt used in each *time-history* analysis was equal to the time step of the accelerogram used in that analysis. This option seems to be the best trade-off between accuracy and time-consuming work. In fact, by choosing such time step one does not disregard any information of the record during the integration process. On the other hand, if one would choose a smaller integration time step the duration of the analyses would increase significantly making the development of the large parametric study herein presented unfeasible.

The integration time step used in the three storey building was 0.01sec and in the five and eight storey buildings was 0.02sec. A good reference minimum value for the time step is $T/10$, where T is the structural period [120]. In order to capture the higher mode effects it is recommended to consider for this calculation the period corresponding to the higher mode that has a considerable influence on the structural response. For the case studies under analysis the structural response was considered to be controlled by the first six modes, corresponding to the first two modes of translation along the X and Y directions and to the first two torsional modes. From Table 3.1 one observes that for the SPEAR building the higher mode has a period of 0.15sec, therefore the time step chosen of 0.01sec is smaller than the reference value of $T/10$. This means that the time step chosen enables the capture of the higher mode effects, which in a three storey building regular along the height do not have much influence. In the five and eight storey building the integration time step (0.02sec) is approximately equal to the higher mode period (see Table 3.1) divided by 10, therefore it also allows the higher mode effects to be captured.

In the adaptive pushover analysis (DAP), the load distribution is updated at every analysis step. In this work it was considered an incremental updating, which means that the load vector for the current step is computed by summing to the load vector of the previous step, a new load vector increment obtained from the product between the current load factor increment, the current modal scaling vector and the initial user-defined nominal load vector. In this work the Complete Quadratic Combination (CQC) method is used in the computation of the modal scaling vector.

The elastic response spectrum analyses performed for the computation of the torsional factors used in this work in the Extended N2 method, in the Extended CSM-

FEMA440 for plan asymmetric buildings, and for the new 3D Pushover procedure, were performed using SAP2000 [121] because SeismoStruct does not include this type of analysis. The same material and geometric properties of the nonlinear models were used in these linear elastic models. It is important to mention that in these analyses, the materials presented an elastic behaviour. The modulus of elasticity (E) of the concrete used in the elastic model is calculated from the compressive strength (f_c) value used in the nonlinear model according to Eq. 3.1:

$$E = 4700 \cdot f_c^{0.5} \qquad \textit{Eq. 3.1}$$

Therefore, for the SPEAR building it was considered that E = 23500MPa, and for the Turkish five and eight storey buildings that E = 19207MPa.

3.2.8 Comparison between experimental and analytical results – SPEAR building

The SPEAR building was pseudo-dynamically tested (Figure 3.25) with a bi-directional loading based on a ground motion recorded at Hercegnovi station during the 1979 Montenegro earthquake and scaled to match with the EC8 type I spectrum for soil type C. This bi-directional record was applied to the structure in three runs of linearly increasing intensity of peak ground acceleration (PGA), such as 0.02g, 0.15g and 0.20g.

Figure 3.25 – SPEAR building experiment specimen.

The very same input motion with a PGA of 0.2g was used to authenticate the adequacy of the current analytical model, so that the same model can be used for further parametric study with confidence.

Table 3.3 shows the comparison between the vibration periods obtained from the experiment specimen and from the analytical model.

Table 3.3 – Periods of vibration: experimental vs. analytical.

Period	Experimental	Analytical
T1	0.85 sec	0.62 sec
T2	0.78 sec	0.53 sec

The results presented in Table 3.3 show that the period of vibration of the experiment specimen and the analytical model are somewhat different. These differences are explained due to the cracking in the columns, occurring when the test specimen was transported from outside the ELSA lab, where it was built, into the inside of the laboratory, where it was tested. Therefore, the stiffness of the experiment specimen was reduced when it was tested, explaining the higher values of periods obtained.

Figure 3.26 and Figure 3.27 show a comparison between experimental and analytical results for displacement and interstorey drift histories in two orthogonal directions for a PGA of 0.2g. For this level of seismic intensity the building was already in the inelastic regime. Despite being a simplified analytical model, it reproduced the experimental results with appreciable accuracy.

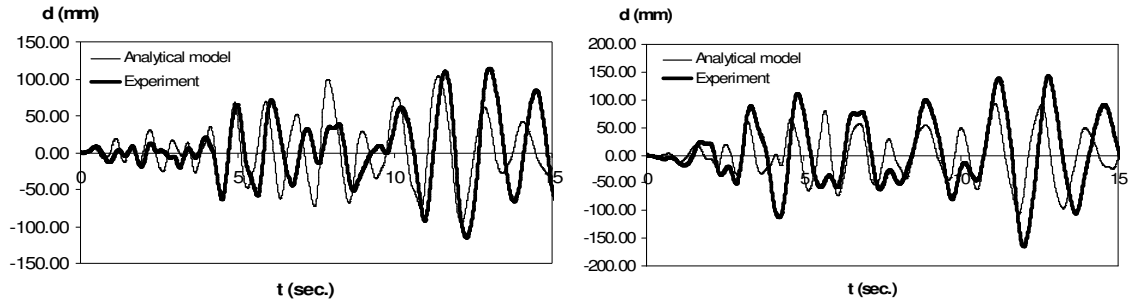

(a) *(b)*

Figure 3.26 – Top displacements, 0.2g a) Node C7, X direction ; b) Node N1, Y direction.

The observed discrepancies are due to the lack of various modelling aspects, like beam-column joints, slippage and pull-out of smooth reinforcing bars, etc., incorporation of which into the current model would considerably increase the computation time and thus make it impossible to perform the large parametric study as required in this work.

The current analytical model provides perhaps the best trade-off between accuracy and efficiency; and therefore it was used for the further parametric study.

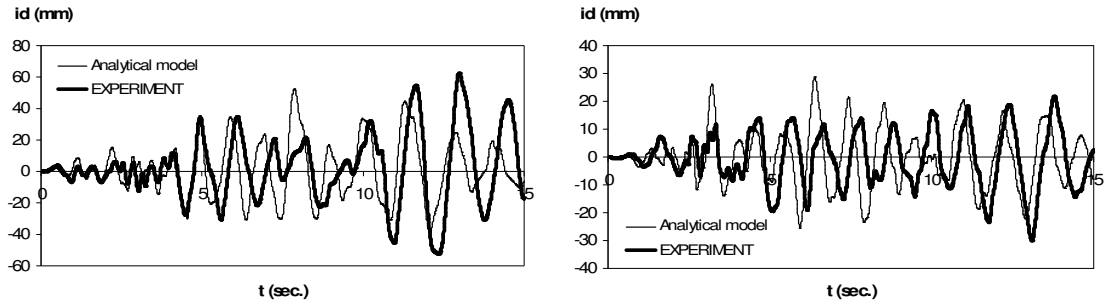

(a) *(b)*

Figure 3.27 – Interstorey drifts, 0.2g a) Node C7, 1st-2nd storeys, X direction ; b) Node C9, 1st storey,Y direction.

The software used in this study takes into account both material inelasticity and geometric nonlinearities, although the authors tend to feel that the P-Δ effects are likely not to play a critical role in the response of structures such as the ones considered in this study.

From the results presented herein one can conclude that the modelling options assumed in this study are acceptable and valid.

Further details on the SPEAR building test in the ELSA laboratory at Ispra can be found in [102].

4. Seismic action and performed analyses

In this section the seismic action definition and the parametric study developed in the present thesis are described.

4.1 Seismic action

For the 3 storey SPEAR building, seven bi-directional semi-artificial ground motion records from the SPEAR project were considered (Table 4.1). These records had been fitted to the Eurocode 8 [25] elastic design spectrum (Type 1, soil C, η=1, S=1.15, β_0=0.02, T_B=0.2sec, T_C=0.6sec, T_D=2sec).

Table 4.1 – Records used in the analyses of the three storey SPEAR building.

Earthquake Name	Station Name
Imperial Valley 1979	Bonds Corner
Loma Prieta 1989	Capitola
Kalamata 1986	Kalamata – Prefecture
Montenegro 1979	Herceg Novi
Friuli 1976	Tolmezzo
Montenegro 1979	Ulcinj2
Imperial Valley 1940	El Centro Array #9

The semi-artificial records used in the three storey building for an intensity of 0.2g are represented in Figure 4.1 and in Appendix A1. For the other intensities, the records were scaled with the respective scaling factor.

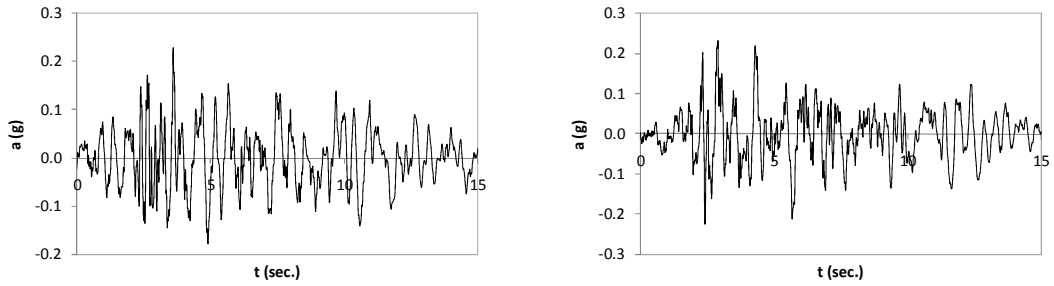

(a) *(b)*

Figure 4.1 - Montenegro earthquake 1979, station Herceg Novi a) component 200x, direction X; b) component 200y, direction Y.

For the Turkish buildings, three bi-directional semi-artificial ground motion records were considered. These three records are real ones (Table 4.2) and were taken from the PEER's database website [122]. They were fitted to the Eurocode 8 elastic design spectrum (with the Turkish code features – Type 1, soil A, η=1, S=1, β_0=0.05, T_B=0.15sec, T_C=0.4sec, T_D=2sec) using the software RSPMatch2005 [123]. This software fits real records to a response spectrum defined by the user through the use of wavelets.

Table 4.2 – Records used in the analyses of the Turkish buildings.

Earthquake Name	YEAR	ClstD (km)	Earthquake Magnitude	Site Classification Campbell's geocode	Mechanism Based on Rake Angle
Tabas, Iran	1978	13.94	7.35	Firm Rock	Reverse
Whittier Narrows-01	1987	40.61	5.99	Very Firm Soil	Reverse - Oblique
Northridge-01	1994	37.19	6.69	Firm Rock	Reverse

The RSPMatch2005 only allows the fitting of one component of a ground motion record. Therefore, the real records (two components each) fitting process was the following:

1) Each real record has two components. One of them has a peak acceleration higher than the other. The ratio between the two peak accelerations was calculated: r = (max peak acceleration of the component with the smaller peak acceleration) / (max peak acceleration of the component with the higher peak acceleration);

2) The component with the higher peak acceleration was fitted, using the RSPMatch2005, to the reference target response spectrum (with the features presented above) with a peak ground acceleration of 0.4g;

3) Afterwards, the component with the smaller peak ground acceleration was fitted (using again the RSPMatch2005) to a target response spectrum equal to the response spectrum used in the previous point 2) multiplying its ordinates by r.

Figure 4.2 shows the two components of the record of Whittier Narrows-01 after being fitted using RSPMatch2005. In this figure one can see that each component fits the respective target response spectrum in a very good manner.

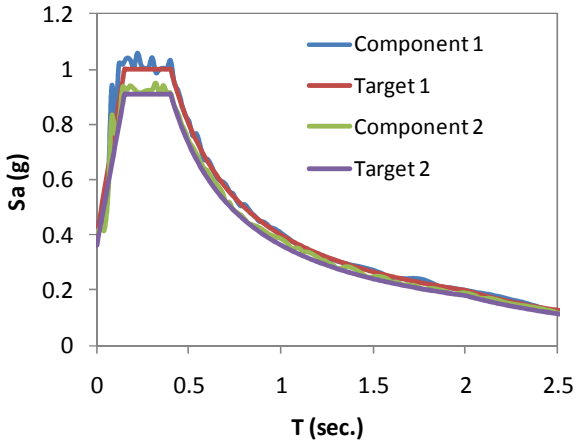

Figure 4.2 - Whittier Narrows-01 record.

By following this fitting process, the ratio of the peak ground accelerations between the two components of the real record stays the same as in the semi-artificial one.

The semi-artificial records used in the five and eight storey buildings for an intensity of 0.4g are represented in Figure 4.3 and in Appendix A2. For the other intensities, the records were scaled with the respective scaling factor.

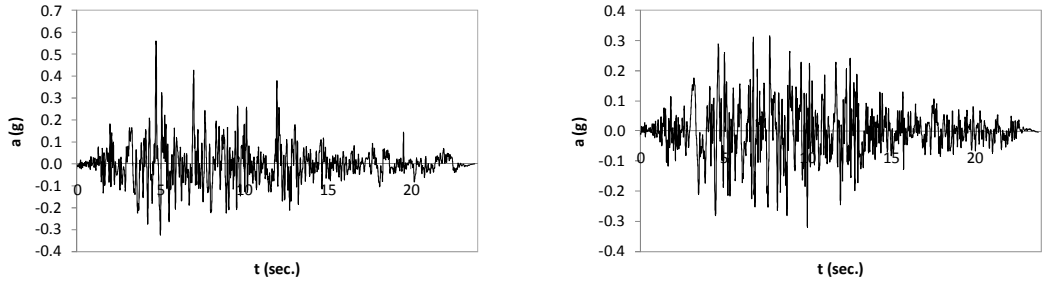

(a) *(b)*

Figure 4.3 - Tabas earthquake 1978 a) component X; b) component Y.

The ground motions were scaled and applied for a wide range of peak ground intensities in order to assess the performance of the NSPs throughout different levels

of structural inelasticity. The accelerograms were scaled for peak ground accelerations of 0.05, 0.1, 0.2 and 0.3g for the three storey building, for 0.1, 0.2, 0.4, 0.6 and 0.8g for the five storey building and for 0.1, 0.2 and 0.4g for the eight storey building.

The median response spectrum of each set of ground motions was used to compute the nonlinear static procedures response. In the three storey building, the median spectrum in the X direction was obtained from the set of response spectra compatible with the X components of the ground motions used. In the Y direction the procedure was the same but now considering the Y components of the accelerograms. These response spectra are represented in Figure 4.4, Figure 4.5 and in Appendix A3.

In Appendix A3 - Figure A. 9 to Figure A. 12 - the median acceleration response spectra are plotted for each intensity level and for each direction. These spectra are calculated as described in the previous paragraph.

In Figure 4.4 and in Appendix A3 - Figure A. 13 to Figure A. 15 - for each intensity level and for each direction, the displacement response spectra compatible with each component of the records used in the three storey building are represented. The median of these compatible spectra are also represented in each plot.

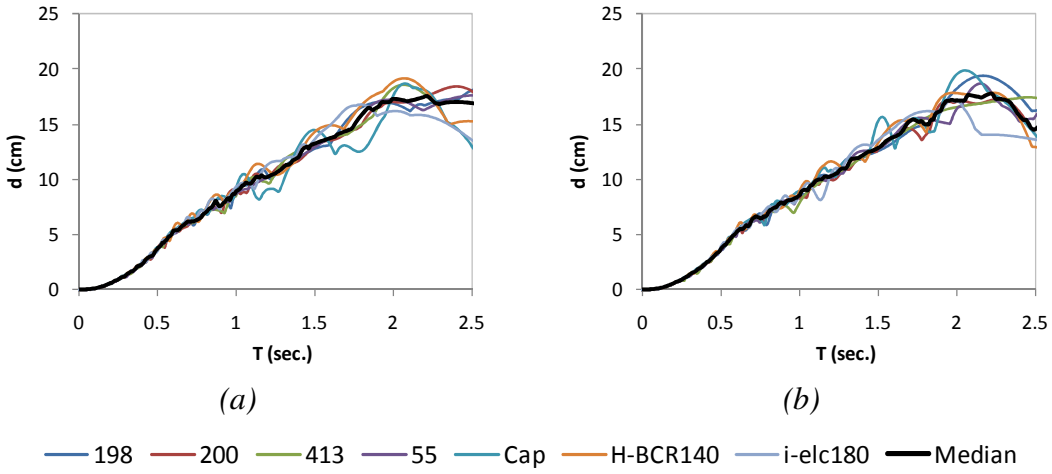

Figure 4.4 – SPEAR building displacement response spectra, 0.2g a) X direction; b) Y direction.

In Figure 4.5 and in Appendix A3 - Figure A. 16 to Figure A. 18 - for each intensity level and for each direction, the median response spectra are plotted in the acceleration-displacement format. These spectra were used in the nonlinear static procedures to calculate the target displacements as described in section 2.4.

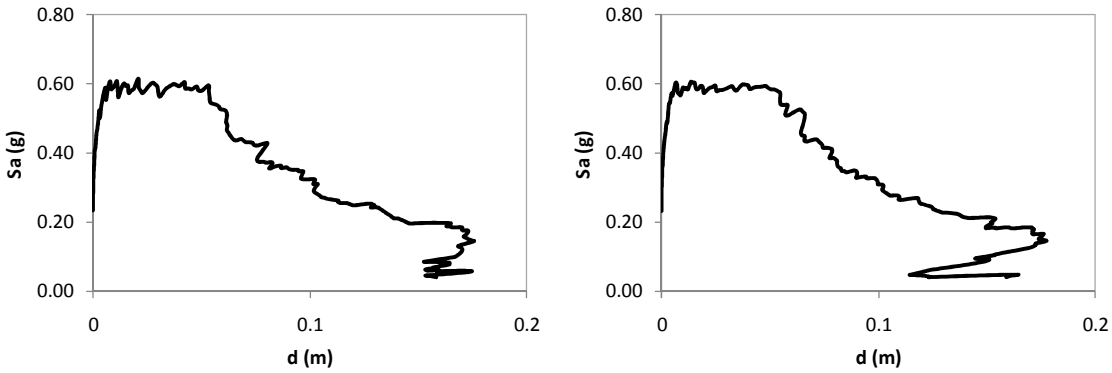

Figure 4.5 – SPEAR building median acceleration-displacement response spectra, 0.2g a) X direction; b) Y direction.

For the five and eight storey buildings, and since each pair of accelerograms was applied twice in the structure changing the direction of the components, the median spectrum in the X direction was obtained from the set of response spectra compatible with all X and Y components of the accelerograms. Therefore the median spectrum in the Y direction is the same as the one used in the X direction. These response spectra are represented in Figure 4.6, Figure 4.7, Figure 4.8 and in Appendix A4.

In Figure 4.6 and in Appendix A4 - Figure A. 19 and Figure A. 20 - for each intensity level, the acceleration response spectra compatible with the records used in the five and eight storey buildings are represented as described in the previous paragraph. For each intensity, the median of these spectra is plotted.

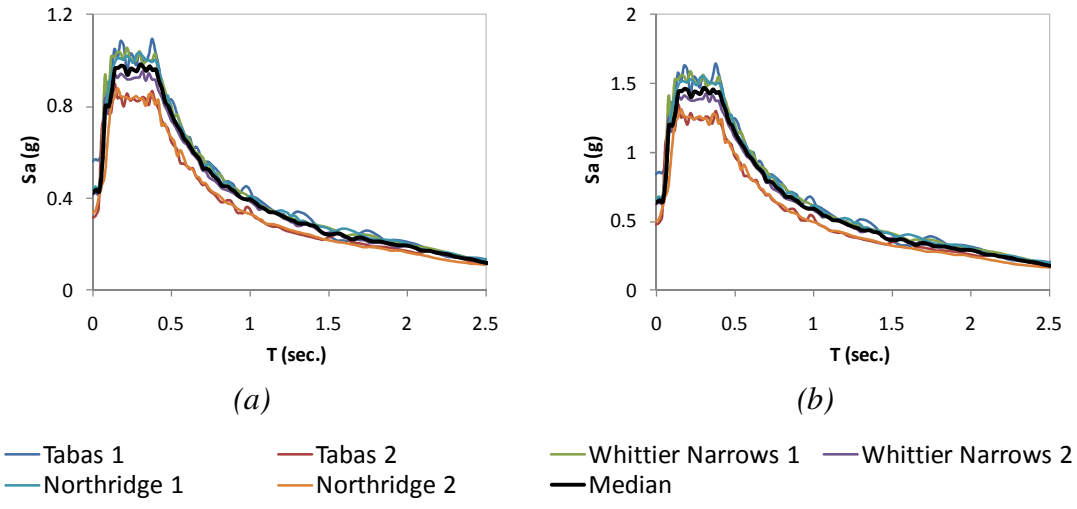

Figure 4.6 - Acceleration response spectra, a) 0.4g; b) 0.6g.

In Figure 4.7 and in Appendix A4 - Figure A. 21 and Figure A. 22 - for each intensity level, the displacement response spectra compatible with the record used as well as the respective median are plotted.

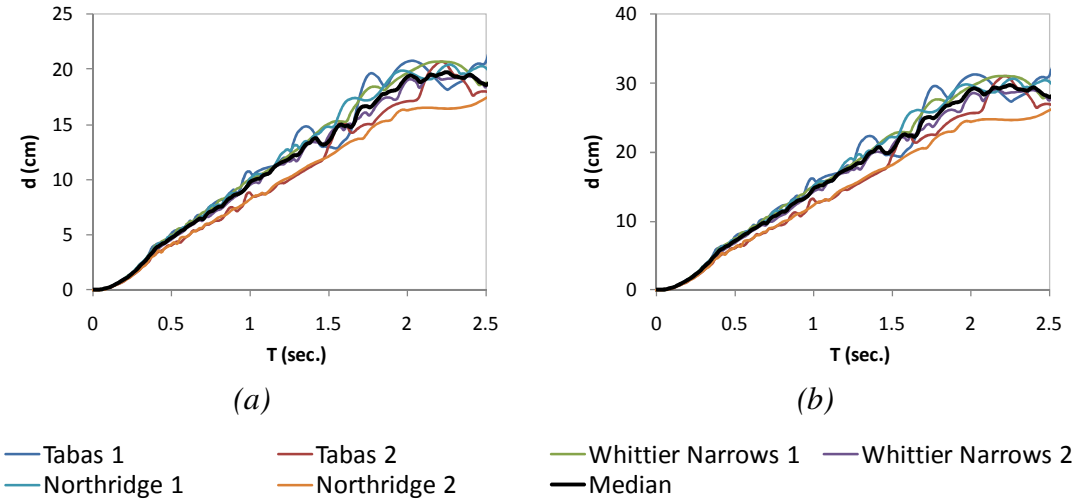

Figure 4.7 – Displacement response spectra, intensity a) 0.4g; b) 0.6g.

In Figure 4.8 and in Appendix A4 - Figure A. 23 and Figure A. 24 - for each intensity level, the median response spectra used in the Turkish buildings are plotted in the acceleration-displacement format. These spectra were used in the NSPs to calculate the target displacements as described in section 2.4.

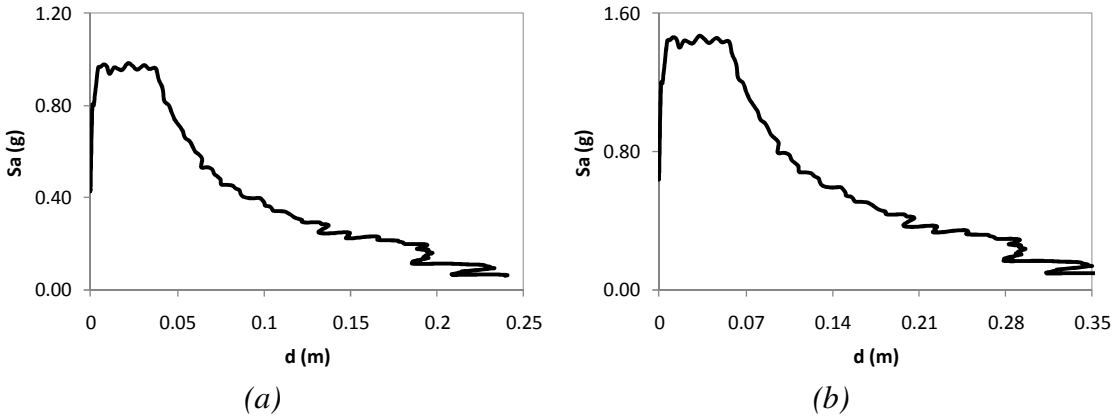

Figure 4.8 – Median acceleration-displacement response spectra a) 0.4g; b) 0.6g.

In Figure 4.9a) and b) the median displacement response spectra are plotted as defined for the three storey building (0.2g) and for the Turkish buildings (0.4g) respectively. The reference response spectra defined according to EC8 are also depicted in these figures.

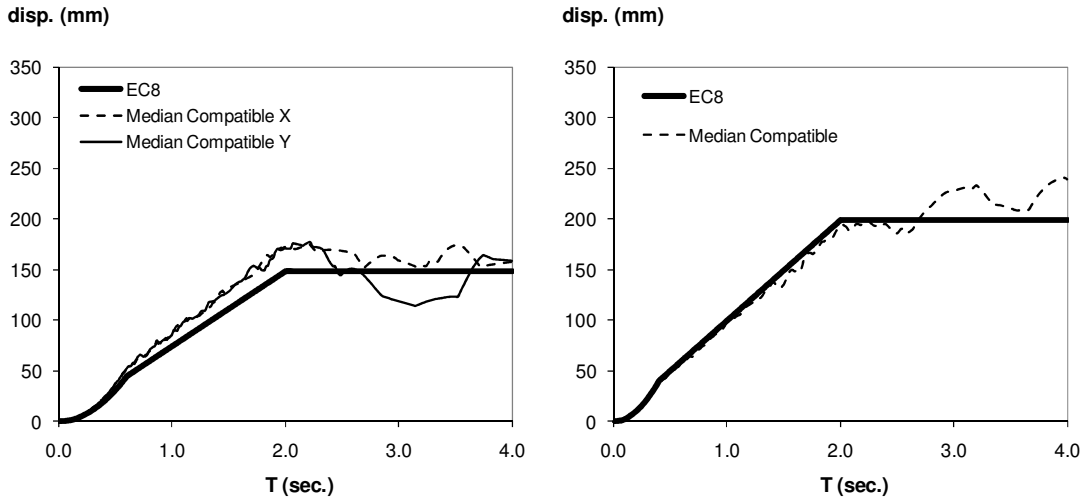

(a) *(b)*

Figure 4.9 – Displacement response spectra a) Three storey building 0.2g; b) Five and eight storey buildings 0.4g.

The main concern about using scaling accelerograms (IDA) lies in the fact that low intensity records are not representative of high intensity ones. In fact, it is important to know if the median results in terms of a certain damage measure (DM) obtained from records scaled for an intensity measure (IM), such as the peak ground acceleration (PGA), accurately estimate the median DM of a set of unscaled records with the same IM. Several questions have been discussed in relation to this topic [124, 125]. In [126] it is stated that IDA leads to accurate estimations of DM if the IM has been chosen such that the regression of DM jointly on IM, magnitude (M) and distance (R) is independent of M and R in the range under analysis.

The IDA is much more practical than a cloud analysis (i.e. selecting several acceleration records that represent various intensity levels from multiple events and running the analyses with these records), because a smaller number of records need to be selected. For the purpose of this thesis, the use of semi-artificial ground motions scaled for different levels of seismic intensity seems to be an optimal solution taking into account the number of analyses performed and the time consumed.

4.2 Structural analyses carried out

Two different classes of nonlinear analyses were performed on the analytical models of the analysed buildings. The first set represents a series of nonlinear static analyses using two different algorithms, namely conventional pushover analysis and displacement based adaptive pushover analysis (DAP) [46]. The second set have consisted of nonlinear dynamic analysis.

Linear elastic analyses were also performed in order to calculate the torsional correction factors used in some NSPs as described during the document.

4.2.1 Nonlinear static analyses

In this work, the most commonly used NSPs are applied and compared: the Capacity Spectrum Method (CSM) with both variants proposed in ATC40 and in FEMA440 guidelines, the original N2 and the Extended N2 methods, the Modal Pushover Analysis (MPA) and the Adaptive Capacity Spectrum Method (ACSM). All these methods are described in section 2.4.

The conventional pushover analyses were performed for different load patterns as required by the different NSPs. For example, the CSM requires a fundamental mode shape proportional load vector (see section 2.4.4), the N2 method calls for at least two different load vectors as proposed in EC8 (see section 2.4.1), namely proportional to fundamental mode shape and proportional to mass distribution over the height, and the MPA warrants load vectors proportional to the vibration mode shapes that contribute significantly to the structural responses (see section 2.4.3). The masses and the modes of vibration of each building used to calculate the load vectors for each method, can be found in section 3.2.

Therefore for each building, in the CSM procedure the load vector used in the pushover analysis in the X direction was proportional to the first mode of vibration of the building with predominant motion along this direction, and in the Y direction this vector was proportional to the first mode of vibration with predominant motion along the Y direction. In the N2 method the load vector proportional to the mode shape was calculated in the same way.

In the MPA procedure, see 2.4.3, in the three storey and in the eight storey buildings the first two modes in each direction (X and Y) were used to compute the load vectors to be applied in the pushover analyses. In the five storey building the first three modes in each direction (X and Y) were used.

The ACSM, on the other hand, employs displacement based adaptive pushover analysis whereby a single displacement vector is imposed on the structure at all beam-column and beam-beam nodes (see section 2.4.5).

Each pushover analysis, be it conventional or adaptive, was performed independently for two orthogonal translational directions with positive and negative signs of the load vector, which resulted in four analyses for each pushover load case. At each storey, the loads (forces or displacements) were applied at every beam-column and beam-beam nodes in order to take into account the torsional motion of the plan asymmetric buildings. The performance points were computed for each pushover curve and the maximum value in each direction was chosen as being the required performance point

for the NSP under consideration. The results were then combined in the two directions using the SRSS combination.

In the present study, the demand was defined by real earthquake spectra rather than a smoothed design spectrum, as mentioned in section 4.1. In these cases, more than one intersection with the capacity curve were found, when using the CSM, ACSM and the new 3D Pushover procedure proposed in chapter 10. It has been verified in [53] that often only one of those intersections leads to convergence with the damping value. Usually it is the one corresponding to the largest displacement value. When more than one intersection provides convergence with the damping, it was concluded that the one corresponding to the largest displacement leads to results closer to the nonlinear dynamic *time-history* analyses. Choosing the largest deformation as the performance point is a conservative assumption, since the different intersections lead to approximate values of base shear (because they happen in the post-elastic range) but different displacement estimations.

The Pushover analysis is used in design offices or by researchers to verify the structural performance of newly designed and existing buildings. Therefore, the results obtained with these methods should first of all be conservative with respect to the *time-history* analysis, in order to never underestimate the structural response of the buildings under analysis. The performance of a specific NSP increases if its results get close to the *time-history* median values, but always on the safe side. In this work, the NSPs are evaluated taking into account these two main characteristics: conservative results and accuracy with respect to the median *time-history* results.

4.2.2 Nonlinear dynamic analyses

The nonlinear dynamic analyses, similar to the static analysis, were performed for four different orientations, on the three storey building, of the aforementioned set of seven semi-artificial ground motions, namely X+Y+, X+Y-, X-Y-, X-Y+, for a set of varying intensity of 0.05g, 0.10g, 0.20g and 0.30g. The median response among all the analyses (7 ground motions x 4 orientations = 28 analyses) for each intensity level was considered as the 'true' response of the building.

For the nonlinear dynamic analysis of the Turkish buildings, the aforementioned three bidirectional semi-artificial ground motion records were employed. Each record was applied twice in the structure changing the direction of the components, resulting in 6 models, each one with five intensity levels for the 5 storey building (0.1g, 0.2g, 0.4g, 0.6g and 0.8g) and three intensity levels for the 8 storey buildings (0.1g, 0.2g and 0.4g). Once again, the median response among all the analyses for each intensity level was considered as the reference response of the corresponding building.

4.2.3 Linear elastic analyses for torsional correction factors calculation

For the calculation of the torsional correction factors for the Extended N2 method (chapters 7 and 8), for the Extended CSM-FEMA440 (chapter 9) and for the new 3D Pushover procedure (chapter 10) it was necessary to perform linear dynamic response spectrum analyses (RSA) in order to evaluate the normalized top displacements at the top of the buildings. In these RSA analyses, the response spectrum was applied simultaneously in the two directions. The results were obtained using the SRSS (square root of sum of squares) combination between the two directions. The combination of the modes of vibration was performed using the CQC (complete quadratic combination) rule. The elastic acceleration response spectra used in each building were the median of the spectra compatible with each set of records as explained in 4.1. The ones used for the three storey building are represented in Appendix A3 – from Figure A. 9 to Figure A. 12. The response spectra used in the five and eight storey buildings are plotted in Figure 4.6 and in Appendix A4 – Figure A. 19 and Figure A. 20.

4.2.4 Analysed measures

As mentioned before, nowadays it is generally recognized that a Performance-Based philosophy is more adequate than a Force-Based approach when performing a seismic analysis of a structure. In fact, the structural behaviour and damage of structures during an earthquake are strongly controlled by the inelastic deformation capacity of its members. Therefore, the seismic evaluation and design of structures should be based on displacements/deformations induced by the earthquake instead of the stresses caused by the computed equivalent seismic forces. Assuming this Performance-based philosophy, in this work all nonlinear static and dynamic analyses are compared and evaluated in terms of displacement patterns, interstorey drifts, chord rotations, top displacements, base shear and normalized top displacements in the two directions and for all seismic intensity levels.

In all case studies it is assumed that all elements have been correctly designed to shear. Therefore, no brittle failure is considered in any of the analysed buildings.

4.3 Safety assessment methods

Two main categories can be mentioned in the evaluation of the seismic safety of structures: probabilistic and deterministic methods. Both procedures can use the same seismic input characterization (response spectra and accelerograms), and the same tools for estimating structural effects (distributed or concentrated plasticity nonlinear models to be used in nonlinear static or nonlinear dynamic analysis). The main difference lies in the way each method considers the uncertainty related to the seismic input, capacity models and analysis procedures, and how it influences the final assessment.

The probabilistic assessment methods are developed via probabilistic concepts. They are mainly applied to calibrate the deterministic approaches prescribed in codes based on the use of safety factors. This approach requires a much higher amount of information than the deterministic one, such as the probabilistic characterization of seismic action, description of the capacity and structural demand, and the respective variability. According to Pinto et al. [127] these methods exhibit a considerable level of mathematical complexity and abstractness, which demand a clear and accurate understanding of the physical features of the problem. For all these reasons, the application of such kind of verification is not yet widespread amongst the professional community.

Deterministic assessment is based on the direct comparison between the capacity and the corresponding demand, member-by-member. The capacity is prescribed by several codes, such as the Eurocode 8 and ATC40, and the safety verification is usually performed according to predefined limit states associated with specific return periods. This approach is the one commonly used in design offices.

In this work the safety verification was performed using the deterministic assessment. The damage limitation control in terms of interstorey drifts according to Eurocode 8 was verified in some members of the three analysed buildings for the different seismic intensities tested, see section 8.4.

The shear capacity according to the specifications of the ATC40 in some members of the three case studies was also compared with the respective demand for several seismic intensities, see section 8.5.

5. Capacity curves

In this chapter, the capacity curves obtained from the conventional force pushover and from the DAP analysis are compared with the incremental *time-history* median results for the three buildings under analysis in both positive and negative senses of the X and Y directions. Each type of analysis was described and explained in section 4.2. The results of this chapter are presented in [128, 129]. In each plot, the "Modal" curve corresponds to the conventional force pushover with a modal proportional load pattern, the "Uniform" curve to the conventional force pushover with a uniform load pattern, the "DAP" curve to the displacement adaptive pushover and the "TH" dots to the *time-history* median results for the different intensity levels analysed. In the X direction the "Modal" corresponds to a load pattern proportional to the first mode of vibration along the X direction, and in the Y direction to the first mode of vibration along the Y direction.

5.1 Three storey building

The *time-history* median results at the centre of mass in terms of displacements (d) and base shear (BS) represented in the plots of the three storey building are summarized in Table 5.1.

Table 5.1 – Time-history median results at the centre of mass, three storey building.

	3 storey X direction		3 storey Y direction	
Intensity	d (m)	BS (kN)	d (m)	BS (kN)
0.05g	0.022	147.033	0.018	174.882
0.1g	0.050	242.266	0.040	281.774
0.2g	0.091	291.542	0.083	378.877
0.3g	0.130	277.463	0.123	416.163

The capacity curves of the three storey building are plotted in Figure 5.1 and Figure 5.2, for the X and Y direction, respectively.

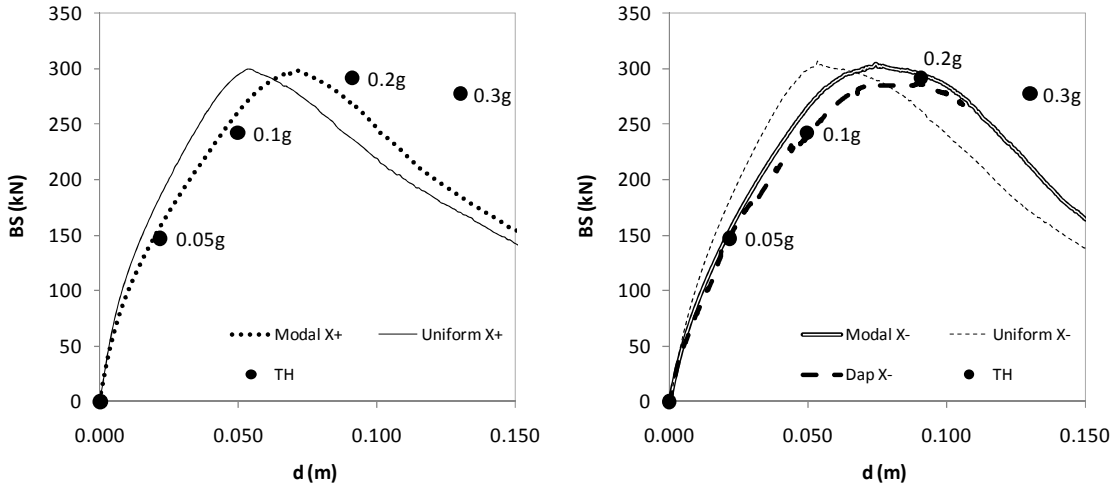

(a) *(b)*

Figure 5.1 – Three storey building, X direction: a) X+; b) X-.

The DAP results are not presented for the X direction in the positive sense (X+) because it was not possible to complete the analysis due to convergence problems.

From the plots it is clear that the DAP and the Modal proportional load pattern lead to the same results in the very elastic range (until 0.05g). For higher seismic intensities, the DAP presents slightly smaller values of base shear for the same level of top displacement in the X direction, and slightly higher in the Y direction. Both curves match pretty much well the *time-history* median results, except for 0.3g which corresponds to a very high level of inelasticity.

The capacity curves obtained with a uniform load pattern present higher values of base shear for the same top displacement than the other curves in both directions in both senses before the peak. In the post peak range – corresponding to the softening of the concrete – the uniform capacity curves present smaller values of base shear for the same displacement when compared with the other curves. The uniform capacity curve is further away from the *time-history* median results than the modal and DAP curves.

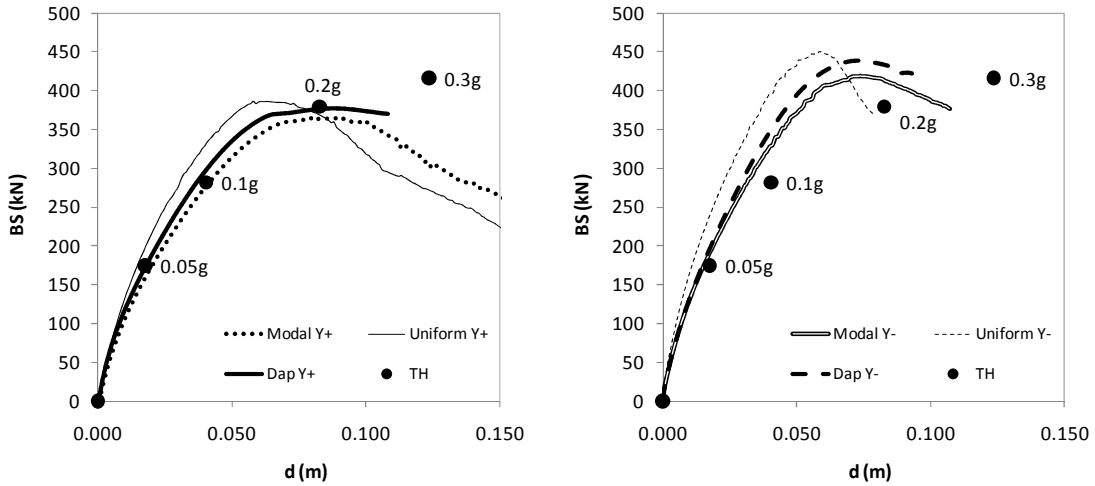

Figure 5.2 – Three storey building, Y direction: a) Y+; b) Y-.

One can observe that the building presents more strength along the Y direction because the only elongated column in the structure (column C6, see Figure 3.2) presents its higher dimension along this direction.

The capacity curves in both positive and negative senses of the X direction are pretty much the same, but they are different in the positive and negative senses of the Y direction. In fact, the capacity curves present more strength when they are obtained with the load applied along Y- because the elongated column C6 is being more compressed than when the load is applied in Y+.

From Figure 5.1 and Figure 5.2, one can observe that the three storey building remains elastic or almost elastic in both X and Y directions for seismic intensities of 0.05g and 0.1g. The building goes through the inelastic range for 0.2g and 0.3g. For this last intensity the building is in a very high stage of inelasticity for which it actually collapses because the plastic behaviour takes place in a sufficient number of sections to create a collapse mechanism.

The capacity curves of the three storey building obtained with load vectors proportional to the first two modes of vibration in both X and Y directions, in positive and negative senses, are represented in Figure 5.3 and Figure 5.4. These curves were used to calculate the response in the Modal Pushover Analysis procedure (MPA).

The second mode proportional capacity curves in the Y direction present a higher base shear than in the X direction for the same top displacement, as expected and confirming the idea that the structure strength was increased more in the Y direction. The building is also stiffer in this direction.

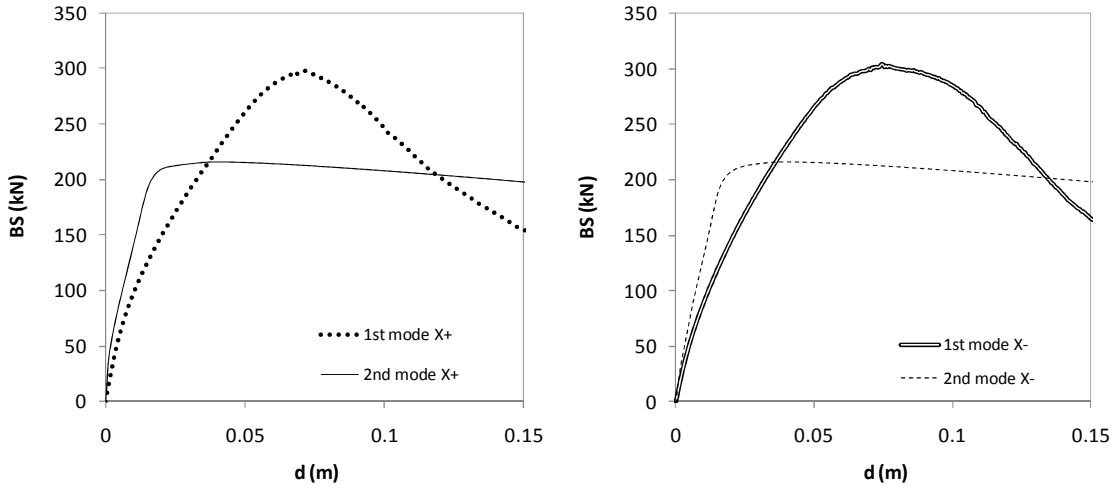

Figure 5.3 – Three storey building 1st mode and 2nd mode curves, X direction: a) X+; b) X-.

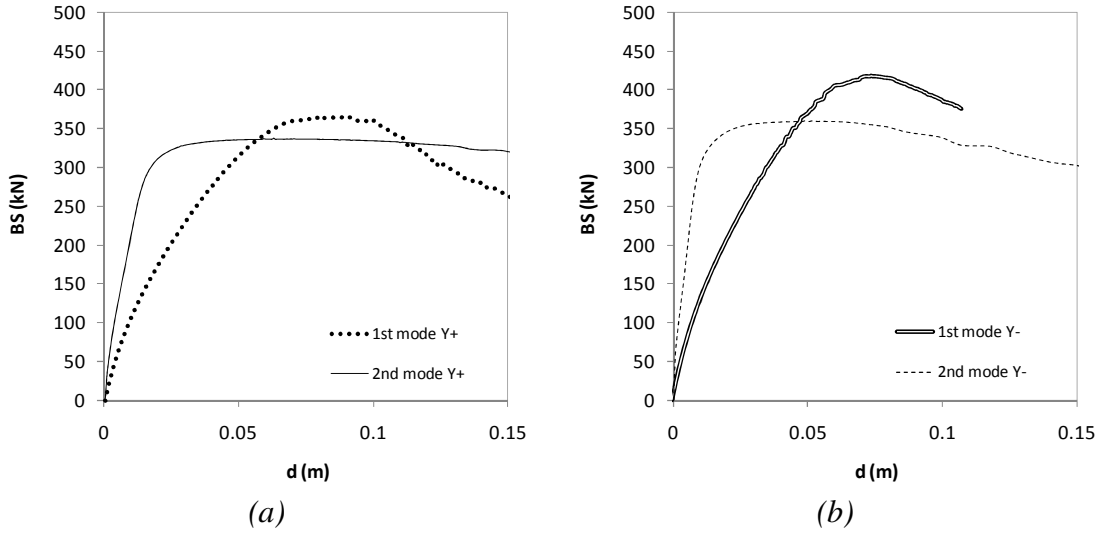

Figure 5.4 – Three storey building 1st mode and 2nd mode curves, Y direction: a) Y+; b) Y-.

The second mode curves seem to have a first range which is almost elastic and a second one with a slightly negative slope explained by the softening of the concrete.

The second mode curves are pretty much the same in both positive and negative senses in the X direction. In the Y direction, the post peak range of the curve obtained in the negative sense has a sharper negative slope than in the positive sense.

The second mode curves have a maximum base shear smaller than the first mode curves. Before the peak, they present a higher stiffness than the first mode curves.

5.2 Five storey building

The capacity curves obtained for the five storey building are plotted in Figure 5.5 and Figure 5.6 together with the *time-history* median results.

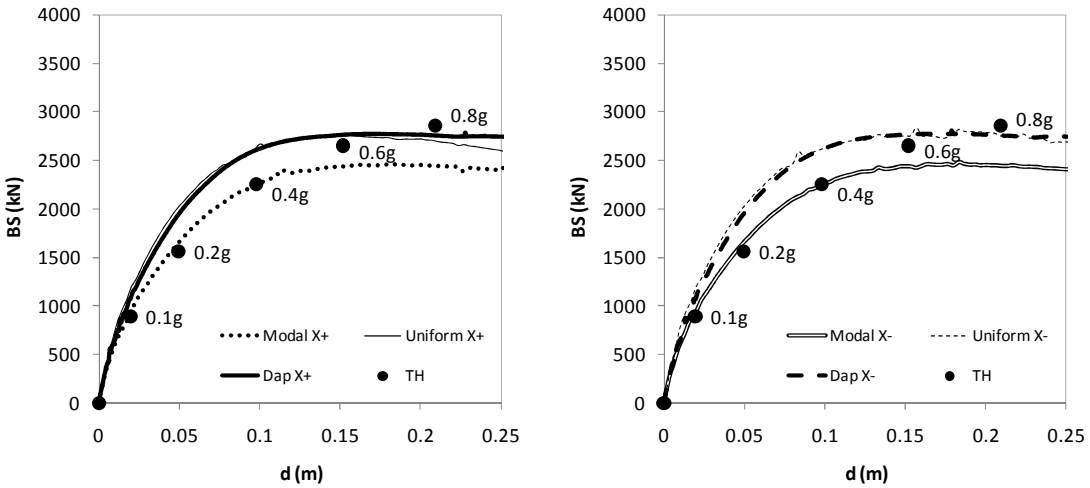

(a) *(b)*

Figure 5.5 – Five storey building, X direction: a) X+; b) X-.

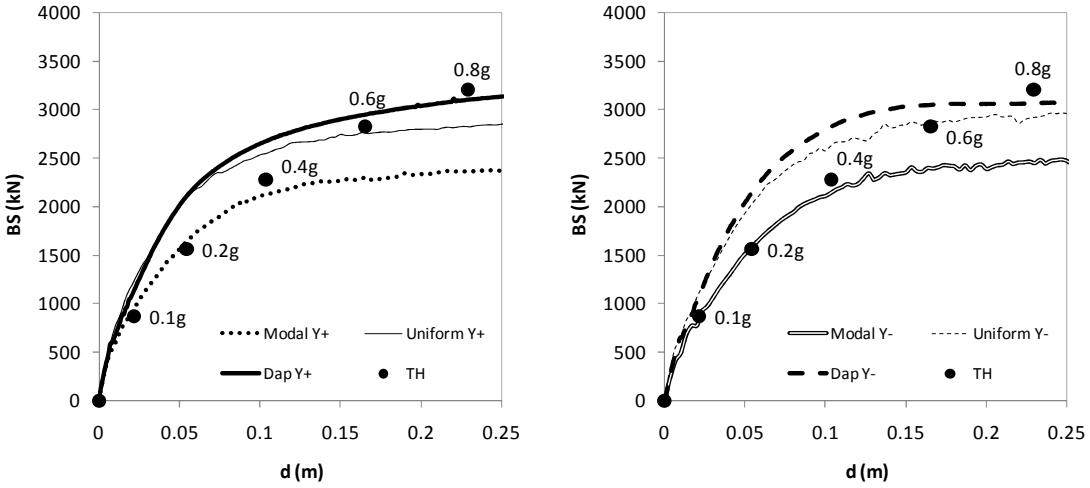

(a) *(b)*

Figure 5.6 – Five storey building, Y direction: a) Y+; b) Y-.

The *time-history* median results at the centre of mass represented in the plots of the five storey building are summarized in Table 5.2.

Table 5.2 – Time-history median results at the centre of mass, five storey building.

	5 storey X direction		5 storey Y direction	
Intensity	d (m)	BS (kN)	d (m)	BS (kN)
0.1g	0.020	894.298	0.022	866.294
0.2g	0.049	1561.200	0.054	1559.600
0.4g	0.098	2252.900	0.104	2275.200
0.6g	0.152	2650.500	0.165	2824.500
0.8g	0.209	2857.500	0.230	3202.300

The pushover curves obtained from a uniform load pattern and from the DAP analysis almost coincide in the X direction for both positive and negative senses. In the Y direction, these curves are equal in the elastic stage, but in the inelastic range the DAP curve tends to present higher values of base shear than the uniform load pattern curve for the same level of top displacement. The curve obtained with a modal proportional load pattern presents lower values of base shear than the other curves for the same top displacement.

From Figure 5.5 and Figure 5.6 one can conclude that for the elastic range, 0.1 and 0.2g, and for medium levels of inelasticity, 0.4g, the *time-history* results perfectly match the pushover curves obtained from a modal proportional load pattern in both X and Y directions, in both positive and negative senses.

Figure 5.5 and Figure 5.6 also show that for higher levels of inelasticity, 0.6 and 0.8g, the *time-history* points match the pushover curves obtained from the uniform load pattern and from the DAP analysis in both X and Y directions, for both positive and negative senses. The pushover curves clearly show that the building has more strength in the Y direction.

The five storey building behaves elastically or almost elastically for seismic intensities of 0.1g and 0.2g, as shown in Figure 5.5 and Figure 5.6. The structure goes through the inelastic stage for 0.4g, 0.6g and 0.8g. For this last intensity the building collapses because the plastic behaviour takes place in a sufficient number of sections to create a collapse mechanism.

The capacity curves of the five storey building obtained with load vectors proportional to the first three modes of vibration in both X and Y directions, in positive and negative senses, are represented in Figure 5.7 and Figure 5.8. These curves were used to calculate the response in the Modal Pushover Analysis procedure (MPA).

The second mode and third mode proportional capacity curves are pretty much the same in both positive and negative senses, in both X and Y directions. These curves have a first range which is almost elastic and a second one almost constant with a slightly positive slope.

In the X direction the second mode and third mode curves almost coincide, except in the first range (the almost elastic one) where the third mode proportional curve exhibits a higher stiffness. In this direction, these two curves present a higher base shear than the first mode curve for the same top displacement level. In the Y direction the third mode proportional capacity curve presents a higher value of base shear than the second mode and the first mode proportional curves, for the same top displacement. Also in this direction, the second mode curve presents a higher base shear value than the first mode curve for the same value of top displacement.

The higher mode proportional curves present higher values of base shear in the Y direction than in the X direction for the same values of top displacement.

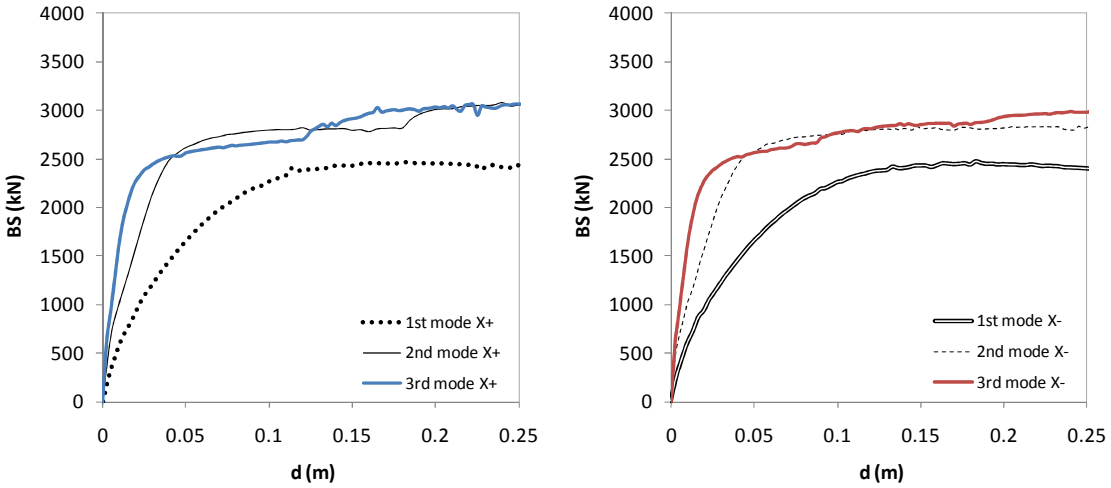

(a) *(b)*

Figure 5.7 – Five storey building 1st mode, 2nd mode and 3rd mode curves, X direction: a) X+; b) X-.

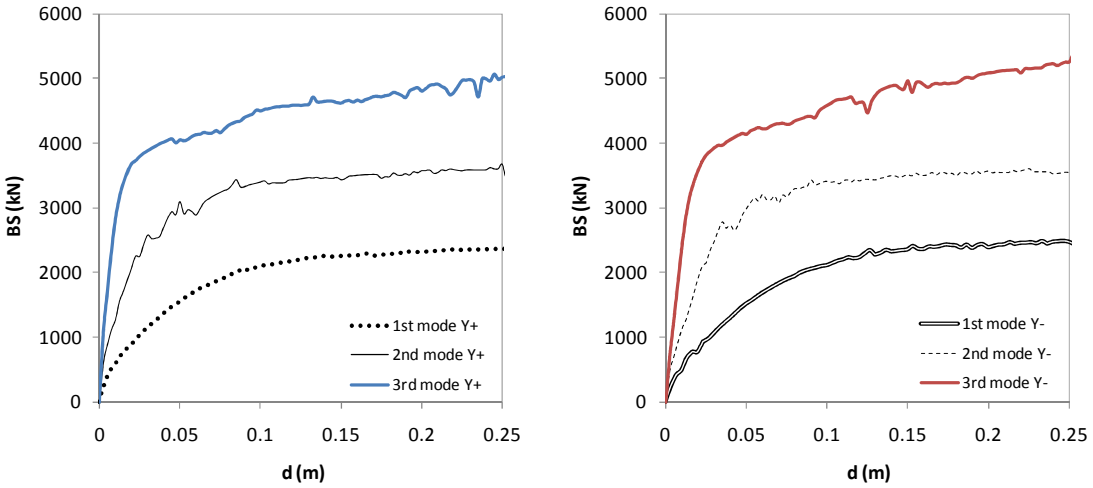

(a) *(b)*

Figure 5.8 – Five storey building 1st mode, 2nd mode and 3rd curves, Y direction: a) Y+; b) Y-.

5.3 Eight storey building

The pushover curves obtained for the eight storey building are plotted against the *time-history* median results in Figure 5.9 and Figure 5.10.

One can observe that in the X direction, Figure 5.9, both DAP and conventional pushover, with a modal proportional and uniform load patterns, lead to the same results. They perfectly match the *time-history* median results for all intensities tested. In the Y direction, Figure 5.10, the three pushover curves lead to approximately the same estimations in the elastic stage. They perfectly match the *time-history* results for this regime. In the inelastic stage, the DAP curve leads to higher base shear values out of all the curves, for the same level of displacement.

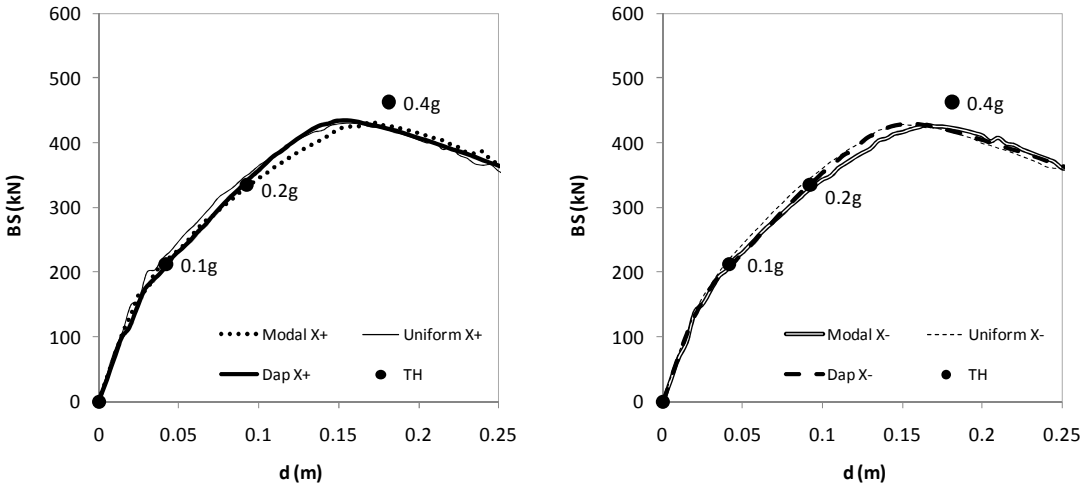

(a) *(b)*

Figure 5.9 – Eight storey building, X direction: a) X+; b) X-.

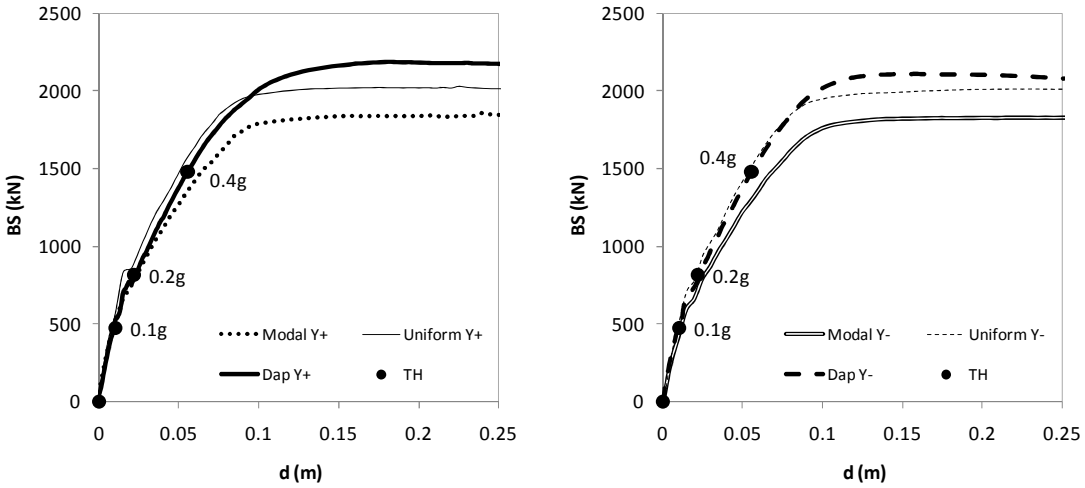

(a) *(b)*

Figure 5.10 – Eight storey building, Y direction: a) Y+; b) Y-.

The *time-history* median results at the centre of mass represented in the plots of the eight storey building are summarized in Table 5.3.

Table 5.3 – Time-history median results at the centre of mass, eight storey building.

	8 storey X direction		8 storey Y direction	
Intensity	d (m)	BS (kN)	d (m)	BS (kN)
0.1g	0.042	212.442	0.010	472.894
0.2g	0.092	334.600	0.022	813.834
0.4g	0.181	463.164	0.056	1478.954

From Figure 5.9 and Figure 5.10, one can conclude that the building presents a clearly unbalanced stiffness and strength distribution between the two directions. In fact, the building is much stiffer and stronger in the Y direction than in the X direction. Figure 5.10 also shows that the building remains elastic in the Y direction through all the seismic intensities analysed.

On the other hand, the structure remains elastic or almost elastic in the X direction only for 0.1g and goes through the inelastic stage for 0.2g and 0.4g. For this last intensity, the building collapses due to a soft storey mechanism in the first floor along the X direction.

The capacity curves of the eight storey building obtained with load vectors proportional to the first two modes of vibration in both X and Y direction, are represented in Figure 5.11. These curves were used for the Modal Pushover Analysis procedure (MPA).

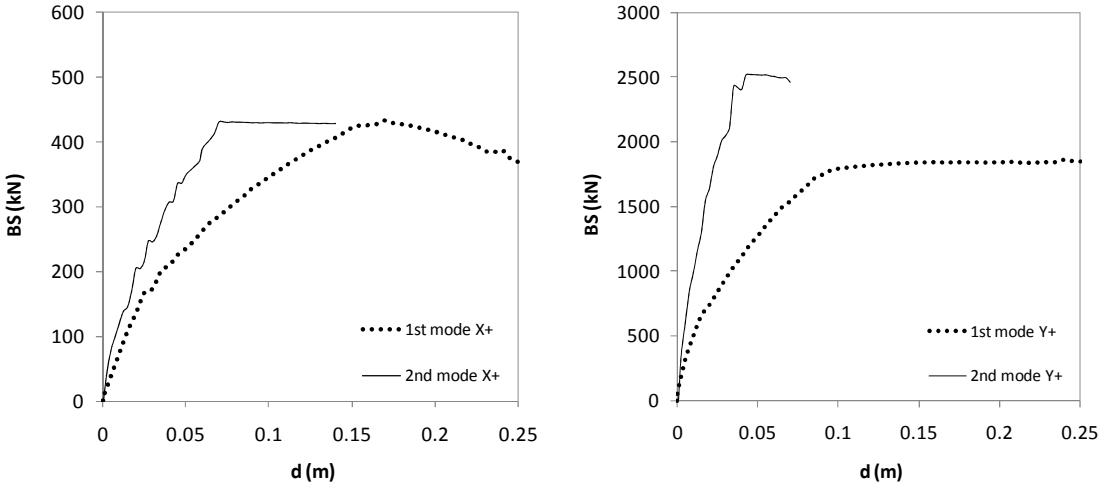

(a) *(b)*

Figure 5.11 – Eight storey building 1st mode and 2nd mode curves: a) X+; b) Y+.

The second mode proportional curves in both X and Y directions have a first range which is almost elastic and a second one practically constant. In the Y direction this last range is very short.

The second mode curves exhibit higher values of base shear than the first mode curves for the same level of top displacement.

The second mode curve has higher values of base shear in the Y direction than in the X direction for the same top displacement level, confirming the idea that the structure has more strength in the Y direction than in the X one.

From the presented plots, one can conclude that:

- The SPEAR building presents low ductility;
- For the Turkish buildings the ductility seems compatible with the 1.2 confinement factor used for concrete;
- Indeed the eight storey building in the X direction shows a sharp softening due to a soft storey mechanism.

6. A comparison between the CSM-ATC40 and the CSM-FEMA440

The Capacity Spectrum method (CSM) has gained considerable popularity amongst pushover users since its introduction in 1975 by Freeman and collaborators [19]. The ATC40 guidelines [21] included it as the recommended nonlinear static procedure to be used, and later the FEMA440 report [16] came out with an updated version of the method increasing the precision of its results.

The good performance of both methods, namely in regular buildings and planar frames, is widely supported by extensive verifications, such as [1, 19]. However, the use of such NSPs in the case of real existing plan asymmetric buildings is currently limited. Since these structures happen to represent the usual case in real life, a verification of such methods in the seismic assessment of irregular structures is needed.

In this chapter, an extensive parametric study is performed in order to compare the CSM with the features recommended in the ATC40 and in the FEMA440 guidelines in the seismic assessment of real existing plan asymmetric buildings. The NSPs are compared with the *time-history* median results for several levels of seismic intensities, so that one can understand the performance of both NSPs through different stages of structural inelasticity. The case studies under analysis are the ones already presented in section 3.1. Discussion of results and conclusions are outlined at the end. The results of this chapter are presented in [130].

The description of the features of both methods is skipped at this point, since they were already presented in sections 2.4.4.1 and 2.4.4.2.

6.1 Analysis results

The comparison of results obtained with the two methods is presented in this section. The *time-history* median results are identified in each graph as TH.

6.1.1 Lateral displacement profiles

The lateral displacement profiles for all the buildings under analysis are compared for the CSM-ATC40, the CSM-FEMA440 and for the *time-history* analysis, from Figure 6.1 to Figure 6.7.

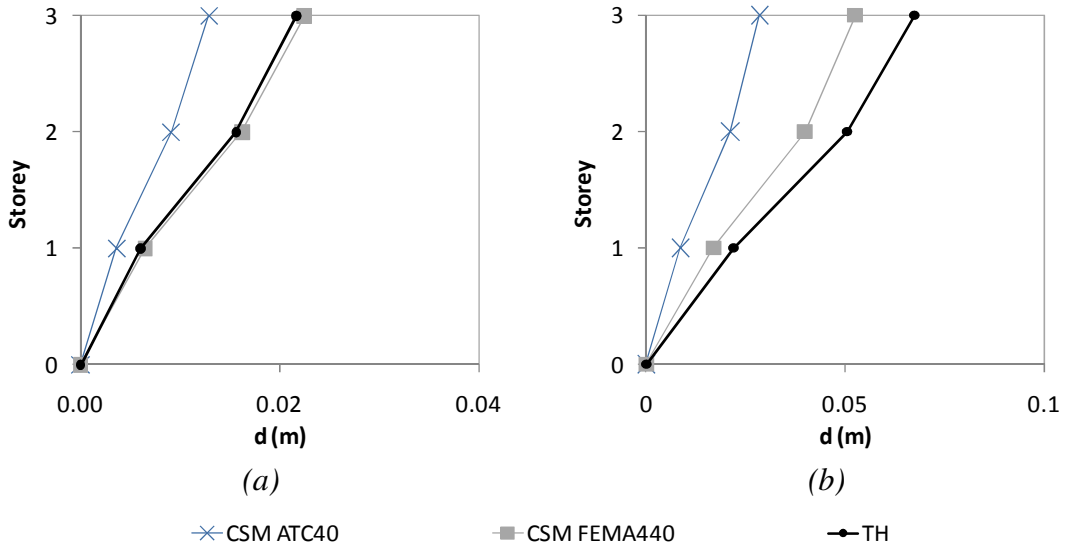

Figure 6.1 – Three storey, X direction: a) Column C3, 0.05g; b) Column C2, 0.1g.

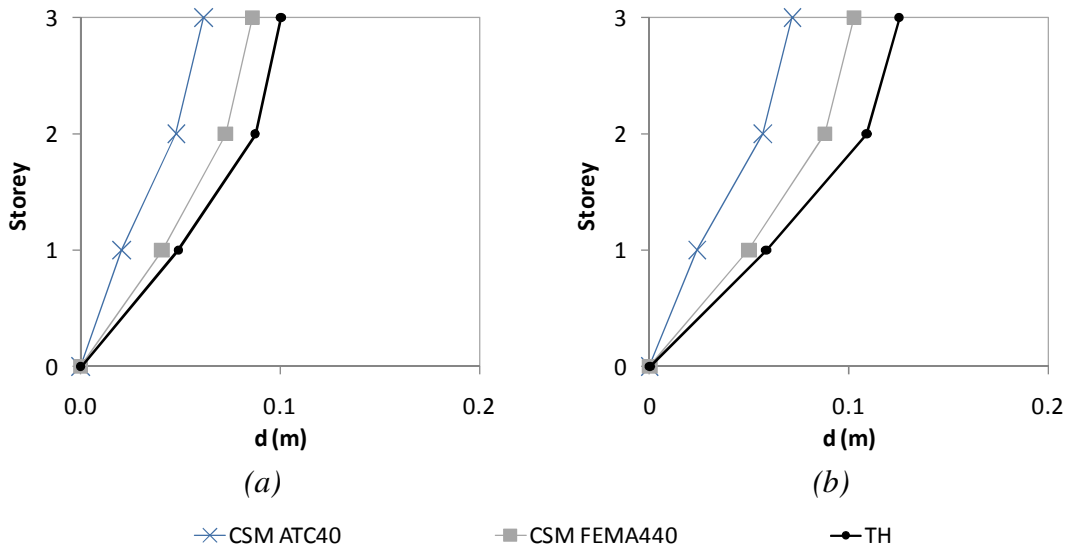

Figure 6.2 – Three storey, X direction: a) Column C8, 0.2g; b) Column C2, 0.2g.

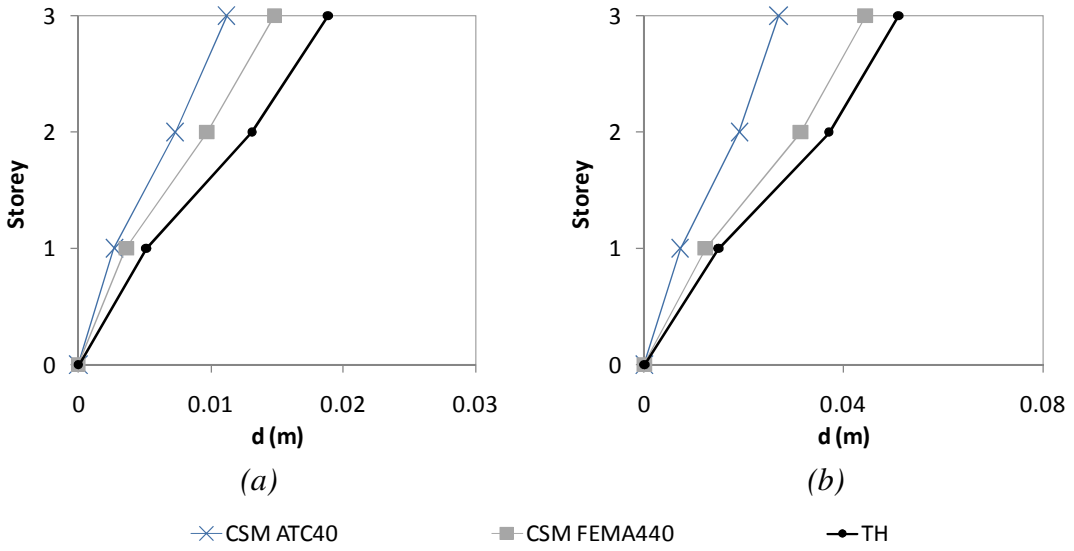

Figure 6.3 – Three storey, Y direction: a) Column C8, 0.05g; b) Column C2, 0.1g.

From Figure 6.1 to Figure 6.4, one can observe that in the three storey building, the lateral displacement profiles can be well captured by CSM-FEMA440 in column C3, the one near the centre of mass. At the edge columns, the method slightly underestimates the response, because it is not able to reproduce the torsional influence on the seismic response. The CSM-ATC40 leads in general to underestimated results in all the columns analysed. These conclusions can be drawn over all the seismic intensities tested.

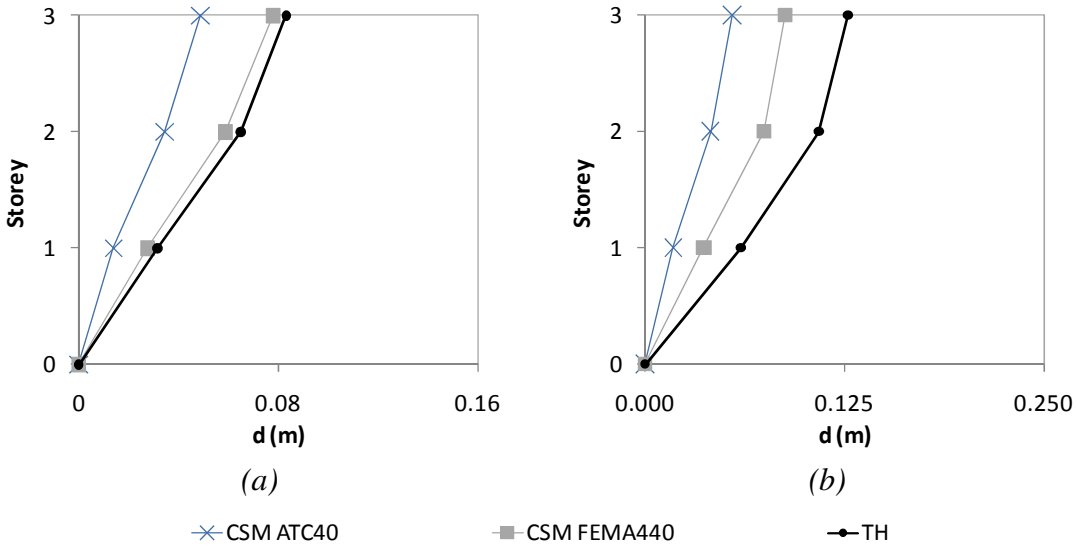

Figure 6.4 – Three storey, Y direction: a) Column C3, 0.2g; b) Column C8, 0.3g.

In the five storey building, Figure 6.5 and Figure 6.6, CSM-FEMA440 is able to reproduce the lateral displacement profiles of the columns located near the centre of mass, in both X and Y directions, over all the seismic levels tested. The method leads to quite good approximation to the *time-history* results for lower levels of intensity, where the structure still behaves elastically or almost elastically, and to conservative results for higher levels of inelasticity. The CSM-ATC40 method leads to under conservative results, with these discrepancies being higher for the upper storeys. The method is able to reproduce the displacement of the first storey in a good fashion.

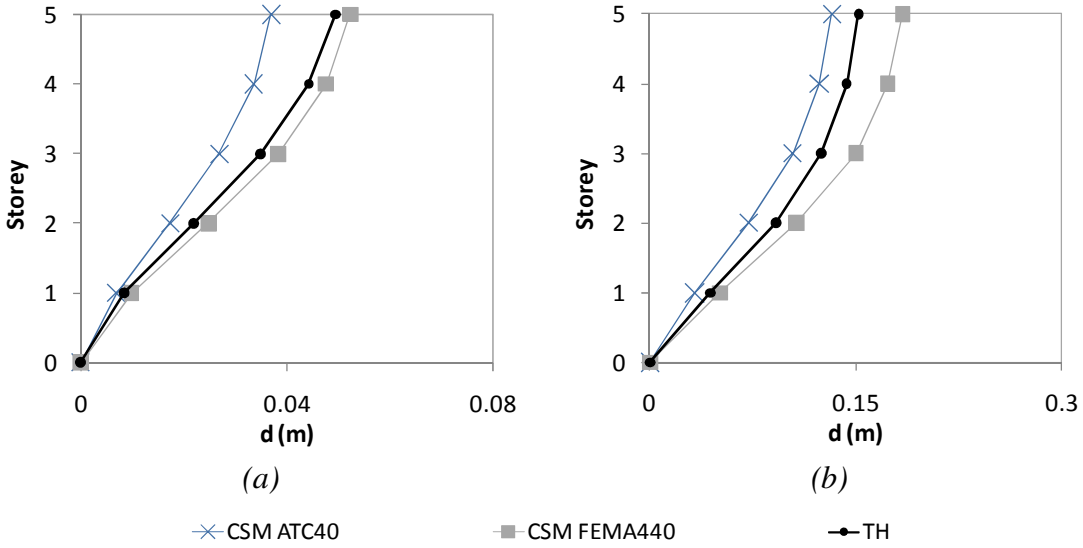

Figure 6.5 – Five storey, X direction: a) Column S14, 0.2g; b) Column S13, 0.6g.

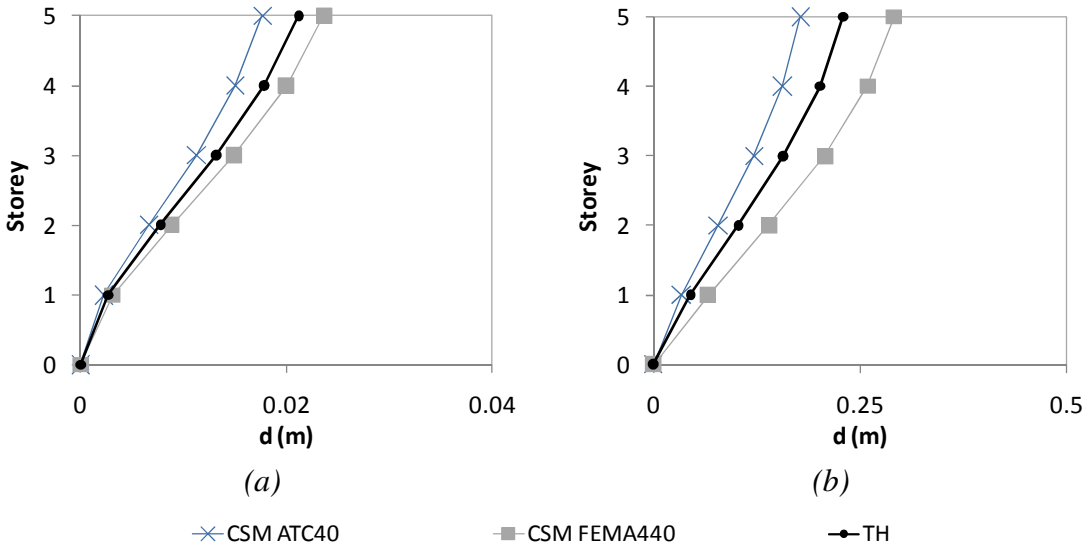

Figure 6.6 – Five storey, Y direction: a) Column S13, 0.1g; b) Column S14, 0.8g.

The same conclusions taken from the five storey building can be drawn for the eight storey building, Figure 6.7. In this case, for 0.4g – corresponding to a very high level of inelasticity – CSM-ATC40 gets close to the *time-history* results, but is still under conservative.

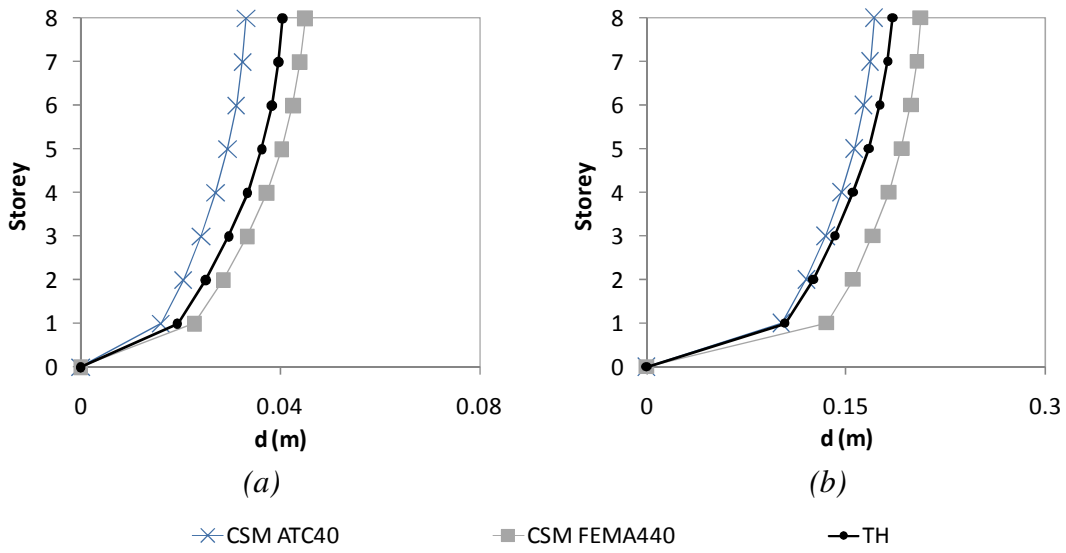

Figure 6.7 – Eight storey, X direction: a) Column S52, 0.1g; b) Column S23, 0.4g.

In terms of lateral displacement profiles, it can be concluded from the previous plots that CSM-FEMA440 presents very good results for the columns located near the centre of mass of the buildings, when compared with the nonlinear dynamic analysis results. For the columns located at the ends of the buildings the method slightly underestimates the response. CSM-ATC40 invariantly gives under conservative results, and they are always smaller than the ones obtained with the FEMA440 guidelines. These conclusions can be taken for both X and Y directions, for all ground shaking intensities and for all the buildings analysed.

6.1.2 Interstorey drifts profiles

The interstorey drifts profiles are plotted from Figure 6.8 to Figure 6.12 and compared for different intensity levels.

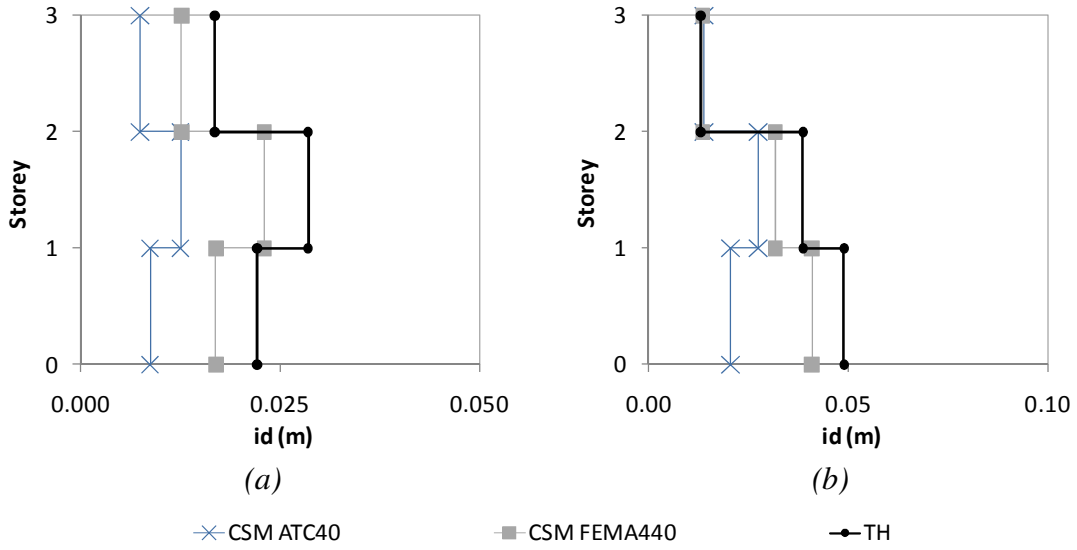

Figure 6.8 – Three storey, X direction: a) Column C2, 0.1g; b) Column C8, 0.2g.

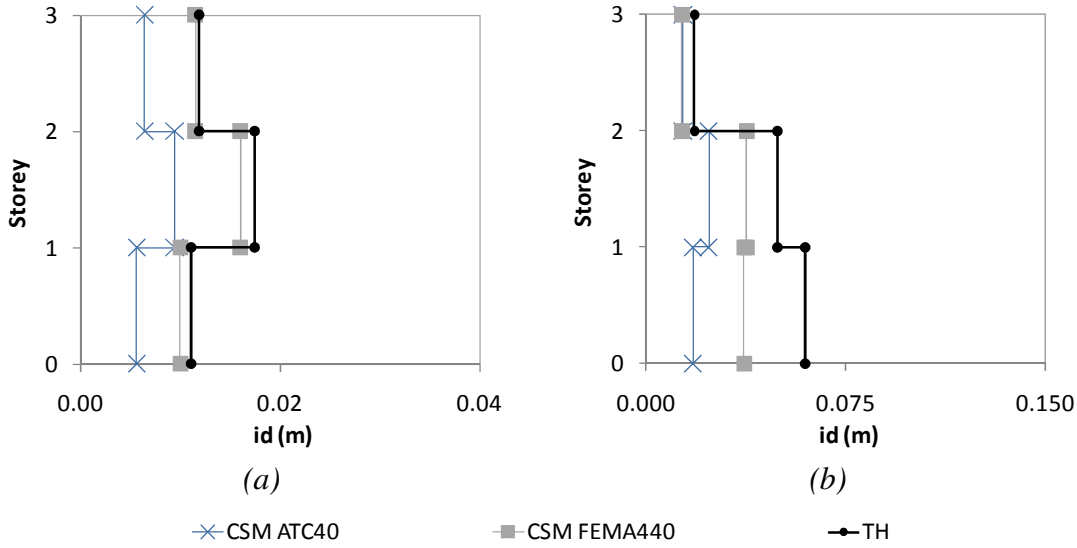

Figure 6.9 – Three storey, Y direction: a) Column C3, 0.1g; b) Column C8, 0.3g.

From Figure 6.8 and Figure 6.9 one can observe that in the three storey building, the CSM-FEMA440 interstorey drifts values are well reproduced in column C3, located near the centre of mass, for the different seismic intensities tested and for both X and Y directions. At the edge columns the method leads to slightly under conservative results, since it is not capable of reproducing the torsional effect. The exceptions are the interstorey drifts between the second and the third floors in column C8, where the method can accurately capture the correct behaviour of the structure.

The CSM-ATC40 gives non conservative results in all the columns analysed, in both directions and for all seismic levels tested. These values are always smaller than the ones obtained using the FEMA440 recommendations, consequently further away from the nonlinear dynamic median results.

In the case of the five storey building, Figure 6.10 and Figure 6.11, CSM-FEMA440 can capture the interstorey drifts profiles in a very good manner for low levels of seismic intensity – elastic or almost elastic structural behaviour. For higher levels of inelasticity the method leads to slightly overestimated results.

The CSM-ATC40 method leads once again to underestimated results, except in the three upper storeys of the five storey building for column S14 in the X direction for a 0.6g seismic intensity where the method leads to good estimations.

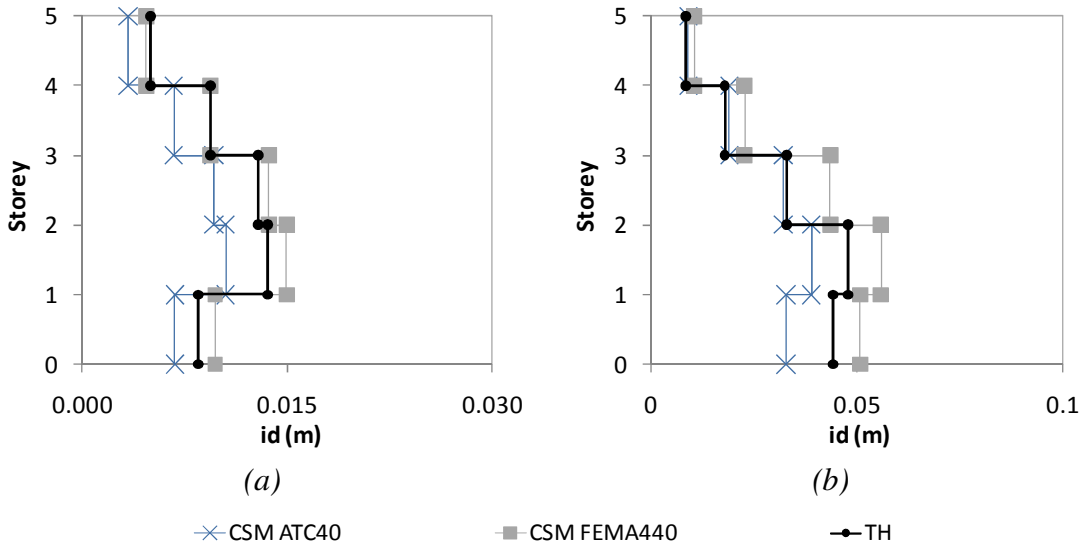

Figure 6.10 – Five storey, X direction: a) Column S13, 0.2g; b) Column S14, 0.6g.

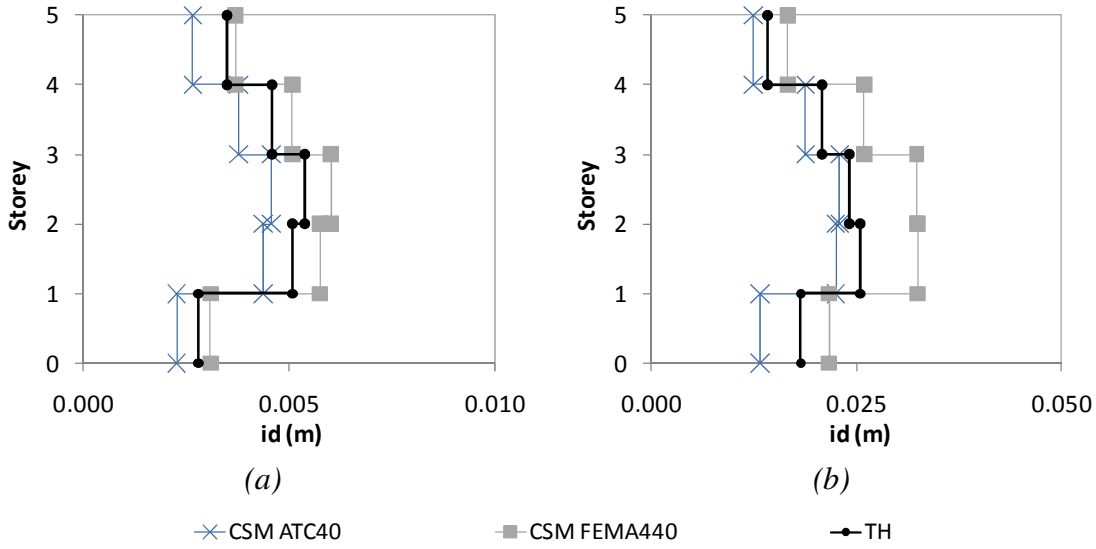

Figure 6.11 – Five storey, Y direction: a) Column S14, 0.1g; b) Column S13, 0.4g.

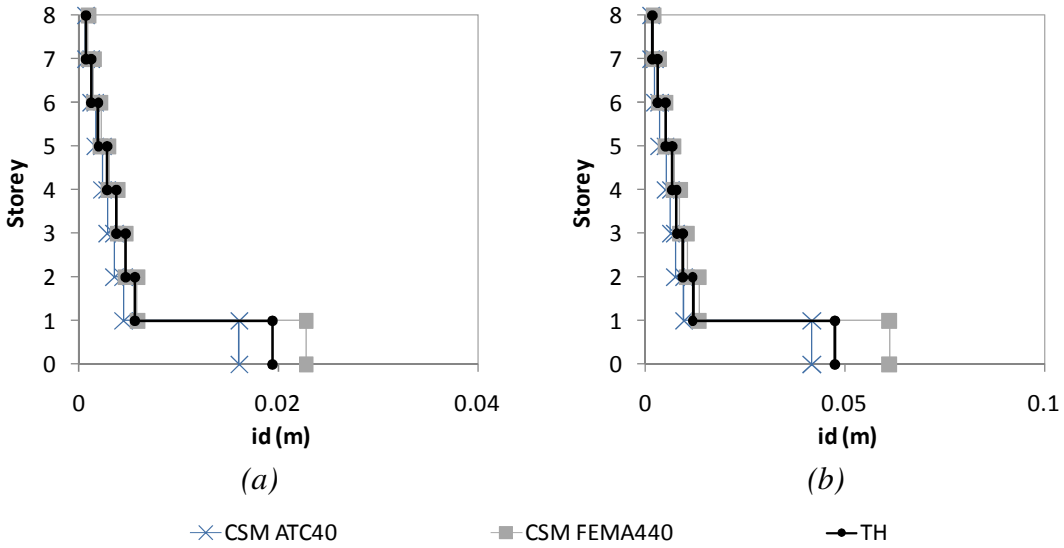

Figure 6.12 – Eight storey, X direction: a) Column S52, 0.1g; b) Column S23, 0.2g.

As is clear from Figure 6.12, the eight storey building presents a soft storey mechanism on the first floor along the X direction. Both methods can reproduce this effect, but while FEMA440 leads to an overestimation of this local mechanism, ATC40 slightly underestimates it. This trend is clear over all the seismic intensities evaluated.

From Figure 6.8 to Figure 6.12 one can observe that CSM-FEMA440 usually leads to better estimations of the interstorey drifts profiles than the CSM-ATC40 for the columns located near the centre of mass of the buildings. For the columns located on the periphery of the buildings the method slightly underestimates the response. The CSM-ATC40 method leads in general to underestimated results and they are always smaller than the ones obtained with FEMA440, therefore further away from the *time-history* median profiles.

6.1.3 Chord rotations profiles

The chord rotations profiles are now presented for the different buildings from Figure 6.13 to Figure 6.15.

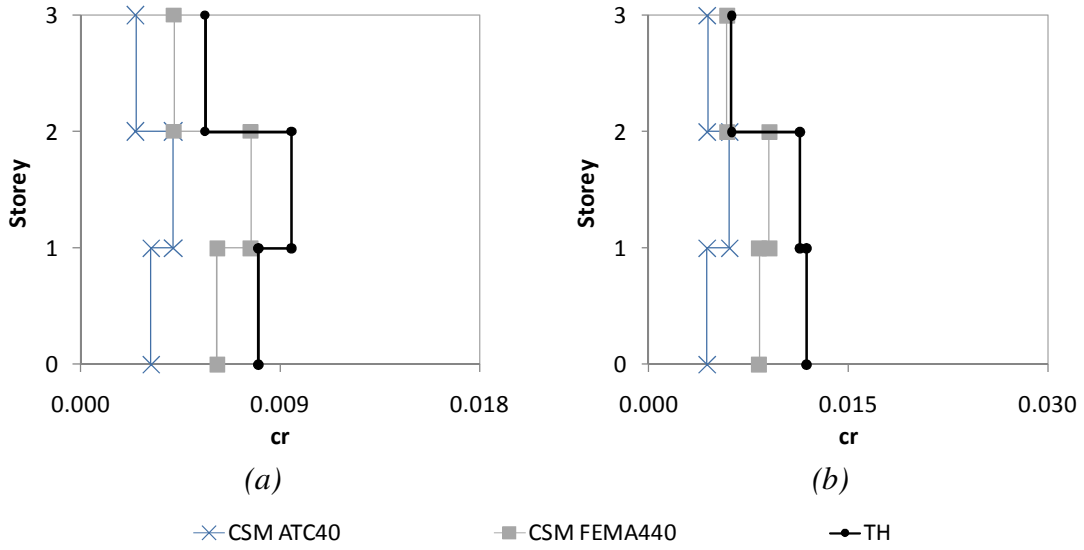

Figure 6.13 – Three storey: a) Column C2, 0.1g, X; b) Column C8, 0.2g, Y.

From the plots, one can observe that CSM-FEMA440 estimates in a very accurate way the chord rotations in columns near the centre of mass. For columns located in the periphery of the buildings, the method cannot perfectly reproduce the structural seismic response. One can also observe that CSM-ATC40 generally underestimates the chord rotations profiles for all the buildings analysed.

Once again it is evident that CSM-FEMA440 can capture the soft storey mechanism on the first floor of the eight storey building in a very good fashion, while CSM-ATC40 slightly underestimates this effect, see Figure 6.15.

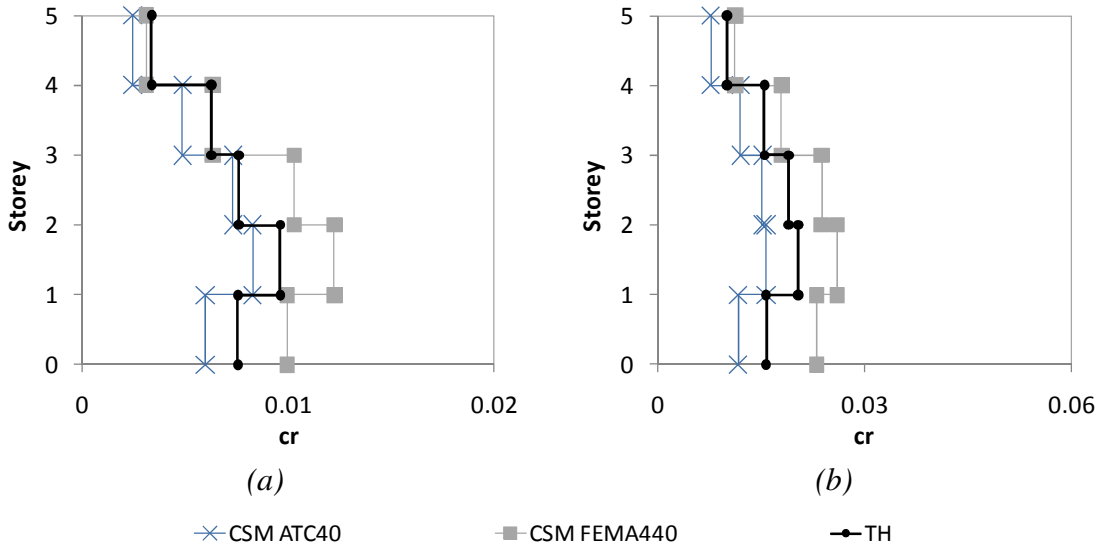

Figure 6.14 – Five storey: a) Column S13, 0.4g, X; b) Column S14, 0.8g, Y.

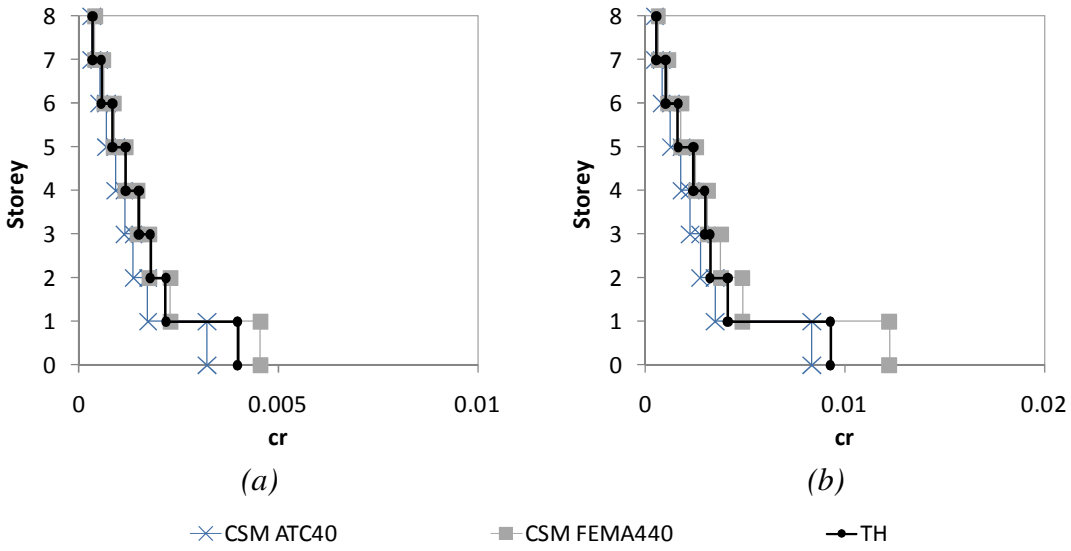

Figure 6.15 – Eight storey, X direction: a) Column S23, 0.1g; b) Column S52, 0.2g.

6.1.4 NSPs and *time-history* ratios

The roof displacements and base shears determined from the NSPs are normalized by the corresponding median responses of dynamic analysis, as shown in Eq. 6.1, which give an estimate of bias – how good or bad is the NSP under scrutiny for predicting that particular response – as the target reference value in ideal conditions should simply be unity. An NSP is said to be biased towards underestimating the response if the normalized response is less than one and overestimating the same if the ratio exceeds one. This provides a point of comparison between different NSPs. As mentioned before, the NSPs must never lead to underestimated results, therefore these ratios should always be higher than one. Ideally one would want such ratios to tend to unity, which means the NSPs would perfectly match the *time-history* median results. Note that the top displacements at the centre of mass correspond to the target displacements.

$$Top\ Displacement\ ratio = \frac{NSP's\ top\ displacement}{Time\ history\ median\ top\ displacement} \qquad Eq.\ 6.1$$

Figure 6.16 to Figure 6.23 illustrate top displacement ratios computed for the three buildings in both directions for different intensity levels.

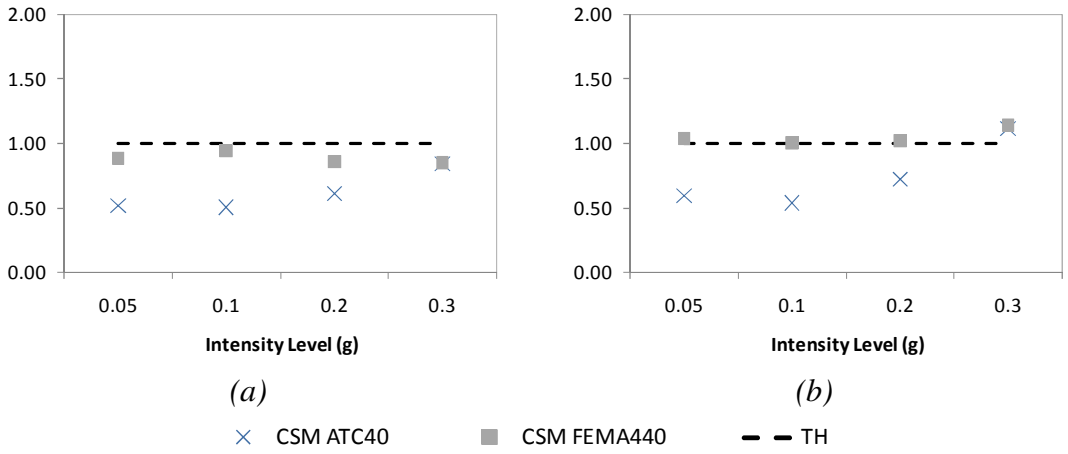

Figure 6.16 – Three storey, X direction: a) Column C8; b) CM.

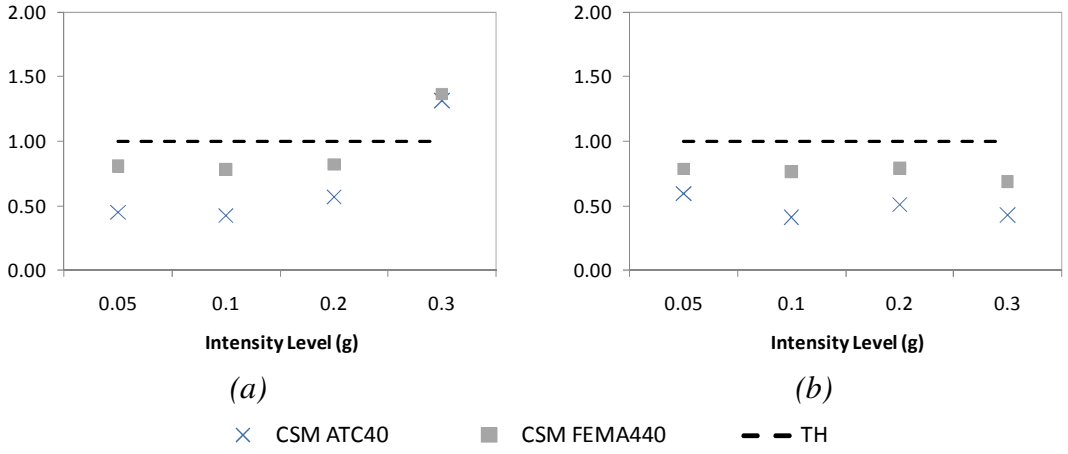

Figure 6.17 – Three storey: a) Column C2, X; b) Column C8, Y.

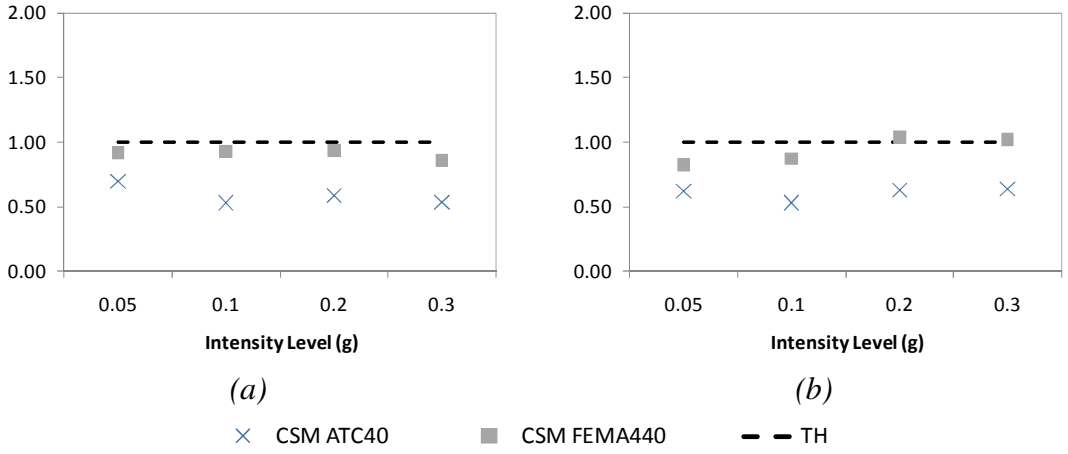

Figure 6.18 – Three storey, Y direction: a) CM; b) Column C2.

From Figure 6.16b) and Figure 6.18a), it is clear that target displacements, i.e. the displacements at the centre of mass at the roof level, computed using the CSM-FEMA440 perfectly match the *time-history* in both directions and for the different intensity levels. The exception occurs in the Y direction for 0.3g, corresponding to a very high level of inelasticity, where the response is under conservative. On the other hand the target displacements computed with the CSM-ATC40 are non conservative in both directions and for the different intensity levels, except in the X direction for 0.3g where the response gets close to the *time-history* results.

In column C8, the stiff edge of the building, FEMA440 leads to under conservative results with the discrepancy to the *time-history* being higher in the Y direction. This method also leads to smaller results than the *time-history* at column C2 (the flexible edge of the building) except in the X direction for 0.3g (very high level of inelasticity) where it leads to significant conservative results, and for 0.2g and 0.3g in the Y direction where the method practically matches the nonlinear dynamic median results. The CSM-ATC40 method invariantly gives under conservative results for columns C2 and C8 in both directions and over the different intensity levels analysed. The exception is at column C2 in the X direction for 0.3g where it leads to the same and conservative result of FEMA440.

The results computed with ACT40 are generally smaller than the ones obtained with FEMA440, therefore further away from the nonlinear dynamic median response.

From Figure 6.19 to Figure 6.21, one can observe that CSM-FEMA440 leads to slightly conservative results of top displacements in all the columns analysed in the five storey building, in both directions and over all the seismic intensities tested. The results are quite close to the *time-history* mainly for lower levels of seismic intensity, where the buildings behave elastically or almost elastically. On the other hand, the results computed with the ATC40 features are always non conservative.

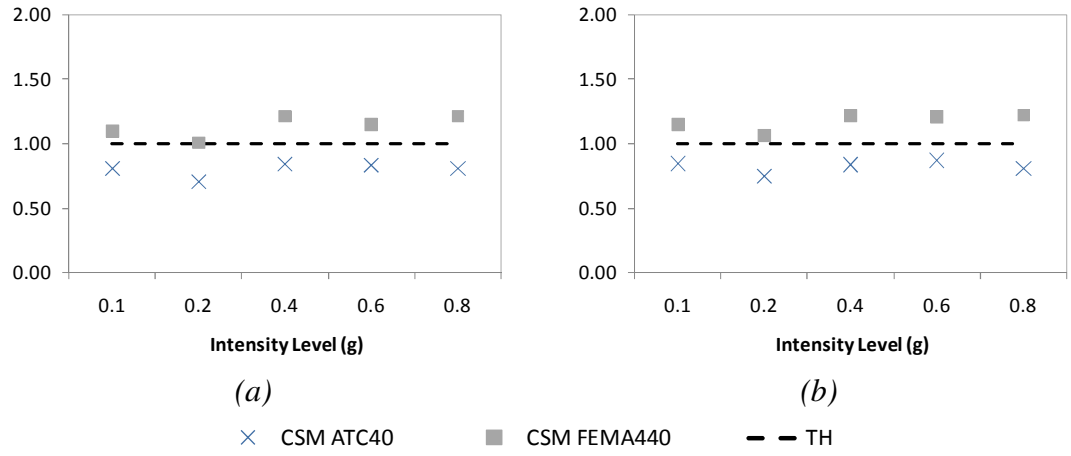

Figure 6.19 – Five storey, X direction: a) Column S1; b) CM.

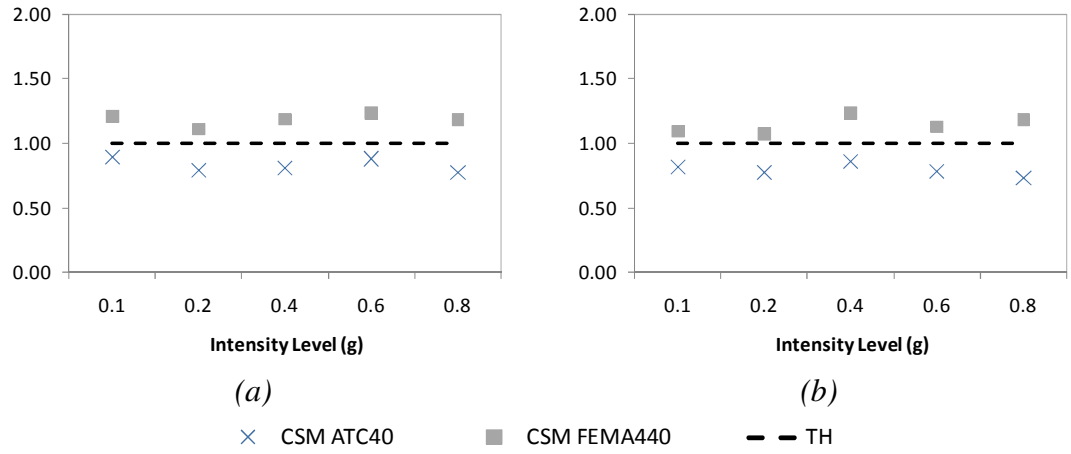

Figure 6.20 – Five storey: a) Column S23, X; b) Column S1, Y.

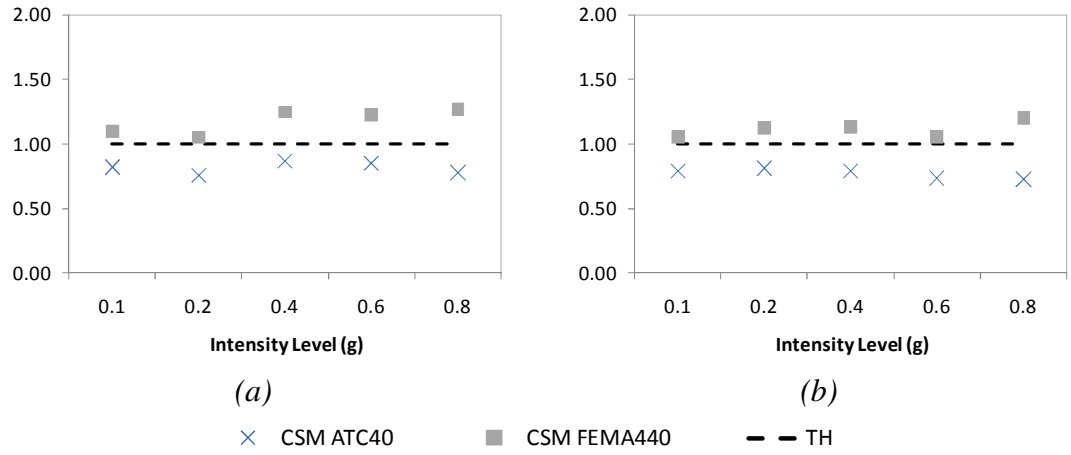

Figure 6.21 – Five storey, Y direction: a) CM; b) Column S23.

From Figure 6.22 and Figure 6.23 it is clear that the CSM-FEMA440 leads to very good estimations of the top displacements in all the columns analysed in the eight storey building. Although, the results are slightly overestimated for an intensity of 0.2g.

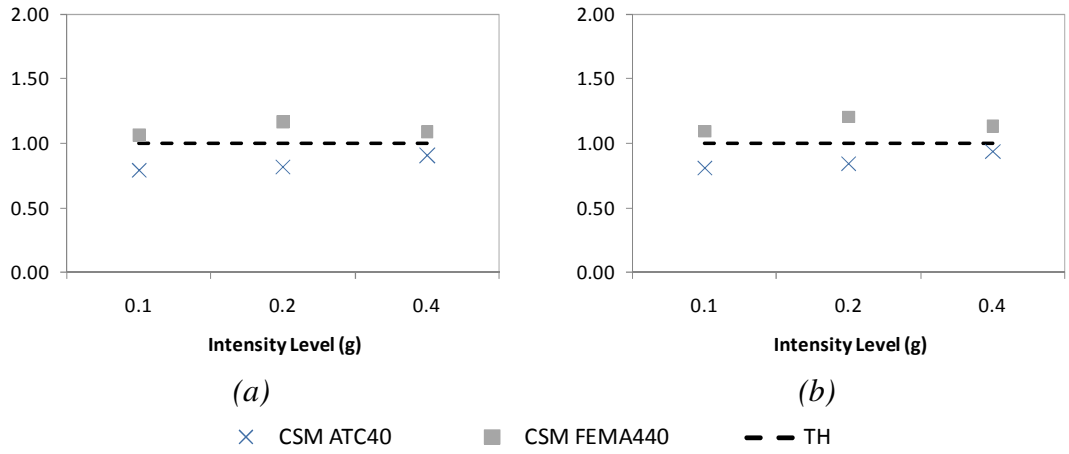

Figure 6.22 – Eight storey, X direction: a) Column S9; b) CM.

The ATC40 underestimates the results, but it gets closer to the *time-history* as the intensity increases. For 0.3g, the method almost matches the nonlinear dynamic median results.

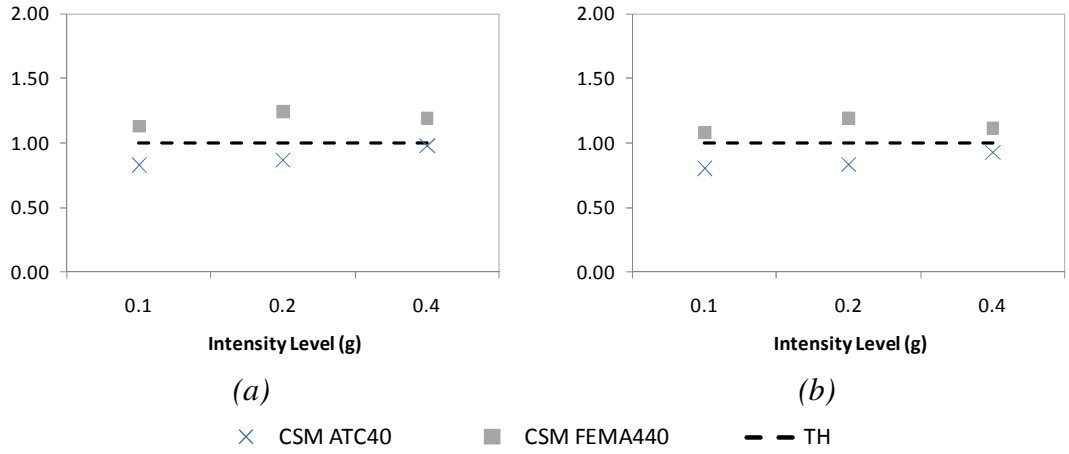

Figure 6.23 – Eight storey, X direction: a) Column S69; b) Column S23.

Similar ratios were computed for base shears in both X and Y directions for the different seismic intensities. They are plotted in Figure 6.24 and Figure 6.25.

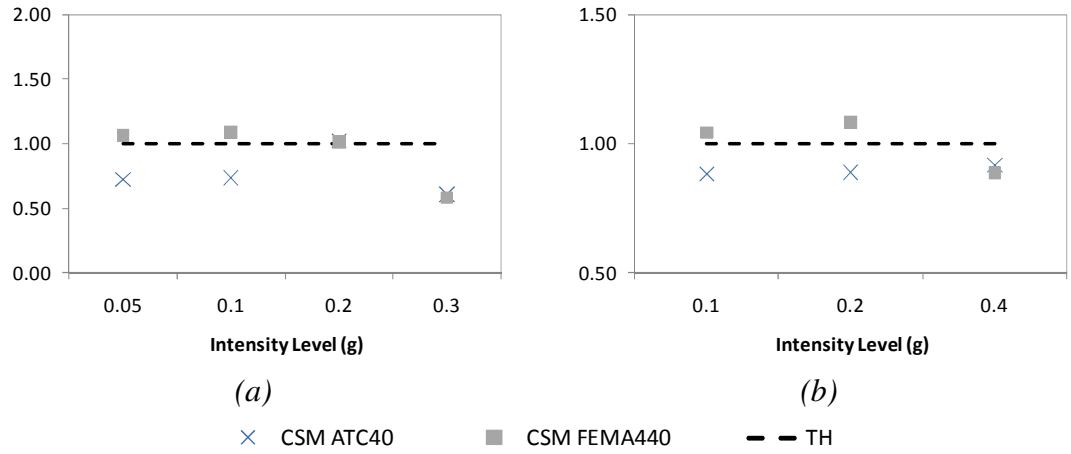

Figure 6.24 – a) Three storey, X direction; b) Eight storey, X direction.

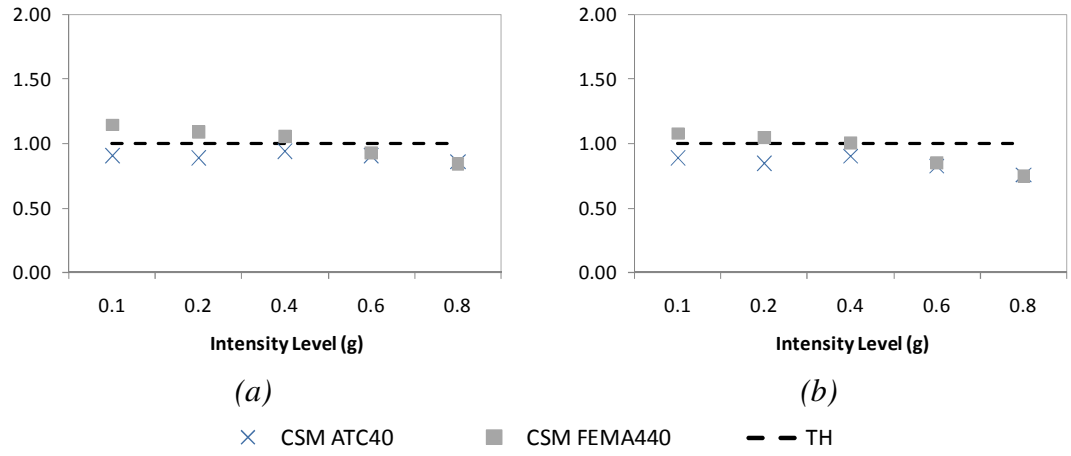

Figure 6.25 – Five storey: a) X direction; b) Y direction.

From the previous plots, it is possible to identify a trend in the base shear index computed using CSM-FEMA440 for the three buildings under study. For increasing seismic intensities, mainly when the building goes through high inelastic ranges, the base shear index tends to decrease in all buildings. For these high levels of inelasticity the method slightly underestimates the response. When the buildings behave elastically and inelastically (but not with a high level of inelasticity) CSM-FEMA440 is able to correctly estimate the base shear response. On the other hand, CSM-ATC40 generally underestimates the base shear response in all buildings, for all intensity levels and in both directions. The exception occurs in the 3 storey building, in the X direction for 0.2g where the method correctly estimates the base shear.

6.1.5 Normalized top displacements

When dealing with plan-asymmetric buildings the normalized top displacements is the measure one should analyse in order to understand the torsional behaviour of the

structure. This measure is obtained by normalizing the edge displacement values with respect to those of the centre of mass. Several plots are presented showing the performance of the analysed procedures in estimating the torsional motion of the evaluated buildings.

From Figure 6.26 and Figure 6.27 one can observe that both methods lead to the same estimations of the normalized top displacements in the three storey building. None of them is able to capture the torsional amplification at the flexible edge, column C2. These conclusions are taken for the different seismic intensities tested in both directions.

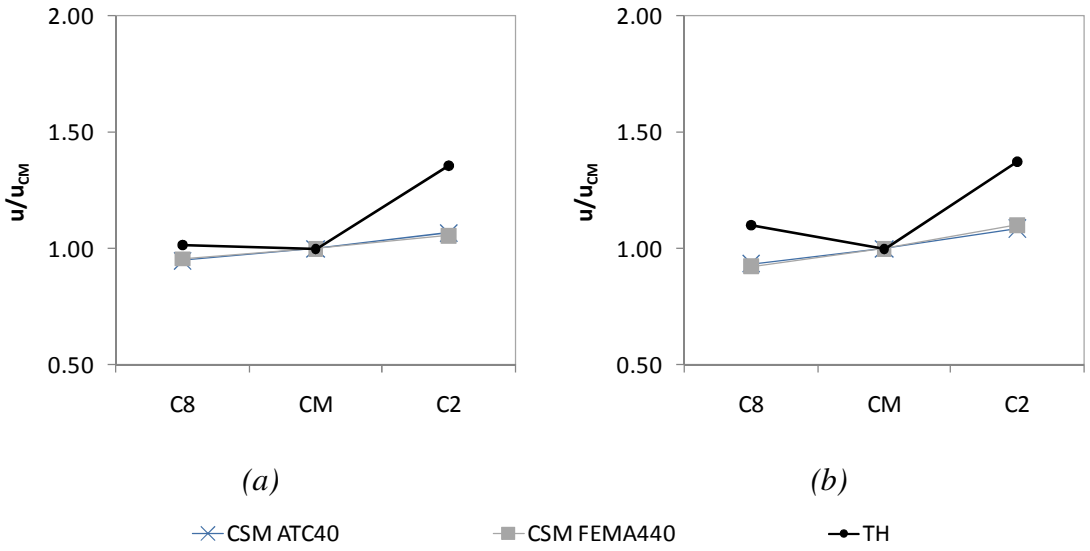

Figure 6.26 – Three storey, X direction: a) 0.1g; b) 0.2g.

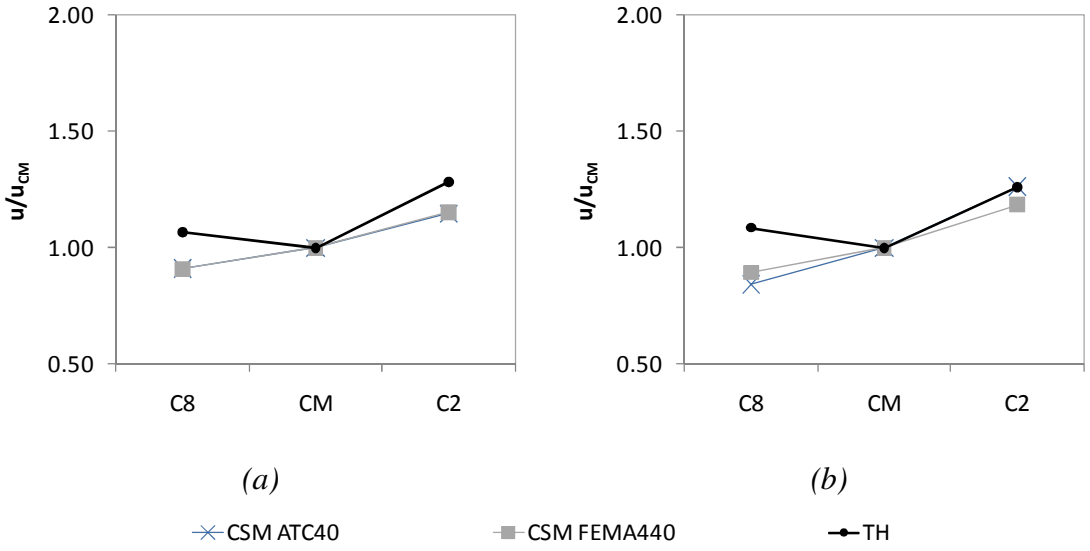

Figure 6.27 – Three storey, Y direction: a) 0.05g; b) 0.1g.

In the five storey building, Figure 6.28, the normalized top displacements computed with both methods are pretty much the same. Generally, they cannot capture the torsional amplification on the flexible side, column S1. This trend is observed over all the seismic levels studied.

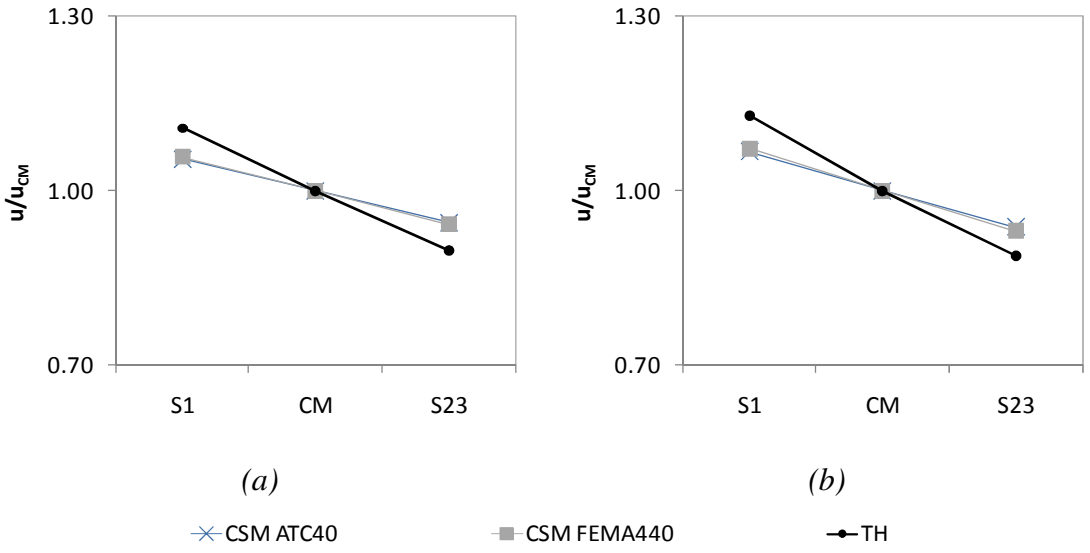

Figure 6.28 – Five storey, X direction: a) 0.1g; b) 0.2g.

Figure 6.29 and Figure 6.30 show that both methods are unable to reproduce the torsional amplification of column S9 in the X direction and of column S69 in the Y direction, over all the seismic levels tested.

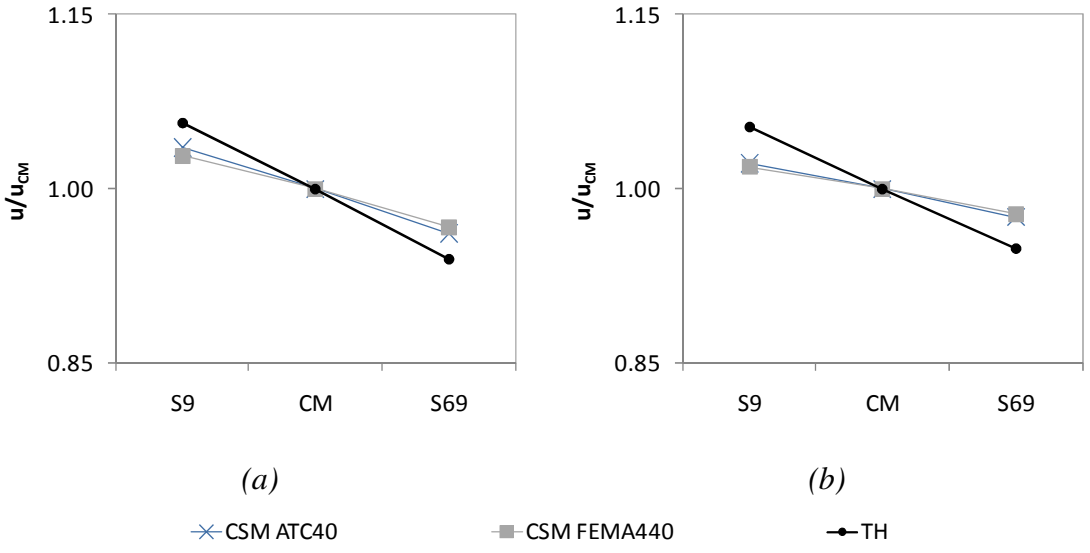

Figure 6.29 – Eight storey, X direction: a) 0.1g; b) 0.2g.

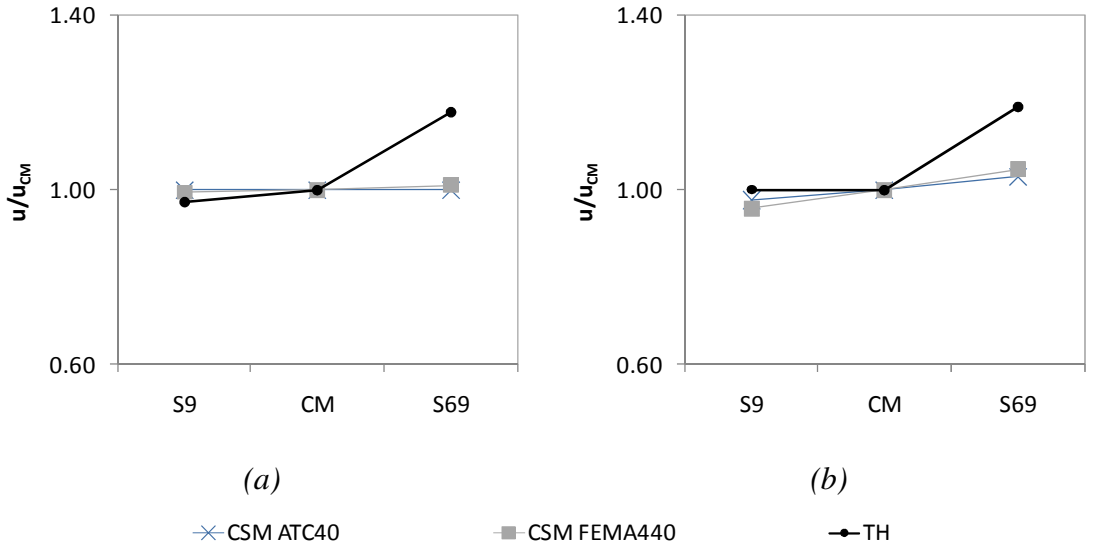

Figure 6.30 – Eight storey, Y direction: a) 0.1g; b) 0.2g.

From the previous plots, it is clear that both CSM-ATC40 and CSM-FEMA440 lead to approximately the same estimations of normalized top displacements. They are unable to reproduce the torsional motion induced by the earthquake in the structure for different levels of inelasticity. In fact, none of the methods can capture the torsional amplification at the flexible edges of the buildings. These conclusions can be drawn for all the buildings analysed over all the seismic levels evaluated.

6.2 Discussion

The results presented above show that CSM-FEMA440 estimates in a very accurate way the response of the centre of mass and the response of the columns located near this node, where the torsional effect is not very marked, over all the seismic intensities analysed. On the other hand, CSM-ATC40 leads to a generally underestimated response of these elements. These differences can be explained due to different estimations of the effective period and damping computed by these two methods. This fact is easily observed in the elastic range, where the effective damping calculated with these procedures should be equal to the viscous damping considered for each building in the nonlinear dynamic analysis. In the case of the three storey building, a 2% viscous damping was used in the nonlinear *time-history*. One can see in Table 6.1 that ATC40 overestimates the damping in both directions for seismic intensities of 0.05g and 0.1g, for which the building remains elastic or almost elastic. On the other hand FEMA440 seems to estimate the damping in a very accurate way. In the five storey and eight storey buildings the viscous damping used in the *time-history* analysis was 5%. The five storey building remains elastic or almost elastic for 0.1g and 0.2g and the eight storey building for 0.1g. It is important to point out that this last case behaves elastically in the Y direction over all the seismic intensities studied. In both five storey, see Table 6.2, and eight storey buildings the ATC40 once again overestimates the damping, while the FEMA440 seems to reproduce it in a very good manner. The overestimation of the damping in the elastic range for the three buildings

under analysis by ATC40, when compared to the viscous damping used in the *time-history*, explains the underestimated results obtained by this method. On the other hand, the innovative methods to compute the effective damping by FEMA440 explain the good results obtained with this method at the centre of mass and in columns near this node.

All the buildings analysed in this study in both X and Y directions have short/medium periods (less than 2 seconds), see Table 6.1 and Table 6.2. The differences in the results of the two NSPs for these short/medium-period buildings in the elastic range can be explained by the high sensitivity of the μ value in the CSM procedure to small errors in estimating the period and damping ratio. In fact, the elastic response spectrum tends to be very jagged in the short-period range. Therefore the calculation of the elastic SDOF system becomes very sensitive to errors in the vibration period and damping ratios. In the elastic range, the values of μ used in ATC40 and in FEMA440 to compute the effective period and the effective damping, may become larger than one (in the elastic range the μ should theoretically be equal to one). Thus the two NSPs lead to different responses for short/medium-period buildings [131]. This fact also explains the differences in the results obtained with the ATC40 and FEMA440 procedures in the elastic range. The elastic response spectrum in the long-period range tends to be smooth, therefore the errors in the vibration period and damping ratio do not affect the target displacement estimation so drastically, and consequently the μ of the long-period buildings in the elastic range. Probably, the results of the two methods would not be so different for long period structures behaving elastically.

In the inelastic range the underestimated results obtained with the ATC40 procedure can also be explained by its overestimation of the effective damping. The three storey building behaves inelastically for 0.2g and for 0.3g, the five storey building for 0.4g, 0.6g and 0.8g, and the eight storey building goes through the inelastic range for 0.2g and 0.4g only in the X direction. From Table 6.1 and Table 6.2 one can observe that the values of effective damping calculated with ATC40 are much higher than the ones obtained with FEMA440 for these seismic intensities. The buildings under analysis are not very ductile so the high values of damping obtained with ATC40 in the inelastic range seem quite unrealistic. This fact confirms the trend previously observed in the elastic range. The results obtained with FEMA440 are close to the *time-history* leading to the conclusion that the effective damping calculated with this method is in fact more realistic.

Table 6.1 - Three storey building - effective damping values.

	Three storey building: 2% viscous damping			
	X (T = 0.617 sec)		Y (T = 0.441 sec)	
Intensity level (g)	ATC40	FEMA440	ATC40	FEMA440
0.05	6.4%	2.1%	5.7%	2.1%
0.1	12.0%	2.2%	10.1%	2.1%
0.2	13.6%	5.8%	10.6%	3.2%
0.3	25.8%	15.9%	15.8%	5.8%

Table 6.2 - Five storey building - effective damping values.

	Five storey building: 5% viscous damping			
	X (T = 0.617 sec)		Y (T = 0.593 sec)	
Intensity level (g)	ATC40	FEMA440	ATC40	FEMA440
0.1	12.8%	5.2%	13.2%	5.4%
0.2	13.8%	5.3%	13.6%	5.3%
0.4	17.3%	6.7%	16.6%	6.4%
0.6	23.0%	10.9%	22.2%	10.0%
0.8	25.5%	18.9%	24.3%	15.6%

Figure 6.31 to Figure 6.33 illustrate the target displacement computation using both methods in the five storey building X direction, for several levels of inelasticity: elastic or almost elastic regime (0.1g), medium level of inelasticity (0.4g) and high level of inelasticity (0.8g). The *time-history* displacement at the centre of mass of the roof is divided by the SDOF to MDOF gamma transformation factor (that is the same in both NSPs methods), see section 2.4.4.1 and 2.4.4.2, in order to compare it with the SDOF target displacements calculated with both methods.

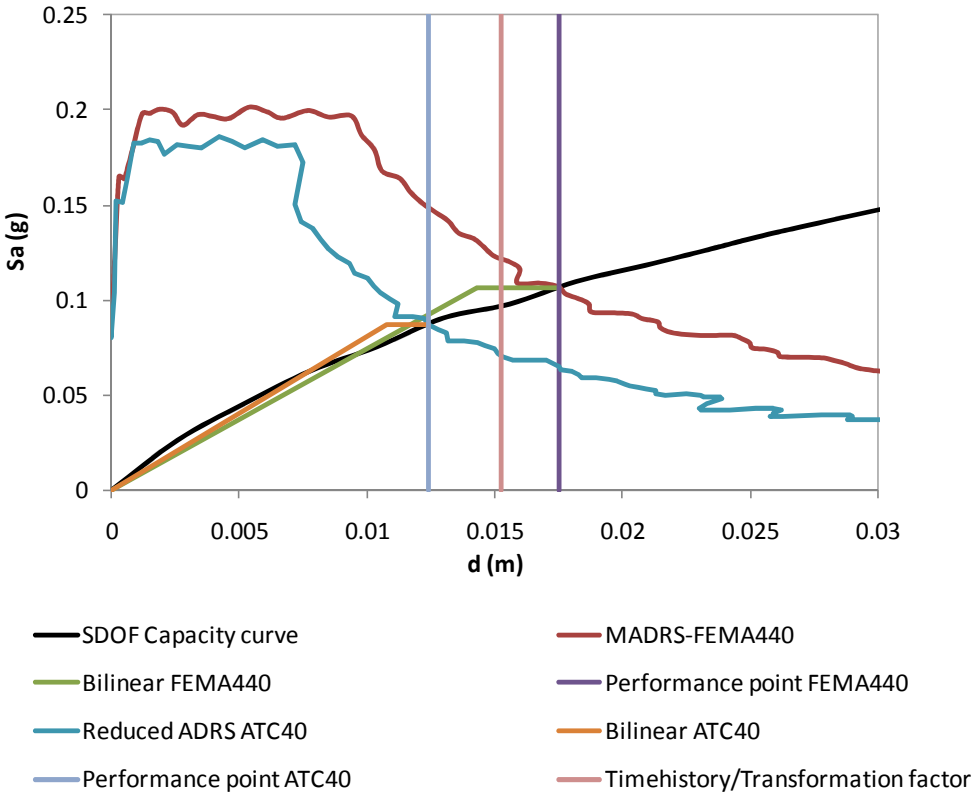

Figure 6.31 – Target displacement calculation, CSM-ATC40 vs CSM-FEMA440. Five storey building, X direction, 0.1g.

From the plots, one can observe that the initial stiffness of the SDOF (corresponding to the slope of the first part of the bilinear curve) is approximately the same for the two methods. The differences in the results are explained by the damping calculation, described in the previous paragraphs, and in the reduced demand spectrum definition. From the previous tables, one could conclude that FEMA440 estimates the damping in a more accurate way than ATC40. From the plots it is evident that the spectral reduction is more accentuated in ATC40 than in FEMA440. Since the ATC40 results are underestimated when compared with the *time-history* median results, one can conclude that the spectral reduction recommended by this code may not be so suitable for the buildings studied herein.

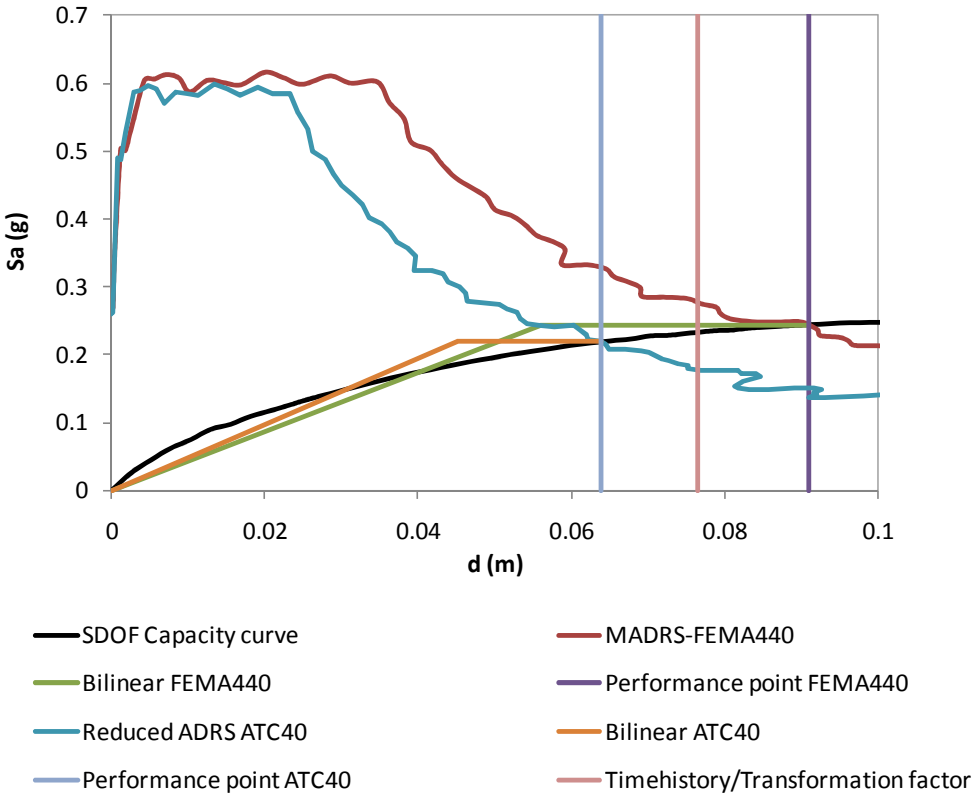

Figure 6.32 – Target displacement calculation, CSM-ATC40 vs CSM-FEMA440. Five storey building, X direction, 0.4g.

One can observe from the plots, that the MADRS recommended in FEMA440 is very close to the reduced spectrum proposed in ATC40 until the second corner period value of the last one. In the elastic range (0.1g), the ATC40 reduced spectrum presents slightly smaller values of acceleration and displacements than those from FEMA440, but they remain close to each other. For periods higher than this, MADRS presents higher values of displacements and accelerations. The FEMA440 procedure leads to conservative results in most of the cases, so it is safer to use this method than ATC40 when designing or assessing irregular structures. Therefore, one can say that the FEMA440 MADRS spectrum represents in a more adequate way the spectral

reduction due to inelastic hysteretic damping than the reduced spectrum computed with the ATC40 formulas.

One can conclude that the satisfactory results obtained with CSM-FEMA440 can be explained by its innovative and accurate algorithm to calculate the damping and the innovative spectral reduction definition (MADRS).

The conclusions presented herein and illustrated for the five storey building, can also be drawn for the other buildings analysed in this study.

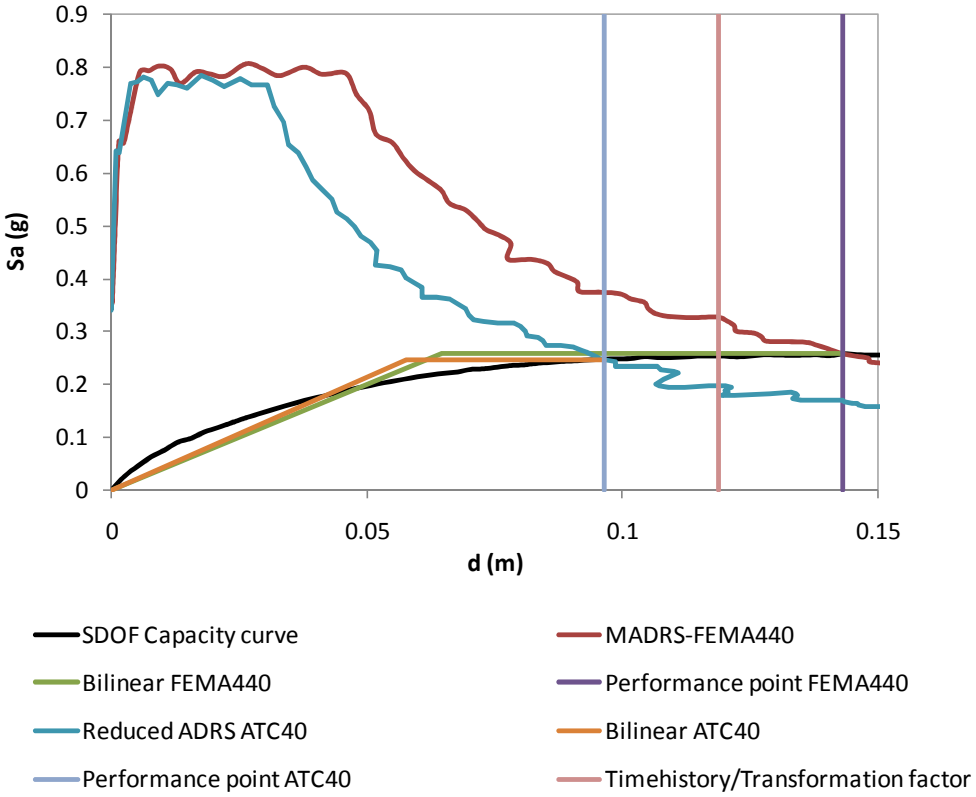

Figure 6.33 – Target displacement calculation, CSM-ATC40 vs CSM-FEMA440. Five storey building, X direction, 0.6g.

In the columns located at the extremities of the buildings (away from the centre of mass) the results obtained with CSM-FEMA440 are closer to the *time-history* than the ones obtained with CSM-ATC40, although they seem to be not so exact as the ones obtained for the columns near the centre of mass. This fact was evident in the SPEAR building response.

Analysing the normalized top displacements, one can get an overview of how well each method is able to reproduce the torsional effects induced by the earthquake in the structure. One can observe that both methods lead in general to the same estimations of normalized top displacements, but none of them can capture the torsional effects. This is evident observing the inability of both methods to capture the torsional amplification at the flexible edge of the buildings. This can be explained because none

of the algorithms contemplate any special feature in order to capture the torsional motion induced by the earthquake, especially regarding torsional amplification.

Since CSM-FEMA440 leads to better results than ATC40, this last method will be disregarded in the comparisons presented in the following chapters.

7. A comparison between the Extended N2 method and the original N2 proposed in EC8

As was mentioned in section 2.3, Eurocode 8 [25] introduced the N2 method developed by Fajfar and his team [2] as the recommended nonlinear static procedure to be used when performing pushover analyses. The problem of the commonly used NSPs, including the N2 method, is their inability to deal with plan-asymmetric buildings. Generally they cannot capture the torsional effects distorting the real structural response. This kind of buildings constitutes the common case in real life so it is urgent to implement updating formulations in these procedures making the structural response as realistic as possible. Eurocode 8-1 (4.3.3.4.2.7 Procedure for the estimation of the torsional effects) includes some guidelines for the determination of torsional effects based on elastic analysis (e.g. an early version of the Extended N2 method), but they are only restricted to torsionally flexible buildings.

Fajfar and his team have developed the Extended N2 method [4, 8] which is able to capture the torsional behaviour of plan-asymmetric buildings. This procedure is based on the application of correction factors to the pushover results obtained with the N2 method. The correction factors depend on a dynamic elastic analysis and on a pushover analysis.

The main objective of this chapter is to assess the seismic behaviour of the buildings, evaluating the accuracy of the Extended N2 method and the original N2 proposed in Eurocode 8. The results will be divided in two main sections: the ones corresponding to the elements located at the centre of the buildings, where the torsional effects are

not so important as the ones at the extremities; and the ones corresponding to the elements located at the edges of the buildings, where the influence of the seismic torsional motion is very important in their structural response. From the first set one expects to make a better evaluation of the accuracy of the N2 method in computing the target displacements and the response in the central columns for different intensity levels. Since the torsional effect is not very evident for such elements, the Extended N2 method uses a correction factor equal to one, see the theoretical background of the method in section 2.4.2. Therefore both original and extended procedures lead to the same results. From the second set, one can compare the performance of the original N2 and its extended version in estimating the torsional response on both stiff and flexible sides of the buildings through increasing seismic intensities. Discussion and conclusions are outlined in the end. The results of this chapter are presented in [132].

7.1 Assessing the seismic response in the central elements of the buildings

The assessment results of the elements located at the centre of the analysed buildings are presented herein. The torsional influence in these elements is not considerable; therefore the results of the original N2 and the Extended N2 method are pretty much the same, as previously explained. The maximum roof displacement at the centre of mass of each building, computed with the N2 method for different seismic intensities, is plotted with the pushover curves and the median *time-history* results. Thus, one can better understand how far in the inelastic range the buildings are deformed.

The plots identified as Modal X+ correspond to the pushover curves obtained in the X direction applying a modal proportional load pattern along the positive sense of the X direction. On the other hand the Modal X- corresponds to the pushover curves obtained with the same load pattern but now applied along the negative sense of the X direction. The same explanation applies to the Y direction. The TH represents the median *time-history* results for the different seismic intensities analysed in each case.

Obviously, the maximum roof displacement at the centre of mass will be the same whether it is computed with the N2 method or with the Extended N2 method, because the correction factor at the centre of mass used in the Extended N2 procedure is equal to one.

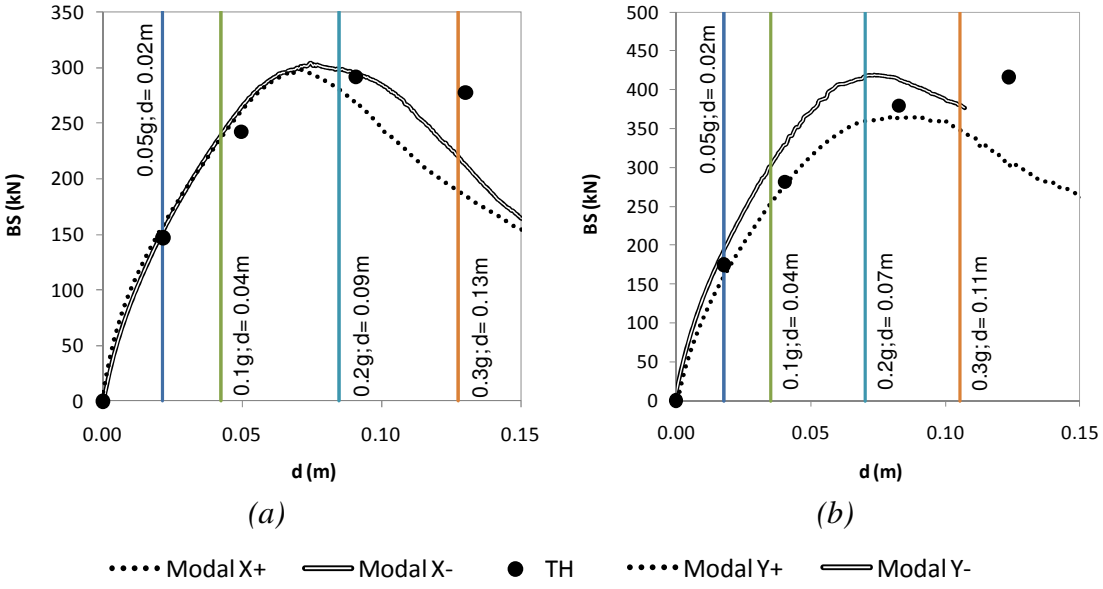

Figure 7.1 – Three storey, max roof displacement computed with the N2 method a) X direction b) Y direction.

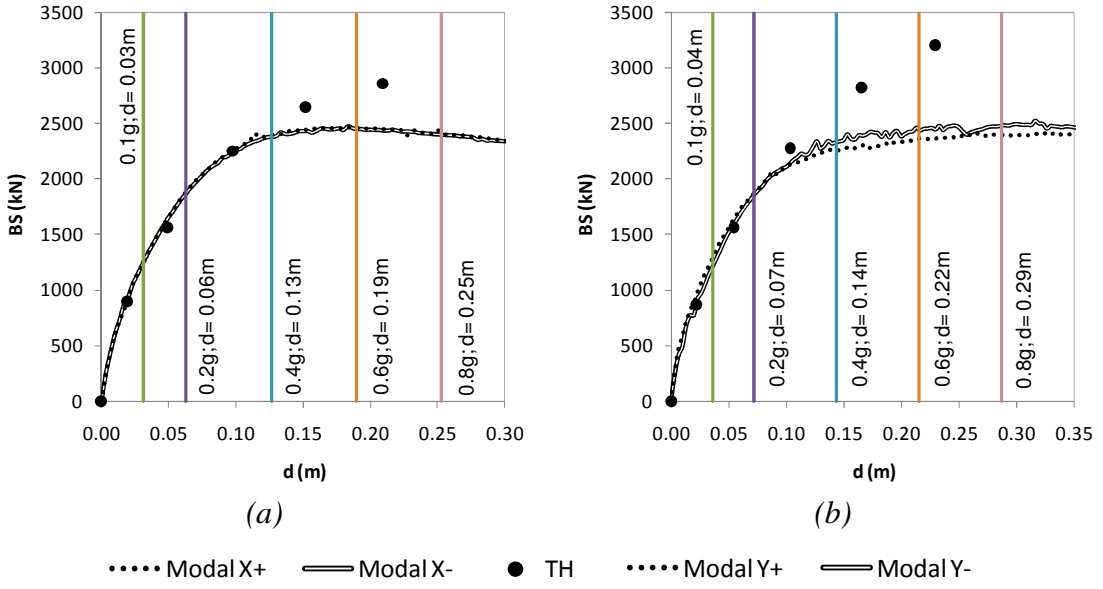

Figure 7.2 – Five storey, max roof displacement computed with the N2 method a) X direction b) Y direction.

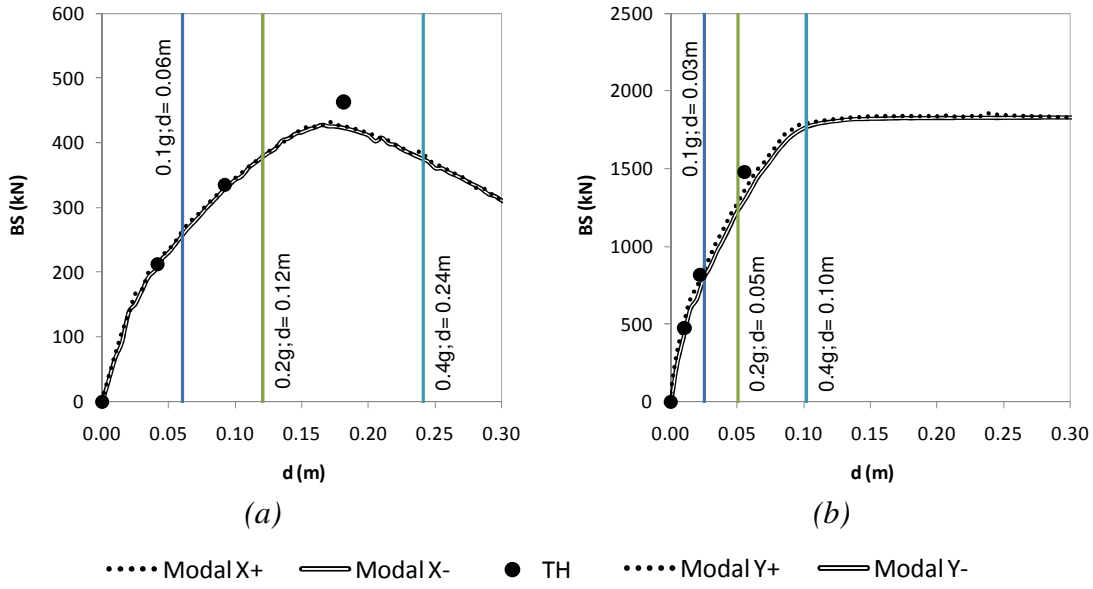

Figure 7.3 – Eight storey, max roof displacement computed with the N2 method a) X direction b) Y direction.

From the presented pushover curves one can observe that the N2 method generally leads to conservative maximum roof displacements when compared with the nonlinear dynamic analysis. The exception is the three storey building where the results have a good match with the *time-history*.

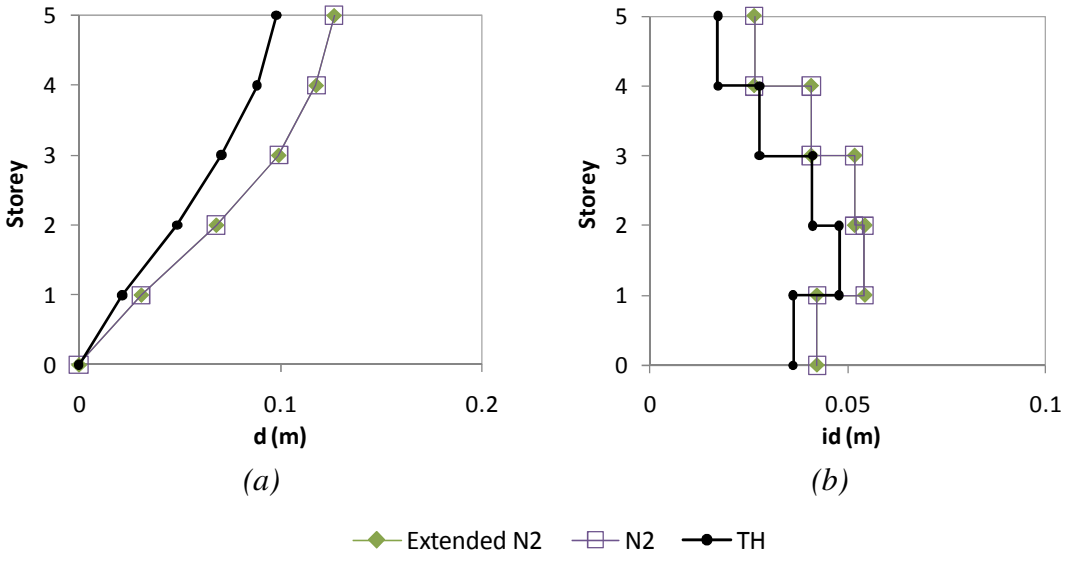

Figure 7.4 – Five storey building, a) Lateral displacement pattern S13, X 0.4g b) Interstorey drifts S14, Y 0.6g.

Figure 7.4 and Figure 7.5 illustrate the lateral displacement pattern, the interstorey drifts and the chord rotations profiles for columns located at the centre of the

buildings near the centre of mass. Once again, both N2 and Extended N2 lead to the same results. Each method is represented in the subsequent plots, where TH stands for *time-history* results.

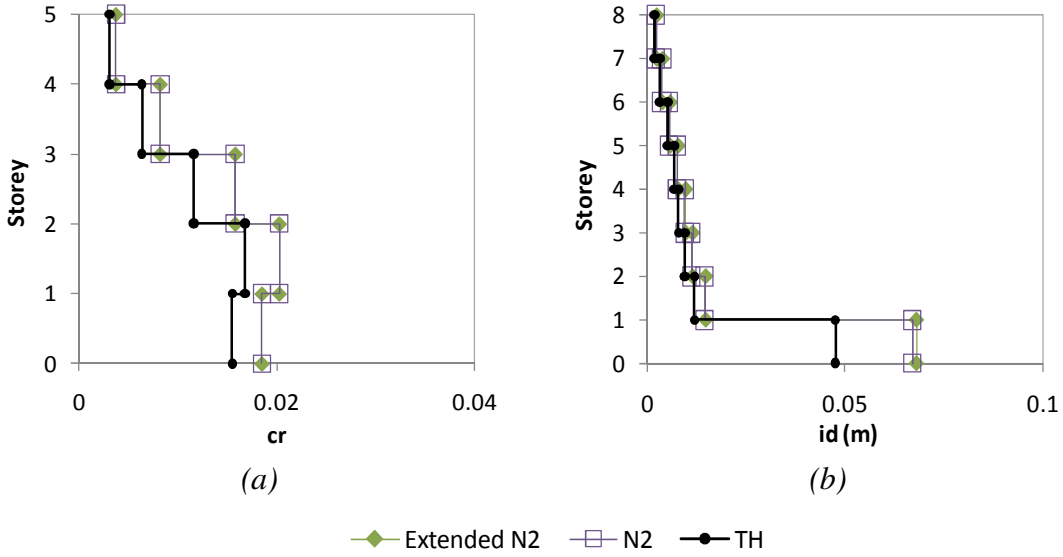

Figure 7.5 – a) Five storey building, chord rotation S13, X 0.6g b) Eight storey building, interstorey drifts S23, X 0.2g.

From the plots above, one can generally conclude that the N2 method reproduces in a good fashion the seismic behaviour of the columns at the centre of the studied buildings through all the seismic intensities tested. Although, the method slightly overestimates the response in such elements. It can capture the soft storey mechanism in the first floor of the eight storey building overestimating its interstorey drift, as shown in Figure 7.5b).

This overestimation of the response by the N2 method can be explained by the following reasons:

1) The N2 method calculates the single degree of freedom (SDOF) period independently of the seismic action intensity, thus also independently of the current structural stage. It uses the point of maximum acceleration of the capacity curve of the SDOF in order to bilinearize it and calculate the period. For SDOF periods higher than the spectral Tc the procedure advocates that the response of the SDOF is elastic. In the case studies analysed, mainly in the Turkish buildings, the periods of the SDOFs are always higher than the respective Tc. For intensity levels in which the response spectrum intersects the SDOF curve before the point of maximum acceleration, the period computed with the N2 method will be higher than the real one. Therefore, the displacements calculated elastically will be conservative. Note that, for instance, the CSM with the features proposed in FEMA440 computes the effective period of the SDOF based on the seismic intensity and on the current structural stage. For this, the method bilinearizes the SDOF capacity curve at the point of intersection with the response spectrum, computing the ductility

and then the effective period.

2) The use of the equal displacement rule assumed by the method for SDOF periods higher than Tc, may lead to conservative results [20]. In fact, the experience in nonlinear analysis shows that the peak responses are usually smoothed in the inelastic stage.

One can conclude that the N2 method gains in simplicity, leading to conservative but not exaggerated results. The use of this simplified procedure in design offices is worthwhile since there is an important and considerable saving on computation time when compared with the *time-history* analysis.

7.2 Assessing the seismic torsional response at the edges of the buildings

In this section the Extended N2 method results are compared with the original N2 method proposed in Eurocode 8 and with the nonlinear dynamic *time-history* median results for the columns located in the extremities of the buildings. Therefore, one can evaluate the performance of each method in estimating the torsional behaviour of the case studies. This comparison is done for all the buildings under analysis and for all seismic ground motion intensities. Next, the interstorey drifts and chord rotations are presented for the three storey building at the flexible edge, column C2, for different seismic intensities.

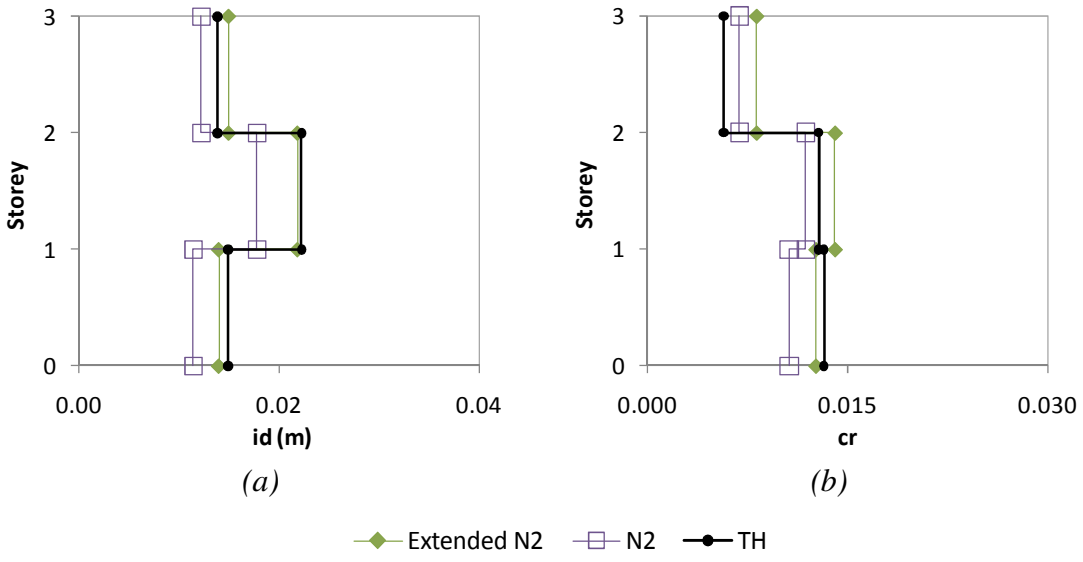

Figure 7.6 – a) Three storey building a) interstorey drifts C2, Y 0.1g b) chord rotation C2, Y 0.2g.

From Figure 7.6, one can see that the N2 method generally underestimates the interstorey drift and the chord rotation profiles over all the intensity levels analysed, on the flexible side of the building. This happens because the method cannot capture the seismic torsional effect that amplifies the response at this extremity of the building. On the other hand, the Extended N2 method can accurately capture this behaviour due to the use of a correction factor based on an elastic response spectrum analysis.

When dealing with plan-asymmetric buildings the normalized top displacements is the measure one should analyse in order to understand the torsional behaviour of the structure [4]. Several plots are presented showing the performance of the analysed procedures in estimating the torsional motion of the evaluated buildings. Figure 7.7 to Figure 7.13 illustrate the torsional response of the three buildings analysed by comparing the results obtained with both original and Extended N2 methods, with the *time-history* and with the response spectrum analysis (RSA). In the response spectrum analysis, the elastic response spectra were applied to the structure in both directions at the same time. The results were combined in the two directions using the SRSS combination, and the modes of vibration were combined using the CQC combination, as explained in section 4.2. The plots legends are represented in each figure, where TH stands for *time-history* and RSA for elastic response spectrum analysis.

From Figure 7.7a) one can see that, for the three storey building, for 0.1g in the X direction, the Extended N2 method captures very well the torsional response on both sides of the building. It perfectly reproduces the amplification of displacements on the flexible side of the building, column C2, while the original N2 method provides non-conservative results for this column. Both methods reproduce in a very good fashion the response at the stiff edge, column C8. The RSA is able to capture the torsional response on both sides of the structure.

Figure 7.7b) shows that the Extended N2 method reproduces in a very accurate way the response of column C8 for 0.3g, in the X direction. In fact, this extended procedure does not consider any de-amplification of displacements on the stiff side. On the contrary, the original N2 considers the de-amplification at this node, leading to underestimated results. The extended method overestimates the response on the flexible side for this intensity, while the original N2 reproduces the *time-history* results in a very good way. The RSA leads to the same results as the ones obtained with the Extended N2 method.

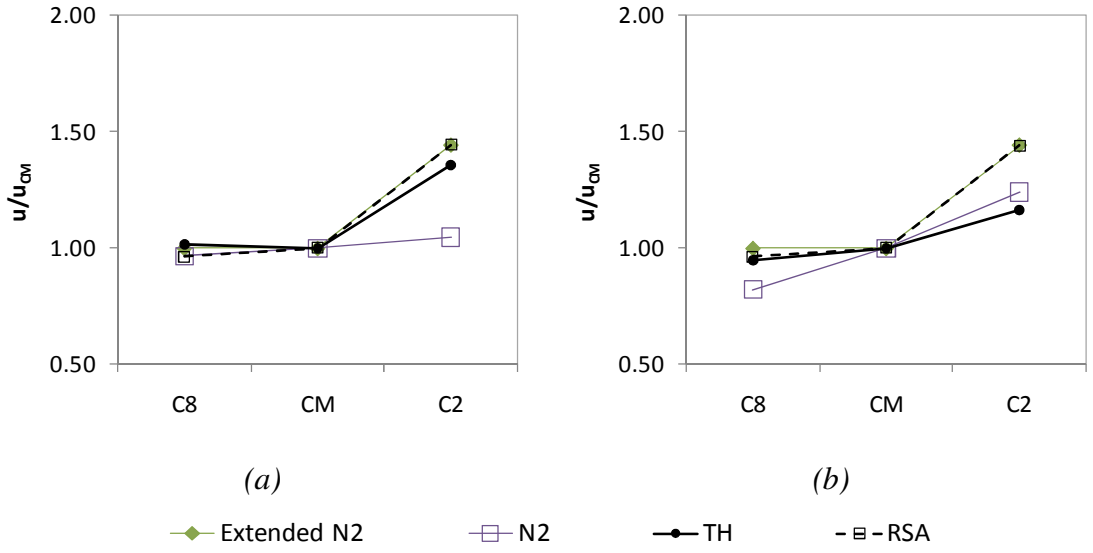

Figure 7.7 – Three storey X direction a) 0.1g, b) 0.3g.

From Figure 7.8, for 0.2g and 0.3g in the Y direction, one can see that the Extended N2 method reproduces in a very good manner the results in column C8 and overestimates the response of column C2. The original N2 method and the RSA underestimate the results at the stiff edge and overestimate the displacements at the flexible edge.

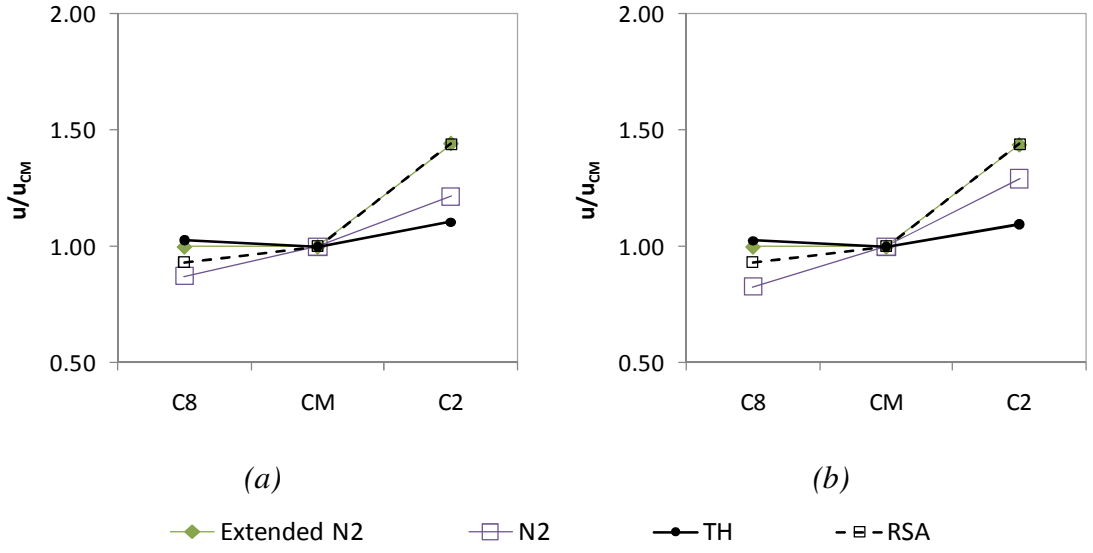

Figure 7.8 – Three storey Y direction a) 0.2g, b) 0.3g.

In the three storey building one can conclude that the N2 method always gives a linear estimation of the structural torsional motion from one side of the building to the other, for all intensity levels analysed. It usually considers the de-amplification at the stiff

edge, leading to underestimated results. On the other hand the Extended N2 method does not consider any de-amplification of displacements due to torsion.

Figure 7.9 to Figure 7.11 illustrate the torsional response of the five storey building in both X and Y directions, for the different intensity levels analysed.

In the five storey building, in the X direction for all intensity levels (except for 0.8g), Figure 7.9 and Figure 7.10, one can observe that the Extended N2 method accurately predicts the response of column S1, the flexible edge of the building, and overestimates the results in column S23, the stiff edge.

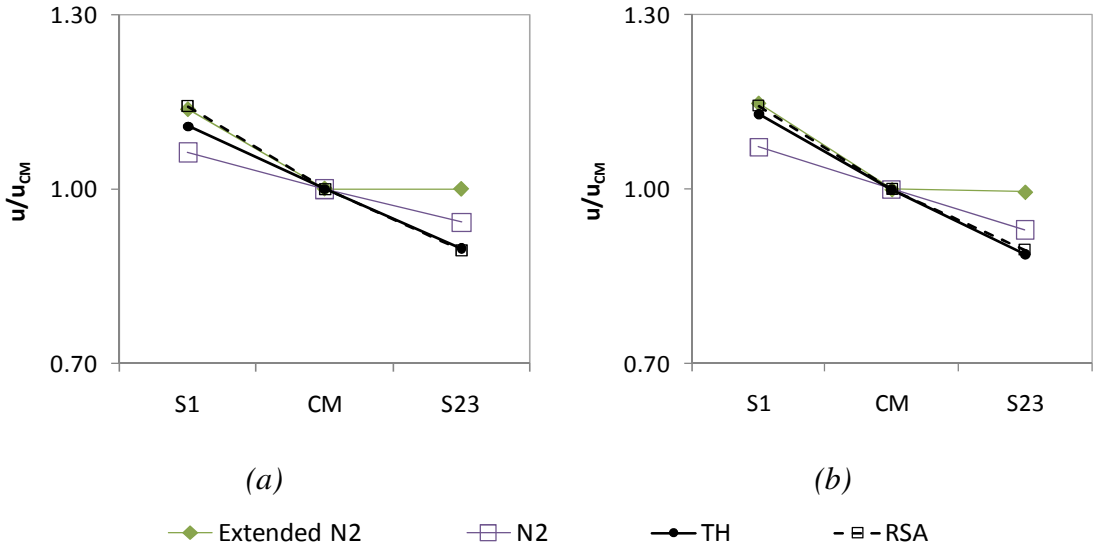

Figure 7.9 – Five storey X direction a) 0.1g, b) 0.2g.

This procedure does not consider the de-amplification of displacements due to torsion in column S23, the stiff side of the building. For 0.8g, Figure 7.11a), the Extended N2 method overestimates the response in column S1 and reproduces in a very accurate fashion the response of column S23.

In the X direction, for 0.1g and 0.2g, Figure 7.9, the N2 method underestimates the results in column S1 and overestimates the response in column S23. This procedure considers the de-amplification of displacements at the stiff edge caused by torsion.

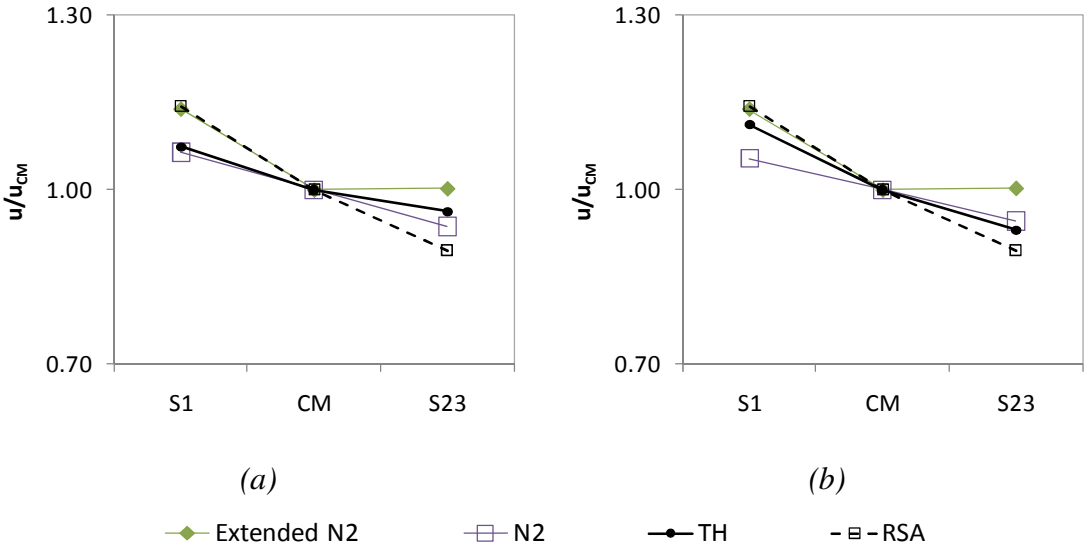

Figure 7.10 – Five storey X direction a) 0.4g, b) 0.6g.

From Figure 7.10 and Figure 7.11a), one can see that the original N2 method estimates correctly the response of the column S1 for 0.4g and 0.8g, and of the column S23 for 0.6g. It underestimates the displacements of column S23 for 0.4g and 0.8g, and of column S1 for 0.6g.

The results obtained by RSA in the X direction match the Extended N2 method on the flexible side of the building for all seismic intensities. This procedure leads to the same results as the *time-history* on the stiff side of the building for 0.1g and 0.2g. For 0.4g, 0.6g and 0.8g the RSA underestimates the results computed with the nonlinear dynamic analysis on this side of the building. Therefore, the theoretical approach of the Extended N2 method, by considering the RSA ratio equal to one when it is in fact smaller than one, allows the method to give conservative results.

In the Y direction, the Extended N2 method reproduces quite well the torsional behaviour of the building. The original N2 method generally underestimates the real response, except in column S1 for 0.1g and 0.4g where it matches the *time-history* median response. The RSA leads to the same results as the Extended N2 procedure on both sides of the building over all the seismic intensities.

For this building one can see that once again the N2 method always provides a linear estimation of the torsional motion for all intensity levels.

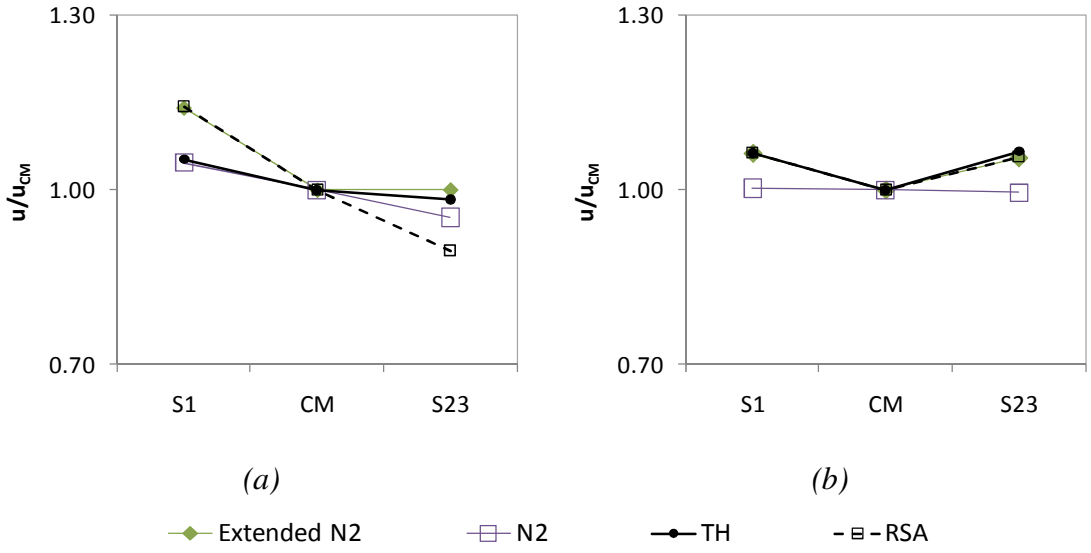

Figure 7.11 – Five storey a) X direction 0.8g, b) Y direction 0.8g.

In Figure 7.12 and Figure 7.13 the torsional behaviour of the eight storey building is plotted.

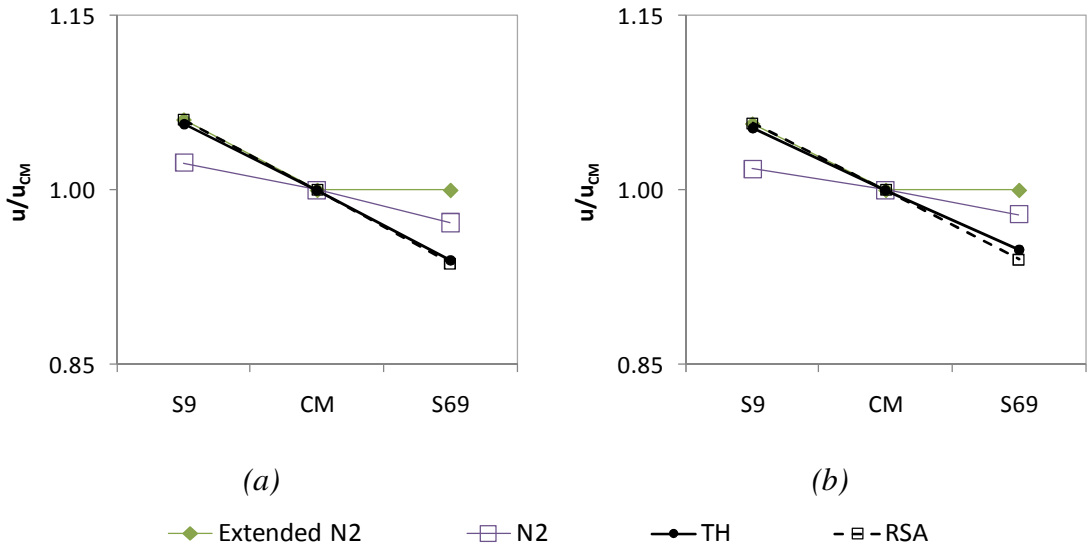

Figure 7.12 – Eight storey X direction a) 0.1g, b) 0.2g.

From Figure 7.12 and Figure 7.13a), it is clear that the Extended N2 method perfectly reproduces the response of column S9 in the X direction. It does not consider the de-amplification of displacements due to torsion in column S69, so the method overestimates the response on this side of the building. The original N2 underestimates the displacements in column S9 and overestimates the response of column S69. Note that the response in the X direction of the original and the Extended

N2 in column S69, gets closer as the ground motion intensity increases. The RSA leads to the same results as the *time-history* on both sides of the building in the X direction, through all the seismic intensities.

In the Y direction the Extended N2 method reproduces perfectly the response of column S9. It slightly overestimates the results of column S69 for 0.4g, Figure 7.13b).

The original N2 slightly underestimates the response in column S9 for 0.2g and 0.4g, and it captures the real motion of this column for 0.1g. In column S69 the method provides non-conservative results for 0.1g and 0.2g and it gets close to the nonlinear dynamic analysis for 0.4g. Along the lines of what happened in the previous two analysed buildings, in the eight storey building the N2 method provides a linear estimation of the structural torsional motion for all intensity levels analysed.

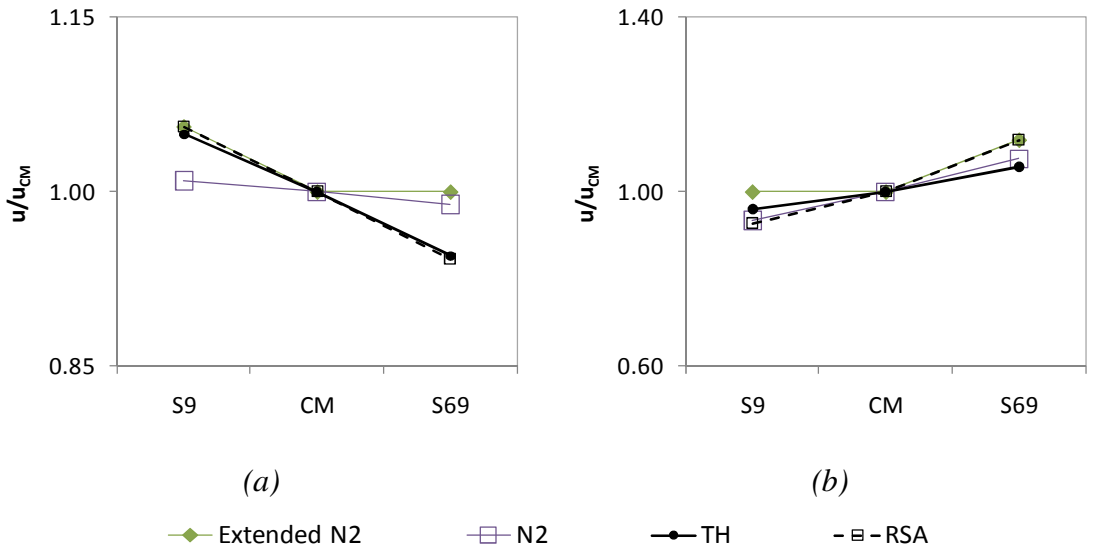

Figure 7.13 – Eight storey a) X direction 0.4g, b) Y direction 0.4g.

The results of the RSA match the Extended N2 method in column S69 in the Y direction for all intensity levels. The method underestimates the *time-history* results in column S9, once again for all seismic intensities.

7.3 Discussion

The obtained results lead to the conclusion that torsional effects are generally higher for lower ground motion intensities. For increasing seismic intensities, one can understand a flattening in the normalized top displacements. This can be seen in all

the buildings analysed. This conclusion confirms the idea that torsional effects are generally smaller in the inelastic range compared to what happens in the elastic one.

The plots clearly show that the RSA estimates an upper bound of the torsional amplification on the flexible side of the buildings, in both elastic and inelastic range.

The Extended N2 method reproduces in a good fashion the nonlinear dynamic results for all the buildings analysed and through all the seismic intensities tested. This method shows, for these case studies, a much better performance in estimating the torsional behaviour of the buildings than the original N2 method. Generally the latter is not capable of reproducing the torsional response of the buildings.

The plots presented above show that the Extended N2 method reproduces in a very accurate way the torsional amplification on the flexible edge in all the buildings analysed over all the increasing intensities. This good performance is explained because this extended procedure uses a correction factor based on a RSA which also leads to very good estimations of the torsional amplifications, as shown in the plots. The original N2 method generally underestimates the torsional amplification of the displacements on the flexible side.

From the plots it is evident that both RSA and the original N2 consider the torsional de-amplification on the stiff side of the buildings, leading in some cases to underestimated results. Figure 7.8 (column C8), Figure 7.10 (column S23), Figure 7.11a) (column S23) and Figure 7.13b) (column S9) illustrate the cases where the RSA leads to normalized top displacements smaller than one at the stiff edge, being these results non-conservative when compared with the *time-history*. Therefore, whenever the RSA leads to normalized top displacements smaller than one, the Extended N2 method considers this value to be equal to one. This recommendation avoids the extended method to produce non-conservative results on this stiff edge.

The N2 method always provides a linear estimation of the torsional motion from one side of the building to the other, through all the seismic intensities. The Extended N2 method does not consider any de-amplification of displacements due to torsion, leading in some cases to very accurate results and in others to conservative responses on the stiff edge of the buildings.

The results obtained herein seem quite optimistic regarding the implementation of this extended procedure in the next version of the Eurocode 8 as a nonlinear static method able to correctly deal with the torsional problems in plan-asymmetric buildings. However, one should be aware that the interplay between ground motion, inelastic

amplification or de-amplification of displacements and the structural system is complex. Therefore, more studies in different buildings should be developed in order to consolidate this nonlinear static approach.

8. Seismic assessment of real plan asymmetric buildings with commonly used Nonlinear Static Procedures

The use of Nonlinear Static Procedures (NSPs) for the seismic assessment of plan irregular buildings is challenging. The most common pushover-based approaches have led to adequate results in regular buildings, and hence, there is a need to verify the validity of such methods on the assessment of irregular structures.

In this chapter, four nonlinear static procedures - CSM-FEMA440, Extended N2, MPA, ACSM - are applied in the assessment of the three case studies used in this thesis. From the previous chapters one could conclude that:

- the CSM with the features proposed in FEMA440 led to better results than CSM-ATC40 in the buildings analysed;
- the Extended N2 method also presented a better performance than its original version.

Therefore, both CSM-ATC40 and the original N2 method will not be used in the next comparisons.

In this chapter, the accuracy of the different NSPs is evaluated through comparisons with the results derived from the most exact nonlinear dynamic analyses. The results are presented in terms of interstorey drifts, normalized top displacements, lateral displacement profiles, chord rotations, base shear and top displacement ratios. In the first three sections of the chapter the results of three case studies will be presented. Afterwards, the performance of the NSPs in evaluating the damage limitation according to Eurocode 8 is verified. In order to confirm that the buildings do not collapse due to brittle failures, the shear strength in some characteristic columns is also evaluated. Discussion and conclusions about the performance of each NSP are outlined at the end. The results of this chapter are presented in [128, 129].

8.1 Three storey SPEAR building

Presented herein are the representative plots that provide an idea about the relative accuracy of the NSPs under consideration in the seismic evaluation of the three storey SPEAR building.

8.1.1 Ratios between NSPs and *time-history*

In order to get a quick overview of how the different NSPs perform, ratios of the values obtained with the latter for different response parameters and the corresponding median estimates from the nonlinear dynamic analysis (Eq. 6.1) are computed.

The top displacement ratios in different locations of the building and in both directions are presented from Figure 8.1 to Figure 8.3. Note that the top displacements at the centre of mass correspond to the target displacements. In each figure and for each level of intensity, a vertical line representing the dispersion of the *time-history* (TH) results ([mean – standard deviation, mean + standard deviation]) is also plotted.

The plots illustrate how prediction of normalized roof displacements from the four above-mentioned NSPs varies with increasing intensity levels. All the NSPs gave reasonably good predictions at the centre of mass location, whereas biasness gets far from unity, albeit inconsistently throughout the intensity range, for normalized ratios at the flexible and stiffer edges.

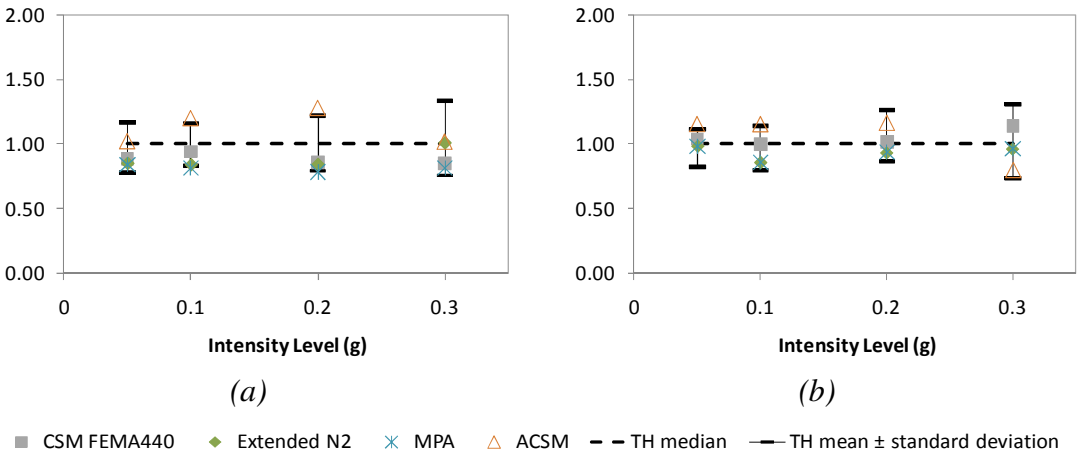

Figure 8.1 – a) Column C8, X; b) CM, X.

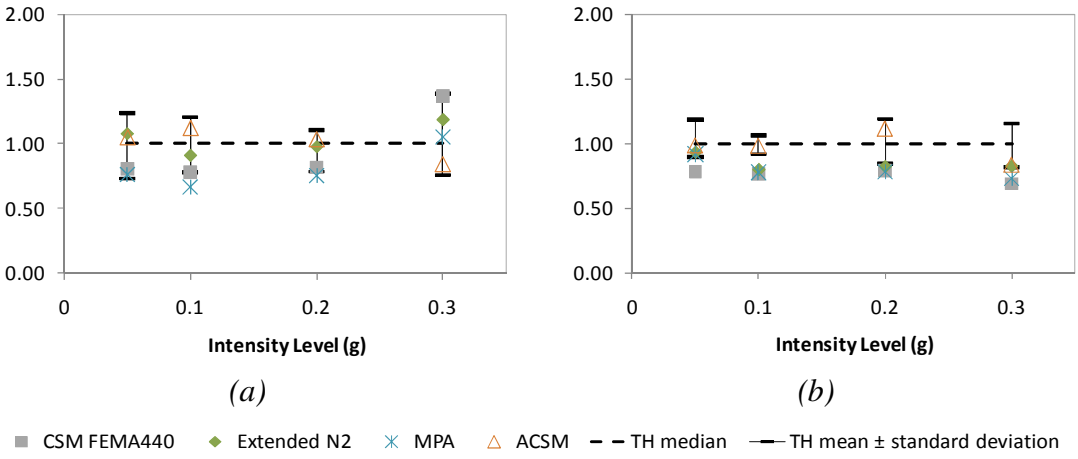

Figure 8.2 – a) Column C2, X; b) C8, Y.

The CSM-FEMA440 and MPA procedures generally underestimated the 'true' responses at the edges for all the intensity levels except at the flexible edge (column C2) for 0.3g where these procedures overestimated the response. In the CM in the X direction, the CSM-FEMA440 leads to very good results except for 0.3g where the method slightly overestimates the response. In the CM in the X direction the MPA perfectly matches the *time-history* results. In the Y direction, both methods lead to results very close to the *time-history* in the CM.

The Extended N2 method leads in general to good results in the CM and at the flexible edge (column C2) in the X direction. In the Y direction the method perfectly matches the *time-history* at the flexible edge.

The ACSM, on the other hand, predicted normalized roof displacement conspicuously well for all intensity levels except at 0.3g where, it underestimated it.

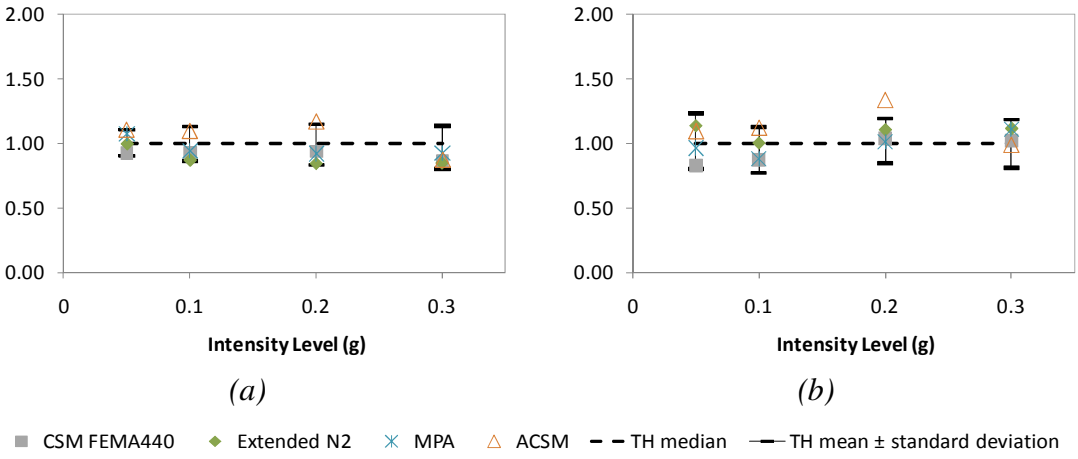

Figure 8.3 – a) Column CM, Y; b) C2, Y.

From the plots one can conclude that the dispersion of the *time-history* results is not very high, confirming that the number and type of records used in the three storey building seem to be sufficient to obtain reliable results. All the methods lead in general to results within the range [mean – standard deviation, mean + standard deviation], through all the seismic intensities in all locations analysed.

The ratios in terms of base shear are presented for both directions in Figure 8.4.

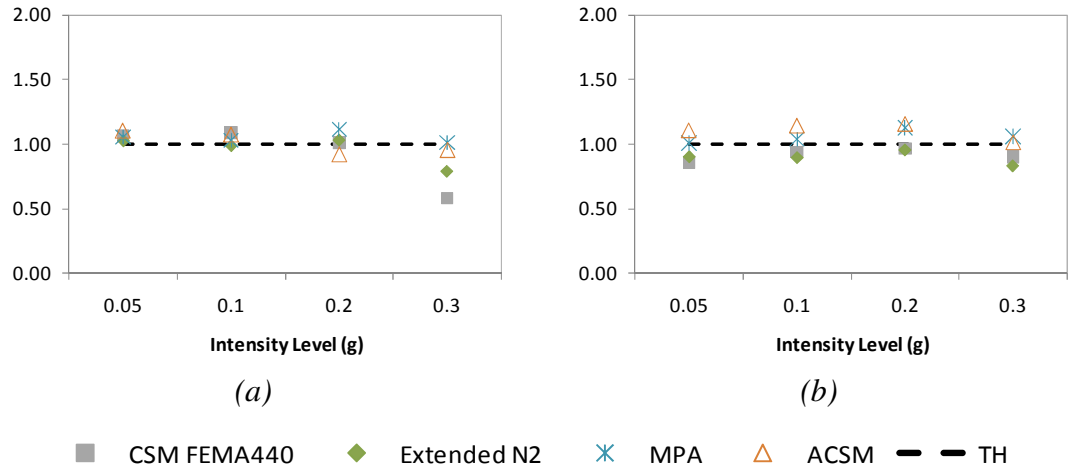

Figure 8.4 – a) X direction; b) Y direction.

Figure 8.4 demonstrates that all the NSPs predicted normalized base shear ratio appreciably well with a slight consistent overestimation by the ACSM in the Y direction. For 0.3g, the Extended N2 method and the CSM-FEMA440 underestimate the response in both directions. In the Y direction, both methods also underestimate the base shear for 0.05g.

8.1.2 Lateral displacement profiles

From Figure 8.5 to Figure 8.8 and in Appendix A5 are presented some representative plots of storey displacement profiles determined from different NSPs comparing with median profiles estimated from nonlinear dynamic analyses.

ACSM leads to conservative results for 0.05g, 0.1g and 0.2g in both directions. For very high levels of inelasticity, 0.3g, the method underestimates the response, except at the stiff edge (column C8) in the X direction and at the flexible edge (column C2) in the Y direction where it practically matches the *time-history*.

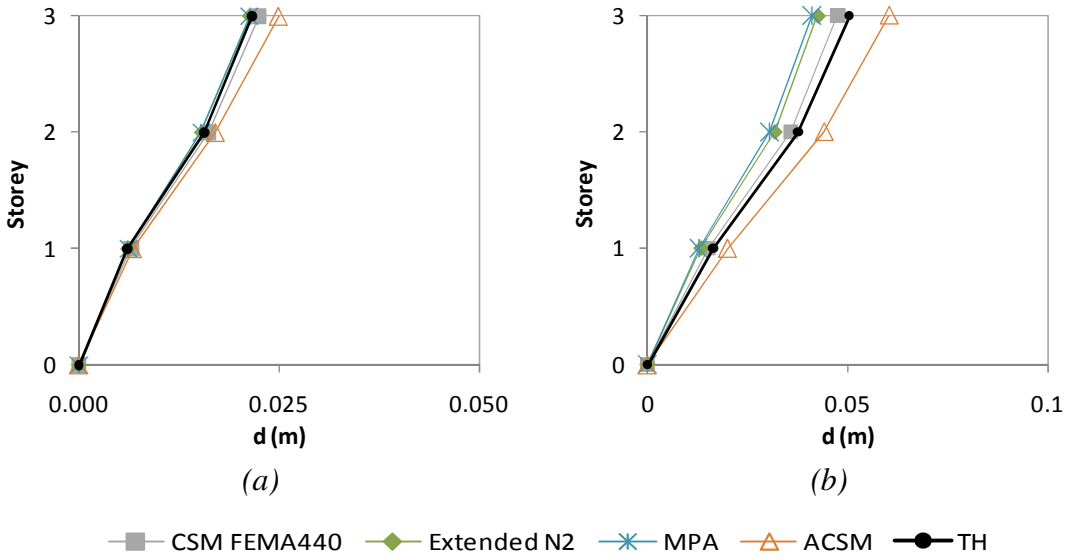

Figure 8.5 – X direction: a) Column C3, 0.05g; b) Column C8, 0.1g.

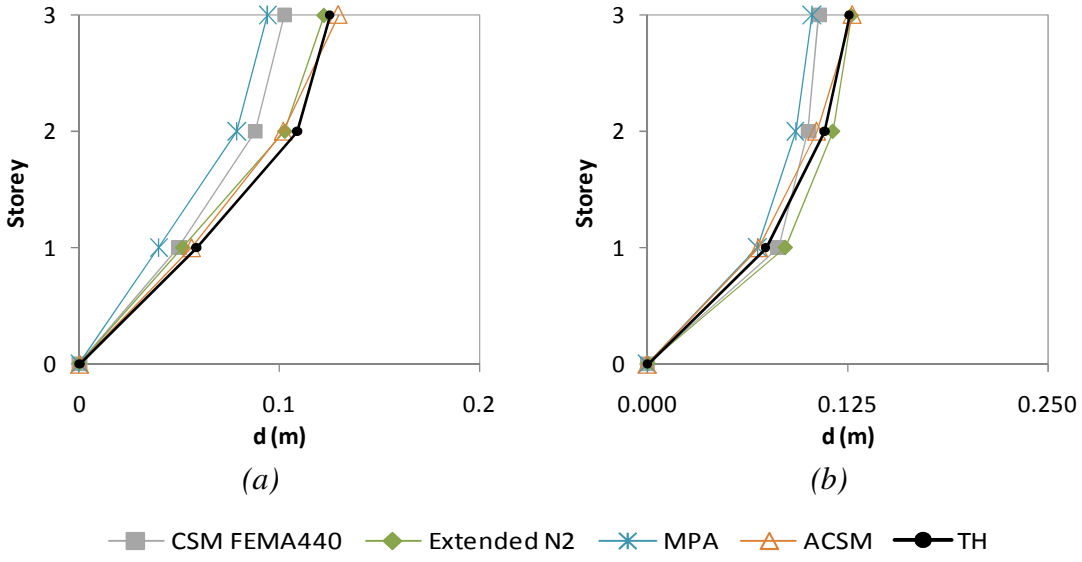

Figure 8.6 – X direction: a) Column C2, 0.2g; b) Column C8, 0.3g.

For 0.05g, 0.1g and 0.2g, the Extended N2 method usually underestimates the lateral displacements at the stiff edge (column C8). At the flexible edge the method gives good estimations, once again in both directions. For very high levels of inelasticity, 0.3g in the X direction, the method leads to good estimations at the stiff edge and at the central column, and it overestimates the response at the flexible edge. For the same intensity but now in the Y direction, the method underestimates the response at the stiff edge, but it practically matches the *time-history* at the flexible edge.

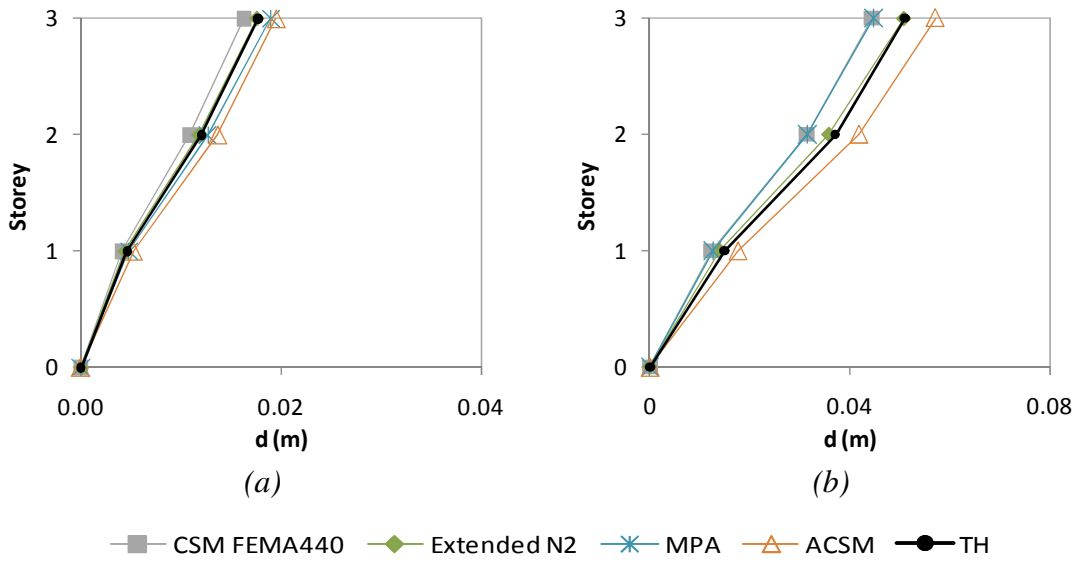

Figure 8.7 – Y direction: a) Column C3, 0.05g; b) Column C2, 0.1g.

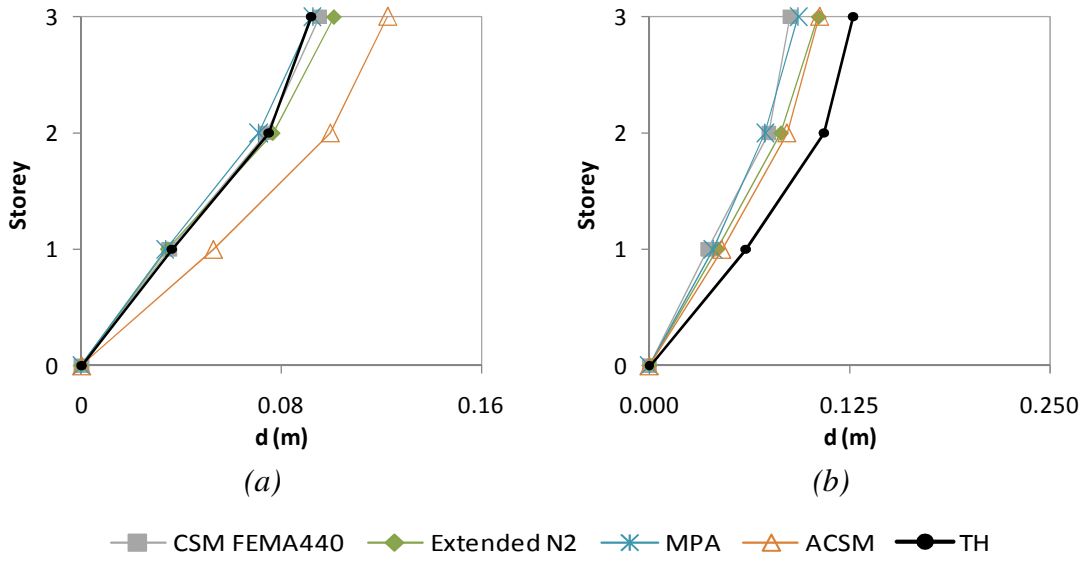

Figure 8.8 – Y direction: a) Column C2, 0.2g; b) Column C8, 0.3g.

For 0.3g in the X direction, the MPA leads to overestimated displacements at the flexible edge, good estimations at the central column, and underestimated displacements at the stiff edge mainly in the upper floors. For the same level of intensity but in the Y direction, the method slightly overestimates the displacements at the flexible edge.

In the X direction the CSM-FEMA440 practically matches the *time-history* in the central column C3, but it underestimates the response at the stiff and flexible edges of the building. For 0.3g (very high level of inelasticity) the method overestimates the displacements at the central column and at the flexible edge, but it underestimates the response on the stiff side of the building, mainly in the upper storeys.

8.1.3 Interstorey drifts and chord rotation profiles

Interstorey drift profiles are presented from Figure 8.9 to Figure 8.12 and in Appendix A6. Chord rotations are depicted in Figure 8.13, Figure 8.14 and in Appendix A7.

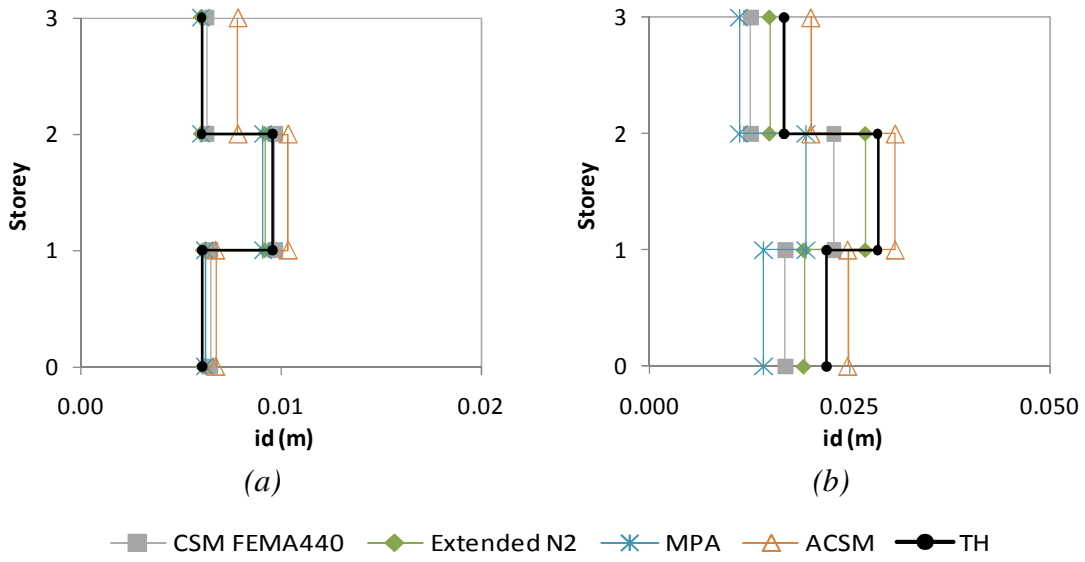

Figure 8.9 – Interstorey drifts X direction: a) Column C3, 0.05g; b) Column C2, 0.1g.

In the X direction, the ACSM usually leads to good estimations of the storey drifts and chord rotations, reproducing in a good way the response pattern. In the inelastic range, 0.2g and 0.3g, the method slightly underestimates the response on the second storey.

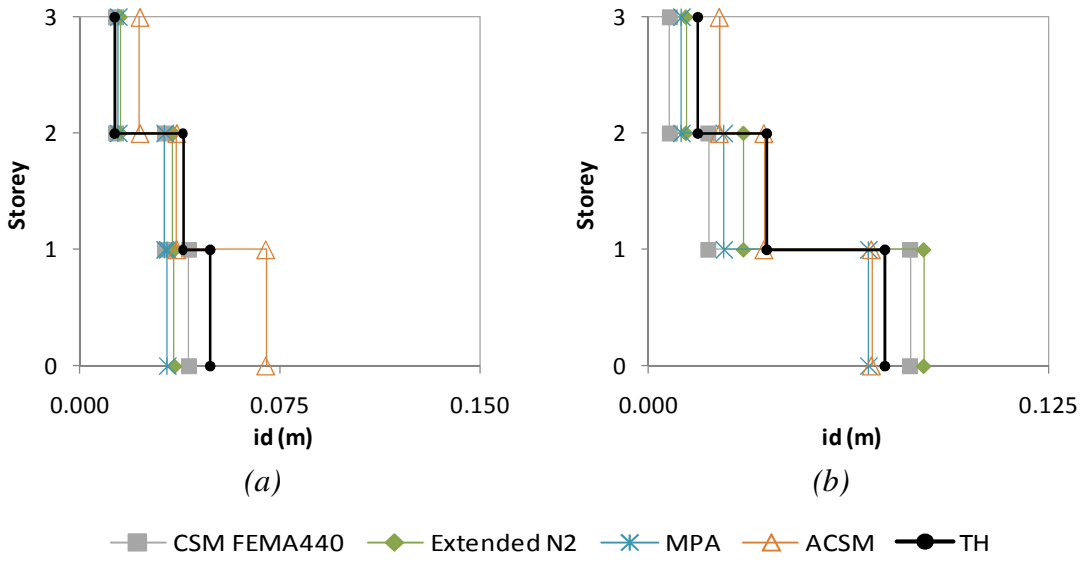

Figure 8.10 – Interstorey drifts X direction: a) Column C8, 0.2g; b) Column C8, 0.3g.

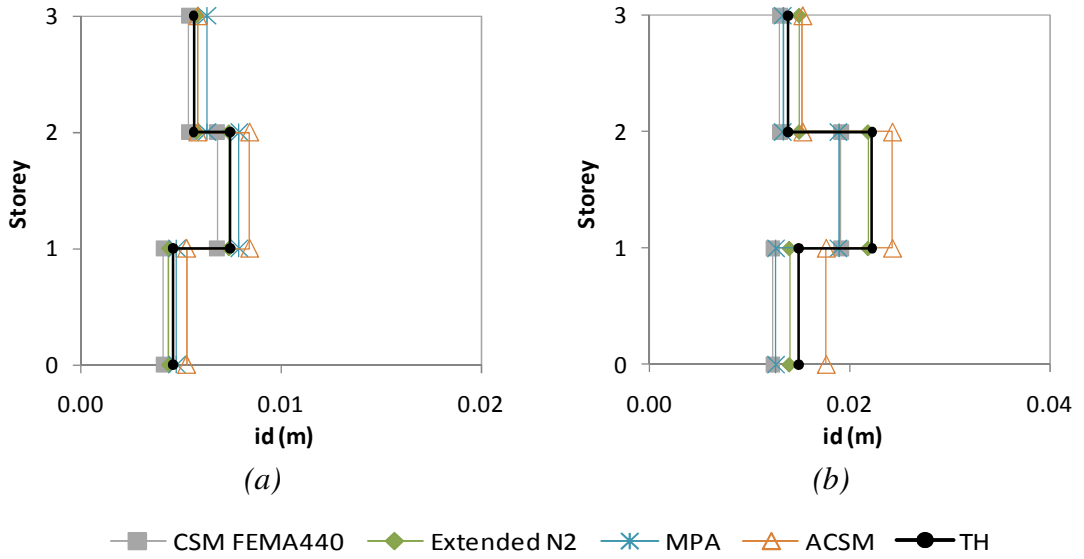

Figure 8.11 – Interstorey drifts Y direction: a) Column C3, 0.05g; b) Column C2, 0.1g.

In the Y direction, in the elastic range the ACSM can reproduce quite well the *time-history* response. For 0.2g, the method cannot completely reproduce the response profile, leading to conservative results on the first two storeys. For very high levels of inelasticity, 0.3g, it leads to underestimated responses on the first and on the second floors.

In the X direction, the Extended N2 method usually leads to non-conservative results on the stiff edge, but to good estimations at the flexible edge.

In the Y direction, the method is able to reproduce in a good way the response in terms of storey drifts and chord rotations at the flexible edge of the building, column C2.

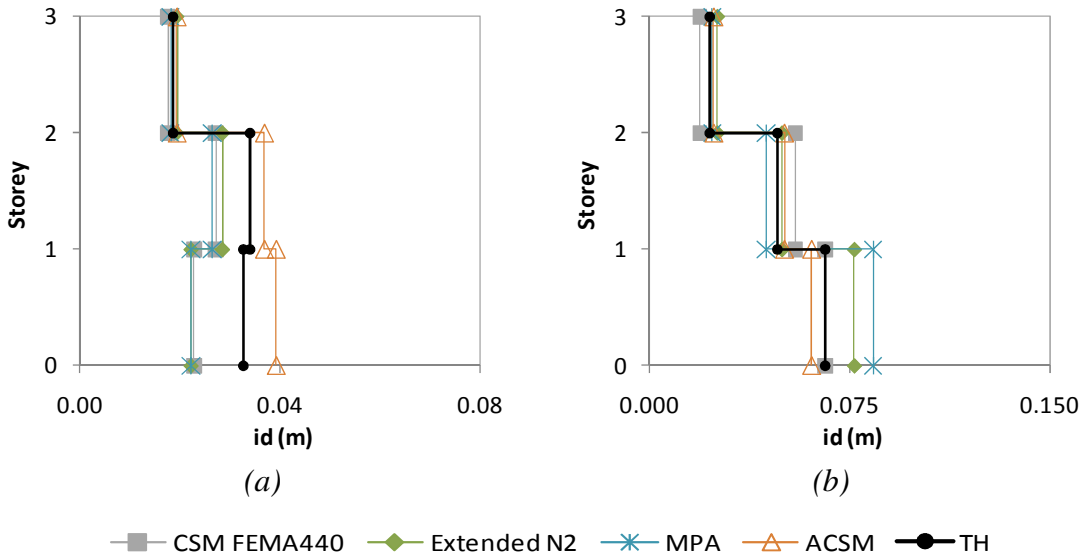

Figure 8.12 – Interstorey drifts Y direction: a) Column C8, 0.2g; b) Column C2, 0.3g.

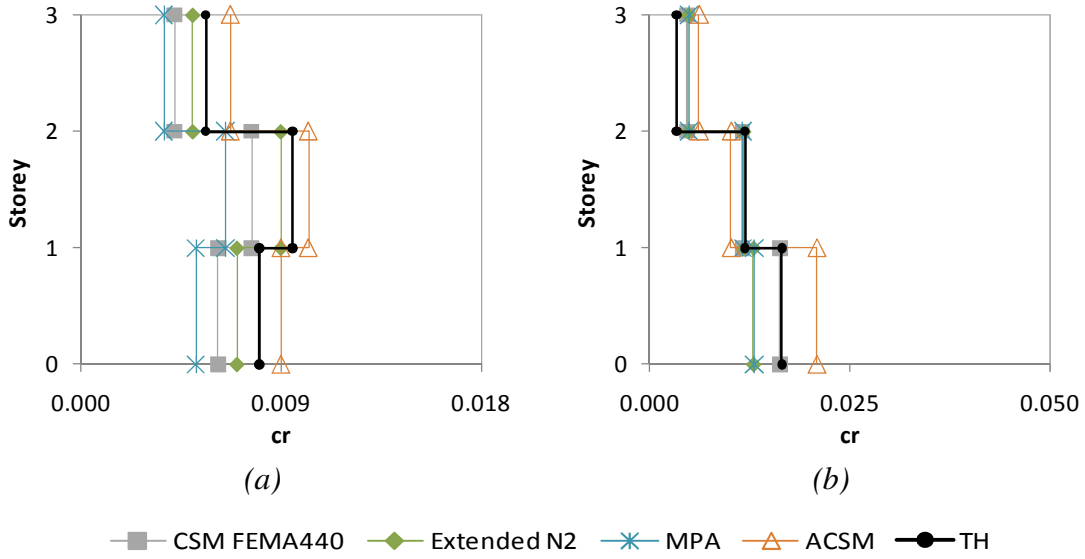

Figure 8.13 – Chord rotations X direction: a) Column C2, 0.1g; b) Column C3, 0.2g.

In both X and Y directions, the CSM-FEMA440 and the MPA usually underestimate the response. The exception occurs in column C3 where the methods are able to capture the response in a good manner.

In general, all NSPs are able to reproduce the storey drifts and chord rotations patterns correctly.

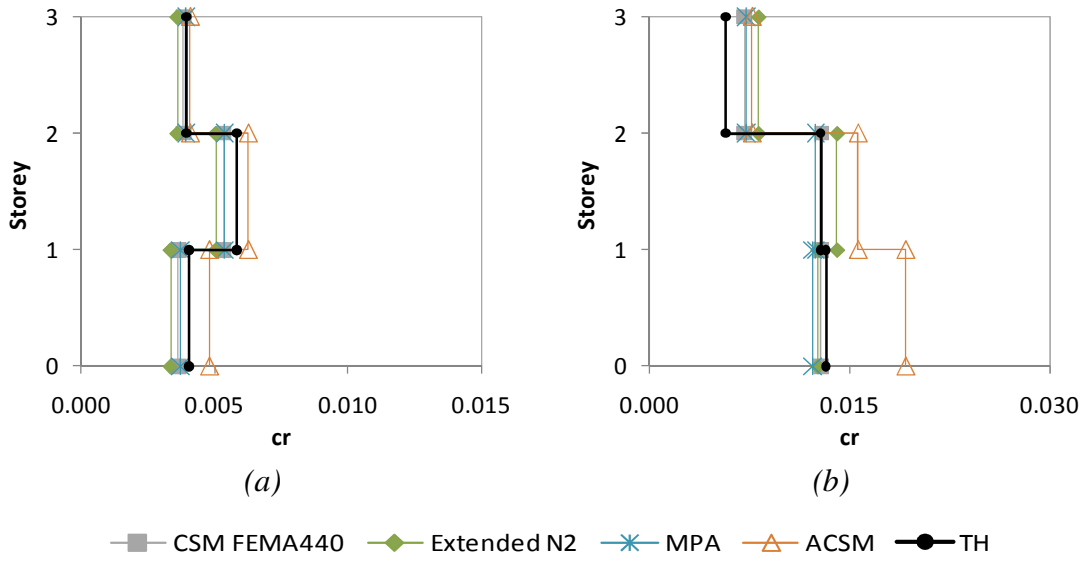

Figure 8.14 – Chord rotations Y direction: a) Column C3, 0.1g; b) Column C2, 0.2g.

8.1.4 Normalized top displacements

The pattern of roof displacements in plan normalized by the same at the centre of mass, as shown in Figure 8.15 and in Figure 8.16, gives an idea of how torsional rotation changes the displacement demands at the edges. Comparing the NSP predictions with the 'true' nonlinear dynamic responses, it is observed that the ACSM and torsional variant of N2 capture reasonably well the dynamic response whilst the MPA and CSM-FEMA440 underestimate it considerably at some locations, for instance at the flexible edge along the X direction and at the stiff edge along the Y direction. The torsional response in the *time-history* is taken from the step of the analysis corresponding to the maximum top displacement (in absolute value) at the centre of mass.

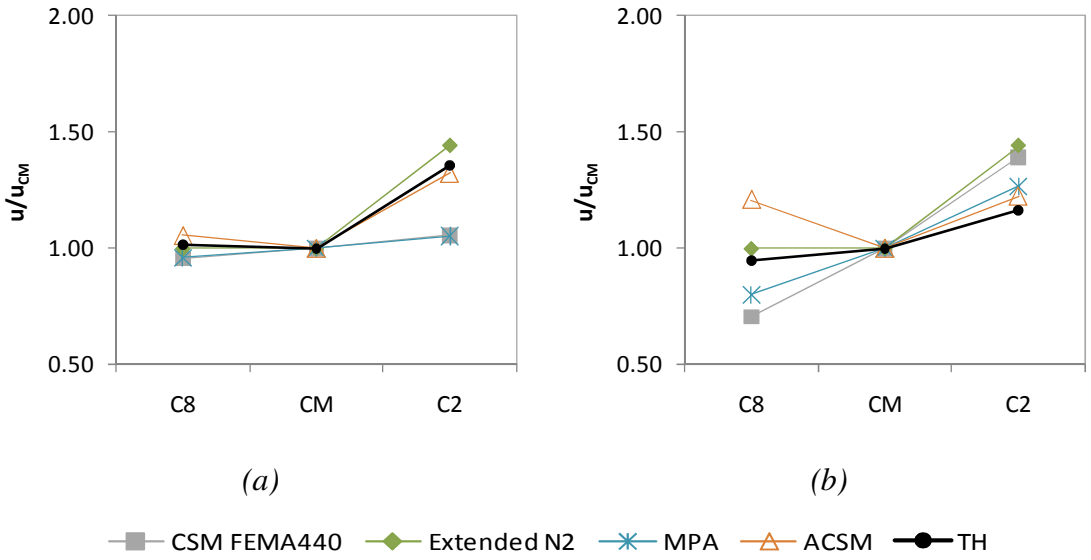

Figure 8.15 – X direction: a) 0.1g; b) 0.3g.

In the X direction, the Extended N2 method perfectly reproduces the response on the stiff edge of the building, column C8. The ACSM estimates in a very good fashion the displacements on this side of the building in the elastic stage but it considerably overestimates them in the inelastic range. The other two methods usually underestimate the response of column C8.

The ACSM perfectly reproduces the torsional amplification at the flexible edge, column C2, in the X direction in both elastic and inelastic range. The Extended N2 method usually overestimates this response. The other two procedures underestimate the torsional amplification on this side of the building in the elastic regime, but they overestimate it in the inelastic range.

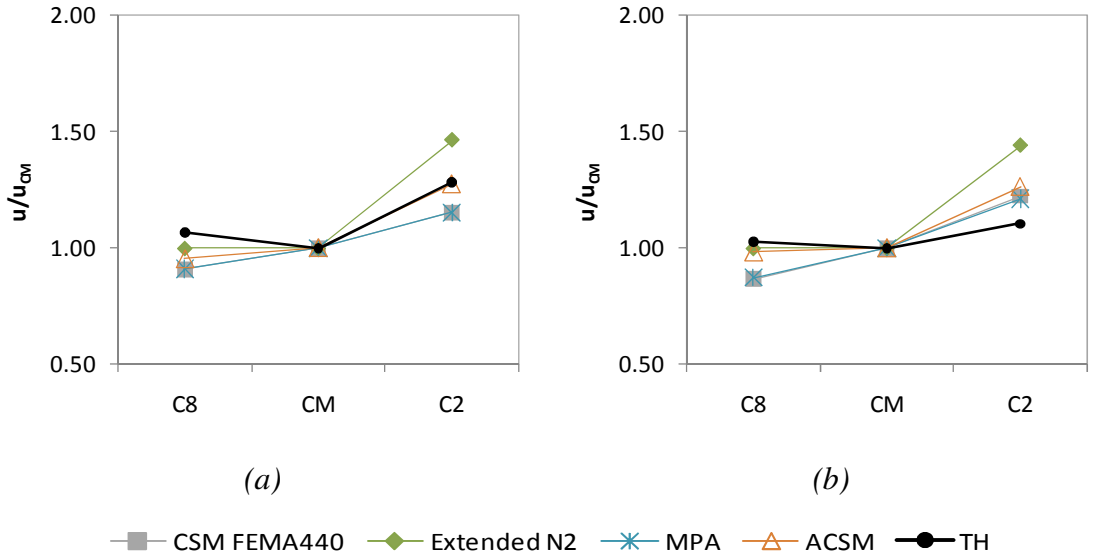

Figure 8.16 – Y direction: a) 0.05g; b) 0.2g.

In the Y direction, all NSPs tend to underestimate the response at the stiff edge, column C8, in the elastic range. In the inelastic stage, the Extended N2 method and the ACSM are able to correctly reproduce the displacements on this side of the building, while CSM-FEMA440 and MPA lead to non-conservative results.

At the flexible edge, column C2, in the Y direction, the Extended N2 method leads in general to overestimated results. The ACSM perfectly matches the *time-history* in the elastic stage and it overestimates the response in the inelastic regime. The other two methods provide underestimated responses in the elastic regime and overestimated normalized top displacements in the inelastic stage.

CSM-FEMA440 and MPA compute in general the same results in terms of normalized top displacements. They always estimate linearly the response from one side of the building to the other.

8.2 Five storey Turkish building

In this section, the five storey building is assessed comparing the NSPs under study with the *time-history* results. The same measures evaluated in the previous section are herein analysed for the five storey building.

8.2.1 Ratios between NSPs and *time-history*

The ratios between the NSPs and the *time-history* in terms of top displacements are plotted from Figure 8.17 to Figure 8.20.

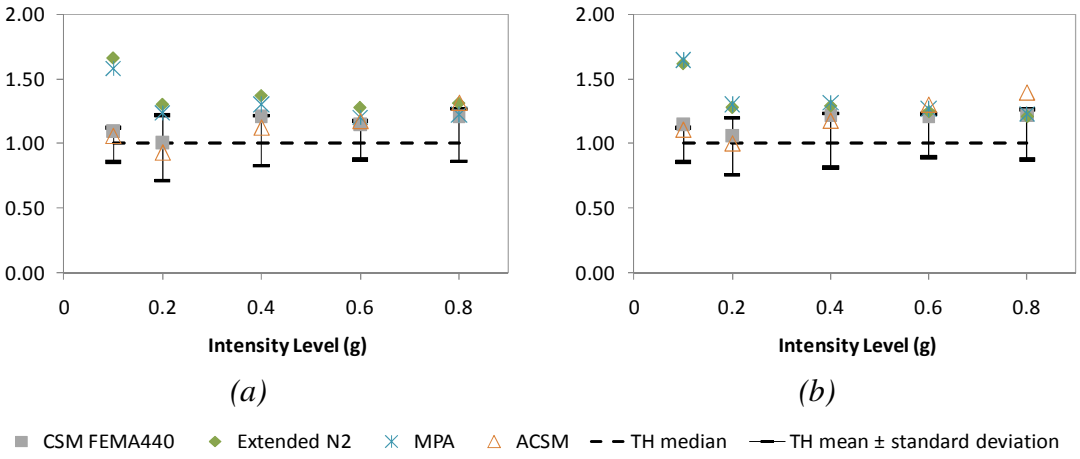

Figure 8.17 – a) Column S1, X; b) CM, X.

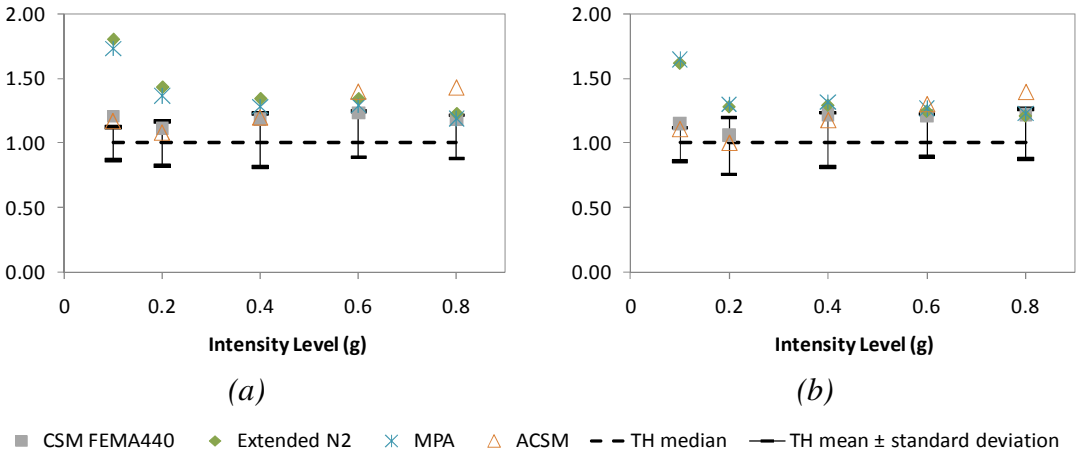

Figure 8.18 – a) Column S23, X; b) S13, X.

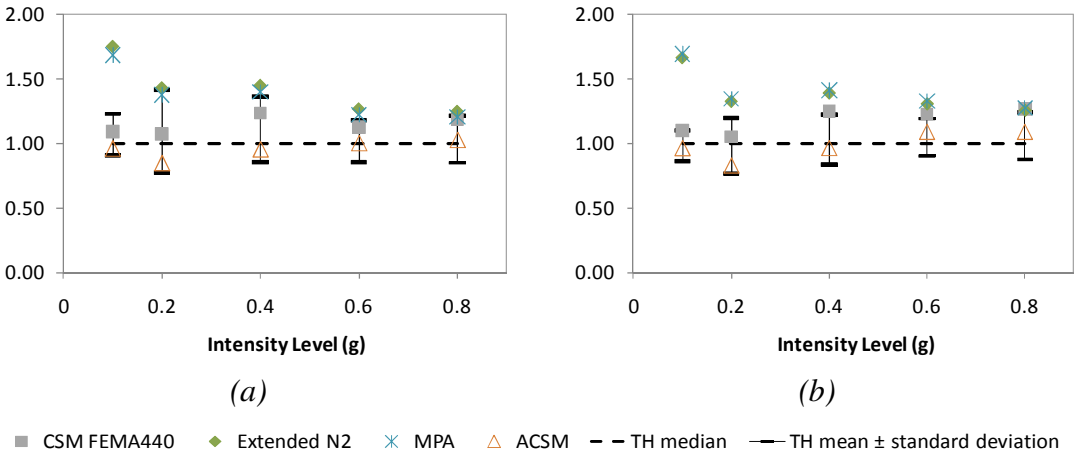

Figure 8.19 – a) Column S1, Y; b) CM, Y.

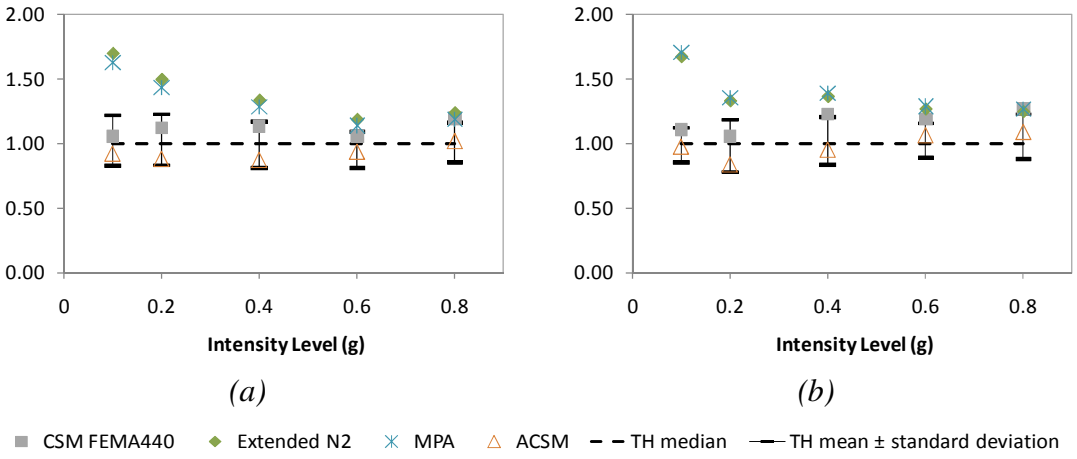

Figure 8.20 – a) Column S23, Y; b) S14, Y.

From the plots one can see that in the elastic or almost elastic stage (0.1g and 0.2g) the CSM-FEMA440 leads to estimations very close to the *time-history* in both directions. For these levels of intensity ACSM leads to very good results in the X direction and it under predicts the estimations in the Y direction. The Extended N2 method and the MPA overestimate the top displacements in this elastic stage.

In the inelastic regime (0.4g to 0.8g) in the X direction all the methods lead to approximately the same predictions and always on the conservative side. The exception occurs for 0.8g where ACSM leads to higher results than the other methods.

In the Y direction for 0.4g, ACSM leads to slightly underestimated results, while the other methods overestimate the response. For 0.6g and 0.8g, ACSM perfectly matches the *time-history* while the other methods lead to approximately the same results and always conservative. The exception occurs for 0.6g at the top of column S23 where ACSM underestimates the top displacement and CSM-FEMA440 matches the nonlinear dynamic results quite well.

From the plots, one can confirm that the dispersion of the *time-history* results is not very high, leading to the conclusion that the number and type of records chosen for this study proved to be sufficient to obtain reliable results in the five storey building. One can also observe that, as far as top displacement ratios are concerned, the ACSM and the CSM-FEMA440 lead in general to results close to the *time-history* median and always within the range [mean – standard deviation, mean + standard deviation]. This fact shows their good performance on estimating such a measure. The Extended N2 method and the MPA are generally close to the upper bound of this range, mean + standard deviation.

The same ratios are now presented for base shear in Figure 8.21.

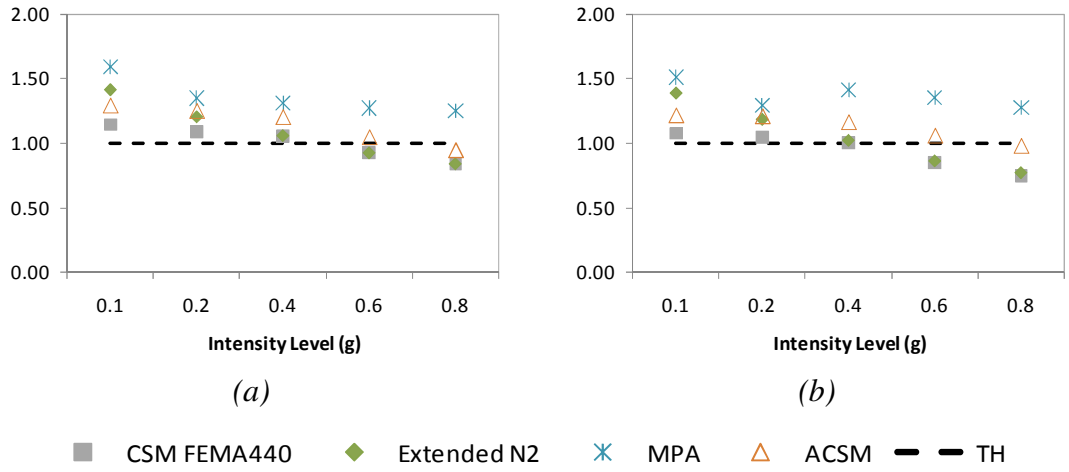

Figure 8.21 – a) X direction; b) Y direction.

From Figure 8.21 one can observe a decreasing linear trend on the base shear indexes in both directions for the ACSM, Extended N2 method and CSM-FEMA440. In the elastic or almost elastic stage these methods lead to conservative results, except CSM-FEMA440 which perfectly matches the *time-history*.

For 0.4g both Extended N2 and CSM-FEMA440 lead to the same results very close to the nonlinear dynamic analysis, whereas ACSM leads to overestimated results.

For 0.6g, the ACSM matches the *time-history*, while the Extended N2 method and the CSM-FEMA440 under predict the response. For 0.8g, these three methods lead to under conservative estimations, but the ACSM is closer to the *time-history*.

The MPA leads to conservative results and always higher than the other three methods.

8.2.2 Lateral displacement profiles

The comparison of the different NSPs and the nonlinear dynamic results in terms of lateral displacement profiles are plotted from Figure 8.22 to Figure 8.26 and in Appendix A8.

The results obtained from the parametric study developed for the five storey building show that the nonlinear static procedures generally lead to conservative results.

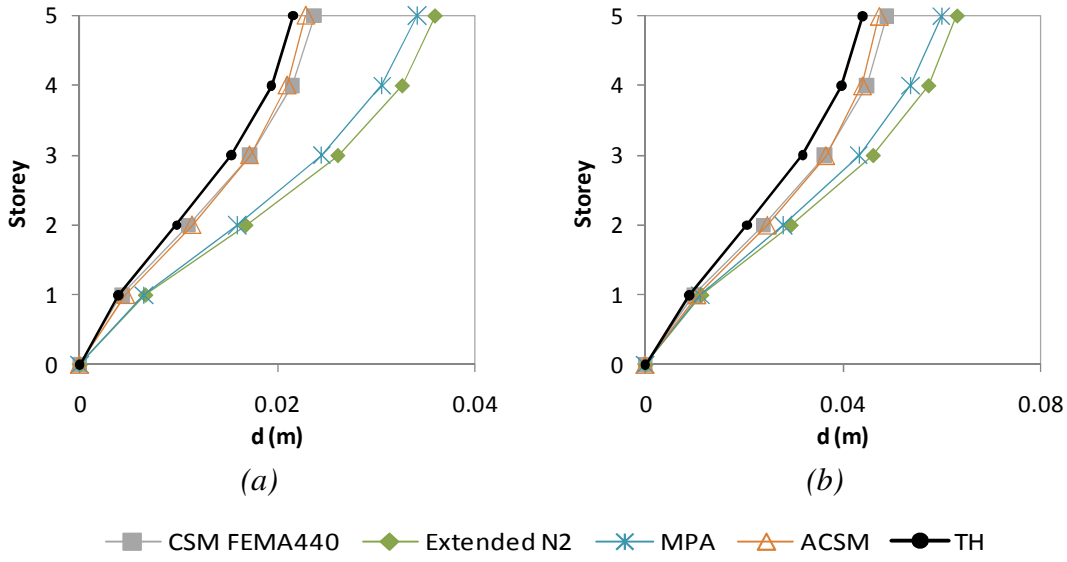

Figure 8.22 – X direction: a) Column S1, 0.1g; b) Column S23, 0.2g.

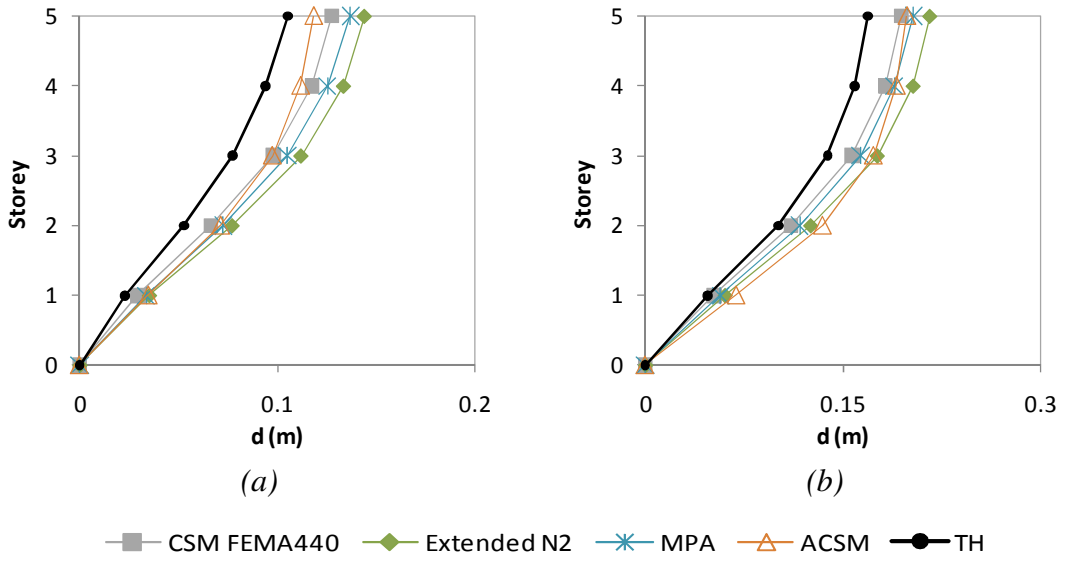

Figure 8.23 – X direction: a) Column S1, 0.4g; b) Column S1, 0.6g.

In the X direction, the asymmetric direction of the building, one can clearly conclude that for the elastic or almost elastic regime:

- The results computed with CSM-FEMA440 and ACSM match the *time-history* analysis;
- Both Extended N2 and MPA procedures generally lead to conservative estimations.

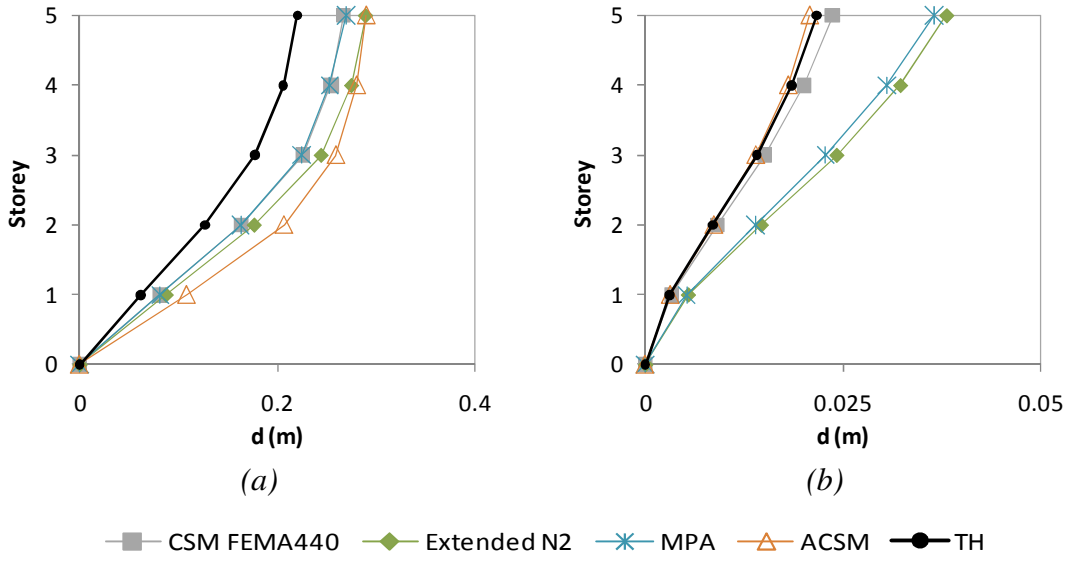

Figure 8.24 – a) Column S1, X 0.8g; b) Column S1, Y 0.1g.

In the inelastic regime, all NSPs tend to reproduce the response of the building in the X direction conservatively.

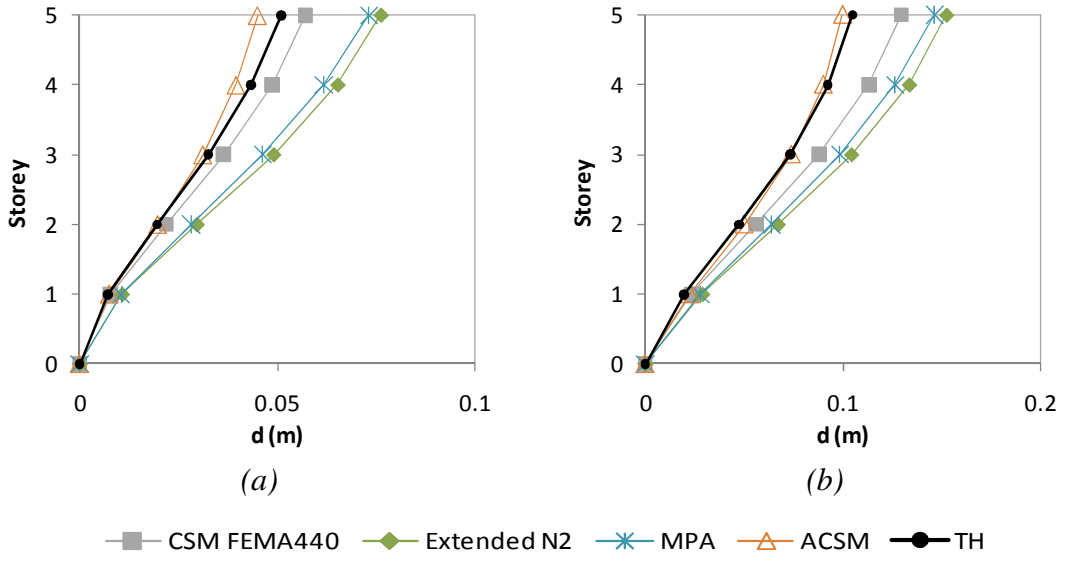

Figure 8.25 – Y direction: a) Column S23, 0.2g; b) Column S1, 0.4g.

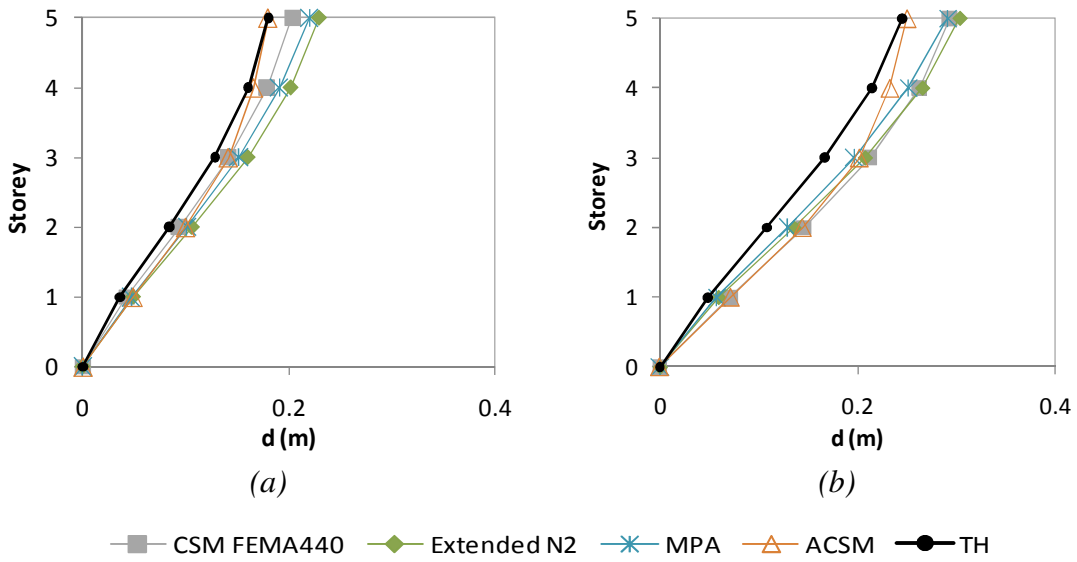

Figure 8.26 – Y direction: a) Column S1, 0.6g; b) Column S23, 0.8g.

In the Y direction, the symmetric direction of the building, the results for the elastic or almost elastic range, show that:

- The CSM-FEMA440 and the ACSM lead to results very close to the nonlinear dynamic analysis. Although, ACSM sometimes leads to under conservative results in the upper floors;
- The Extended N2 and the MPA methods lead to conservative results.

For medium levels of inelasticity (0.4g) in the Y direction one can observe that:

- The ACSM matches the *time-history* analysis. However this method sometimes leads to non conservative results in the upper floors;
- The other three methods lead to conservative results, but CSM-FEMA440 is the method closer to the nonlinear dynamic results.

For higher levels of inelasticity (0.6g and 0.8g) in the Y direction:

- The results computed with ACSM get close to the *time-history* response;
- The CSM-FEMA440, the Extended N2 method and the MPA lead to similar and conservative results.

8.2.3 Interstorey drift and chord rotation profiles

The interstorey drift profiles obtained using the different NSPs are presented from Figure 8.27 to Figure 8.31 and in Appendix A9.

The corresponding chord rotation profiles are plotted in Figure 8.32 and Figure 8.33 and in Appendix A10 .

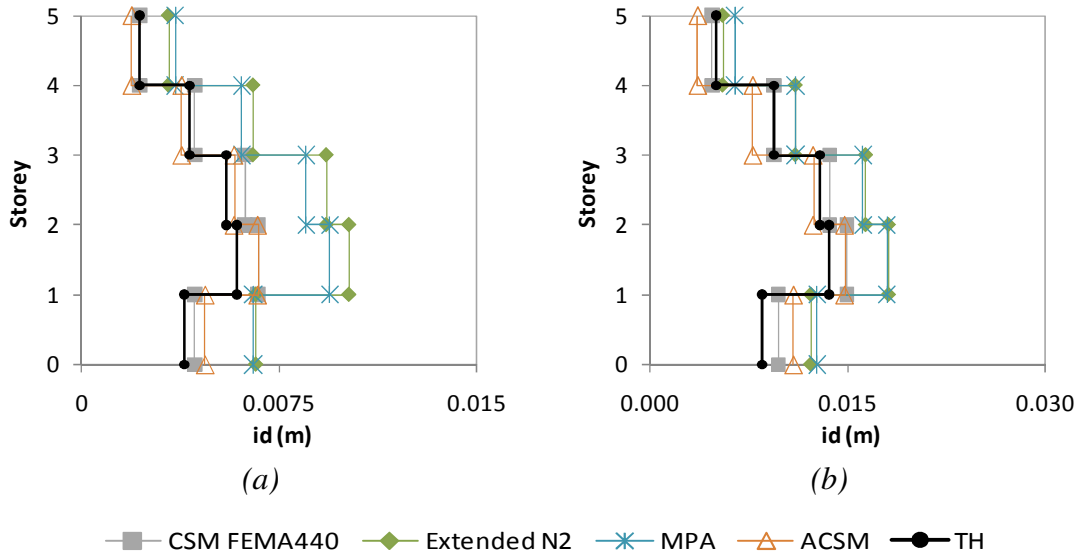

Figure 8.27 – Interstorey drifts X direction: a) Column S1, 0.1g; b) Column S13, 0.2g.

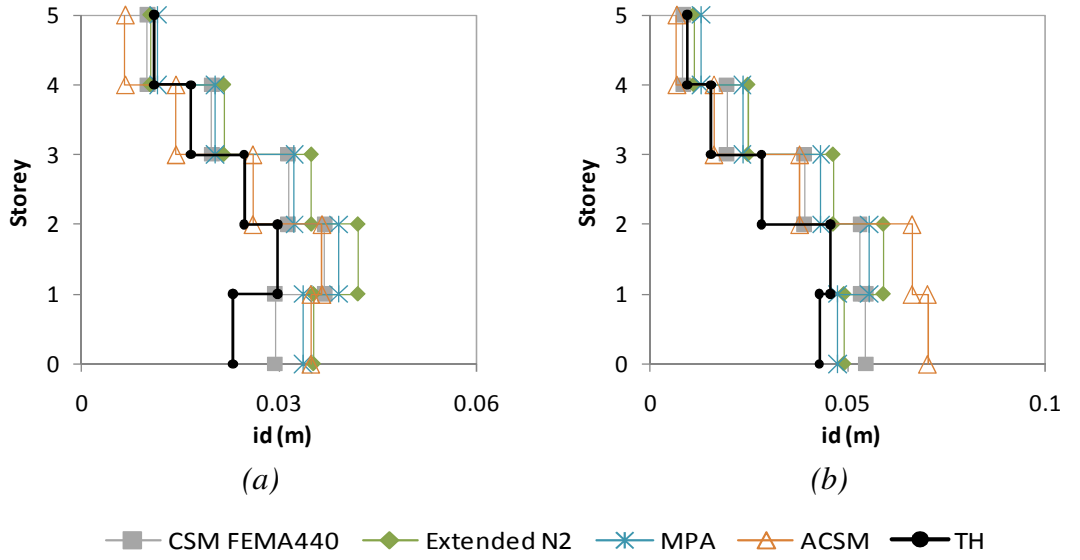

Figure 8.28 – Interstorey drifts X direction: a) Column S1, 0.4g; b) Column S23, 0.6g.

From the plots one can conclude that in the X direction for the elastic or almost elastic range:

- The CSM-FEMA440 matches the *time-history* results quite perfectly;
- The ACSM leads to good results in the first three floors, but it slightly underestimates the response in the two upper floors;
- The Extended N2 method and the MPA lead to conservative results although, they get close to the *time-history* for 0.2g;
- All the methods can reproduce the response patterns in all the floors in the elastic or almost elastic stage.

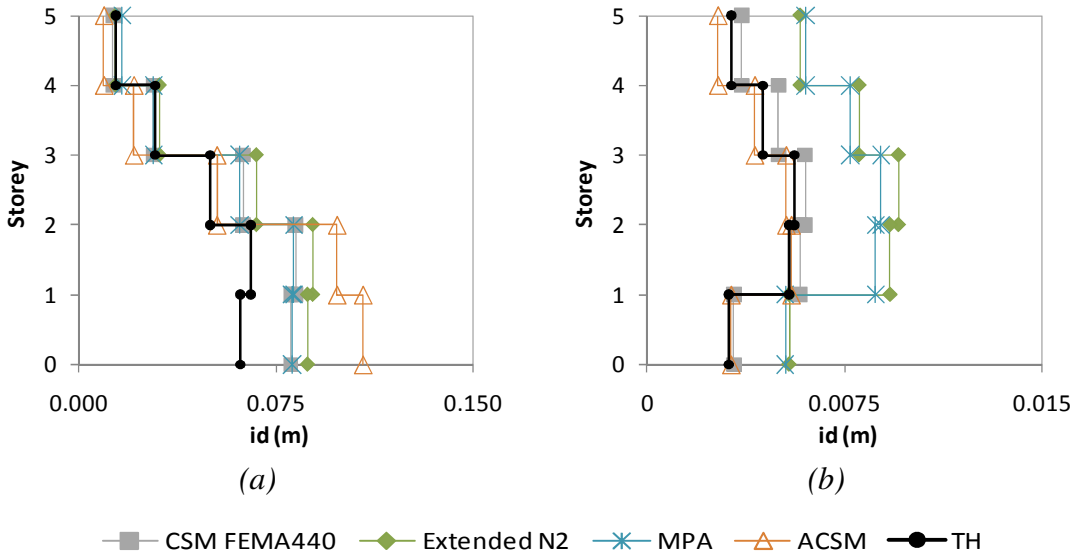

Figure 8.29 – Interstorey drifts a) Column S1, X, 0.8g; b) Column S1, Y, 0.1g.

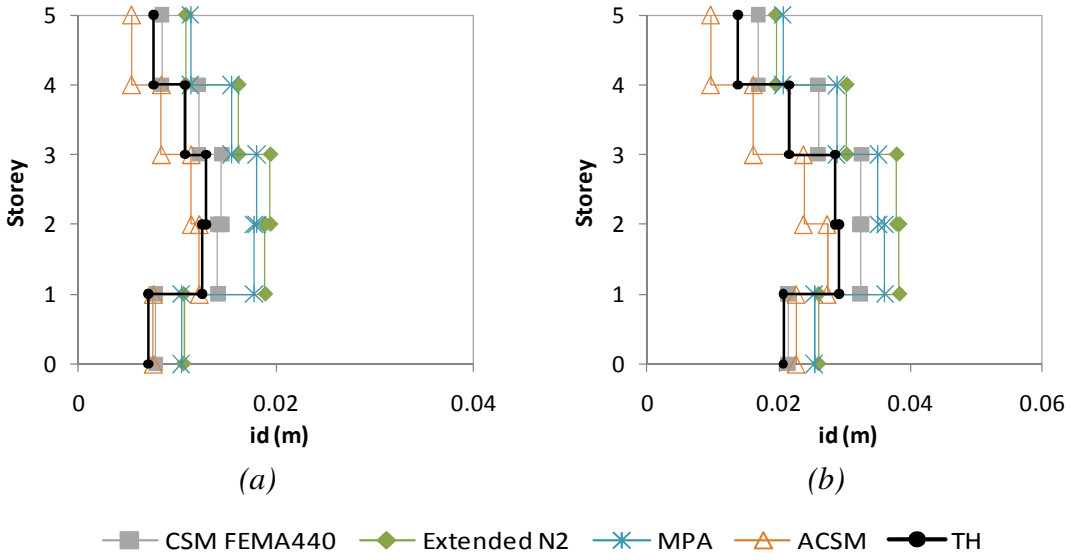

Figure 8.30 – Interstorey drifts Y direction: a) Column S1, 0.2g; b) Column S23, 0.4g.

In the X direction and in the inelastic range:

- The Extended N2 method, the MPA and the CSM-FEMA440 lead to slightly conservative results but generally close to the *time-history*;
- The ACSM leads to conservative results in the lower floors and to slightly non-conservative estimations in the upper floors;
- For high levels of inelasticity (0.6g and 0.8g), ACSM cannot reproduce the interstorey drift nor the chord rotation patterns, mainly in the first two floors;
- The other three methods reproduce in a very good fashion the response patterns through all inelastic stages in all the floors.

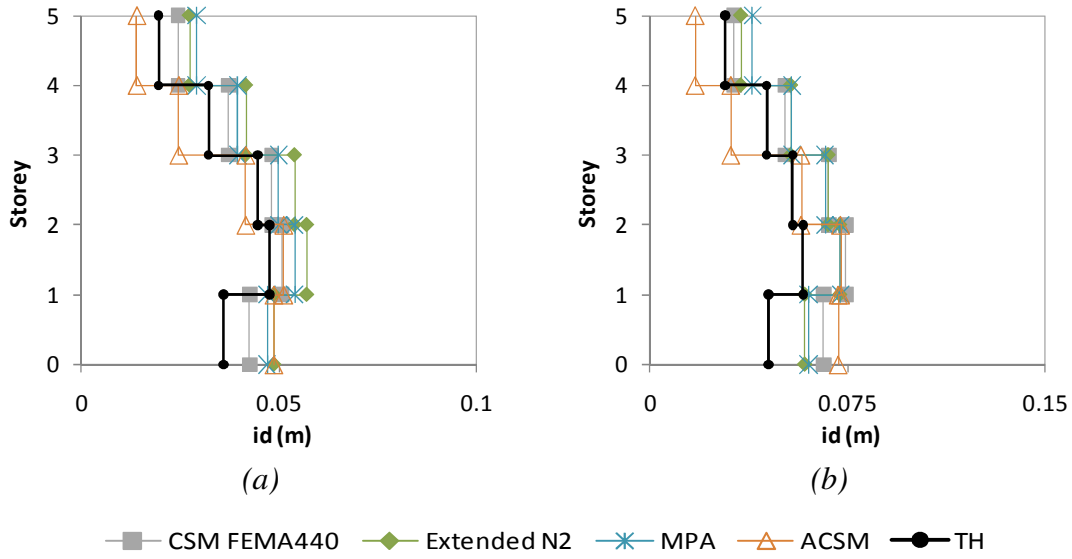

Figure 8.31 – Interstorey drifts Y direction: a) Column S1, 0.6g; b) Column S14, 0.8g.

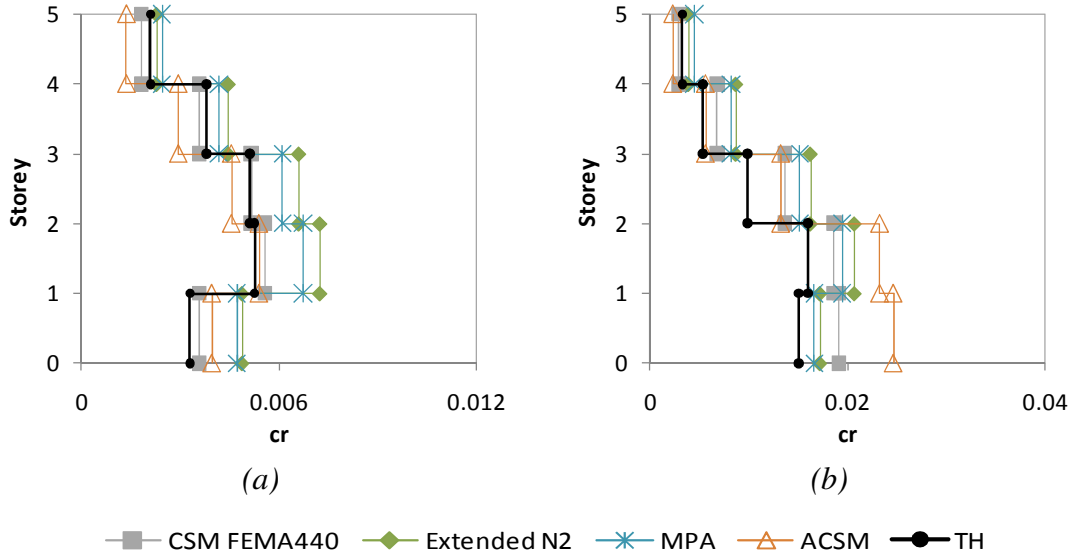

Figure 8.32 – Chord rotations X direction: a) Column S1, 0.2g; b) Column S23, 0.6g.

In the Y direction for the elastic or almost elastic range:

- The CSM-FEMA440 perfectly matches the *time-history* results;
- The ACSM leads to results very close to the *time-history* but slightly underestimated in the upper floors;
- The Extended N2 and the MPA lead to conservative results;
- All methods are able to correctly reproduce the response patterns in all the floors.

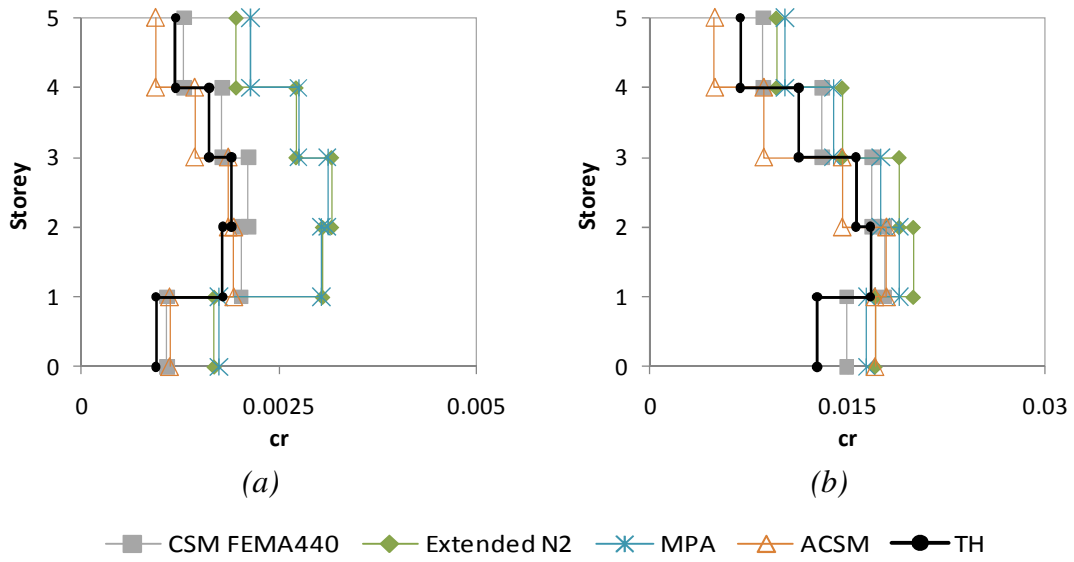

Figure 8.33 – Chord rotations Y direction: a) Column S13, 0.1g; b) Column S1, 0.6g.

In the Y direction for medium levels of inelasticity:

- The CSM-FEMA440 leads to slightly conservative results;
- The ACSM leads to slightly underestimated responses;
- The other two methods lead to conservative results;
- All methods are able to correctly reproduce the response patterns in all the floors.

In the Y direction for high levels of inelasticity:

- The CSM-FEMA440, the Extended N2 and the MPA lead to slightly conservative results;
- The ACSM leads to slightly non-conservative estimations on the upper floors and to conservative results on the lower floors;
- All methods are able to correctly reproduce the response patterns in all the floors, except ACSM which is not able to reproduce the pattern on the first storey.

8.2.4 Normalized top displacements

In order to study the torsional behaviour of the building, the trend of normalized top displacements are also analysed in this section.

These measures are plotted in Figure 8.34 and Figure 8.35, in the X direction for increasing seismic intensities.

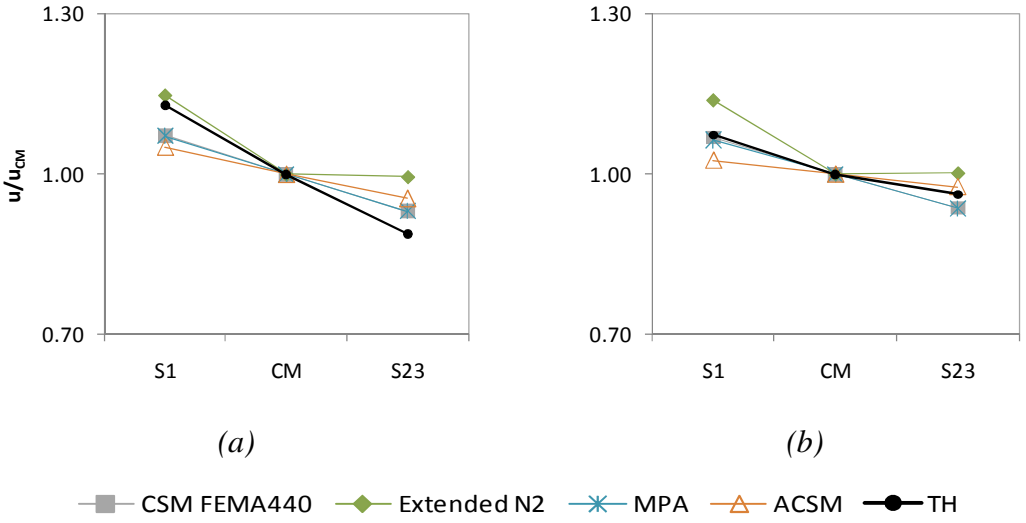

Figure 8.34 – X direction: a) 0.2g; b) 0.4g.

In terms of normalized top displacements, the Extended N2 was the method that better reproduced the torsional motion of the building in the X direction (the asymmetric direction of the structure). In fact, the method perfectly captures the torsional amplification at the flexible edge of the building, column S1, for 0.2g and 0.6g. For 0.4g and 0.8g it slightly overestimates the response. The Extended N2 method led to conservative results on the stiff side of the building, column S23, over all the seismic intensities, because it does not consider any de-amplification effect due to torsion.

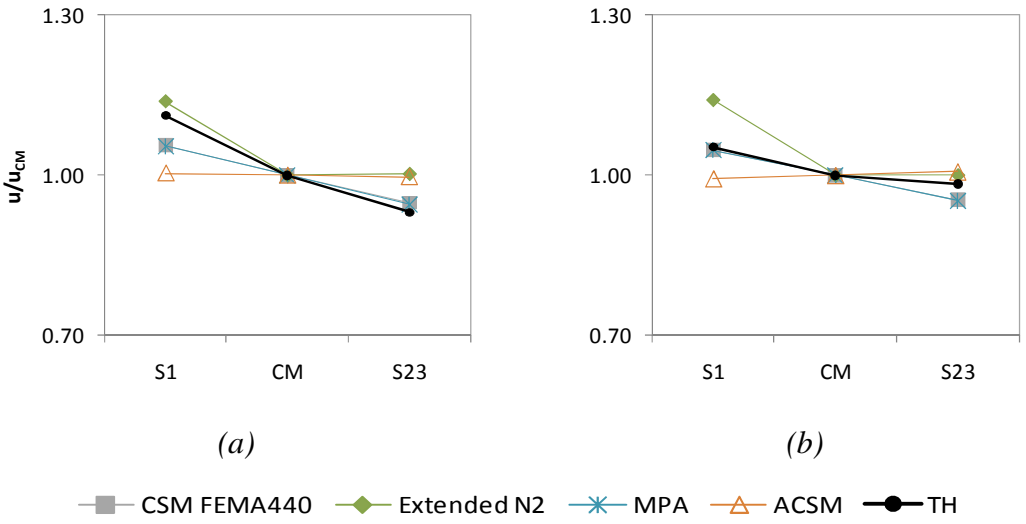

Figure 8.35 – X direction: a) 0.6g; b) 0.8g.

The CSM-FEMA440 and the MPA led to the same normalized top displacements results. They perfectly reproduced the *time-history* on the flexible side for 0.4g and 0.8g, but they underestimated the results for 0.2g and 0.6g. The methods slightly overestimate the response on the stiff side for 0.2g and 0.6g, but they led to non conservative estimations for 0.4g and 0.8g.

The ACSM generally underestimated the results at the flexible side through all the seismic intensities tested. On the other hand, the procedure led to overestimated results at the stiff edge for 0.2g and 0.6g. For 0.4g and 0.8g the method reproduced in a very good manner the response on this side of the building.

The CSM-FEMA440, the MPA and the ACSM always predicted the torsional motion of the building in a linear way from one side of the building to the other. The Extended N2 method does not estimate this motion linearly because no de-amplification due to torsion is taken into account in its theoretical background.

One can also notice a flattening in the normalized top displacements curves as the seismic intensity increases. This fact confirms the idea that the torsional effects are higher for lower levels of seismic intensity, reducing its effect for major seismic intensity levels.

8.3 Eight storey Turkish building

The results obtained for the eight storey building are presented in this section. As was concluded from section 5.3, the eight storey building behaves inelastically only in the X direction, but it remains elastic along the Y direction. Therefore, the results presented herein are mainly focused on the X direction.

8.3.1 Ratios between NSPs and *time-history*

The ratios of top displacements at the centre of mass and of the base shear, for all the seismic intensities studied, are plotted from Figure 8.36 to Figure 8.38 and in Appendix A11. The dispersion of the *time-history* results in terms of top displacements is also plotted in the figures.

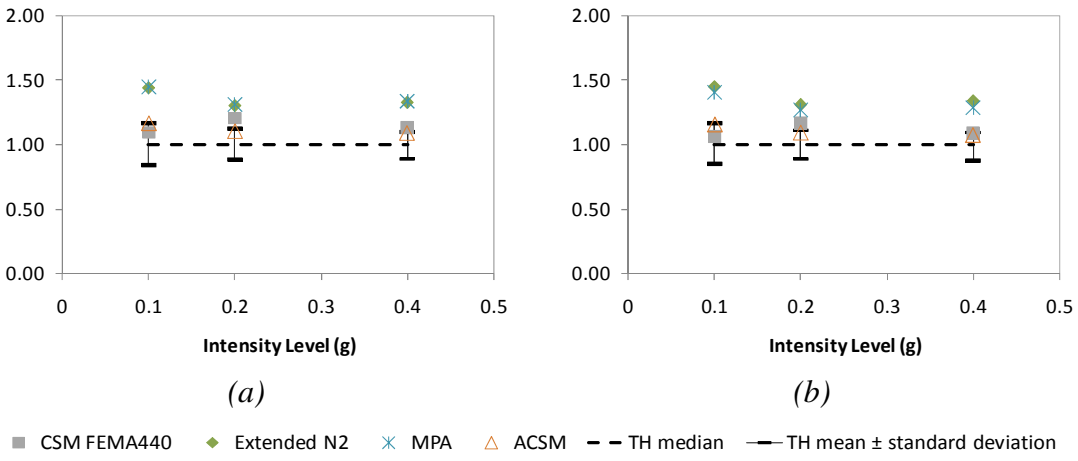

Figure 8.36 – a) Top displacements ratios at the centre of mass X direction; b) Top displacements ratios in column S9 X direction.

In terms of top displacements, one can observe that ACSM practically matches the *time-history* results over all the seismic intensities. The CSM-FEMA440 almost matches the *time-history* for 0.1g and 0.4g, but it slightly overestimates the results for a seismic intensity of 0.2g. The Extended N2 and the MPA generally lead to conservative results.

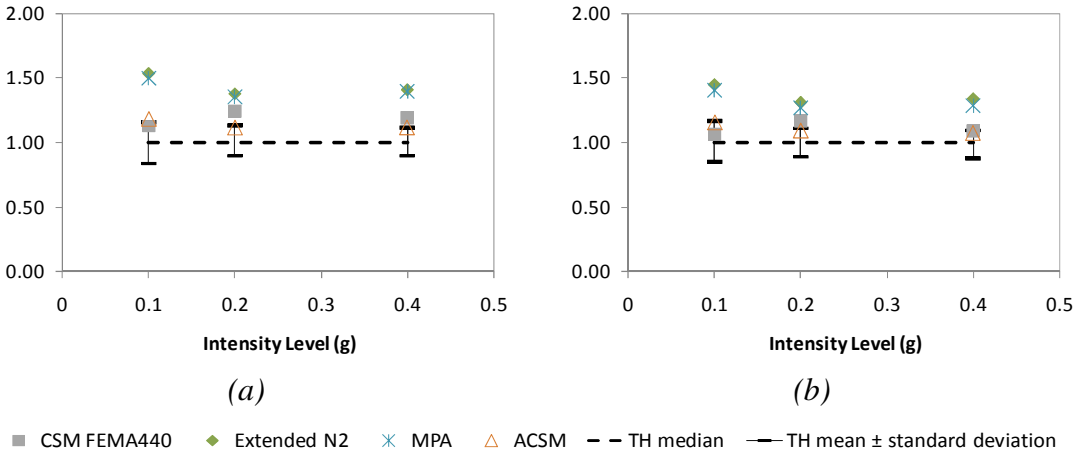

Figure 8.37 – a) Top displacements ratios in column S69 X direction; b) Top displacements ratios in column S15 X direction.

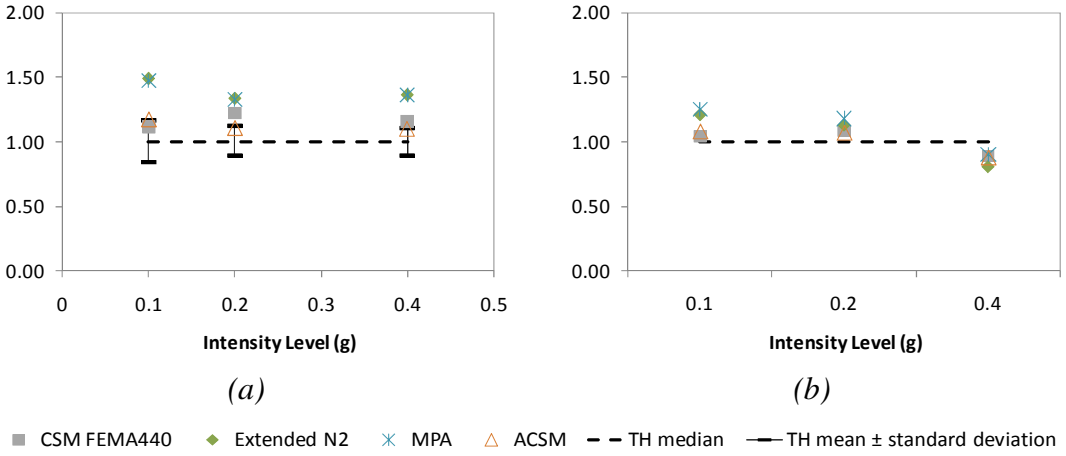

Figure 8.38 – a) Top displacements ratios in column S52 X direction; b) Base shear ratios X direction.

From the figures representing the top displacement ratios, it is evident that the distribution of the *time-history* results has a relatively small dispersion. This corroborates the idea that the number and type of records used in this study seem to be sufficient to obtain reliable results in the eight storey building. One can also observe that the ACSM and the CSM-FEMA440 lead to top displacement ratios very close to the upper bound of the *time-history* distribution range – mean + standard deviation – while the other two methods lead to values slightly above this range.

As far as base shear ratios are concerned, Figure 8.38b), once again the ACSM and the CSM-FEMA440 lead to almost perfect predictions for 0.1g and 0.2g, while the

other two methods slightly overestimate the response. For 0.4g, corresponding to a high level of inelasticity, all the NSPs lead to the same results but slightly non conservative.

8.3.2 Lateral displacement, interstorey drift and chord rotation profiles

The results in terms of lateral displacement profiles, interstorey drifts and chord rotations for the eight storey building are plotted from Figure 8.39 to Figure 8.42. More results are presented in Appendix A12, A13 and A14.

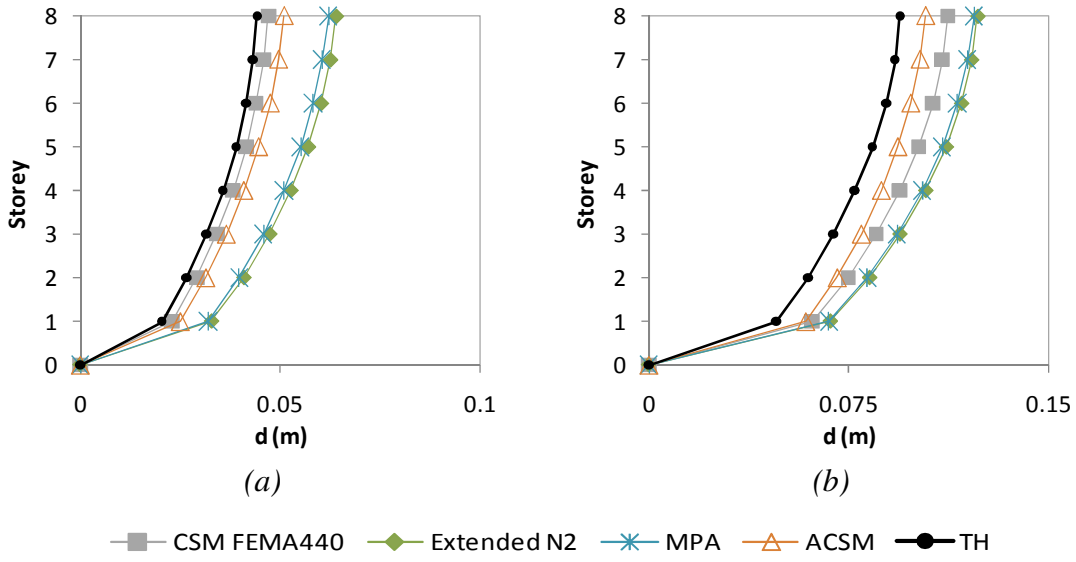

Figure 8.39 – Lateral displacement profiles X direction: a) Column S9, 0.1g; b) Column S23, 0.2g.

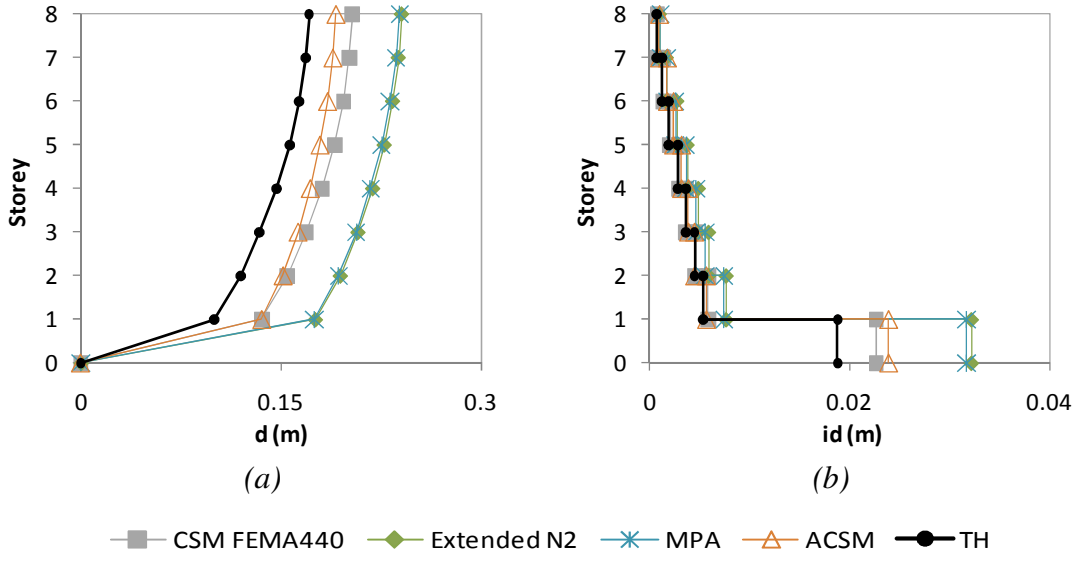

Figure 8.40 – a) Lateral displacement profile X direction, Column S69, 0.4g; b) Interstorey drifts profile X direction, Column S69, 0.1g.

Figure 8.39 to Figure 8.42 clearly illustrate the soft storey mechanism on the first floor along the X direction of the eight storey building. In fact, the interstorey drifts and chord rotations are much higher on the first storey than in the upper floors. This trend is observed over all the seismic intensities tested. The ACSM and the CSM-FEMA440 are the methods that better reproduce this phenomenon. The Extended N2 and the MPA slightly overestimate this mechanism. In fact, the ACSM is able to correctly predict the soft storey mechanism because it uses the DAP where the properties of the damaged structures are updated and fed into the model in each analysis step. The soft storey mechanism on the first floor can be explained by the considerable difference between the heights of the first and the second floors, inducing a considerable difference in the stiffness between these two storeys. In fact, the first storey height amounts to 5m and the upper floors to 2.70m; therefore the first floor is more flexible than the upper ones, leading to a local mechanism. This phenomenon also explains why the pushover curves of the building present less strength and stiffness in the X direction, as illustrated in Figure 5.9 and Figure 5.10.

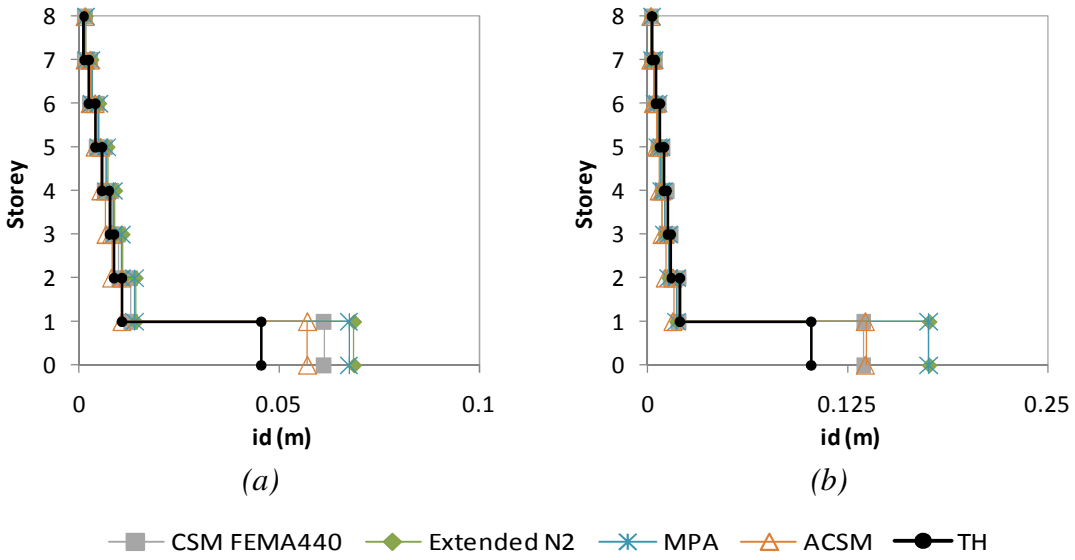

Figure 8.41 – Interstorey drifts profile X direction a) Column S72, 0.2g; b) Column S52, 0.4g.

From Figure 8.39 and Figure 8.40a), one can observe that for the elastic or almost elastic stage, corresponding to 0.1g, both ACSM and CSM-FEMA440 match almost perfectly the lateral displacement profile obtained from the *time-history* analysis in the X direction. On the other hand, the Extended N2 and the MPA overestimate the response. As the intensity increases and the structure goes through higher levels of inelasticity, all the methods seem to overestimate the lateral displacement profiles. However, the ACSM and the CSM-FEMA440 are the methods that lead to results closer to the nonlinear dynamic analysis. This trend is mainly clear on the first floor where the soft storey mechanism is quite well reproduced by these two methods.

In terms of interstorey drifts and chord rotations, Figure 8.40b) to Figure 8.42, one can observe that the ACSM and the CSM-FEMA440 are the methods that better

reproduce the soft storey mechanism on the first floor. The other two procedures lead to conservative estimations. For the upper storeys, all the NSPs lead to the same results, very close to the *time-history*.

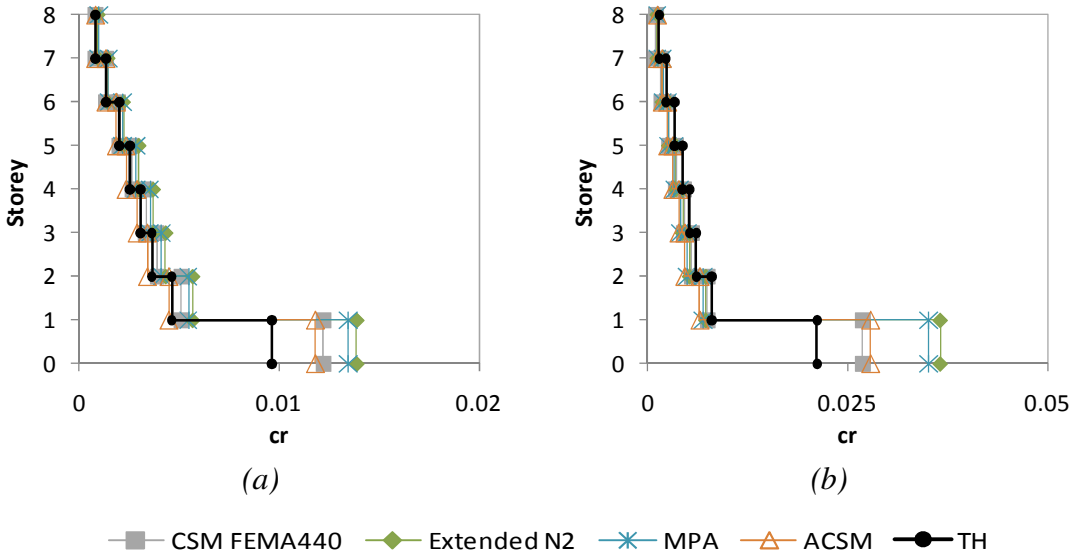

Figure 8.42 – Chord rotations profiles X direction a) Column S15, 0.2g; b) Column S9, 0.4g.

It is interesting to note that all pushover methods could reproduce in a very good way the specific characteristics of the building's structural response through all the seismic intensities tested, namely:

- The unbalanced stiffness distribution between the two directions;
- The Y direction is much stiffer than the X direction;
- The response of the building remains elastic in the Y direction over all the intensity levels analysed;
- The collapse of the building due to a soft storey mechanism in the first floor along the X direction.

8.3.3 Normalized top displacements

The normalized top displacements in both X and Y directions are plotted from Figure 8.43 to Figure 8.46, for increasing seismic intensities.

In Figure 8.43 and Figure 8.44a) it is shown that the Extended N2 method could perfectly capture the torsional amplification on column S9 in the X direction. At the opposite edge, the method overestimates the seismic response because it does not consider any de-amplification due to torsion.

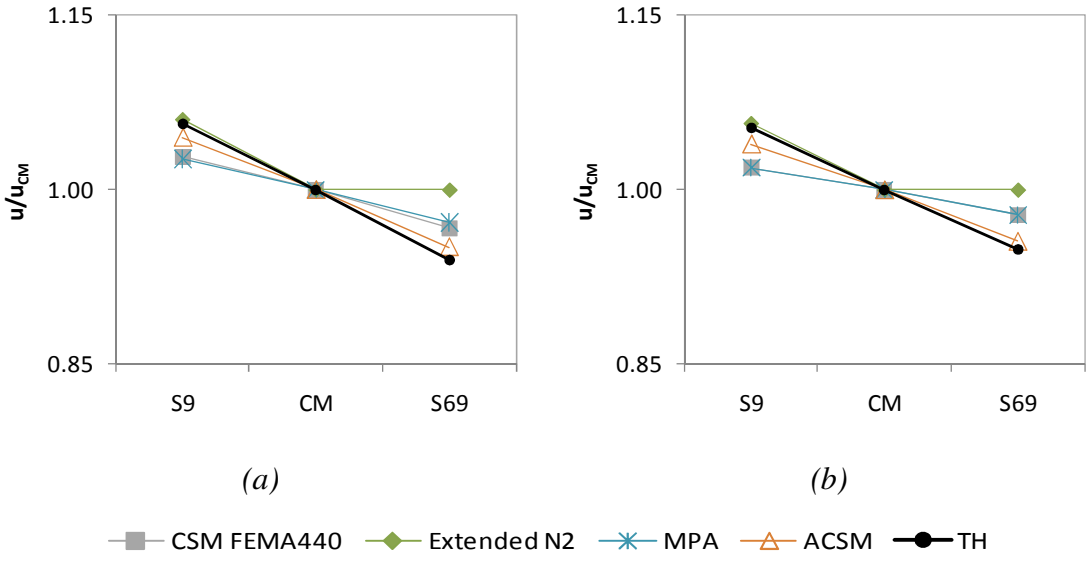

Figure 8.43 – X direction: a) 0.1g; b) 0.2g.

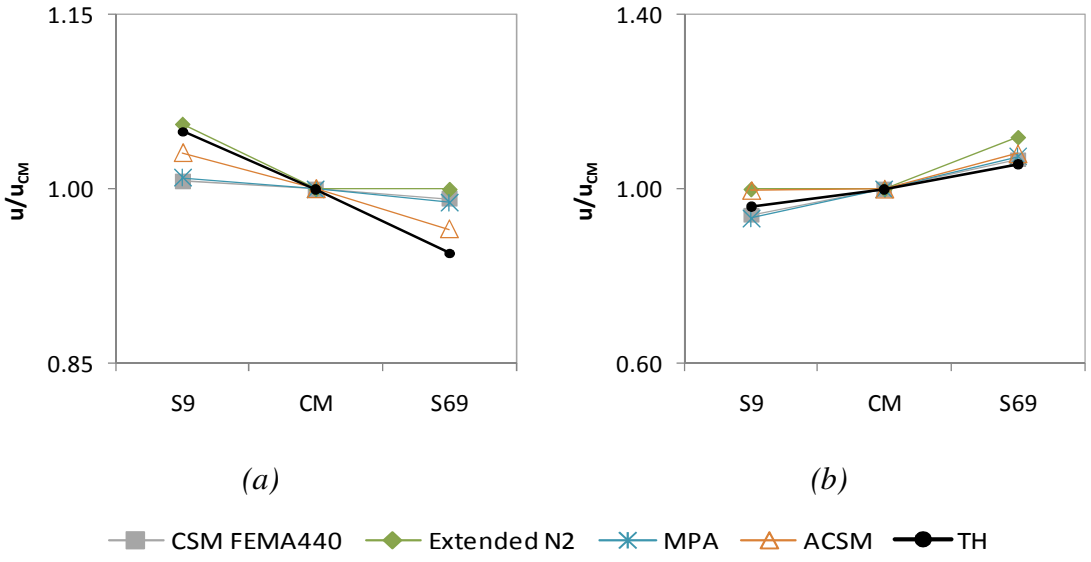

Figure 8.44 – a) X direction 0.4g; b) Y direction 0.4g.

The CSM-FEMA440 and the MPA lead to similar results in the X direction. They estimate the response linearly from one side of the building to the other, underestimating the torsional amplification on column S9 and overestimating the results on column S69. The ACSM could perfectly capture the torsional de-amplification on column S69, but it slightly underestimated the amplification at the opposite edge.

In the Y direction, Figure 8.44b), it is clear that all the NSPs predict in a very good way the torsional amplification on column S69. On the opposite edge, the Extended

N2 and the ACSM slightly overestimate the response while the other two methods slightly underestimate the response.

From Figure 8.45 and Figure 8.46a) one can conclude that in the X direction, the Extended N2 method is the only method able to correctly capture the torsional amplification on column S15 over all the intensity levels analysed. This method overestimates the response on column S72.

The CSM-FEMA440 and the MPA lead to approximately the same results. Once again they estimate the response linearly from one side of the building to the other, underestimating the torsional amplification on column S15 and overestimating the response on column S72.

The ACSM captures in quite a good manner the response of column S72 through all the seismic intensities analysed, but it underestimates the torsional amplification on column S15.

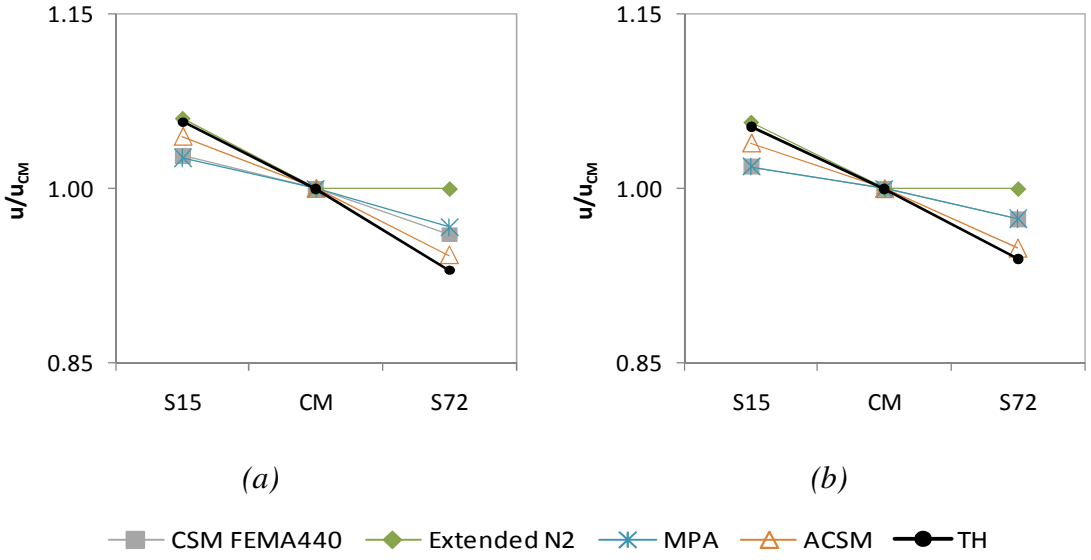

Figure 8.45 – X direction: a) 0.1g; b) 0.2g.

In the Y direction, Figure 8.46b), all the methods are in general able to capture the torsional amplification on column S15. On column S72 the Extended N2 and the ACSM lead to conservative results, and the CSM-FEMA440 and the MPA lead to slightly non-conservative estimations.

Once again, it is evident from the plots that the torsional effect decreases as the seismic intensity increases. This can be concluded by the flattening of the normalized top displacements from 0.1g to 0.4g.

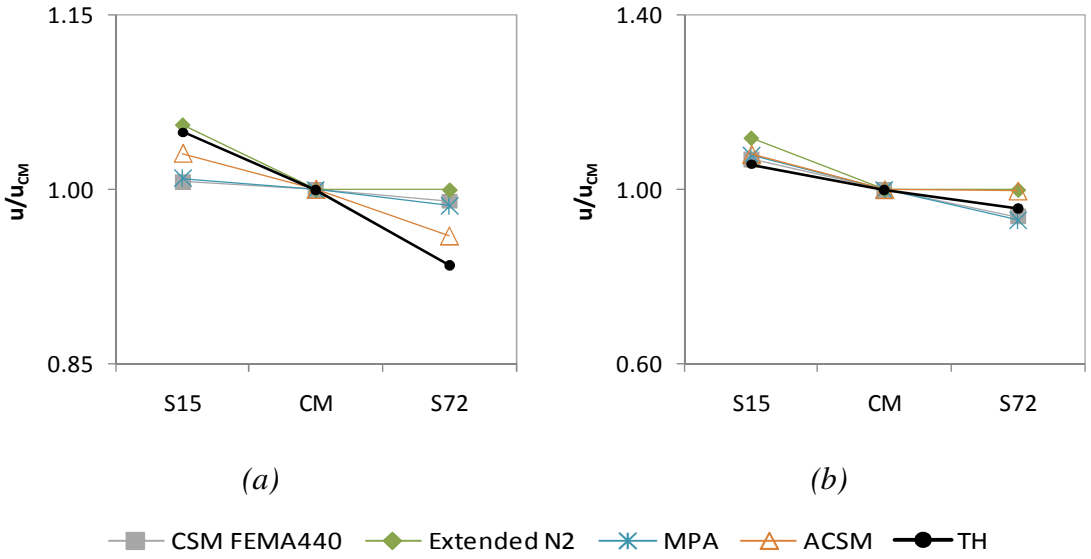

Figure 8.46 – a) X direction 0.4g; b) Y direction 0.4g.

8.4 Damage Limitation Control According to Eurocode 8

In this section, the damage limitation (DL) requirement according to Eurocode 8 is evaluated. This verification is performed in terms of interstorey drift limitation. Since the buildings under analysis have non-structural elements of brittle materials attached to the structure, the interstorey drift limit is defined in Eq. 8.1:

$$d_r \nu \leq 0.005h \qquad \textit{Eq. 8.1}$$

where,

d_r is the design interstorey drift;

h is the storey height;

ν is the reduction factor, which takes into account the lower return period of the seismic action associated with the damage limitation requirement.

The value of ν depends on the importance class of the building. Since the case studies under analysis belong to an importance class II, the value ascribed to ν is 0.5.

The elements analysed within this damage limitation verification were: columns C8, C3 and C2 in the three storey building; columns S1, S23, S13 and S14 in the five storey building; and columns S9, S69, S15, S72, S23 and S52 in the eight storey building. These columns were verified in all storeys, in both X and Y directions, over all the seismic intensities tested. The number of columns evaluated in each building is

sufficient so one can understand the trend of how accurately each NSP performs in finding when the damage limitation criterion is exceeded.

The last column of Table 8.1 to Table 8.6 presents the number of elements that exceeded the interstorey drift damage limitation defined according to EC8, resulting from the *time-history* analysis. The other columns give an insight of how many of these exceedances were captured by each NSP. These comparisons are made for all seismic intensities tested, in both X and Y directions, for the three buildings analysed.

Table 8.1 - Three storey building: Interstorey drifts Damage Limitation EC8 - X direction.

	CSM FEMA440	Extended N2	MPA	ACSM	*Time-history*
0.05g	0	0	0	0	0
0.1g	0	0	0	1	1
0.2g	3	4	3	6	6
0.3g	6	6	6	6	6

Table 8.2 - Three storey building: Interstorey drifts Damage Limitation EC8 - Y direction.

	CSM FEMA440	Extended N2	MPA	ACSM	*Time-history*
0.05g	0	0	0	0	0
0.1g	0	0	0	0	0
0.2g	3	2	3	6	6
0.3g	6	6	6	6	6

Table 8.1 and Table 8.2 summarize the number of elements that exceeded their storey drift capacities at the DL limit state for different levels of seismic intensity determined from different analysis procedures in the three storey building. Similar to the previous comparisons, the median of dynamic analyses provides the benchmark numbers. At a high intensity level of 0.3g, all the NSPs predicted the number of elements exceeding DL capacities very well, whereas at moderate intensity levels, 0.1g and 0.2g, it is only ACSM that matched with the prediction of dynamic analysis well. Note that the ACSM is the only method that always provided results similar to the median dynamic response.

From Table 8.3 and Table 8.4 one can conclude that in the five storey building the *time-history* results indicate no elements exceeding in the elastic or almost elastic stage, 0.1g and 0.2g. For lower levels of inelasticity, 0.4g, the number of exceeding elements is very small, and once again all NSPs could generally capture this

behaviour, except the ACSM in the Y direction. In the inelastic stage, 0.6g and 0.8g, there is a large increase in exceeding elements. For 0.6g, all NSPs could reproduce the *time-history* results, except the ACSM in the Y direction where it slightly underestimated the response. For very high levels of inelasticity, 0.8g, all the NSPs tend to slightly underestimate the results obtained with the nonlinear dynamic analysis in the X direction. In the Y direction they could capture the real response of the building, except the ACSM which underestimated it.

Table 8.3 - Five storey building: Interstorey drifts Damage Limitation EC8 - X direction.

	CSM FEMA440	Extended N2	MPA	ACSM	*Time-history*
0.1g	0	0	0	0	0
0.2g	0	0	0	0	0
0.4g	1	1	1	1	1
0.6g	11	11	11	11	11
0.8g	12	13	13	12	16

Table 8.4 - Five storey building: Interstorey drifts Damage Limitation EC8 - Y direction.

	CSM FEMA440	Extended N2	MPA	ACSM	*Time-history*
0.1g	0	0	0	0	0
0.2g	0	0	0	0	0
0.4g	2	2	2	0	2
0.6g	14	14	14	12	14
0.8g	19	19	19	16	19

The ACSM usually reproduces quite well the *time-history* response profiles over different seismic intensities. Despite its accuracy in terms of profile shapes, the method sometimes leads to non-conservative estimations when compared with the nonlinear dynamic median results. This fact is more relevant when analysing damage limitation criteria. In fact, if the method leads to a response which is smaller than the damage limitation, even if it is a slight underestimation, the element under consideration is not considered to exceed the damage criterion. This explains why the ACSM underestimates the number of damaged elements even though it reproduces in a good fashion the *time-history* response profiles.

From Table 8.5, it is clear that the eight storey building did not present any element exceeding the damage limitation criterion for 0.1g and 0.2g in the X direction. For 0.4g, 6 elements exceeded the limit, being well captured by all the NSPs.

The results obtained by the NSPs were the same from those of *time-history*, through all the seismic intensities tested.

Table 8.5 - Eight storey building: Interstorey drifts Damage Limitation EC8 - X direction.

	CSM FEMA440	Extended N2	MPA	ACSM	*Time-history*
0.1g	0	0	0	0	0
0.2g	0	0	0	0	0
0.4g	6	6	6	6	6

Table 8.6 - Eight storey building: Interstorey drifts Damage Limitation EC8 - Y direction.

	CSM FEMA440	Extended N2	MPA	ACSM	*Time-history*
0.1g	0	0	0	0	0
0.2g	0	0	0	0	0
0.4g	0	0	0	0	0

Table 8.6 shows that any element exceeded the damage limitation in the Y direction of the eight storey building. As was mentioned before the building remains elastic in this direction over all the seismic intensities tested.

8.5 Shear strength verification

The Turkish buildings analysed herein are constituted by wall-like columns. When these kinds of structures are not properly designed, the sensitiveness to shear actions can increase. This effect is more evident in old structures where there is a lack of design and construction against brittle failures.

This aspect is actually very relevant because if brittle failure occurs the structure loses ductility, and the building will be subjected to an undesirable brittle collapse.

In this thesis it was considered that the buildings analysed were properly designed to shear, and that therefore they do not have brittle failures. In order to confirm this assumption, some characteristic columns were analysed in terms of shear capacity for the higher seismic intensities tested in the three buildings assessed. This capacity was calculated based on the ATC40 recommendations according to equations Eq. 8.2, Eq. 8.3 and Eq. 8.4:

$$V_n = V_C + V_S \qquad \textit{Eq. 8.2}$$

$$V_C = 35 \cdot \lambda \cdot \left(k + \frac{N}{2000 \cdot A_g} \right) \cdot \sqrt{f_c^{'}} \cdot b_w \cdot d \qquad \textit{Eq. 8.3}$$

$$V_S = \frac{A_v \cdot f_y \cdot d}{0.6 \cdot s} \qquad \textit{Eq. 8.4}$$

Where,

$k = 1$ in regions of low ductility and 0 in regions of moderate and high ductility

$\lambda = 1$ for normal-weight aggregate concrete

N - axial compression force in pounds (zero for tension force)

V_n - total shear strength

V_C - shear strength due to the concrete

V_S - shear strength due to the transverse reinforcement

$f_c^{'}$ - design strength of the concrete

b_w - section width

d - section useful height

A_g - gross section

f_y - design strength of the transverse reinforcement steel

A_v - transverse reinforcement area

s - spacing of the transverse reinforcement

All units in the formulas are expressed in pounds and inches.

The comparison between the maximum shear value (Vsd) obtained from the *time-history* analysis in each column, for each level of intensity, and the shear capacity (Vrd) are presented in Table 8.7 to Table 8.12, for the three, five and eight storey buildings.

In each column, the shear verification was performed for the yielding regions at the column ends – plastic hinge zones. Since the transverse reinforcement is constant along the height of the column and the shear demand is also constant at each storey, the conditioning zone is the region of moderate or high ductility corresponding to the plastic hinge zone. In this case, the shear strength in the midheight region of the columns is always higher than in the plastic hinge zone. In the near midheight region

of the columns (low ductility zones) the shear capacity is always higher than the shear demand for the case studies analysed. The results presented in the tables correspond to the verification at the column ends.

Table 8.7 – Three storey building: Shear vs. Shear capacity - X direction (units kN)

	C8		C3		C2	
Intensity level (g)	Vsd	Vrd	Vsd	Vrd	Vsd	Vrd
0.3g	30	62	38	308	34	165

Table 8.8 – Three storey building: Shear vs. Shear capacity - Y direction (units kN)

	C8		C3		C2	
Intensity level (g)	Vsd	Vrd	Vsd	Vrd	Vsd	Vrd
0.3g	22	62	38	308	33	165

Table 8.7 and Table 8.8 show that in the three storey building, there is no brittle failure, because the shear demand is always smaller than the shear strength for the higher intensity level analysed – 0.3g.

Table 8.9 – Five storey building: Shear vs. Shear capacity - X direction (units kN)

	S1		S13		S14		S23	
Intensity level (g)	Vsd	Vrd	Vsd	Vrd	Vsd	Vrd	Vsd	Vrd
0.6g	47	156	400	490	346	491	52	149
0.8g	51	156	556	490	465	491	60	149

Table 8.10 - Five storey building: Shear vs. Shear capacity - Y direction (units kN)

	S1		S13		S14		S23	
Intensity level (g)	Vsd	Vrd	Vsd	Vrd	Vsd	Vrd	Vsd	Vrd
0.6g	216	318	91	365	80	366	91	203
0.8g	245	318	94	365	96	366	154	203

From Table 8.9 and Table 8.10, one can observe that in the five storey building brittle failure only occurs for a seismic intensity of 0.8g, because in column S13 the shear demand in the X direction is slightly higher than its capacity in the same direction. This was the last and the highest seismic intensity level tested in this building, corresponding to the structural collapse. For the other seismic intensities there are no problems related with brittle failure.

Table 8.11 - Eight storey building: Shear vs. Shear capacity - X direction (units kN)

	S15		S23		S72	
Intensity level (g)	Vsd	Vrd	Vsd	Vrd	Vsd	Vrd
0.4g	28	176	62	224	29	177

Table 8.12 - Eight storey building: Shear vs. Shear capacity - Y direction (units kN)

	S15		S23		S72	
Intensity level (g)	Vsd	Vrd	Vsd	Vrd	Vsd	Vrd
0.4g	100	343	123	422	109	345

From Table 8.11 and Table 8.12, one can conclude that there is no brittle failure in the eight storey building for any seismic intensity tested, as the shear capacity of the analysed columns is always higher than the shear demand for 0.4g – the higher seismic level tested in this building.

8.6 Discussion

In Figure 4.4 and Appendix A3 - Figure A. 13 to Figure A. 15 - are plotted the response spectra compatible with each record used in the three storey building, as well as the median of these spectra, for the different seismic intensities analysed. In Figure 4.6, Figure 4.7, Appendix A4 - Figure A. 19 to Figure A. 22 - are plotted the response spectra compatible with the records used in the Turkish buildings and the correspondent median spectra. From the plots one can conclude that the dispersion of the records used in the three buildings is relatively small. The median of the spectra compatible with the records in the analysed buildings has a good fit with the respective target spectrum (calculated from the code), see Figure 4.9. This happens because the records were modified using wavelets. This scaling process increases the fitting level of the records. As a consequence, the dispersion of the *time-history* results is relatively small in the three storey building, Figure 8.1 to Figure 8.3, and in the Turkish buildings, Figure 8.17 to Figure 8.20 (in the five storey building) and Figure 8.36 to Figure 8.38 and Figure A. 96 (in the eight storey building). This fact shows that the number and type of records used in each case were sufficient to obtain reliable results.

As was previously mentioned, the records used in this work were semi-artificial. The use of modified records compatible with the target response spectrum, lead in general to smaller response dispersions, when compared with the ones obtained from real

records which are usually very high. As a consequence, it is generally accepted that the number of real records needed to obtain reliable results is much higher than by using modified records. Since the 3D models developed herein have an extremely large memory size, the time-consuming of each nonlinear dynamic analysis is also considerable. If one would use real records, the number of accelerograms would be much higher, making the large parametric study developed herein much more time-consuming.

However, modified records compatible with the target spectrum lead to conservative results of the median structural responses when compared to the real records. As an example, Figure 8.47 shows the 5% damped target spectrum as well as the spectrum compatible with the real Tabas ground motion and the spectrum compatible with the semi-artificial Tabas ground motion used in the Turkish buildings. These plots refer to the component of the Tabas ground motion with the highest peak ground acceleration.

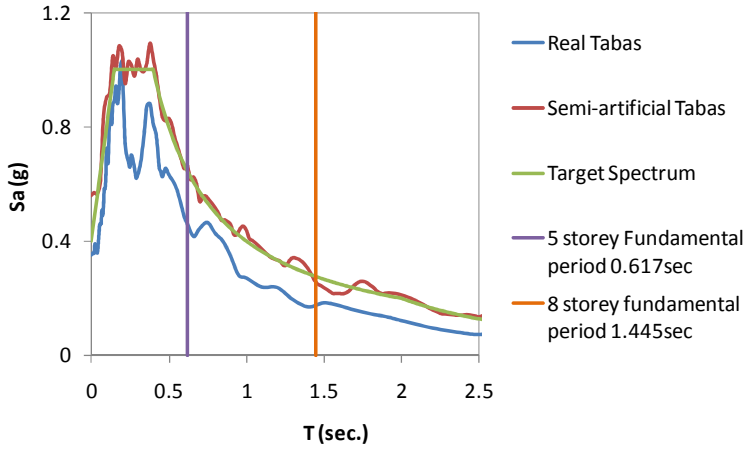

Figure 8.47 – Tabas ground motion .

In the five storey building, the spectrum values for the periods beyond the fundamental period 0.617sec are larger for the spectrum compatible with the semi-artificial record, influencing the nonlinearity effect. For periods less than 0.617sec the spectrum values are also amplified significantly for the spectrum compatible with the semi-artificial record, influencing the higher modes effect. The same conclusions can be drawn for the eight storey building with a fundamental period of 1.445sec. Therefore one can conclude that modified records lead to larger response estimations when compared with the respective real records.

The results obtained in this study, in terms of top displacements, lateral displacement profiles, interstorey drifts and chord rotations, showed that the CSM-FEMA440 and the ACSM were the methods that better reproduced the nonlinear dynamic median response profiles/values, although the ACSM was usually closer to the *time-history*. The exception occurs in the edge columns of the three storey building, where the CSM-FEMA440 led to underestimated responses.

The good performance of the CSM-FEMA440 can be explained by its accurate procedure for calculating the target displacement that includes: a new and efficient

algorithm to compute the effective period and the effective damping; an accurate demand spectrum reduction factor coupled with the new concept of the modified acceleration-displacement response spectrum (MADRS).

The ACSM apparently managed to follow slightly better the change of response characteristics with the increase of seismic intensity, most likely because of the fact that such a method uses an adaptive displacement pushover (DAP) and an equivalent SDOF structural displacement built on the current deformed pattern (which can turn out to be very useful when dealing with 3D plan asymmetric buildings).

The CSM-FEMA440 and the ACSM have two essential differences:

- The CSM-FEMA440 uses a conventional non-adaptive force-based pushover and the ACSM uses a displacement based adaptive pushover (DAP);
- The post-yield equivalent period, equivalent viscous damping ratio and the spectrum reduction factor used to calculate the target displacement are obtained by using different sets of equations (see section 2.4.4.2 and 2.4.5). Both methods use reduction factors depending on the damping.

The damping ratios obtained using the CSM-FEMA440 and the ACSM procedures are represented in Table 8.13 to Table 8.15, for the three buildings under analysis. Since the reduction factors used by both methods are damping dependent, the damping ratio values and the reduction factors are correlated, as explained in sections 2.4.4.2 and 2.4.5.

At the lower seismic intensities for which the buildings remain elastic, the damping ratio calculated by the methods should be equal to the viscous damping used in the nonlinear dynamic analysis in the elastic range – 2% for the three storey building, and 5% for the five and eight storey buildings.

Table 8.13 - Three storey building - effective damping ratios (%).

	Three storey building: 2% viscous damping			
	X (T = 0.617 sec)		Y (T = 0.441 sec)	
Intensity level (g)	ACSM	FEMA440	ACSM	FEMA440
0.05	3.5	2.1	3.8	2.1
0.1	5.2	2.2	4.4	2.1
0.2	11.9	5.8	9.8	3.2

In the three storey building, for the elastic or almost elastic regime 0.05g and 0.1g, the ACSM overestimates the damping while the CSM-FEMA440 calculates damping ratios very close to the 2% considered in the *time-history* analysis, see Table 8.13.

Also in the inelastic regime, the ACSM leads to higher values of damping than the CSM-FEMA440.

Table 8.14 - Five storey building - effective damping ratios (%).

	Five storey building: 5% viscous damping			
	X (T = 0.617 sec)		Y (T = 0.593 sec)	
Intensity level (g)	ACSM	FEMA440	ACSM	FEMA440
0.1	6.5	5.2	6.8	5.4
0.2	7.3	5.3	7.0	5.3
0.4	10.2	6.7	9.3	6.4
0.6	14.0	10.9	11.8	10.0

Table 8.15 - Eight storey building - effective damping ratios (%).

	Eight storey building: 5% viscous damping	
	X (T = 1.445 sec)	
Intensity level (g)	ACSM	FEMA440
0.1	7.3	5.3
0.2	7.7	5.4
0.4	12.3	9.2

Table 8.14 shows that in the five storey building in the elastic or almost elastic regime, 0.1g and 0.2g, the ACSM overestimates the damping in both directions while the CSM-FEMA440 leads to damping ratios quite close to 5%. The same conclusion can be drawn for the eight storey building for an intensity of 0.1g (elastic regime), see Table 8.15.

In the inelastic range, the ACSM continues to calculate values of damping larger than the ones obtained using the CSM-FEMA440 in both five and eight storey buildings.

By using the sophisticated and powerful DAP algorithm [46] the ACSM could in theory perfectly match the *time-history* response. In fact, this type of pushover takes into account the stiffness degradation, the period elongation and the progressive structural damage. At each step, the eigenvalues and modes of vibration of the building are calculated considering the current structural stiffness state. The load pattern to be applied in the next step is obtained by performing a combination of these different mode shapes, so that the higher mode effects are taken into account. Despite all these powerful features of DAP, the ACSM uses equations to calculate the damping (proposed by Gulkan and Sozen [58] based on the Takeda model without hardening) and the spectral reduction factor proposed by Lin and Chang [57], (see section 2.4.5), that proved to be not so accurate, since the method overestimated the damping ratios in the structures under analysis. Therefore, the final results obtained

with the method were not as accurate as expected. In fact, this overestimation of the damping can explain why the ACSM leads in certain cases to underestimated results when compared with the *time-history* median, especially in terms of damage criteria such as interstorey drifts and chord rotations.

The less accurate conventional force-based non-adaptive pushover analysis used by the CSM-FEMA440 is somewhat compensated by the accurate procedure to calculate the target displacement. As was described in section 2.4.4.2, it uses innovative methods to compute the effective period, the effective damping and the demand spectrum reduction factors, as well as the innovative modified acceleration-displacement response spectrum (MADRS) [16]. As can be concluded from the results in the previous tables, the method correctly estimates the damping ratios. For this reason the CSM-FEMA440 leads to results close to the ACSM, even though it uses a less accurate pushover procedure.

However, some underestimated results obtained with the method when compared with the nonlinear dynamic median, can be explained due to the conventional pushover used. A clear example happens in the three storey building, where the method leads to good and slightly conservative response estimations in the central columns, but it underestimates the response at the edges of the building. This happens because the conventional pushover procedure used is not able to capture the torsional motion of the building. This pushover has a lack of accuracy in reproducing in a correct manner the stiffness degradation and the progressive structural damage along the elements. This influences the ability of the pushover method in reproducing in a correct fashion the torsional behaviour of the structure, namely the response at the edges where this effect is more accentuated. From the obtained results, one can conclude that in the three storey building the conventional pushover underestimated the stiffness degradation mainly on the edge elements, underestimating their displacements. So, despite the CSM-FEMA440 calculate correctly the target displacement at the centre of mass of the last floor (where the torsional effect is not very significant), the response on the peripheral columns was underestimated. On the other hand, the ACSM was able to estimate in a good fashion the response of the columns located at the edges because of the DAP. The good performance of the ACSM at the extremities of the three storey building can also be explained, because the method instead of using a single control node like the other NSPs, computes the equivalent SDOF structural displacement built on the current deformed pattern, which can turn out to be very useful in the 3D case, see section 2.4.5. The other NSPs consider a single control node for the SDOF characterization, usually the centre of mass of the roof.

So, despite the fact of calculating in a correct way the target displacement (where torsion does not have an important effect), the results obtained by a certain NSP on the columns located at the edges of the buildings strongly depend on the accuracy of the pushover method used.

The conclusions obtained herein with these case studies confirm the idea that in a pushover analysis procedure all steps of a NSP are equally important – the pushover algorithm and the definition of the pushover curve, the MDOF to SDOF

transformation and the calculation of the target displacement. A less accurate approach in one of the steps can explain some inadequate results.

The Extended N2 was the method that in general led to the most conservative results in the analysed buildings, in terms of lateral displacement profiles, top displacements, interstorey drifts and chord rotations. From Figure 8.48 to Figure 8.50, are plotted the SDOF capacity curves against the demand ADRS spectrum, showing the target displacement calculation by the N2 method and the CSM-FEMA440 for different seismic intensities. The figures correspond to the pushover curve in the X direction of the five storey building using a conventional non-adaptive force based load pattern proportional to the first mode of vibration in this direction. The two methods consider a single control node for the SDOF characterization - the centre of mass of the roof. In the N2 method both displacements and forces of the MDOF are multiplied with the same gamma factor that depends on the mass of each storey, the modal displacement at each floor normalized to the roof's centre of mass and of the equivalent mass, in order to obtain the SDOF curve force vs. displacement. The CSM-FEMA440 uses two different coefficients for the transformation of displacements and accelerations, in order to calculate the SDOF curve in terms of the acceleration vs. displacement format. Note that, if one divides the SDOF forces in the N2 method by the equivalent mass (as defined by the method) in order to obtain the SDOF curve acceleration vs. displacement, the equation of the SDOF accelerations will be the same as the one presented by FEMA440. The equations of the SDOF displacement transformation are the same in Eurocode 8 and in FEMA440, see sections 2.4.1 and 2.4.4.2.

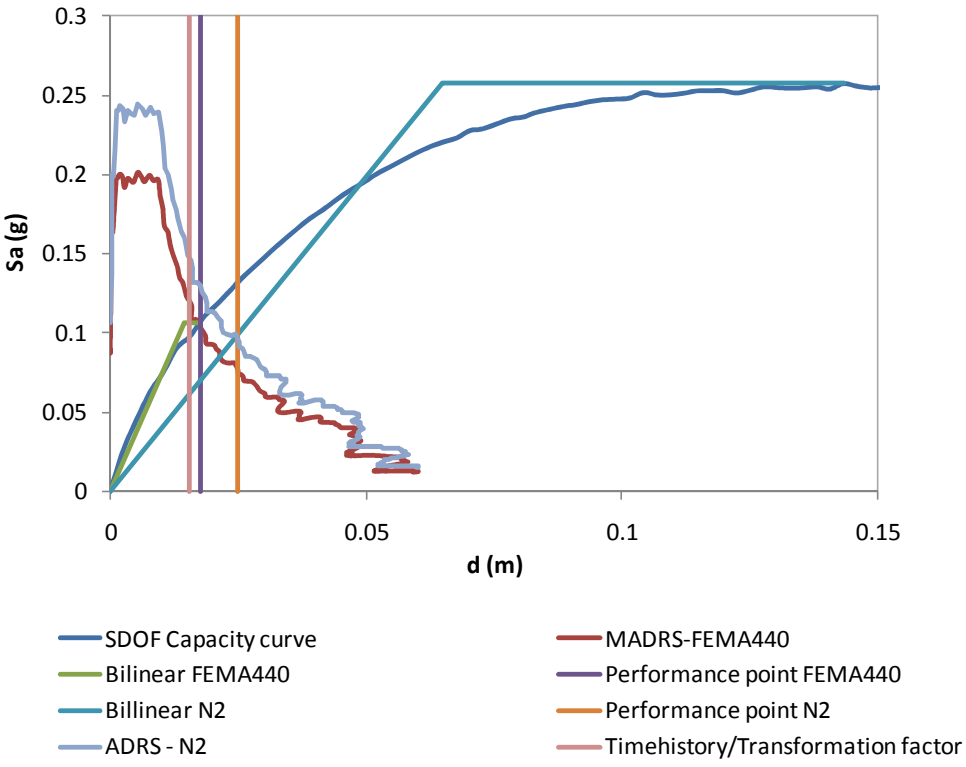

Figure 8.48 – Target displacement calculation. CSM-FEMA440 vs. N2 method. Five storey building, X direction, 0.1g.

In the plots, the *time-history* median top displacement at the centre of mass is divided by the gamma factor (MDOF to SDOF transformation factor) which is the same for both CSM-FEMA440 and N2 method as explained before. Therefore, the *time-history* results can be compared with the SDOF target displacements computed with the two methods. Note that the target displacement (displacement at the centre of mass of the roof) calculated with the N2 method is equal to the one computed with the Extended N2 procedure, because the torsional correction factor at this location is one. In fact, the torsional effect at the centre of mass is not significant.

During this study, one could conclude that the Extended N2 method overestimated the response when the Turkish buildings were still in the elastic regime. This is easily explained analysing Figure 8.48 which illustrates the target displacement calculation to a seismic intensity of 0.1g, for which the five storey building remains elastic. One can observe that the N2 method bilinearizes the SDOF capacity curve at the point of maximum acceleration, while the CSM-FEMA440 bilinearizes the curve at the intersection point between the capacity curve and the reduced demand spectrum. Therefore, the initial stiffness (the slope of the first part of the bilinear curve) of the SDOF will be smaller using the N2 method than using the FEMA440 recommendations. In fact, the effective period obtained with the N2 method in this case is 1.006sec and from the FEMA440 is 0.623sec. As a consequence, the displacement obtained in the elastic regime by the N2 method is larger than the one obtained by the CSM-FEMA440. The latter is closer to the *time-history* result, as can be observed in Figure 8.48. The fundamental elastic period in the X direction of the five storey building is 0.617sec, therefore one can conclude that the CSM-FEMA440 estimates it better than the N2 method.

The SDOF effective period calculated by the N2 method is independent of the seismic intensity, while the one computed using the CSM-FEMA440 depends on the intersection of the spectrum with the capacity curve, therefore it depends on the intensity of the seismic action. Table 8.16 to Table 8.18 compare the effective periods calculated with both methods for the buildings under analysis in the elastic regime, see the formulas for each method in sections 2.4.1 and 2.4.4.2. From the results, one can confirm that the N2 method overestimates the period and therefore underestimates the stiffness of the SDOF systems in the elastic regime, while the CSM-FEMA440 reproduces these characteristics in a very good manner. These conclusions can be drawn for all the buildings analysed in both X and Y directions.

Table 8.16 - Three storey building: effective periods (N2 and CSM-FEMA440) in the elastic/almost elastic regime (sec) vs. Fundamental period (sec).

	3 storey building periods (sec)					
	X			Y		
Intensity	N2	CSM-FEMA440	Fundamental Period	N2	CSM-FEMA440	Fundamental Period
0.05g	1.003	0.622	0.617	0.703	0.532	0.527
0.1g	1.003	0.625	0.617	0.703	0.533	0.527

Table 8.17 - Five storey building: effective periods (N2 and CSM-FEMA440) in the elastic/almost elastic regime (sec) vs. Fundamental period (sec).

	5 storey building periods (sec)					
	X			Y		
Intensity	N2	CSM-FEMA440	Fundamental Period	N2	CSM-FEMA440	Fundamental Period
0.1g	1.006	0.623	0.617	0.674	0.596	0.593

Table 8.18 - Eight storey building: effective periods (N2 and CSM-FEMA440) in the elastic/almost elastic regime (sec) vs. Fundamental period (sec).

	8 storey building periods (sec)		
	X		
Intensity	N2	CSM-FEMA440	Fundamental period
0.1g	2.007	1.463	1.445

The N2 method defines that for effective periods higher than Tc, the inelastic target displacement is equal to the elastic displacement – equal displacement rule, see section 2.4.1. In this case, the Tc is 0.4sec, therefore the displacement obtained by the N2 method is equal to the elastic displacement corresponding to the effective period calculated. In the elastic regime (0.1g), this value should in theory be close to the real one (*time-history* median) if the SDOF effective period was correctly estimated. However, as was observed before, the effective period calculated with this method is overestimated (the stiffness is underestimated) leading to conservative responses. On the other hand, in the CSM-FEMA440 the demand spectrum is reduced (MADRS) in order to take into account the hysteretic damping in the inelastic regime. In Figure 8.48 one can observe that the reduced demand spectrum used in the CSM-FEMA440 is very close to the initial ADRS spectrum (used in the N2 method), because for 0.1g (elastic or almost elastic regime) the hysteretic damping is very small. Note that, the target displacement in the CSM-FEMA440 procedure is obtained by intersecting the SDOF capacity curve with the MADRS, as explained in section 2.4.4.2. The CSM-FEMA440 procedure leads to results very close to the *time-history* in the elastic range.

The overestimation of the results by the N2 method is more evident in the elastic regime. In fact, according to Fajfar (the creator of the method) the N2 method was not developed to be applied in the elastic regime, but only when the structure presents inelastic behaviour.

For medium levels of inelasticity 0.4g (Figure 8.49) and for high levels of inelasticity 0.6g (Figure 8.50), the SDOF stiffness (slope of the initial part of the bilinear curve) is practically the same in both methods. The difference in the results between the two methods is justified by the equal displacement rule used by the N2 method to compute

the target displacements, which is proven to be conservative. In fact it is generally recognized that in the inelastic range the peak responses get smoother, so by considering the elastic displacements in the inelastic regime one may be too conservative. This explains the overestimation of the results by the N2 method. On the other hand, the CSM-FEMA440 considers the reduction of the demand spectrum (MADRS) to take into account the hysteretic damping in the inelastic regime. As one can observe from Figure 8.49 and Figure 8.50, the difference between the elastic spectrum (ADRS) and the reduced inelastic one (MADRS), for each intensity level, is significant.

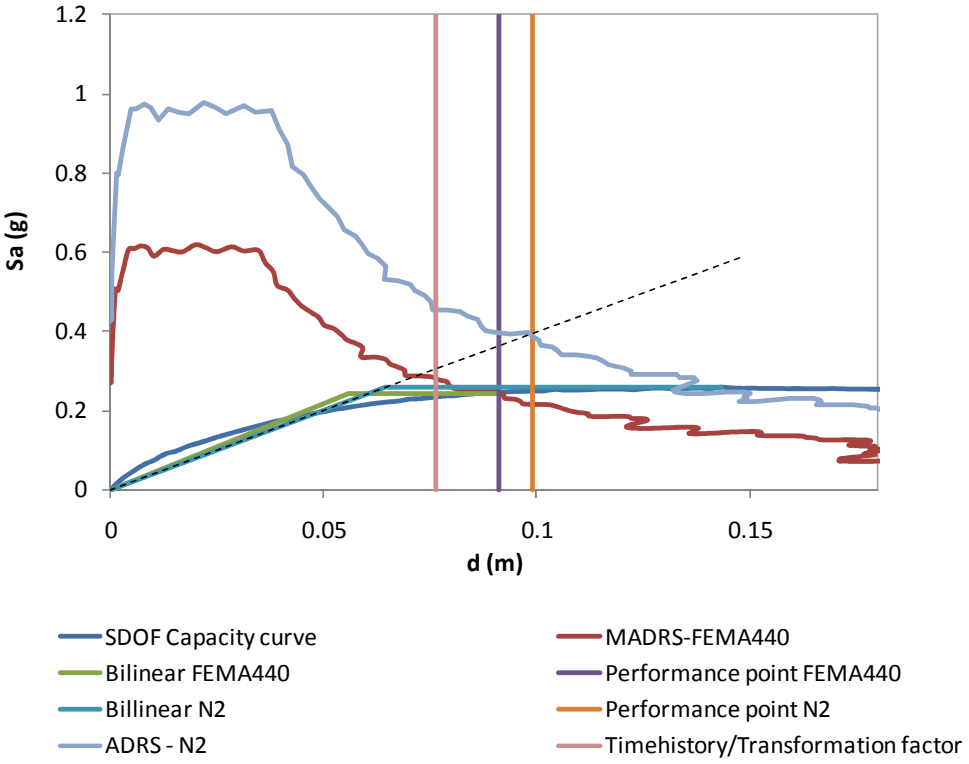

Figure 8.49 – Target displacement calculation. CSM-FEMA440 vs. N2 method. Five storey building, X direction, 0.4g.

The explanations presented herein for the conservative results of the Extended N2 method at the centre of mass and in columns near the centre of mass, illustrated for the five storey building case, can also be made for the other analysed buildings.

In the three storey building, the inability of the conventional pushover to reproduce the torsional behaviour of the structure (mainly on the peripheral columns) was overcome by the use of torsional correction factors that took into account the elastic spectrum results, see chapter 7. It was stated in section 2.4.2 that the dynamic elastic response spectrum analysis gives a good estimation of the torsional behaviour of the structure even in the inelastic regime. This explains the generally good results of the

Extended N2 method mainly at the flexible edge of the three storey building. However, the method sometimes underestimated the response at the stiff edge.

As was previously described, the MPA is a multi-run method that uses in each run a different load pattern proportional to each mode of vibration of the structure. The final response is obtained by combining the results computed from each pushover curve presented in chapter 5, taking into account the higher mode effects. The results obtained herein in terms of lateral displacement profiles, top displacements, interstorey drifts and chord rotations, showed that the MPA leads to results close to the ones obtained by the original N2 method. In fact, both methods use the same inelastic spectrum for the target displacement calculation. The method underestimated the results in the edge columns of the three storey building, due to its incapability to capture the torsional effect of the structure.

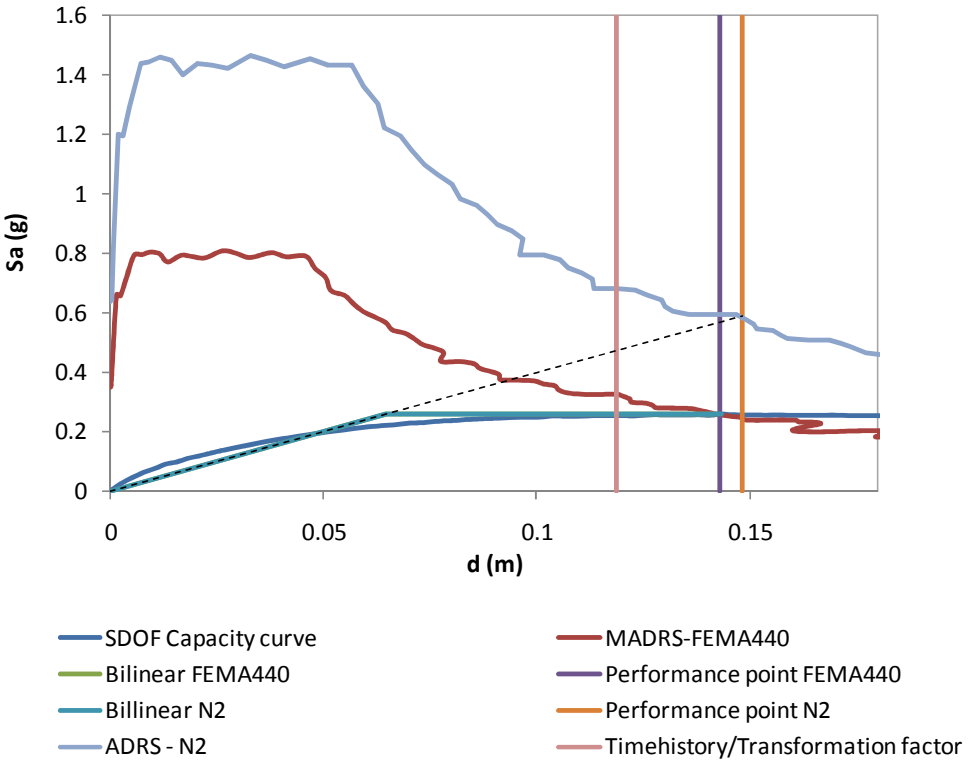

Figure 8.50 – Target displacement calculation. CSM-FEMA440 vs. N2 method. Five storey building, X direction, 0.6g.

All the methods seemed to lead to approximate and conservative results for high levels of inelasticity, in terms of lateral displacements profiles, top displacements, interstorey drifts and chord rotations.

In terms of normalized top displacements, the Extended N2 method was the only method capable of reproducing the torsional motion of the buildings over increasing seismic intensities. The reason for this trend lies in the fact that such a method uses

correction factors based on an elastic response spectrum analysis, without considering any de-amplification of displacements due to torsion. Therefore the method is able to capture the torsional amplification at the flexible edge of the buildings, and it generally led to conservative results on the stiff side. The other NSPs generally reproduced in a linear way the torsional motion from one side of the building to the other. For each intensity level in each direction, these methods were only able to capture the torsional behaviour of just one side of the building, under predicting the other. The ACSM could reproduce in a good manner the torsional motion of the three storey building, but it could not keep this good performance in the five and eight storey buildings. This measure is very important to evaluate the relative displacements in plan between the top floor edge columns and the centre of mass, and consequently evaluate the ability of the method to correctly reproduce the torsional motion of the structure. Apart from the Extended N2 method, all the other analysed NSPs should be improved in order to correctly reproduce this measure.

The eight storey building has a bad stiffness distribution between the two orthogonal directions, collapsing due to a soft storey mechanism on the first floor along the X direction. All NSPs were able to reproduce this local mechanism and the specific features in the seismic response of the building over all the intensity levels tested.

The conclusions drawn herein are based on the general response of the NSPs evaluated and illustrated in the plots presented in this thesis. Of course, there are some particular responses of certain methods that are exceptions to the conclusions outlined: in the three storey building the Extended N2 method leads in some particular cases to slightly underestimated results on the columns near the centre of mass and at the flexible edge; in the same building, the CSM-FEMA440 and the MPA lead in certain cases to slight underestimations of the response on columns near the centre of mass.

The NSPs are used to assess new or existing buildings, therefore it is required that such methods lead to safe results. The principal aspect when evaluating a NSP is to verify that the method never leads to underestimated results, i.e. it should produce conservative estimations with respect to the *time-history* median results. A second aspect consists of evaluating the capability of a NSP to produce results close to the *time-history* median values. Considering these two aspects, the study carried out showed that the Extended N2 method was the most powerful and complete NSP, out of all the evaluated procedures, for analysing the real existing plan asymmetric buildings considered herein. In fact, the method was the only one to always present conservative results in all the analysed measures over all the seismic intensities tested albeit, in some cases, it is significantly conservative. This was evident when analysing the normalized top displacements. The other NSPs analysed were not able to correctly reproduce the torsional motion of the analysed structures. They should be improved in order to better capture the torsional behaviour in this type of buildings.

9. An extension of the CSM-FEMA440 to plan asymmetric real buildings

As was observed during this thesis, the big issue when dealing with plan-asymmetric buildings, which usually leads to a less accurate performance of the currently used nonlinear static procedures, is torsion.

The results presented in the previous chapters show that the existing nonlinear static procedures cannot deal with this torsional problem in plan irregular buildings. The exception is the Extended N2 method which is the only one able to capture the torsional effects in these kinds of structures. However, this method ends up by leading to conservative results as was concluded in chapter 8. Therefore it is urgent to improve the actual existing NSPs in order to upgrade their performance in the seismic assessment of such torsional sensitive buildings.

In chapter 6 it was shown that the CSM-FEMA440 leads to far more accurate results than its predecessor CSM-ATC40 when comparing with the most exact nonlinear dynamic analysis. This was concluded for a wide range of seismic intensities, in different kinds of buildings. However, the method is not able to reproduce the seismic torsional behaviour in plan asymmetric structures. In chapter 8, it was also concluded that besides the Extended N2 method, the CSM-FEMA440 and the ACSM were the procedures that led to better results although, these two methods could not reproduce the torsional motion of such irregular structures correctly. In order to overcome the torsional issue, improvements to these two methods will be proposed in this thesis.

In this chapter an extension of the CSM-FEMA440 is proposed to overcome the torsional problem in plan irregular buildings. This proposal was based on the results presented by Fajfar and collaborators [4] and advocates that torsional amplification can be computed through the combination of a linear elastic analysis and a pushover analysis. The outcomes outlined by this team were taken to extend the N2 method to

the case of buildings with this kind of irregularities, as explained in section 2.4.2. It was concluded that in the majority of buildings an upper bound of the torsional amplifications can be determined by a linear dynamic (response spectrum) analysis also in the inelastic range.

In the first part of the chapter, the Extension of CSM-FEMA440 is described. Afterwards, the precision of the proposed method to plan asymmetric buildings is illustrated with the normalized top displacements of the structures under analysis for different levels of seismic intensity. Other plots representing the response of the analysed case studies are also presented. The results of this chapter are presented in [130].

9.1 The procedure

The extended version of the CSM-FEMA440 proposed herein takes into account the contribution of a pushover analysis, with the calculation of the target displacement based on the FEMA440 recommendations, and the contribution of a linear response spectrum analysis in order to capture the amplification due to torsion. The reduction of demand due to torsion is neglected. The entire procedure can be summarized in the following steps:

1) Perform pushover analyses with positive and negative sign for each X and Y direction of a 3D numerical model. Compute the target displacement – displacement demand at the CM at roof level – for each direction as the larger value of the + and – sign pushover. For this calculation use the CSM-FEMA440 recommendations described in section 2.4.4.2;
2) Perform a linear modal response spectrum analysis in two X and Y direction combining the results according to the SRSS rule;
3) Determine the torsional correction factors. This factor is computed doing the ratio between the normalized roof displacements obtained by the elastic response spectrum analysis and by the pushover analysis. The normalized roof displacement is obtained by normalizing the displacement value at a specific location with respect to those of the centre of mass (CM). If the normalized roof displacement obtained from the elastic response spectrum analysis is smaller than 1.0, one should consider 1.0 to avoid any favourable torsional effect (reduction of displacements) given by the elastic analysis;
4) Multiply the quantity under study for a certain location by the correction factor calculated for that location.

9.2 Assessment of the new procedure

The proposed procedure is applied to the three, five and eight storey buildings under analysis. In order to evaluate the torsional response of the buildings the results are presented in terms of normalized top displacements.

In each of the subsequent plots, RSA represents the results of the elastic response spectrum analysis and TH the median results of the *time-history* analysis.

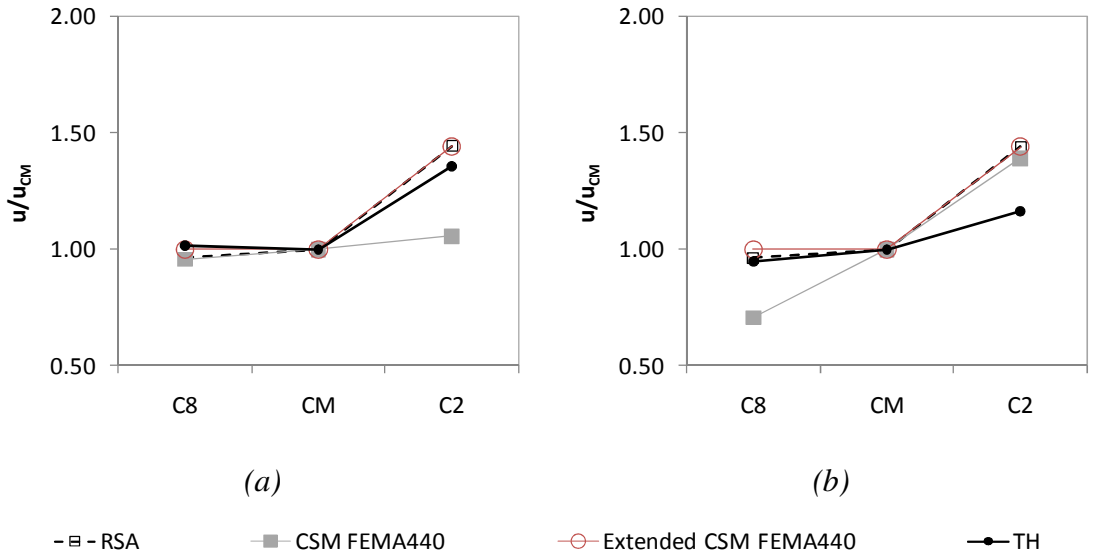

Figure 9.1 – Three storey building, X direction: a) 0.1g; b) 0.3g.

In Figure 9.1a) the good agreement is observed between the Extended CSM-FEMA440 and the *time-history* results for the 3 storey building in the X direction for an intensity level of 0.1g. The original CSM-FEMA440 presents a good match with the *time-history* in the column C8, while in column C2 this method significantly underestimates the response. The torsional amplification in column C2 is correctly captured by the Extended CSM-FEMA440. The RSA leads to underestimated results in column C8 when compared with the *time-history*, but it matches quite perfectly the response of column C2. Note that in this last column the results of RSA are the same as the ones obtained with the Extended CSM-FEMA440.

In Figure 9.1b), for 0.3g also in the X direction, one can observe the good performance of the proposed method for the column C8. In fact, the results perfectly match the *time-history* ones. For this column the original method presents under conservative results. For column C2 both original and Extended CSM-FEMA440 presents conservative estimations. The RSA reproduces in a very good fashion the behaviour of column C8, and it overestimates the response in column C2. The RSA results in column C2 correspond to the ones of the Extended CSM-FEMA440.

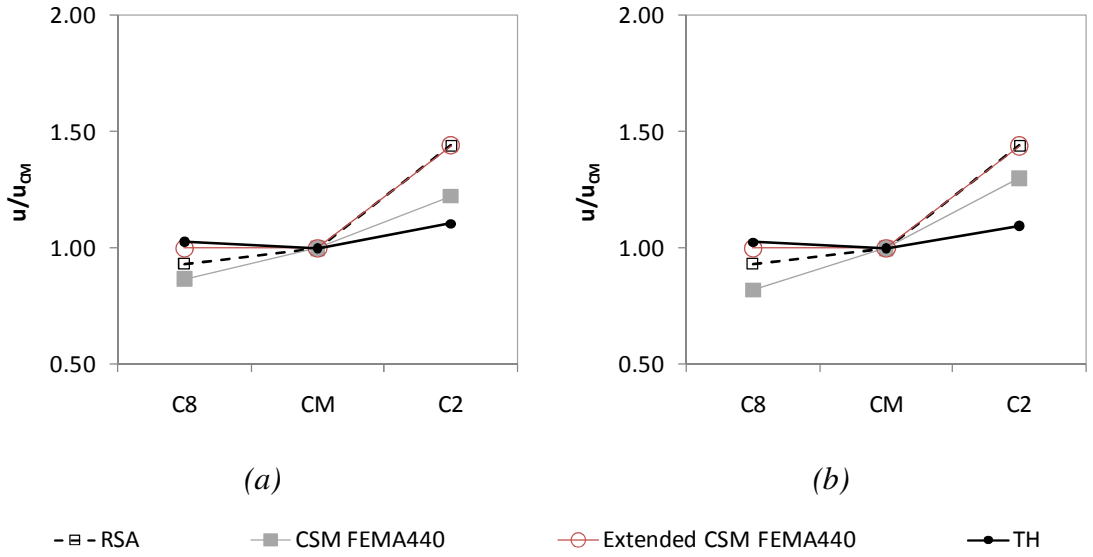

Figure 9.2 – Three storey building, Y direction: a) 0.2g; b) 0.3g.

In the Y direction, for the 3 storey building, for both 0.2 and 0.3g, Figure 9.2, the response of the column C8 is perfectly reproduced by the proposed procedure, while the original method underestimates the results. In fact, the unrealistic favourable effect of torsion (de-amplification of displacements) given by the original CSM-FEMA440 on this side of the building is not considered by the extended procedure. For both intensity levels, the results for the column C2 are overestimated by both methods. The RSA underestimates the results in column C8 for both intensities, but it matches the response of the Extended CSM-FEMA440 in column C2.

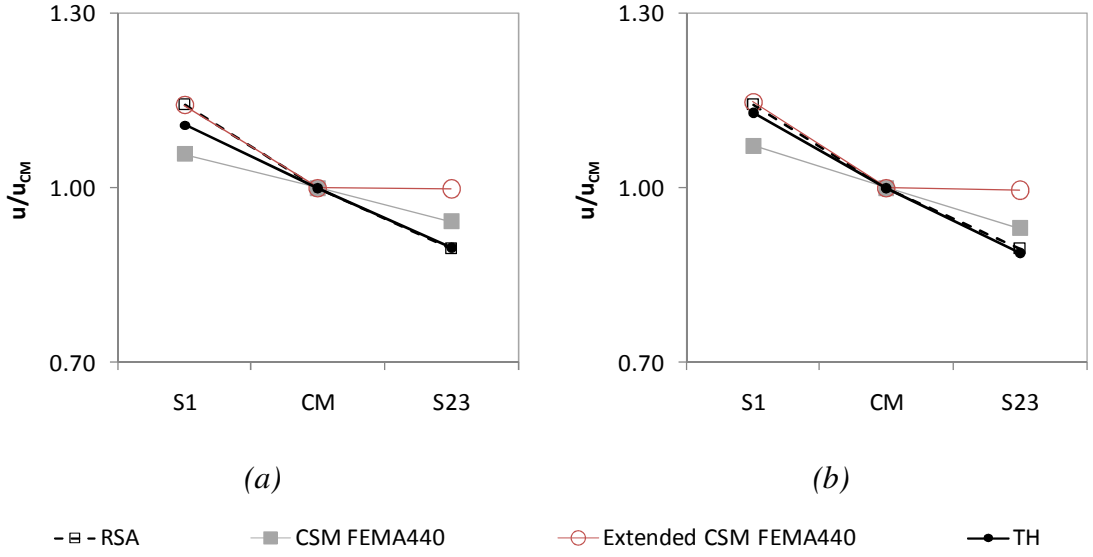

Figure 9.3 – Five storey building, X direction: a) 0.1g; b) 0.2g.

Figure 9.3 represents the response of the 5 storey building in the X direction for 0.1g and 0.2g. Based on the results obtained one can conclude that for column S1 the proposed procedure perfectly reproduces the realistic response, while the original

procedure leads to underestimated results. In column S23 both methods lead to conservative results. The RSA reproduces in a very accurate manner the *time-history* results on both sides of the building for both intensity levels.

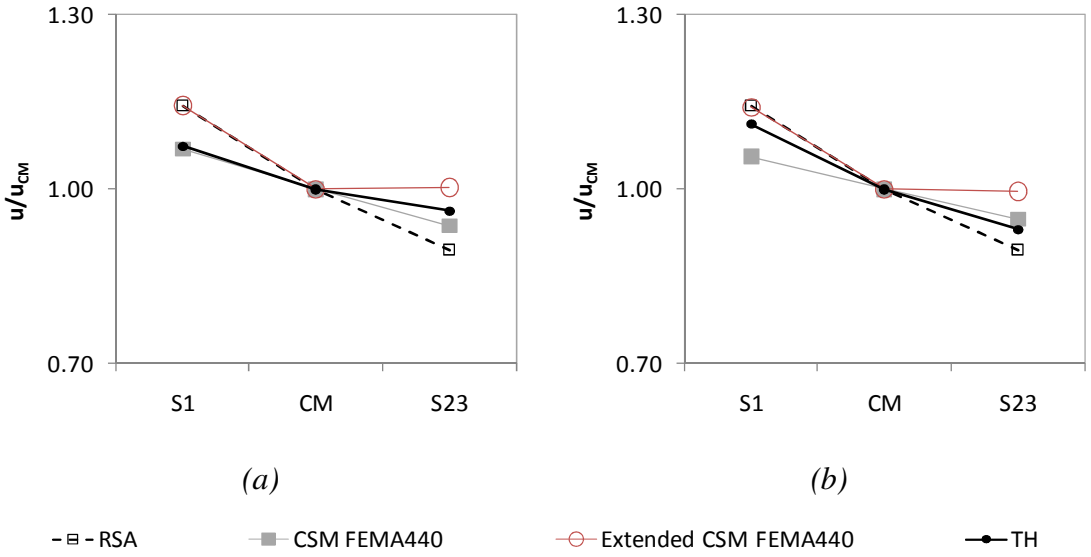

Figure 9.4 – Five storey building, X direction: a) 0.4g; b) 0.6g.

From the plots of Figure 9.4 it can be seen that for column S1 the proposed method gives conservative results for 0.4g and a good match for 0.6g.

For the same column, the original procedure leads to a good response for 0.4g and to under conservative estimations for 0.6g. In column S23, the Extended CSM-FEMA440 always gives conservative results, while the original method leads to an under conservative response for 0.4g and to a good match for 0.6g. The RSA considerably underestimates the response of column S23 for both intensities and it matches the Extended CSM-FEMA440 results in column S1.

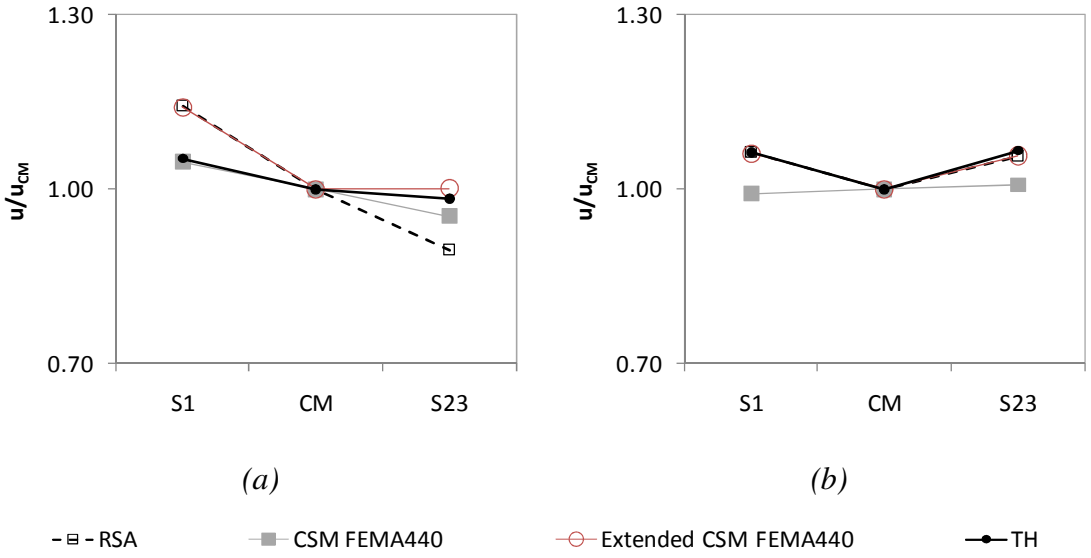

Figure 9.5 – Five storey building: a) X direction, 0.8g; b) Y direction, 0.8g.

For the X direction but for 0.8g, Figure 9.5a), once again the extended method proposed herein leads to conservative results in column S1 and to a very good match in column S23. The original method perfectly matches the response of column S1 but underestimates the results for column S23. The response of column S23 is once again underestimated by the RSA for this intensity level.

In the Y direction for 0.8g, Figure 9.5b), the torsional motion of the building is perfectly reproduced by the Extended CSM-FEMA440 and by RSA. The original method underestimates the response on both sides of the building.

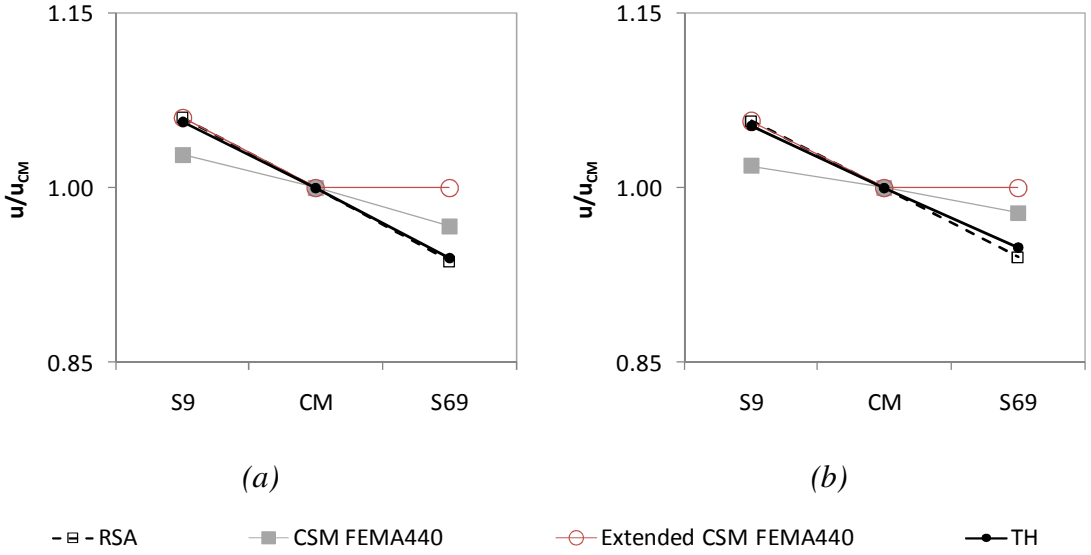

Figure 9.6 – Eight storey building, X direction: a) 0.1g; b) 0.2g.

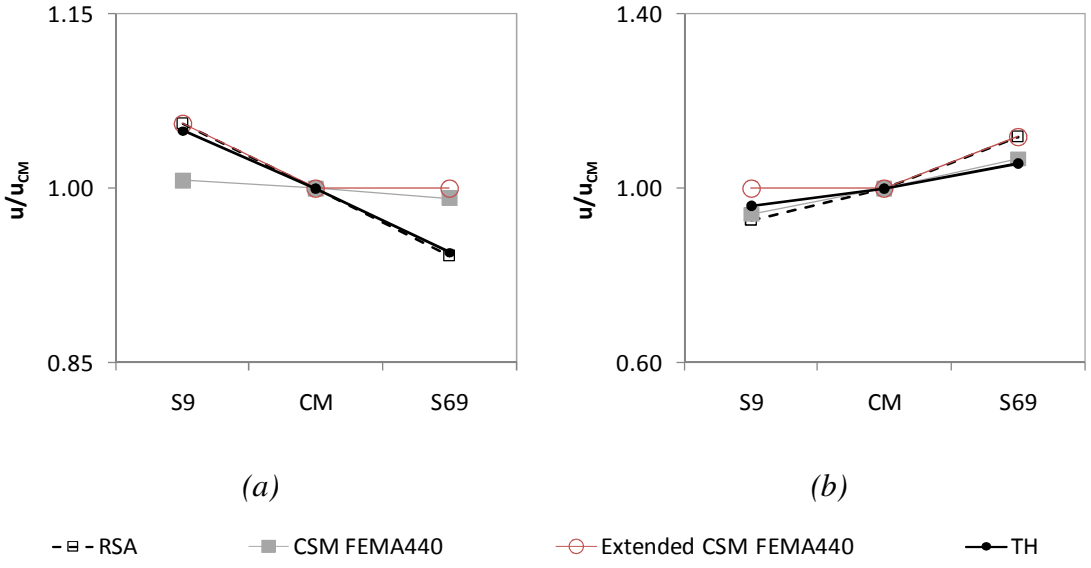

Figure 9.7 – Eight storey building: a) X direction 0.4g; b) Y direction 0.4g.

In the 8 storey building the Extended CSM-FEMA440 perfectly captures the response of the column S9 for both 0.1g and 0.2g in the X direction, Figure 9.6. For this column the original procedure leads to non conservative results. The response of column S69 is overestimated by both methods. The same conclusions can be drawn for the X direction for 0.4g, Figure 9.7a). The RSA perfectly reproduces the *time-history* results in the X direction for all the intensity levels analysed.

In the Y direction for 0.4g, Figure 9.7b), both methods reproduce the torsional motion of the building quite well, except the original procedure which slightly underestimates the response of the column S9. The RSA underestimates the results in column S9 in the Y direction for 0.4g, but it matches the Extended CSM-FEMA440 in column S69.

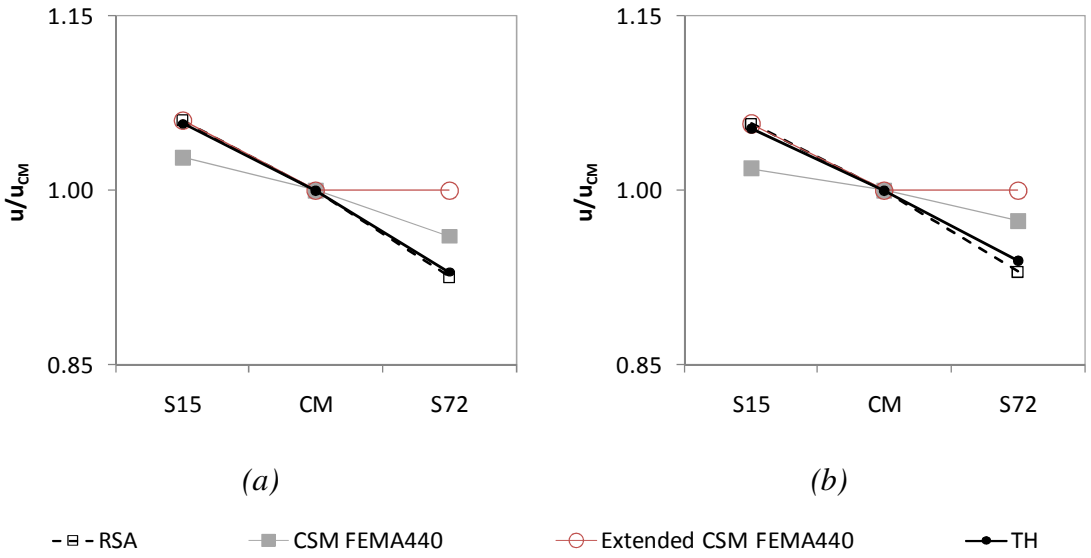

Figure 9.8 – Eight storey building, X direction: a) 0.1g; b) 0.2g.

For the same building, Figure 9.8 shows that the Extended CSM-FEMA440 reproduces in a very good fashion the response of the column S15 for both 0.1g and 0.2g in the X direction. On the other hand, the original procedure leads to under conservative results in exactly the same column. The response of column S72 is overestimated by both methods. The same conclusions can be drawn for the X direction for 0.4g, Figure 9.9a). Once again, the RSA perfectly reproduces the *time-history* median results in the X direction over all the seismic intensities tested.

In the Y direction for 0.4g, Figure 9.9b), both methods capture in a very good manner the torsional behaviour of the building, except the original procedure that slightly underestimates the response of the column S72. The RSA slightly underestimates the results in column S72 in the Y direction for 0.4g, but it perfectly matches the Extended CSM-FEMA440 in column S15.

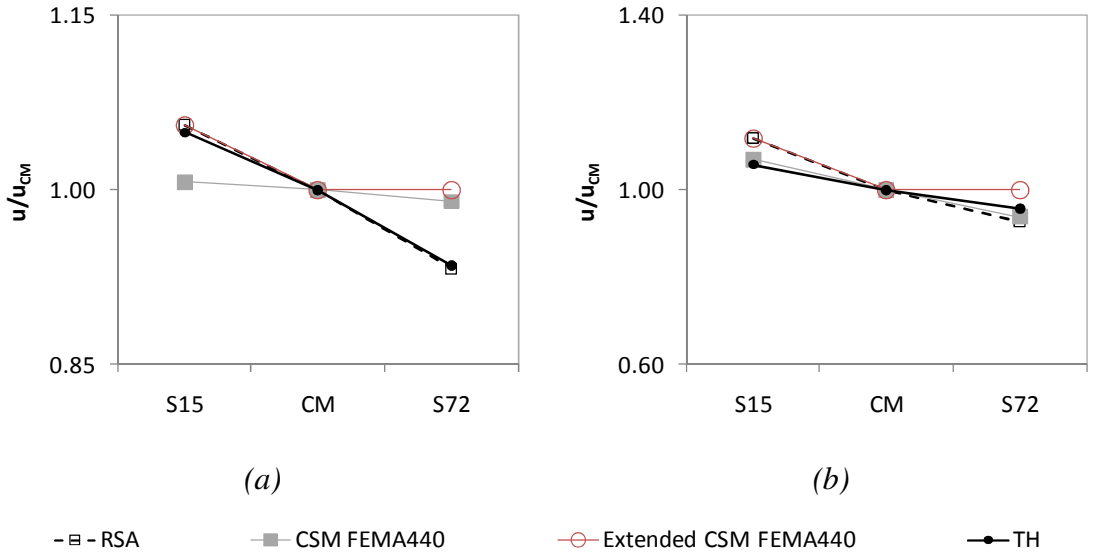

Figure 9.9 – Eight storey building: a) X direction 0.4g; b) Y direction 0.4g.

The improvement in the performance of the proposed Extended CSM-FEMA440 when compared with its original version is evident in the response of the flexible edge, column C2, of the three storey building, Figure 9.10 to Figure 9.19. For this element, the original CSM-FEMA440 is not able to capture the torsional amplification, leading to under conservative results in terms of lateral displacement profiles, interstorey drifts, chord rotations and top displacement ratios. On the other hand, the Extended CSM-FEMA440 using the proposed torsional correction factors, is able to reproduce these amplifications.

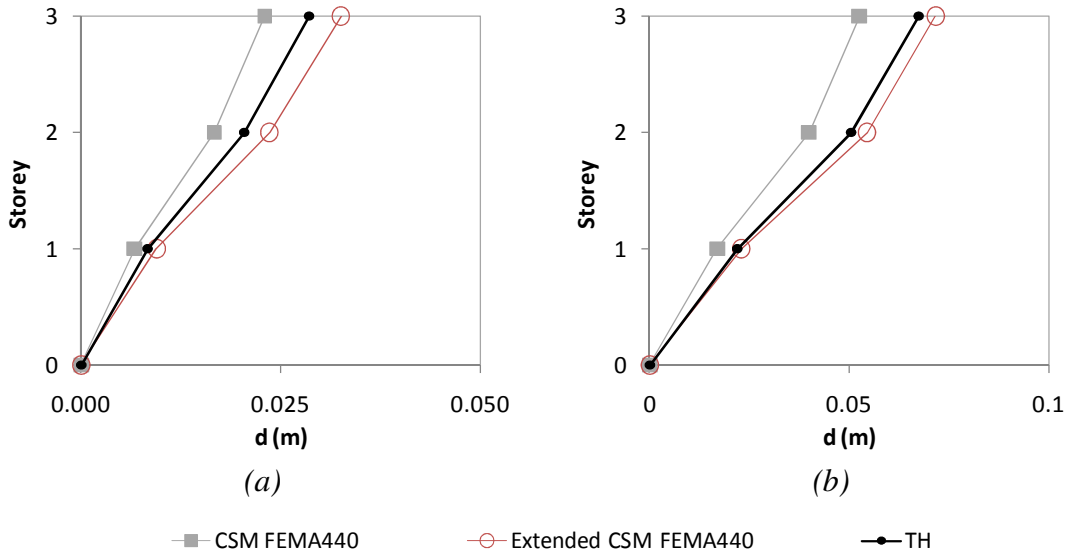

Figure 9.10 – Lateral displacement profiles, X direction: a) 0.05g; b) 0.1g.

Figure 9.10 to Figure 9.12 show the lateral displacement profiles on the flexible edge, column C2, of the three storey building, in both X and Y directions through different levels of inelasticity.

From the plots, one can observe that the original CSM-FEMA440 leads to under conservative results in terms of lateral displacements. The extended procedure can accurately capture the amplification of the displacements due to torsion on this flexible side of the structure.

In the Y direction for 0.3g, where the building presents a very high level of inelasticity, the original method computes very good results while the extended procedure leads to slightly conservative estimations.

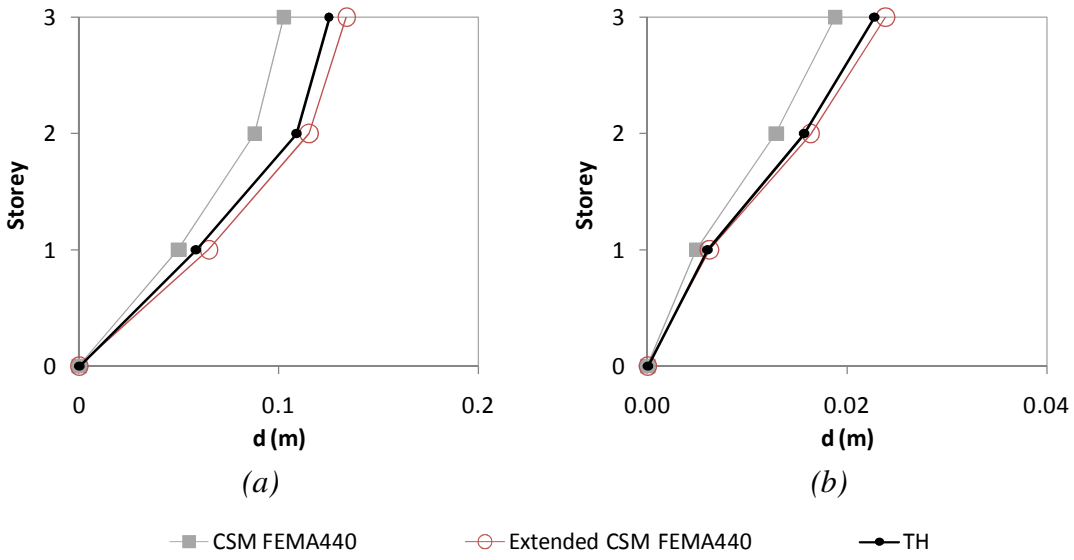

Figure 9.11 – Lateral displacement profiles: a) X direction, 0.2g; b) Y direction, 0.05g.

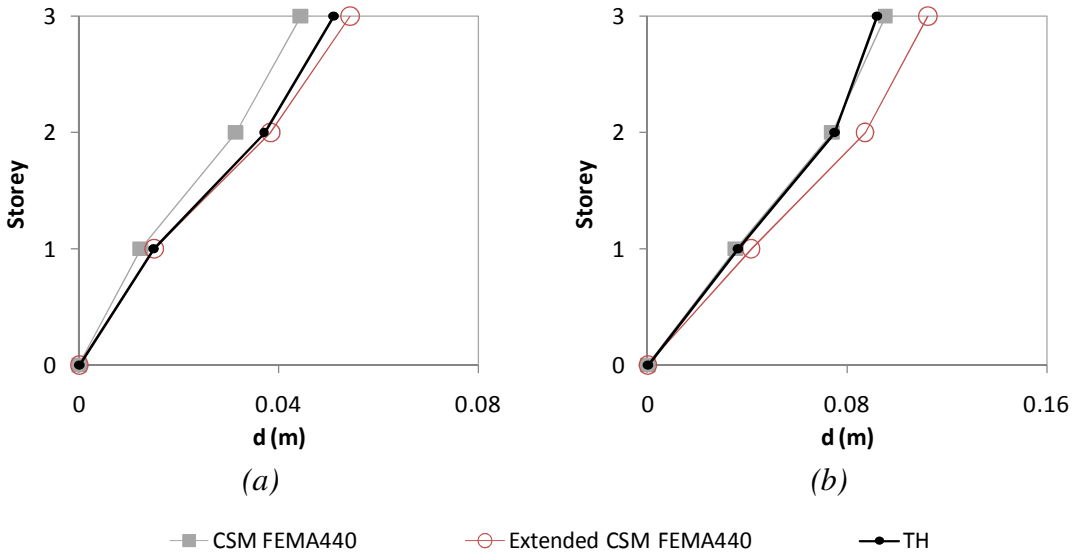

Figure 9.12 – Lateral displacement profiles, Y direction: a) 0.1g; b) 0.2g.

Figure 9.13 to Figure 9.15, show the interstorey drifts at the same flexible edge, over several seismic intensities.

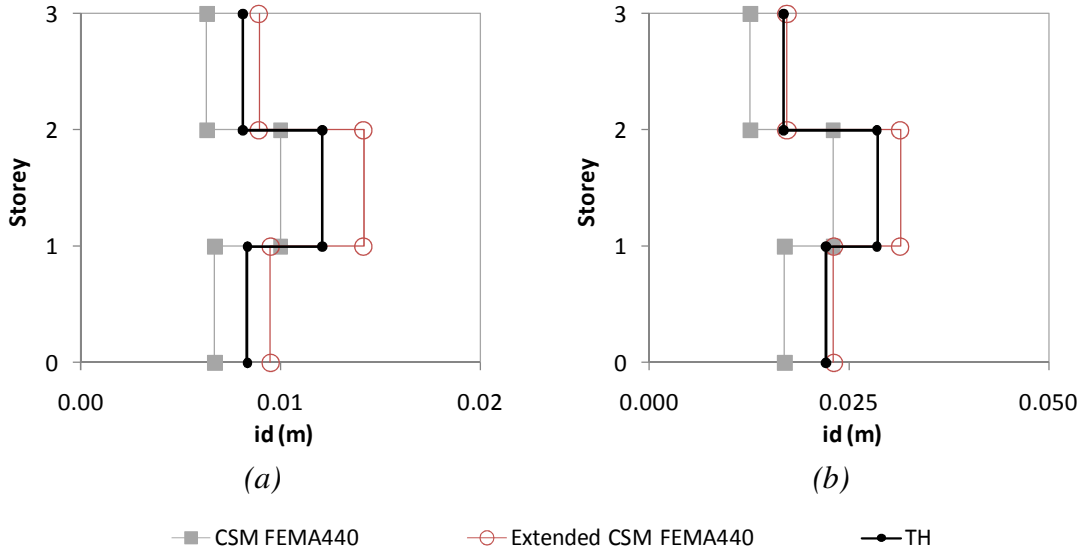

Figure 9.13 – Interstorey drifts, X direction: a) 0.05g; b) 0.1g.

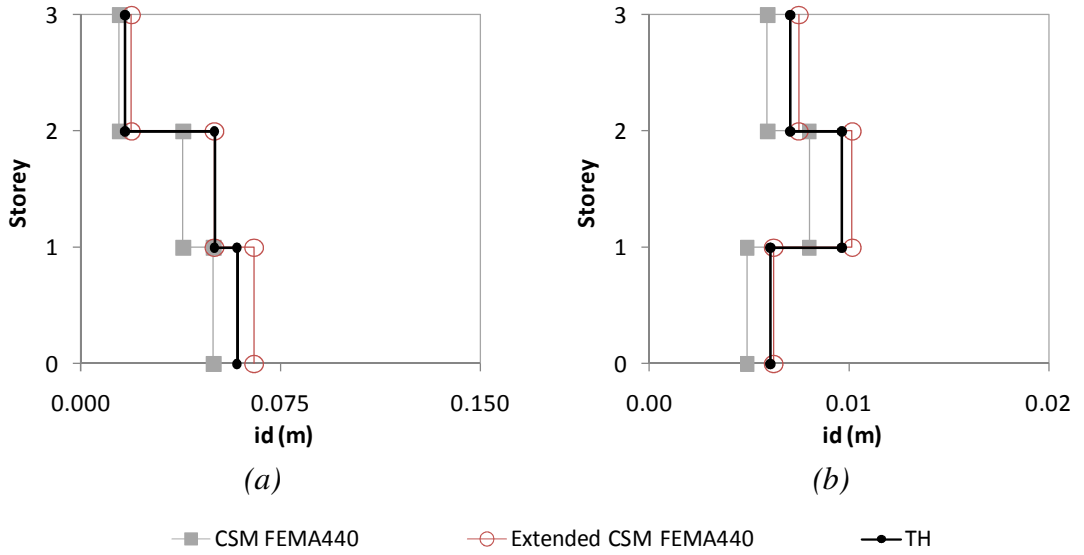

Figure 9.14 – Interstorey drifts: a) X direction, 0.2g; b) Y direction, 0.05g.

From the plots, one can conclude once again, that the original CSM-FEMA440 invariantly leads to under conservative results, while the extended procedure can capture in a very good fashion the amplification of the interstorey drift profiles due to torsion.

In the Y direction for 0.3g, the original method can reproduce quite well the *time-history* median results and the extended procedure is slightly conservative. This happens for a very high level of structural inelasticity.

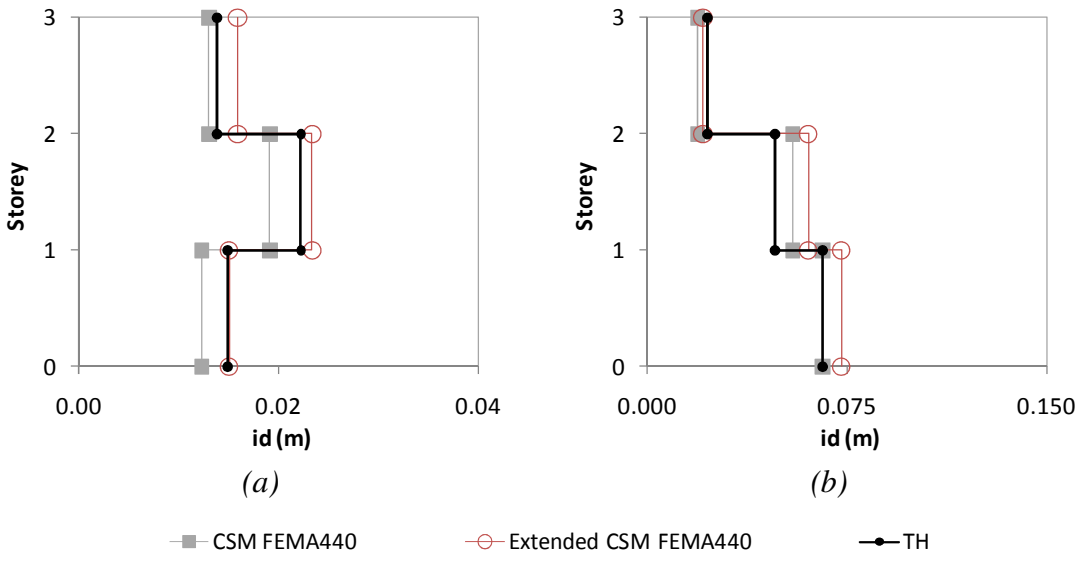

Figure 9.15 – Interstorey drifts, Y direction: a) 0.1g; b) 0.3g.

Chord rotations are represented from Figure 9.16 to Figure 9.18. The same conclusion made for the previous plots can also be drawn herein.

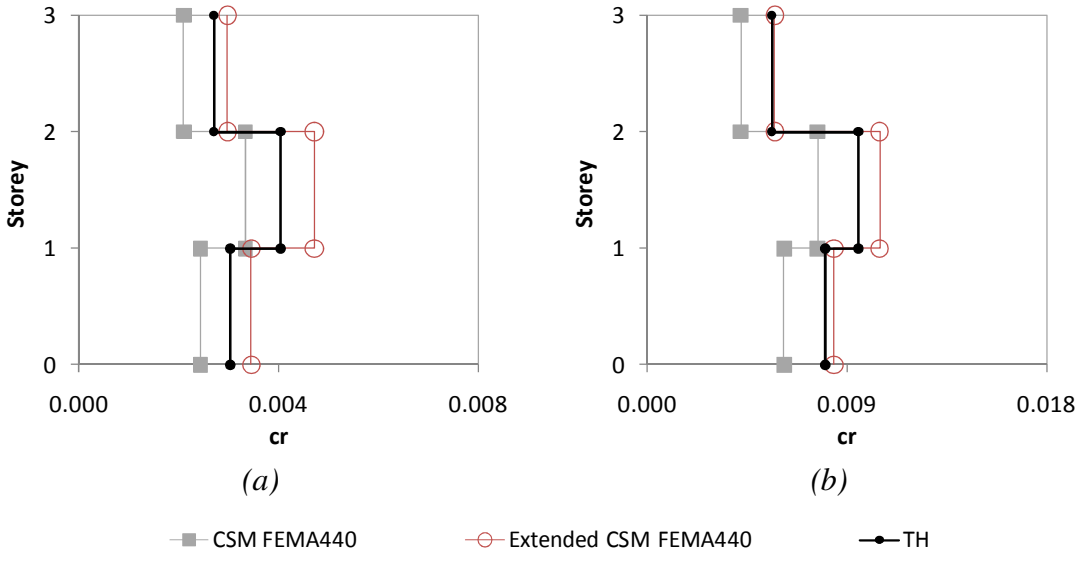

Figure 9.16 – Chord rotations, X direction: a) 0.05g; b) 0.1g.

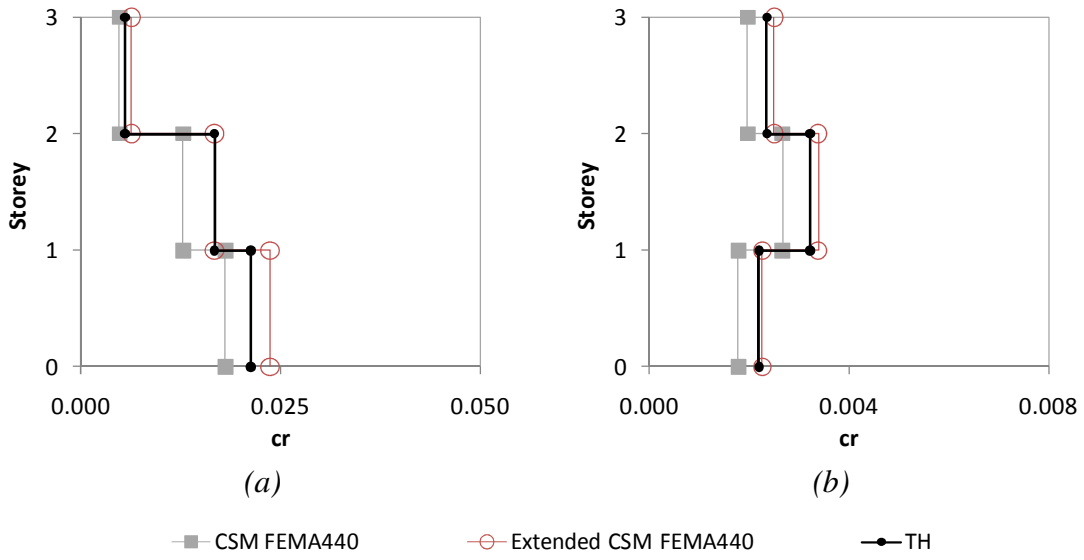

Figure 9.17 – Chord rotations: a) X direction, 0.2g; b) Y direction, 0.05g.

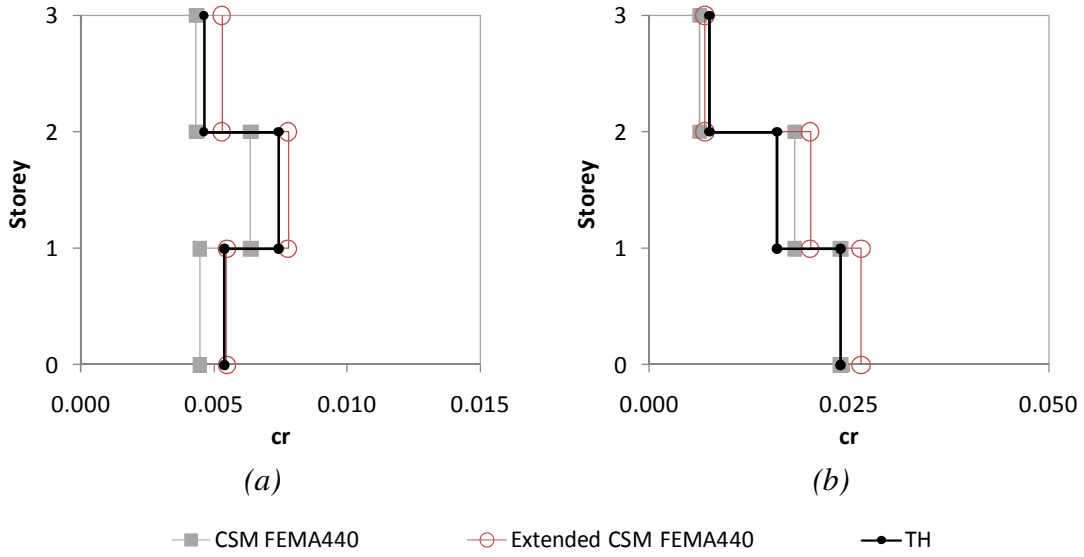

Figure 9.18 – Chord rotations, Y direction: a) 0.1g; b) 0.3g.

Figure 9.19 shows the top displacement ratios between the NSPs under analysis and the *time-history* median results, at the flexible edge.

One can conclude that in the X direction, the original method leads to under conservative top displacements while the extended procedure perfectly matches the nonlinear dynamic results. The exception occurs for a seismic intensity of 0.3g where

both original and Extended CSM-FEMA440 lead to the same and conservative results.

In the Y direction, the original method leads to under conservative top displacements in the elastic range, 0.05g and 0.1g. For the inelastic stage, 0.2g and 0.3g, the method correctly estimates the *time-history* results. The Extended CSM-FEMA440 perfectly matches the nonlinear dynamic analysis for 0.05g and 0.1g, and slightly overestimates it for 0.2g and 0.3g.

Once again, the Extended CSM-FEMA440 seems to capture the torsional amplification on the flexible side of the SPEAR building, while the original method generally leads to underestimated responses.

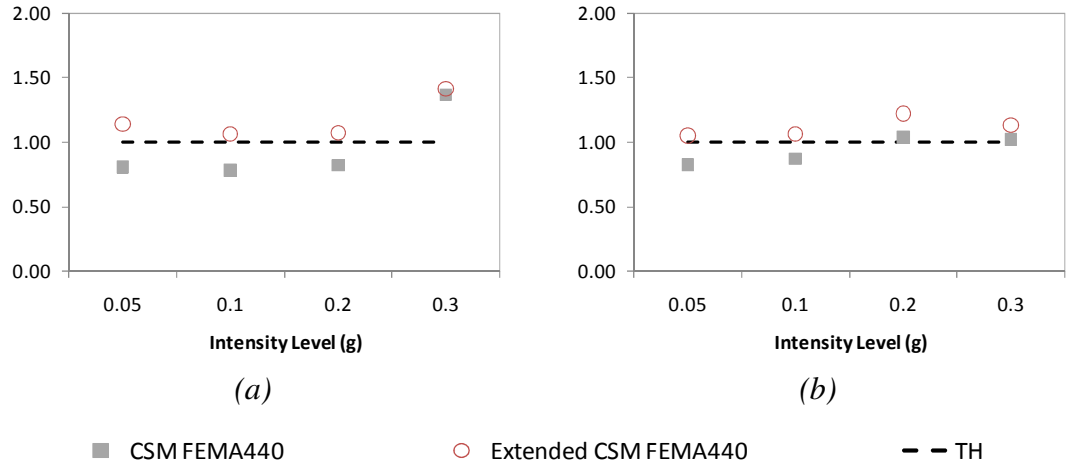

Figure 9.19 – Top displacements ratios: a) X direction; b) Y direction.

9.3 Discussion

From the presented results one can conclude that the Extended CSM-FEMA440 proposed herein captures in a more accurate fashion the torsional motion of the studied buildings for all seismic intensities than the original CSM-FEMA440 procedure.

From the plots presented above it is observed that the Extended CSM-FEMA440 adequately reproduces the torsional amplification in all buildings through all the seismic intensities in both directions. This happens because the method uses a correction factor based on a RSA which also leads to very good estimations of the torsional amplifications, as shown in the plots. The original CSM-FEMA440 generally underestimates the torsional amplification in the buildings.

The plots also show that both RSA and the original CSM-FEMA440 consider the torsional de-amplification. In some cases these methods led to underestimated results.

On the other hand the Extended CSM-FEMA440 does not consider any positive effect due to torsion, as explained before in the description of the procedure, leading in some cases to very accurate results and in others to conservative responses. One can say that this is a safe criterion for designing. In fact it must not be forgotten that these simplified procedures are developed to be applied in design offices where the results should rather be conservative than almost close to *time-history* but slightly underestimated.

The results obtained herein seem quite optimistic regarding the implementation of this extended procedure in future codes, namely in the ATC guidelines. Nevertheless, more studies in different buildings should be developed in order to consolidate this nonlinear static approach.

10. A new 3D Pushover Procedure for seismic assessment of plan irregular buildings

From the results obtained in chapters 6, 7 and 8 one can conclude that the most commonly used NSPs nowadays, are not able to give completely reliable results when assessing 3D buildings irregular in plan. In fact, the torsional motion of these structures is not well captured by these methods. The exception was the Extended N2 method, although this NSP usually led to significant conservative results, namely in the five and eight storey buildings studied in this work.

The CSM, with both features of ATC40 and FEMA440, the original N2 and the MPA, had a lack of accuracy in determining the response, in terms of damage measures such as lateral displacement profiles, top displacements, interstorey drifts, and chord rotations, of the columns located on the edges of the three storey building. The methods were not able to correctly reproduce the torsional motion which has an important role in the structural behaviour of such elements. The Extended N2 method could generally capture the response in a good fashion at the centre of mass and at the flexible edge of the three storey building but it usually overestimated the response in the other buildings. However, in some cases the method underestimated the response at the stiff edge of the three storey building in terms of lateral displacement profiles, interstorey drifts, chord rotations and top displacement ratios.

As was mentioned before, the normalized top displacements is a measure that expresses the ability of each method in reproducing the relative displacements in plan between the extremities and the centre of mass, giving an idea about how good a NSP estimates the torsional motion of the building. The Extended N2 method was the only method to estimate this measure in a conservative way in the three buildings over all the seismic intensities analysed. The ACSM could only reproduce the torsional

behaviour of the three storey building, but it was not able to do it adequately in the five and eight storey buildings, where it usually underestimated the normalized top displacement at one of the edges of the building. The other methods were not able to reproduce the torsional motion of the buildings analysed in this work in a correct manner.

Chapter 9 proposed an extension of the CSM-FEMA440 in order to increase its capabilities of estimating the torsional behaviour of plan irregular structures. The results obtained were quite good, although they can be improved.

Therefore, in this chapter a new 3D Pushover methodology is presented. The new procedure combines the most advanced and accurate features of some of the methods analysed, and it intends to be a powerful tool to perform nonlinear static analysis in 3D buildings asymmetric in plan leading to reliable and accurate responses. The results obtained herein, show that the proposed methodology seems to be able to handle the torsional problem in a very smart fashion, invariantly leading to better results than the most commonly used NSPs.

In the first part of the chapter the features of the new procedure are described. Afterwards, the new 3D Pushover procedure is duly compared with each of the existing NSPs and the advantages over the existing procedures are outlined. Final observations are pointed out at the end. The results of this chapter are presented in [133].

10.1 Description of the new 3D Pushover procedure

The new 3D Pushover methodology is based on some of the best features of the most commonly used NSPs. The steps of the proposed procedure are described herein.

Step 1: Perform a displacement based adaptive pushover (DAP)

The first step of the procedure consists of the development of a 3D nonlinear model of the building, in which the nonlinear monotonic behaviour of the materials is perfectly defined. For this, one can adopt a distributed plasticity strategy through the use of fibre elements, or a concentrated plasticity option through the definition of plastic hinges - in terms of Moment-Curvature section behaviour and plastic hinge length. As was previously mentioned, in this work a distributed plasticity strategy has been adopted. For this model and in the case of reinforced concrete structures, one has to define the geometry of the section and the amount of longitudinal reinforcement in order to correctly calculate the sectional nonlinear relationships. It is also necessary to estimate the mass supported by each beam-column and beam-beam joint, at each storey level.

Afterwards, one should perform a displacement based adaptive pushover (DAP) [46] on the 3D model defined. The pushover is performed separately in each X and Y directions, with the + and – sense in each direction, resulting in four analyses per building. The DAP algorithm is available in several software packages, such as SeismoStruct [104] and OpenSees [134]. The innovative features of the algorithm are described in section 2.4.5.

Step 2: Characterization of the equivalent SDOF

At this stage, the characterization of the adaptive capacity curve of the SDOF is computed step by step from the DAP analysis performed in step 1 of the procedure. This transformation was proposed by Casarotti and Pinho in 2007 [53], and is based on the principle of Substitute Structure analogy which was also derived using the principle of equal work developed, as described in section 2.4.5.

The adaptive SDOF curve is obtained step by step, according to equations Eq. 2.55, Eq. 2.56 and Eq. 2.57.

The procedure described in this step has to be repeated for the four DAP analyses performed in step 1 (curves obtained in the X and Y directions, in both positive and negative senses). Therefore, one obtains four equivalent SDOF adaptive capacity curves.

Step 3: Calculation of the target displacement

In this step, the target displacement of the equivalent SDOF is calculated by intersecting the adaptive capacity curve obtained in step 2 with the reduced elastic response spectrum (in the acceleration-displacement format) corresponding to the seismic action considered, Figure 10.1.

The intersection point is called the performance point, and corresponds to the inelastic acceleration and to the target displacement of the equivalent SDOF.

Note that, in this work the demand was defined by a real earthquake spectrum rather than a smoothed design spectrum. Therefore more than one intersection with the capacity curve may be obtained. The intersection point chosen was the one corresponding to the largest deformation as explained in the last paragraph of section 4.2.1.

As was previously mentioned, the elastic response spectrum is reduced using factors dependent on the effective damping. Its formulation is based on the proposals recommended in the FEMA440 report presented in 2005 [16], and described in section 2.4.4.2.

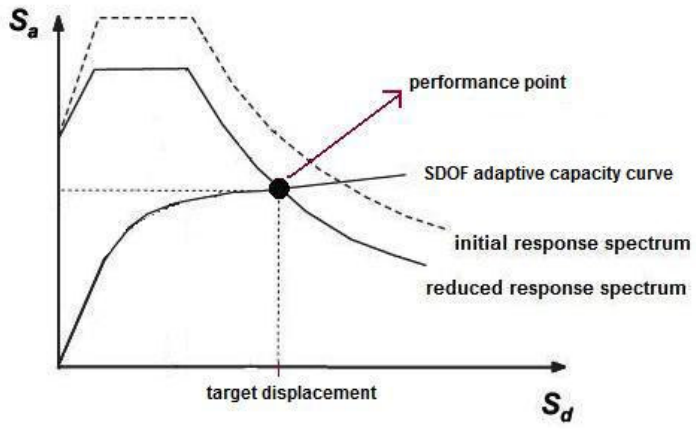

Figure 10.1 – Calculation of the performance point and the target displacement of the equivalent SDOF.

Effective damping

The effective damping depends on the ductility level μ of the structure and it is calculated using equations Eq. 2.43, Eq. 2.44 and Eq. 2.45. The effective damping-ductility function is plotted in Figure 2.22. These formulas apply to any capacity curve, independent of hysteretic model type or post-elastic stiffness value (α) used.

Effective Period

The effective period depends on the ductility level and it is calculated using equations Eq. 2.46, Eq. 2.47 and Eq. 2.48. The effective period-ductility function is plotted in Figure 2.23. Once again, these equations apply to any capacity spectrum independent of hysteretic model type or post-elastic stiffness value.

Spectral reduction factor for effective damping

The spectral reduction factor is a function of the effective damping and is called the damping coefficient, $B(\beta_{eff})$ and is calculated using Eq. 2.50. It is used to adjust spectral acceleration ordinates as shown in Eq. 2.49. The reduction factor B as a function of the effective damping β_{eff} is illustrated in Figure 2.24.

Modificated acceleration-displacement response spectrum (MADRS)

After reducing the initial ADRS by using the $B(\beta_{eff})$ factor as described, one should multiply the acceleration ordinates (i.e. not the displacement ordinates) of the new reduced ADRS by the modification factor, M. This factor is determined using the calculated effective period, T_{eff}, as shown in Eq. 2.51 and Eq. 2.52, in order to compute the modified acceleration-displacement response spectrum (MADRS). See Figure 2.25.

Where α is the post-elastic stiffness, and μ the ductility, calculated according to equations Eq. 2.53 and Eq. 2.54.

At this stage, the target displacement is calculated by an iterative process described as follows:

a) Consider an initial value for the ductility μ;
b) Calculate the effective period based on equations Eq. 2.46, Eq. 2.47 and Eq. 2.48;
c) Calculate the effective damping based on equations Eq. 2.43, Eq. 2.44 and Eq. 2.45;
d) Calculate the reduction factor *B*, according to equation Eq. 2.50, to be applied to the initial elastic acceleration-displacement response spectrum (ADRS), according to equation Eq. 2.49;
e) Calculate the modification factor *M*, based on equations Eq. 2.51 and Eq. 2.52;
f) Multiply the spectral accelerations of the ADRS reduced in d) by the modification factor *M*, in order to get the modified acceleration-displacement response spectrum (MADRS);
g) Intersect the SDOF adaptive capacity curve with the modified acceleration-displacement response spectrum (MADRS). The intersection point is called the performance point. The abscissa of this point corresponds to a first trial of the target displacement, see Figure 10.1;
h) Bilinearize the SDOF adaptive capacity curve at the performance point calculated in g);
i) Calculate the ductility μ as the ratio between the target displacement (calculated in g)) and the displacement corresponding to the yielding point of the bilinear curve calculated in h), see Eq. 2.54;
j) If the ductility μ calculated in i) is close to the initial trial defined in a) – within an error range of 5% – the process ends and the target displacement of the SDOF system is the one calculated in g). Otherwise, the cycle should be repeated. Therefore, one should return to a) using for the ductility μ, the value calculated in i) of the previous cycle. This procedure should be repeated until the convergence of the ductility value μ is reached.

The previously described procedure should be repeated for each one of the SDOF adaptive capacity curves defined in step 2 (curves obtained for the X and Y directions, in both + and – senses). Therefore, two target displacements in the X direction (+ and – senses) are obtained as well as two target displacements in the Y direction (+ and – senses). The target displacement chosen in each direction should be the larger of the + and – senses.

Step 4: Determination of MDOF response parameters in correspondence to the Performance Point (converted from SDOF to MDOF)

To calculate the structural response in each direction, one should check the step *k* of the SDOF curve corresponding to the target displacement calculated in step 3, and go to the same step *k* of the MDOF pushover curve in order to take the displacement at the centre of mass of the roof. For that level of displacement, take the response parameters of the building.

Example: if the target displacement of the SDOF in the X direction calculated in step 3 corresponds to the DAP analysis along the + sense, then:

a) One should define the step *k* of the SDOF capacity curve corresponding to this target displacement;
b) One should return to the step *k* of the DAP analysis along the X direction in the + sense, and take the displacement at the centre of mass of the roof;
c) For the displacement calculated in b), take the response parameters of the building.

The final results in both directions of the structure are combined at the end using the SRSS (square root of the sum of squares) rule.

Step 5: Calculation of the torsional correction factors

In this step a linear response spectrum analysis of the 3D mathematical model is performed, applying the excitation in both directions and combining them using the SRSS rule. In this analysis, the materials that constitute the building have an elastic behaviour, and the response spectrum used is the elastic one.

The torsional correction factors calculated herein are based on the proposal of Fajfar and his team [4, 8], previously presented in chapters 7 and 8, to the extension of the N2 method for plan asymmetric buildings. The conclusions drawn by Fajfar and his team showed that in the majority of the buildings it is possible to calculate an upper bound of the torsional amplifications through a linear response spectrum analysis.

The torsional correction factors are determined calculating the ratio between the normalized top displacements (in the last floor) obtained from the linear response spectrum analysis and from the pushover analysis (steps 1, 2, 3 and 4 of this procedure). The normalized top displacements are obtained normalizing the displacement at a certain location of the roof with respect to those at the centre of mass of the roof. If the normalized top displacement obtained from the linear response spectrum analysis is smaller than 1.0, one should consider it 1.0 in order to avoid any de-amplification of displacements due to torsion given by this elastic analysis. Note that, each location has a torsional correction factor for the X direction and another one for the Y direction.

Step 6: Final structural performance

Multiply the quantity under analysis in an element, at a certain location in plan, by the torsional correction factor calculated for that location.

10.2 Performance of the new 3D Pushover procedure

In this section, the results obtained with the new 3D Pushover procedure are presented and compared with the commonly used NSPs analysed in the previous chapters. The comparisons are presented in terms of lateral displacement profiles, interstorey drifts, chord rotation profiles, top displacement ratios and normalized top displacements.

More results of the comparisons between the new 3D Pushover procedure and the CSM-FEMA440, the ACSM, the Extended N2 and the MPA are plotted in Appendix A15, Appendix A16, Appendix A17 and in Appendix A18 respectively.

10.2.1 Lateral displacement profiles

Comparisons of lateral displacement profiles between the proposed procedure and other NSPs are presented from Figure 10.2 to Figure 10.13

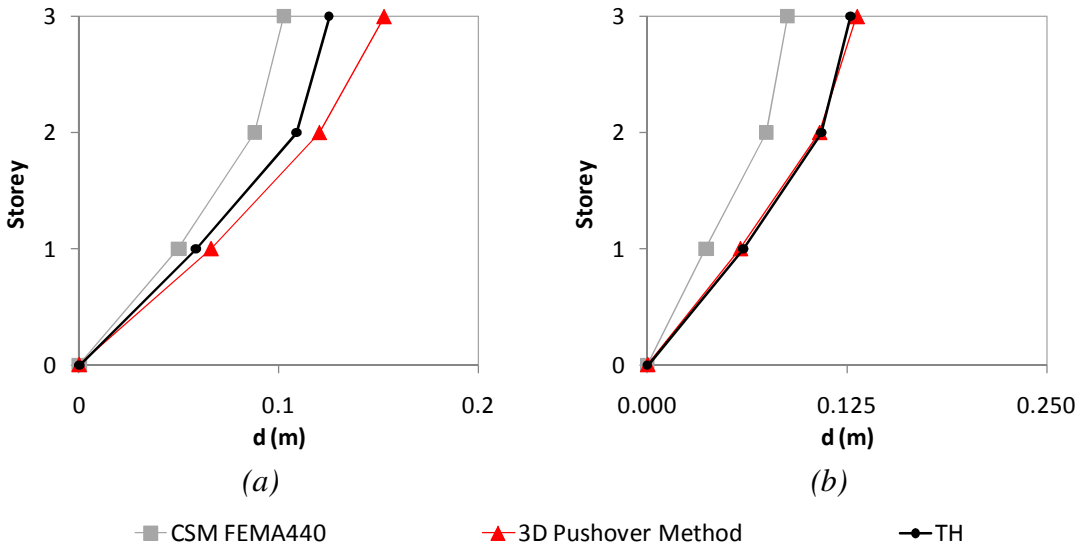

Figure 10.2 – Lateral displacement profiles, three storey building: a) column C2, X, 0.2g; b) column C8, Y, 0.3g.

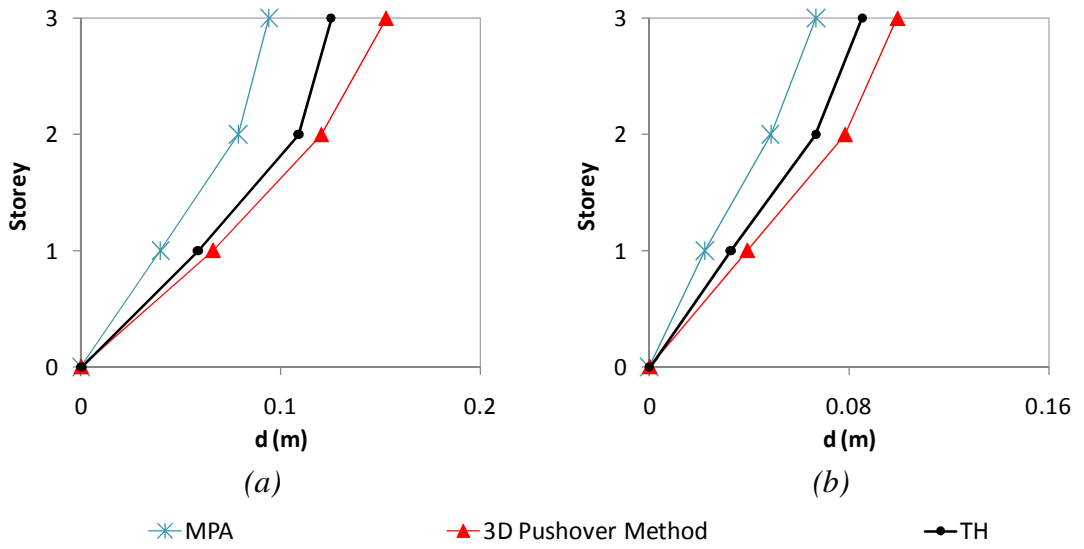

Figure 10.3 – Lateral displacement profiles, three storey building: a) column C2, X direction 0.2g; b) column C8, Y direction 0.2g.

In terms of lateral displacement profiles, one can observe that in the three storey building, the proposed 3D Pushover method leads to better estimations than CSM-FEMA440 and MPA, especially on the edge columns. In fact, in the peripheral columns of this building both CSM-FEMA440 and MPA cannot reproduce the torsional motion, leading to underestimated displacement profiles. The new 3D Pushover method generally leads to responses very close to the *time-history*, or slightly conservative responses. These conclusions are valid for all the seismic intensities analysed.

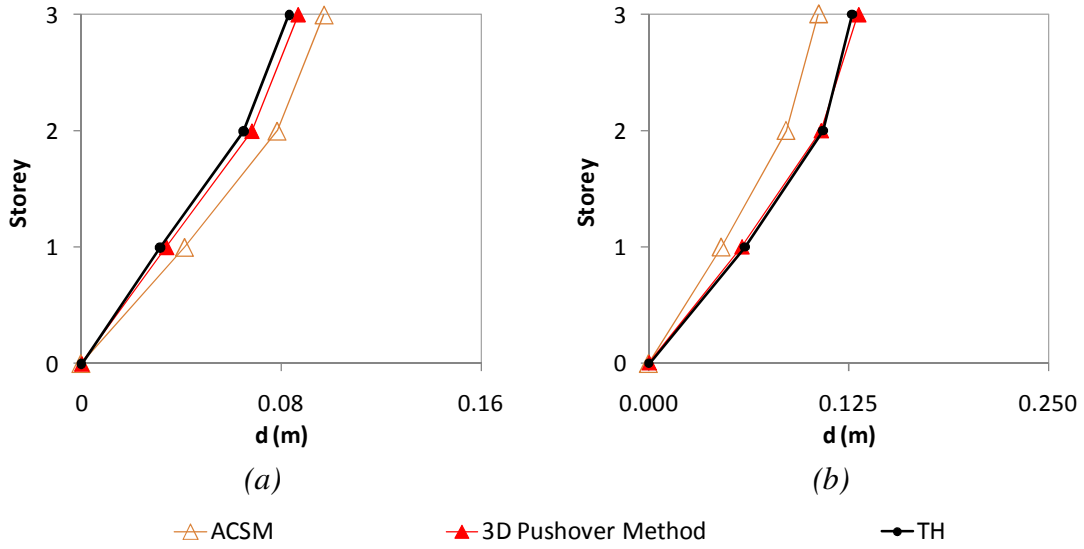

Figure 10.4 – Lateral displacement profiles, three storey building, Y direction: a) column C3 0.2g; b) column C8 0.3g.

In the same building, the original ACSM leads in certain cases to slightly non conservative estimations at the stiff edge, column C8. On the other hand, the proposed

method is able to adequately reproduce the torsional motion of the building. The new 3D Pushover method leads to results closer to the *time-history* than the ACSM as happens in the central column C3.

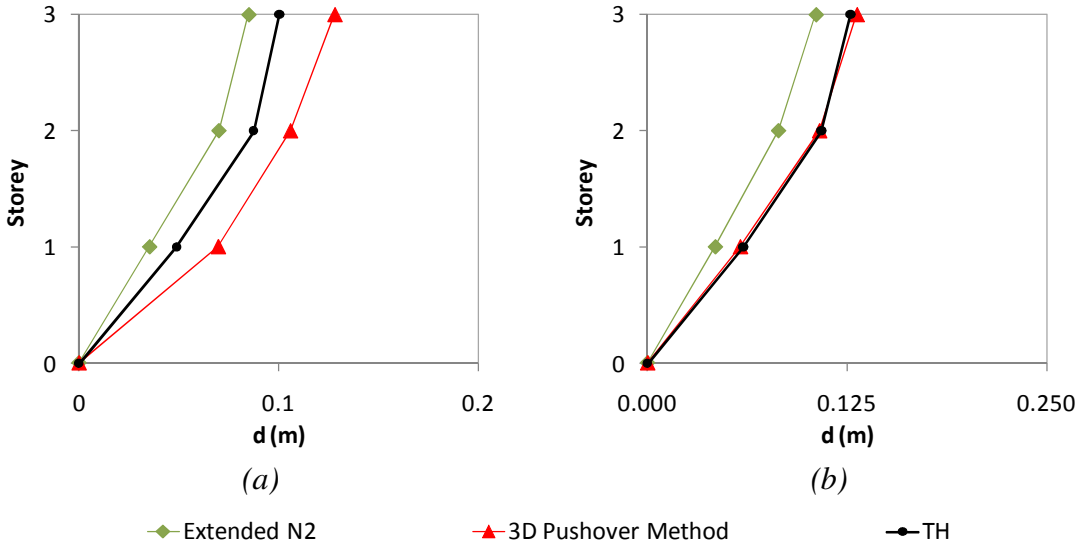

Figure 10.5 – Lateral displacement profiles, three storey building, column C8: a) X direction 0.2g; b) Y direction 0.3g.

As was explained in chapters 7 and 8 the Extended N2 method reproduces in a very good fashion the torsional motion of the three storey building and therefore the response on the edge columns. Despite this generally good performance, the method sometimes underestimates the lateral displacements at the stiff edge, column C8, as one can observe in Figure 10.5. On the contrary, the proposed method reproduces in a good manner the response in terms of lateral displacement profiles, never underestimating the *time-history* results.

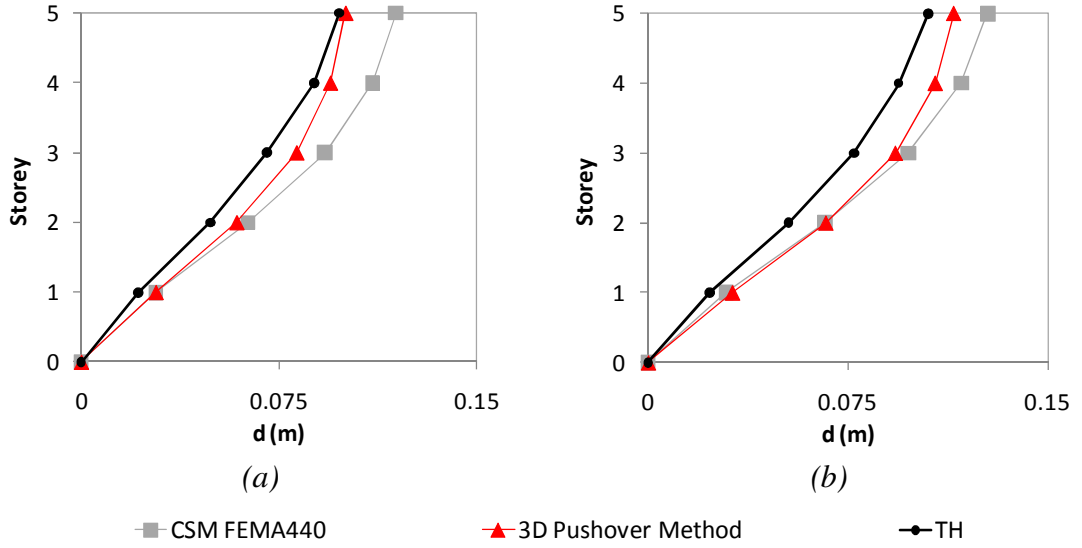

Figure 10.6 – Lateral displacement profiles, five storey building, X direction: a) column S13, 0.4g; b) column S1, 0.4g.

In the five storey building one can conclude that both methods lead to conservative estimations of the lateral displacement profiles. The results are very similar for the first two storeys, but the 3D Pushover method proposed herein presents a better match with the *time-history* response for the three upper storeys. These conclusions can be drawn for all the seismic intensities tested in the five storey building.

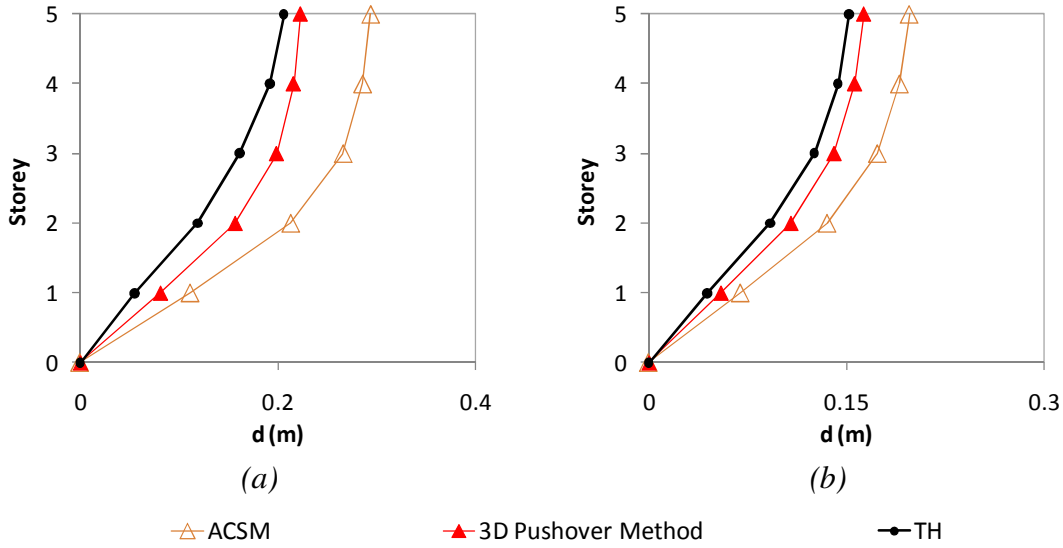

Figure 10.7 – Lateral displacement profiles, five storey building, X direction: a) column S23, 0.8g; b) column S14 0.6g.

The new 3D Pushover procedure leads to results close to the *time-history*, while the ACSM provides conservative estimations of the lateral displacement profiles in the five storey building.

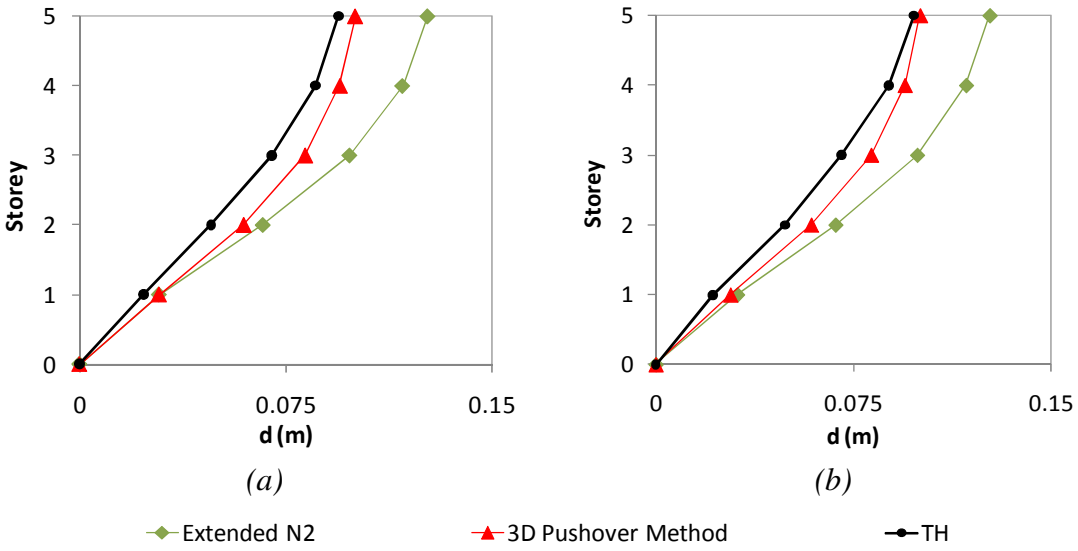

Figure 10.8 – Lateral displacement profiles, five storey building: a) column S23, X direction 0.4g; b) column S13, X direction 0.4g.

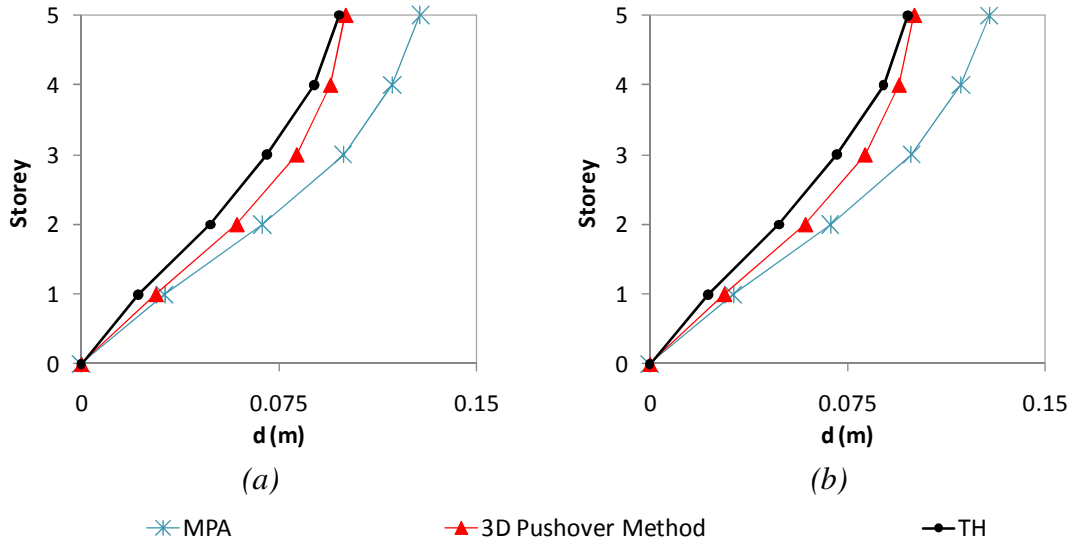

Figure 10.9 – Lateral displacement profiles, five storey building: a) column S13, X direction 0.4g; b) column S14, X direction 0.4g.

In the five storey building, the Extended N2, the MPA and the new 3D Pushover method are able to reproduce quite perfectly the lateral displacement profiles in the first two storeys. However, in the upper floors the proposed procedure is able to reproduce in a more accurate fashion the pattern of the lateral displacement profiles than the other two methods. In fact, by using the DAP the 3D Pushover method is able to capture in a more accurate way the evolution of the nonlinearity in the structure and the contribution of the higher mode effects. On the other hand, the other two methods lead invariantly to conservative estimations of the structural response.

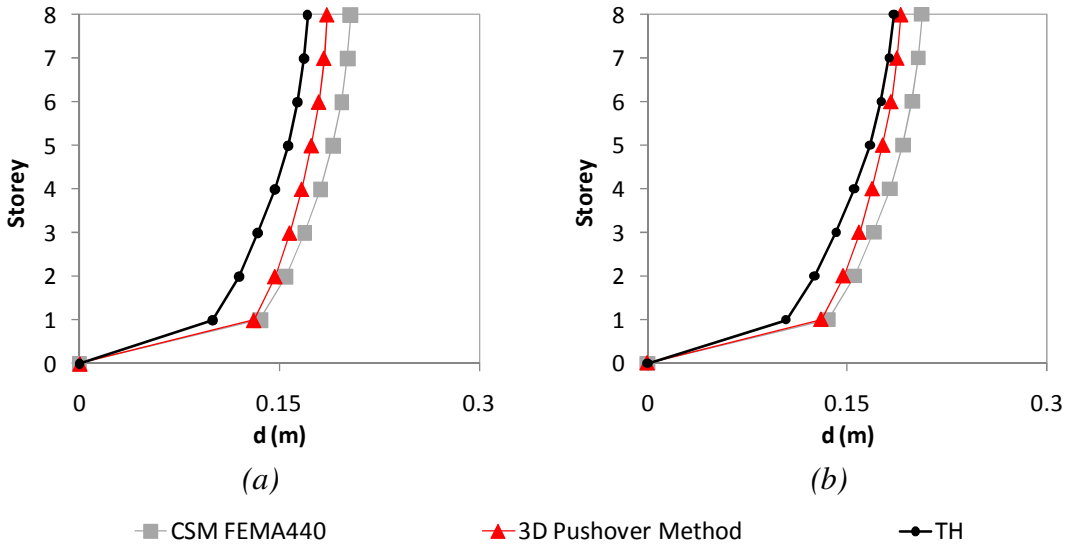

Figure 10.10 – Lateral displacement profiles, eight storey building, X direction: a) column S69, 0.4g; b) column S23, 0.4g.

In the eight storey building, both CSM-FEMA440 and the new 3D Pushover method lead to slightly conservative estimations of the lateral displacement profiles.

Although, the proposed procedure suggested herein leads to better results than the CSM-FEMA440. In fact, as the height increases, the proposed method leads to results which are closer to the *time-history* than the method proposed in FEMA440. As the inelastic behaviour increases, the accuracy of the proposed method also increases. Both methods reproduce in a good manner the soft storey mechanism on the first floor, but the 3D Pushover method leads to better estimations on the upper floors.

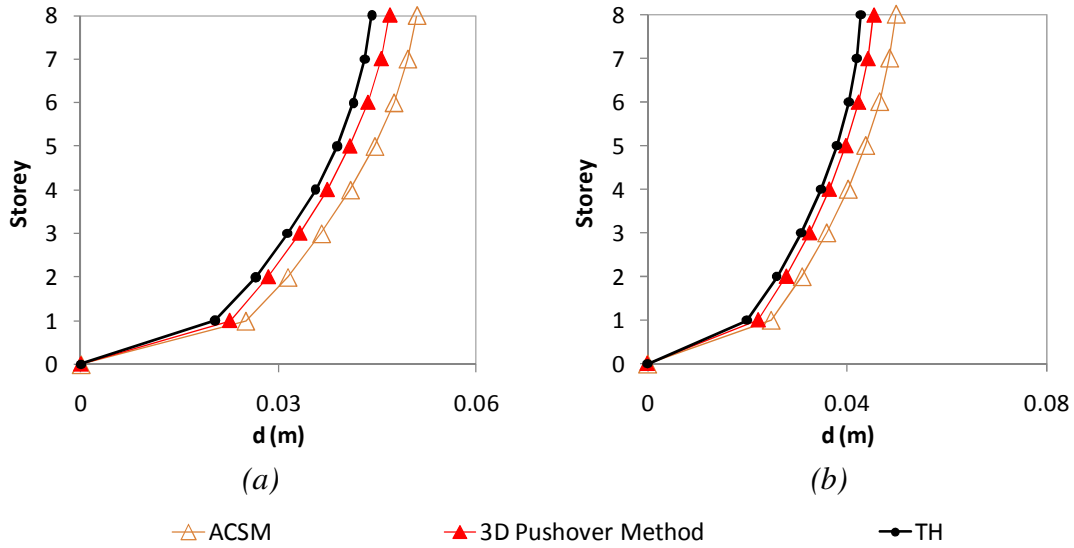

Figure 10.11 – Lateral displacement profiles, eight storey building, X direction, 0.1g: a) column S9; b) column S23.

The ACSM and the new 3D Pushover methods are able to correctly reproduce the soft storey mechanism on the first floor of the eight storey building. However, the proposed procedure matches in a more accurate fashion the *time-history* profiles than the original ACSM on the upper floors, but always on the conservative side.

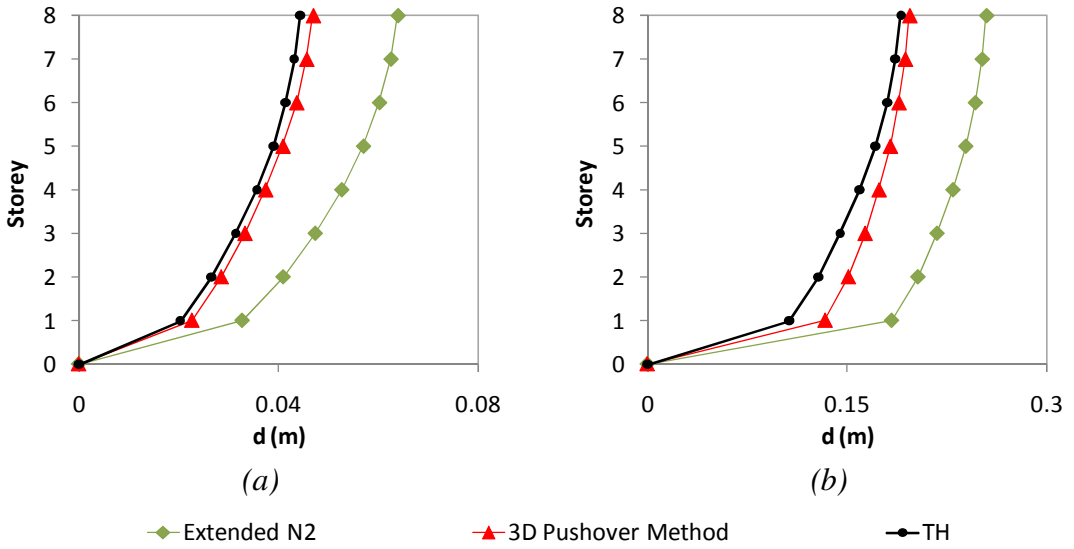

Figure 10.12 – Lateral displacement profiles, eight storey building: a) column S15, X direction 0.1g; b) column S9, X direction 0.4g.

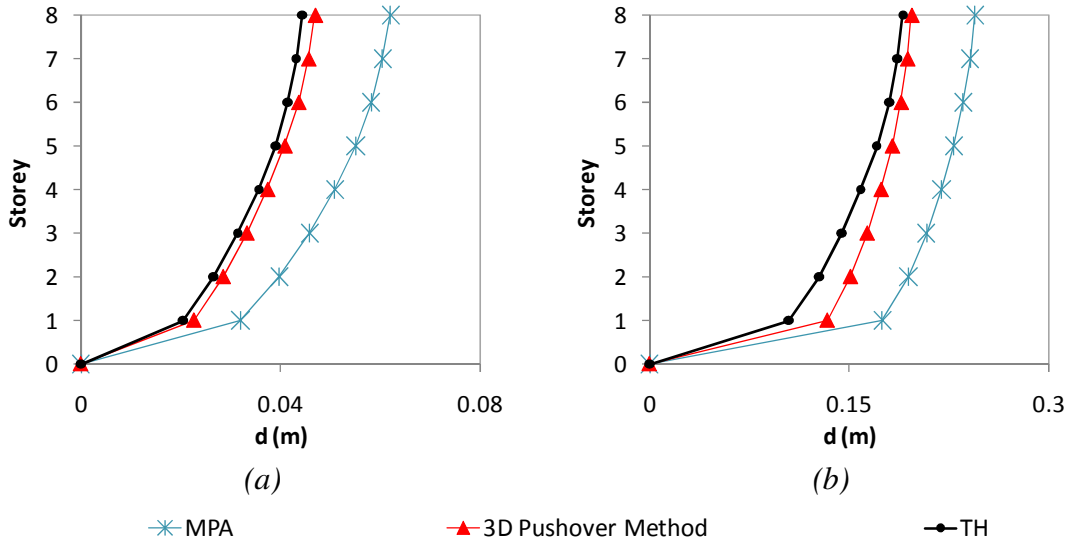

Figure 10.13 – Lateral displacement profiles, eight storey building: a) column S9, X direction 0.1g; b) column S15, X direction 0.4g.

In the eight storey building, the Extended N2 method and the MPA overestimate the soft storey mechanism in the first floor, while the proposed procedure leads to results closer to the *time-history*. In fact, by using DAP the method is able to capture in a better manner the development of the structural damage.

10.2.2 Interstorey drifts and chord rotations profiles

Figure 10.14 to Figure 10.21 illustrate the comparisons between the proposed method and the other NSPs in terms of interstorey drifts and chord rotation profiles.

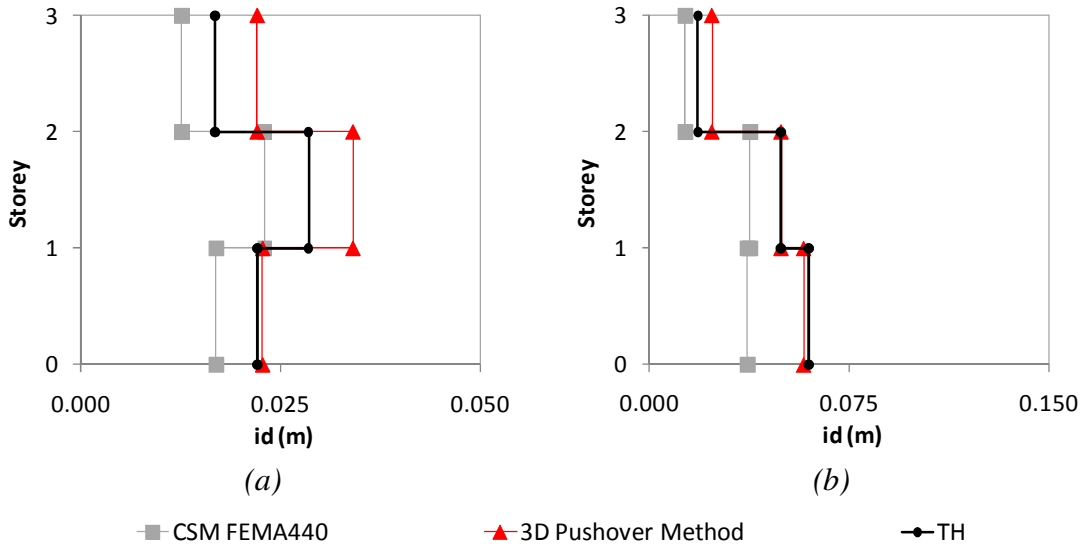

Figure 10.14 – Interstorey drifts profiles, three storey building: a) column C2 X direction 0.1g; b) column C8 Y direction 0.3g.

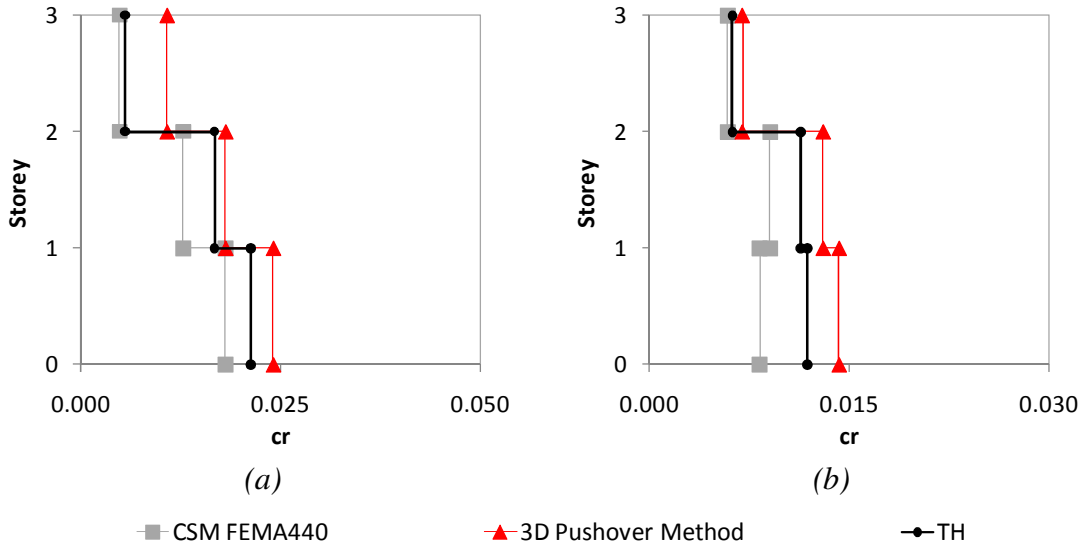

Figure 10.15 – Chord rotations profiles, three storey building: a) column C2 X direction 0.2g; b) column C8 Y direction 0.2g.

In terms of interstorey drifts and chord rotation profiles, one can observe that the new 3D Pushover method captures in a good fashion the response at the edges of the three storey building. On the other hand, the CSM-FEMA440 underestimates these measures on the same extremity columns.

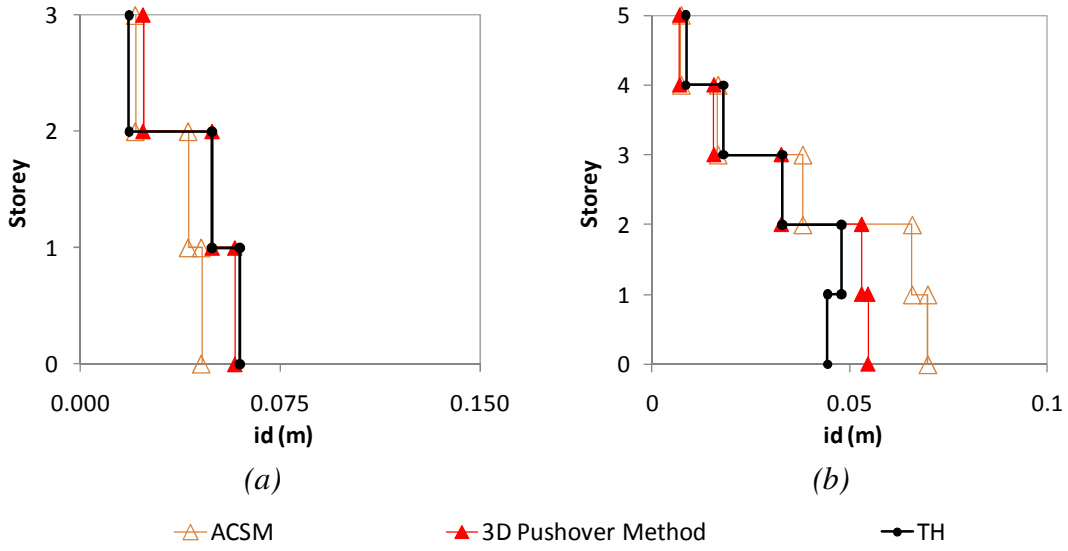

Figure 10.16 – Interstorey drifts profiles: a) three storey building, column C8, Y direction 0.3g; b) five storey building, column S14, X direction 0.6g.

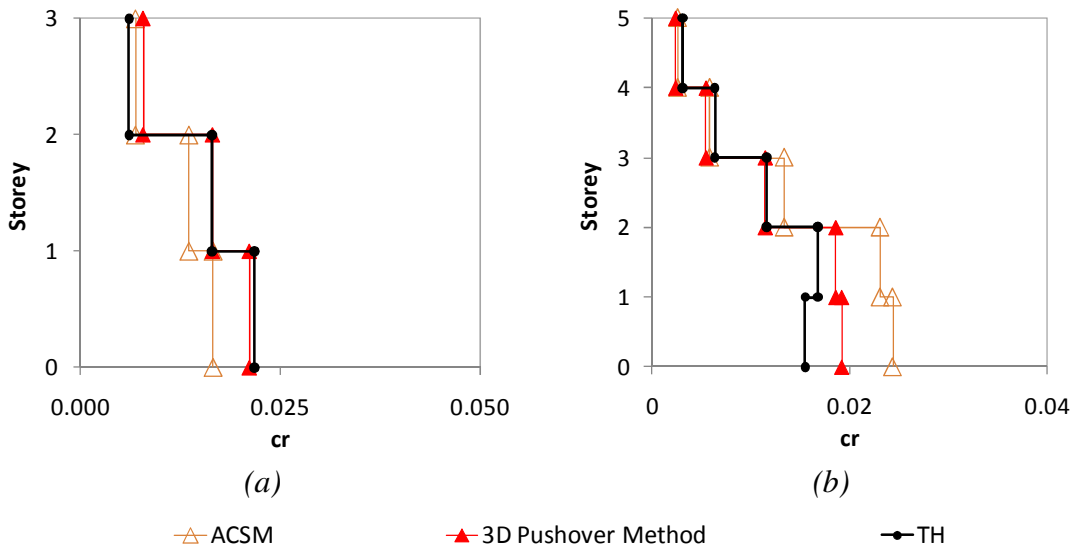

Figure 10.17 – Chord rotations profiles: a) three storey building, column C8, Y direction 0.3g; b) five storey building, column S14, X direction 0.6g.

In the three storey building, the original ACSM leads in some cases to underestimated interstorey drifts and chord rotations mainly on the first and second floors of the stiff edge column, because the method is not able to reproduce in a perfect fashion the torsional behaviour of the building. The new 3D Pushover method reproduces adequately both interstorey drifts and chord rotations profiles.

In the five storey building, the proposed 3D Pushover method practically matches the *time-history* results in the three upper storeys, leading to slightly conservative estimation on the first two storeys, but still close to the *time-history* profiles. The original ACSM leads to the same results of the proposed procedure in the upper floors, but in the first two storeys it overestimates the response.

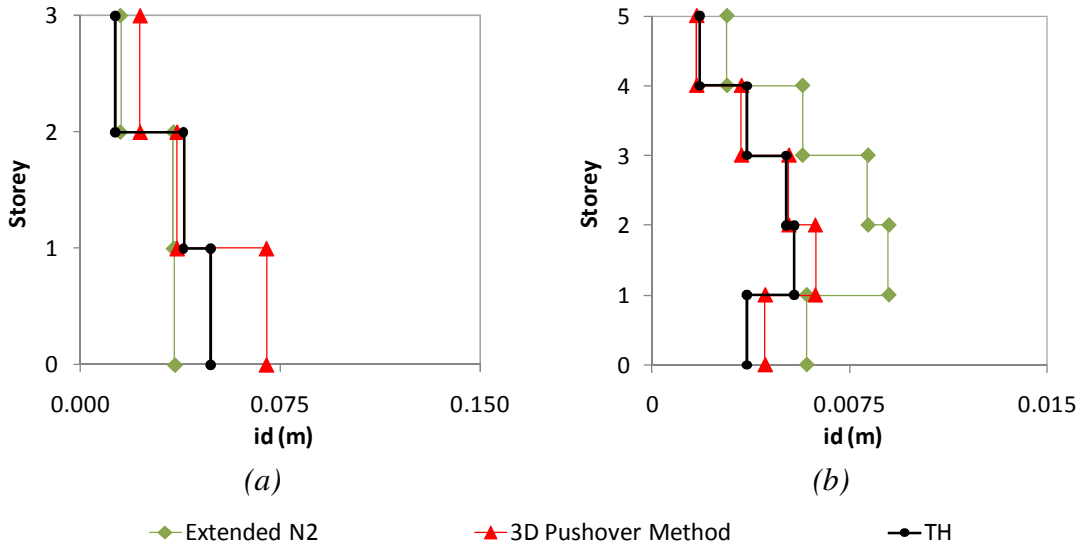

Figure 10.18 – Interstorey drifts profiles, X direction: a) three storey building, column C8, 0.2g; b) five storey building, column S13, 0.1g.

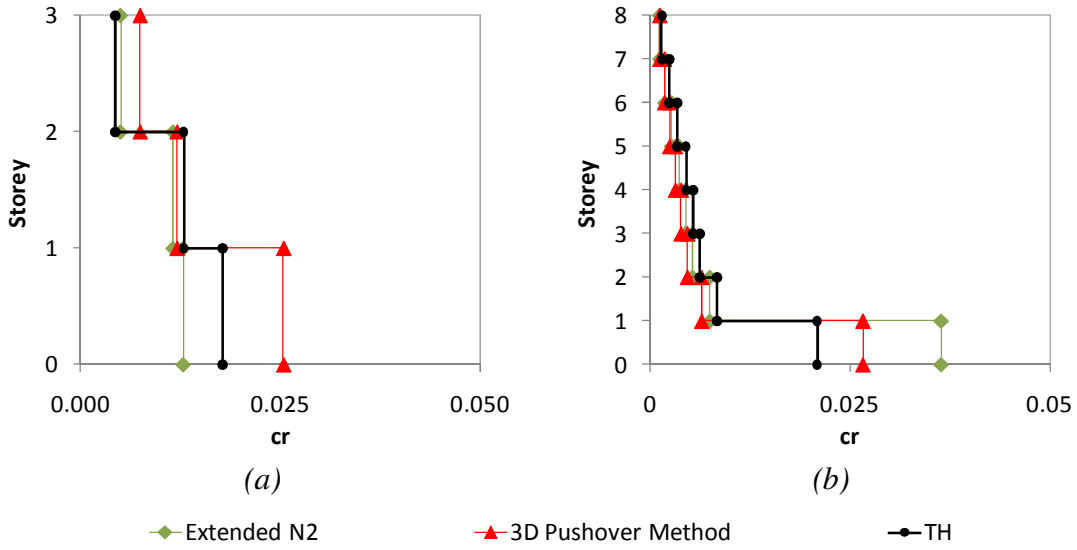

Figure 10.19 – Chord rotations profiles, X direction: a) three storey building, column C8, 0.2g; b) eight storey building, column S15, 0.4g.

As happens with the lateral displacement profiles, the Extended N2 method leads to good estimations of interstorey drifts and chord rotations in the three storey building, including the flexible edge column. However, in some cases the method slightly underestimates the response at the stiff edge, column C8. The proposed method usually reproduces in a very good manner the *time-history* response in all the analysed columns.

In the five storey buildings, the proposed procedure leads to results closer to the *time-history* than the Extended N2 method that leads to conservative estimations.

In the eight storey building the Extended N2 method overestimates the soft storey mechanism on the first floor, while the 3D Pushover method gets closer to the *time-history* response, but always on the conservative side. This improved performance can be explained mainly because of DAP and its ability in reproducing the stiffness degradation and the progressive structural damage.

In terms of interstorey drifts and chord rotations, one can observe that in the three storey building, the MPA underestimates the response on the edge columns while the 3D Pushover method is able to correctly reproduce the torsional response of the building.

In the five and eight storey buildings, the proposed procedure showed once again a better performance in estimating the response than the MPA. The latter usually led to conservative results.

In the eight storey building, the MPA overestimated once again the soft storey mechanism, while the proposed procedure reproduced it in a good fashion.

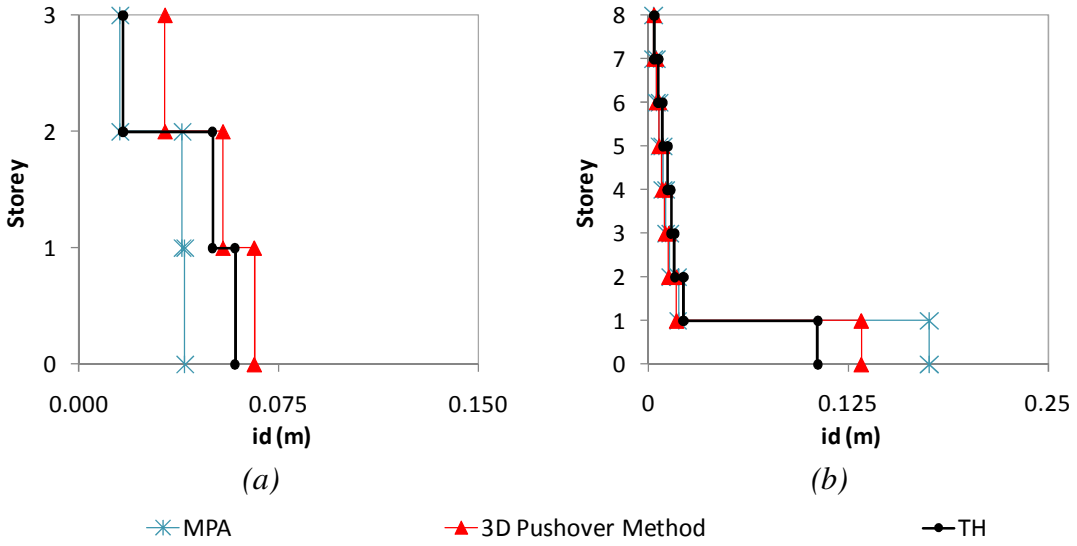

Figure 10.20 – Interstorey drift profiles, X direction: a) three storey building, column C2, 0.2g; b) eight storey building, column S9, 0.4g.

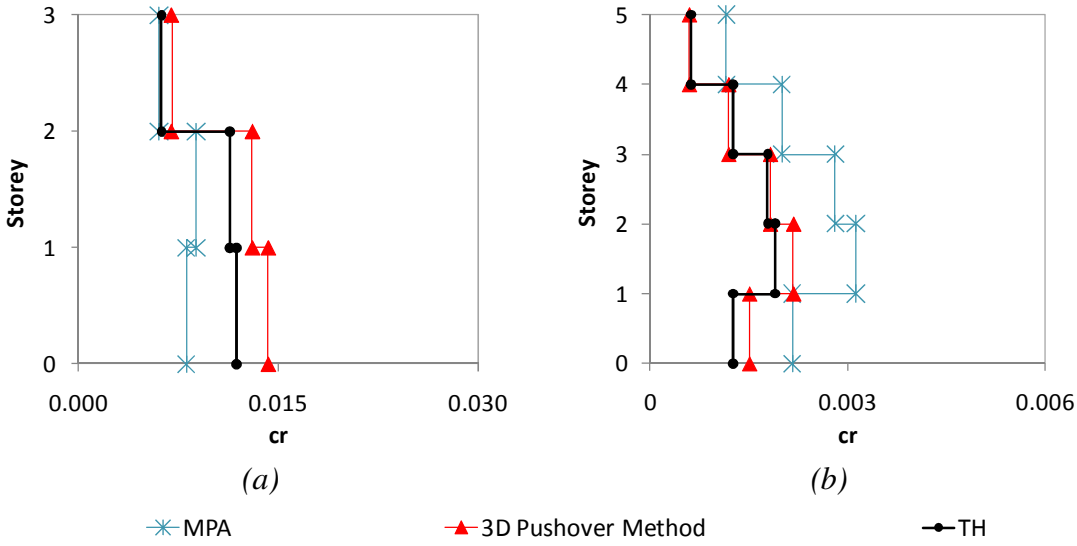

Figure 10.21 – Chord rotations profiles: a) three storey building, column C8, Y direction, 0.2g; b) five storey building, column S13, X direction, 0.1g.

10.2.3 Top displacement ratios

The comparisons between the proposed method and the other NSPs in terms of top displacements ratios are plotted from Figure 10.22 to Figure 10.25.

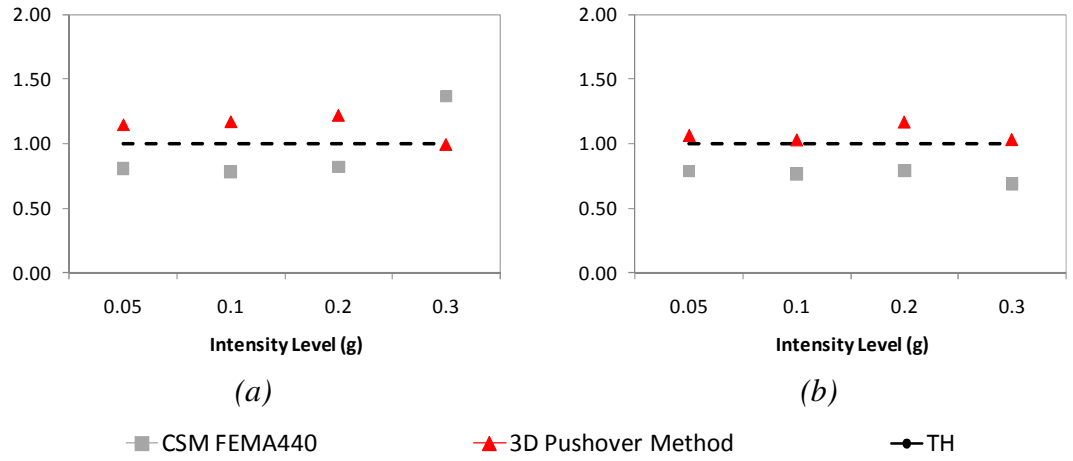

Figure 10.22 – Top displacements ratios three storey building: a) column C2 X direction; b) column C8 Y direction.

In terms of top displacement ratios, one can conclude that the 3D Pushover method leads to better estimations than CSM-FEMA440. In the three storey building, the results on the edge columns are underestimated by CSM-FEMA440. In the five storey building, both methods lead to conservative results, but the ones obtained with the proposed method are closer to the *time-history*.

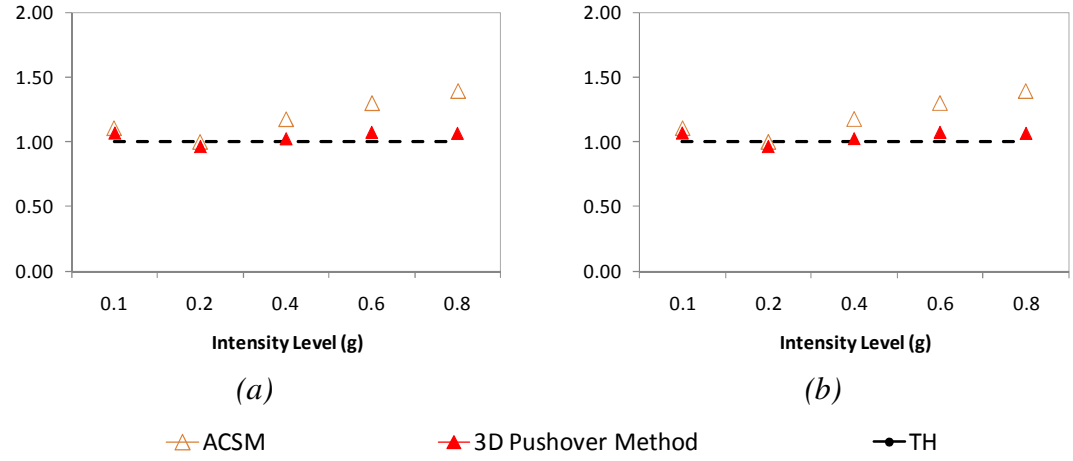

Figure 10.23 – Top displacement ratios, five storey building, X direction: a) CM; b) column S14.

In terms of top displacement ratios in the five storey building, one can observe that both ACSM and the new 3D Pushover method perfectly match the *time-history* for lower levels of intensity (elastic regime). However, for higher levels of inelasticity, the proposed procedure maintains the good matching with the *time-history* results while the original ACSM overestimates the response. It is interesting to note that the overestimation of the original ACSM in the inelastic regime increases as the seismic intensity increases, i.e. as the structure increases its level of nonlinear behaviour.

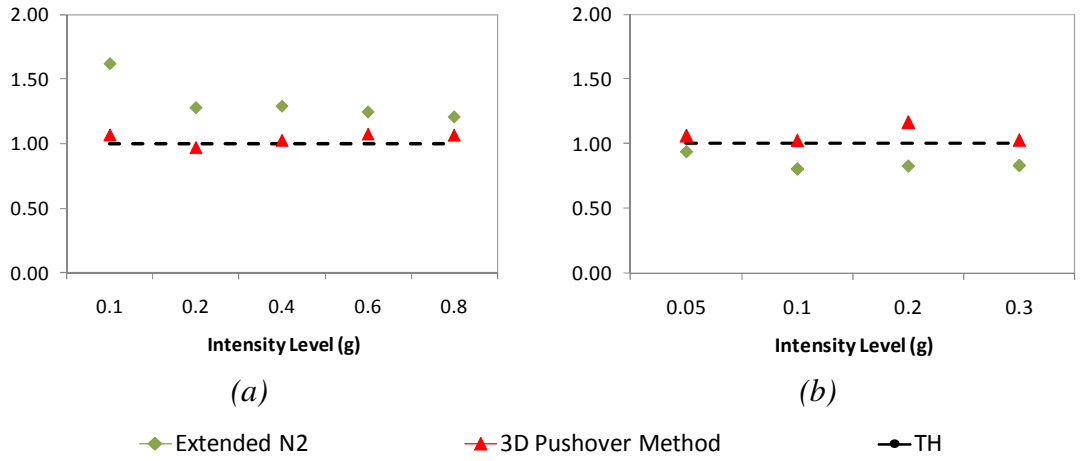

Figure 10.24 – Top displacements ratios a) five storey building, X direction, CM; b) three storey building, Y direction, column C8.

In terms of top displacement ratios, one can observe that the Extended N2 method usually leads to conservative results over all the seismic intensities tested. Note that this conservativeness is higher in the elastic range (example: 0.1g in the five storey building). However, the method leads to slightly underestimated results at the stiff edge of the three storey building. The proposed procedure matches in a good manner the *time-history* results.

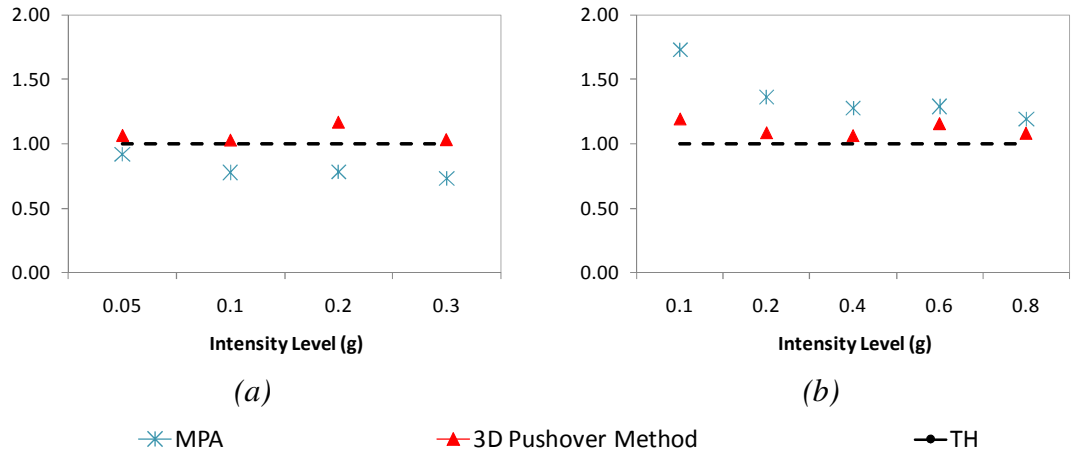

Figure 10.25 – Top displacement ratios: a) three storey building, column C8, Y direction; b) five storey building, column S23, X direction.

In terms of top displacement ratios, one can observe that in the three storey building on the top of the edge columns, the MPA led to underestimated results, and in the five and eight storey buildings it overestimated the response. On the other hand, the proposed procedure adequately matched the *time-history* results in all the buildings, through all the seismic intensities tested.

10.2.4 Normalized top displacements

From Figure 10.26 to Figure 10.29 the normalized top displacements in the three case studies evaluated for the new 3D Pushover method and for the other NSPs are plotted.

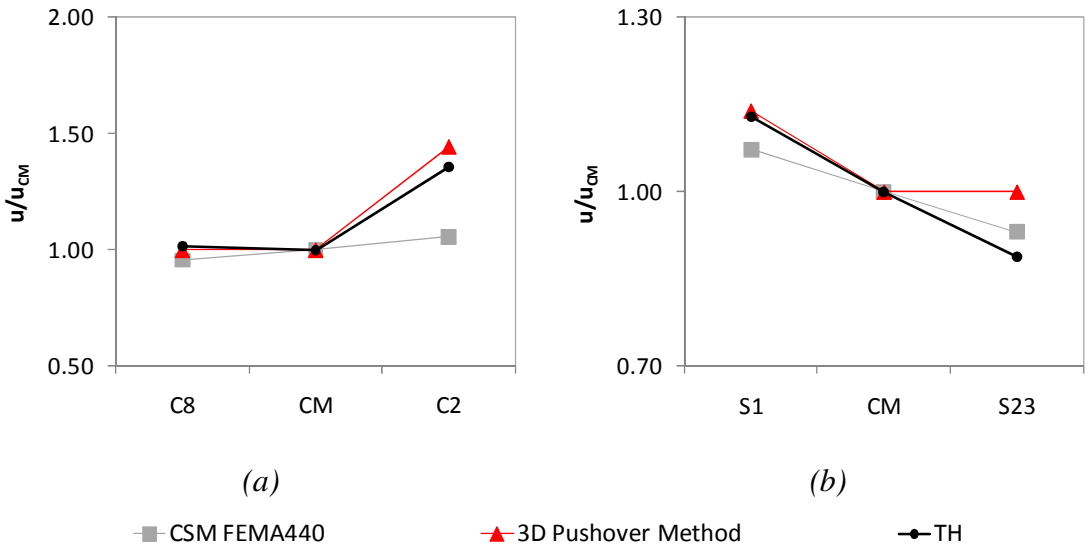

Figure 10.26 – Normalized top displacements, X direction: a) three storey building, 0.1g; b) five storey building, 0.2g.

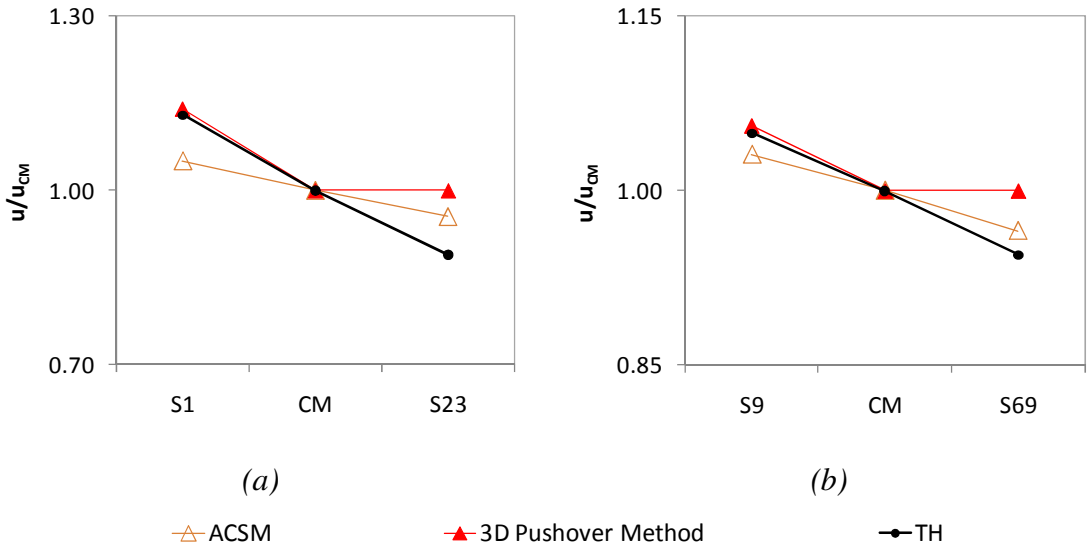

Figure 10.27 – Normalized top displacements, X direction: a) five storey building, 0.2g; b) eight storey building, 0.4g.

In terms of normalized top displacements one can observe that the new 3D Pushover method and the Extended N2 are able to reproduce the torsional motion of the buildings in a good fashion, due to the use of torsional correction factors.

These methods are able to capture the torsional amplification at the flexible edge, and they usually overestimate or reproduce in an exact way the response at the stiff edge.

These correction factors do not consider any de-amplification of displacements due to torsion, as was previously explained, therefore the response at the stiff edge is invariantly overestimated. This conservativeness is quite acceptable in terms of designing.

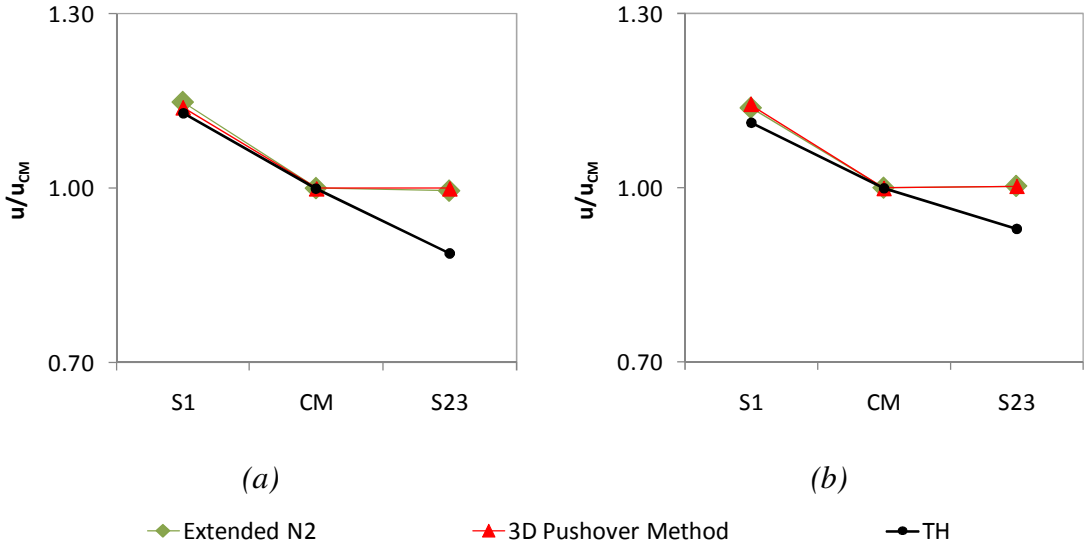

Figure 10.28 – Normalized top displacements, five storey building, X direction: a) 0.2g; b) 0.6g.

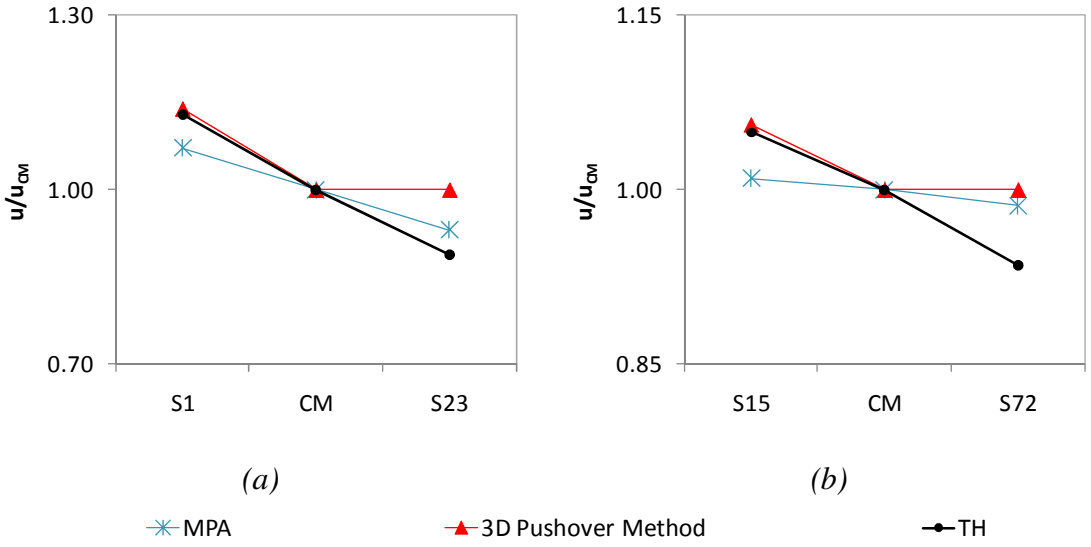

Figure 10.29 – Normalized top displacements, X direction: a) five storey building 0.2g; b) eight storey building, 0.4g.

The other NSPs estimate the torsional motion of the buildings linearly from one side of the building to the other, usually underestimating one of the edges.

The conclusions drawn herein are valid for all the seismic intensities analysed.

10.3 The advantages of the new 3D Pushover methodology when compared with the evaluated NSPs

The 3D Pushover methodology proposed presents a better performance in the seismic assessment of the three plan irregular buildings studied in this thesis than the most commonly used NSPs – CSM-FEMA440, Extended N2 method, MPA and ACSM. The explanation of this is based on its specific features described in the following sections.

10.3.1 DAP analysis

The proposed methodology uses a displacement based adaptive pushover (DAP) that updates the load pattern to be applied in each step, based on the modal properties of the structure in that step of the analysis. Therefore, the method takes into account the stiffness degradation, the period elongation and the progressive structural damage. The other methods evaluated herein (except the ACSM), use a conventional force based non-adaptive pushover, i.e. the incremental load to be applied in the structure maintains the same pattern. For this reason, the abovementioned methods are not able to reproduce the structural specificities mentioned in the DAP case. The good performance of the method in estimating the interstorey drifts and chord rotation profiles is clear in the case studies analysed, namely in the eight storey building where the proposed procedure estimates in an accurate fashion the development of the soft storey mechanism on the first floor. One of the explanations for this good performance is the use of DAP which is able to take the progressive structural damage into account.

The CSM-FEMA440 and the Extended N2 method use a force based load pattern proportional to the mass and to the elastic first mode of vibration of the structure in the direction under analysis. Therefore, none of the methods takes into account the contribution of the higher modes. The DAP used in the ACSM and in the proposed methodology, builds the displacement pattern to be applied in each step of the analysis considering the contribution of a pre-defined number of modes of vibration calculated based on the actual structural stiffness of that step. Therefore, the method takes into account the contribution of the higher modes of vibration of the structure. This is clear in the five and eight storey buildings, where the method led to more accurate results in the upper floors in terms of lateral displacements than the procedures that use conventional pushovers.

The MPA considers the contribution of the higher modes by a multi-run method, where each run corresponds to a pushover where the load pattern is proportional to the elastic modes of vibration of the building. However, these multi-run pushovers are not

adaptive, therefore, the capability of the method in capturing the previously described structural features decreases.

By using DAP, the proposed method is able to capture in a more accurate manner the response profiles, namely in terms of lateral displacements, interstorey drifts and chord rotations.

10.3.2 MDOF to SDOF transformation

For the definition of the SDOF capacity curve, the CSM-FEMA440, MPA and the Extended N2 method only consider one single control node – usually the centre of mass of the last floor, thus not contributing to a correct estimation of the structural torsional response.

On the other hand, the ACSM and the methodology proposed herein compute the SDOF capacity curve taking into account all beam-column and beam-beam nodes of the structure, therefore the torsional response can be better reproduced.

10.3.3 Target displacement calculation

In the proposed procedure, in CSM-FEMA440 and in ACSM the target displacement is calculated intersecting the SDOF capacity curve with the reduced ADRS spectrum. The new 3D Pushover procedure uses the innovative algorithm presented in FEMA440 for the computation of the effective period, effective damping and spectral reduction factors. It also uses the new modified acceleration-displacement response spectrum (MADRS), introduced in this guideline. As was concluded in chapter 6 and 8, this new algorithm leads to better estimations of the damping than the one used in ATC40. As was mentioned before [54], it was concluded that the reduction factor and the damping estimation formulas that lead the ACSM to the best performance in planar frames are the ones proposed by Lin and Chang [57] and by Gulkan and Sozen [58]. In chapter 8 it was concluded that the formulas proposed by FEMA440 led to better estimations of the damping than the ones used in ACSM.

It is important to mention that the new 3D Pushover procedure and the CSM-FEMA440 lead to similar estimations of the damping in the elastic range for the three buildings analysed. Table 10.1, Table 10.2, Table 10.3 show the damping ratios calculated by both methods in all case studies.

In the analysed buildings, one can observe that in the elastic and near elastic range - 0.05g and 0.1g for the three storey building, 0.1g and 0.2g for the five storey building, 0.1g for the eight storey building - both methods lead to similar estimations of the viscous damping used in the nonlinear *time-history* analysis – 2% in the three storey building and 5% in the five and eight storey buildings. This fact is justified by the

accuracy of the formulas proposed in FEMA440 and used by both methods, and because both adaptive and conventional pushover curves are very similar in the elastic range.

Table 10.1 - Three storey building - effective damping ratios (%).

	Three storey building: 2% viscous damping			
	3D Pushover		CSM-FEMA440	
Intensity level (g)	X	Y	X	Y
0.05g	2.2	2.1	2.1	2.1
0.1g	3.0	2.5	2.2	2.1
0.2g	9.7	6.4	5.8	3.2

In the inelastic range, the 3D Pushover method leads in general to larger estimations of the damping than the CSM-FEMA440. This fact is one of the justifications of the more conservative results obtained by the last one.

Notwithstanding both methods use the same formulas for the damping calculation, the differences in the damping values obtained in the inelastic range are due to the differences between the adaptive and conventional pushover curves used by each method based on which the damping is calculated. Since the results of the new 3D Pushover procedure are closer to the *time-history* than the ones obtained with CSM-FEMA440 in the inelastic range (especially in the columns near the centre of mass of the buildings where the torsional effects are not significant and therefore the comparison between the methods is not influenced by the torsional correction factors), one can conclude that the damping estimations in the inelastic regime obtained with the proposed procedure seem to be more realistic.

Since the two curves (adaptive and conventional) are very similar in the elastic or almost elastic regime for each building, the damping ratios computed by both methods are also very similar in this range.

Table 10.2 - Five storey building - effective damping ratios (%).

	Five storey building: 5% viscous damping			
	3D Pushover		CSM-FEMA440	
Intensity level (g)	X	Y	X	Y
0.1g	5.1	5.1	5.2	5.4
0.2g	5.3	5.2	5.3	5.3
0.4g	7.2	6.5	6.7	6.4
0.6g	12.5	8.8	10.9	10.0

Table 10.3 - Eigth storey building - effective damping ratios (%).

	Eight storey building: 5% viscous damping	
	3D Pushover	CSM-FEMA440
Intensity level (g)	X	X
0.1g	5.3	5.3
0.2g	5.5	5.4
0.4g	8.8	9.2

Table 10.4, Table 10.5 and Table 10.6 show the damping values calculated by the new 3D Pushover method and by the ACSM in the analysed buildings. One can observe that in the elastic or almost elastic range - 0.05g and 0.1g for the three storey building, 0.1g and 0.2g for the five storey building, 0.1g for the eight storey building – the 3D Pushover procedure estimates the damping in an accurate way, being very close to the viscous damping values used in the *time-history* analysis – 2% in the three storey building and 5% in the Turkish buildings. On the other hand the ACSM, using the reduction factor proposed by Lin and Chang [57] with damping based on the formulas of Gulkan and Sozen [58], overestimates the damping values in the elastic regime. As previously mentioned the formulas for the damping calculation proposed in FEMA440 seem to be more accurate than the ones proposed by Gulkan and Sozen used in ACSM.

In the inelastic range, the ACSM leads to larger damping estimations than the 3D pushover method.

Table 10.4 - Three storey building - effective damping ratios (%).

	Three storey building: 2% viscous damping			
	3D Pushover		ACSM	
Intensity level (g)	X	Y	X	Y
0.05g	2.2	2.1	3.5	3.8
0.1g	3.0	2.5	5.2	4.4
0.2g	9.7	6.4	11.9	9.8

Table 10.5 - Five storey building - effective damping ratios (%).

	Five storey building: 5% viscous damping			
	3D Pushover		ACSM	
Intensity level (g)	X	Y	X	Y
0.1g	5.1	5.1	6.5	6.8
0.2g	5.3	5.2	7.3	7.0
0.4g	7.2	6.5	10.2	9.3
0.6g	12.5	8.8	14.0	11.8

Even though the damping estimations of the ACSM are larger, the results obtained by this method seem to be more conservative than the ones obtained with the proposed procedure. Since both methods use a DAP capacity curve, this difference can be explained due to the different reduction factors used by each method. Since the results obtained by the 3D Pushover procedure are closer to the *time-history* (mainly in the columns near the centre of mass of the buildings where the torsional effects are not significant and therefore the comparison between the methods is not influenced by the torsional correction factors), one can conclude that the combination of the reduction factors and damping formulas proposed in FEMA440 seems to be more accurate than the one used in ACSM (reduction factor proposed by Lin and Chang [57] with damping based on the formulas of Gulkan and Sozen [58]).

Table 10.6 - Eight storey building - effective damping ratios (%).

	Eight storey building: 5% viscous damping	
	3D Pushover	ACSM
Intensity level (g)	X	X
0.1g	5.3	7.3
0.2g	5.5	7.7
0.4g	8.8	12.3

Both original and Extended N2, and MPA use the equal displacement rule for the calculation of the target displacement, leading in general to conservative results, as was shown in chapter 8.

The conservativeness of the Extended N2 method increases in the elastic range. In fact, according to Fajfar the method was not developed for the elastic range, since it considers an inelastic period independently of the seismic action intensity, calculated based on the SDOF capacity curve point corresponding to the maximum base shear, see chapter 8, Figure 8.48. At this elastic stage, the 3D Pushover method leads to better estimations because it calculates the target displacement by intersecting the reduced spectrum with the SDOF capacity curve, therefore considering the effective SDOF period and damping associated with the seismic action under analysis, as explained before. In fact, by using the new algorithms presented in FEMA440 to compute the effective damping, the effective period and the reduction factor, the method is able to lead to very good response estimations. Table 10.7, Table 10.8 and Table 10.9 show the effective periods calculated with both procedures. One can find that in the elastic range, the effective periods calculated by the proposed method are very close to the elastic periods in both directions of the analysed buildings, confirming once again the accuracy of the formulas proposed in FEMA440.

Table 10.7 - Three storey building: effective periods (N2 and 3D Pushover method) in the elastic/almost elastic regime (sec.) vs. Fundamental period (sec.).

	3 storey building periods (sec)					
	X			Y		
Intensity	N2	3D Pushover	Fundamental Period	N2	CSM-FEMA440	Fundamental Period
0.05g	1.003	0.625	0.617	0.703	0.443	0.527
0.1g	1.003	0.645	0.617	0.703	0.449	0.527

Table 10.8 - Five storey building: effective periods (N2 and 3D Pushover method) in the elastic/almost elastic regime (sec.) vs. Fundamental period (sec.).

	5 storey building periods (sec)					
	X			Y		
Intensity	N2	3D Pushover	Fundamental Period	N2	CSM-FEMA440	Fundamental Period
0.1g	1.006	0.623	0.617	0.674	0.600	0.593

Table 10.9 - Eight storey building: effective periods (N2 and 3D Pushover method) in the elastic/almost elastic regime (sec.) vs. Fundamental period (sec.).

	8 storey building periods (sec)		
	X		
Intensity	N2	3D Pushover	Fundamental period
0.1g	2.007	1.466	1.445

10.3.4 Torsional correction factors

Only the Extended N2 and the new procedure use correction factors in order to take into account the torsional effects. These correction factors based on Pushover and linear elastic analyses, were found to estimate in a good manner the torsional motion of plan irregular buildings. In fact, the only NSPs that were able to reproduce in a good or conservative fashion the normalized top displacements were the ones that use these correction factors. The other NSPs generally underestimated the normalized top displacements at one of the edges of the analysed buildings.

By using torsional correction factors, the 3D Pushover method leads to good estimations of the torsional motion of the buildings. As an example, the response at both flexible and stiff edges of the three storey building in terms of lateral displacement, interstorey drifts, chord rotation profiles and top displacement ratios, is reproduced in an accurate manner by the method. On the other hand, the CSM-FEMA440 and the MPA usually underestimate the response at these edges, over all the seismic intensities tested. Despite using torsional correction factors, the Extended

N2 method leads in certain cases to underestimated responses at the stiff edge of this building.

In terms of normalized top displacements, the proposed method was able to capture the torsional amplification at the flexible edges and it usually overestimated the response at the stiff edges of the three analysed buildings. The CSM-FEMA440, the MPA and the ACSM generally estimated in a linear way the response from one side of the building to the other, underestimating one of the edges. These conclusions were observed for all the seismic intensities tested. As mentioned before, the ACSM was able to correctly reproduce this parameter in the three storey building, but it could not keep the good performance in the other two case studies.

10.4 Final observations

The 3D Pushover procedure presented in this chapter led in general to better results than the most well known nonlinear static procedures. This conclusion was supported by the extensive parametric study presented herein. For the buildings analysed and for different seismic intensities, the proposed method led to better estimations of the lateral displacement profiles, interstorey drifts, chord rotations, top displacement ratios and normalized top displacements. The results obtained with the method were generally close to the *time-history* and always on the conservative side.

As was previously mentioned, the use of pushover analysis in planar frames and bridges is widespread due to the extensive published studies that support the performance of such a procedure. However, its application to plan irregular buildings (the majority of existing ones) is still limited due to the small number of scientific studies on this topic. During this work it was pointed out that the biggest problem of the majority of the existing NSPs is their inability to capture the torsional behaviour of these kind of buildings. The 3D Pushover procedure presented in this chapter, contemplates the best features of the most commonly used NSPs. Its good performance in estimating the *time-history* response, always on the conservative side, increases its potential to be included in future seismic codes, as a nonlinear static procedure able to accurately predict the torsional and structural response of plan irregular buildings.

It is recognized worldwide that *time-history* analysis leads to more accurate results. Although, it still presents some difficulties in practical applications, such as: a correct record selection, the post-processing of results and the time-consuming nature of the analyses. The procedure presented herein, leads to results close to the *time-history* requiring a much smaller computation time, and are easy and simple to be applied. Therefore, it can emerge as a valuable solution to develop nonlinear seismic analysis either in research or design offices where time constraints are a reality. It will allow the widespread use of nonlinear seismic analyses among design engineers, increasing the quality of design projects. In fact, if the procedure proposed herein is programmed in a single software package, it can turn out to be a valuable and practical tool in design offices.

The method can be used to assess existing buildings for rehabilitation, as presented during this work, or it can be used to design new buildings. In the second case, the design methodology is iterative, starting with a preliminary design of the building using for instance a traditional procedure (linear dynamic modal analysis by means of a response spectrum) or ideally a Displacement Based Design procedure, and afterwards verifying the reinforcement using the 3D pushover method. If the code limits are verified the process ends, otherwise the iteration continues changing the reinforcement and verifying once again with the pushover analysis until one reaches the desired performance.

11. Concluding remarks and future developments

In the first part of this section, the final conclusions obtained from each chapter are presented. In the second part some ideas for future work are outlined and suggested.

11.1 Concluding remarks

The three case studies evaluated in this work are real existing structures asymmetric in plan.

The three storey SPEAR building was designed only for gravity loads following Greece's concrete design code in force between 1954 and 1995 and the construction practice applied in the early 1970s. The five and eight storey Turkish buildings were designed according to the 1975 Seismic Code of Turkey.

During this work it was concluded that the three buildings have inadequate seismic design. A clear example is the existence of beams framing into beams which are potential weak locations when the earthquake acts on the structure.

From the dynamic properties presented in section 3.2.6, one can conclude that the three and eight storey buildings are classified as torsionally stiff in the X direction and torsionally flexible in the Y direction. The five storey building is torsionally stiff in both X and Y directions.

From the capacity curves presented in chapter 5 one can conclude that the three storey building have poor ductility. The poor confinement effect provided by the small amount of transverse reinforcement, especially in the columns, is one of the reasons for this low ductility. The eight storey building exhibits a pronounced softening in the X direction because of the soft storey mechanism.

11.1.1 CSM-ATC40 vs. CSM-FEMA440

In chapter 6, a comparison between the performance of the CSM-ATC40 and the CSM-FEMA440 recommendations was carried out.

From the obtained results, it was concluded that the features presented in the FEMA440 report led to better results than its predecessor when compared with nonlinear dynamic *time-history* analyses.

For the CM and for the columns located near this node the results obtained with CSM-FEMA440 are close to the *time-history*, while the ones obtained with the ATC40 are invariantly underestimated.

This happens both for the elastic and inelastic range because the ATC40 procedure overestimates the effective damping while the FEMA440 calculates it in a very accurate way.

In fact, the innovative methods to compute the effective damping, the effective period, the demand spectrum reduction factors and the new concept of Modified ADRS introduced in FEMA440 seem to provide more realistic results than the procedure proposed in ATC40.

The results of both methods for columns located at the extremities of the buildings were usually underestimated.

11.1.2 Original N2 method vs. Extended N2 method

In chapter 7, the Extended N2 method was compared with the original N2, recommended in Eurocode 8, and with the *time-history* median response. The study presented in this endeavour aimed to continue the work developed by Peter Fajfar and his team for the development of the Extended N2 method for plan irregular buildings.

This procedure consists of the application of a correction factor to the pushover analysis results determined by the original N2 method. These correction factors are calculated based on a linear elastic analysis and on a pushover analysis.

In the first part of the chapter, the seismic response was assessed at the centre of the analysed buildings. The torsional effects were not so evident at this location, therefore the results obtained with both the original and the Extended N2 method were pretty much the same. The results at the centre of mass and columns near this point, were generally overestimated for all seismic intensities analysed. This trend was the result of the features of the procedure. Despite this fact, the method seems to gain in simplicity and its use is certainly worthwhile, mainly in design offices where the time saving is considerable when compared with the *time-history* analysis.

In the second part, the seismic assessment was performed on the elements located at the edges of the buildings in order to evaluate their torsional response. The results obtained from this study showed that torsional effects are in general higher for lower ground motion intensities. In fact, for increasing seismic intensities, one can notice a flattening in the normalized top displacements of each building. This confirms the idea that torsional effects are generally smaller in the inelastic range than in the elastic stage.

The Extended N2 method performed in a much more accurate way than its original counterpart in estimating the torsional behaviour of all buildings analysed over all the seismic intensities tested. It generally captured in a very precise manner the torsional amplification in terms of displacements on the flexible side of the buildings.

The Extended N2 method does not take into account any de-amplification of displacements due to torsion. Therefore, the response on the stiff side of the buildings was in some cases estimated in a precise way by the method, and overestimated in others.

The N2 method is not capable in general to reproduce the torsional motion of the buildings, usually leading to a linear estimation of the torsional motion from one side of the building to the other.

The original method considered the de-amplification on the stiff side of the buildings, underestimating their response through all the seismic intensities tested. On the flexible side, the normalized top displacements were also generally non conservative with respect to the *time-history* results.

Recently, several procedures have been proposed taking torsion into account in simplified nonlinear static procedures, however definitive answers have not yet been reached. This work certainly does not present a breakthrough, but it does make a step forward. The results obtained herein added to the ones already published [4, 6, 79], confirm the idea that the Extended N2 method has the potential to be implemented in the next version of Eurocode 8 in order to correctly estimate the torsional response in real plan-asymmetric RC buildings through the use of pushover analysis.

11.1.3 Performance evaluation of commonly used NSPs on the seismic assessment of plan irregular buildings

In chapter 8, four commonly used nonlinear static procedures - the Extended N2 method, the CSM-FEMA440, the MPA and the ACSM - were applied to real existing plan asymmetric RC buildings. The results were compared with the *time-history* nonlinear dynamic analyses through the use of semi-artificial ground motions. Several seismic intensities were tested in order to evaluate the NSPs performance in different inelastic structural stages.

The results obtained in this study, in terms of top displacement ratios, lateral displacement profiles, interstorey drifts and chord rotations, showed that the CSM-FEMA440 and the ACSM were the methods that better reproduced the nonlinear dynamic median response profiles. The ACSM estimations were usually closer to the *time-history*. The exception to these conclusions occurred on the edge columns of the three storey building, where CSM-FEMA440 led to underestimated responses.

The general good results obtained by the ACSM are justified by the use of an adaptive displacement pushover (DAP) and an equivalent SDOF structural displacement based on the current deformed pattern.

The set of equations used by the ACSM to calculate the damping ratio (proposed by Gulkan and Sozen) and the spectral reduction factor (proposed by Lin and Chang) led to an overestimation of the damping ratio in the elastic regime in all the buildings analysed. On the other hand, the formulas proposed by the FEMA440 led to damping estimations very close to the ones considered in the *time-history* analysis. In the inelastic range, the ACSM continued to calculate values of damping larger than the ones obtained using the CSM-FEMA440.

Despite using the powerful DAP algorithm, the ACSM uses equations to calculate the damping and the spectral reduction factor that proved to be not so accurate, leading to final results sometimes far from the expected. The overestimation of the damping can explain why the ACSM leads in certain cases to underestimated results when compared with the *time-history* median, especially in terms of damage criteria such as interstorey drifts and chord rotations.

The less accurate conventional pushover curve used by CSM-FEMA440, when compared with the sophisticated DAP used by ACSM, is somehow compensated by the accurate procedure to calculate the target displacement that includes: a new and efficient algorithm to compute the effective period and the effective damping; an accurate demand spectrum reduction factor coupled with the new concept of the modified acceleration-displacement response spectrum (MADRS). This explains the generally good performance of the CSM-FEMA440 when calculating the target displacement of the buildings under analysis.

The CSM-FEMA440 leads to good estimations of the target displacement in the three storey building, although it underestimated the results on the edge columns. This can be justified by the conventional pushover used by the method, which cannot accurately reproduce the stiffness degradation and the progressive structural damage along the elements. This leads to a worse reproduction of the torsional motion of the building. Since torsion does not significantly influence the target displacement calculation, this parameter is well estimated by the method. However the response on peripheral columns, strongly influenced by torsion, cannot be reproduced in a correct fashion by CSM-FEMA440. On the other hand, the ACSM is able to reproduce the response on these columns better than CSM-FEMA440 mainly because of the DAP.

These conclusions confirm the idea that all steps of a nonlinear static procedure are important: from the pushover curve definition, to the MDOF to SDOF transformation, and to the target displacement calculation. A less accurate approach in one of the steps can be the explanation for some undesirable results.

The Extended N2 was the method that in general led to the most conservative results in the analysed buildings, in terms of lateral displacement profiles, top displacements, interstorey drifts and chord rotations. This is because the method considers the equal displacement rule which is proven to lead to conservative response estimations.

The overestimation of the results by the N2 method is more evident in the elastic regime. This happens because the method bilinearizes the SDOF capacity curve at the point of maximum acceleration, underestimating the stiffness and therefore overestimating the period of the SDOF system in the elastic regime.

In terms of lateral displacements profiles, top displacements, interstorey drifts and chord rotations, all the methods seemed to lead to approximate and conservative estimations for high levels of inelasticity.

The normalized top displacements indicate the relative displacements in plan between the top floor edge columns and the centre of mass. Therefore, it is very important to evaluate the ability of a NSP in reproducing the torsional motion of plan irregular buildings.

In terms of normalized top displacements, the Extended N2 method was the only procedure able to reproduce in a correct manner the torsional motion of all the analysed buildings for increasing levels of seismic intensity.

This good performance in estimating the torsional motion of the buildings is because the method uses correction factors based on a linear elastic response spectrum analysis, without considering any de-amplification of displacements due to torsion.

The Extended N2 method is able to capture the torsional amplification at the flexible edge of the buildings, leading in general to conservative response estimations on the stiff side.

The other NSPs evaluated in this chapter generally reproduced in a linear way the normalized top displacements from one side of the building to the other. They were only able to capture the torsional motion of just one side of the building, underestimating the other.

The ACSM was able to correctly reproduce the torsional motion of the three storey building, but its performance decreased for the other two buildings, leading to the response described in the previous paragraph.

All the NSPs studied in chapter 8, except the Extended N2 method, should be developed in order to correctly capture the torsional motion of plan irregular buildings.

All NSPs were able to reproduce the soft storey mechanism and the specific features of the seismic response of the eight storey building over all the intensity levels tested.

The study carried out in this chapter showed that the Extended N2 method was the most complete and reliable NSP, amongst all the evaluated procedures to analyse the real existing plan asymmetric buildings, because the method never underestimated the *time-history* response. On the other hand, the other NSPs generally underestimated the torsional motion of the case studies evaluated herein.

11.1.4 Extension of the CSM-FEMA440 to plan asymmetric buildings

In chapter 9, an Extended version of the CSM-FEMA440 was proposed in order to overcome the torsional problem of plan-asymmetric buildings.

This extension was conceived based on the results presented by Fajfar and his team and used to extend the N2 method for plan asymmetric buildings. This extension consists on the application of a correction factor to the pushover results determined by the CSM-FEMA440 recommendations. These correction factors are computed based on a linear RSA and on a pushover analysis.

This procedure was assessed by comparing the results in terms of normalized top displacements of the three case studies and different ground motion intensities.

As far as the torsional effect is concerned it was possible to achieve more realistic and conservative results using the proposed extension than the original CSM-FEMA440 version for all the studied buildings.

The proposed extension should be further tested and, if the results came in line with the ones obtained for the three buildings studied herein, it should be incorporated in

future codes, namely the ATC guideline, as a methodology capable of estimating the torsional amplification in plan-asymmetric buildings.

11.1.5 A New 3D Pushover procedure

In chapter 10 a new 3D Pushover procedure is proposed for the seismic assessment of plan irregular buildings.

This procedure combines the most efficient and accurate features of some of the most commonly used NPSs, which were evaluated in the previous chapters of the thesis.

The method was tested in the three case studies used in this work, for several seismic intensities and compared with the original CSM-FEMA440, the ACSM, the MPA and the Extended N2 method.

The good results obtained with the proposed methodology can be explained due to the following reasons:

1) The method uses a displacement based adaptive pushover (DAP);
2) For the SDOF capacity curve definition, the procedure calculates the equivalent SDOF structural displacement based on the current deformed pattern. This concept can be useful in the 3D case;
3) The computation of the target displacement is made using the innovative and accurate algorithm proposed in FEMA440 for the calculation of the effective period, damping, reduction factor and the new MADRS. The good performance of this algorithm was also confirmed in previous chapters of the thesis;
4) In order to take into account the torsional effects, the new 3D Pushover procedure uses correction factors, as proposed in the Extended N2 method.

The new 3D Pushover Procedure showed a better performance than the previously analysed NSPs in estimating the seismic response of plan asymmetric buildings.

In terms of normalized top displacements, which clearly illustrate the torsional motion of the structures, one could conclude that the MPA, the CSM-FEMA440 and the ACSM generally underestimated the response at one of the edges of the buildings. On the other hand, the Extended N2 method and the new 3D Pushover procedure could reproduce in a good manner the torsional motion of the case studies.

In terms of lateral displacement profiles, interstorey drifts, chord rotations and top displacement ratios one can conclude that the new 3D Pushover procedure leads to results closer to the *time-history* than the Extended N2 method. In fact, the latter generally leads to conservative response estimations. The better performance of the proposed method when compared with the Extended N2 can be explained by the use

of DAP, the transformation of MDOF to SDOF, and the algorithm for the damping and effective period computation used in the target displacement calculation.

Despite both methods using the DAP and the same MDOF to SDOF transformation, the new 3D Pushover procedure leads to results closer to *time-history* than the ACSM due to the more efficient and accurate algorithm for the damping and reduction factor calculation. In fact, the formulas used by the ACSM invariantly lead to overestimations of the damping. In terms of normalized top displacements, the proposed method provides better results than the ACSM due to the use of torsional correction factors.

The proposed method also leads to better results than the original CSM-FEMA440 and the MPA, namely in terms of normalized top displacements.

These conclusions were drawn for all the seismic intensities tested and consequently for different stages of structural inelasticity of each building.

The results obtained herein with the analysed structures, indicate that the method has potential to be implemented in future seismic codes as a more refined nonlinear static procedure able to accurately estimate the seismic response of plan asymmetric buildings.

The new 3D Pushover procedure can be called as the 3DISP method, which means 3D Irregular Structures Pushover method.

11.1.6 3D Pushover on the seismic assessment of existing buildings

The results obtained from this thesis clarify the robustness and applicability of each of the most popular NSPs on the seismic assessment of plan irregular existing buildings. The results showed that the CSM-ATC40, the CSM-FEMA440, the original N2 method, the MPA and the ACSM were not able in general to reproduce in an accurate fashion the torsional response of the analysed buildings through all the seismic intensities tested.

As previously mentioned, the use of NSPs in design engineering offices has not been widespread because their accuracy in the seismic assessment of plan irregular buildings has not been sufficiently proven. In fact, this is a major drawback since these buildings represent the common case in real life. The results obtained in this thesis proved the good accuracy of the Extended N2 method, the Extended CSM-FEMA440 method, and the new 3D Pushover Procedure in the seismic evaluation of such kind of structures. These procedures can be used in the design of new structures and in the assessment and rehabilitation of existing ones.

One can say that in terms of normalized top displacements, the three abovementioned NSPs present the same level of accuracy in estimating this measure. In terms of lateral displacement profiles, interstorey drifts, chord rotations, top displacements and base shear ratios, the new 3D Pushover procedure is the one that leads to more accurate results, followed by the CSM-FEMA440 (leads to slightly overestimated results) and finally by the Extended N2 method (leads to considerably overestimated results). In terms of computation time one can say that the Extended N2 method is the fastest and more practical method, followed by the Extended CSM-FEMA440 and finally by the new 3D Pushover procedure. The DAP analysis used by this last method is more time-consuming than the conventional pushovers used by the other two procedures (it usually takes 25% more time), therefore increasing the computation time of the proposed methodology. However, the accuracy gain provided by this adaptive method somewhat justifies the modest increase in computing time. Both the Extended CSM-FEMA440 and the new proposed methodology need an iterative process for this purpose. Therefore, the Extended N2 method is the one that takes less time to be computed.

The use of *time-history* analysis seems to be not very attractive in design offices due to its large time-consuming (long computation time) and complexity namely in terms of record selection. In fact, this is a topic for which the scientific community has not yet found any definitive answers. The relatively simple methodology of these NSPs as well as their fast applicability will facilitate their use in design offices. Therefore, they will increase the accuracy and quality of seismic design projects.

The use of these more accurate methods will allow a more effective design of new structures or the strength of existing ones, reducing the probability of disasters such as the ones which recently occurred in Chile, Haiti or L'Aquila.

Figure 11.1 and Figure 11.2 illustrate some of the catastrophic consequences of the L'Aquila earthquake, taken during the IST Mission to L'Aquila [135] in which the author of the thesis participated. Figure 11.1 shows an example of a soft storey mechanism that caused the collapse of the Duca Degli Abruzzi Hotel. This kind of collapse mechanism was studied in this thesis in the eight storey building.

The results indicated that the abovementioned NSPs presented a good performance in the estimation of the soft storey mechanism. The use of such methods to evaluate the Hotel Duca Degli Abruzzi would most probably lead to a correct evaluation of the structural response features of the building allowing a more efficient reinforcement, avoiding this kind of collapse.

One would hope that gradually the linear dynamic response spectrum analysis with the use of behaviour factors, commonly used in design offices, will be replaced by the more accurate methods presented herein.

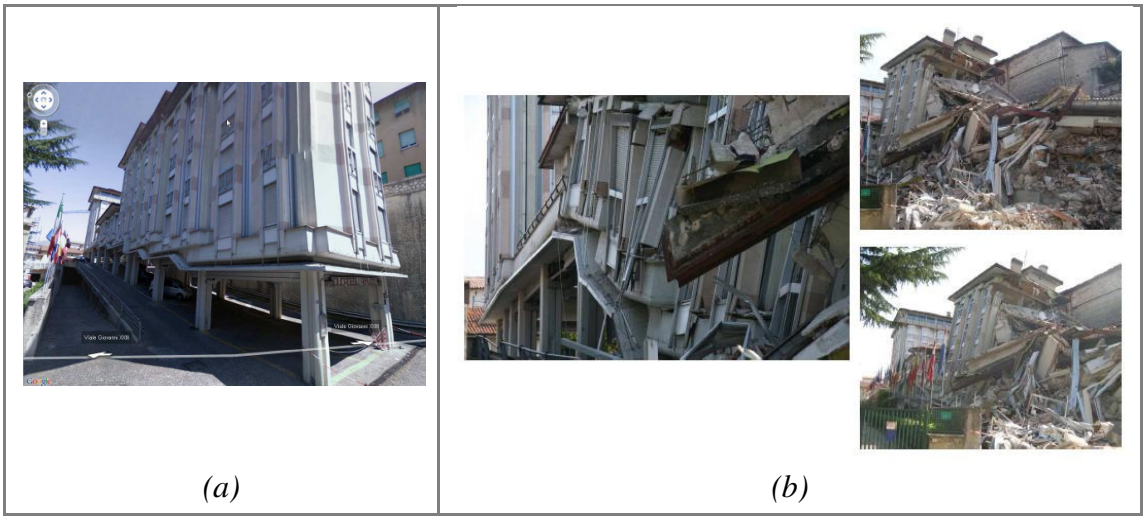

(a) *(b)*

Figure 11.1 – Duca Degli Abruzzi Hotel destroyed after the L'Aquila earthquake due to a soft storey mechanism [135]: a) before the earthquake; b) after the earthquake.

Figure 11.2 – Destroyed buildings after the L'Aquila earthquake [135].

11.2 Future developments

As far as future work is concerned, one may say that the analysed NSPs should be also tested considering the effect of masonry infill panels. This effect has been omitted in this work for reasons of a more thorough research. The non-uniform (not simultaneous) failure of masonry infill panels during the non-linear seismic response of a structure, may increase its torsional behaviour and, thus, should be taken into account. This may increase the asymmetry and consequently increase the torsional effects. Therefore, the effect of infills from modelling until their non-uniform failure may become important.

Buildings with higher ductility should be further tested in order to confirm the conclusions obtained herein for such kind of structures.

The influence of modelling issues on nonlinear static and dynamic analysis of 3D irregular structures should be studied. This topic intends to evaluate several modelling options and compare the structural response when performing nonlinear static and nonlinear dynamic analysis on 3D irregular structures. This issue was dealt by Sashi Kunnath and presented at the international Workshop in Lisbon 2008 [80]. It is clear that due attention and care should be paid to modelling issues (e.g. by means of accurately devised sensitivity studies).

Performance verification of the generalised pushover curve proposed by Goel [80] for 3D irregular structures. It is intended to test the applicability of such generalised pushover curve and the rules to convert it to the force-deformation relationship of the nth-"mode" inelastic SDOF system that is needed in the implementation of the MPA procedure or any other NSPs. The generalized pushover curve is shown to be especially attractive for nonlinear static analysis of 3D structures in which modes excited during the earthquake ground motion may induce little or no base shear.

The extension of the N2 method to take into account the higher mode effects proposed by Fajfar and his team [36] and presented in chapter 2, should be tested in different buildings in order to consolidate the results presented by the authors.

This method should be tested together with the extension of the N2 method to plan irregular buildings in order to evaluate the performance of both extensions simultaneously. The case studies should be irregular in plan and high rise buildings. The results should be compared with nonlinear dynamic analyses for several levels of intensity in order to evaluate the performance of the method for different stages of structural inelasticity. The method can also be compared with the new 3D Pushover procedure proposed in this thesis.

References

1. **Freeman.** *Development and use of capacity spectrum method.* Proceedings of the Sixth U.S. National Conf. Earthquake Engineering. Seattle, Oakland, USA, 1998.
2. **Fajfar P., Fischinger M.** *N2 - A method for non-linear seismic analysis of regular buildings.* Proceedings of the Ninth World Conference in Earthquake Engineering. pp. 111-116. Tokyo-Kyoto, Japan, 1988.
3. **Chopra A.K., Goel R.K.** A modal pushover analysis procedure for estimating seismic demands for buildings. *Earthquake Engineering and Structural Dynamics.* 2002, Vol. 31, pp. 561-582.
4. **Fajfar P., Marusic D., Perus I.** Torsional effects in the pushover-based seismic analysis of buildings. *Journal of Earthquake Engineering.* 2005, Vol. 9(6), pp. 831-854.
5. **Chopra A.K., Goel R.K.** A modal pushover analysis procedure to estimate seismic demands for unsymmetric-plan buildings. *Earthquake Engineering and Structural Dynamics.* 2004, Vol. 33, pp. 903-927.
6. **D'Ambrisi A., Stefano M., Tanganelli M.** Use of Pushover Analysis for Predicting Seismic Response of Irregular Buildings: a Case Study. *Journal of Earthquake Engineering.* 2009, Vol. 13, pp. 1089-1100.
7. **Erduran E., Ryan K.** Effects of torsion on the behaviour of peripheral steel-braced frame systems. *Earthquake Engineering and Structural Dynamics.* 2010, DOI: 10.1002/eqe.1032.
8. **Fajfar P., Marušic D., Perus I.** *The extension of the N2 method to asymmetric buildings.* Proceedings of the 4th European workshop on the seismic behaviour of irregular and complex structures, CD ROM. Thessaloniki, 2005.
9. **Biot, MA.** Analytical and experimental methods in engineering seismology. *ASCE Transactions.* 1942, Vol. 108, pp. 365–408.
10. **Chopra, A. K.** *Dynamic of Structures, Theory and Applications to Earthquake Engineering, 3rd edition.* Pearson Prentice Hall, 2007.
11. **Priestley, MJN.** *Myths and Fallacies in Earthquake Engineering (Revisited).* Pavia : IUSS Press, 2003.

12. **Gutierrez J., Alpizar M.** *An effective method for displacement-based earthquake design of buildings.* Proceedings of the 13th World Conference on Earthquake Engineering. Paper No. 1512. Vancouver, 2004.
13. **Fajfar P., Krawinkler H.** *Seismic Design Methodologies for the Next Generation of Codes.* Balkema, Rotterdam, 1997.
14. **Priestley, M.J.N.** *Performance based seismic design.* Proceedings of 12th World Conference on Earthquake Engineering. Paper No. 2831. New Zealand, 2000.
15. **Priestley M.J.N., Calvi G.M., Kowalsky M.J.** *Displacement Based Seismic Design of Structures.* Pavia, Italy : IUSS Press - Istituto Universitario di Studi Superiori, 2007.
16. **ATC, Applied Technology Council.** *Improvement of Nonlinear Static Seismic Analysis Procedures, FEMA440 Report.* Redwood City, CA, 2005.
17. **Chopra, A.K.** *Estimating seismic demands for performance-based engineering of buildings.* Key-note Lecture at the 13th World Conference on Earthquake Engineering. Paper No. 5007. Vancouver, 2004.
18. **Elnashai, A.S.** Do we really need inelastic dynamic analysis? *Journal of Earthquake Engineering.* 2002, Vol. 6, pp. 123-130.
19. **Freeman S.A., Nicoletti J.P., Tyrell J.V.** *Evaluation of existing buildings for seismic risk - A case study of Puget Sound Naval Shipyard, Bremerton, Washington.* Proceedings of U.S. National Conference on Earthquake Engineering. pp. 113-122. Berkeley, USA, 1975.
20. **Fajfar.** A nonlinear analysis method for performance-based seismic design. *Earthquake Spectra* . 2000, Vol. 16(3), pp. 573-592.
21. **ATC, Applied Technology Council.** *Seismic Evaluation and Retrofit of Concrete Buildings, vol. 1 and 2, Report No. ATC-40.* Redwood City, CA, 1996.
22. **FEMA, Federal Emergency Management Agency.** *NEHRP guidelines for the seismic rehabilitation of buildings (FEMA 273).* Washington D.C., 1997.
23. **ASCE, American Society of civil Engineers.** *Prestandard and commentary for the seismic rehabilitation of buildings, FEMA-356.* Washington D.C., 2000.
24. **MLIT, Ministry of Land Infrastructure and Transport.** *Design example and commentary for the calculation of response and limit strength (in Japanese).* Japan, 2001.
25. **CEN, Comité Européen de Normalisation.** *Eurocode 8: Design of structures for earthquake resistance. Part 1: general rules, seismic actions and rules for buildings. EN 1998-1:2004.* Brussels, Belgium, 2004.
26. **Gupta B., Kunnath S.K.** Adaptive spectra-based pushover procedure for seismic evaluation of structures. *Earthquake Spectra* . 2000, Vol. 16(2), pp. 367-391.
27. **Kunnath S.K., Kalkan E.** Evaluation of seismic deformation demands using nonlinear procedures in multistorey steel and concrete moment frames. *ISET, Journal of Earthquake Technology* . 2004, Vol. 41(1), pp. 159-82.
28. **Kalkan E., Kunnath S.K.** *Method of modal combinations for pushover analysis of buildings.* Proceedings of the 13th world conference on earthquake engineering. Paper No. 2713. Vancouver, 2004.
29. **Goel R.K., Chopra A.K.** Evaluation of modal and FEMA pushover analyses:SAC buildings. *Earthquake Spectra* . 2004, Vol. 20(1), pp. 225-254.
30. **Paret T.F., Sasaki K.K., Eilbeck D.H., Freeman S.A.** *Approximate inelastic procedures to identify failure mechanisms from higher mode effects.* Proceedings of the 11th World Conference in Earthquake Engineering. Paper No. 996. Acapulco, Mexico, 1996.

31. **Moghadam A.S., Tso W.K.** *A pushover procedure for tall buildings.* Proceedings of the 12th European Conference in Earthquake Engineering. Paper No. 395. London, UK, 2002.
32. **Jan T.S., Liu M.W., Kao Y.C.** An upper-bound pushover analysis procedure for estimating seismic demands of high-rise buildings. *Engineering Structures.* 2004, Vol. 26, pp. 117-128.
33. **Hernández-Montes E., Kwon O-S, Aschheim M.** An energy-based fomrulation for first and multiple-mode nonlinear static (pushover) analyses. *Journal of Earthquake Engineering.* 2004, Vol. 8(1), pp. 69-88.
34. **Chopra A.K., Goel R.K., Chintanapakdee C.** Evaluation of a modified MPA procedure assuming higher modes as elastic to estimate seismic demands. *Earthquake Spectra.* 2004, Vol. 20(3), pp. 757-778.
35. **Kunnath, S.K.** Identification of modal combinations for nonlinear static analysis of building structures. *Comput. Aided Civ. Infrastruct. Eng.* 2004, Vol. 19(4), pp. 246-259.
36. **Kreslin M., Fajfar P.** The extended N2 method taking into account higher mode effects in elevation. *Earthquake Engineering and Structural Dynamics.* 2011, DOI: 10.1002/eqe.1104.
37. **Krawinkler H., Seneviratna G.** Pros and cons of a pushover analysis of seismic performance evaluation. *Engineering and Structures.* 1998, Vols. 20(4-6), pp. 452-464.
38. **Aydinoglu, M.N.** An incremental response spectrum analysis procedure based on inelastic spectral deformation for multi-mode seismic performance evaluation. *Bulletin of Earthquake Engineering.* 2003, Vol. 1, pp. 3-36.
39. **Bracci J.M., Kunnath S.K., Reinhorn A.M.** Seismic performance and retrofit evaluation for reinforced concrete structures. *ASCE Journal of Structural Engineering.* 1997, Vol. 123, pp. 3-10.
40. **Sasaki K.K., Freeman S.A., Paret T.F.** *Multi-mode pushover procedure (MMP) - a method to identify the effects of higher modes in a pushover analysis.* Proceedings of the 6th US National Conference on Earthquake Engineering. Seatle, Washington - Earthquake Engineering Research Institute, Oakland, California, 1998.
41. **Satyarno I., Carr A.J., Restrepo J.** *Refined pushover analysis for the assessment of older reinforced concrete buildings.* Proceedings of the New Zealand Society for Earthquake Engineering Technology Conference. pp. 75-82. Wairakei, New Zealand, 1998.
42. **Matsumori T., Otani S., Shiohara H., Kabeyasawa T.** *Earthquake member deformation demands in reinforced concrete frame structures.* Proceedings of the US-Japan Workshop on Performance-Based Earthquake Engineering Methodology for RC building structures. pp. 79-94. Maui, Hawaii : PEER Center Report, UC Berkeley, 1999.
43. **Kalkan E., Kunnath K.** Adaptive Modal Combination Procedure for Nonlinear Static Analysis of Building Structures. *Journal of Structural Engineering.* 2006, Vol. 132(11), pp. 1721-1731.
44. **Requena M., Ayala G.** *Evaluation of a simplified method for the determination of the nonlinear seismic response of RC frames.* Proceedings of the 12th World Conference on Earthquake Engineering. Paper No. 2109. Auckland, New Zealand, 2000.
45. **Elnashai, A.S.** Advanced inelastic static (pushover) analysis for earthquake applications. *Structural Engineering and Mechanics.* 2001, Vol. 12(1), pp. 51-69.

46. **Antoniou S., Pinho R.** Development and verification of a displacement based adaptive pushover procedure. *Journal of Earthquake Engineering* . 2004, Vol. 8(5), pp. 643-661.
47. **Freeman, S., Sasaki, K., Paret, T.** *Multi-mode pushover procedure (MMP) - A method to identify the effects of higher modes in a pushover analysis.* Proceedings of the 6th National Conference on Earthquake Engineering. [ed.] EERI. Seattle,WA, 1998.
48. **Valles, R., Reinhorn, A., Kunnath, S.K., Li, C., Madan, A.** *IDARC2D version 4.0: A computer program for the inelastic analysis of buildings.* National Center for Earthquake Engineering Research. Buffalo, NY, USA, 1996.
49. **Kunnath S.K., John A.Jr.** *Validity of static procedures in performance-based seismic design.* Proceedings of ASCE Structures Congress. Philadelphia, USA, 2000.
50. **Antoniou S., Pinho R.** Advantages and limitations of adaptive and non-adaptive force-based pushover procedures. *Journal of Earthquake Engineering.* 2004, Vol. 8(4), pp. 497-522.
51. **López-Menjivar, M.A.** *Verification of a displacement-based Adaptive Pushover method for assessment of 2-D Reinforced Concrete Buildings.* European School for Advanced Studies in Reduction of Seismic Risk (ROSE School), University of Pavia. Pavia, Italy, 2004. PhD Thesis.
52. **Pinho R., Antoniou S., Casarotti C., López M.** *A displacement-based adaptive pushover for assessment of buildings and bridges.* Proceedings of the NATO International Workshop on Advances in Earthquake Engineering for Urban Risk Reduction. Istanbul, Turkey, 2005.
53. **Casarotti C., Pinho R.** An Adaptive Capacity Spectrum Method for assessment of bridges subjected to earthquake action. *Bulletin of Earthquake Engineering* . 2007, Vol. 5(3), pp. 377-390.
54. **Pinho R., Marques M., Monteiro R., Casarotti C.** *Using the adaptive capacity spectrum method for seismic assessment of irregular frames.* Proceedings of the 5th European Workshop on the Seismic Behaviour or Irregular and Complex Structures. Catania, Italy, 2008.
55. **Newmark N.M., Hall W.J.** *Earthquake spectra and design.* Earthquake Engineering Research Institute. Oakland, California, U.S.A., 1982.
56. **Ramirez O.M., Constantinou M.C., Whittaker A.S., Kircher C.A., Chrysostomou C.Z.** Elastic and inelastic seismic response of buildings with damping systems. *Earthquake Spectra.* 2002, Vol. 18(3), pp. 531–547.
57. **Lin Y. Y., Chang K. C.** A study on damping reduction factors for buildings under earthquake ground motions. *ASCE Journal of Structural Engineering* . 2003, Vol. 129(2), pp. 206-214.
58. **Gulkan P., Sozen M.** Inelastic response of reinforced concrete structures to earthquakes motions. *ACI Journal* . 1974, Vol. 71, pp. 604-610.
59. **Kowalsky M., Priestley M.J.N., McRae G.A.** Displacement-based design of RC bridge columns in seismic regions. *Earthquake Engineering and Structural Dynamics.* 1995, Vol. 24, pp. 1623–1643.
60. **Grant, D.N., Blandon, C.A., and Priestley, M.J.N.** *Modelling inelastic response in direct displacement-based design.* European School of Advanced Studies in Reduction of Seismic Risk. Pavia, Italy, 2004. ROSE 2004/02.
61. **Dwairi H., Kowalsky M.J., Nau J.M.** Equivalent damping in support of direct displacement-based design. *Journal of Earthquake Engineering.* 2007, Vol. 11(4), pp. 512–530.

62. **Iwan, W. D.** Estimating inelastic response spectra from elastic spectra. *Earthquake Engineering and Structural Dynamics.* 1980, Vol. 8, pp. 375–388.
63. **Kwan W.P., Billington S.L.** Influence of hysteretic behaviour on equivalent period and damping of structural systems. *Journal of Structural Engineering.* 2003, Vol. 129(5), pp. 576–585.
64. **Guyader A.C., Iwan W.D.** Determining equivalent linear parameters for use in a capacity spectrum method of analysis. *Journal of Structural Engineering.* 2006, Vol. 132(1), pp. 59–67.
65. **Vidic T., Fajfar P., Fischinger M.** Consistent inelastic design spectra: strength and displacement. *Earthquake Engineering and Structural Dynamics.* 1994, Vol. 23, pp. 502–521.
66. **Miranda, E.** Inelastic displacement ratios for structures on firm sites. *Journal of Structural Engineering.* 2000, Vol. 126(10), pp. 1150–1159.
67. **Miranda E., Akkar S.D.** *Evaluation of approximate method to estimate target displacements in PBEE.* The 4th U.S. - Japan Workshop on Performance-Based Earthquake Engineering Methodology for Reinforced Concrete Building Structures, PEER Rep. No. 2002/21. pp. 75-86. Berkeley, California, 2002.
68. **Kilar V., Fajfar P.** Simple push-over analysis of asymmetric buildings. *Earthquake Engineering and Structural Dynamics.* 1997, Vol. 26, pp. 233-249.
69. **Faella G., Kilar V.** *Asymmetric multistorey R/C frame structures: push-over versus nonlinear dynamic analysis.* Proceedings of the 11th European Conference on Earthquake Engineering. Balkema, Rotterdam, 1998.
70. **De Stefano M., Rutenberg A.** *Predicting the dynamic response of asymmetric multistorey wall-frame structures by pushover analysis: two case studies.* Proceedings of the 11th European Conference on Earthquake. Balkema, Rotterdam, 1998.
71. *Uniform Building Code.* UBC. International Conference of Building Officials. pp. 37-60. USA, 1996.
72. **Azuhata, T., Saito, T., Takayama, M., andNagahara, K.** *Seismic performance of asymmetric buildings based on the capacity spectrum method.* Proceedings of 12th World Conference on Earthquake Engineering. Paper No. 2322. Auckland, New Zealand, 2000.
73. **Ozaki, M., Azuhata, T., Takahashi, T., and Mu, S.** Inelastic deformation of one-story asymmetric-plan systems subjected to strong earthquake ground motions. *Earthquake Spectra.* 1994, Vol. 10(4), pp. 777-790.
74. **Moghadam, A.S. and Tso,W.K.** *Pushover analysis for asymmetric and set-back multi-story buildings.* Proceedings of 12th World Conference on Earthquake Engineering. Paper No. 1093. Auckland, New Zealand, 2000.
75. **Ayala A.G., Tavera E.A.** *A new approach for the evaluation of the seismic performance of asymmetric buildings.* Proceeding of 7th National Conference on Earthquake Engineering. EERI, Boston, USA, 2002.
76. **Penelis G.G., Kappos A.J.** *3D pushover analysis: the issue of torsion.* Proceedings of 12th European Conference on Earthquake Engineering. Paper No. 015. London, UK, 2002.
77. **Penelis G.G., Kappos A.J.** *Inelastic torsional effects in 3D pushover analysis of buildings.* Proceedings of 4th European workshop on the seismic behaviour of irregular and complex structures. Paper No. 51. Greece, 2005.
78. **Reyes J.C., Chopra A.K.** Three-dimensional modal pushover analysis of buildings subjected to two components of ground motion, including its evaluation for tall buildings. *Earthquake Engineering and Structural Dynamics.* 2011, Vol. 40, pp. 789–806.

79. **Koren D., Kilar V.** The applicability of the N2 method to the estimation of torsional. *Earthquake Engineering and Structural Dynamics.* 2011, Vol. 40, pp. 867–886.
80. **R. Bento, R. Pinho.** *3D Pushover 2008 – Nonlinear Static Methods for Design Assessment of 3D Structures.* IST Press, 2009, http://www.3dpushover.org/.
81. **Fujii, K., Nakano, Y., Sanada, Y.** *Simplified nonlinear analysis procedure for asymmetric buildings.* Proceedings of the 13th World Conference on Earthquake Engineering. Paper No. 149. Vancouver, Canada, 2004.
82. **Yu, Q. S. K., Pugliesi, R., Allen, M., Bischoff, C.** *Assessment of modal pushover analysis procedure and its application to seismic evaluation of existing building.* Proceedings of the 13th World Conference on Earthquake Engineering. Paper No. 110. Vancouver, Canada, 2004.
83. **Stefano M., Pintucchi B.** Predicting torsion-induced lateral displacements for pushover analysis: influence of torsional system characteristics. *Earthquake Engineering and Structural Dynamics.* 2010, DOI: 10.1002/eqe.1002.
84. **Fajfar P., Fischinger M.** Non-linear seismic analysis of RC buildings: Implications of a case study. *European Earthquake Engineering.* 1987, Vol. 1, pp. 31-43.
85. **Saiidi M., Sozen M.** Simple nonlinear seismic analysis of R/C structures. *Journal of Structural Division, ASCE.* 1981, Vol. 107, pp. 937-952.
86. **Fajfar P., Gaspersic P.** The N2 method for the seismic damage analysis of RC buildings. *Earthquake Engineering and Structural Dynamics.* 1996, Vol. 25, pp. 23-67.
87. **Fajfar P., Gaspersic P., Drobnic D.** *A simplified nonlinear method for seismic damage analysis of structures.* Seismic design methodologies for the next generation of codes. pp. 183-194. Balkema, Rotterdam: P. Fajfar and H. Krawinkler. 1997.
88. **Fajfar, P.** Capacity spectrum method based on inelastic demand spectrum. *Earthquake Engineering and Structural Dynamics.* 1999, Vol. 28, pp. 979-993.
89. **Baez J., Miranda E.** *Amplification factors to estimate inelastic displacement demands for the design structures in the near field.* Proceedings of the 12th World Conference on Earthquake Engineering. Paper 1561. Auckland, New Zealand : New Zealand Society for Earthquake Engineering, 2000.
90. **Rahnama M., Krawinkler H.** *Effects of soft soil and hysteresis model on seismic demands.* The John A. Blume Earthquake Engineering Center, Stanford University. Stanford, CA, 1993. Report No. 108.
91. **Whittaker A., Constantinou M., Tsopelas P.** Displacement estimates for performance-based seismic design. [ed.] ASCE. *Journal of Structural Engineering.* 1998, Vol. 124, pp. 905-912.
92. **Miranda, E.** Site-dependent strength-reduction factors. *Journal of Structural Engineering (ASCE).* 1993, Vol. 119, pp. 3503-3519.
93. **Riddell, R.** Inelastic design spectra accounting for soil conditions. *Earthquake Engineering and Structural Dynamics.* 1995, Vol. 24, pp. 1491-1510.
94. **Chintanapakdee C., Chopra A.K.** Evaluation of modal pushover analysis using generic frames. *Earthquake Engineering and Structural Dynamics.* 2003, Vol. 32, pp. 417-442.
95. **Chintanapakdee C., Chopra A.K.** Seismic response of vertically irregular frames: response history and modal pushover anlayses. *Journal of Structural Engineering (ASCE).* 2004, Vol. 130(8), pp. 1177-1185.

96. **Miranda E., Ruiz-García J.** Evaluation of approximate methods to estimate maximum inelastic displacement demands. *Earthquake Engineering and Structural Dynamics.* 2002, pp. 539-560.
97. **Monteiro R., Marques M., Adhikari G., Casarotti C., Pinho R.** Spectral Reduction Factors Evaluation for Seismic Assessment of Frame Buildings. *Earthquake and Structures.* 2011, Under review.
98. **Rosenblueth E., Herrera I.** On a kind of hysteretic damping. [ed.] ASCE. *Journal of Engineering Mechanics Division.* 1964, Vol. 90, pp. 37-48.
99. **Kowalsky M.J., Priestley M.J.N., MacRae G.A.** *Displacement-based design: a methodology for seismic design applied to single degree of freedom reinforced concrete structures.* University of California. San Diego, La Jolla, CA, 1994. Structural Systems Research Project SSRP - 94=16.
100. **Pinho R., Monteiro R., Casarotti C., Delgado R.** Verification of Nonlinear Static Procedures (NSP) for Assessment of Bridges. *Nonlinear Static Methods for Design/Assessment of 3D Structures* [book auth.] Bento R. and Pinho R.. Lisbon, Portugal : IST Press, 2008.
101. **Fardis, M.N.** *Design of an Irregular Building for the SPEAR Project - Description of the 3-Storey Structure. Research Report, University of Patras.* Greece, 2002.
102. **Fardis M.N., Negro P.** *SPEAR - Seismic performance assessment and rehabilitation of existing buildings.* Proceedings of the International Workshop on the SPEAR Project. Ispra, Italy, 2006.
103. **Vuran, E.** *Comparison of nonlinear static and dynamic analysis results for 3D dual structures.* Rose School. Pavia, Italy, 2007. MSc Thesis.
104. **Seismosoft.** *Seismostruct - A computer program for static and dynamic nonlinear analysis of framed structures. Available online from URL: www.seismosoft.com.* 2006.
105. **Calabrese A., Almeida J. P., Pinho R.** Numerical issues in distributed inelasticity modelling of RC frame elements for seismic analysis. *Journal of Earthquake Engineering* . 2010, Vol. 14(1).
106. **Mander J.B., Priestley M.J.N., Park R.** Theoretical stress-strain model for confined concrete. *ASCE Journal of Structural Engineering* . 1988, Vol. 114(8), pp. 1804-1826.
107. **Martinez-Rueda, J.E., Elnashai, A.S.** Confined concrete model under cyclic load. *Materials and Structures* . 1997, Vol. 30(197), pp. 139-147.
108. **Menegotto M., Pinto P.E.** *Method of analysis for cyclically loaded RC plane frames including changes in geometry and non-elastic behaviour of elements under combined normal force and bending.* Symposium on the Resistance and Ultimate Deformability of Structures anted on by well defined loads, International Association for Bridges and Structural Engineering. pp. 15-22. Zurich, Switzerland, 1973.
109. **Filippou F.C., Popov E.P., Bertero V.V.** Modelling of R/C joints under cyclic excitations. *Journal of Structural Engineering* . 1983, Vol. 109(11), pp. 2666-2684.
110. **Bal I., Crowley H., Pinho R., Gulay G.** Detailed assessment of structural characteristics of Turkish RC building stock for loss assessment models. *Soil Dynamics and Earthquake Engineering* . 2008, Vol. 28, pp. 914-932.
111. **Priestley M.J.N., Grant D.N.** Viscous damping in seismic design and analysis. *Journal of Earthquake Engineering* . 2005, Vol. 9 (SI1), pp. 229-255.
112. **Pinho R., Bhatt C., Antoniou S., Bento R.** *Modelling of the horizontal slab of a 3D irregular building for nonlinear static assessment.* Proceedings of the 14th World Conference on Earthquake Engineering. pp. 05-01-0159. Beijing, China, 2008.

113. **Hilber H.M., Hughes T.J.R., Taylor R.L.** Improved numerical dissipation for time integration algorithms in structural dynamics. *Earthquake Engineering and Structural Dynamics* . 1977, Vol. 5(3), pp. 283-292.
114. **Irons, B.** A frontal solution program for finite element analysis. *International Journal for Numerical Methods in Engineering.* 1970, Vol. 2, pp. 5-32.
115. **Izzuddin, B.** *Nonlinear Dynamic Analysis of Framed Structures.* Imperial College, University of London. London, UK, 1991. PhD Thesis.
116. **Cook R.D., Malkus D.S., Plesha M.E.** *Concepts and Applications of Finite Elements Analysis.* John Wiley & Sons, 1989.
117. **Zienkiewicz O.C., Taylor R.L.** *The Finite Element Method.* 4th Edition. McGraw Hill, 1991.
118. **Bathe, K.** *Finite Element Procedures in Engineering Analysis.* 2nd Edition. Prentice Hall, 1996.
119. **Felippa, C.** *Introduction to Finite Element Methods, Available from URL: http://www.colorado.edu/engineering/CAS/courses.d/IFEM.d/Home.html.* Centre for Aerospace Structure, College of Engineering, University of Colorado. USA, 2004. Lecture Notes.
120. **Bento R., Lopes M.** *Modelação Fisicamente Não Linear de Estruturas de Betão.* Civil Engineering and Architecture, Instituto Superior Técnico (IST). 1999.
121. **Computers and Structures, Inc.** Sap2000. 1995.
122. **PEER.** *Strong Ground Motion Database, Available from: http://peer.berkeley.edu/nga/.* 2009.
123. **Hancock J., Watson-Lamprey J., Abrahamson N.A., Bommer J.J., Markatis A., McCoy E., Mendis R.** An improved method of matching response spectra of recorded earthquake ground motion using wavelets. *Journal of Earthquake Engineering* . 2006, Vol. 10(S1), pp. 67-89.
124. **Shome N., Cornell C.A.** *Normalization and scaling accelerograms for non-linear structural analysis.* Proceedings of the 6th U.S. National Conference on Earthquake Engineering. Paper No. 243, 1-12. EERI: El Cerrito, CA: Seatle, Washington, 1998.
125. **Shome N., Cornell C.A.** *Probabilistic seismic demand analysis of non-linear structures, Report No. RMS-35, RMS Program.* Stanford University. 1999.
126. **Vamvatsikos D., Cornell C.A.** Incremental dynamic analysis. *Earthquake Engineering and Structural Dynamics* . 2002, Vol. 31, pp. 491-514.
127. **Pinto P.E., Fajfar P., Chryssanthopoulos M., Franchin P., Dolsek M. and Kazantzi A.** *Probabilistic Methods for Seismic Assessment of Existing Structures".* LESSLOSS report Nº 2007/06. Pavia, Italy : IUSS Press, 2007.
128. **Bento R., Bhatt C., Pinho R.** Using Nonlinear Static Procedures for Seismic Assessment of the 3D Irregular SPEAR Building. *Earthquakes and Structures* . 2010, Vol. 1(2), pp. 177-195.
129. **Bhatt C., Bento R.** Comparison of Nonlinear Static Methods for the Seismic Assessment of Plan Irregular Frame Buildings with Non-Seismic Details. *Journal of Earthquake Engineering, Accepted for publication.* 2011.
130. **Bhatt C., Bento R.** Extension of the CSM-FEMA440 to Plan-Asymmetric Real Building Structures. *Earthquake Engineering and Structural Dynamics.* 2011, Vol. 40(11), pp. 1263-1282.
131. **Goel, R.** *Evaluation of current nonlinear static procedures for reinforced concrete buildings.* Proceedings of the 14th World Conference on Earthquake Engineering. Beijing, China, 2008.

132. **Bhatt, C., Bento R.** Assessing the Seismic Response of Existing RC Buildings Using the Extended N2 Method. *Bulletin of Earthquake Engineering.* 2011, Vol. 9(4), pp. 1183-1201.
133. **Bhatt C., Bento R.** A New 3D Pushover Procedure for Seismic Assessment of Plan Asymmetric Buildings. *Earthquake Spectra, under review.*
134. **Mckenna F., Fenves G.L., Filippou F.C, Mazzoni S.** OpenSees - Open System for Earthquake Engineering Simulation, available from: http://opensees.berkeley.edu/. 1999.
135. **Oliveira C., Azevedo J., Bento R., Proença J., Lopes M., Guerreiro L., Ferreira M., Bhatt C.** *"A Missão do IST".* Workshop Sismo de L'Aquila - Ensinamentos para Portugal, LNEC, 2009, available from: http://www-ext.lnec.pt/LNEC/sismo_laquila/IST_LG.pdf.

Appendix

A1. Three storey building records

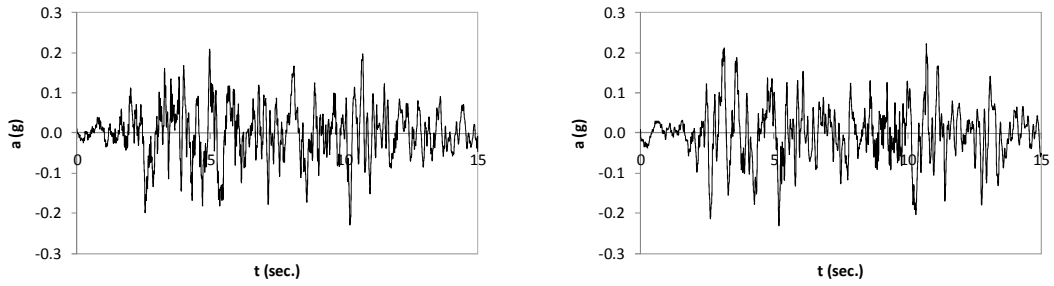

(a) *(b)*

Figure A. 1 - Montenegro earthquake 1979, station Ulcinj2 a) component 198x, direction X; b) component 198y, direction Y.

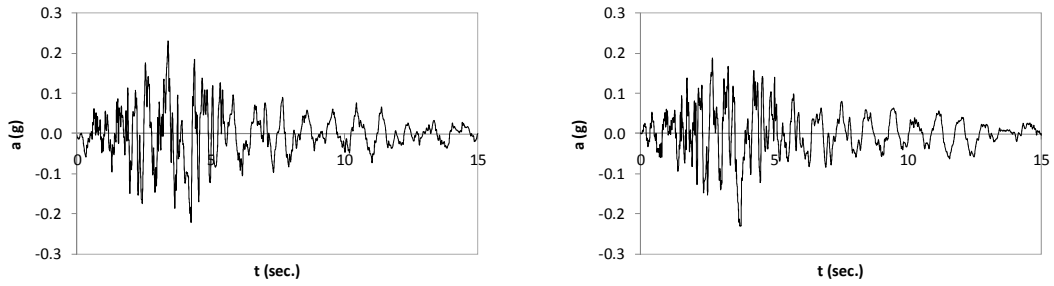

(a) *(b)*

Figure A. 2 - Kalamata earthquake 1986, station Kalamata – Perfecture a) component 413x, direction X; b) component 413y, direction Y.

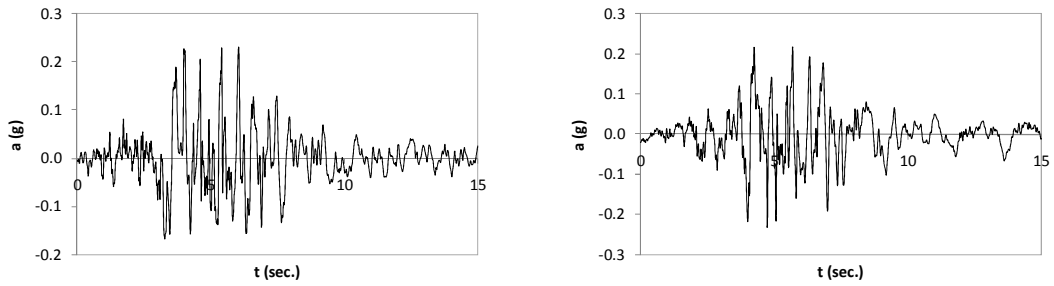

(a) *(b)*

Figure A. 3 - Friuli earthquake 1976, station Tolmezzo a) component 55x, direction X; b) component 55y, direction Y.

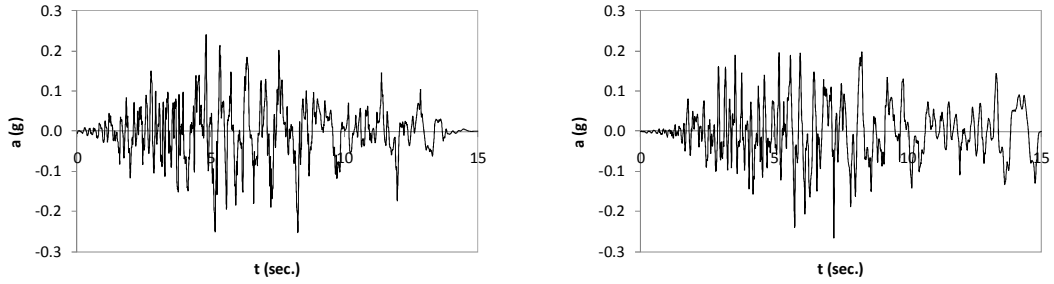

(a) *(b)*

Figure A. 4 - Loma Prieta earthquake 1989, station Capitola a) component Cap000, direction X; b) component Cap090, direction Y.

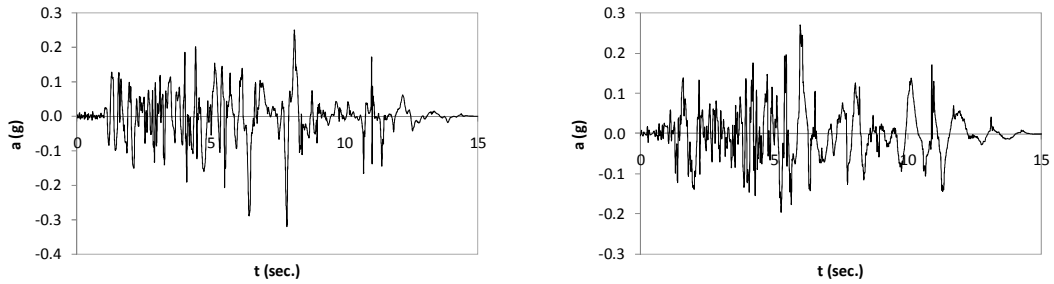

(a) *(b)*

Figure A. 5 - Imperial Valley earthquake 1979, station Bonds Corner a) component H-BCR140, direction X; b) component H-BCR230, direction Y.

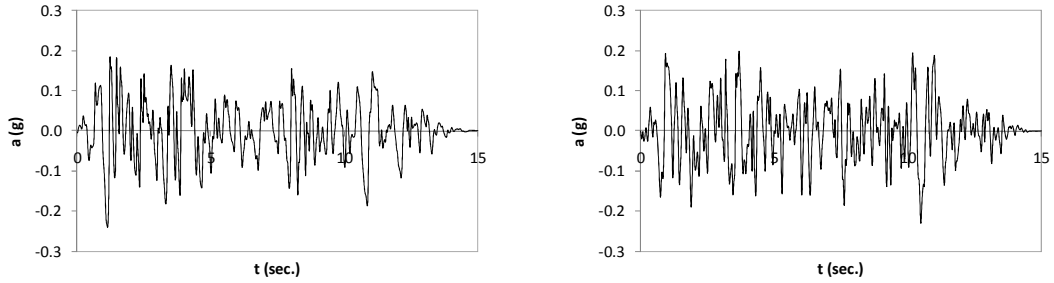

(a) *(b)*

Figure A. 6 - Imperial Valley earthquake 1940, station El Centro Array #9 a) component i-elc180, direction X; b) component i-elc270, direction Y.

A2. Five and eight storey buildings records

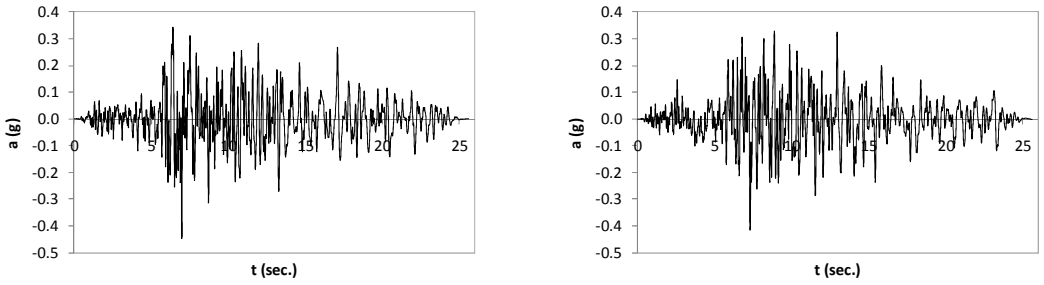

(a) *(b)*

Figure A. 7 - Whittier Narrows-01 earthquake 1987 a) component X; b) component Y.

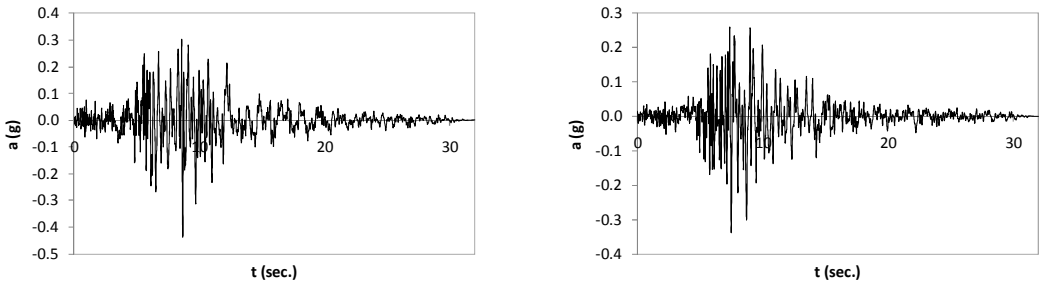

(a) *(b)*

Figure A. 8 - Northridge-01 earthquake 1994 a) component X; b) component Y.

A3. Spectra compatible with the records: three storey building

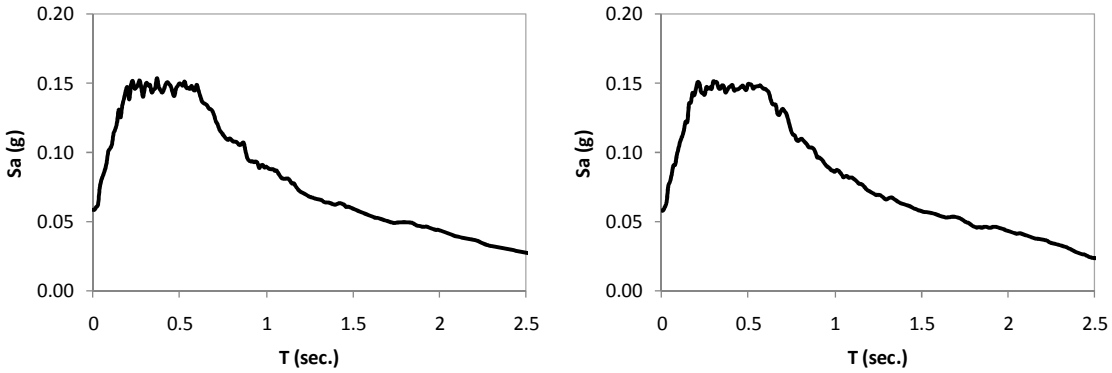

(a) *(b)*

Figure A. 9 – Median acceleration response spectra, 0.05g a) X direction; b) Y direction.

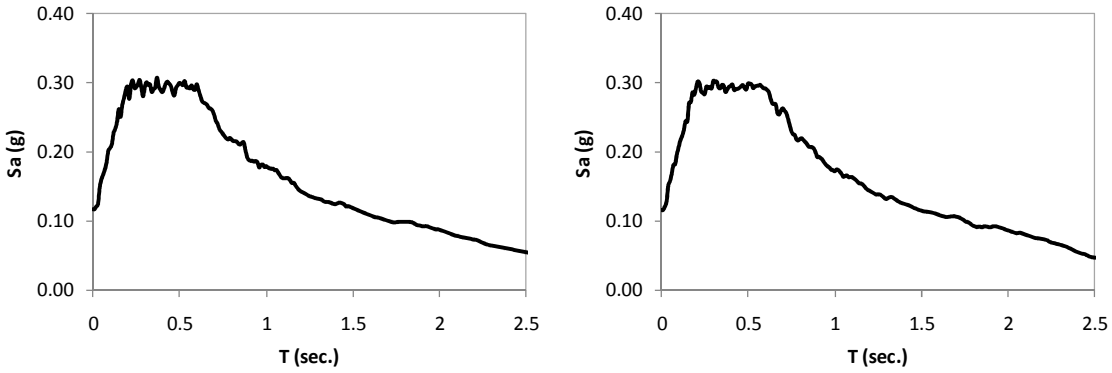

(a) *(b)*

Figure A. 10 – Median acceleration response spectra, 0.1g a) X direction; b) Y direction.

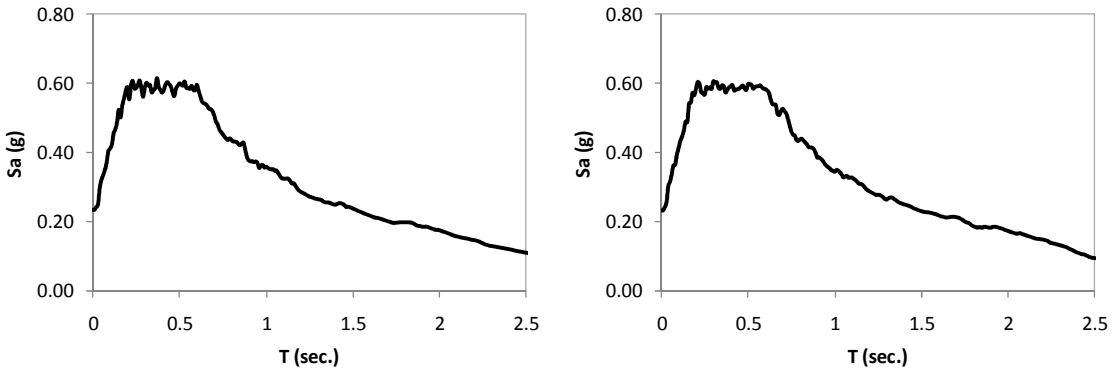

(a) *(b)*

Figure A. 11 – Median acceleration response spectra, 0.2g a) X direction; b) Y direction.

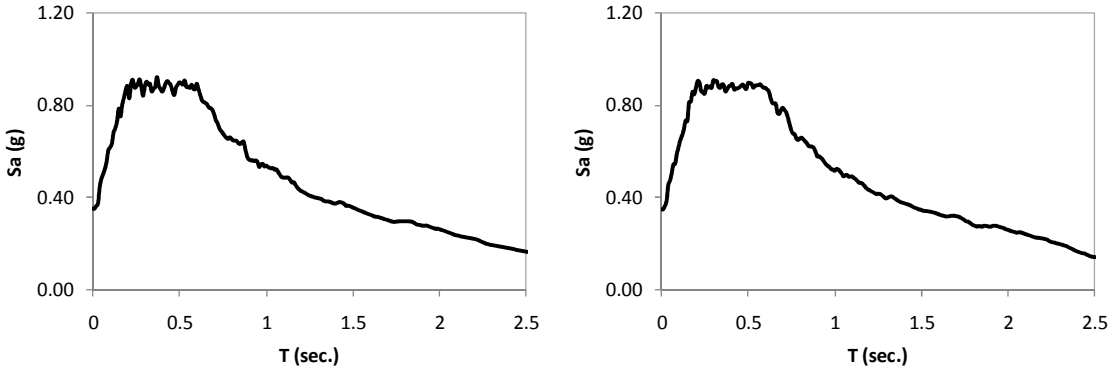

Figure A. 12 – Median acceleration response spectra, 0.3g a) X direction; b) Y direction.

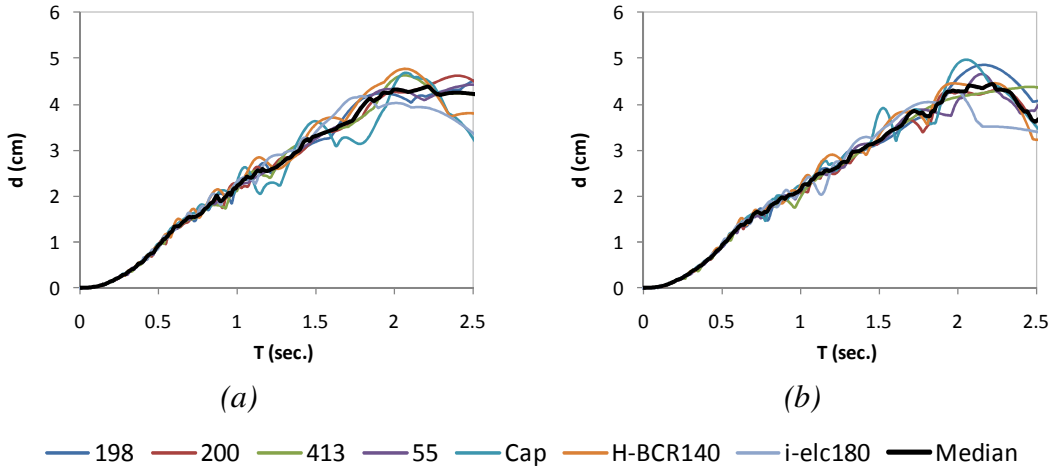

Figure A. 13 - Displacement response spectra, 0.05g a) X direction; b) Y direction.

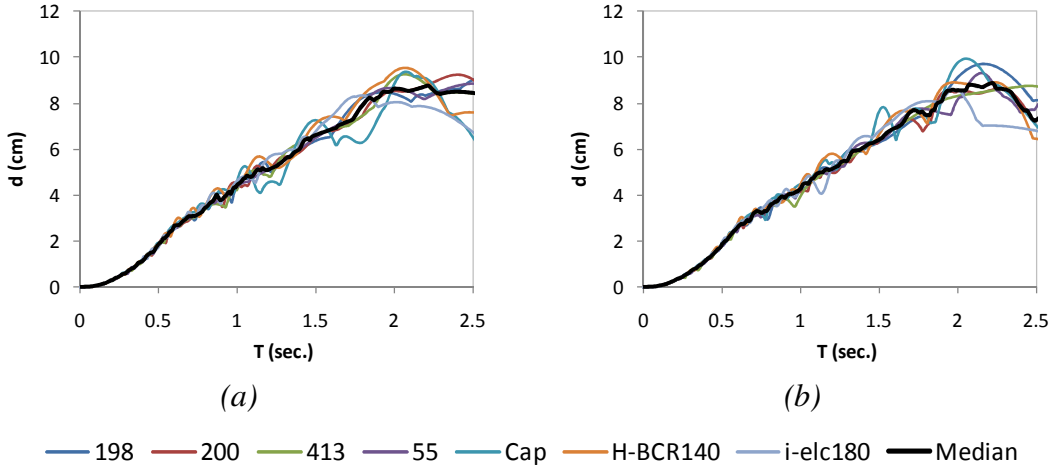

Figure A. 14 - Displacement response spectra, 0.1g a) X direction; b) Y direction.

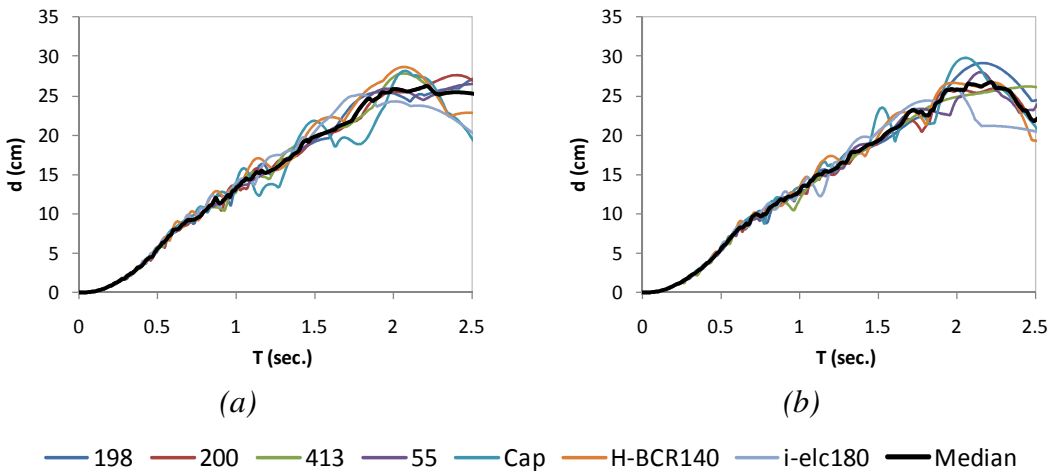

(a) *(b)*

Figure A. 15 - Displacement response spectra, 0.3g a) X direction; b) Y direction.

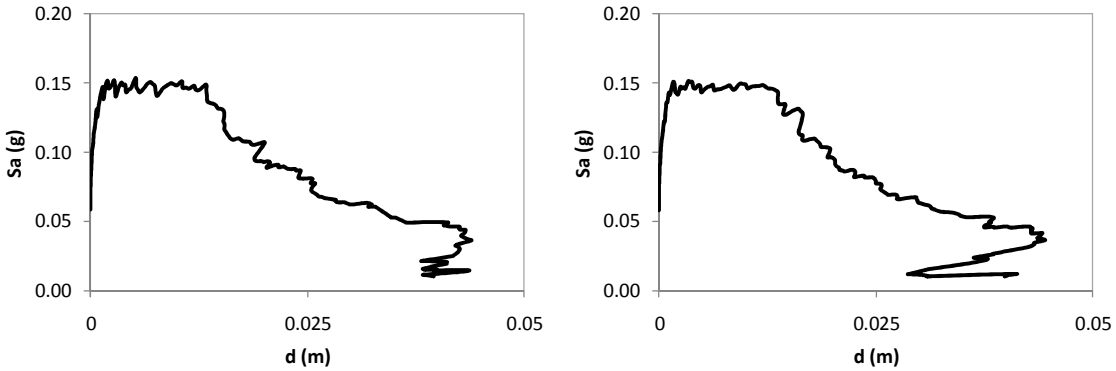

(a) *(b)*

Figure A. 16 – Median acceleration-displacement response spectra, 0.05g a) X direction; b) Y direction.

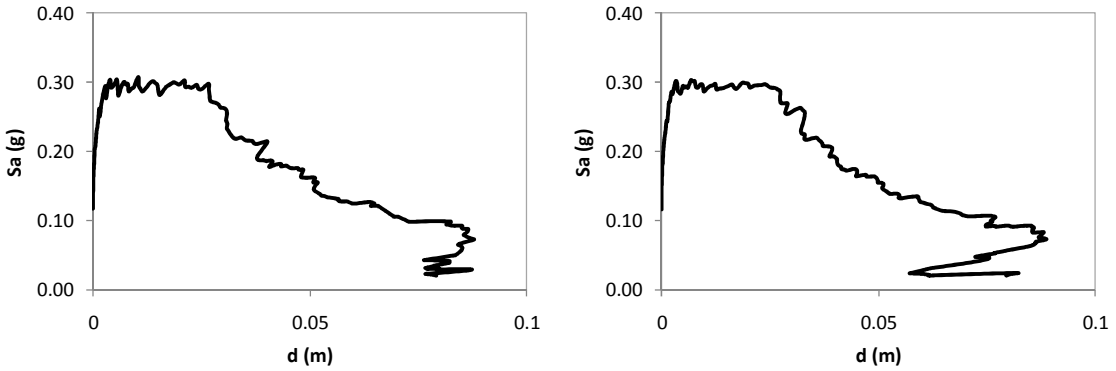

(a) *(b)*

Figure A. 17 – Median acceleration-displacement response spectra, 0.1g a) X direction; b) Y direction.

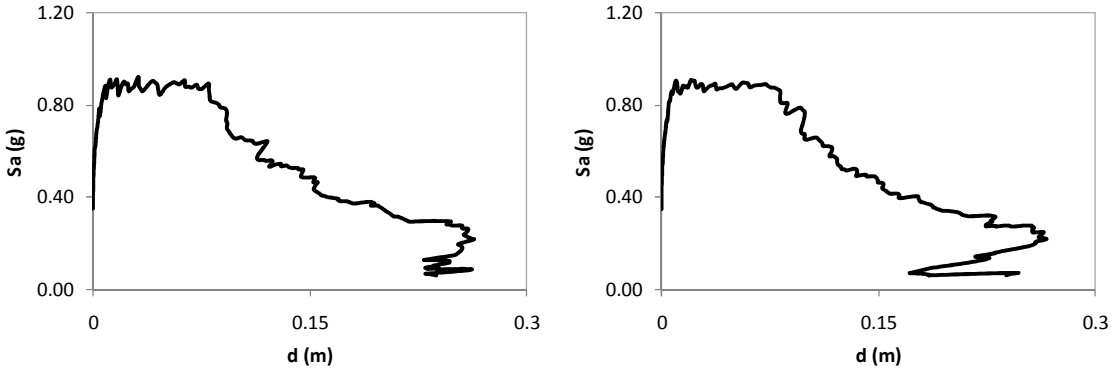

(a) *(b)*

Figure A. 18 – Median acceleration-displacement response spectra, 0.3g a) X direction; b) Y direction.

A4. Spectra compatible with the records: five and eight storey building

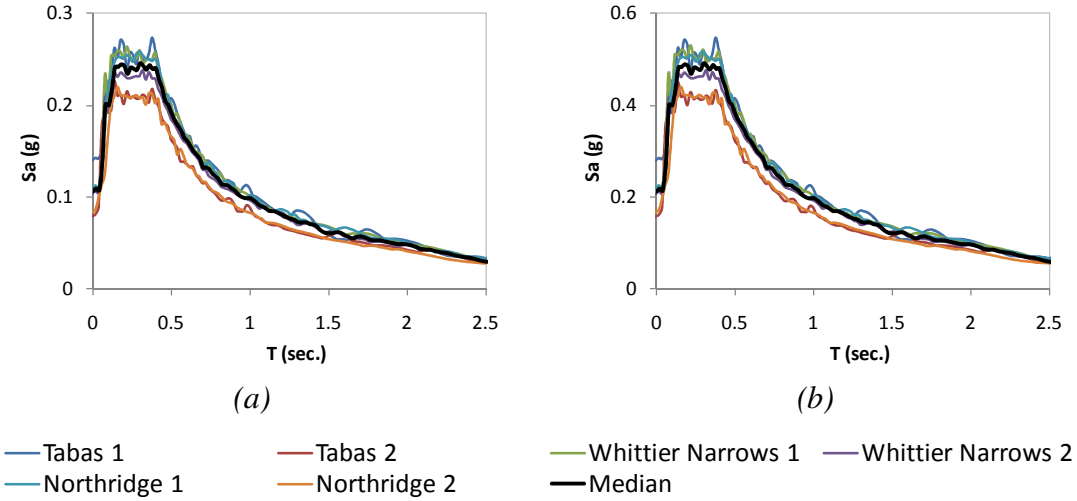

Figure A. 19 - Acceleration response spectra, a) 0.1g; b) 0.2g.

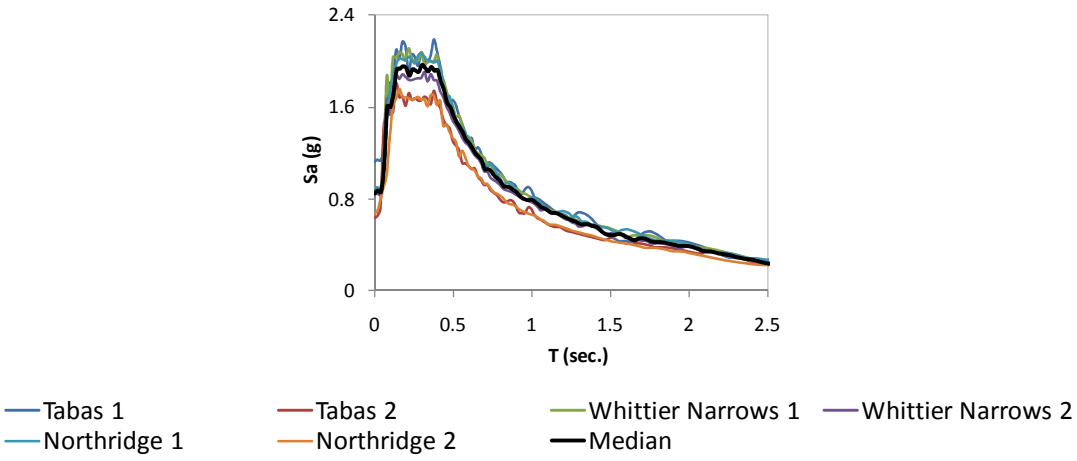

Figure A. 20 - Acceleration response spectra, 0.8g.

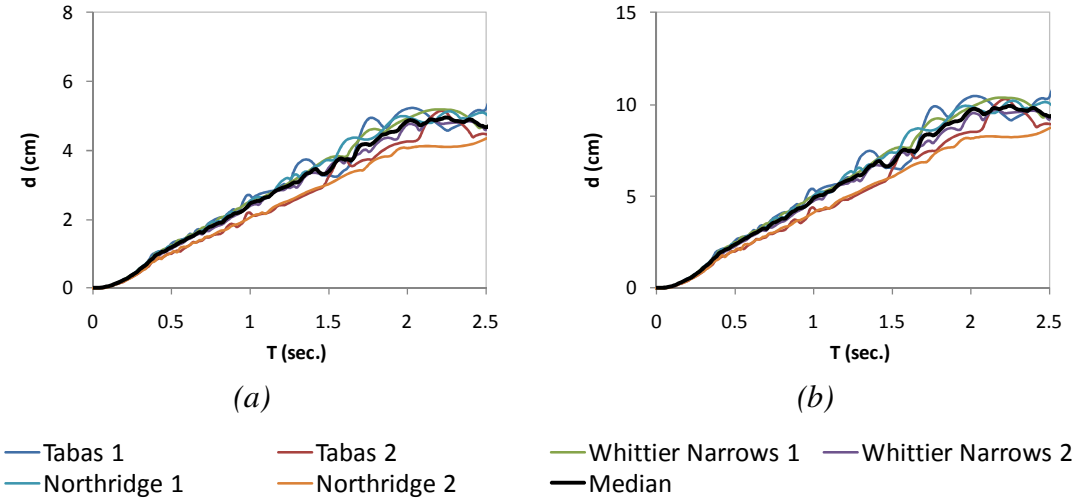

Figure A. 21 - Displacement response spectra, a) 0.1g; b) 0.2g.

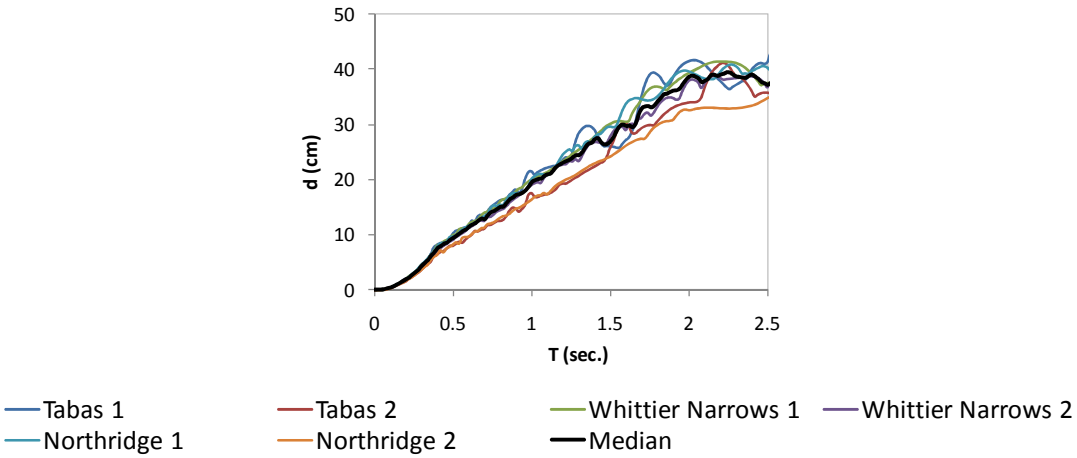

Figure A. 22 - Displacement response spectra, 0.8g.

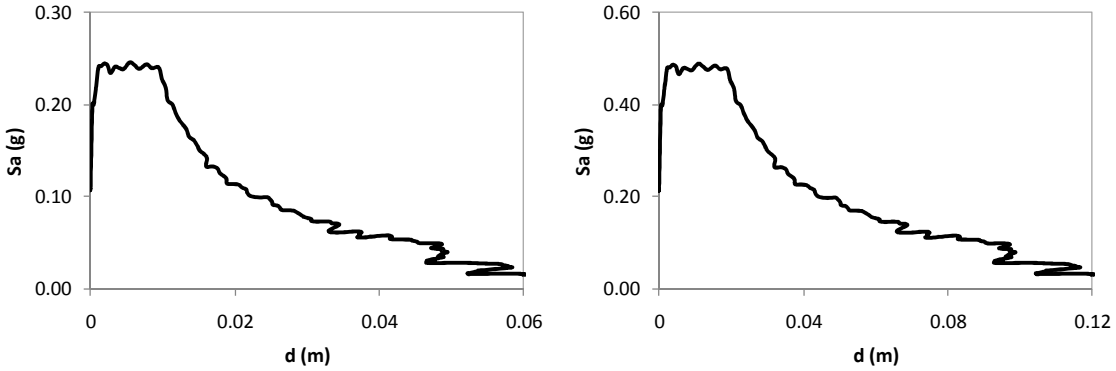

(a) *(b)*

Figure A. 23 – Median acceleration-displacement response spectra a) 0.1g; b) 0.2g.

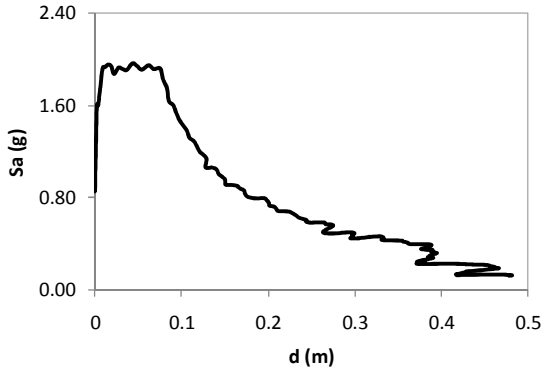

Figure A. 24 – Median acceleration-displacement response spectrum 0.8g.

A5. Lateral displacement profiles three storey building

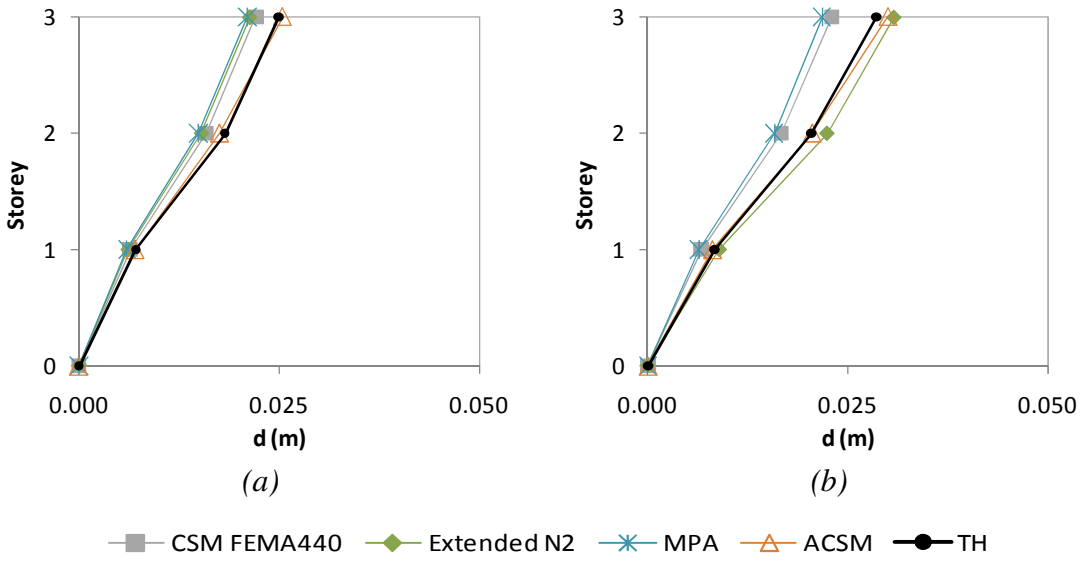

Figure A. 25 – Lateral displacement profiles X direction: a) Column C8, 0.05g; b) Column C2, 0.05g.

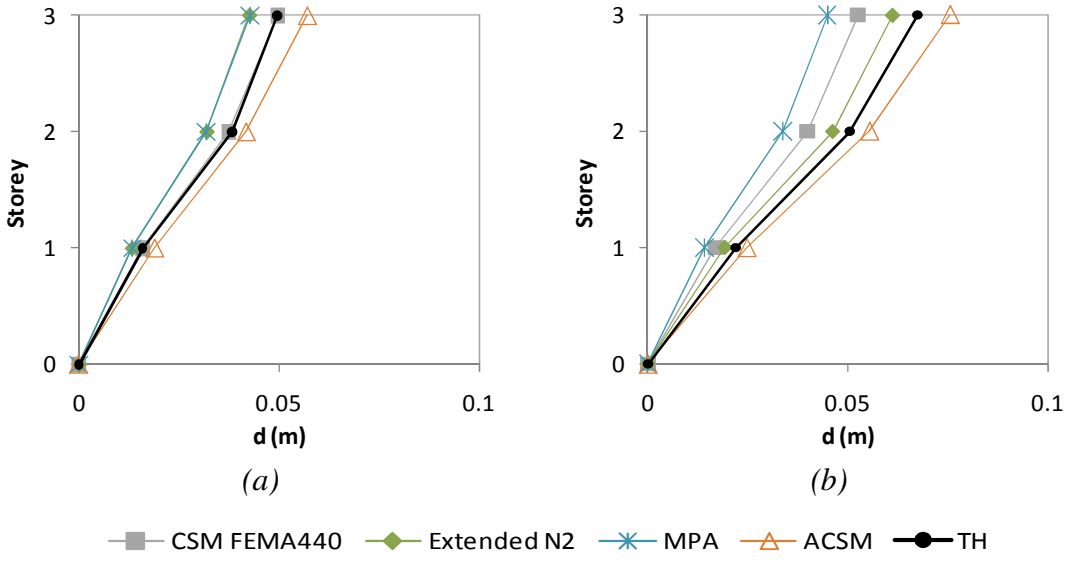

Figure A. 26 – Lateral displacement profiles X direction: a) Column C3, 0.1g; b) Column C2, 0.1g.

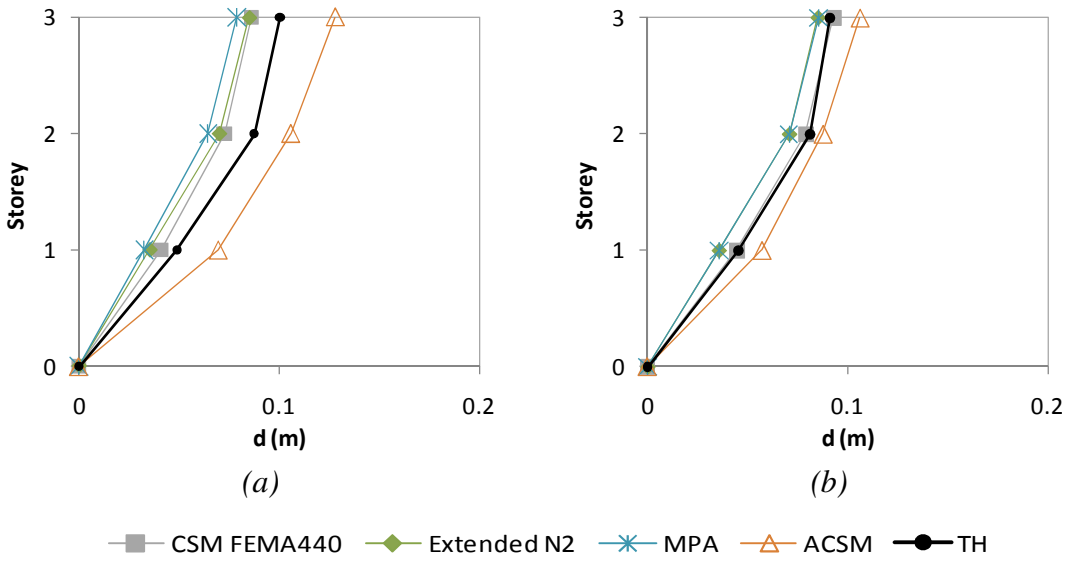

Figure A. 27 – Lateral displacement profiles X direction: a) Column C8, 0.2g; b) Column C3, 0.2g.

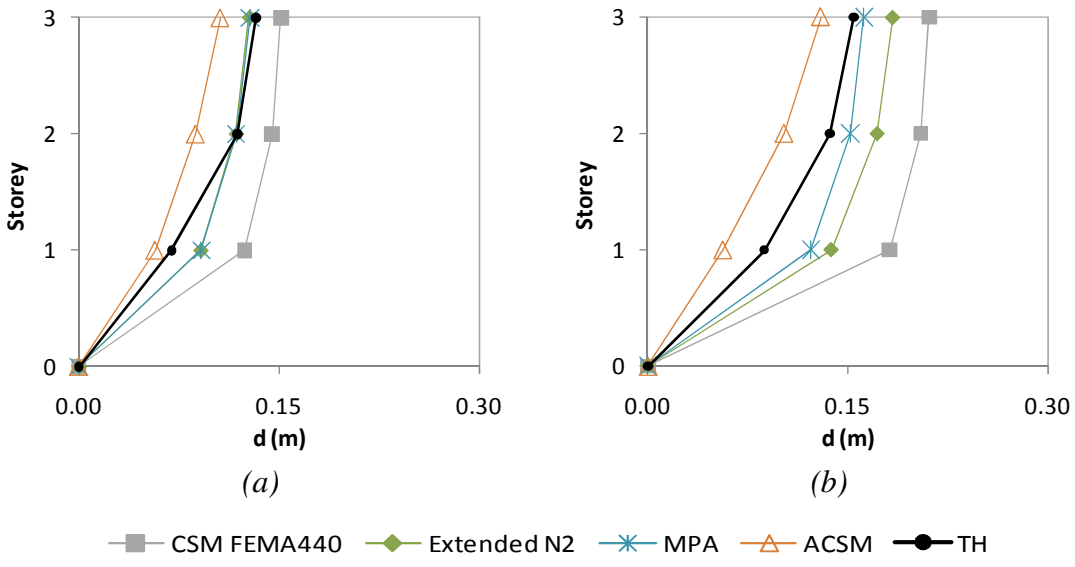

Figure A. 28 – Lateral displacement profiles X direction: a) Column C3, 0.3g; b) Column C2, 0.3g.

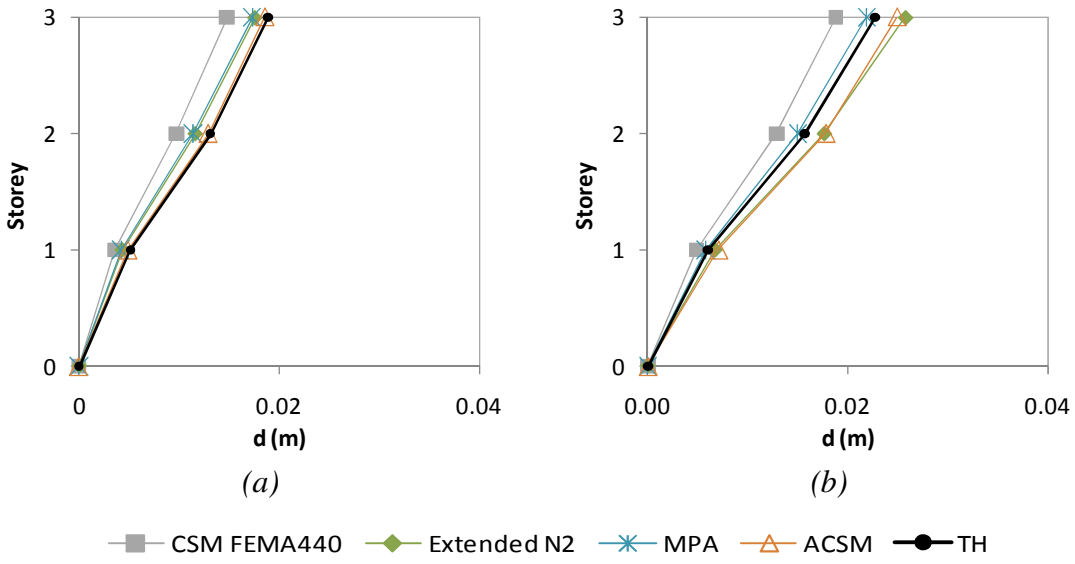

Figure A. 29 – Lateral displacement profiles Y direction: a) Column C8, 0.05g; b) Column C2, 0.05g.

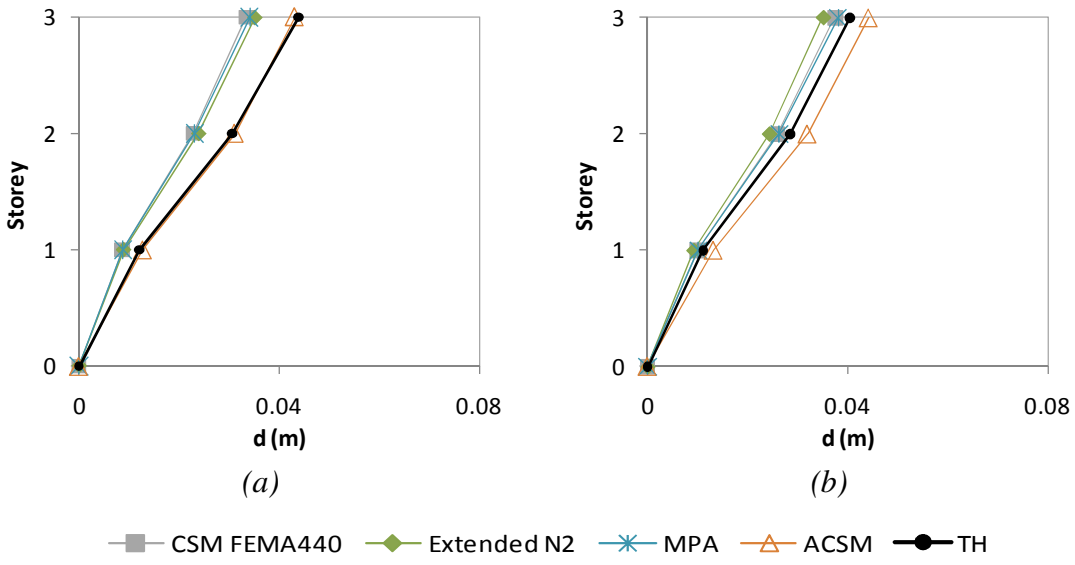

Figure A. 30 – Lateral displacement profiles Y direction: a) Column C3, 0.1g; b) Column C8, 0.1g.

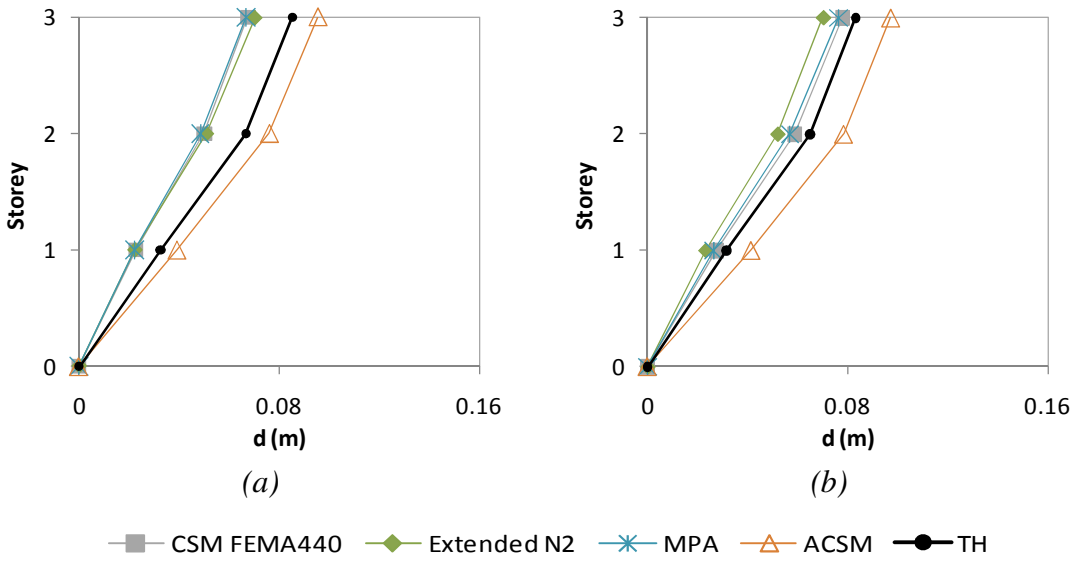

Figure A. 31 – Lateral displacement profiles Y direction: a) Column C8, 0.2g; b) Column C3, 0.2g.

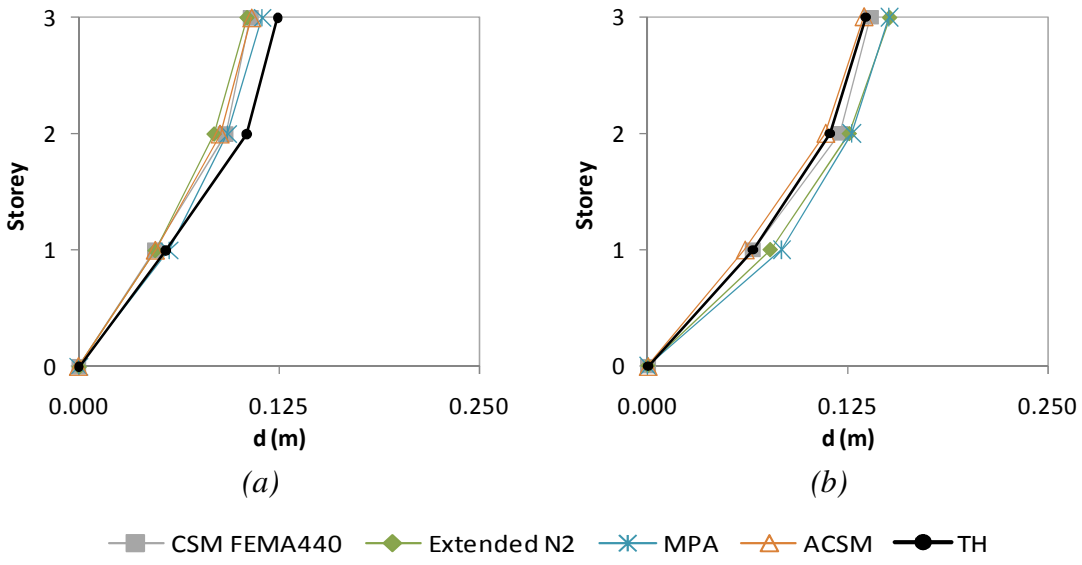

Figure A. 32 – Lateral displacement profiles Y direction: a) Column C3, 0.3g; b) Column C2, 0.3g.

A6. Interstorey drifts profiles three storey building

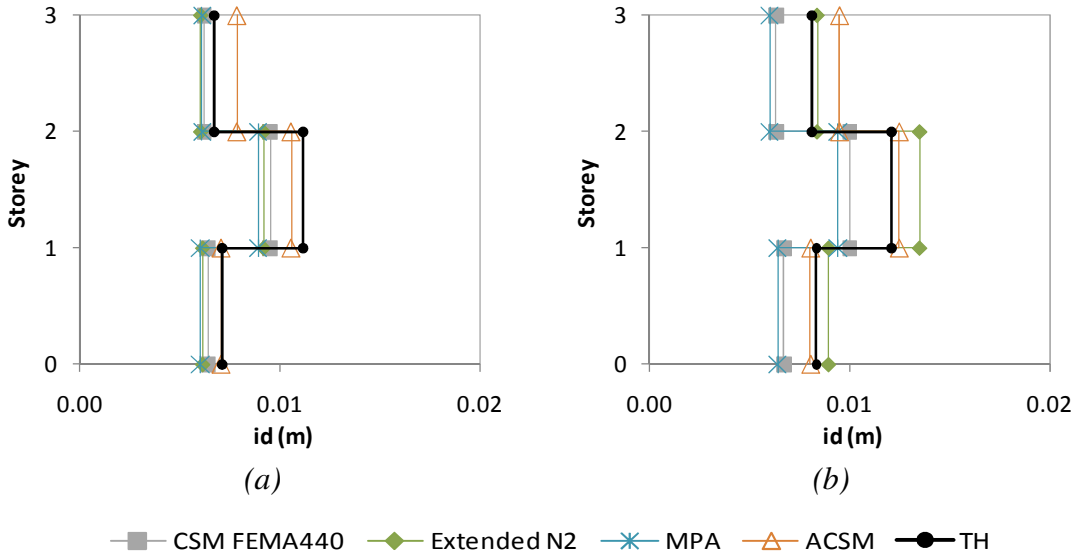

Figure A. 33 – Interstorey drifts profiles X direction: a) Column C8, 0.05g; b) Column C2, 0.05g.

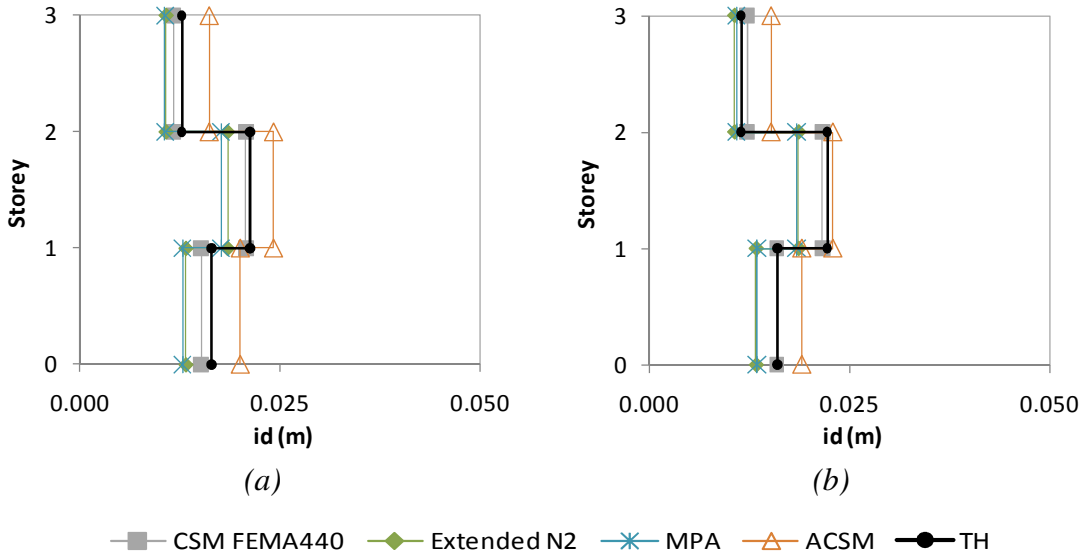

Figure A. 34 – Interstorey drifts profiles X direction: a) Column C8, 0.1g; b) Column C3, 0.1g.

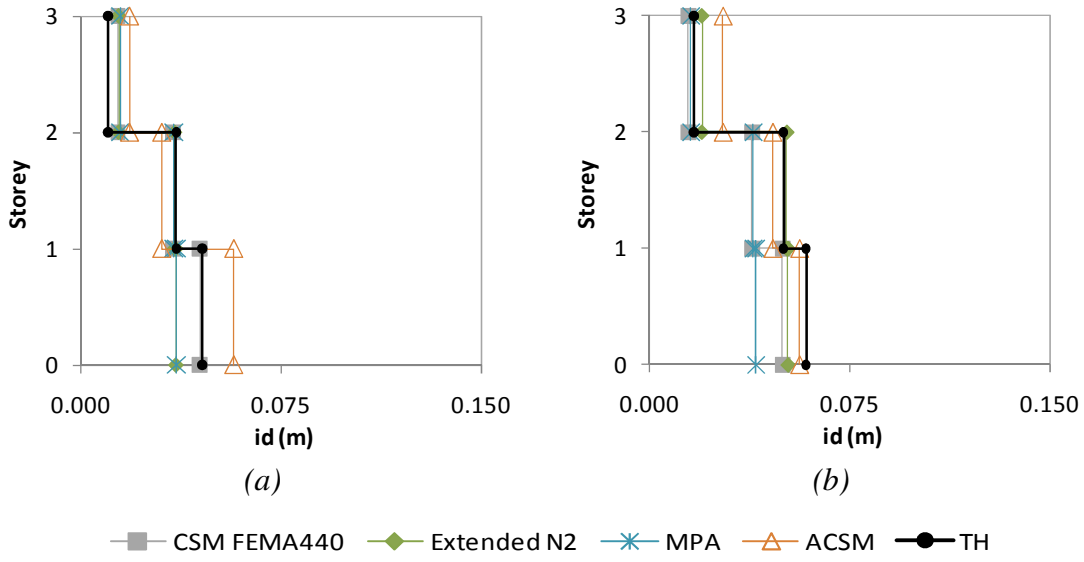

Figure A. 35 – Interstorey drifts profiles X direction: a) Column C3, 0.2g; b) Column C2, 0.2g.

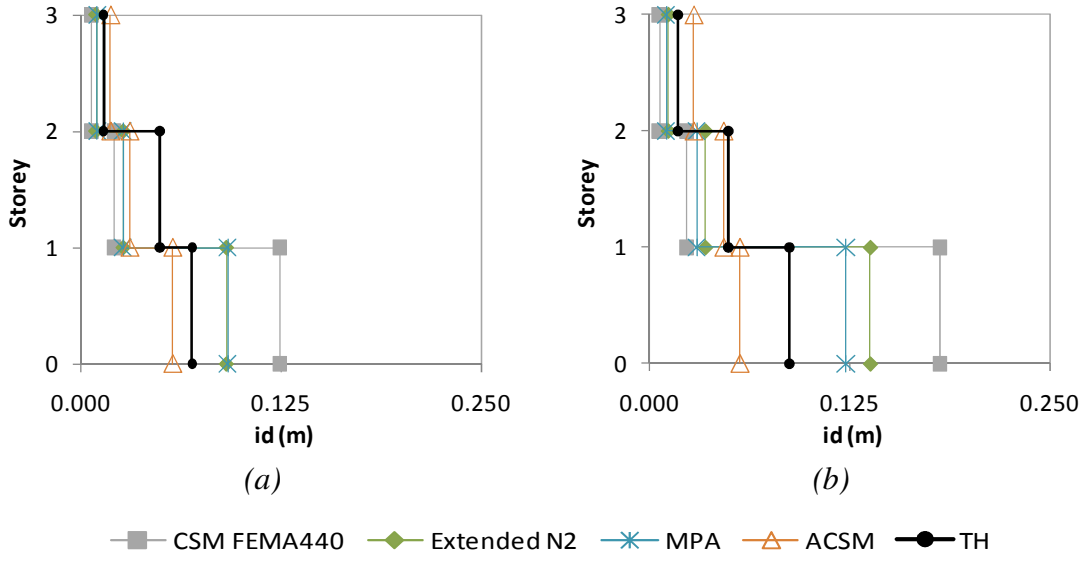

Figure A. 36 – Interstorey drifts profiles X direction: a) Column C3, 0.3g; b) Column C2, 0.3g.

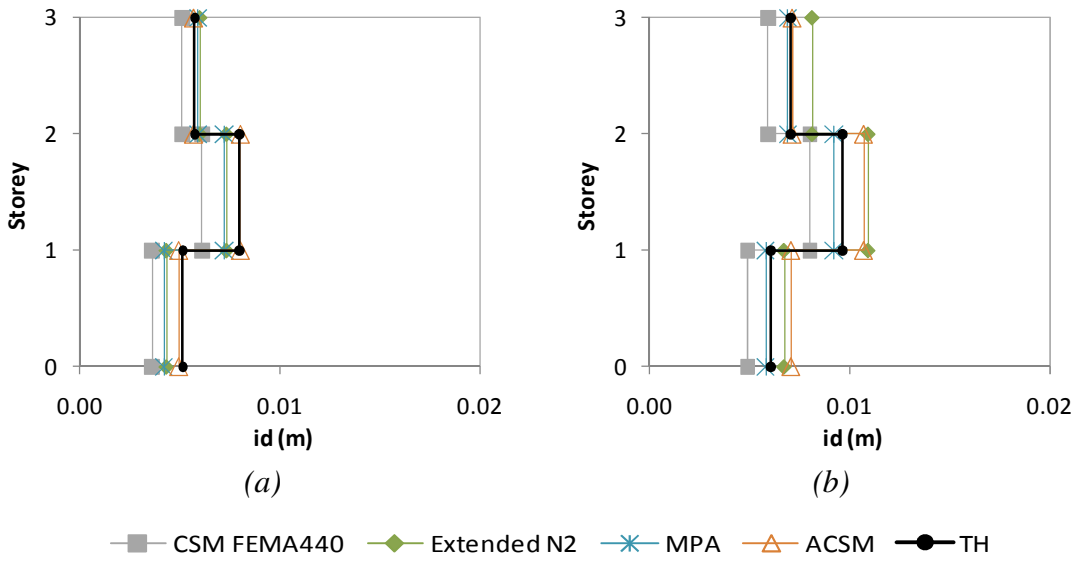

Figure A. 37 – Interstorey drifts profiles Y direction: a) Column C8, 0.05g; b) Column C2, 0.05g.

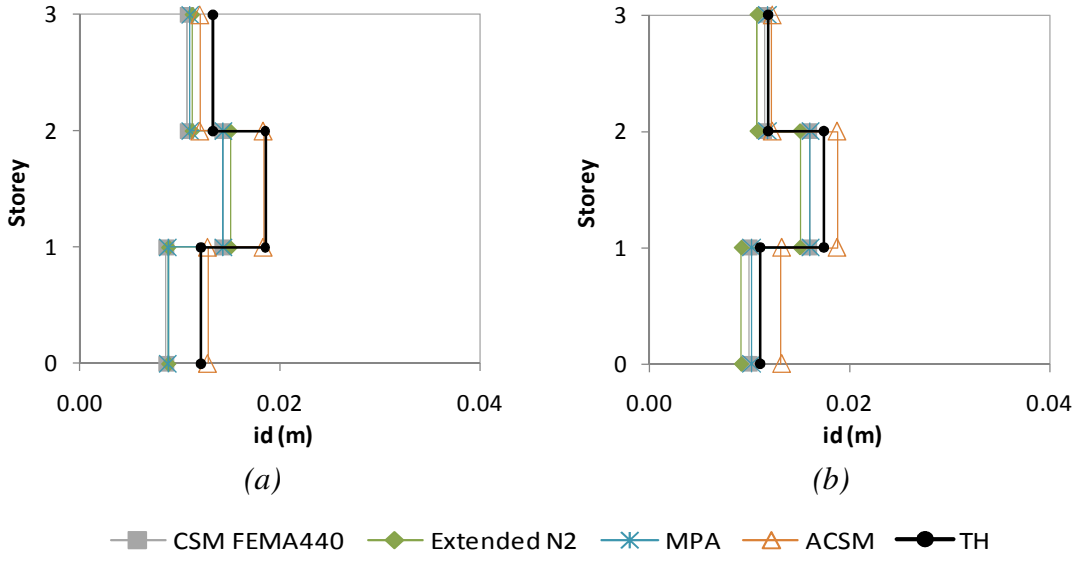

Figure A. 38 – Interstorey drifts profiles Y direction: a) Column C8, 0.1g; b) Column C3, 0.1g.

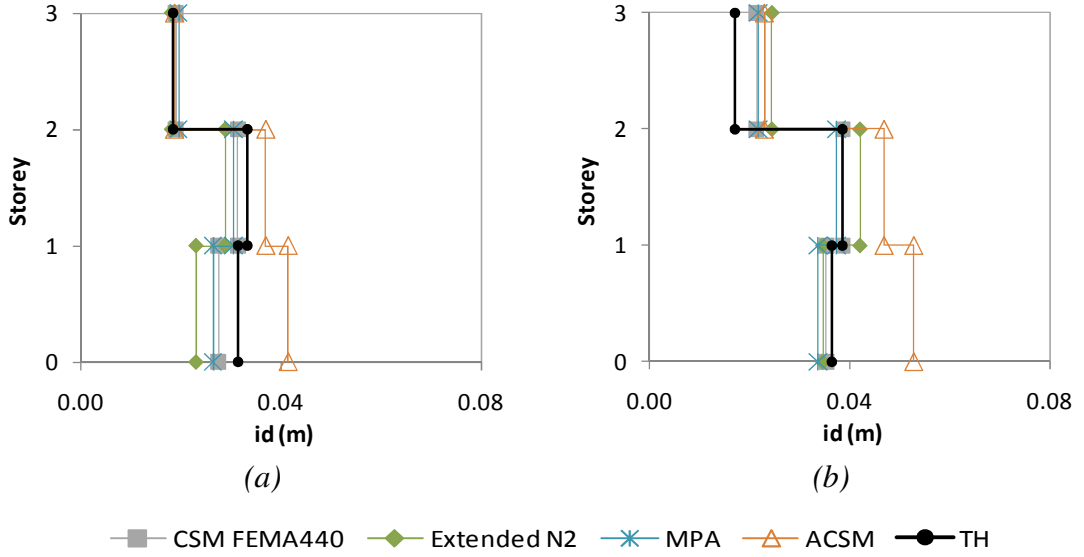

Figure A. 39 – Interstorey drifts profiles Y direction: a) Column C3, 0.2g; b) Column C2, 0.2g.

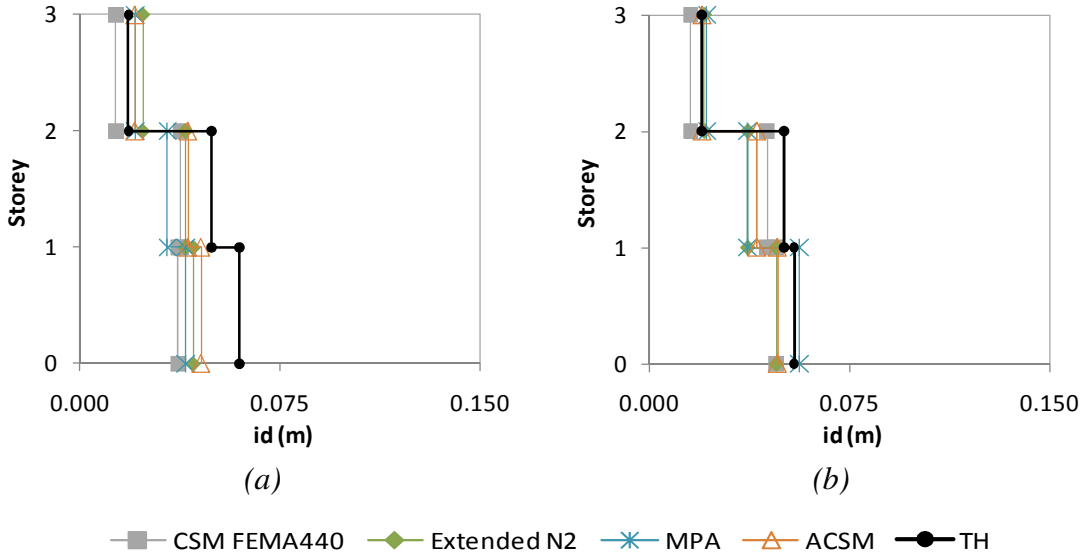

Figure A. 40 – Interstorey drifts profiles Y direction: a) Column C8, 0.3g; b) Column C3, 0.3g.

A7. Chord rotation profiles three storey building

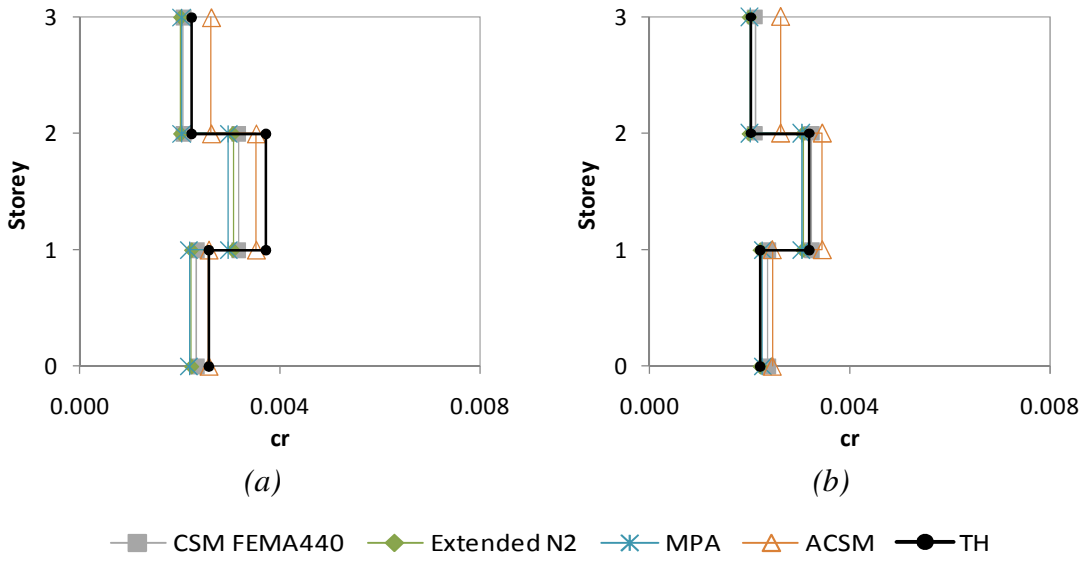

Figure A. 41 – Chord rotation profiles X direction: a) Column C8, 0.05g; b) Column C3, 0.05g.

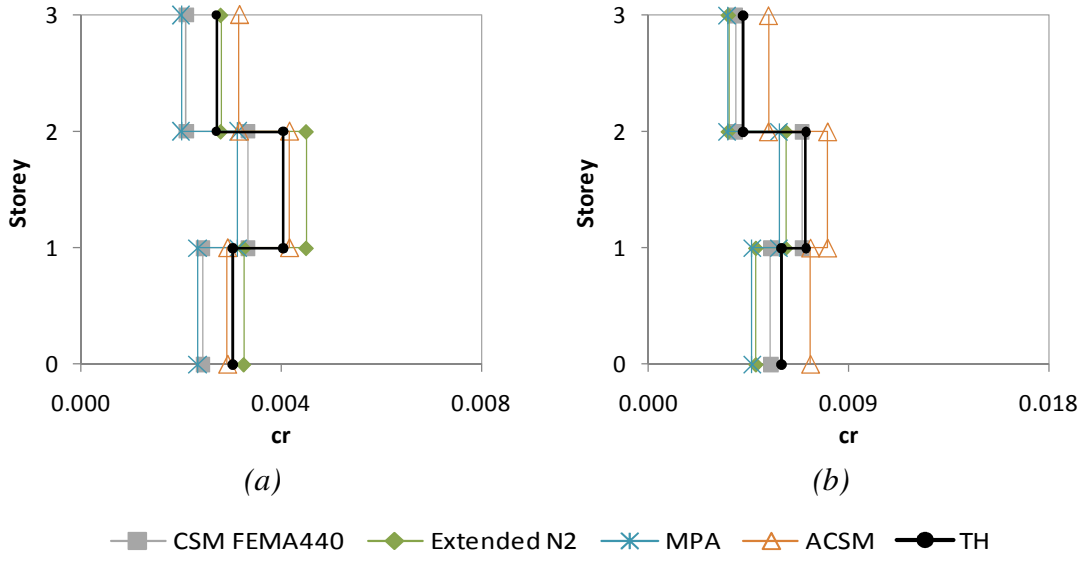

Figure A. 42 – Chord rotation profiles X direction: a) Column C2, 0.05g; b) Column C8, 0.1g.

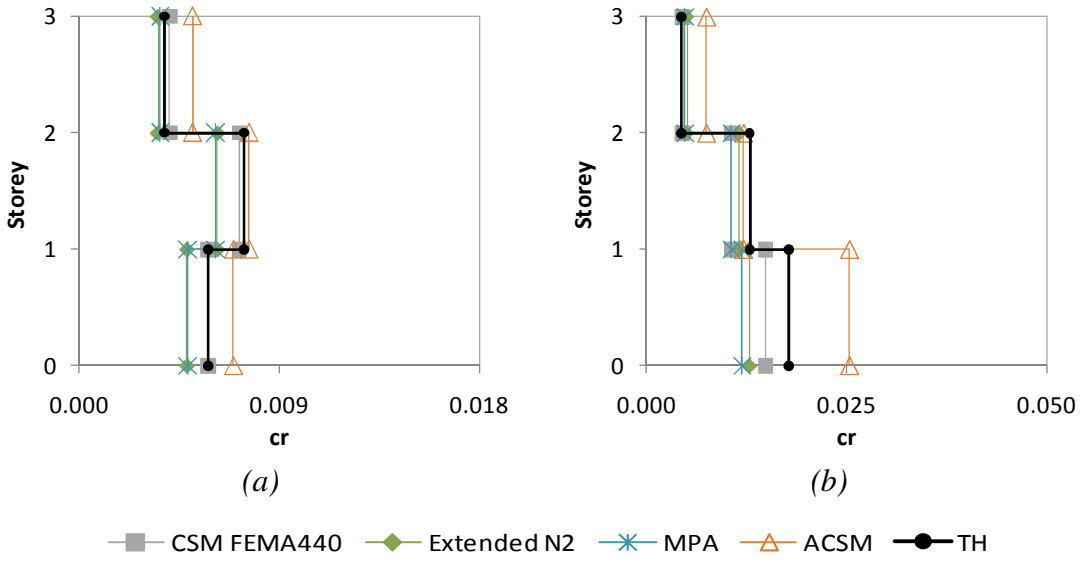

Figure A. 43 – Chord rotation profiles X direction: a) Column C3, 0.1g; b) Column C8, 0.2g.

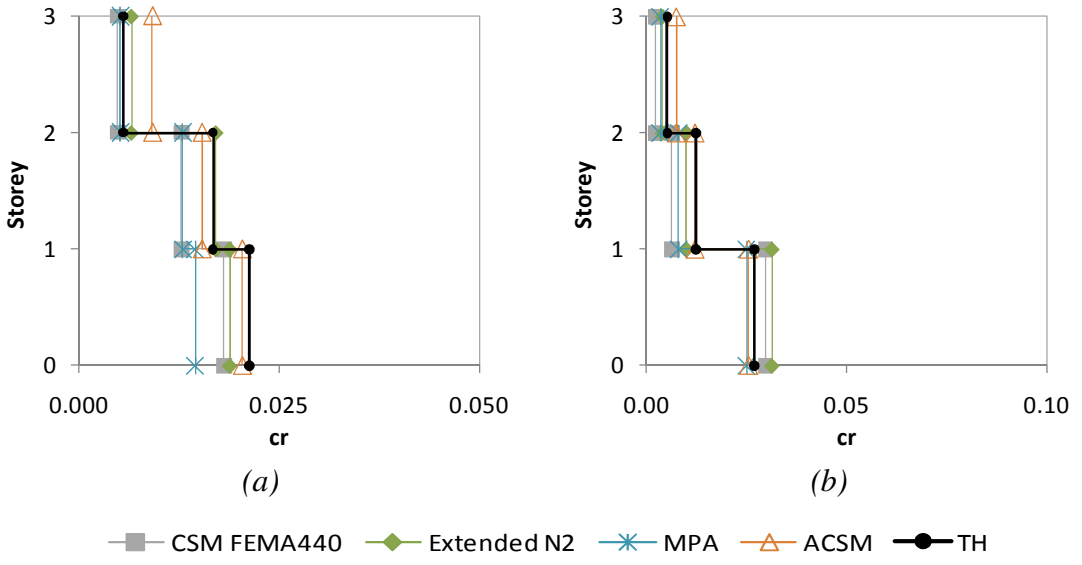

Figure A. 44 – Chord rotation profiles X direction: a) Column C2, 0.2g; b) Column C8, 0.3g.

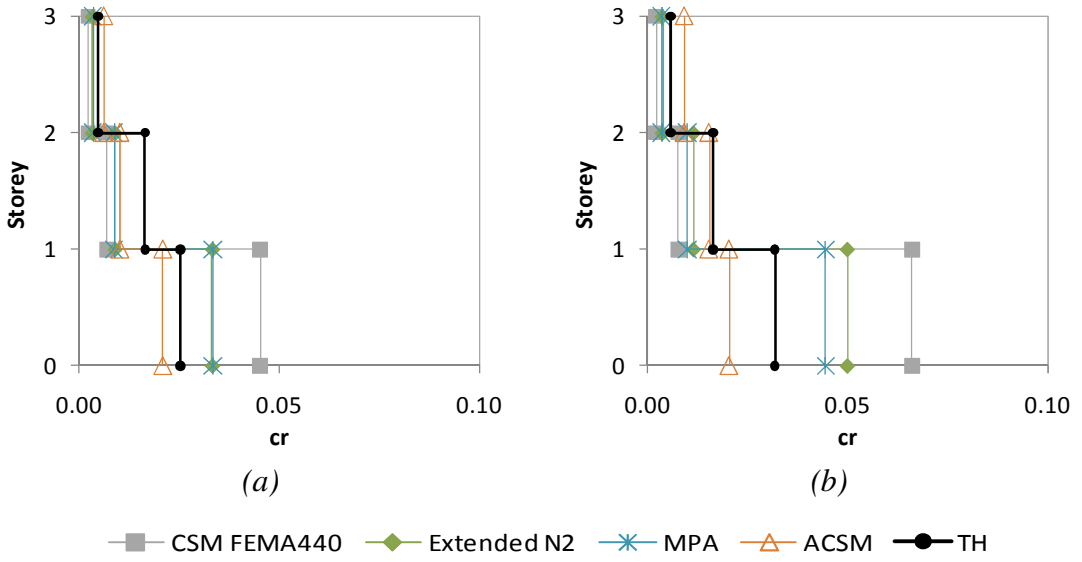

Figure A. 45 – Chord rotation profiles X direction: a) Column C3, 0.3g; b) Column C2, 0.3g.

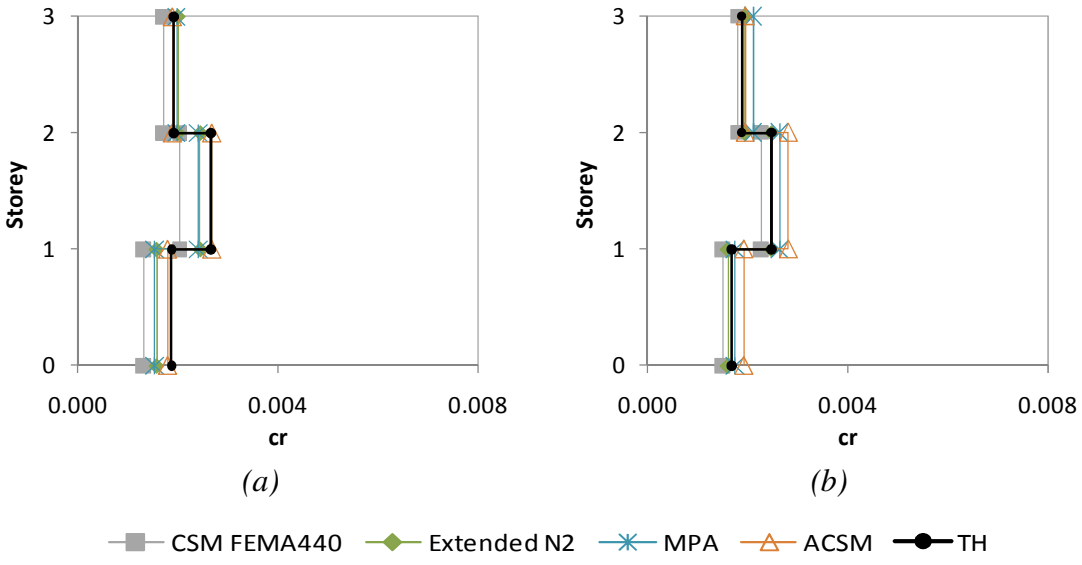

Figure A. 46 – Chord rotation profiles Y direction: a) Column C8, 0.05g; b) Column C3, 0.05g.

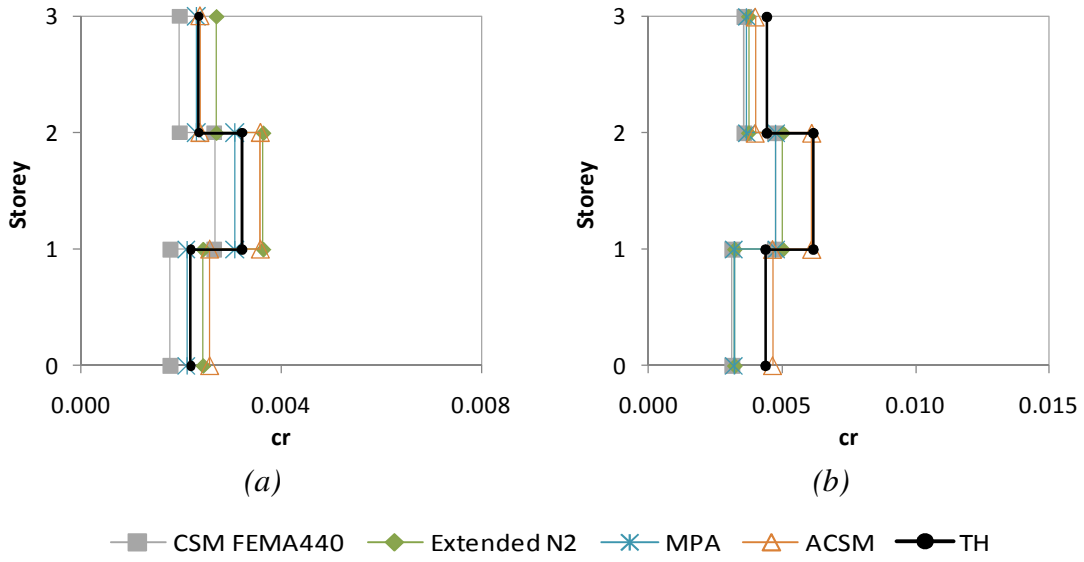

Figure A. 47 – Chord rotation profiles Y direction: a) Column C2, 0.05g; b) Column C8, 0.1g.

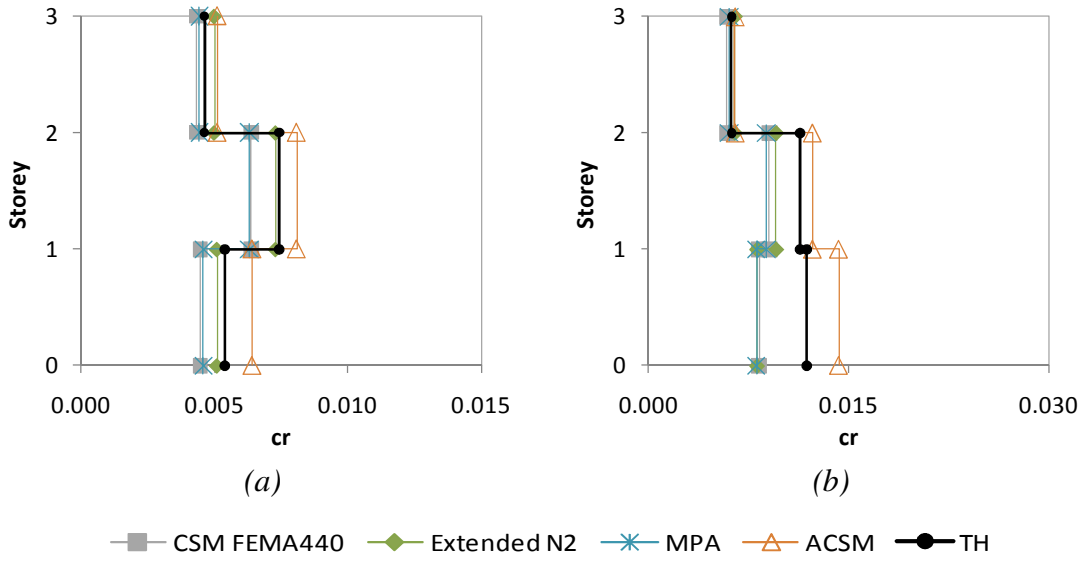

Figure A. 48 – Chord rotation profiles Y direction: a) Column C2, 0.1g; b) Column C8, 0.2g.

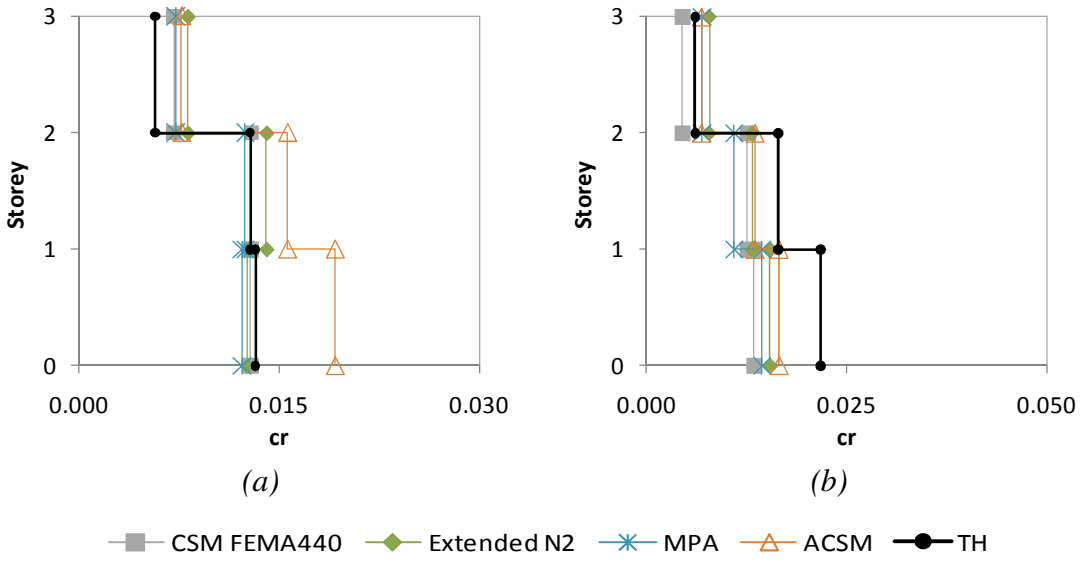

Figure A. 49 – Chord rotation profiles Y direction: a) Column C2, 0.2g; b) Column C8, 0.3g.

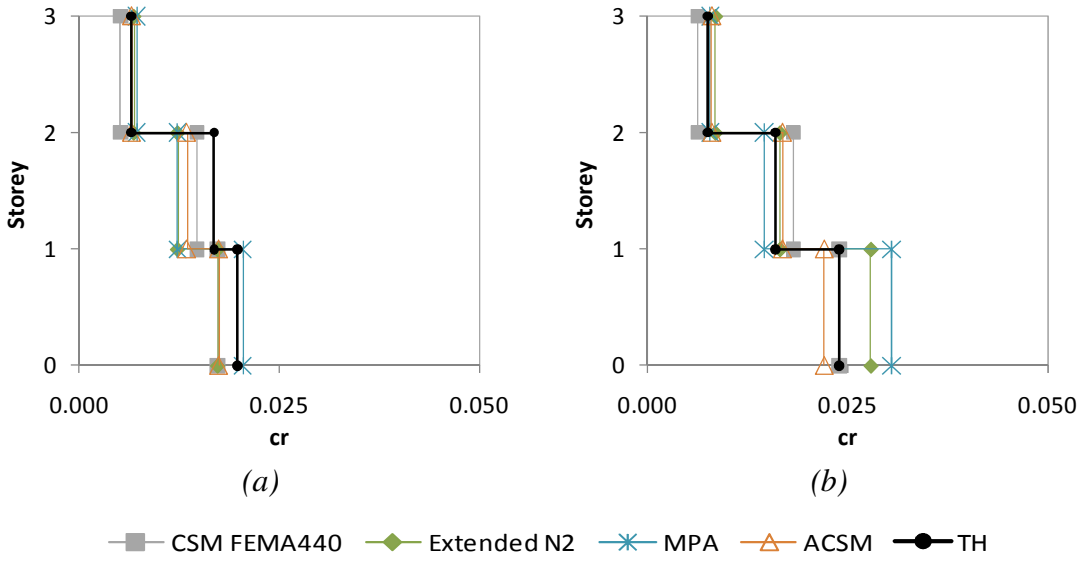

Figure A. 50 – Chord rotation profiles Y direction: a) Column C3, 0.3g; b) Column C2, 0.3g.

A8. Lateral displacements profiles five storey building

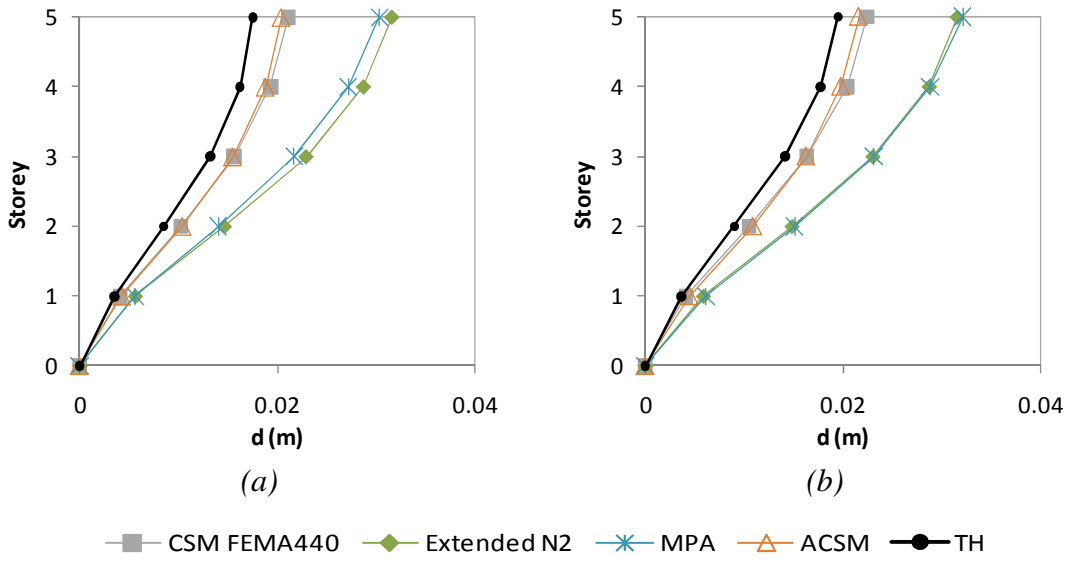

Figure A. 51 – Lateral displacement profiles X direction: a) Column S23, 0.1g; b) Column S13, 0.1g.

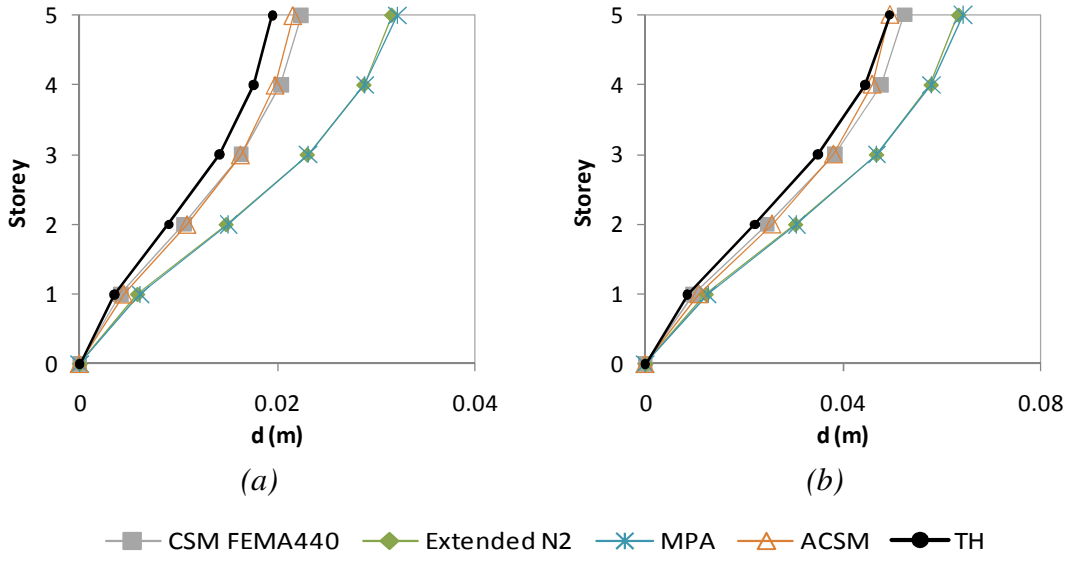

Figure A. 52 – Lateral displacement profiles X direction: a) Column S14, 0.1g; b) Column S13, 0.2g.

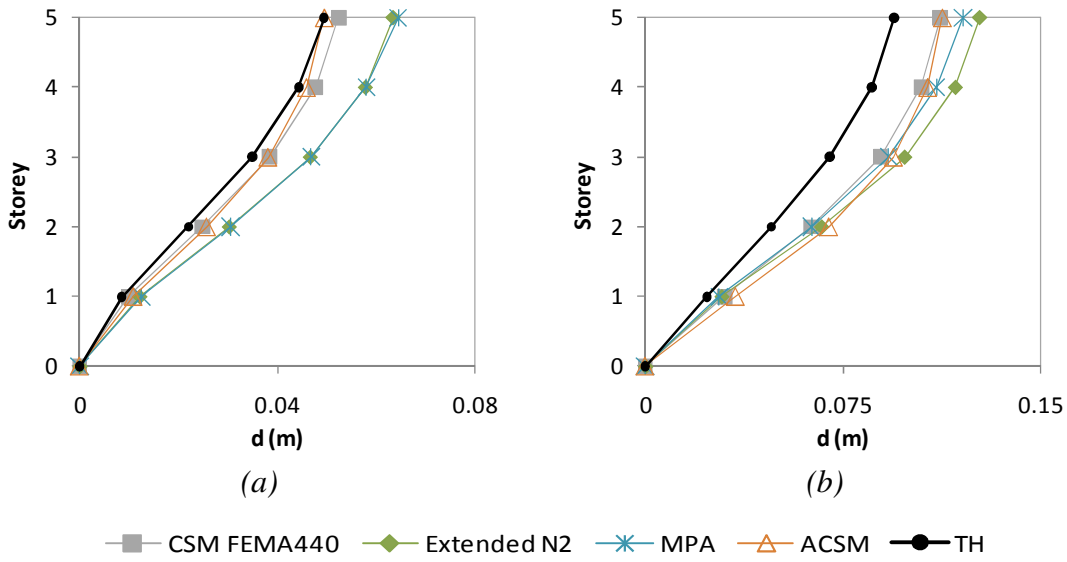

Figure A. 53 – Lateral displacement profiles X direction: a) Column S14, 0.2g; b) Column S23, 0.4g.

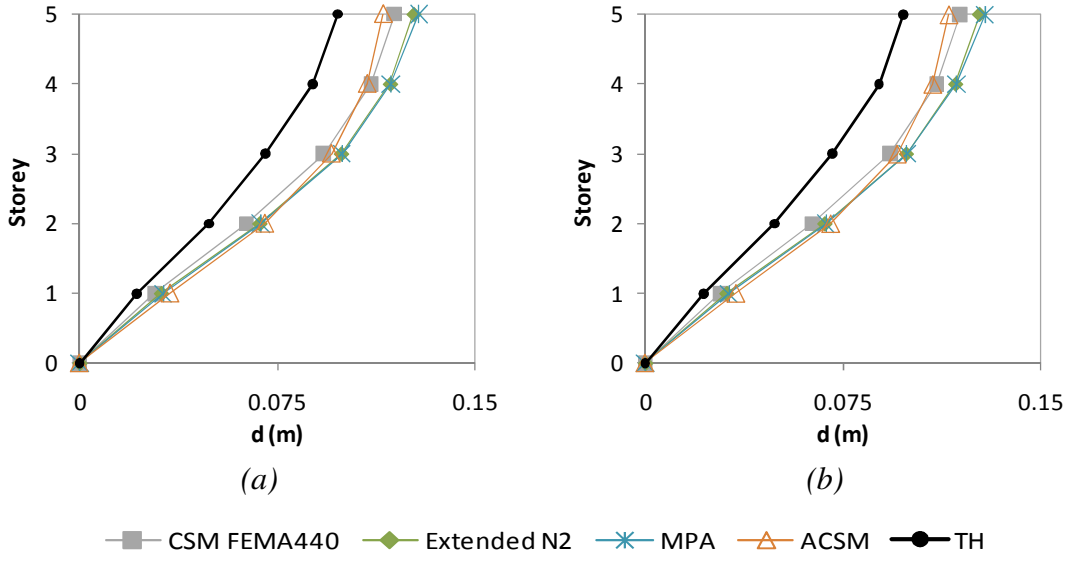

Figure A. 54 – Lateral displacement profiles X direction: a) Column S13, 0.4g; b) Column S14, 0.4g.

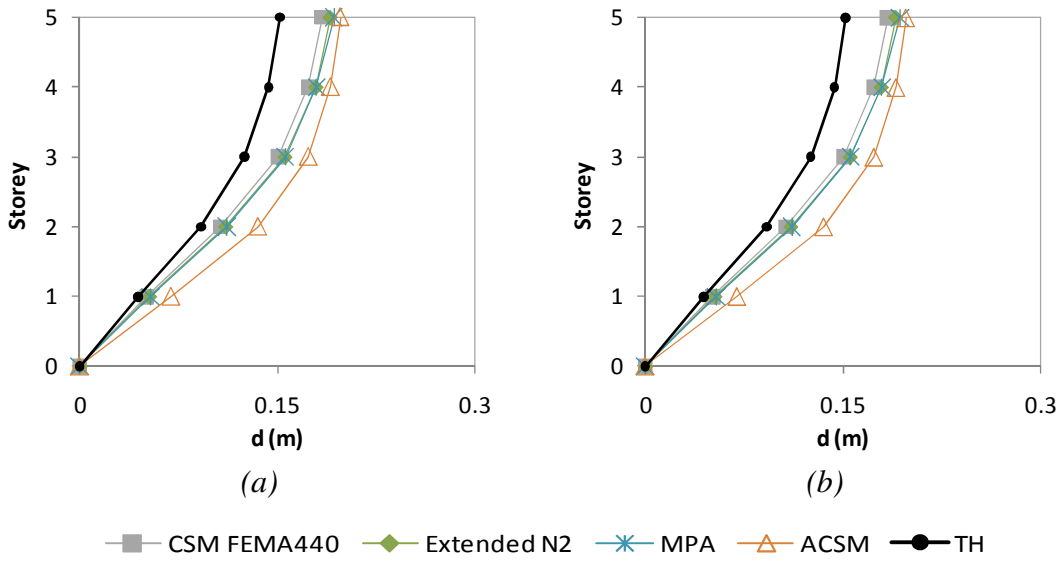

Figure A. 55 – Lateral displacement profiles X direction: a) Column S13, 0.6g; b) Column S14, 0.6g.

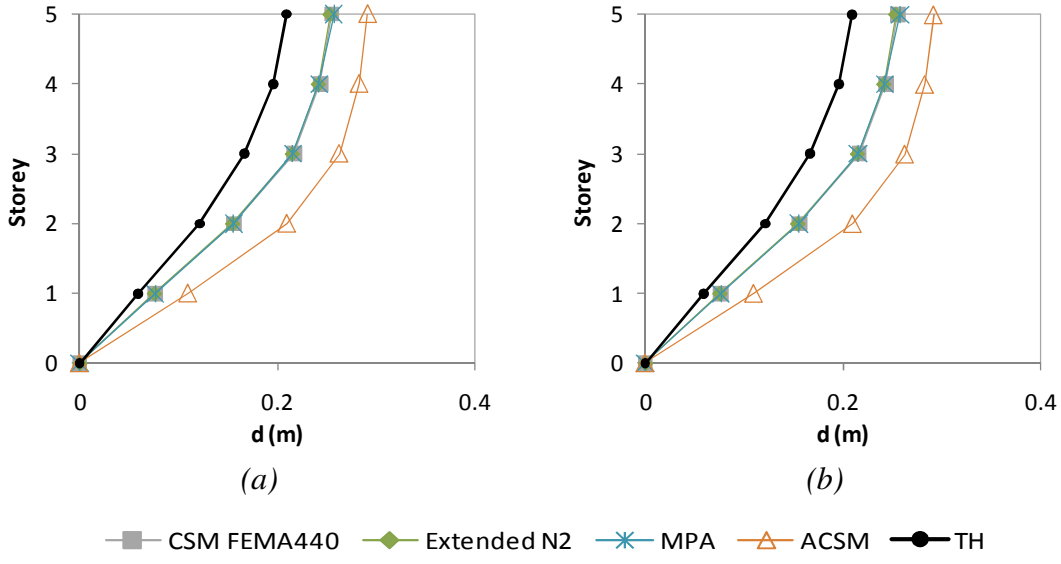

Figure A. 56 – Lateral displacement profiles X direction: a) Column S13, 0.8g; b) Column S14, 0.8g.

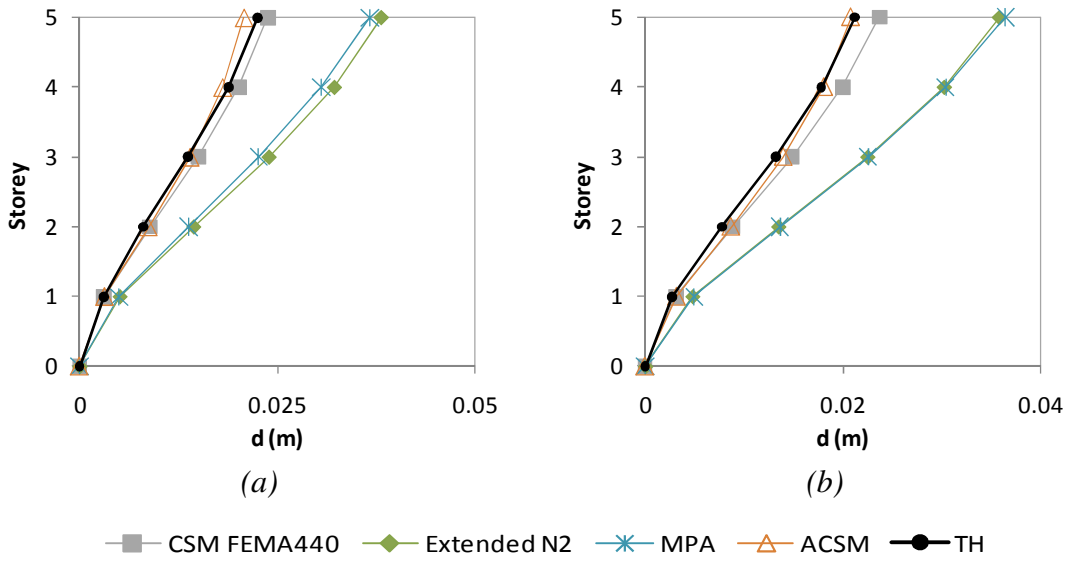

Figure A. 57 – Lateral displacement profiles Y direction: a) Column S23, 0.1g; b) Column S13, 0.1g.

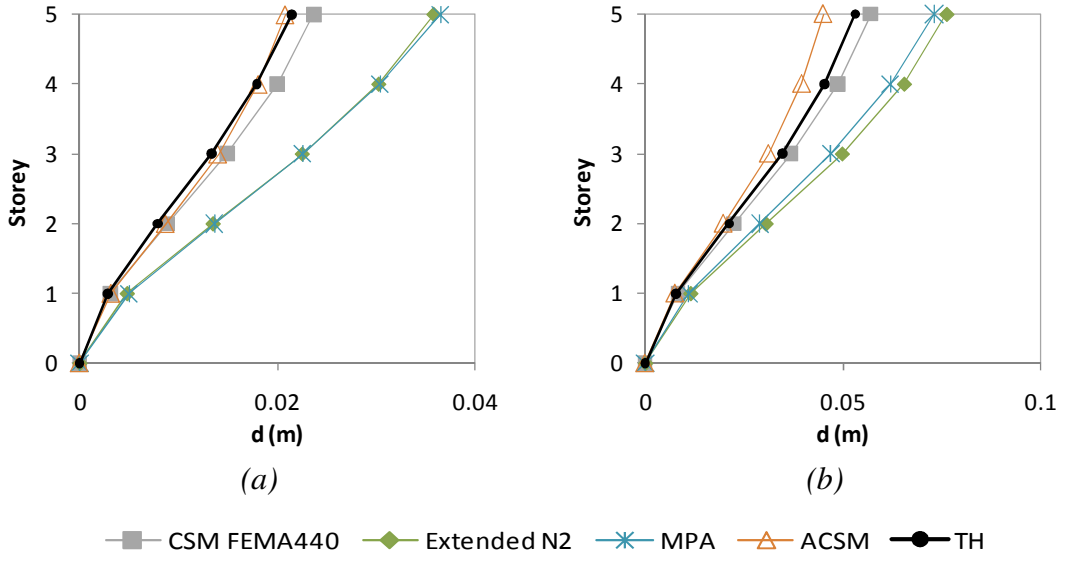

Figure A. 58 – Lateral displacement profiles Y direction: a) Column S14, 0.1g; b) Column S1, 0.2g.

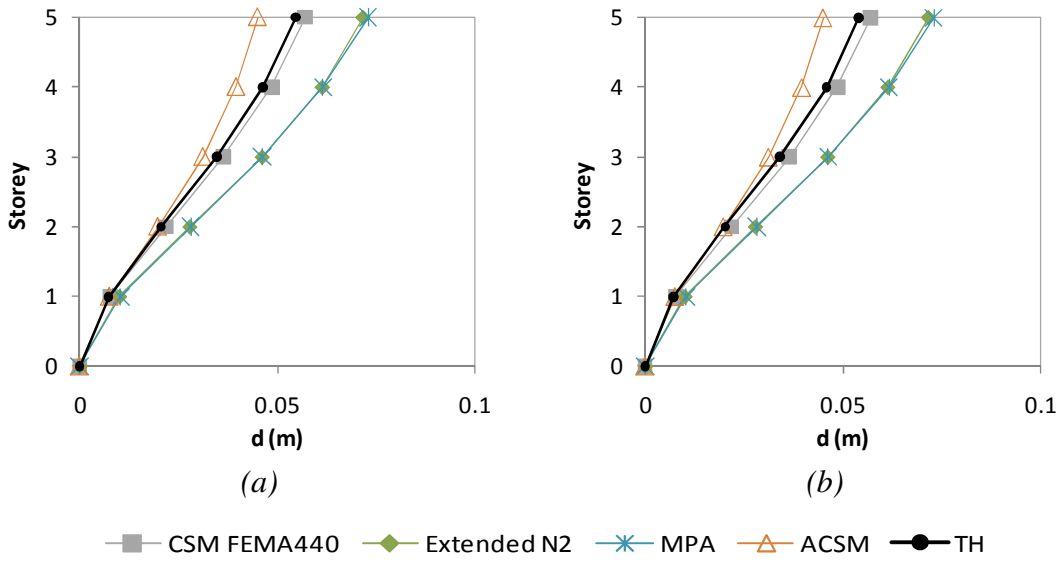

Figure A. 59 – Lateral displacement profiles Y direction: a) Column S13, 0.2g; b) Column S14, 0.2g.

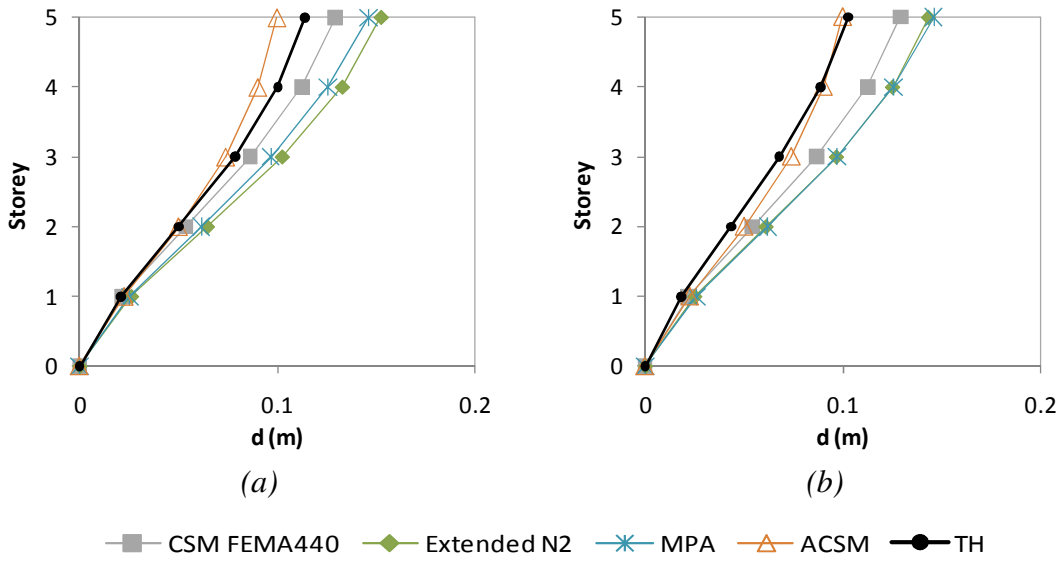

Figure A. 60 – Lateral displacement profiles Y direction: a) Column S23, 0.4g; b) Column S13, 0.4g.

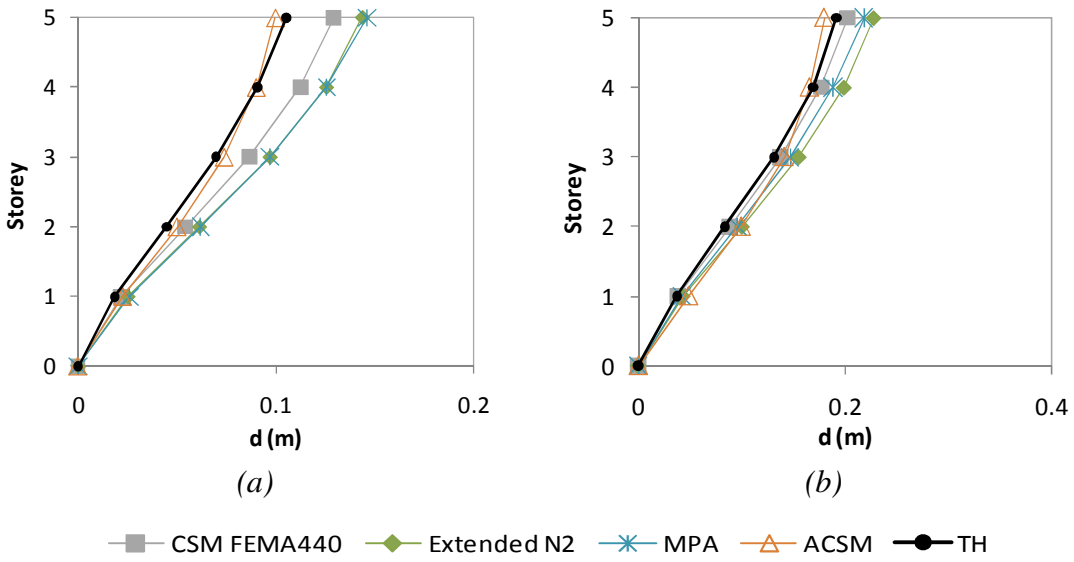

Figure A. 61 – Lateral displacement profiles Y direction: a) Column S14, 0.4g; b) Column S23, 0.6g.

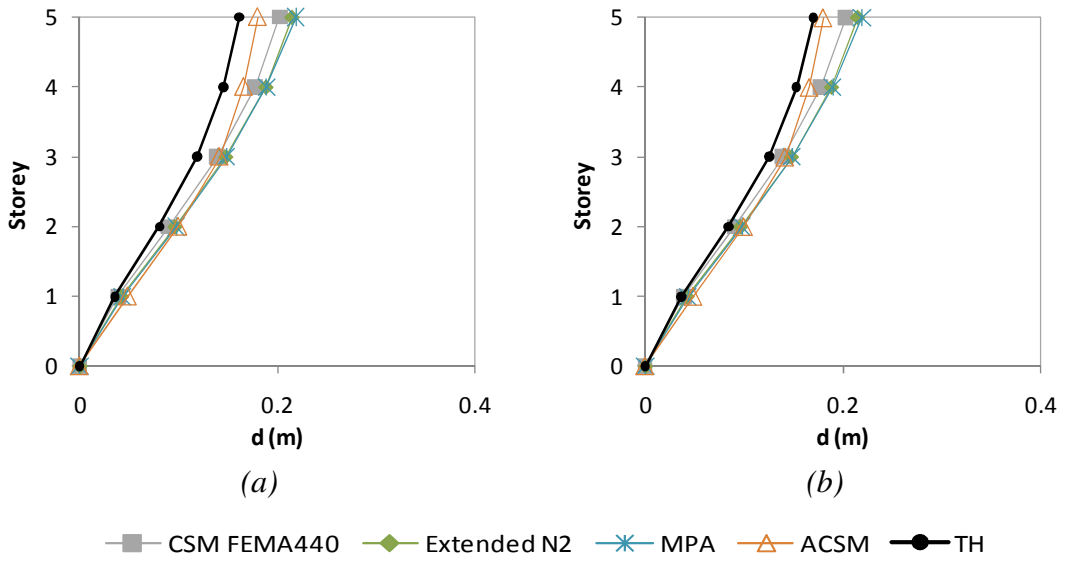

Figure A. 62 – Lateral displacement profiles Y direction: a) Column S13, 0.6g; b) Column S14, 0.6g.

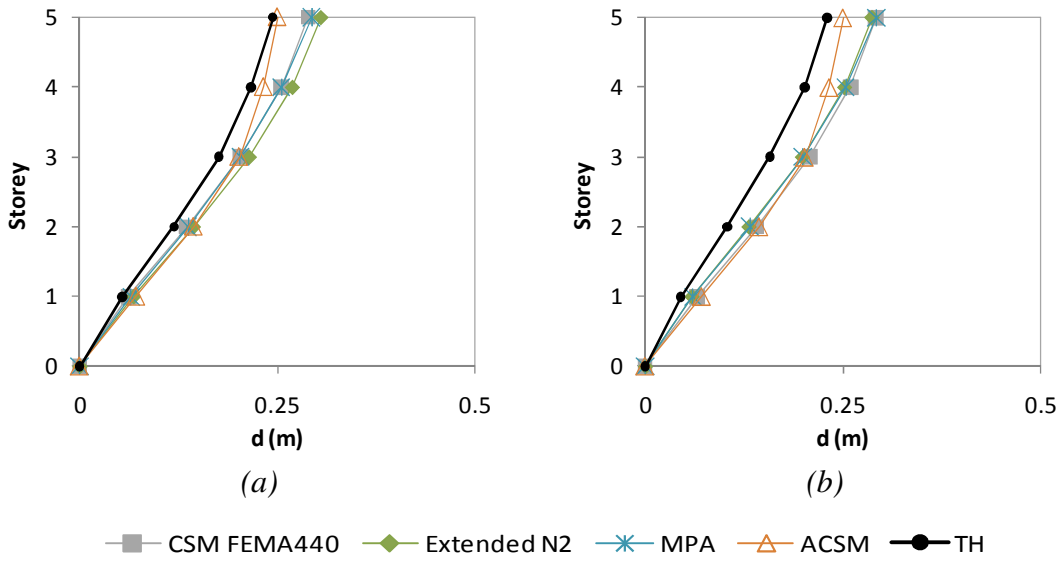

Figure A. 63 – Lateral displacement profiles Y direction: a) Column S1, 0.8g; b) Column S14, 0.8g.

A9. Interstorey drifts profiles five storey building

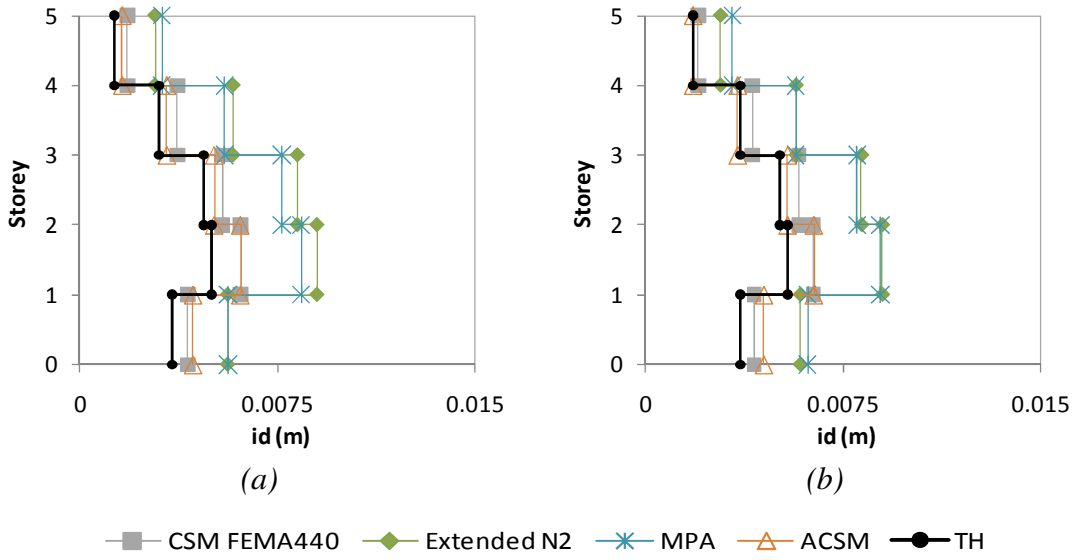

Figure A. 64 – Interstorey drifts profiles X direction: a) Column S23, 0.1g; b) Column S13, 0.1g.

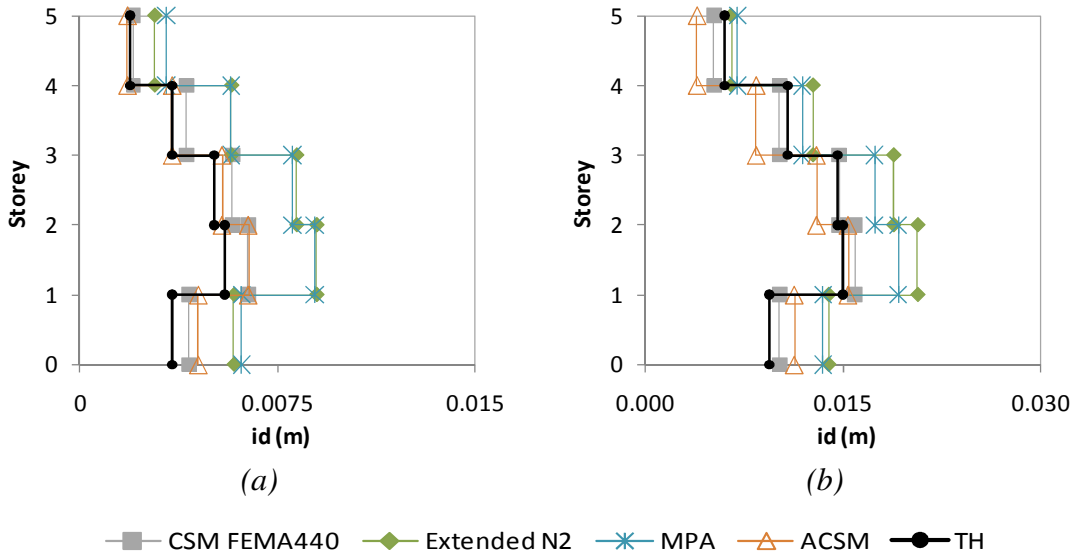

Figure A. 65 – Interstorey drifts profiles X direction: a) Column S14, 0.1g; b) Column S1, 0.2g.

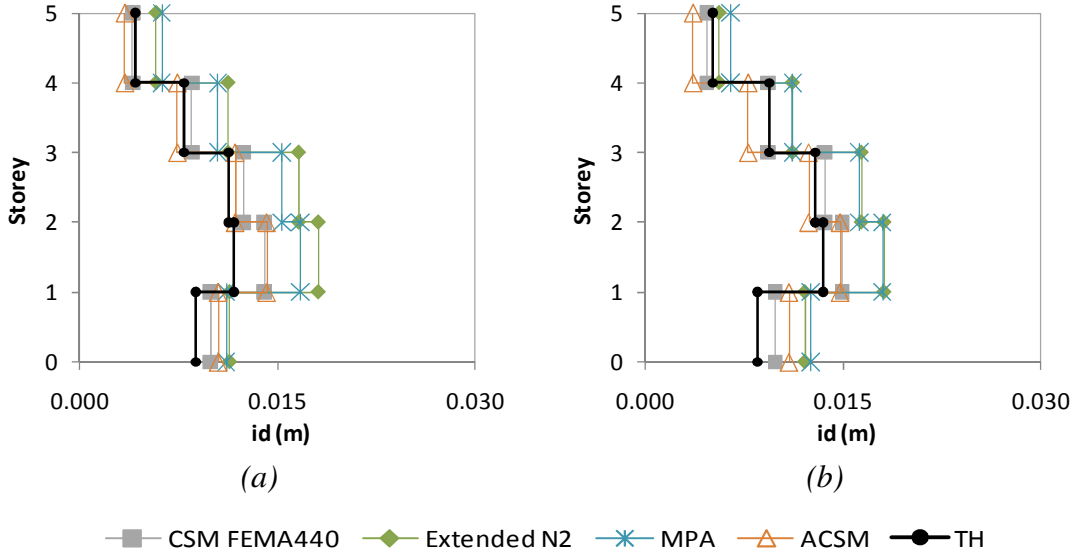

Figure A. 66 – Interstorey drifts profiles X direction: a) Column S23, 0.2g; b) Column S14, 0.2g.

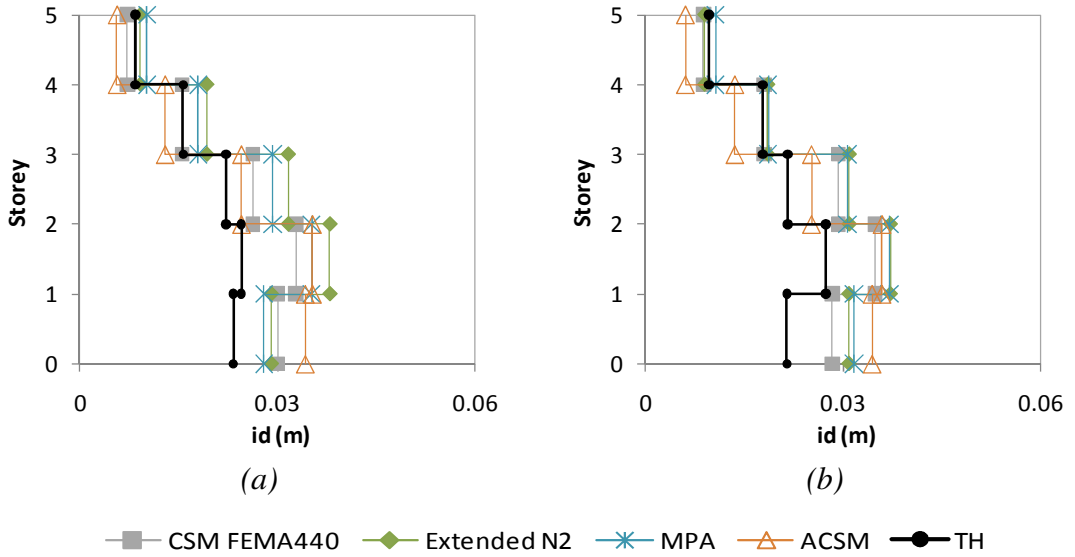

Figure A. 67 – Interstorey drifts profiles X direction: a) Column S23, 0.4g; b) Column S13, 0.4g.

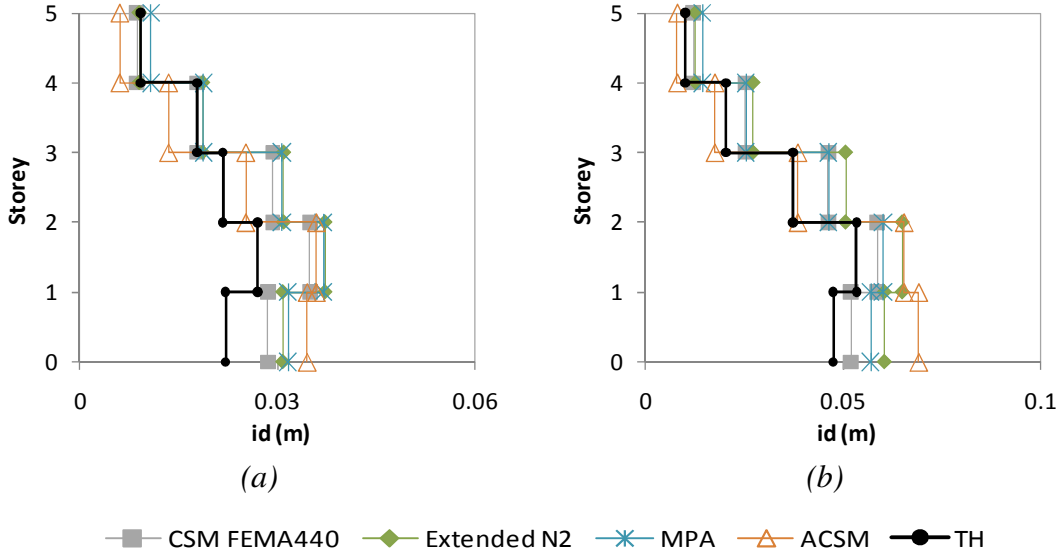

Figure A. 68 – Interstorey drifts profiles X direction: a) Column S14, 0.4g; b) Column S1, 0.6g.

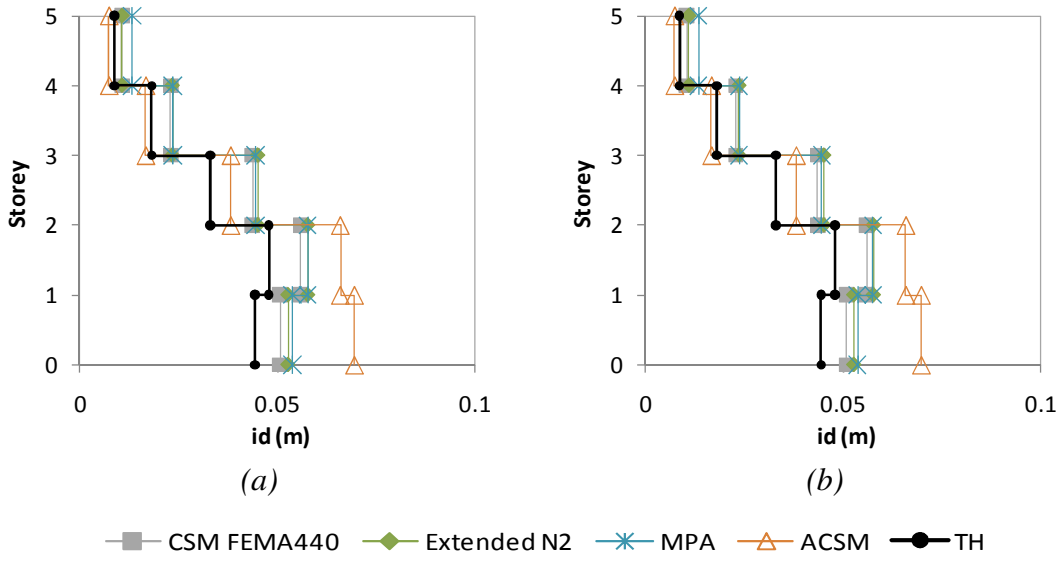

Figure A. 69 – Interstorey drifts profiles X direction: a) Column S13, 0.6g; b) Column S14, 0.6g.

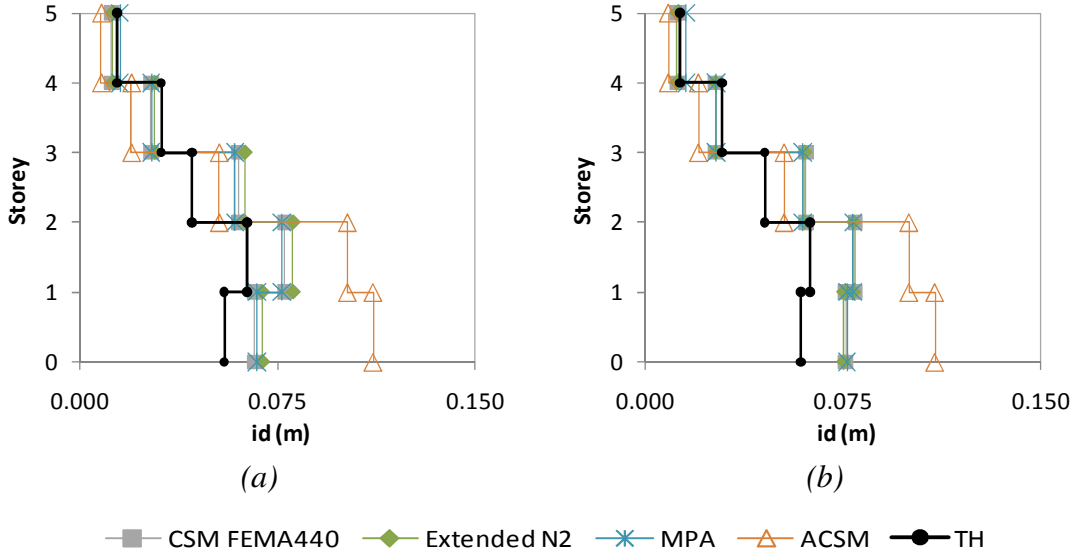

Figure A. 70 – Interstorey drifts profiles X direction: a) Column S23, 0.8g; b) Column S14, 0.8g.

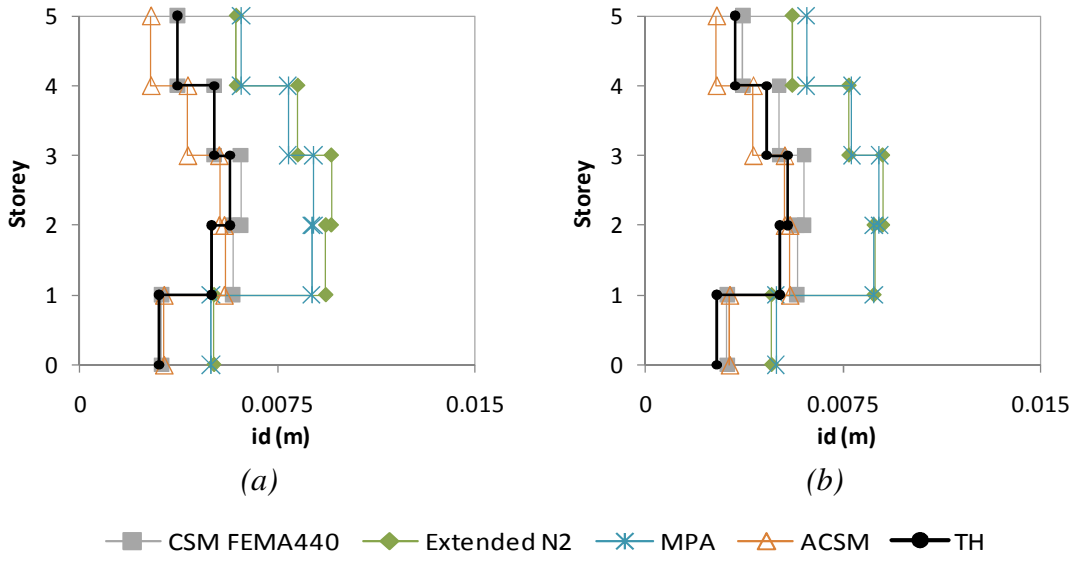

Figure A. 71 – Interstorey drifts profiles Y direction: a) Column S23, 0.1g; b) Column S13, 0.1g.

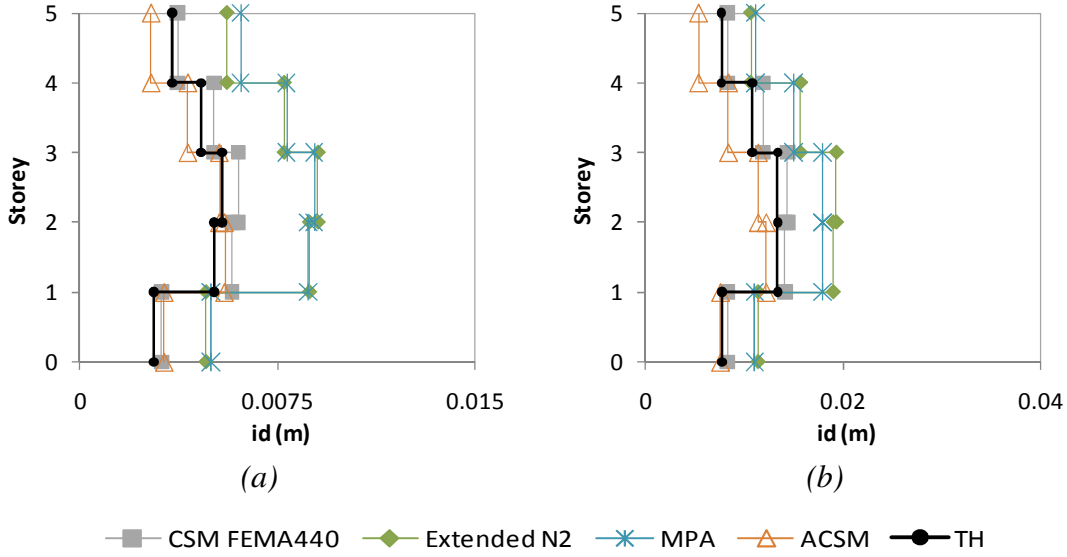

Figure A. 72 – Interstorey drifts profiles Y direction: a) Column S14, 0.1g; b) Column S1, 0.2g.

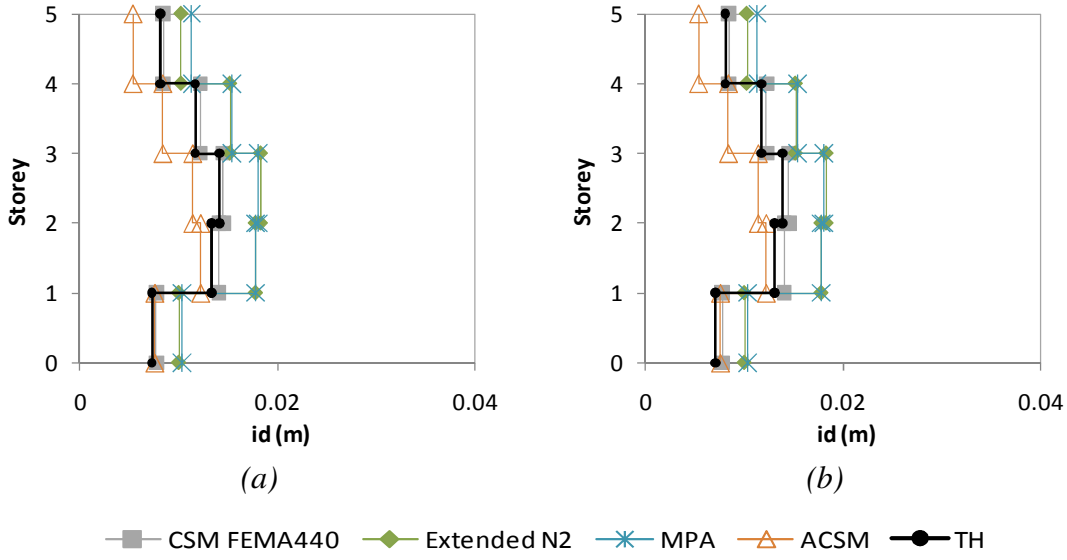

Figure A. 73 – Interstorey drifts profiles Y direction: a) Column S13, 0.2g; b) Column S14, 0.2g.

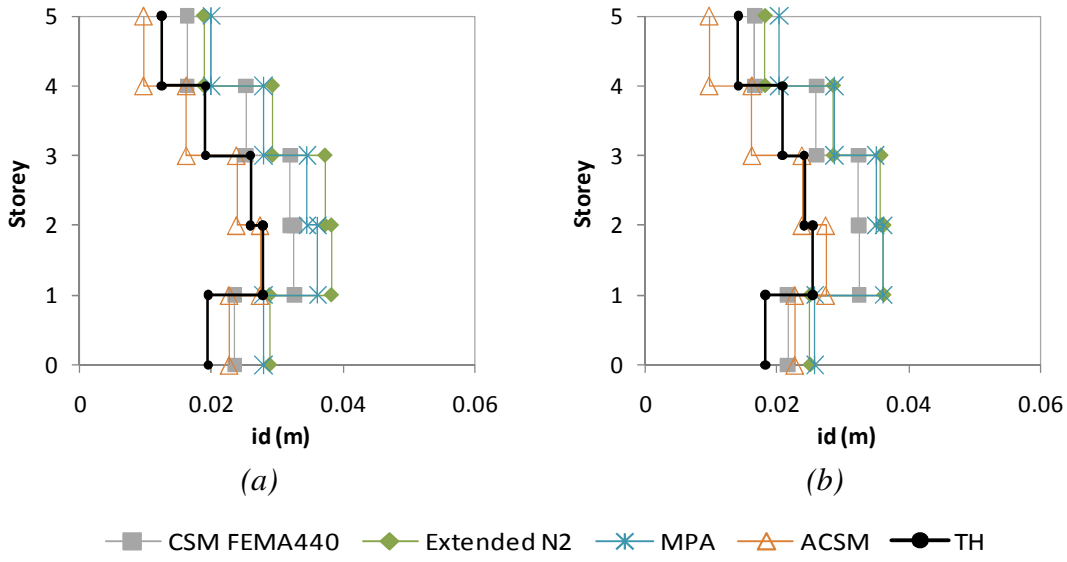

Figure A. 74 – Interstorey drifts profiles Y direction: a) Column S1, 0.4g; b) Column S13, 0.4g.

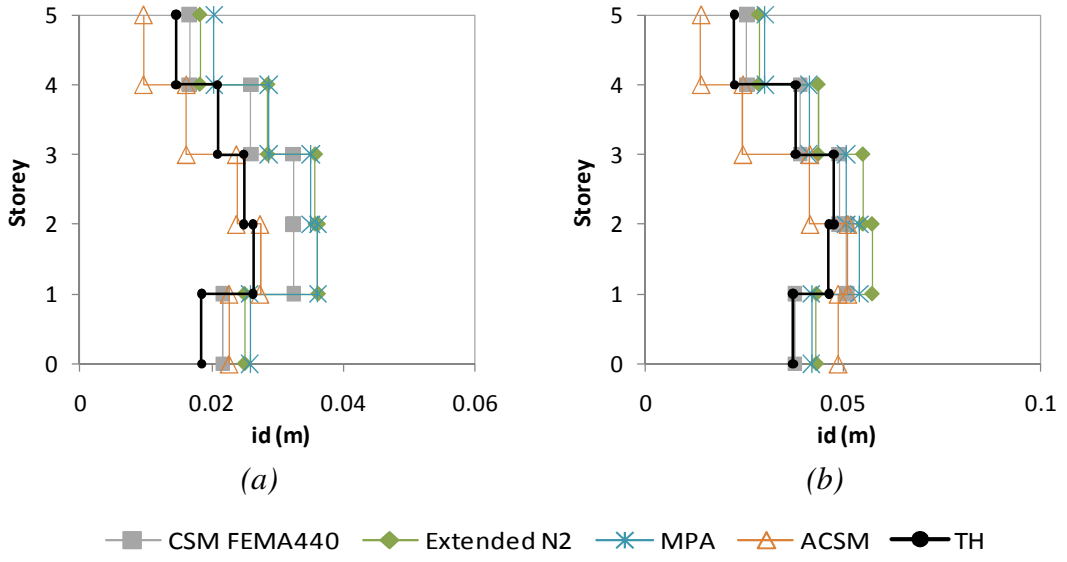

Figure A. 75 – Interstorey drifts profiles Y direction: a) Column S14, 0.4g; b) Column S23, 0.6g.

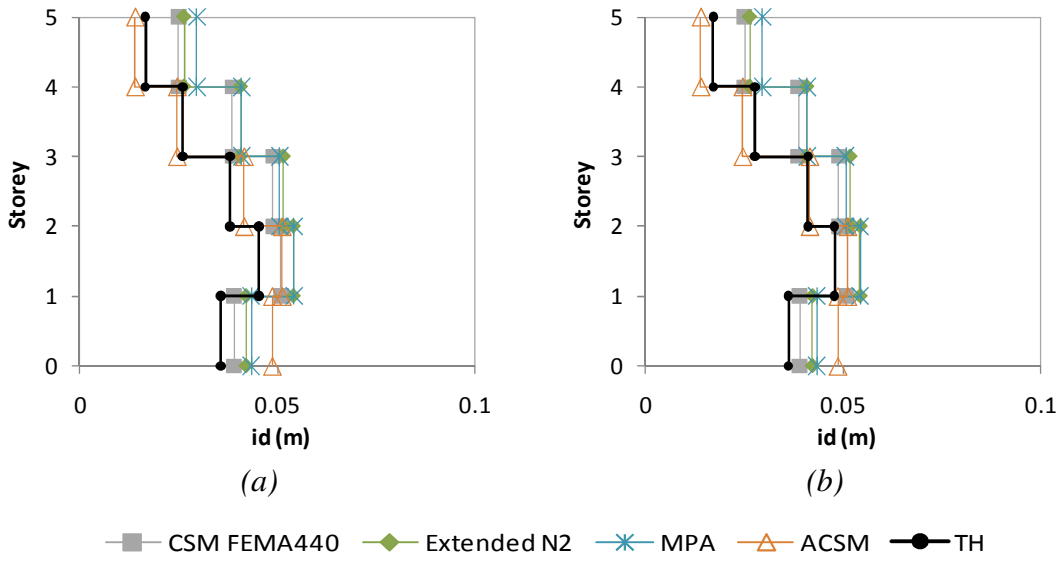

Figure A. 76 – Interstorey drifts profiles Y direction: a) Column S13, 0.6g; b) Column S14, 0.6g.

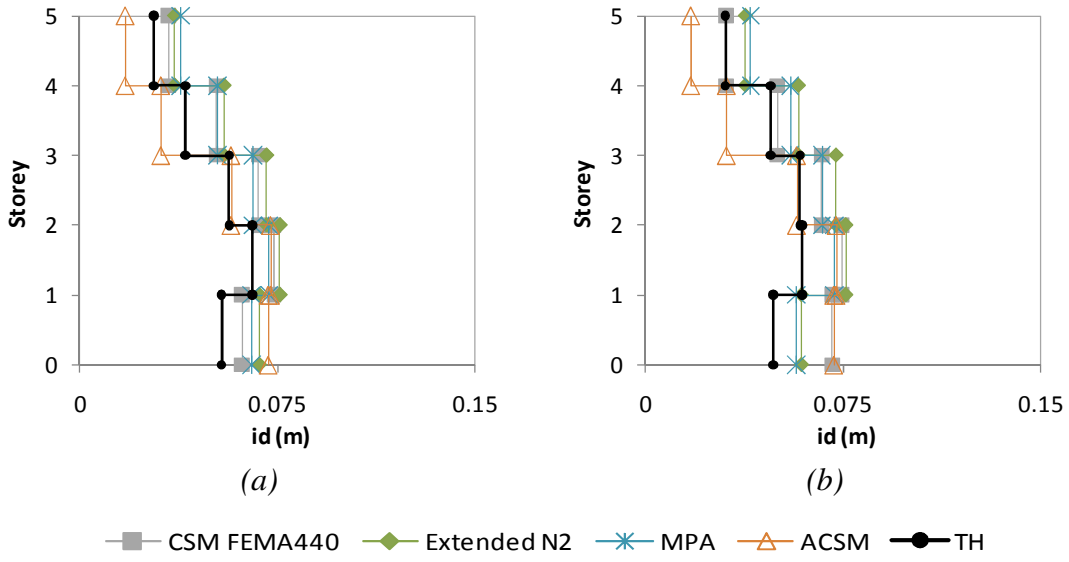

Figure A. 77 – Interstorey drifts profiles Y direction: a) Column S1, 0.8g; b) Column S23, 0.8g.

A10. Chord rotation profiles five storey building

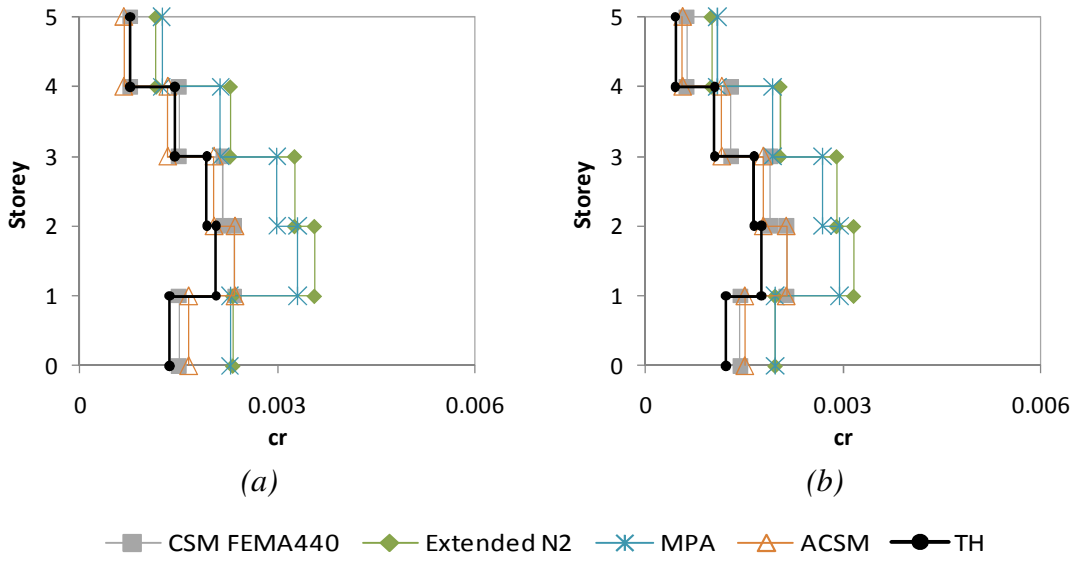

Figure A. 78 – Chord rotation profiles X direction: a) Column S1, 0.1g; b) Column S23, 0.1g.

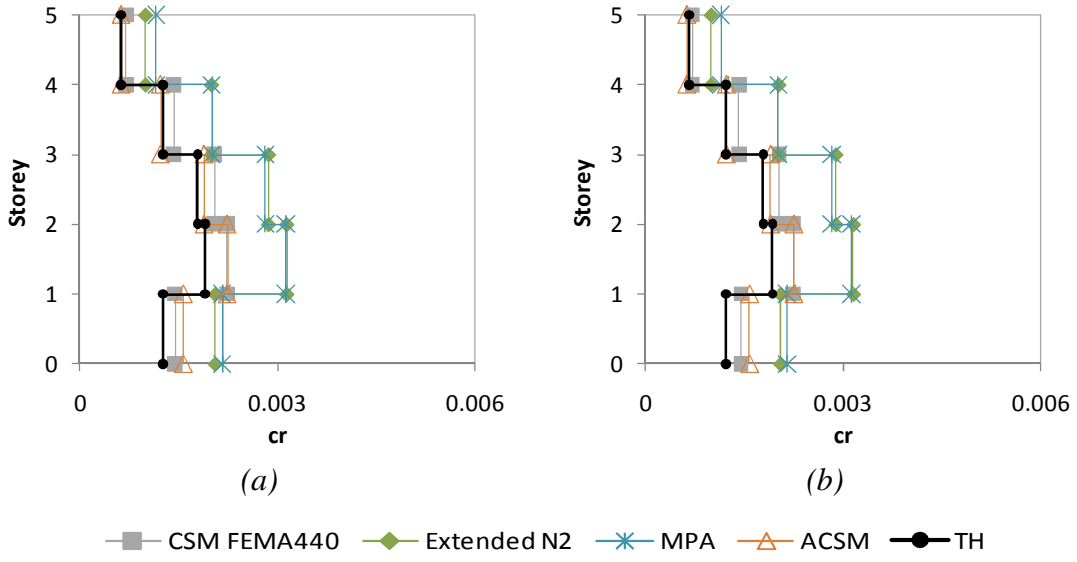

Figure A. 79 – Chord rotation profiles X direction: a) Column S13, 0.1g; b) Column S14, 0.1g.

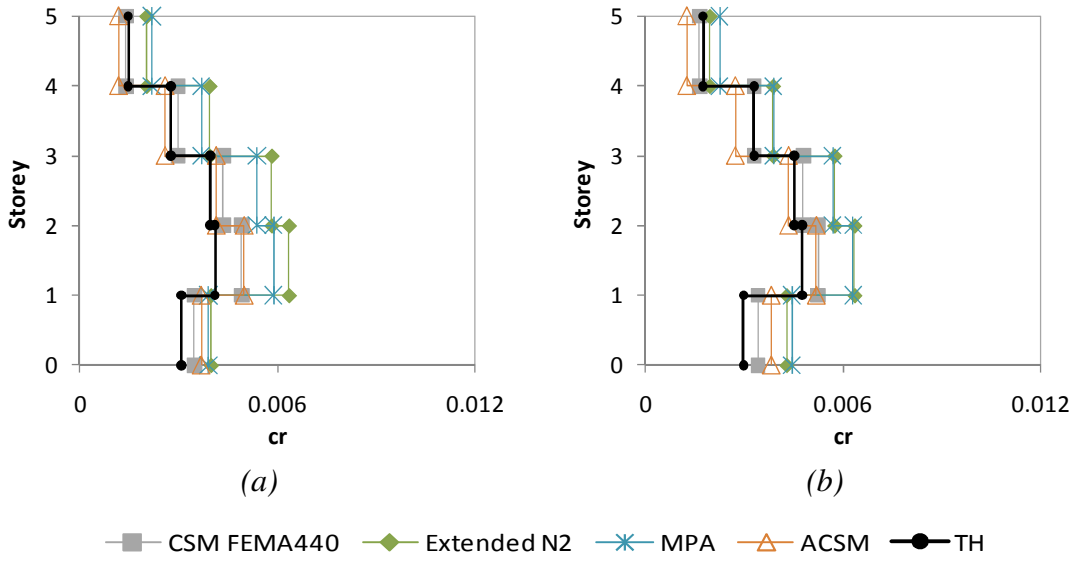

Figure A. 80 – Chord rotation profiles X direction: a) Column S23, 0.2g; b) Column S13, 0.2g.

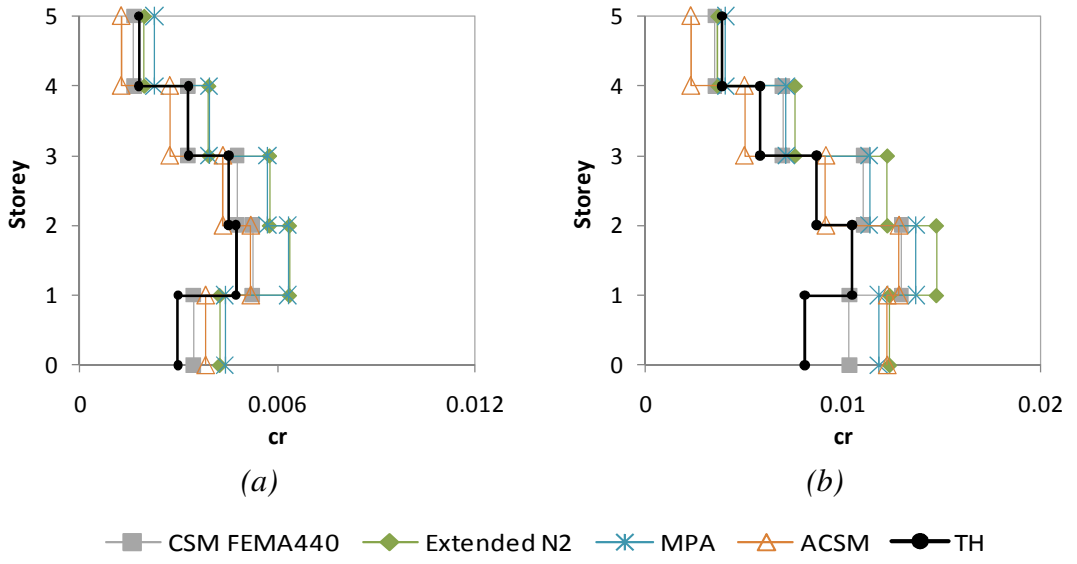

Figure A. 81 – Chord rotation profiles X direction: a) Column S14, 0.2g; b) Column S1, 0.4g.

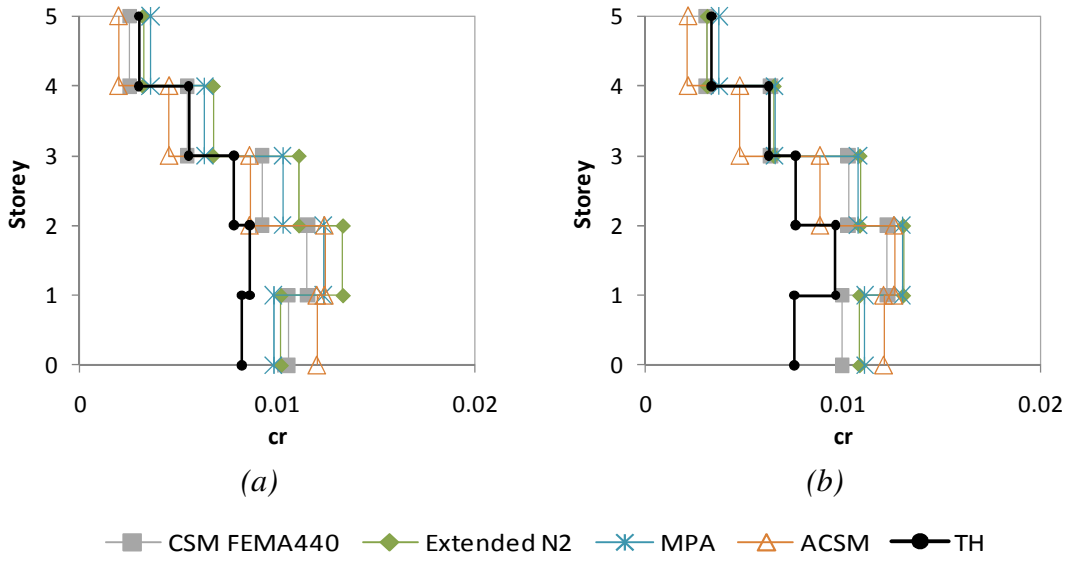

Figure A. 82 – Chord rotation profiles X direction: a) Column S23, 0.4g; b) Column S13, 0.4g.

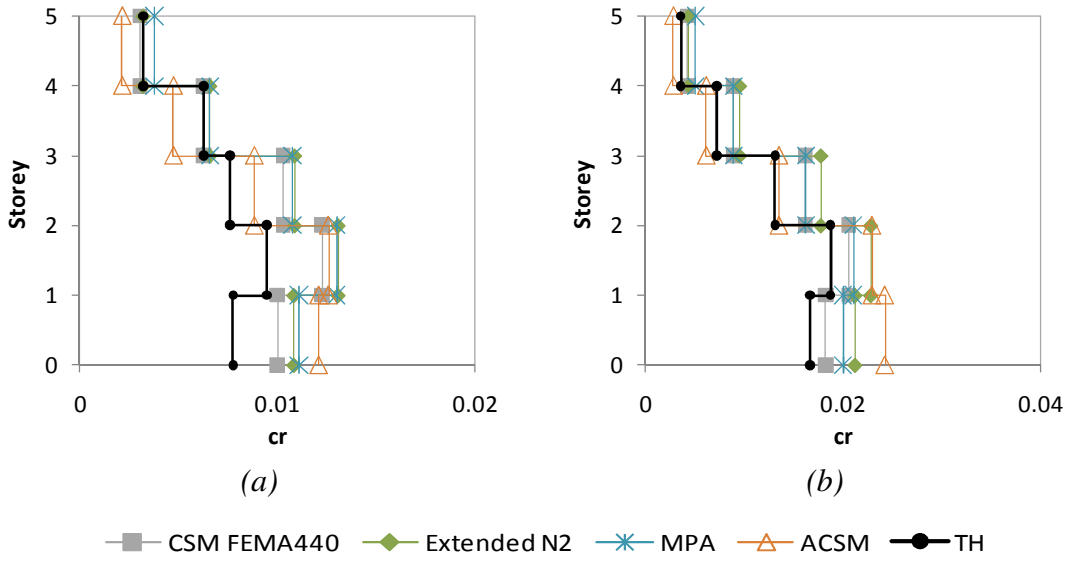

Figure A. 83 – Chord rotation profiles X direction: a) Column S14, 0.4g; b) Column S1, 0.6g.

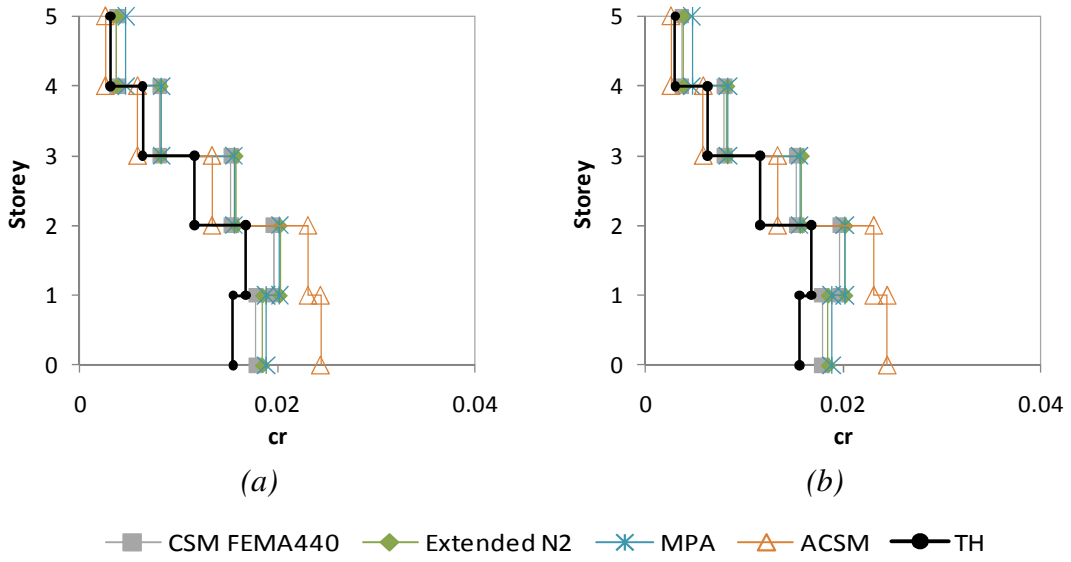

Figure A. 84 – Chord rotation profiles X direction: a) Column S13, 0.6g; b) Column S14, 0.6g.

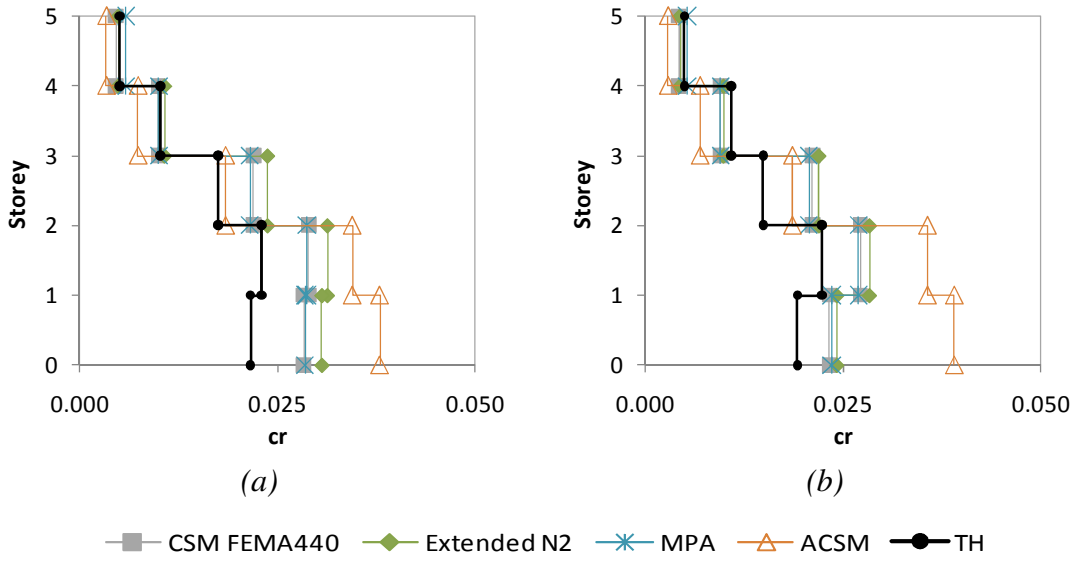

Figure A. 85 – Chord rotation profiles X direction: a) Column S1, 0.8g; b) Column S23, 0.8g.

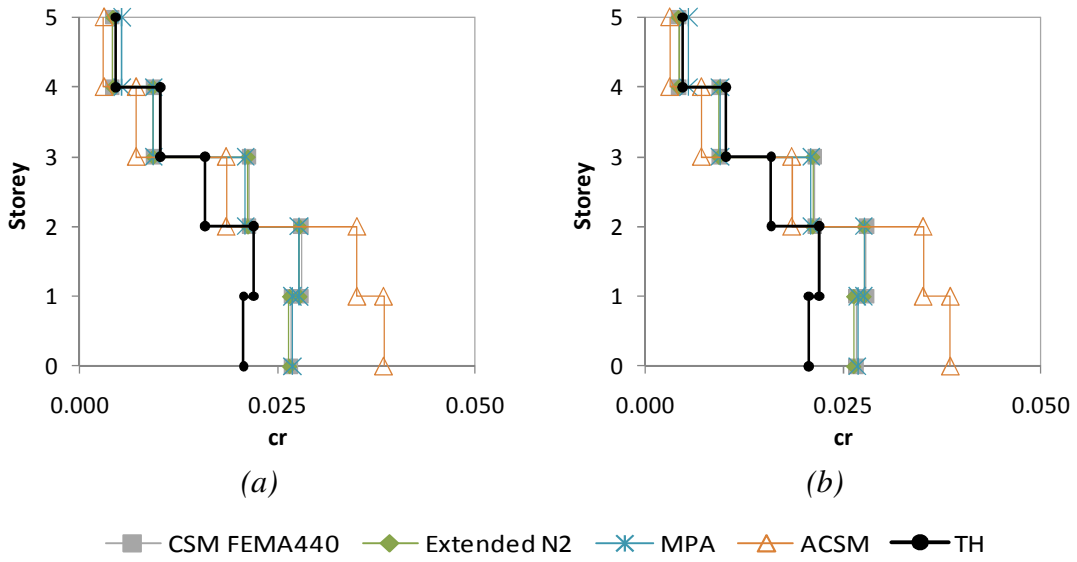

Figure A. 86 – Chord rotation profiles X direction: a) Column S13, 0.8g; b) Column S14, 0.8g.

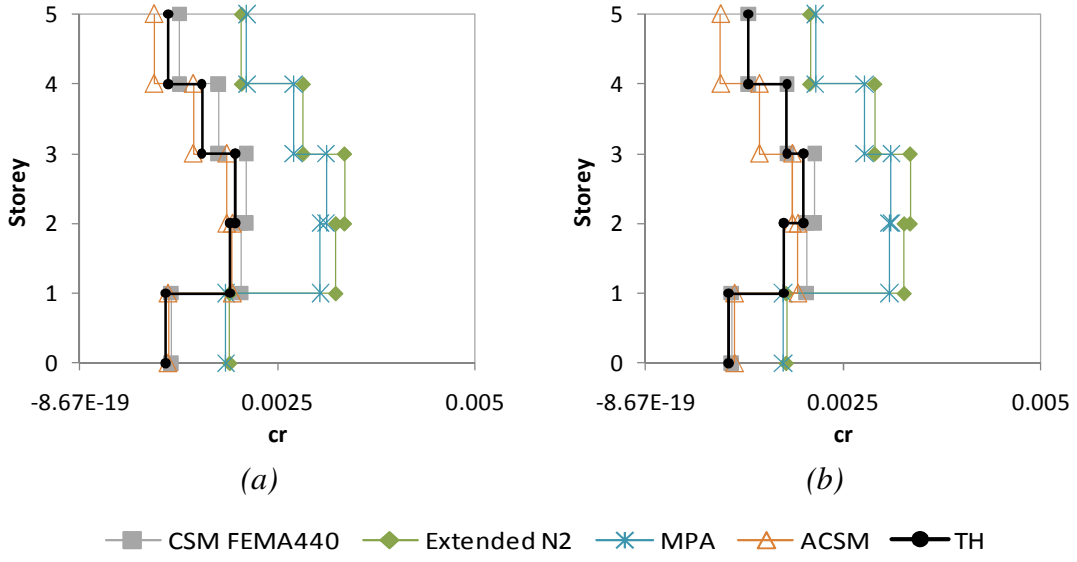

Figure A. 87 – Chord rotation profiles Y direction: a) Column S1, 0.1g; b) Column S23, 0.1g.

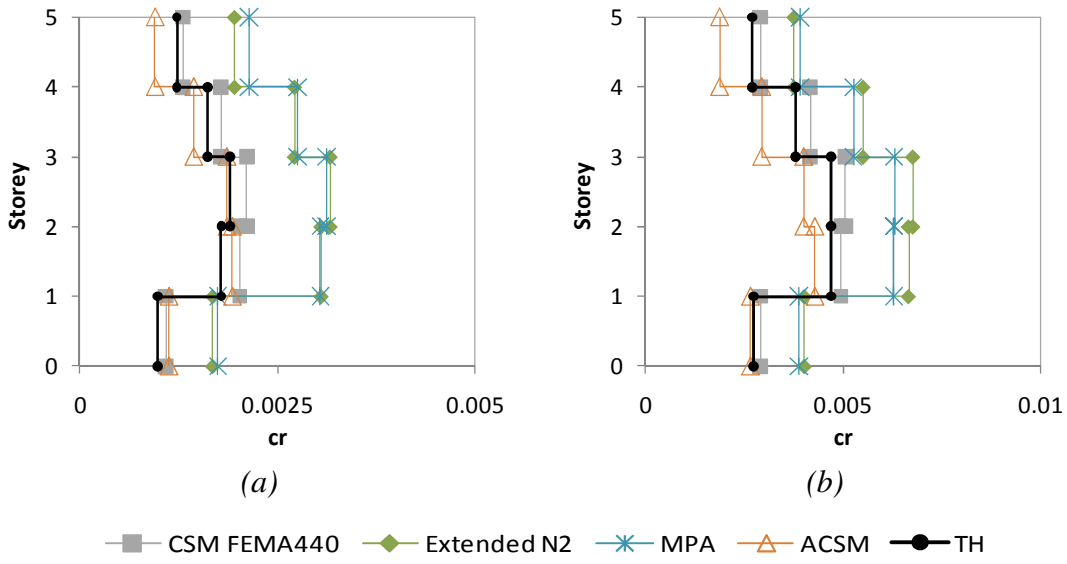

Figure A. 88 – Chord rotation profiles Y direction: a) Column S14, 0.1g; b) Column S1, 0.2g.

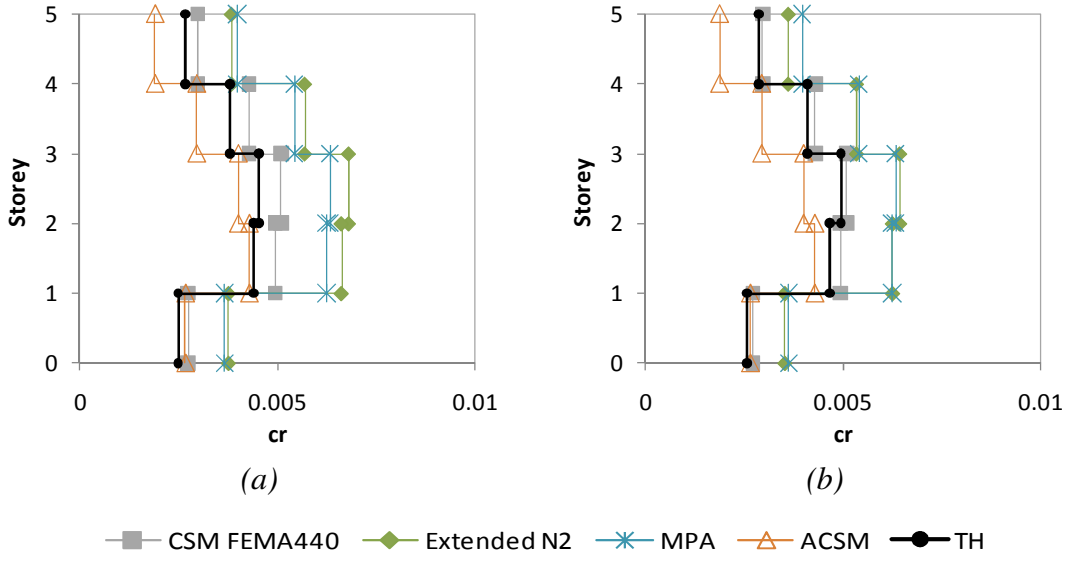

Figure A. 89 – Chord rotation profiles Y direction: a) Column S23, 0.2g; b) Column S13, 0.2g.

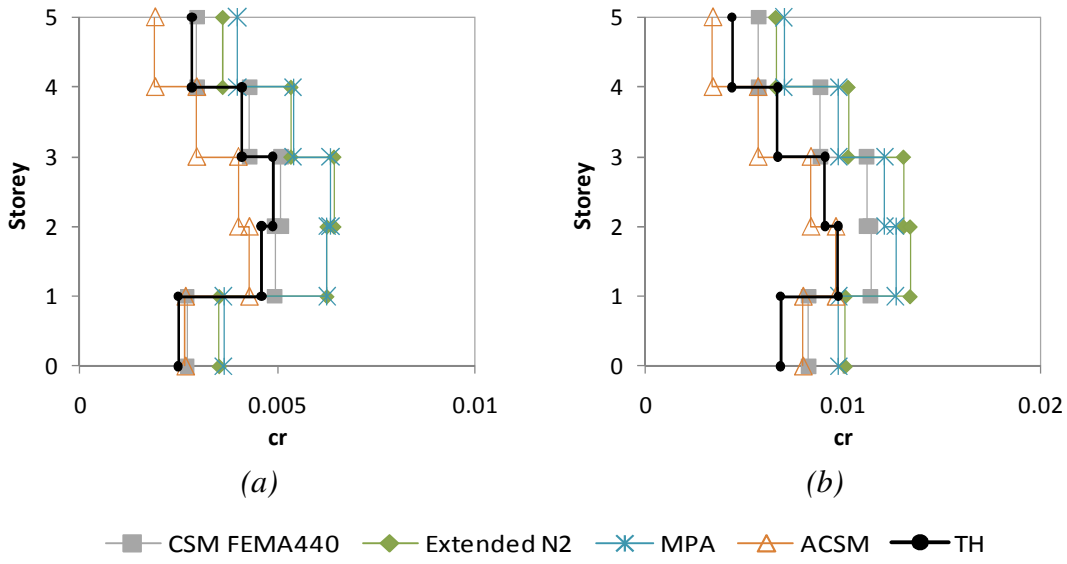

Figure A. 90 – Chord rotation profiles Y direction: a) Column S14, 0.2g; b) Column S1, 0.4g.

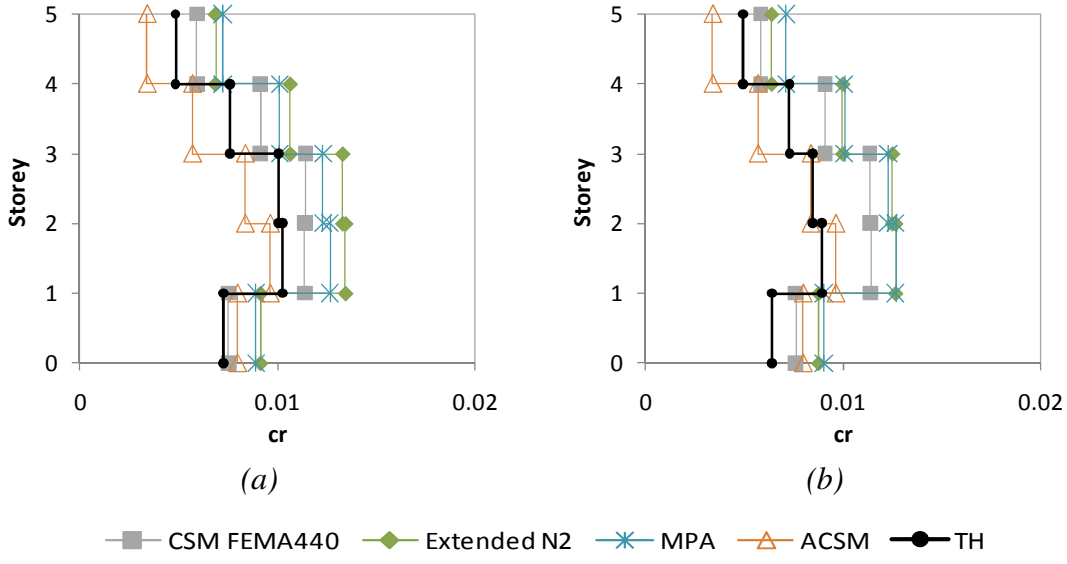

Figure A. 91 – Chord rotation profiles Y direction: a) Column S23, 0.4g; b) Column S13, 0.4g.

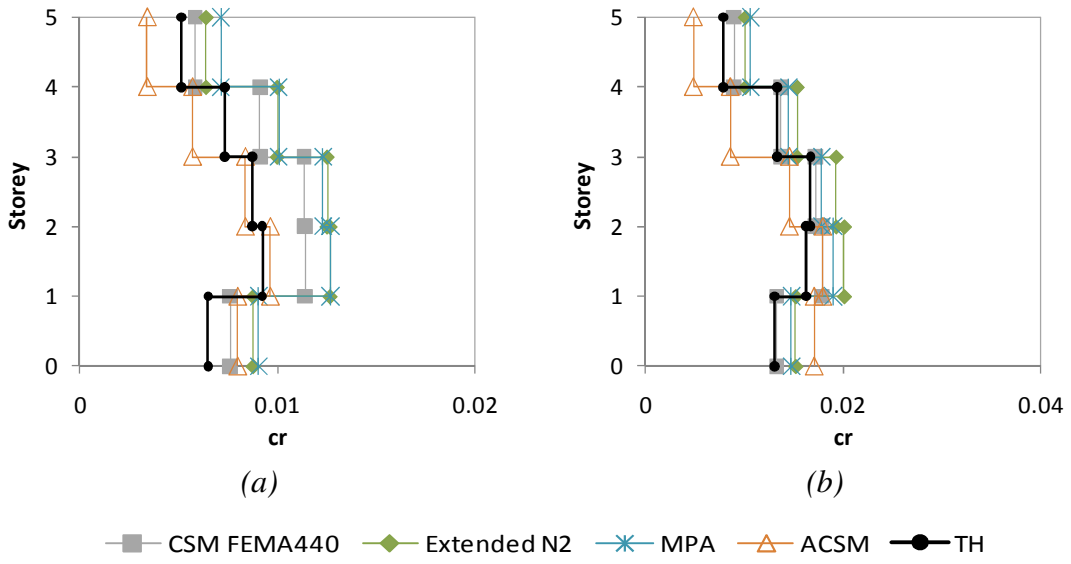

Figure A. 92 – Chord rotation profiles Y direction: a) Column S14, 0.4g; b) Column S23, 0.6g.

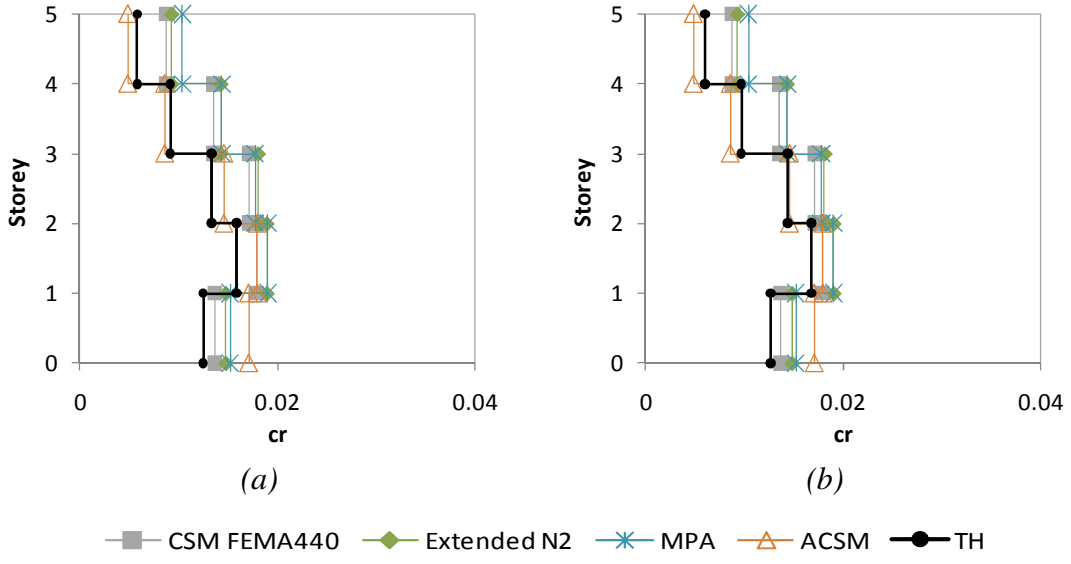

Figure A. 93 – Chord rotation profiles Y direction: a) Column S13, 0.6g; b) Column S14, 0.6g.

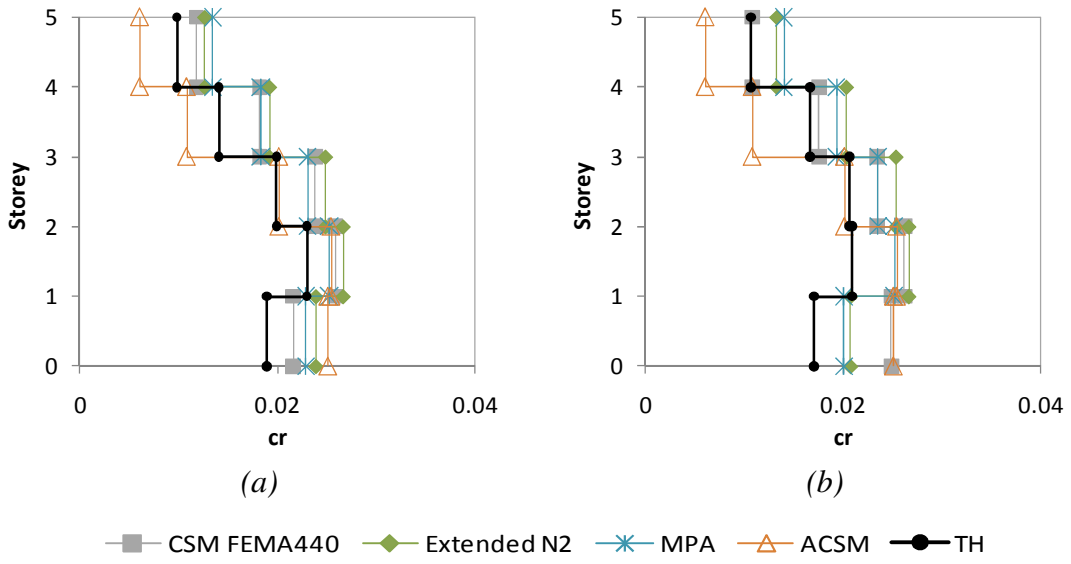

Figure A. 94 – Chord rotation profiles Y direction: a) Column S1, 0.8g; b) Column S23, 0.8g.

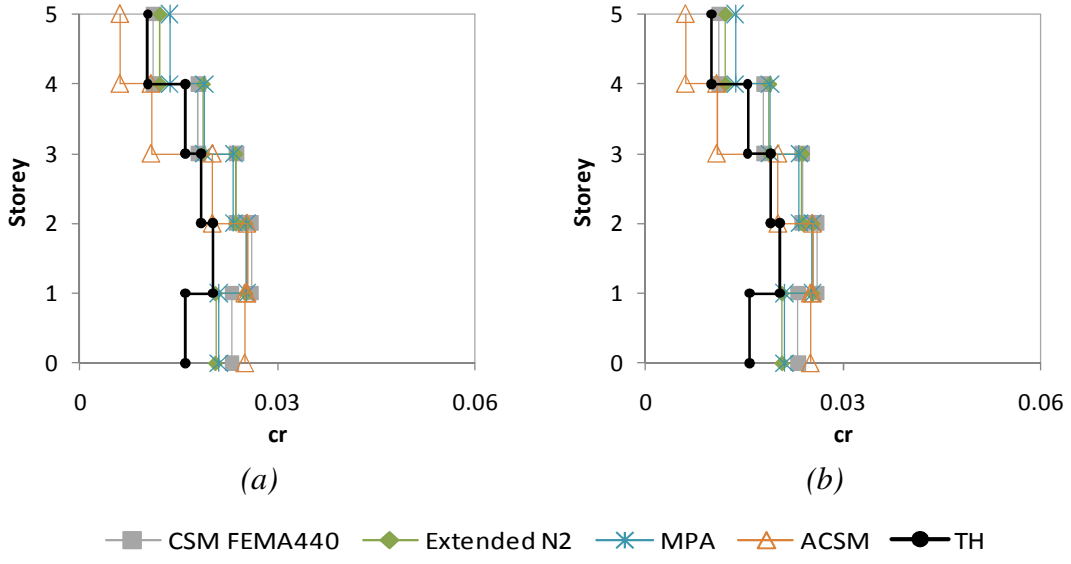

Figure A. 95 – Chord rotation profiles Y direction: a) Column S13, 0.8g; b) Column S14, 0.8g.

A11. Top displacements ratios eight story building

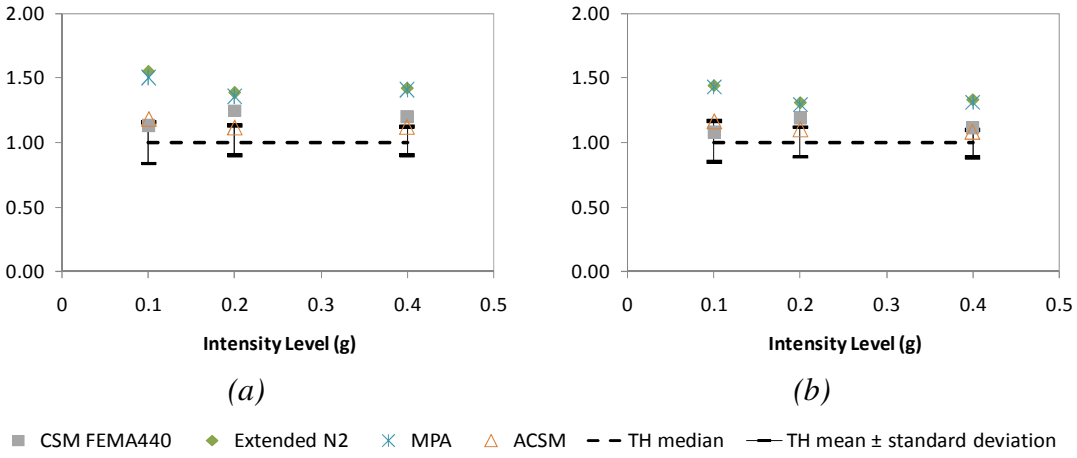

Figure A. 96 – a) Top displacements ratios in column S72 X direction; b) Top displacements ratios in column S23 X direction.

A12. Lateral displacement profiles eight story building

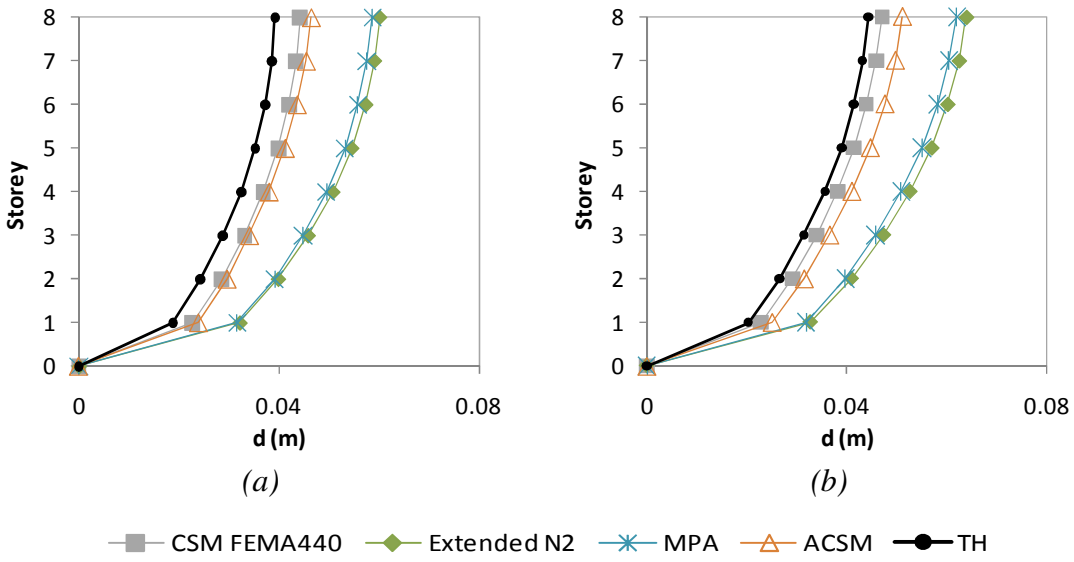

Figure A. 97 – Lateral displacement profiles X direction: a) Column S69, 0.1g; b) Column S15, 0.1g.

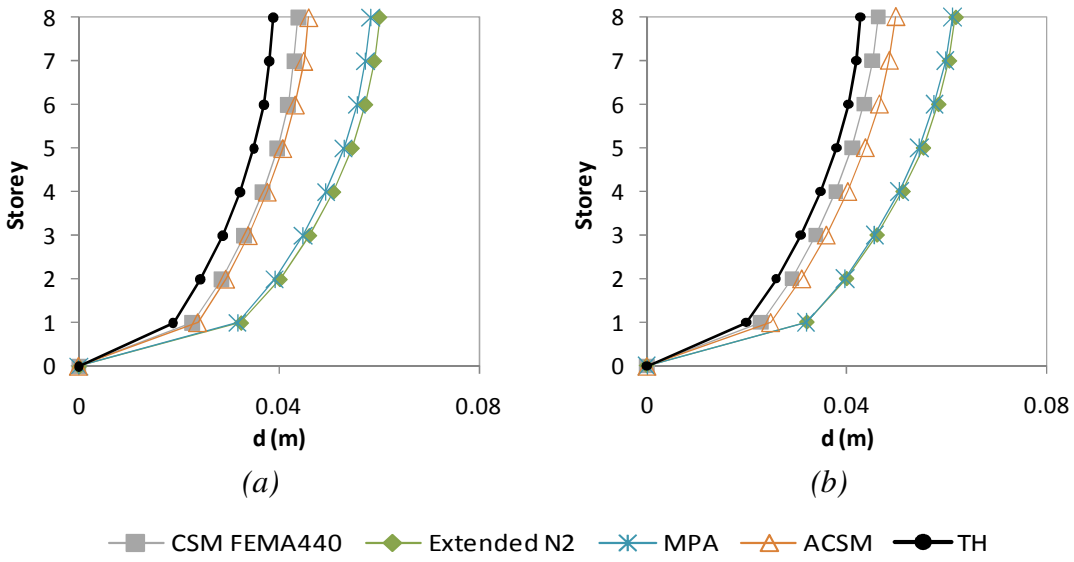

Figure A. 98 – Lateral displacement profiles X direction: a) Column 72, 0.1g; b) Column S23, 0.1g.

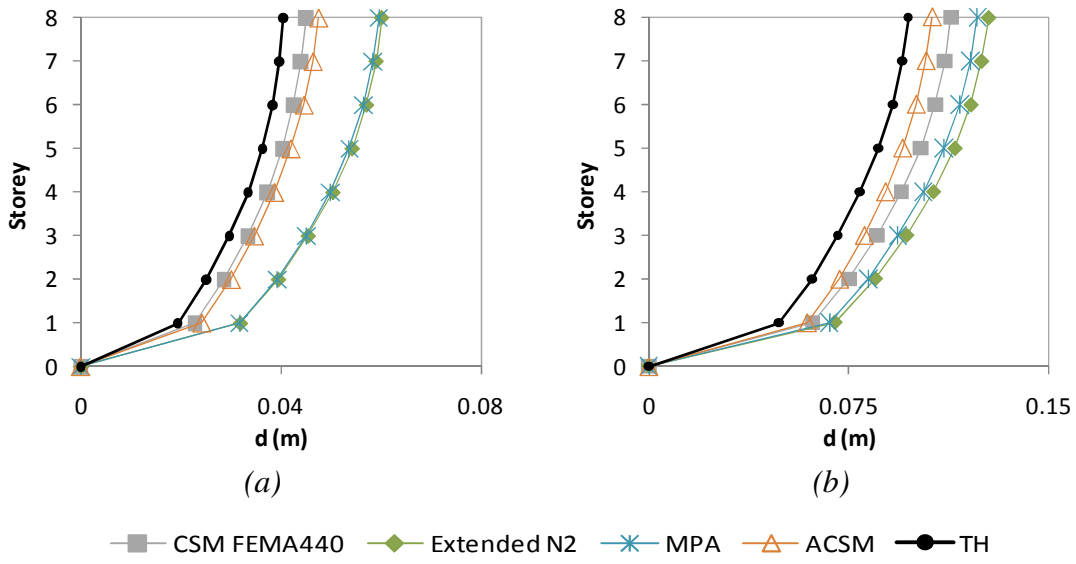

Figure A. 99 – Lateral displacement profiles X direction: a) Column S52, 0.1g; b) Column S9, 0.2g.

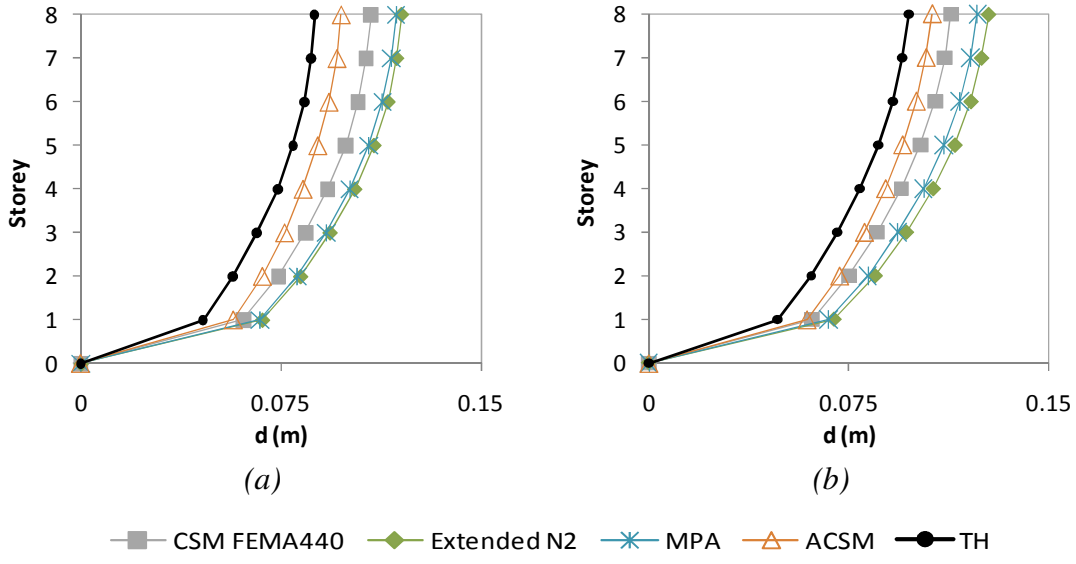

Figure A. 100 – Lateral displacement profiles X direction: a) Column S69, 0.2g; b) Column S15, 0.2g.

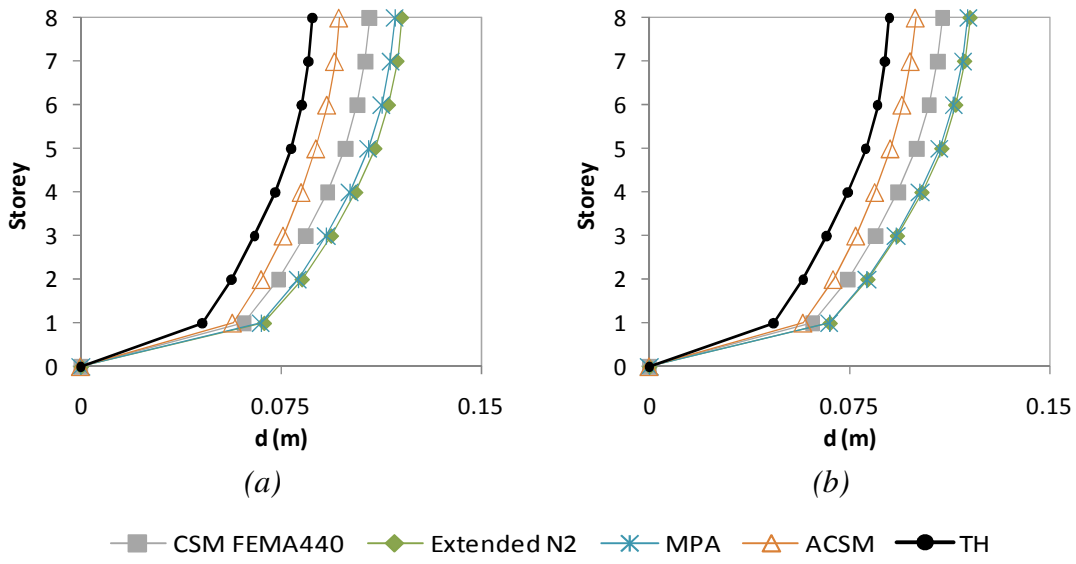

Figure A. 101 – Lateral displacement profiles X direction: a) Column S72, 0.2g; b) Column S52, 0.2g.

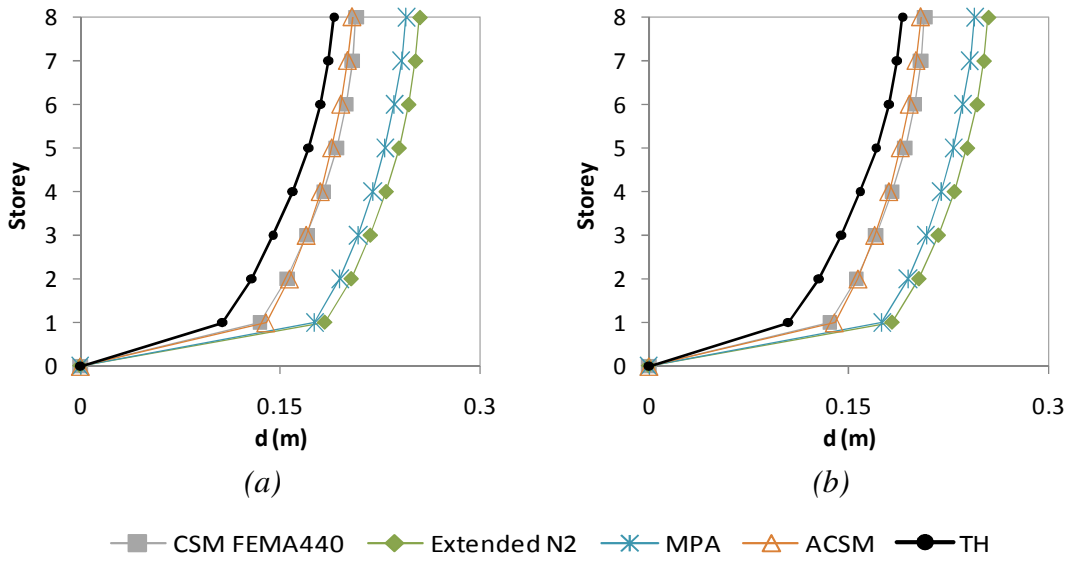

Figure A. 102 – Lateral displacement profiles X direction: a) Column S9, 0.4g; b) Column S15, 0.4g.

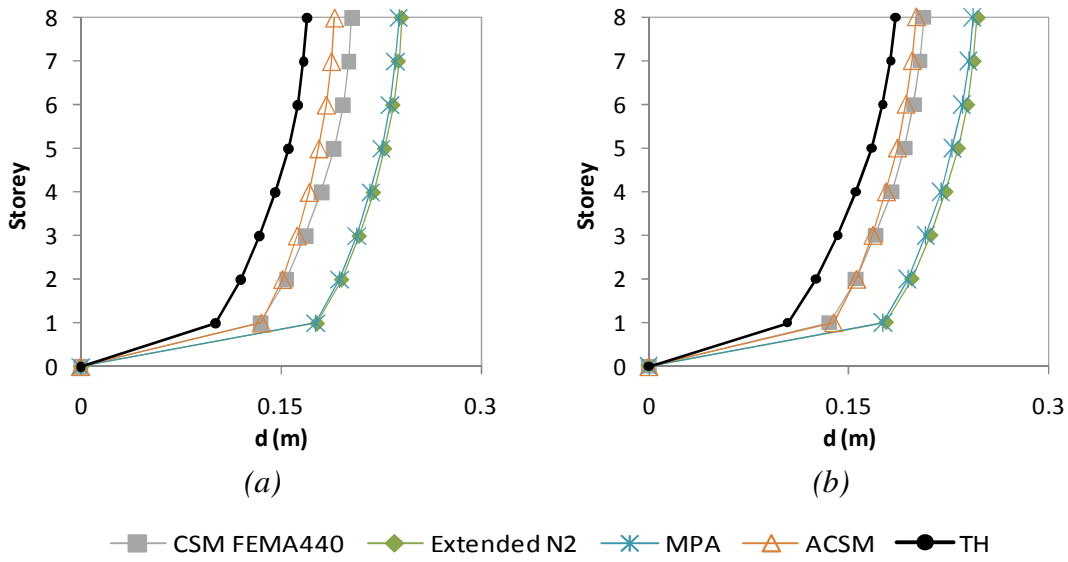

Figure A. 103 – Lateral displacement profiles X direction: a) Column S72, 0.4g; b) Column S23, 0.4g.

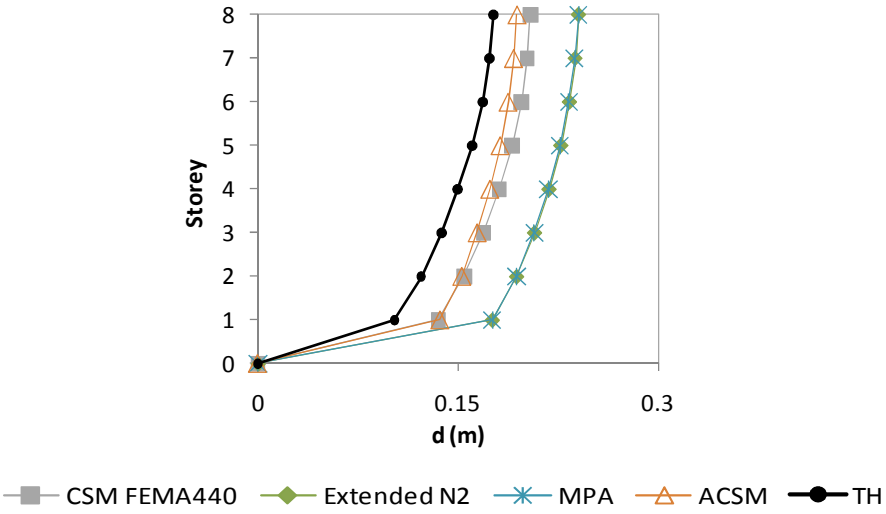

Figure A. 104 – Lateral displacement profile X direction, Column S52, 0.4.

A13. Interstorey drift profiles eight storey building

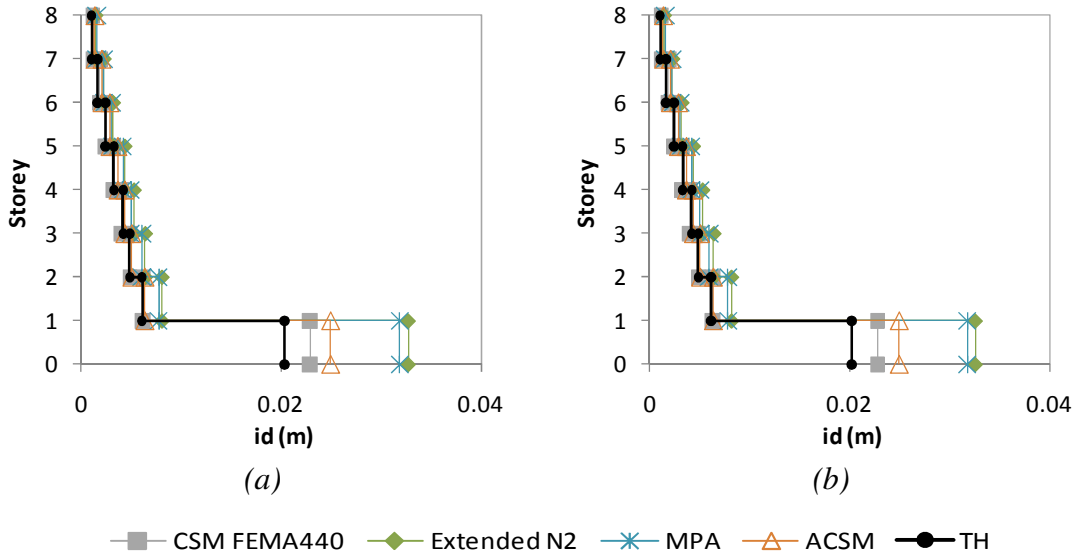

Figure A. 105 – Interstorey drifts profiles X direction: a) Column S9, 0.1g; b) Column S15, 0.1g.

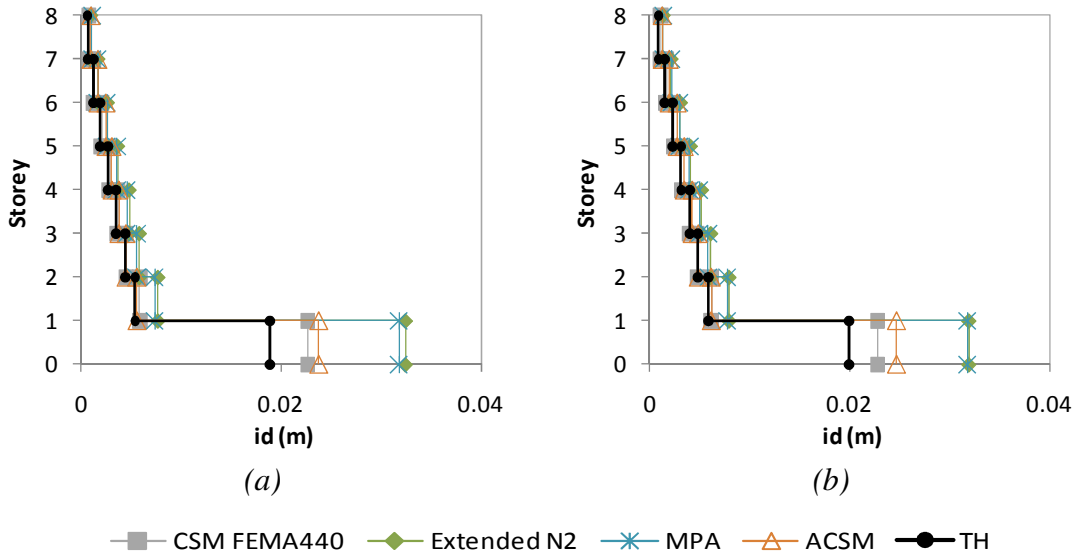

Figure A. 106 – Interstorey drifts profiles X direction: a) Column S72, 0.1g; b) Column S23, 0.1g.

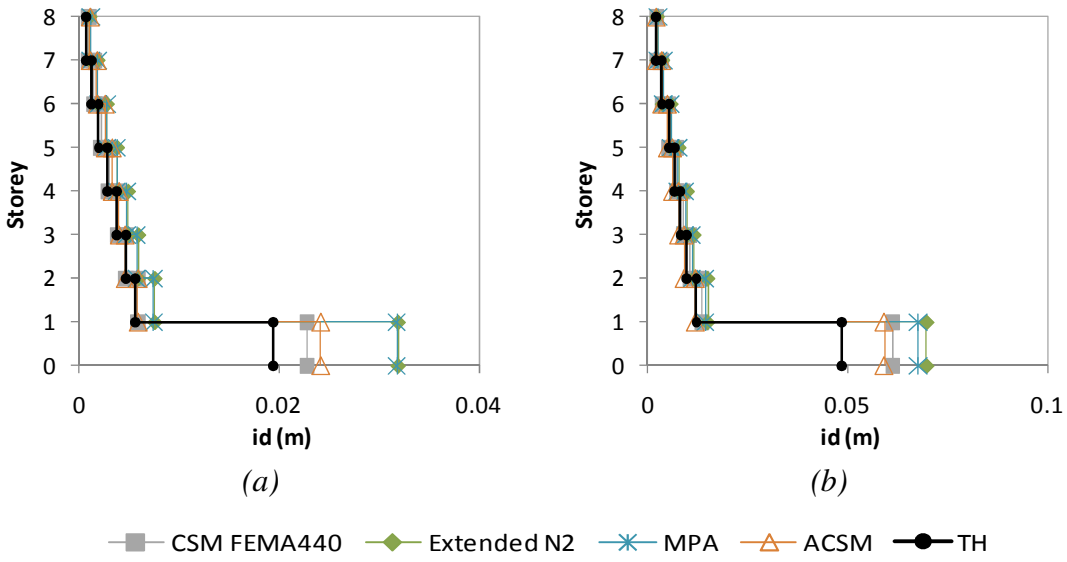

Figure A. 107 – Interstorey drifts profiles X direction: a) Column S52, 0.1g; b) Column S9, 0.2g.

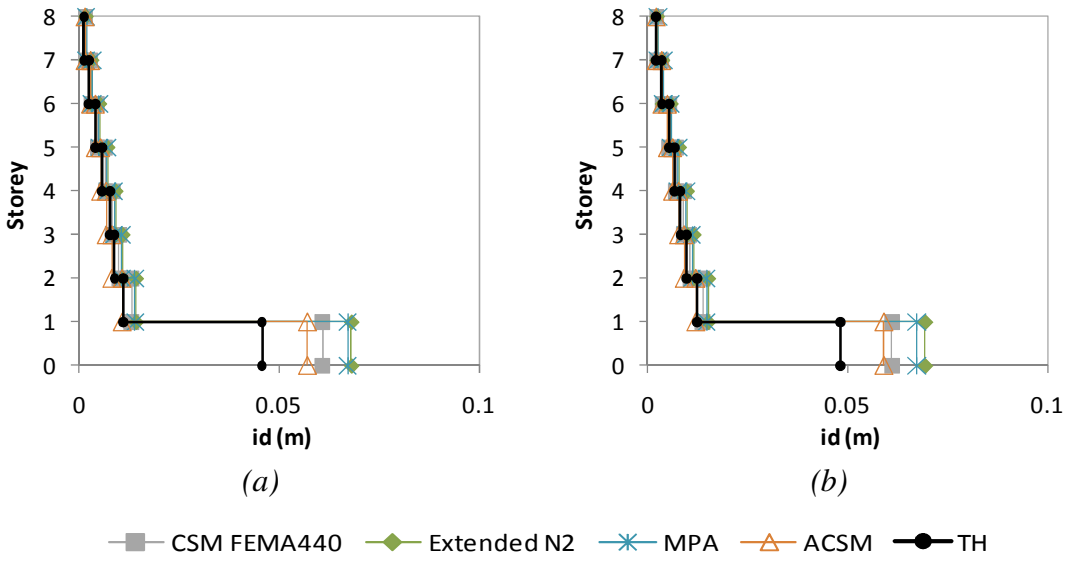

Figure A. 108 – Interstorey drifts profiles X direction: a) Column S69, 0.2g; b) Column S15, 0.2g.

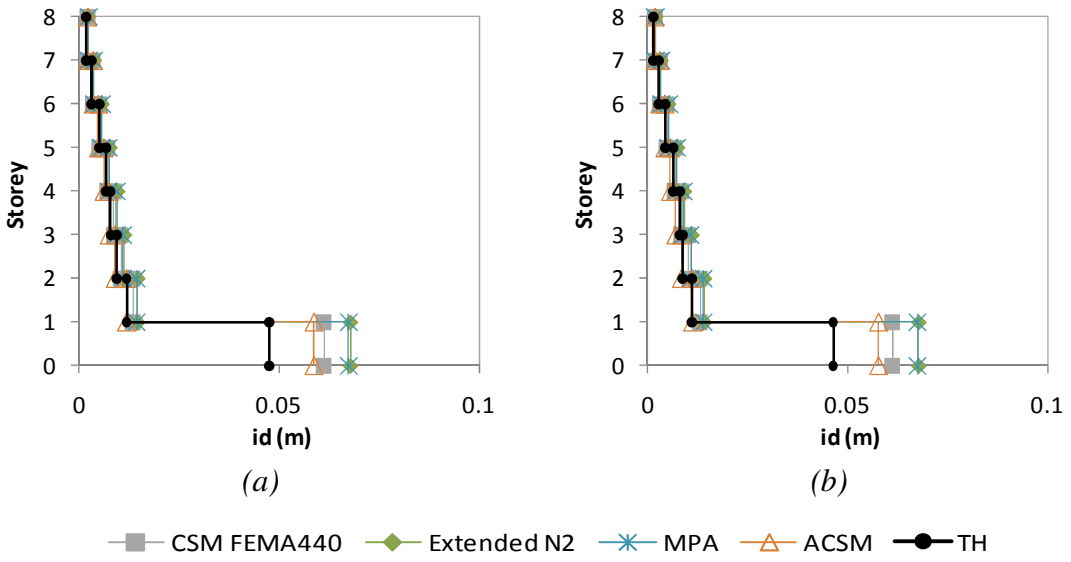

Figure A. 109 – Interstorey drifts profiles X direction: a) Column S23, 0.2g; b) Column S52, 0.2g.

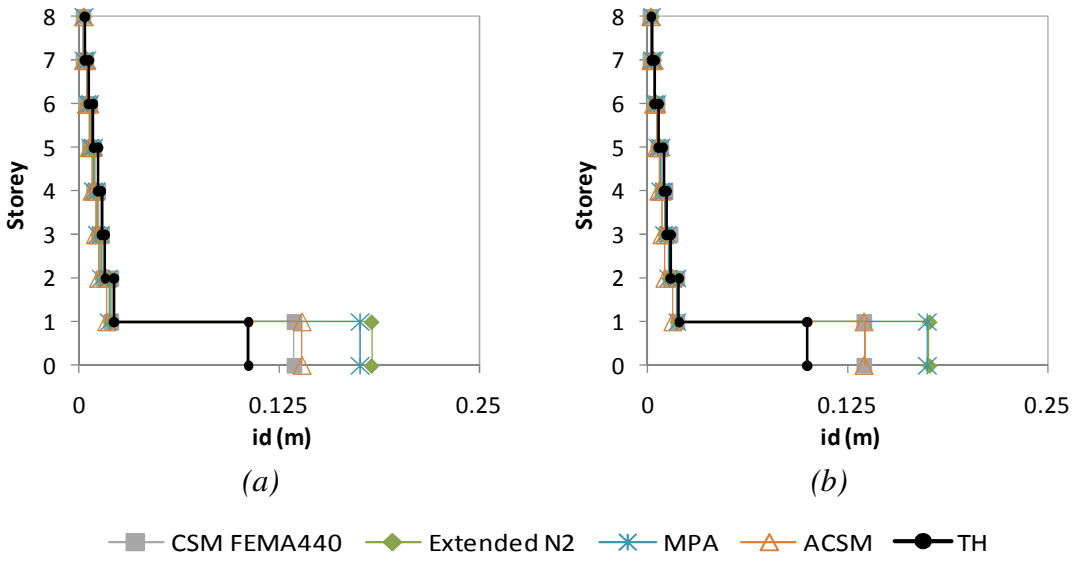

Figure A. 110 – Interstorey drifts profiles X direction: a) Column S9, 0.4g; b) Column S69, 0.4g.

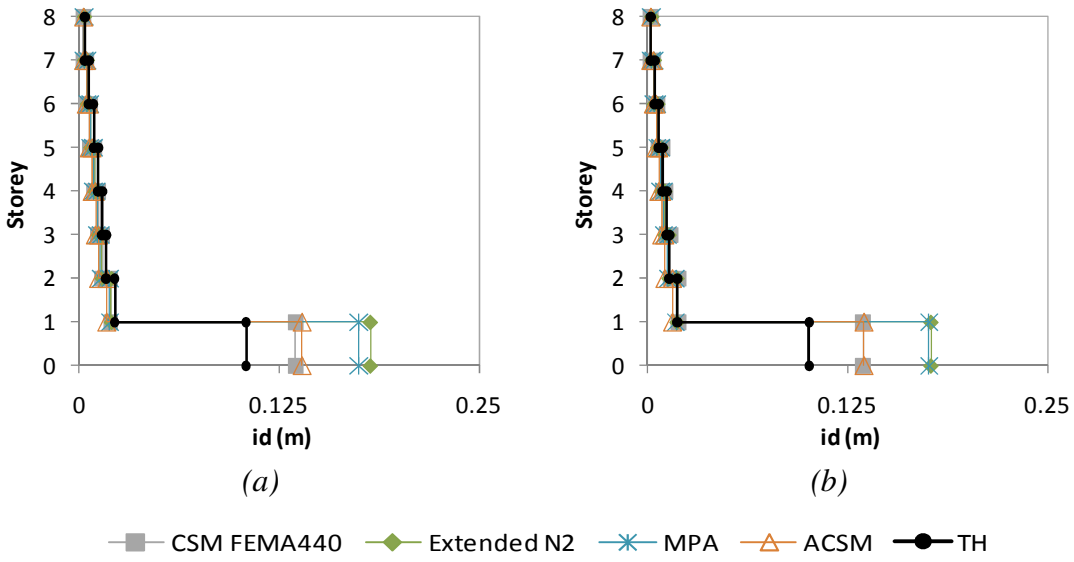

Figure A. 111 – Interstorey drifts profiles X direction: a) Column S15, 0.4g; b) Column S72, 0.4g.

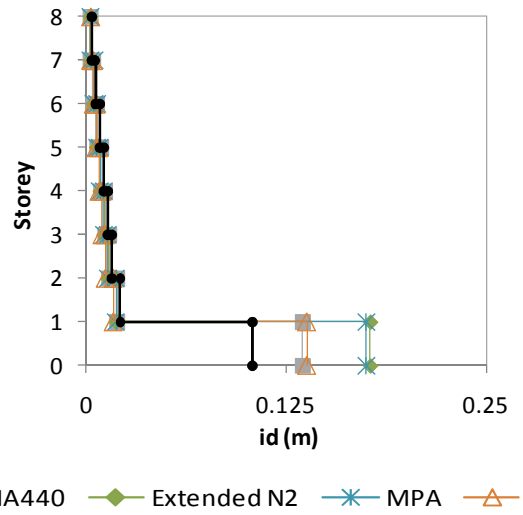

Figure A. 112 – Interstorey drifts profile X direction, Column S23, 0.4g.

A14. Chord rotation profiles eight storey building

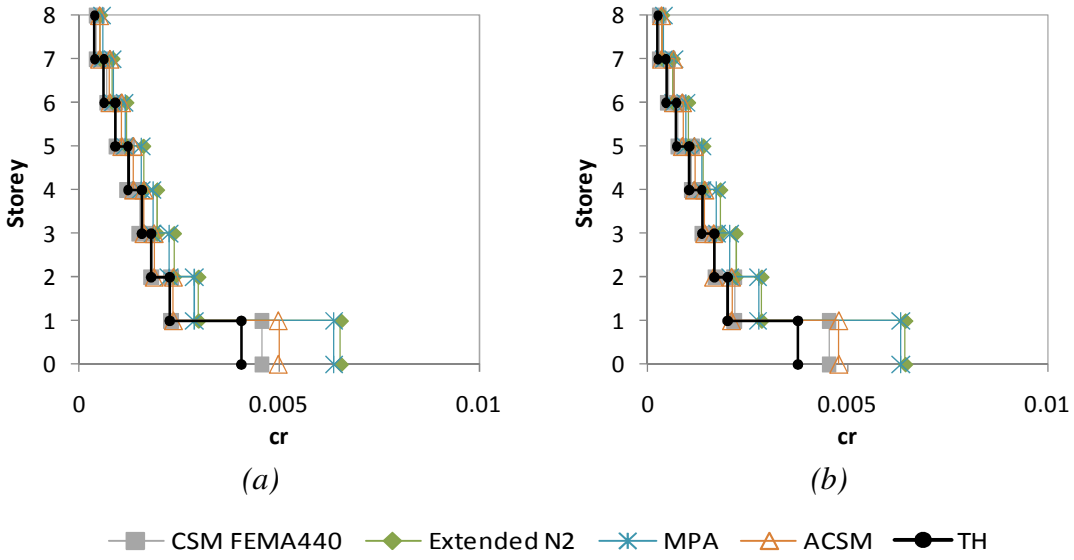

Figure A. 113 – Chord rotation profiles X direction: a) Column S9, 0.1g; b) Column S69, 0.1g.

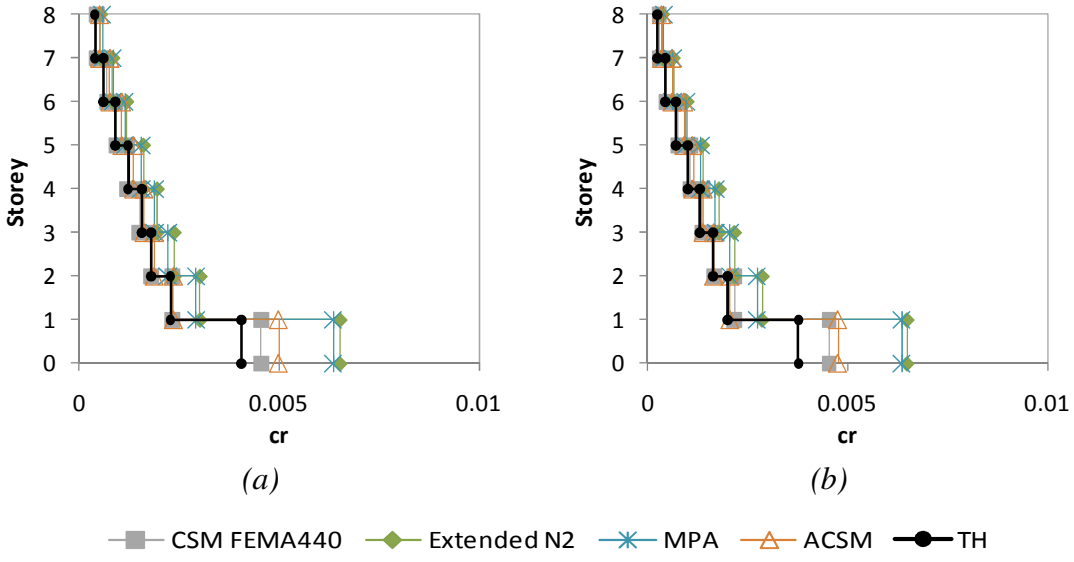

Figure A. 114 – Chord rotation profiles X direction: a) Column S15, 0.1g; b) Column S72, 0.1g.

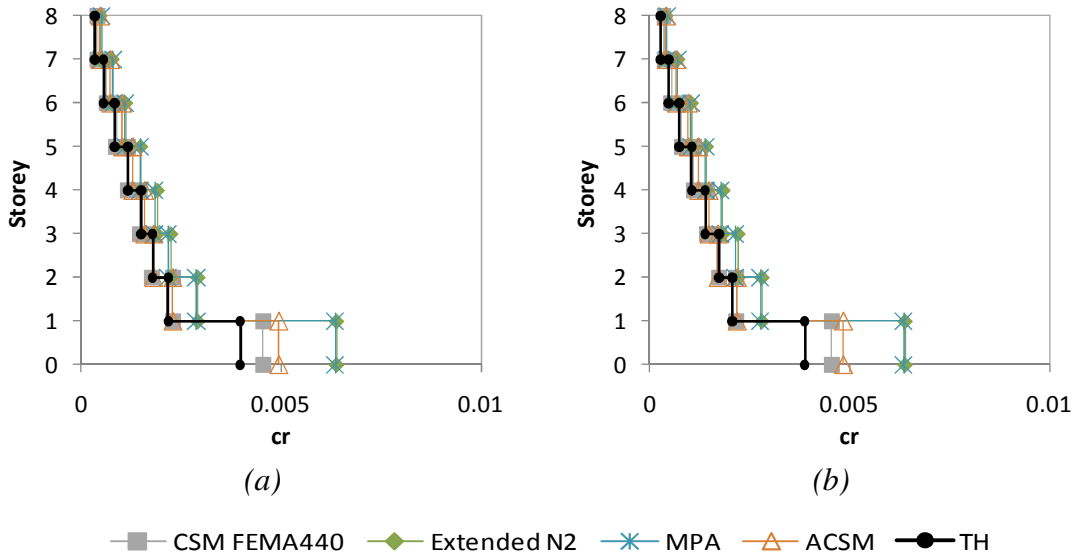

Figure A. 115 – Chord rotation profiles X direction: a) Column S23, 0.1g; b) Column S52, 0.1g.

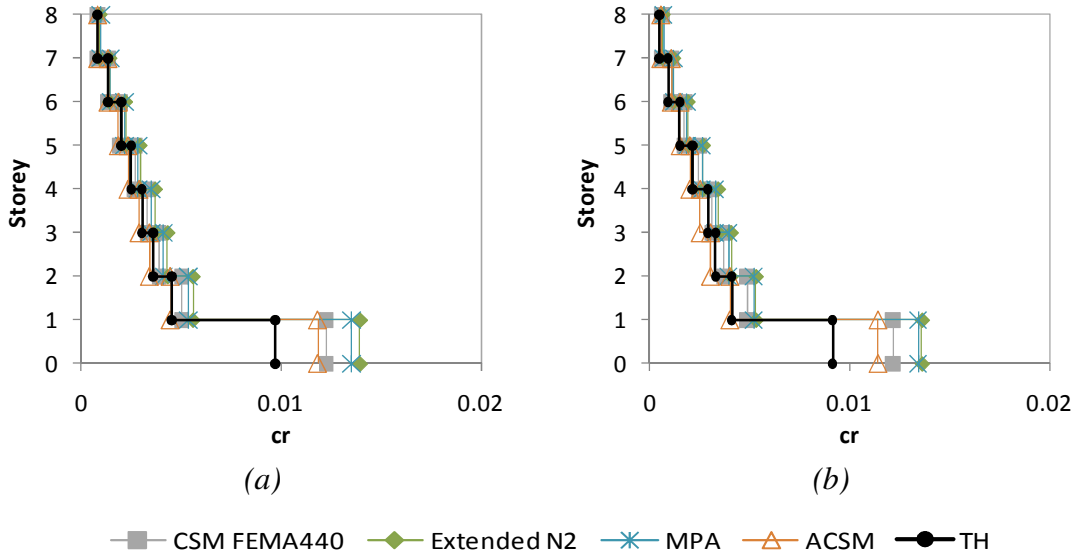

Figure A. 116 – Chord rotation profiles X direction: a) Column S9, 0.2g; b) Column S69, 0.2g.

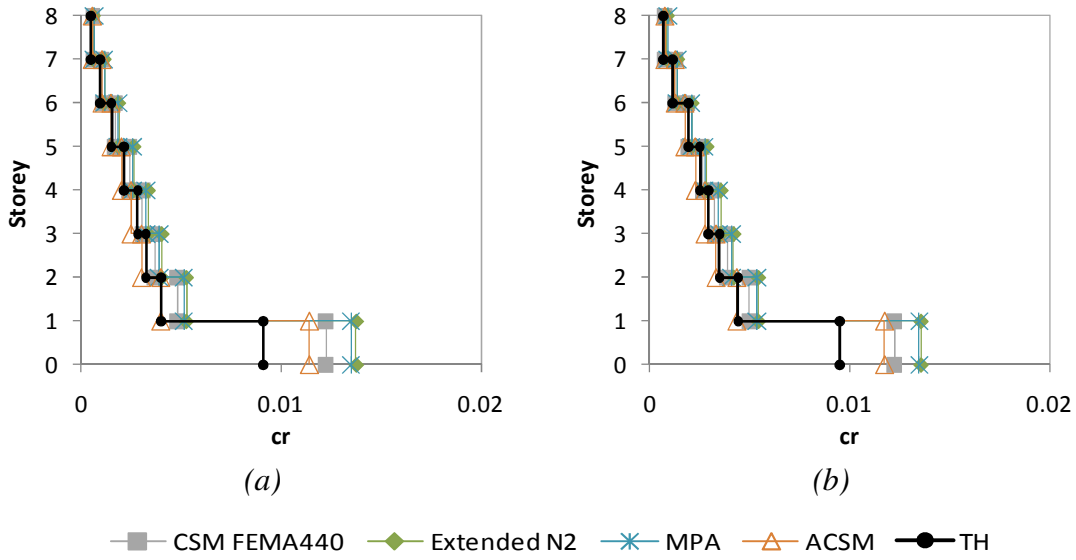

Figure A. 117 – Chord rotation profiles X direction: a) Column S72, 0.2g; b) Column S23, 0.2g.

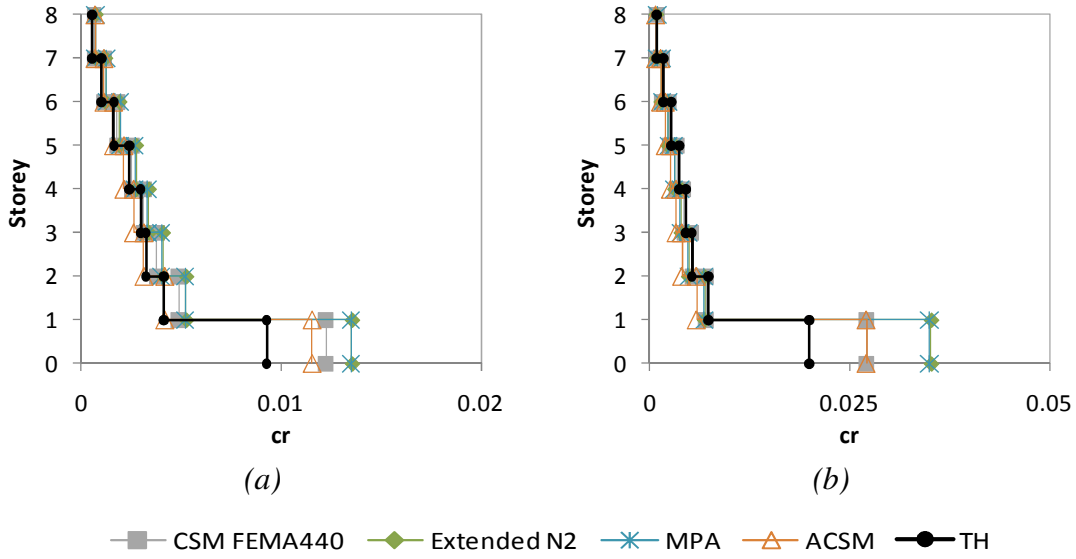

Figure A. 118 – Chord rotation profiles X direction: a) Column S52, 0.2g; b) Column S69, 0.4g.

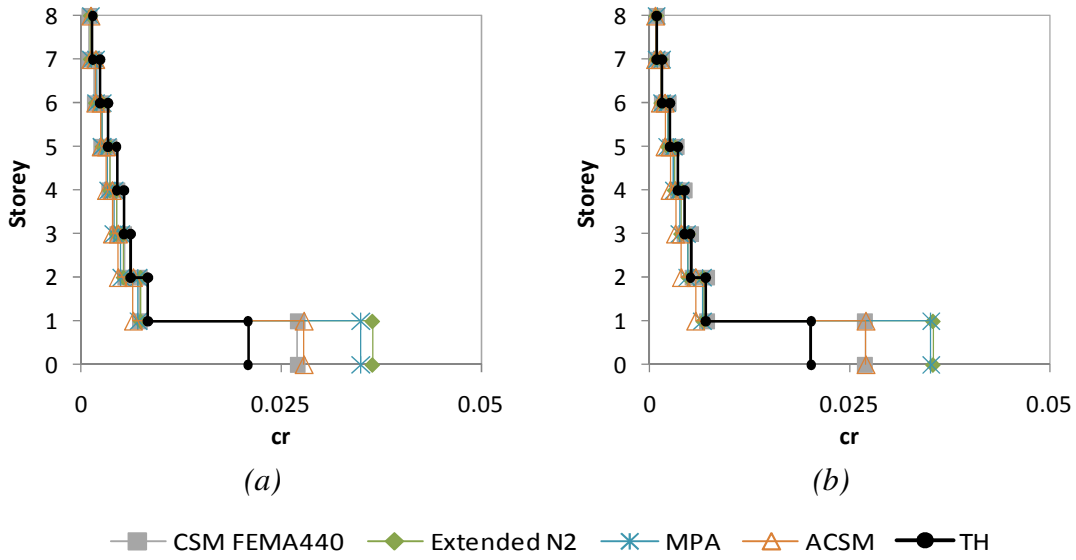

Figure A. 119 – Chord rotation profiles X direction: a) Column S15, 0.4g; b) Column S72, 0.4g.

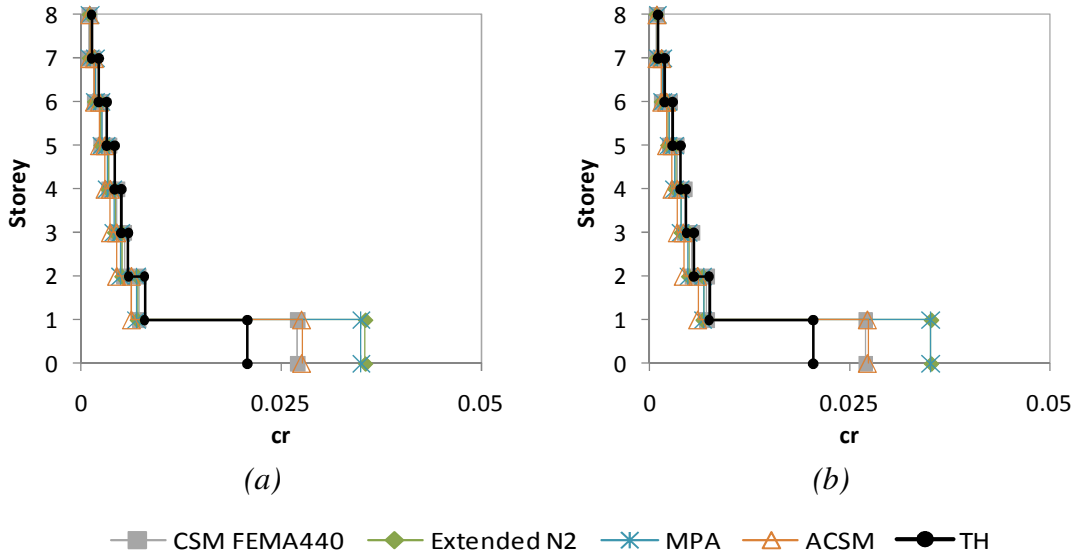

Figure A. 120 – Chord rotation profiles X direction: a) Column S23, 0.4g; b) Column S52, 0.4g.

A15. 3D Pushover procedure *vs.* CSM-FEMA440

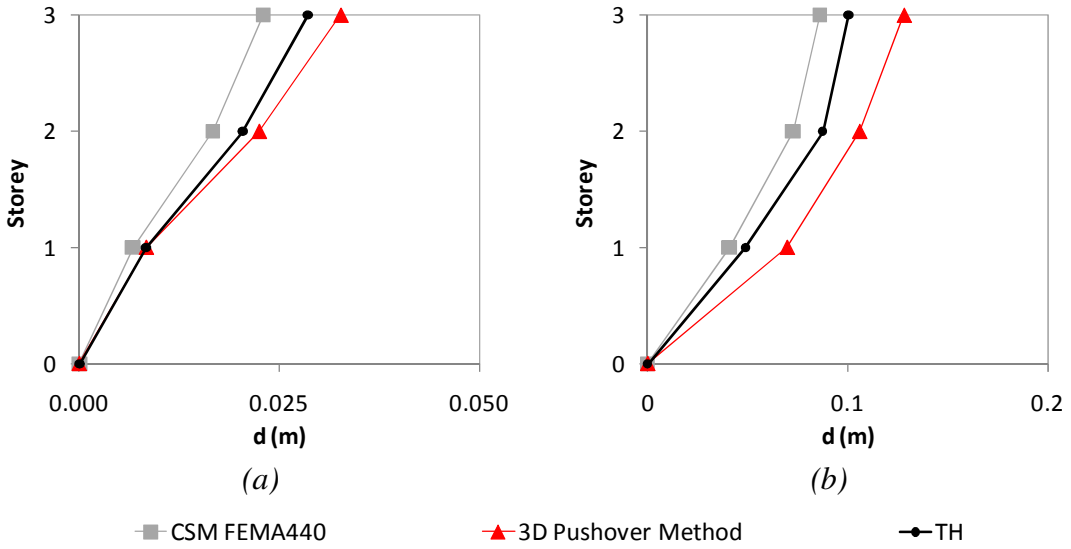

Figure A. 121 – Lateral displacement profiles, three storey building: a) Column C2, X direction, 0.05g; b) Column C8, X direction, 0.2g.

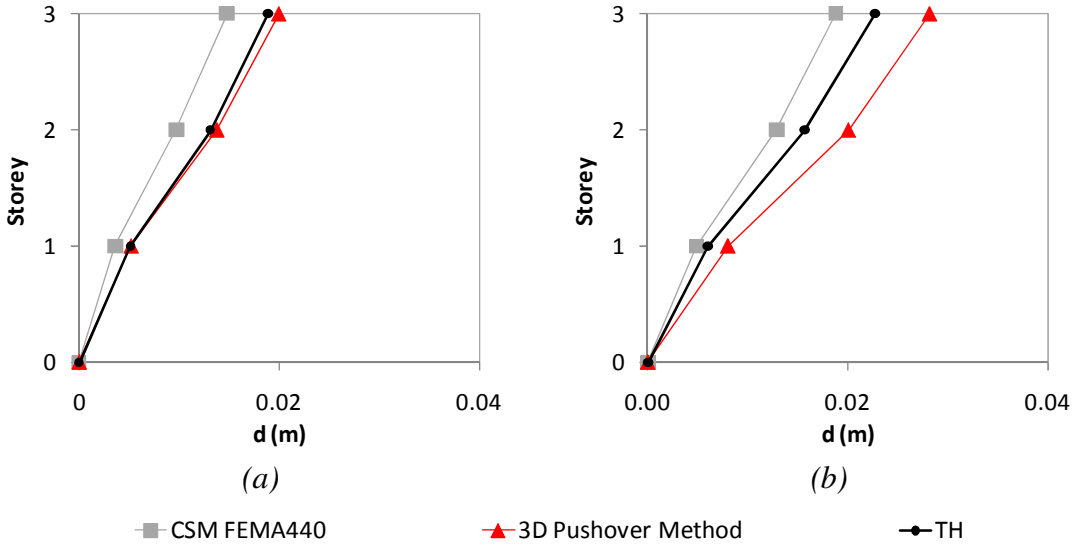

Figure A. 122 – Lateral displacement profiles, three storey building: a) Column C8, Y direction, 0.05g; b) Column C2, Y direction, 0.05g.

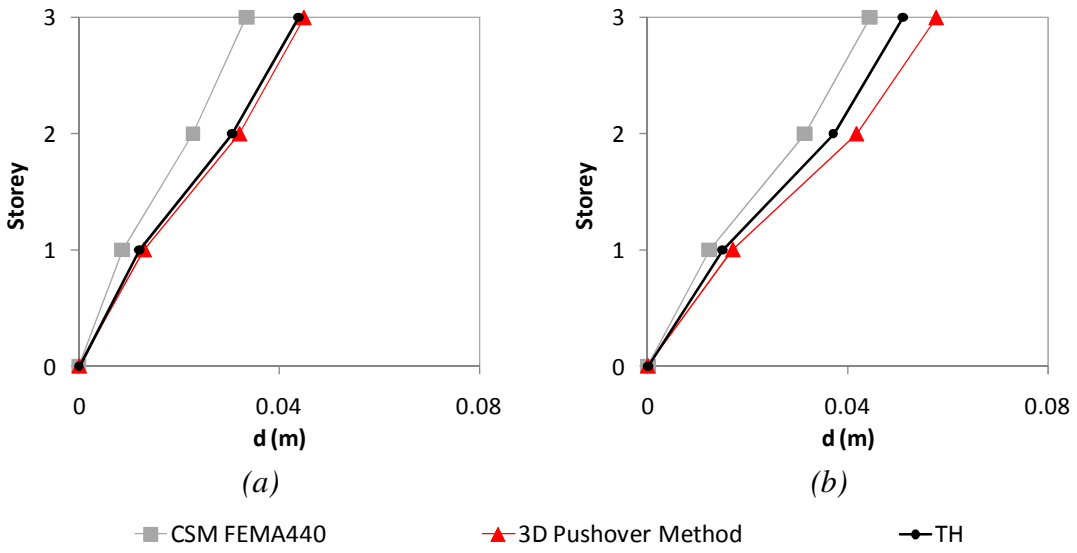

Figure A. 123 – Lateral displacement profiles, three storey building: a) Column C8, 0.1g; b) Column C2, 0.1g.

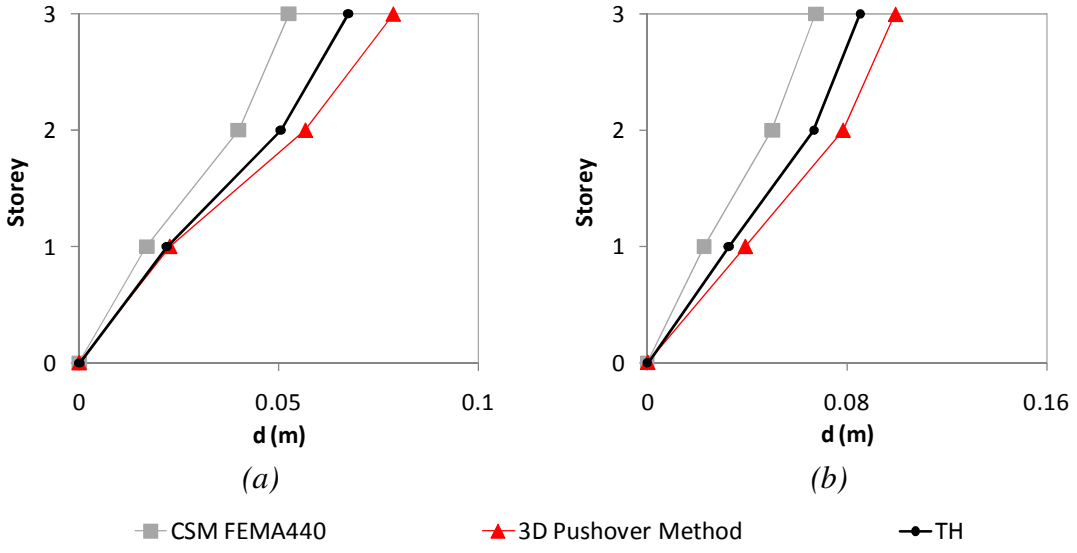

Figure A. 124 – Lateral displacement profiles, three storey building: a) column C2 X 0.1g; b) column C8, Y, 0.2g.

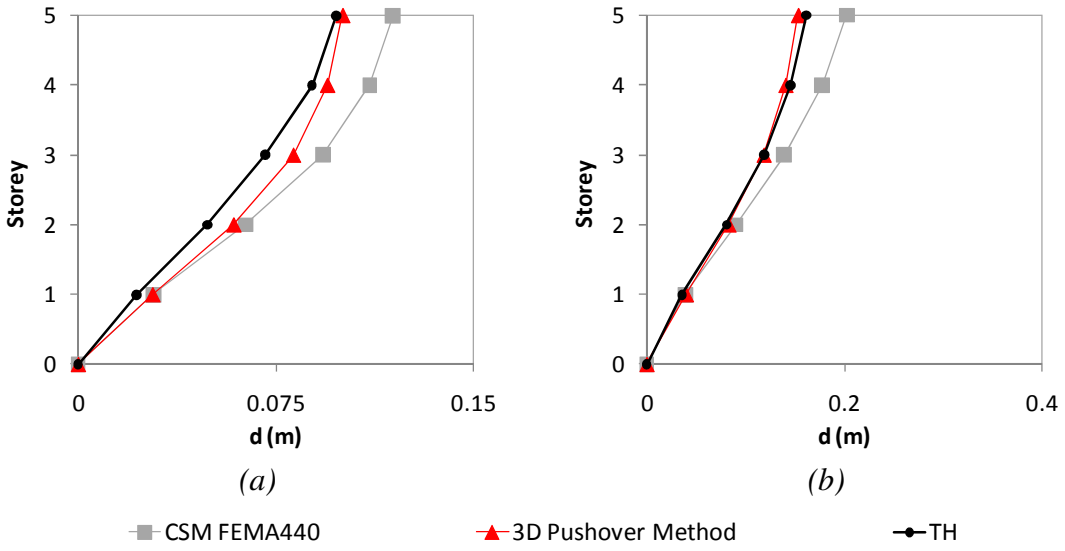

Figure A. 125 – Lateral displacement profiles, five storey building: a) Column S14,X direction, 0.4g; b) Column S13, Y direction, 0.6g.

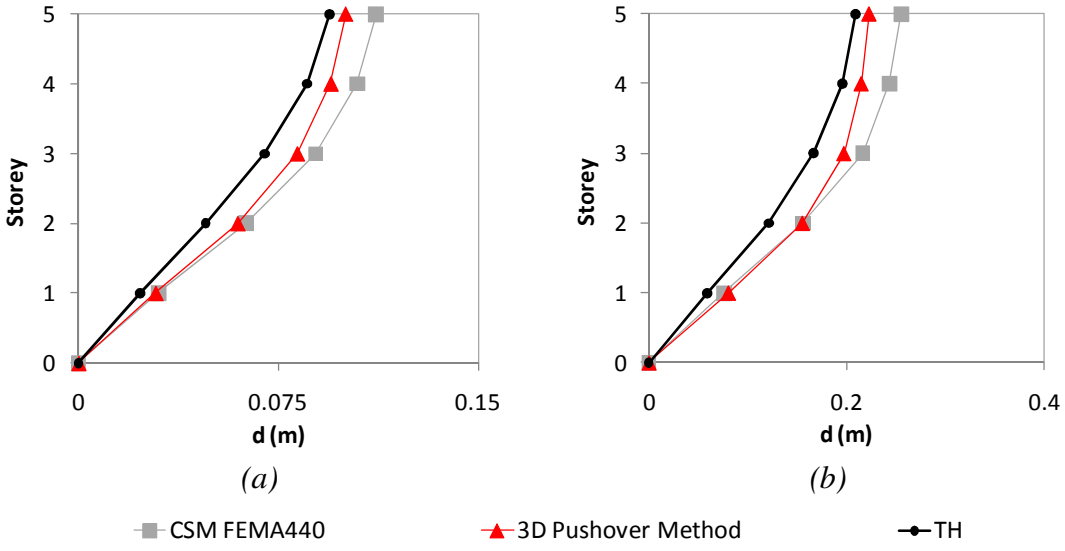

Figure A. 126 – Lateral displacement profiles, five storey building, X direction: a) column S23, 0.4g; b) column S14, 0.8g.

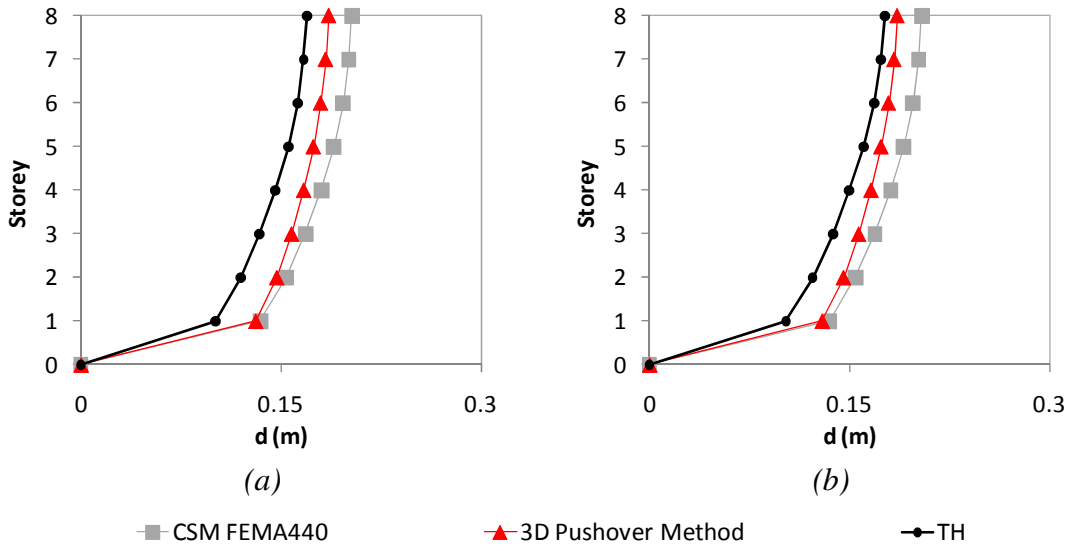

Figure A. 127 – Lateral displacement profiles, eight storey building: a) Column 72, X direction, 0.4g; b) Column S52, X direction, 0.4g.

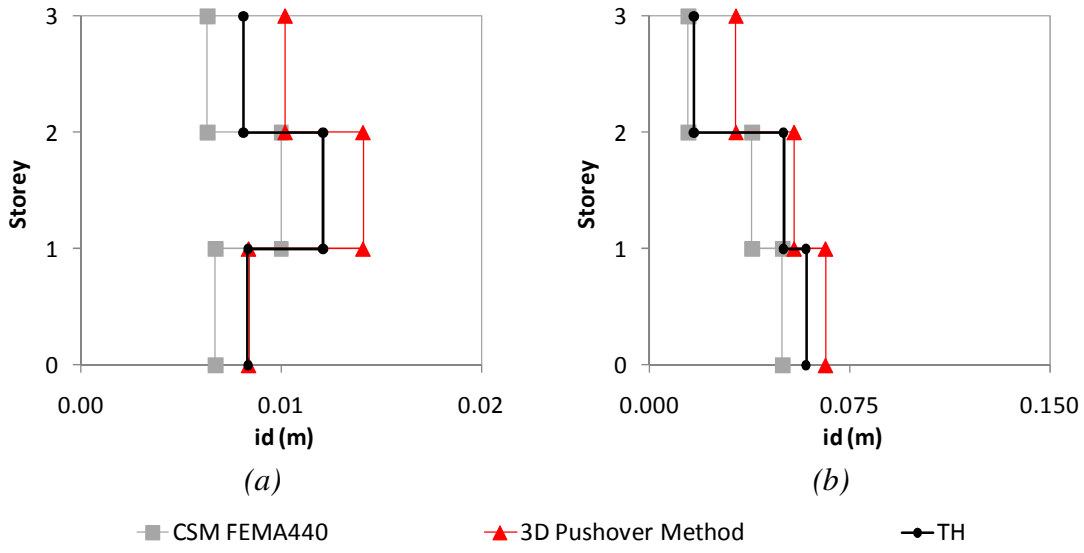

Figure A. 128 – Interstorey drifts profiles, three storey building: a) Column C2, X direction, 0.05g; b) Column C2, X direction, 0.2g.

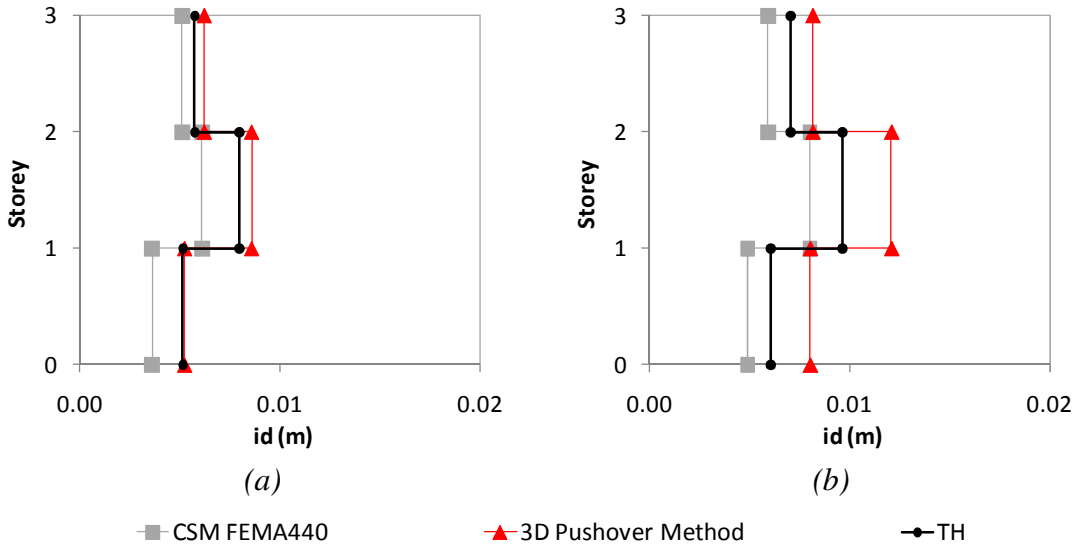

Figure A. 129 – Interstorey drifts profiles, three storey building: a) Column C8, Y direction, 0.05g; b) Column C2, Y direction, 0.05g.

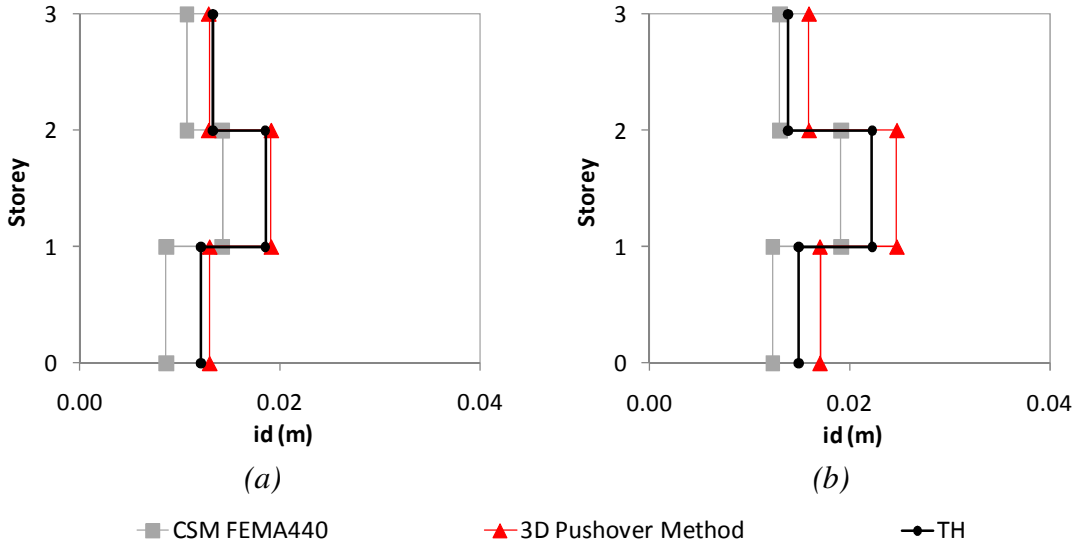

Figure A. 130 – Interstorey drifts profiles, three storey building: a) Column C8, Y direction, 0.1g; b) Column C2, Y direction, 0.1g.

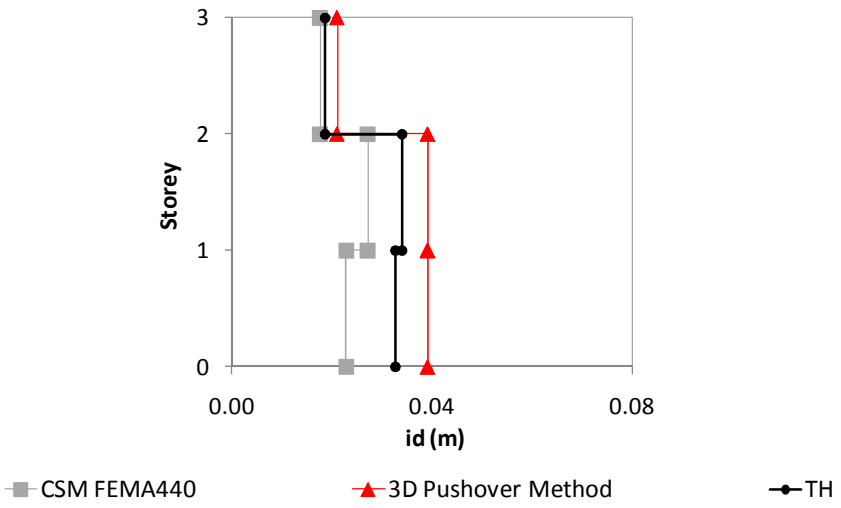

Figure A. 131 – Interstorey drifts profiles, three storey building, Column C8, Y direction, 0.2g.

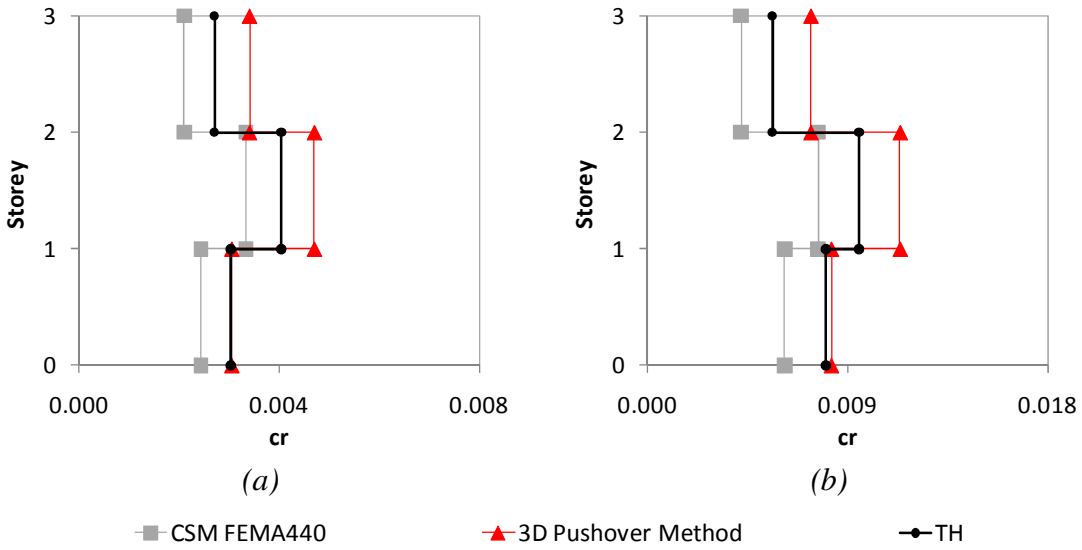

Figure A. 132 – Chord rotation profiles, three storey building: a) Column C2, X direction, 0.05g; b) Column C2, X direction, 0.1g.

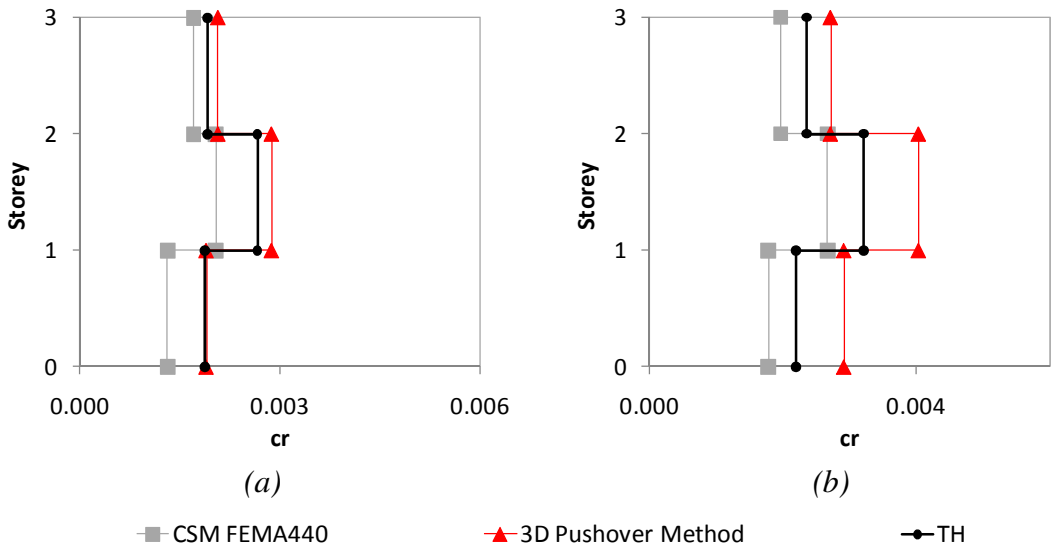

Figure A. 133 – Chord rotation profiles, three storey building: a) Column C8, Y direction, 0.05g; b) Column C2, Y direction, 0.05g.

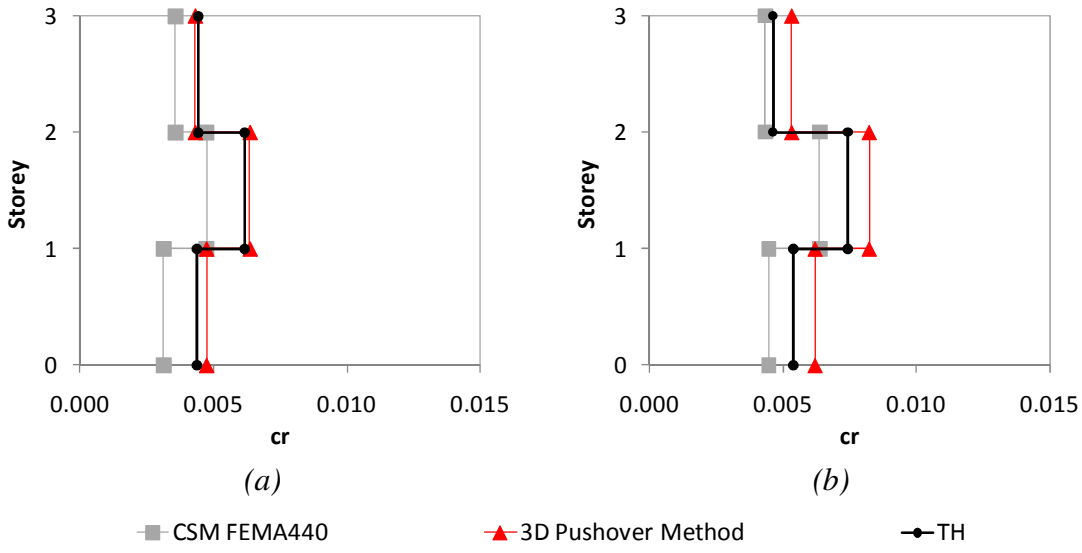

Figure A. 134 – Chord rotation profiles, three storey building: a) Column C8, Y direction, 0.1g; b) Column C2, Y direction, 0.1g.

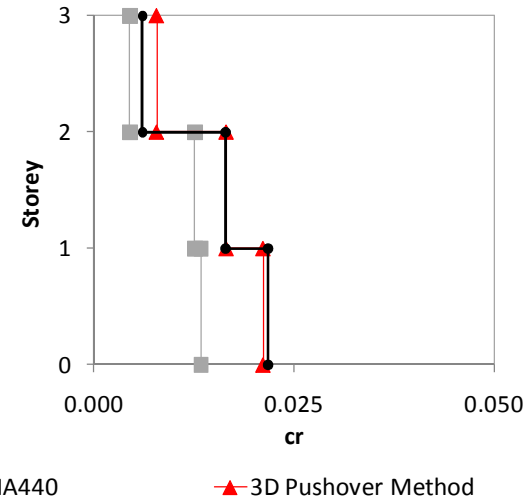

Figure A. 135 – Chord rotation profiles, three storey building, Column C8, Y direction, 0.3g.

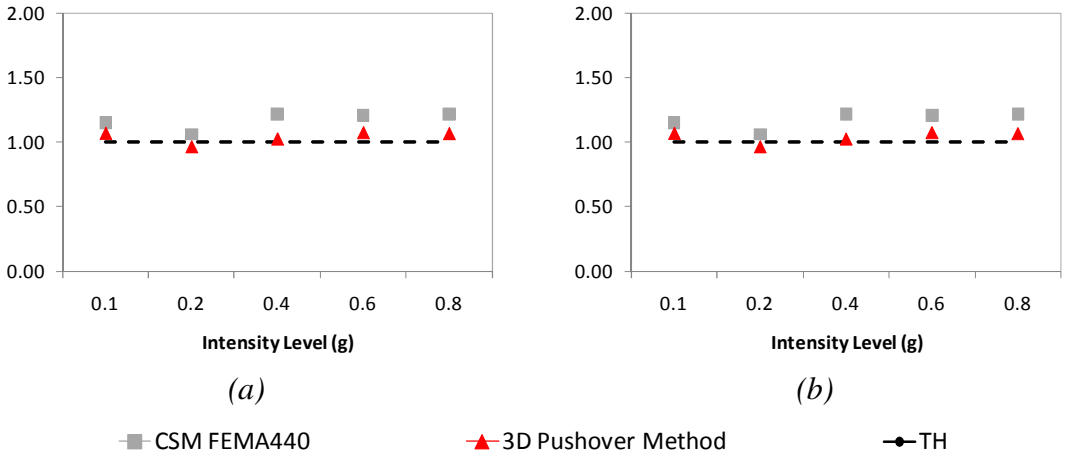

Figure A. 136 – Top displacements ratios five storey building: a) column S13 X direction; b) column CM Y direction.

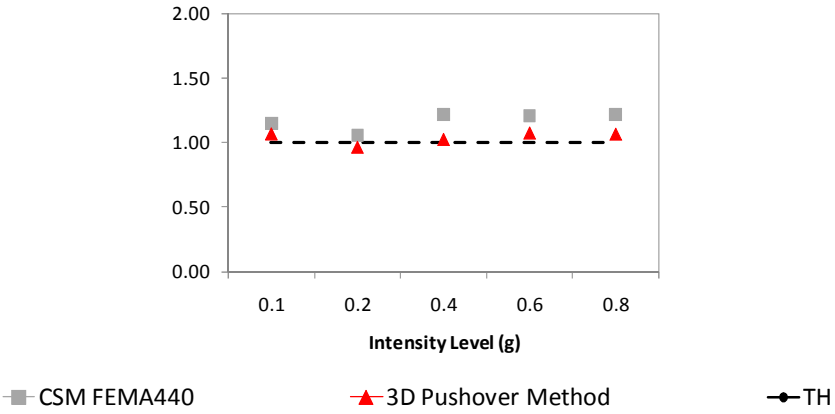

Figure A. 137 – Top displacements ratios five storey building: a) column S14 X direction; b) column CM Y direction.

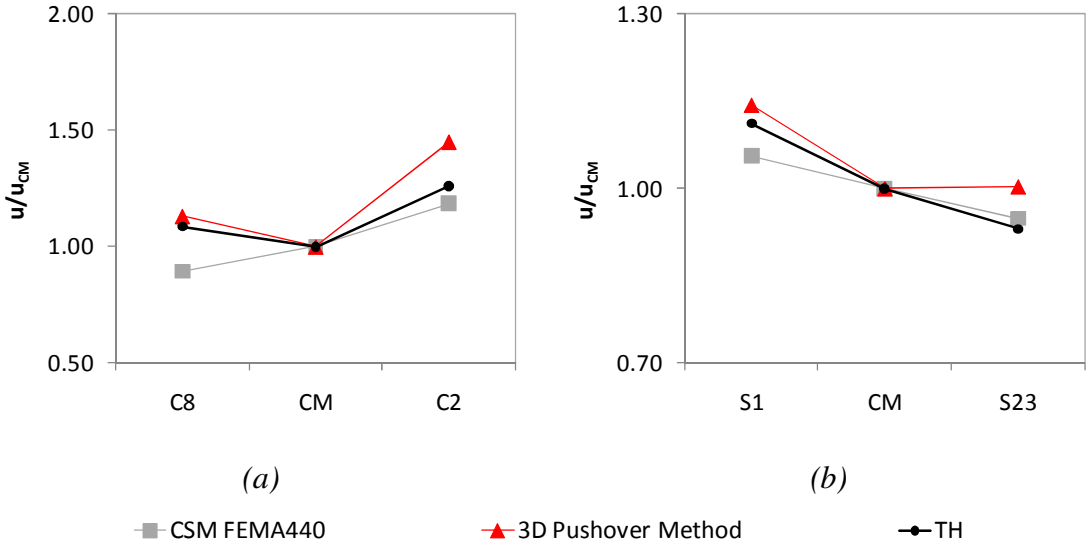

Figure A. 138 – Normalized top displacements: a) three storey building, 0.1g, Y direction; b) five storey building, 0.6g, X direction.

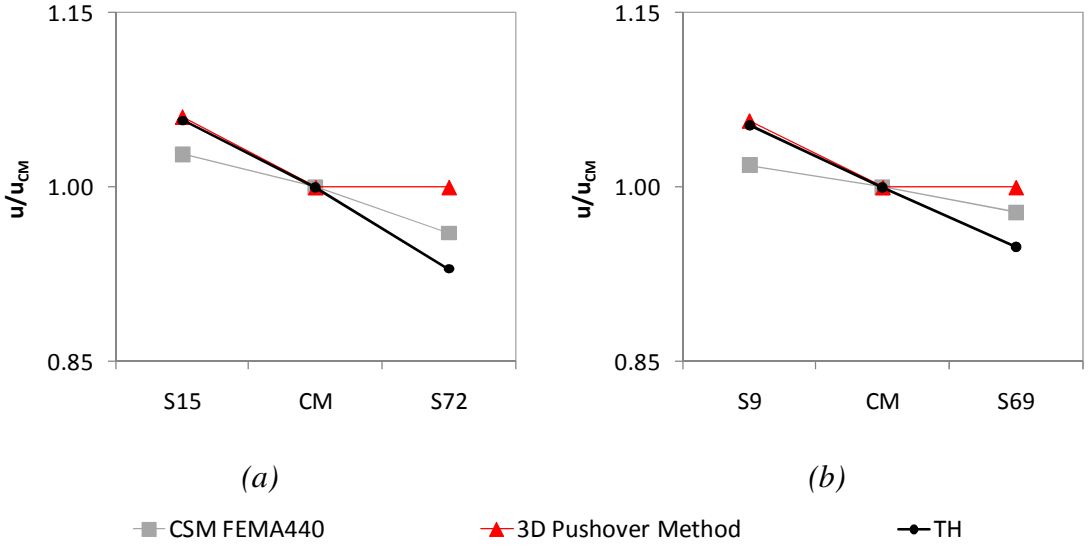

Figure A. 139 –Normalized top displacements eight storey building, X direction: a) 0.1g; b) 0.2g.

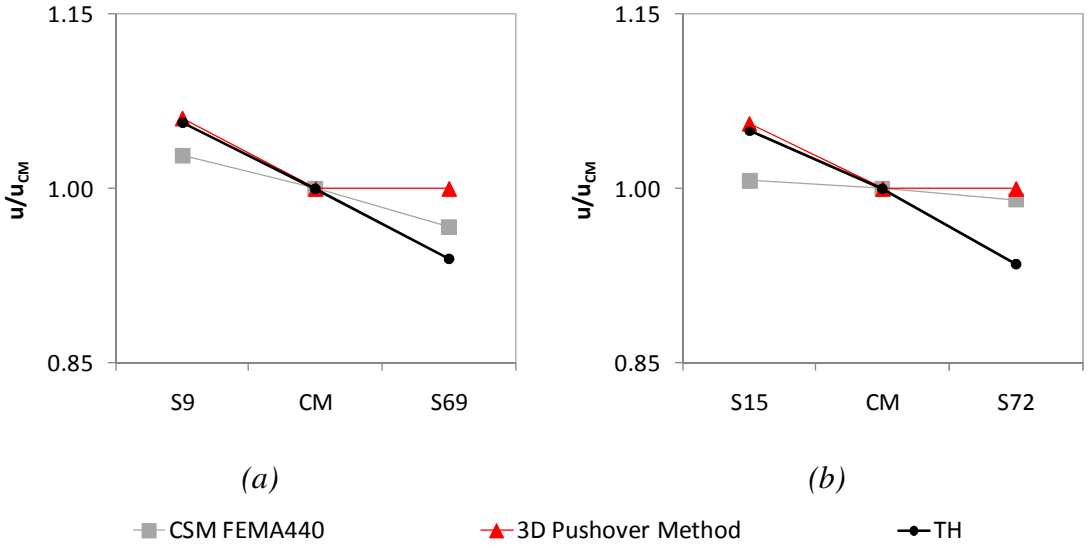

Figure A. 140 – Normalized top displacements eight storey building, X direction: a) 0.1g; b) 0.4g.

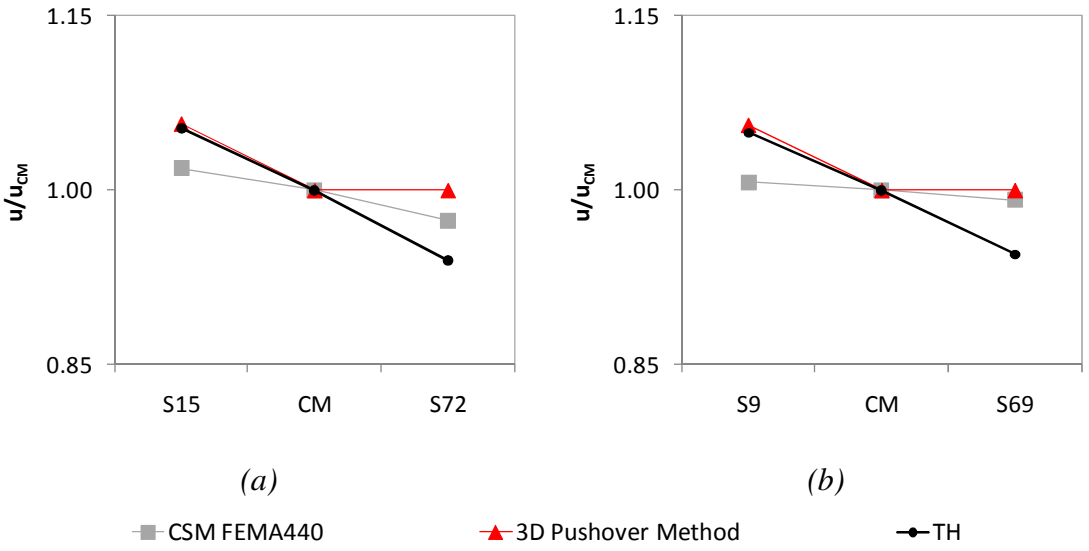

Figure A. 141 – Normalized top displacements eight storey building, X direction: a) 0.2g; b) 0.4g.

A16. 3D Pushover procedure *vs.* ACSM

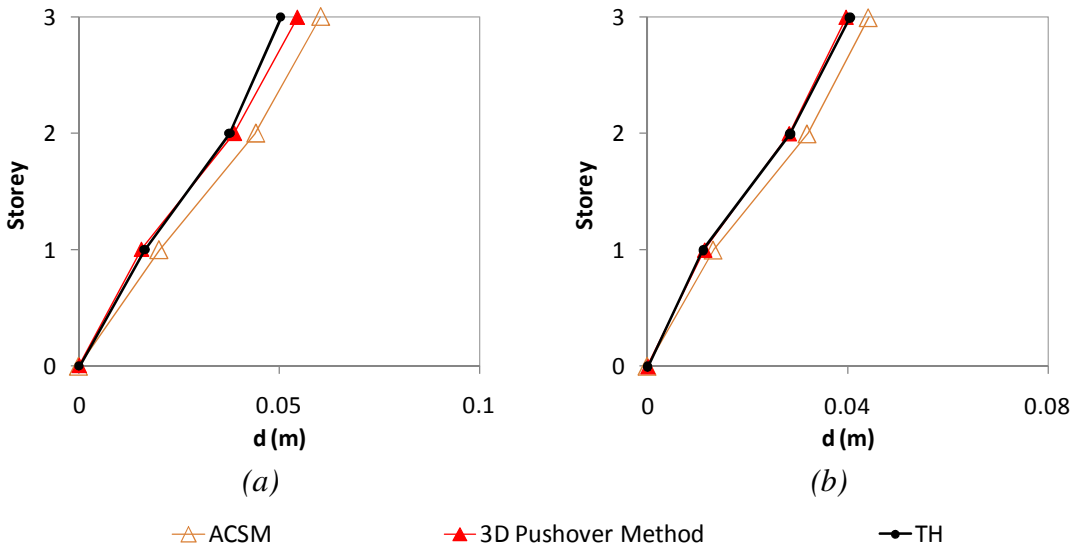

Figure A. 142 – Lateral displacement profiles, three storey building: a) column C8, X direction, 0.1g; b) column C3, Y direction, 0.1g.

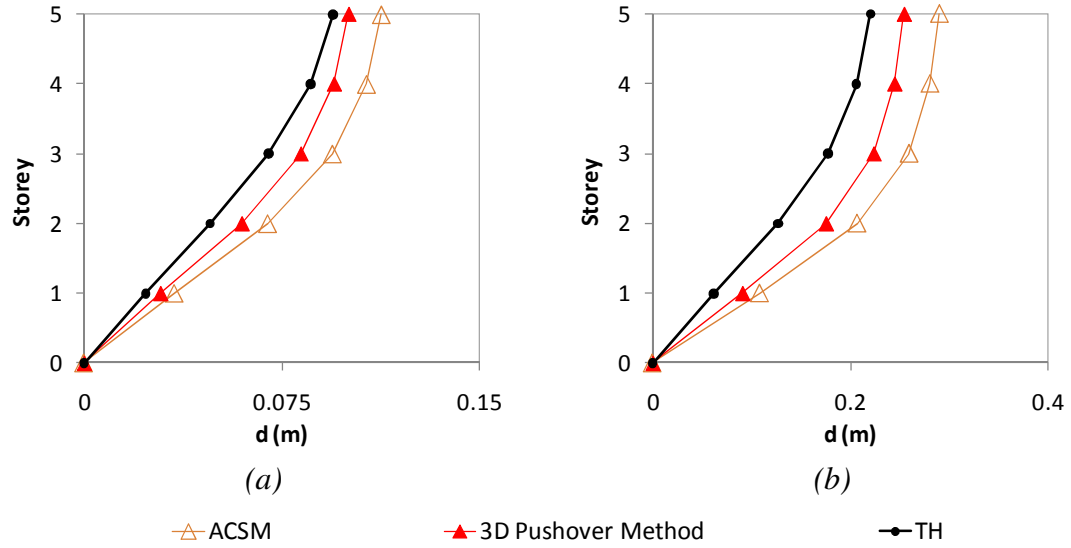

Figure A. 143 – Lateral displacement profiles, five storey building: a) column S23, X direction, 0.4g; b) column S1, X direction, 0.8g.

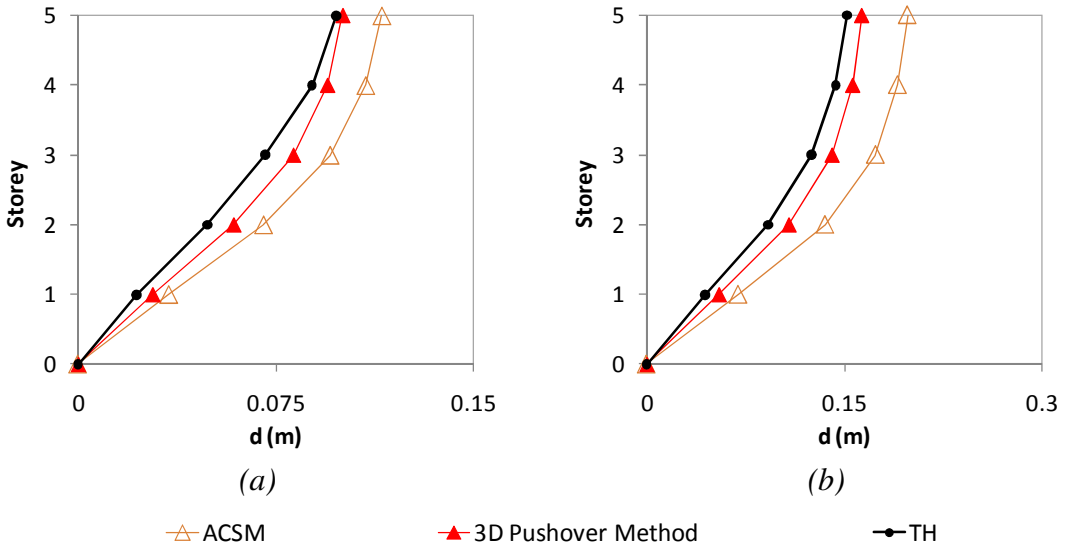

Figure A. 144 – Lateral displacement profiles, five storey building: a) column S14, X direction, 0.4g; b) column S13, X direction, 0.6g.

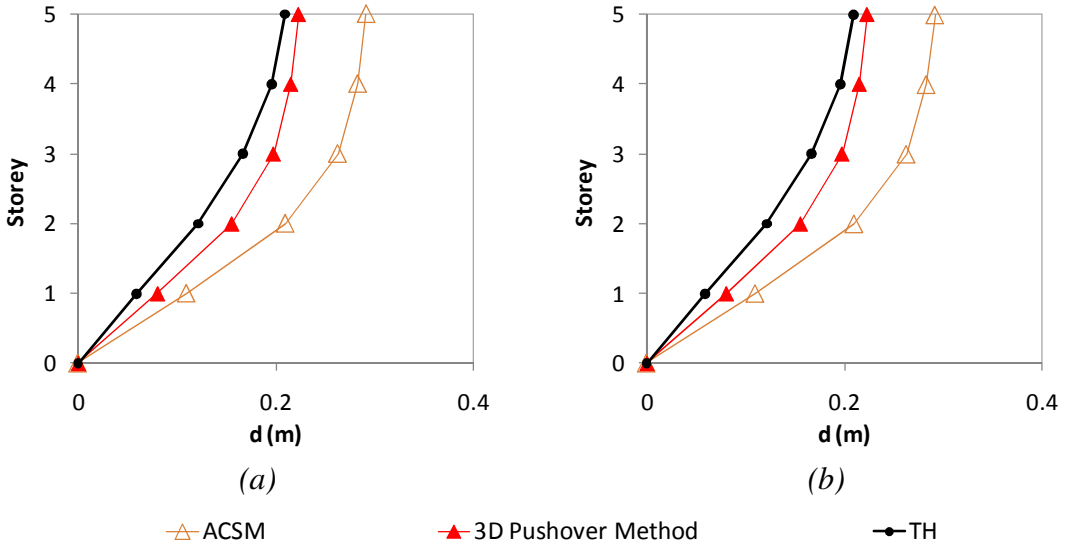

Figure A. 145 – Lateral displacement profiles, five storey building: a) column S13, X direction, 0.8g; b) column S14, X direction, 0.8g.

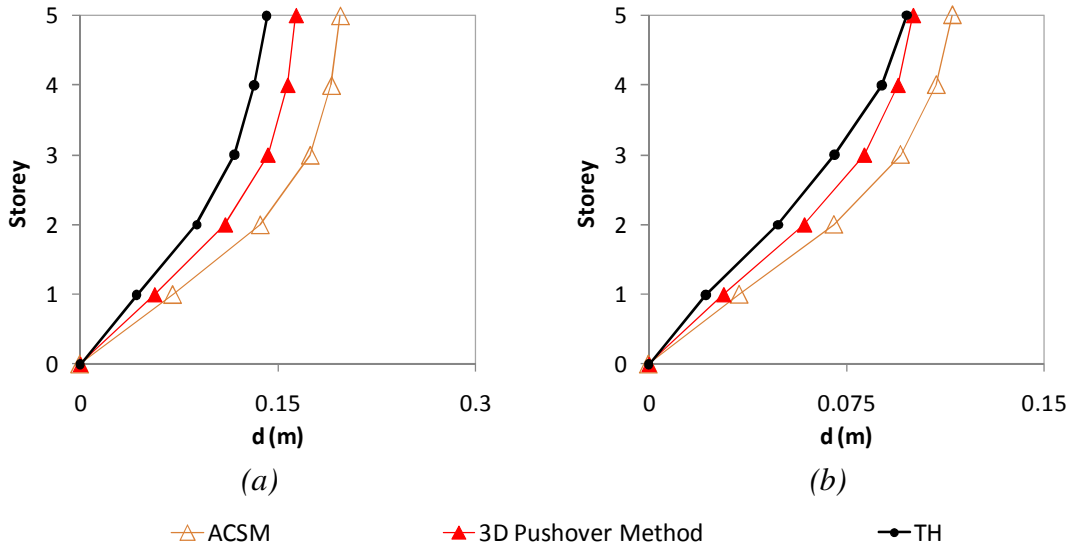

Figure A. 146 – Lateral displacement profiles, five storey building, X direction: a) column S23, 0.6g; b) column S13, 0.4g.

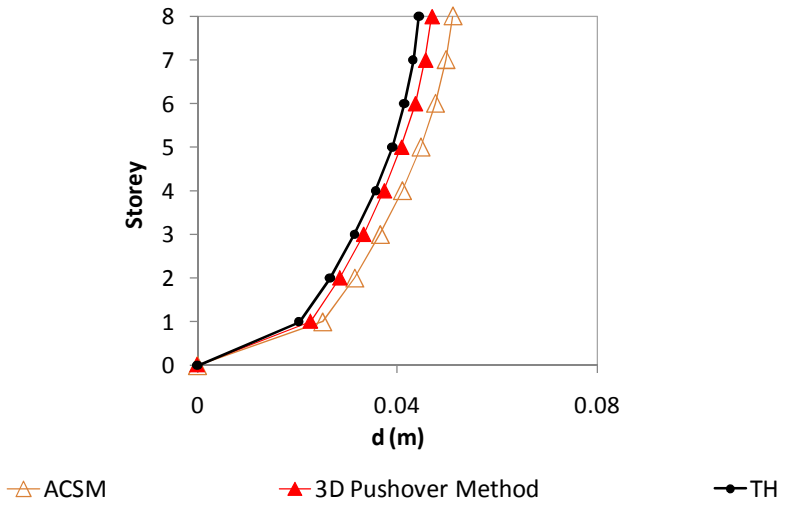

Figure A. 147 – Lateral displacement profiles, eight storey building, column S15, X direction, 0.1g.

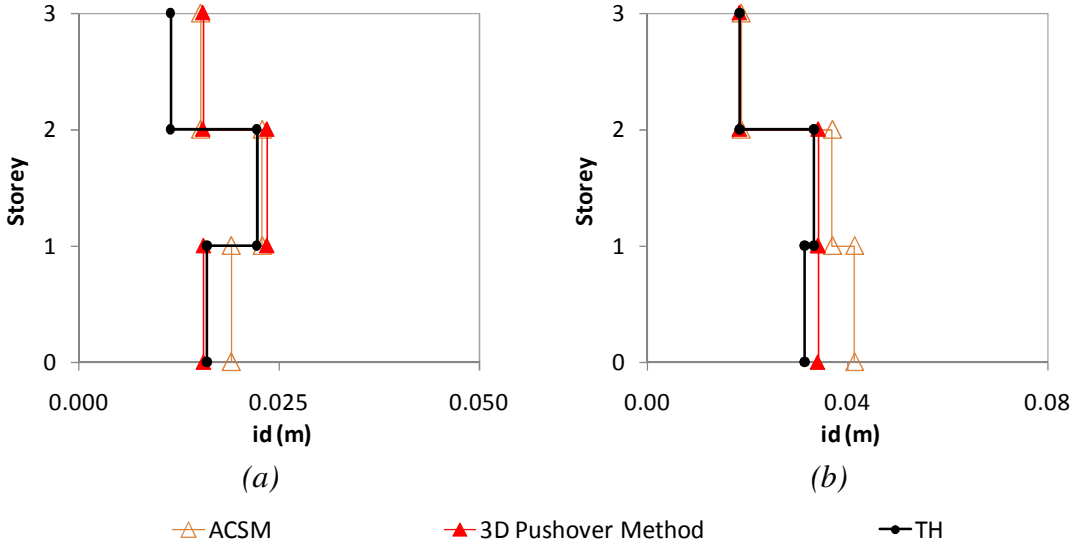

Figure A. 148 – Interstorey drifts profiles, three storey building: a) column C3, X direction, 0.1g; b) column C3, Y direction, 0.2g.

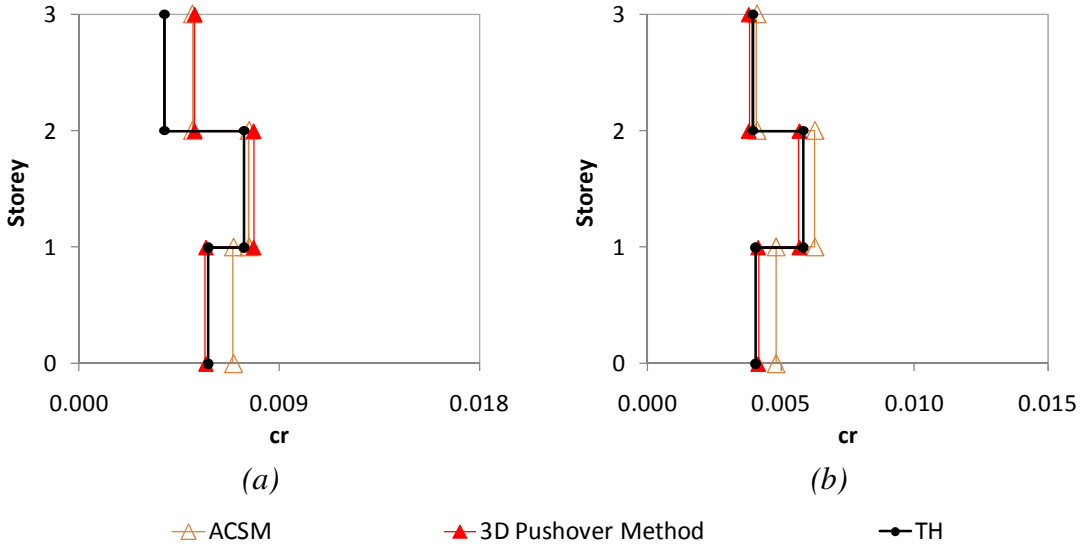

Figure A. 149 – Chord rotations profiles, three storey building: a) column C3, X direction, 0.1g; b) column C3, Y direction, 0.1g.

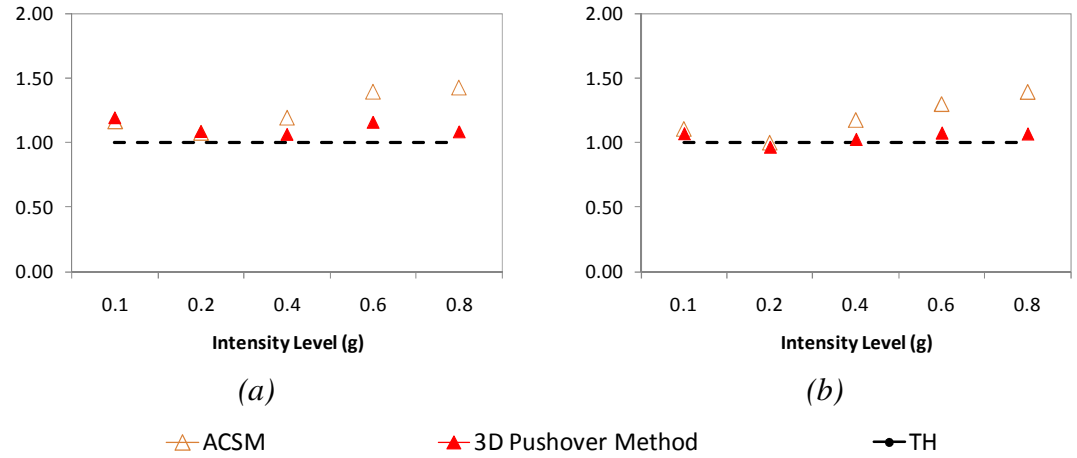

Figure A. 150 – Top displacement ratios, five storey building, X direction: a) S23; b) column S13.

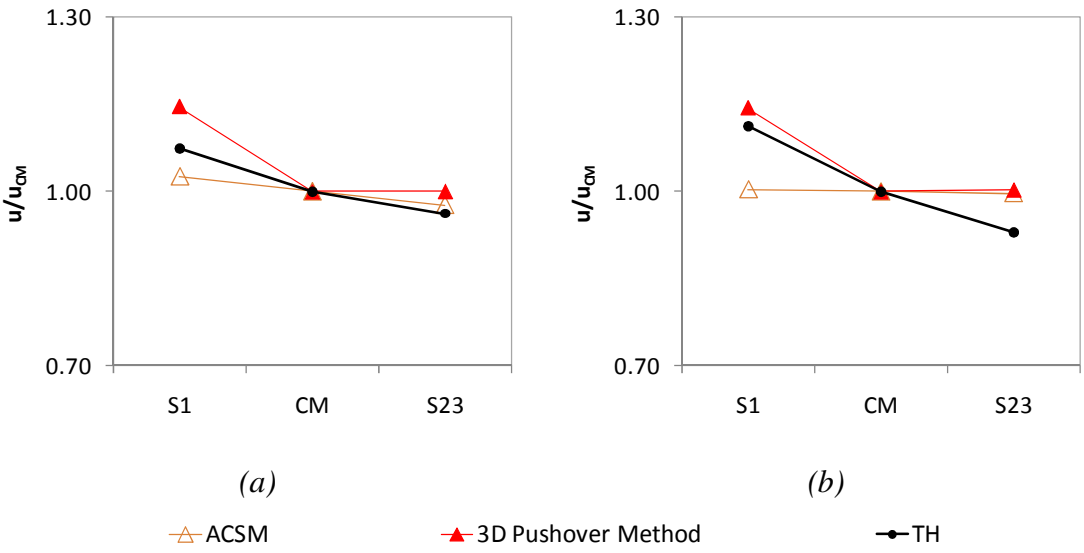

Figure A. 151 – Normalized top displacements, five storey building, X direction: a) 0.4g; b) 0.6g.

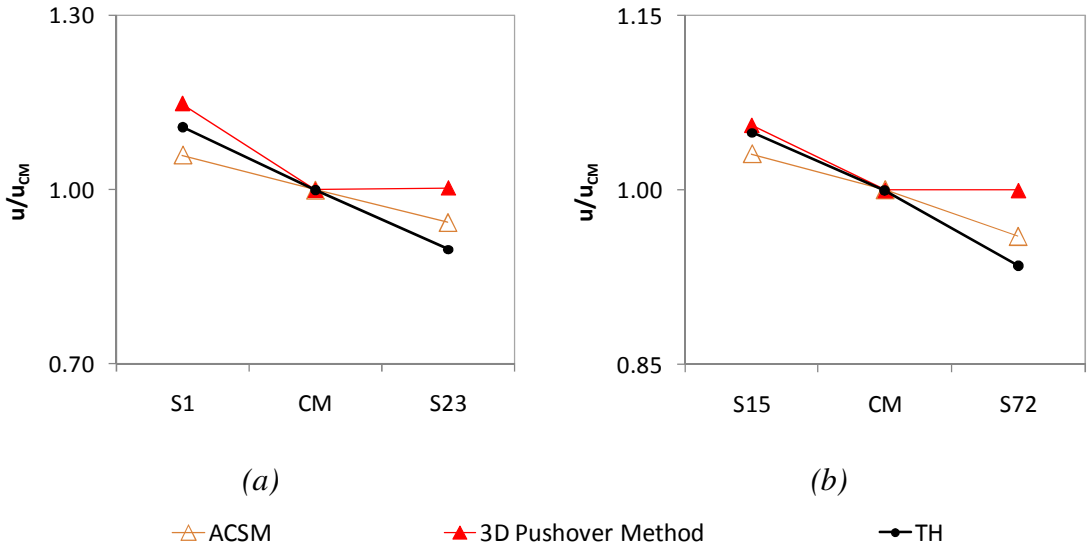

Figure A. 152 – Normalized top displacements, X direction: a) five storey building, 0.1g; b) eight storey building, 0.4g.

A17. 3D Pushover procedure *vs.* Extended N2

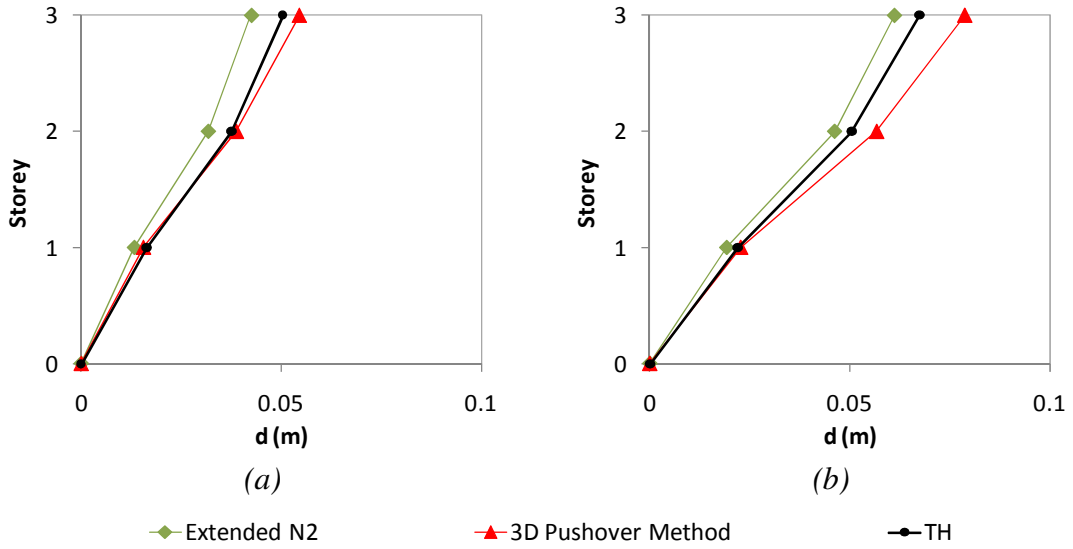

Figure A. 153 – Lateral displacement profiles, three storey building: a) column C8, X direction, 0.1g; b) column C2, X direction, 0.1g.

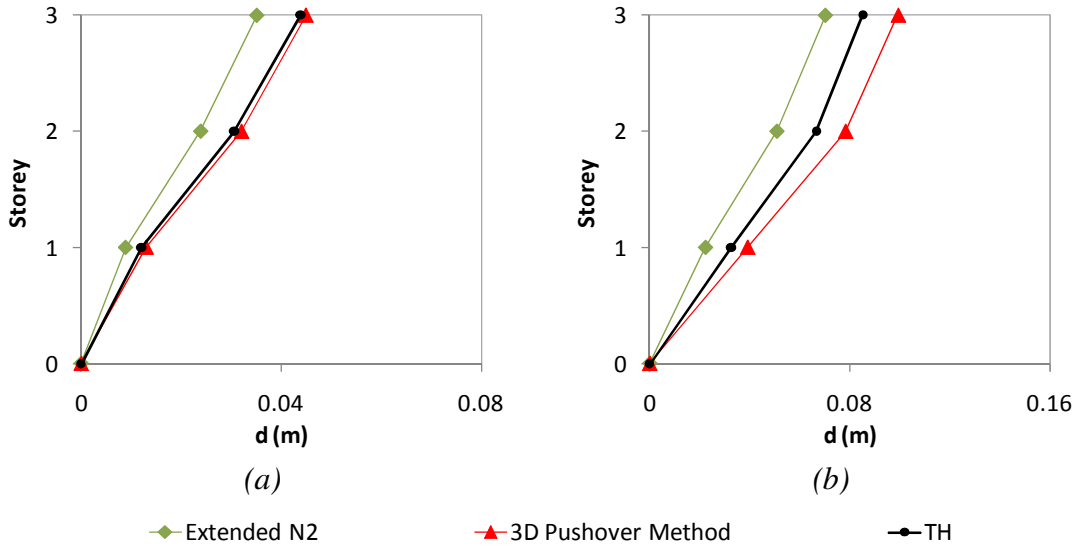

Figure A. 154 – Lateral displacement profiles, three storey building: a) column C8, Y direction, 0.1g; b) column C8, Y direction, 0.2g.

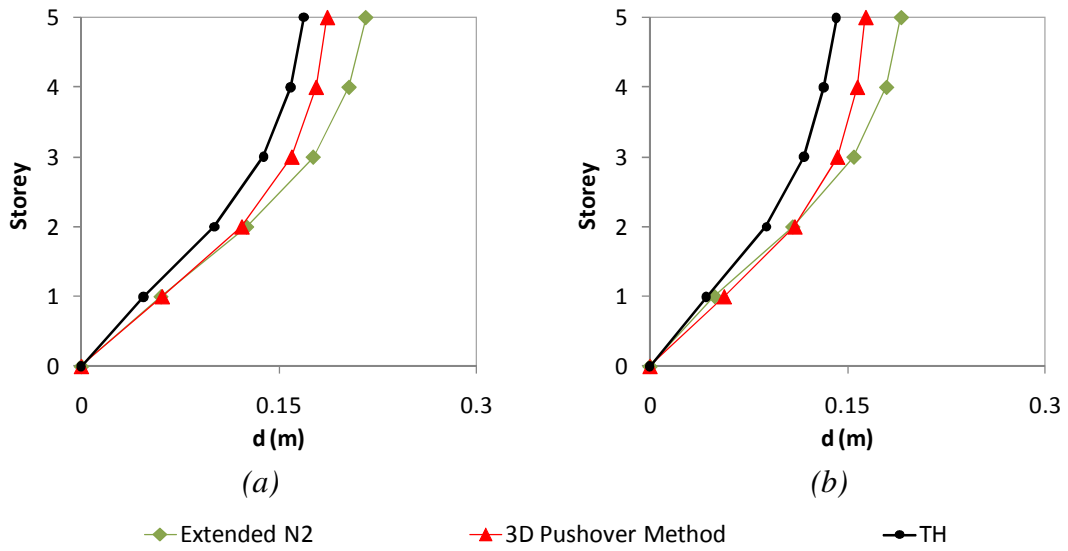

Figure A. 155 – Lateral displacement profiles, five storey building: a) column S1, X direction, 0.6g; b) column S23, X direction, 0.6g.

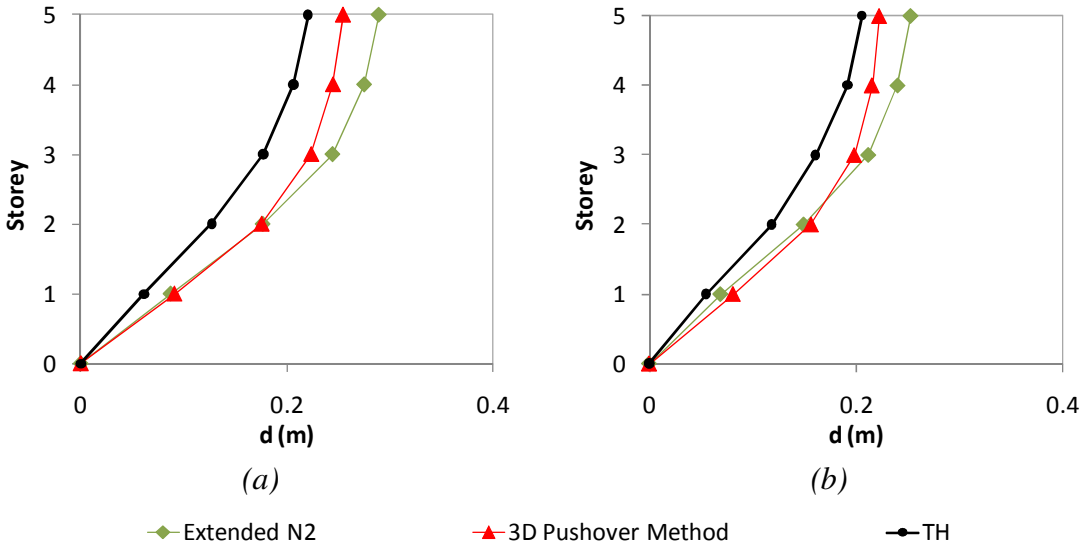

Figure A. 156 – Lateral displacement profiles, five storey building: a) column S1, X direction, 0.8g; b) column S23, X direction, 0.8g.

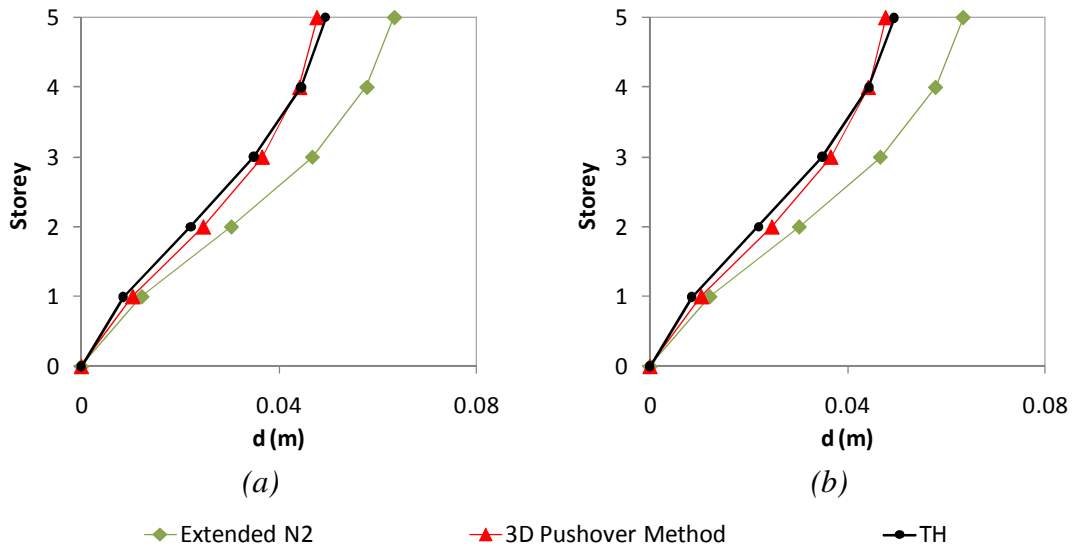

Figure A. 157 – Lateral displacement profiles, five storey building: a) column S13, X direction, 0.2g; b) column S14, X direction, 0.2g.

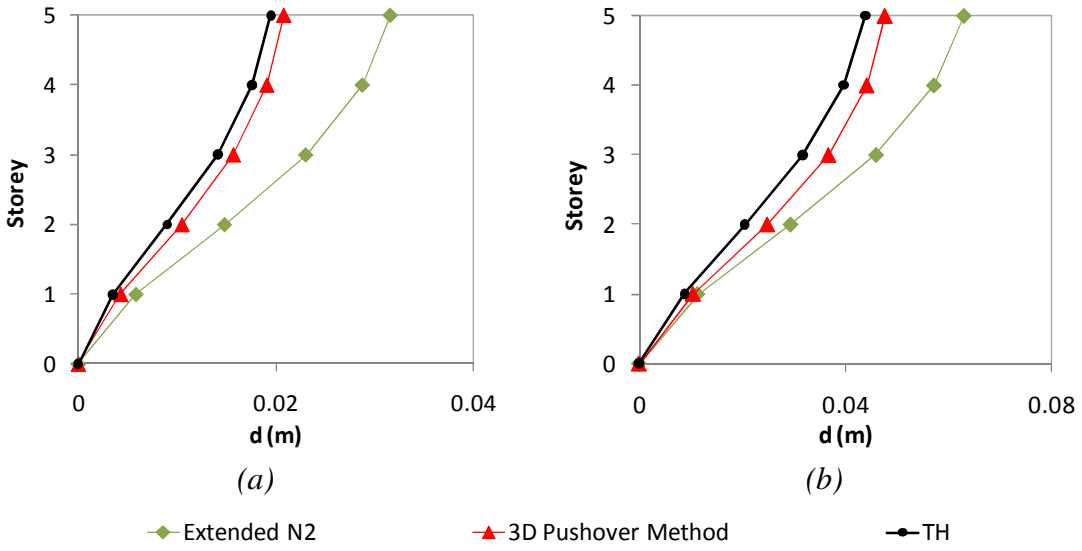

Figure A. 158 – Lateral displacement profiles, five storey building: a) column S14, X direction 0.1g; b) column S23, X direction 0.2g.

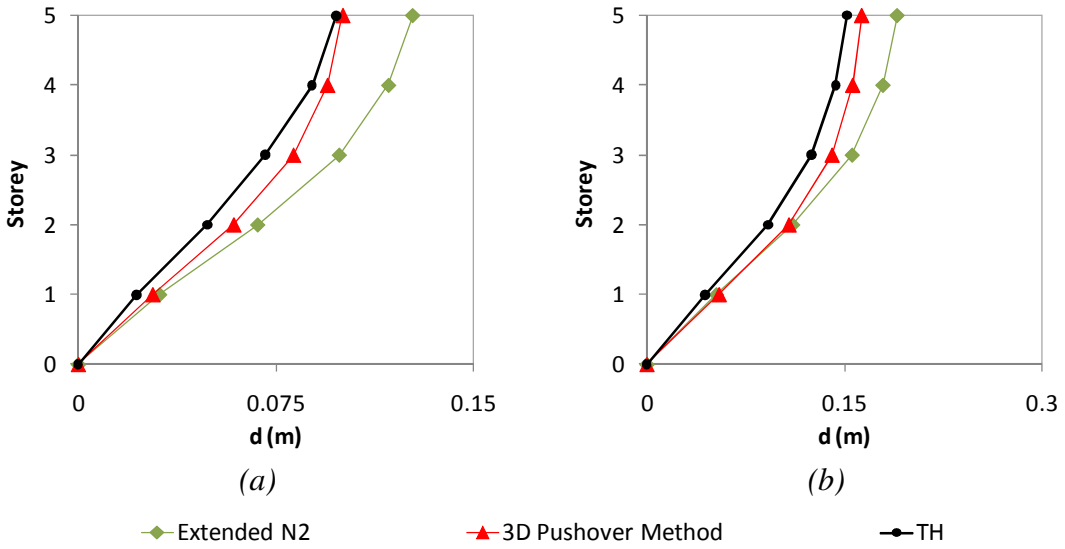

Figure A. 159 – Lateral displacement profiles, five storey building: a) column S14, X direction, 0.4g; b) column S13, X direction, 0.6g.

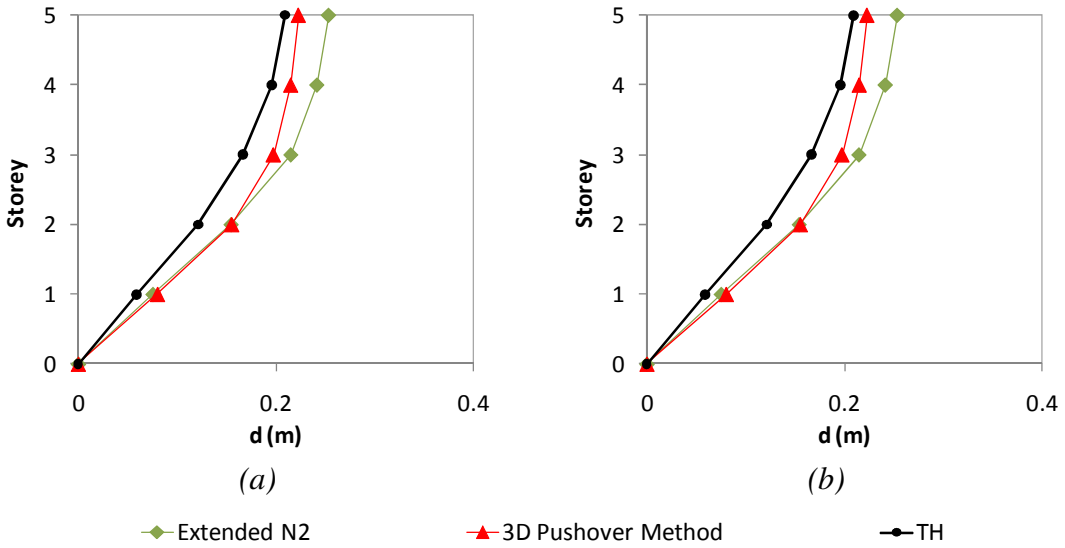

Figure A. 160 – Lateral displacement profiles, five storey building: a) column S13, X direction, 0.8g; b) column S14, X direction, 0.8g.

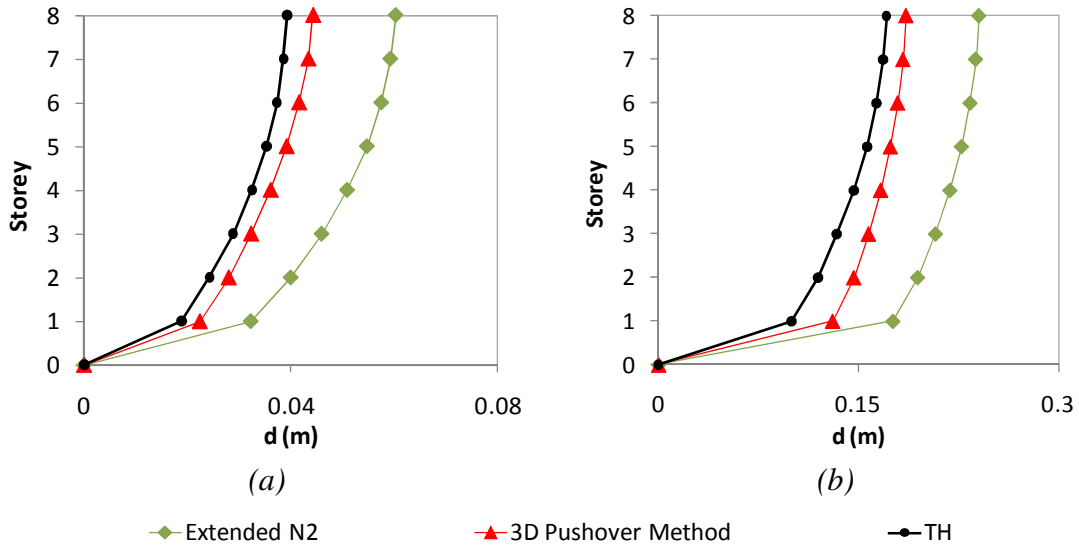

Figure A. 161 – Lateral displacement profiles, eight storey building: a) column S69, X direction, 0.1g; b) column S69, X direction, 0.4g.

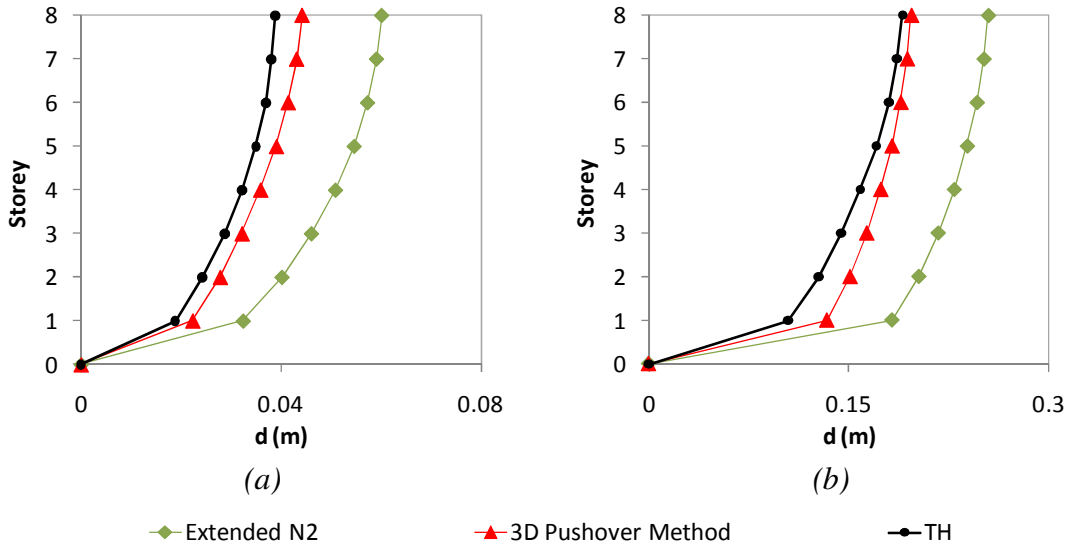

Figure A. 162 – Lateral displacement profiles, eight storey building: a) column S72, X direction, 0.1g; b) column S15, X direction, 0.4g.

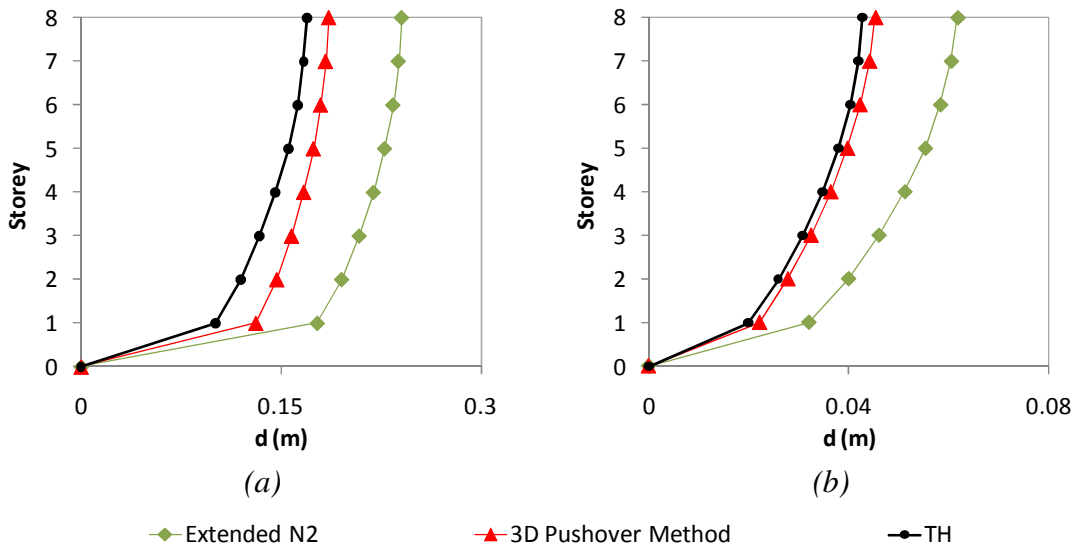

Figure A. 163 – Lateral displacement profiles, eight storey building: a) column S72, X direction, 0.4g; b) column S23, X direction, 0.1g.

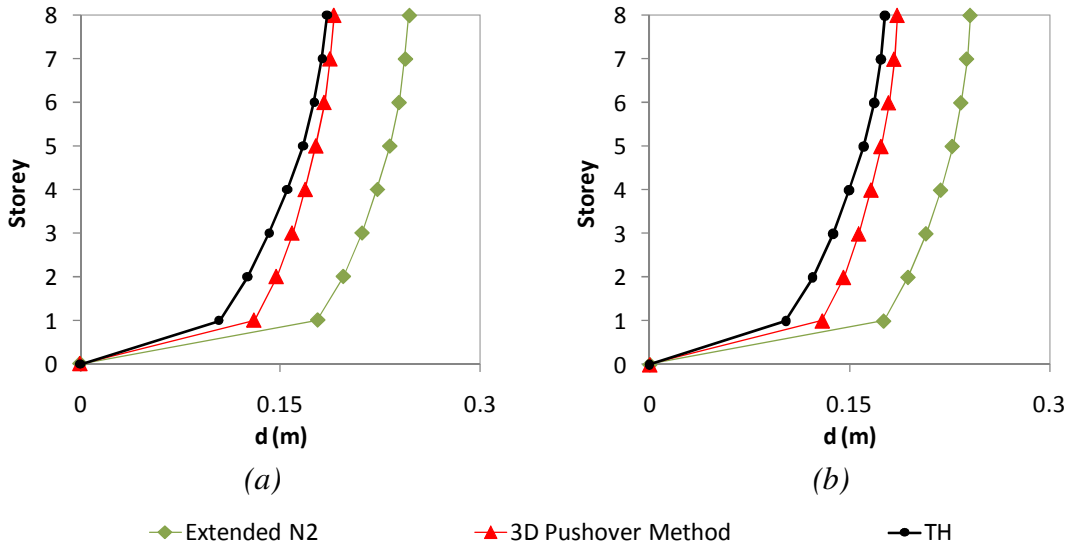

Figure A. 164 – Lateral displacement profiles, eight storey building: a) column S23, X direction, 0.4g; b) column S52, X direction, 0.4g.

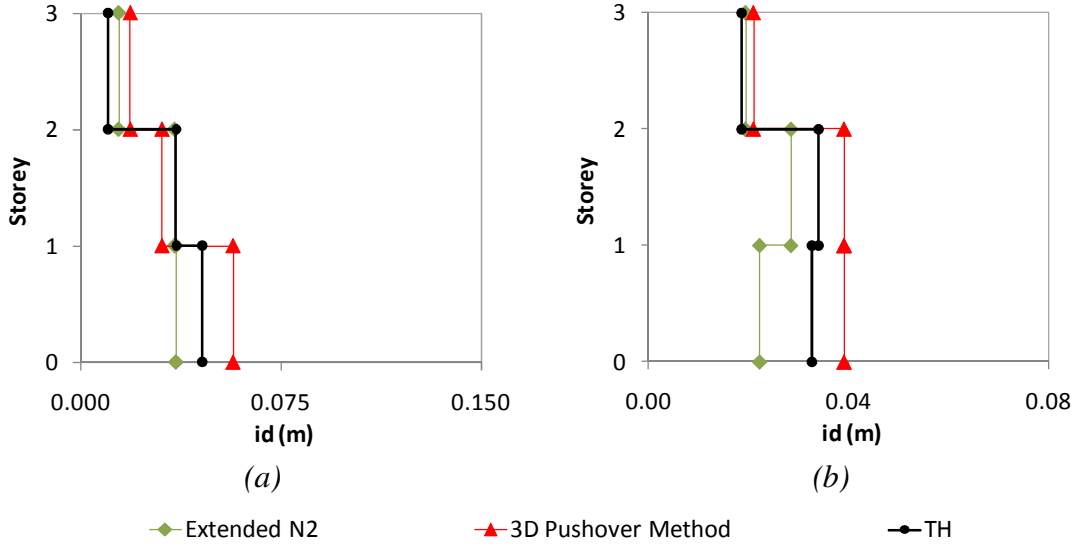

Figure A. 165 – Inter storey drifts profiles, three storey building: a) column C2, X direction, 0.2g; b) column C8, Y direction, 0.2g.

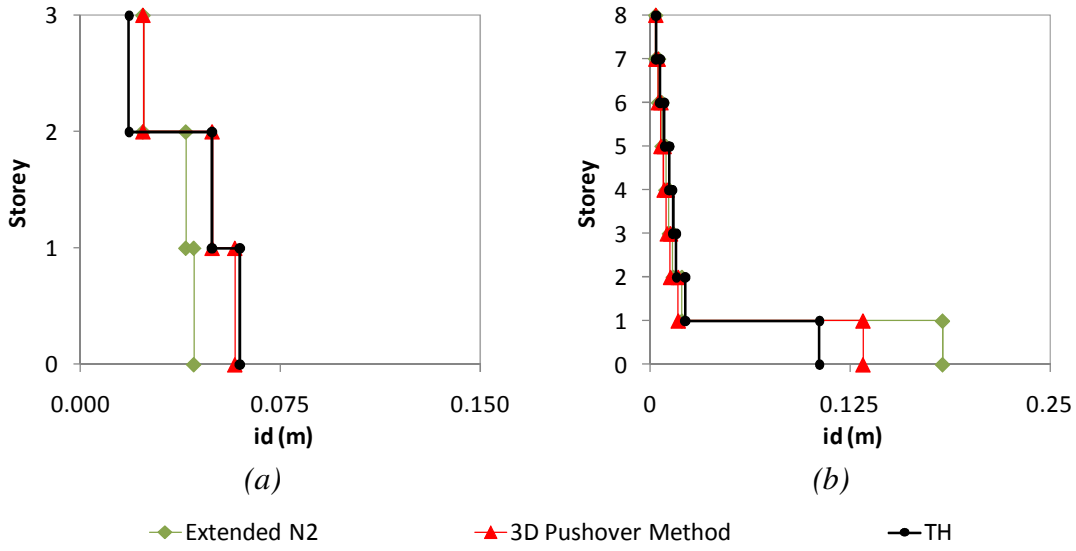

Figure A. 166 – Interstorey drifts profiles: a) three storey building, column C8, Y direction, 0.3g; b) eight storey building, column S9, X direction 0.4g.

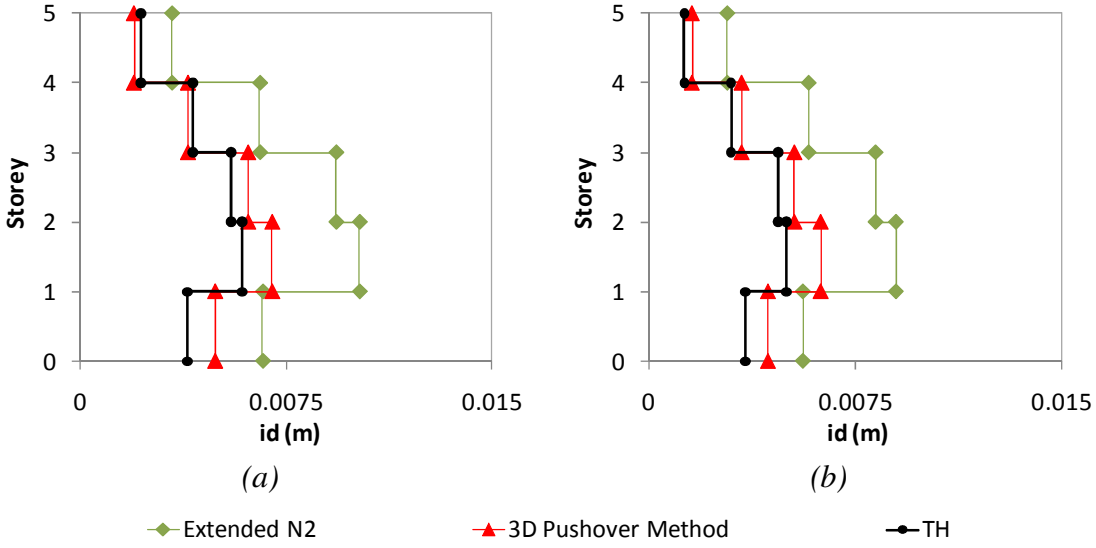

Figure A. 167 – Inter storey drifts profiles, five storey building: a) column S1, X direction, 0.1g; b) column S23, X direction, 0.1g.

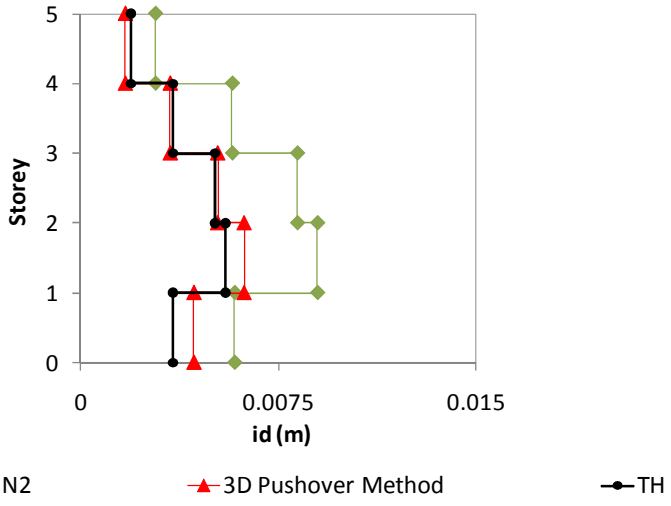

Figure A. 168 – Inter storey drifts profiles, five storey building, column S14, X direction, 0.1g.

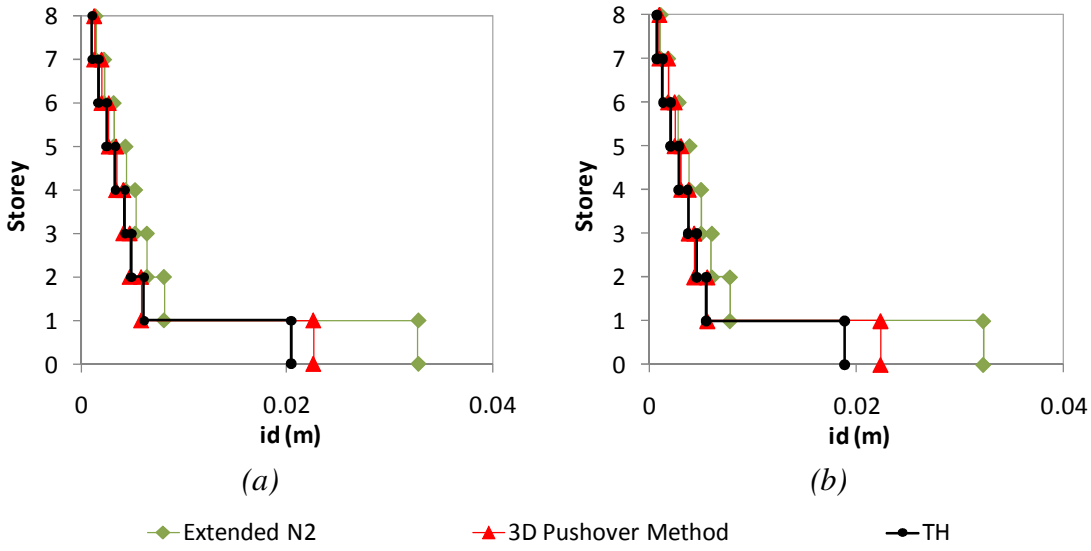

Figure A. 169 – Inter storey drifts profiles, eight storey building: a) column S9, X direction, 0.1g; b) column S69, X direction, 0.1g.

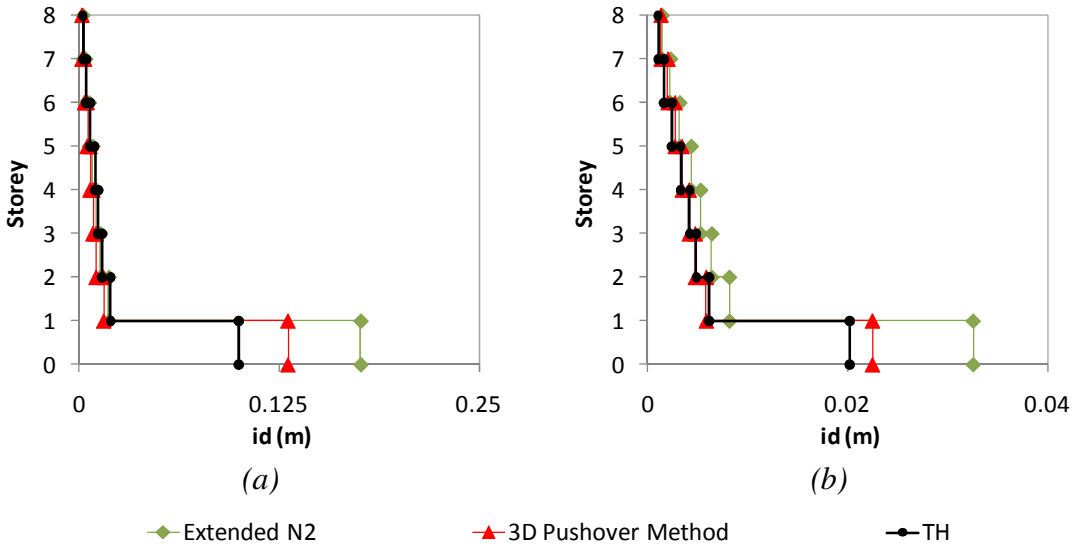

Figure A. 170 – Inter storey drifts profiles, eight storey building: a) column S69, X direction, 0.4g; b) column S15, X direction, 0.1g.

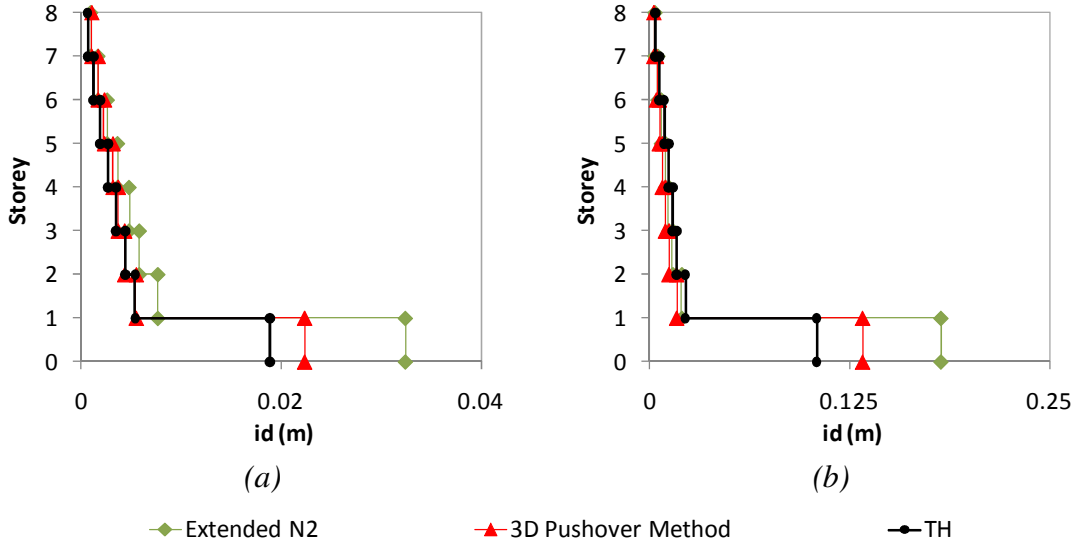

Figure A. 171 – Inter storey drifts profiles, eight storey building: a) column S72, X direction, 0.1g; b) column S15, X direction, 0.4g.

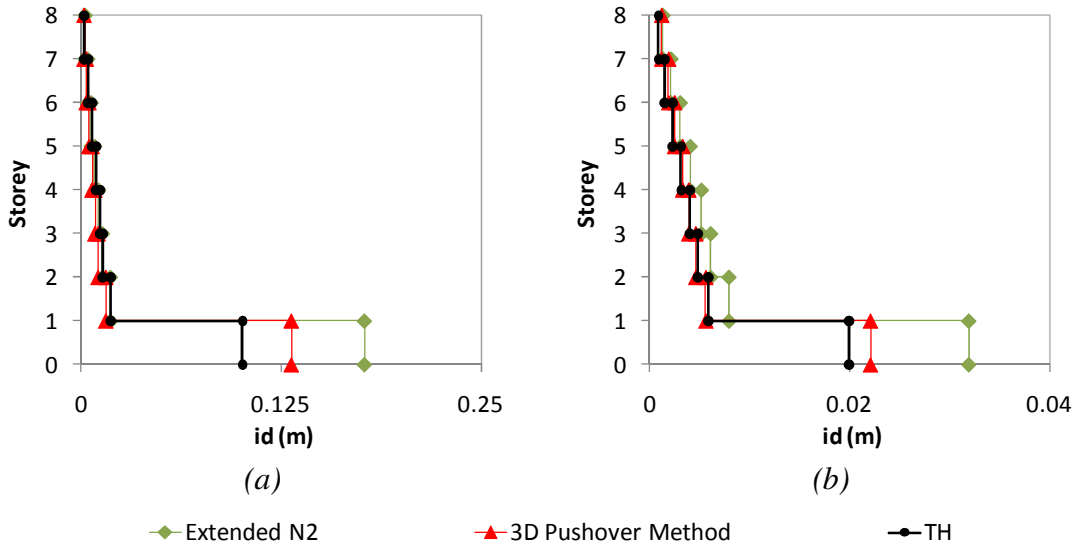

Figure A. 172 – Inter storey drifts profiles, eight storey building: a) column S72, X direction, 0.4g; b) column S23, X direction, 0.1g.

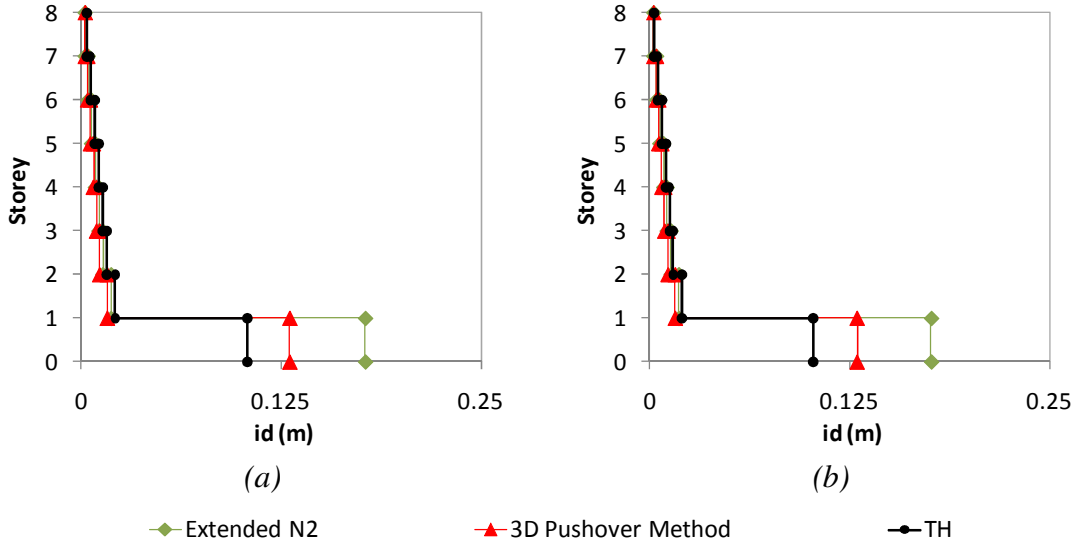

Figure A. 173 – Inter storey drifts profiles, eight storey building: a) column S23, X direction, 0.4g; b) column S52, X direction, 0.4g.

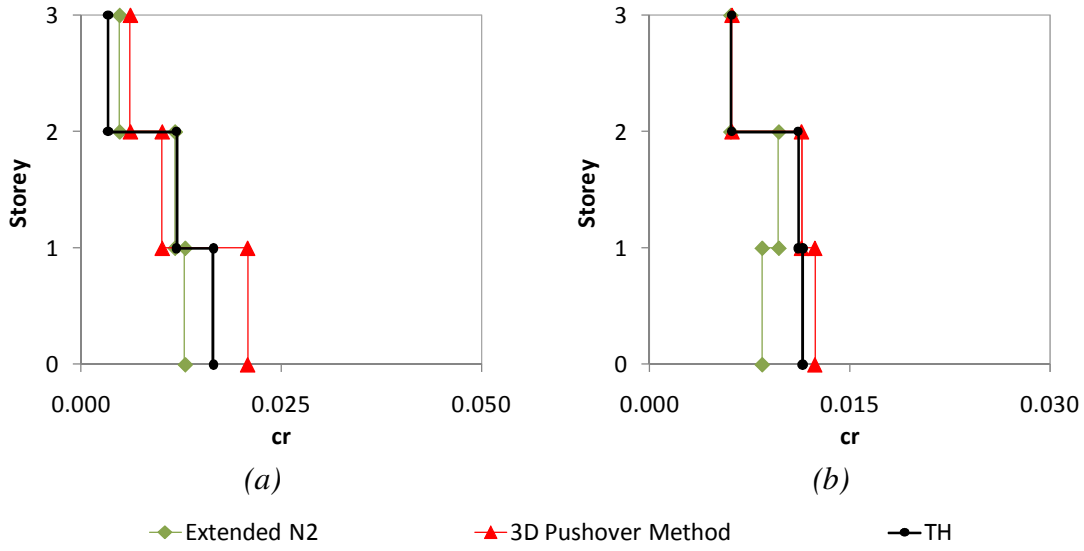

Figure A. 174 – Chord rotations profiles, three storey building: a) column C3, X direction, 0.2g; b) column C3, Y direction, 0.2g.

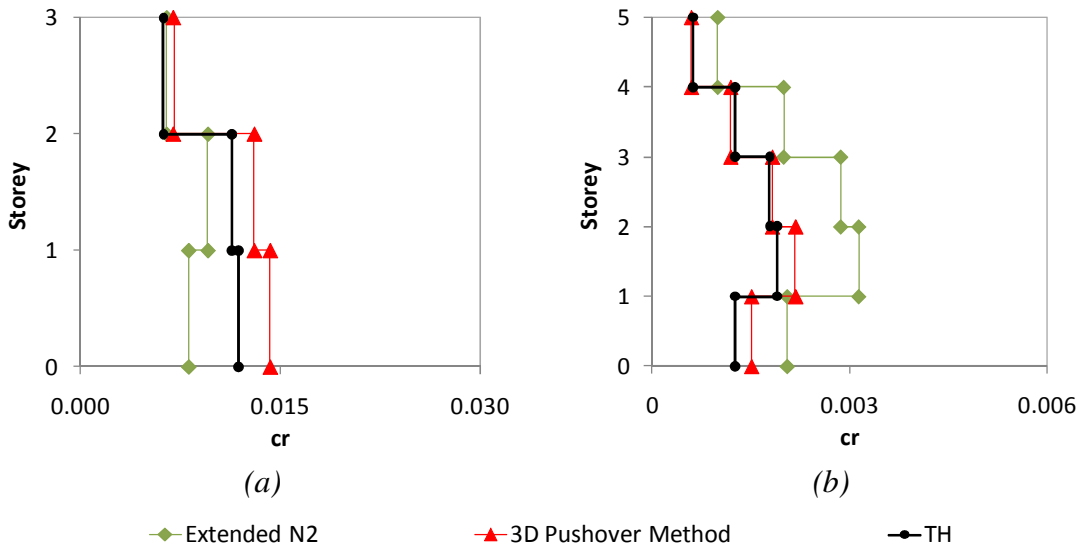

Figure A. 175 – Chord rotations profiles: a) three storey building, column C8, Y direction, 0.2g; b) five storey building, column S13, X direction, 0.1g.

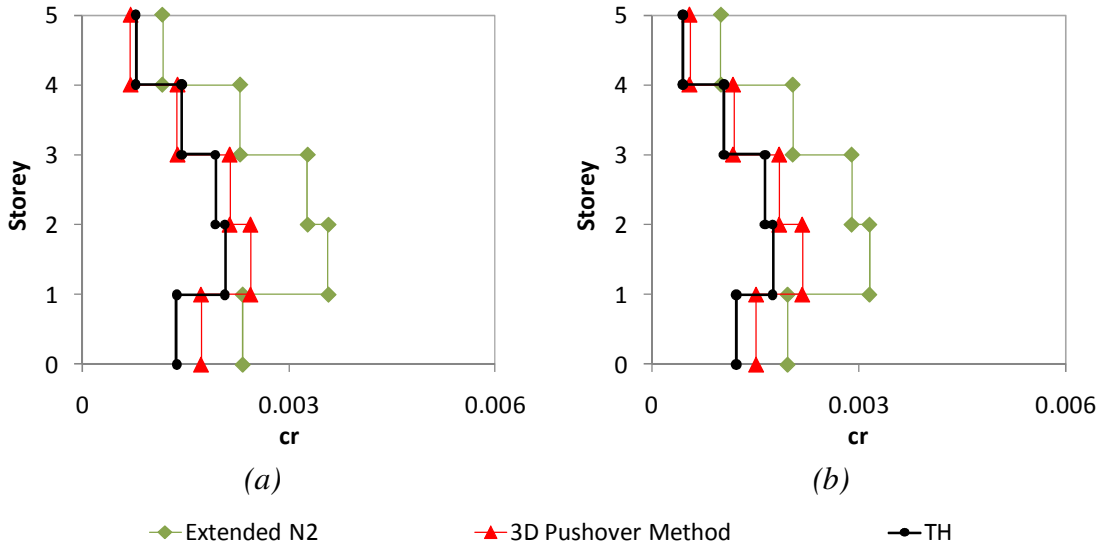

Figure A. 176 – Chord rotations profiles, five storey building: a) column S1, X direction, 0.1g; b) column S23, X direction, 0.1g.

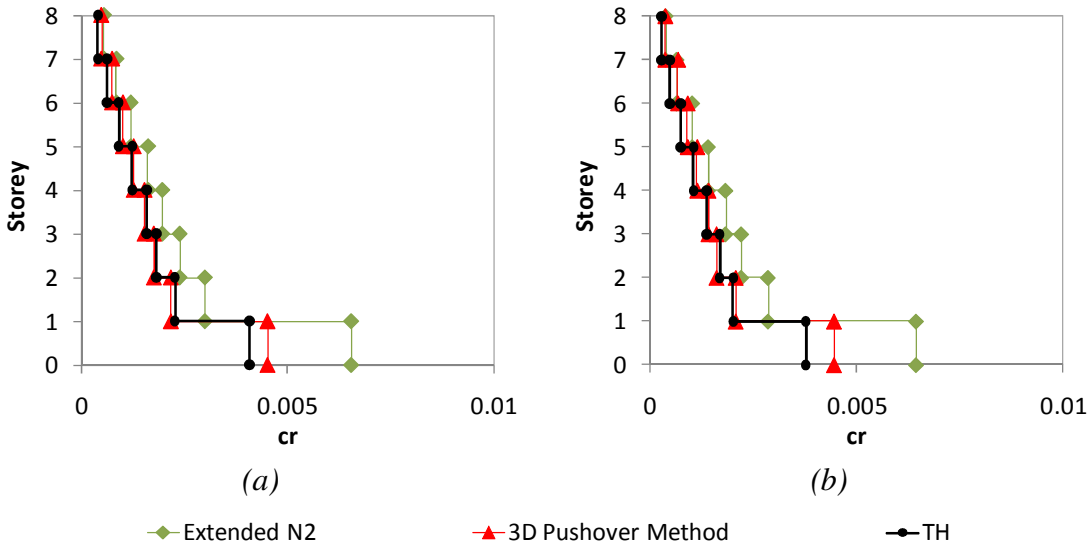

Figure A. 177 – Chord rotations profiles, eight storey building: a) column S9, X direction, 0.1g; b) column S69, X direction, 0.1g.

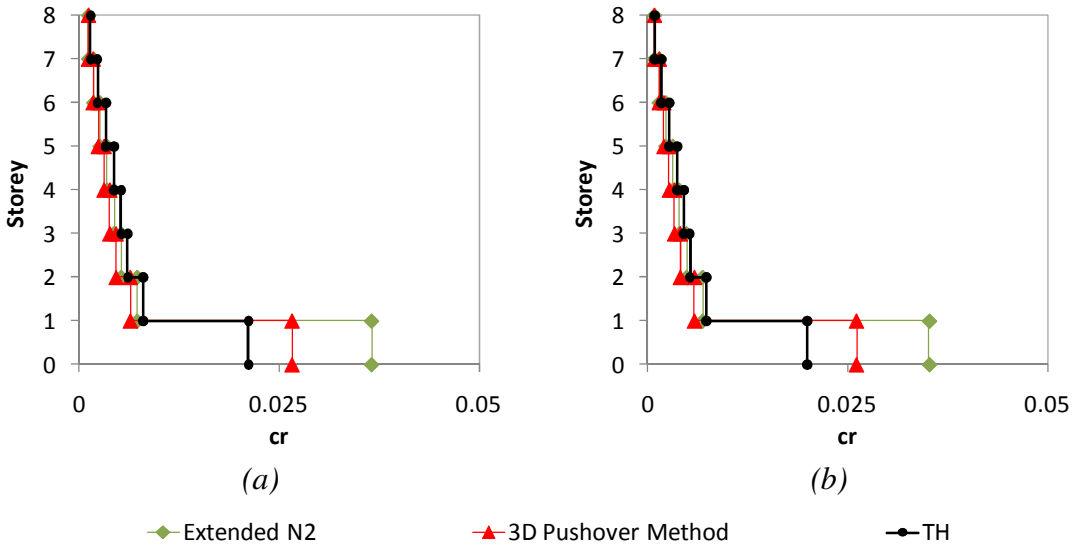

Figure A. 178 – Chord rotations profiles, eight storey building: a) column S9, X direction, 0.4g; b) column S69, X direction, 0.4g.

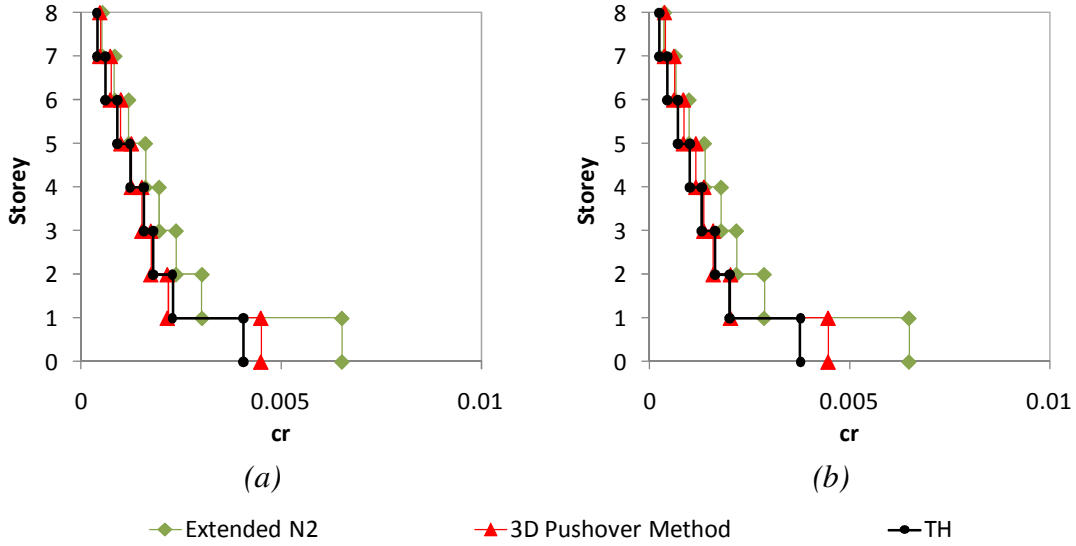

Figure A. 179 – Chord rotations profiles, eight storey building: a) column S15, X direction, 0.1g; b) column S72, X direction, 0.1g.

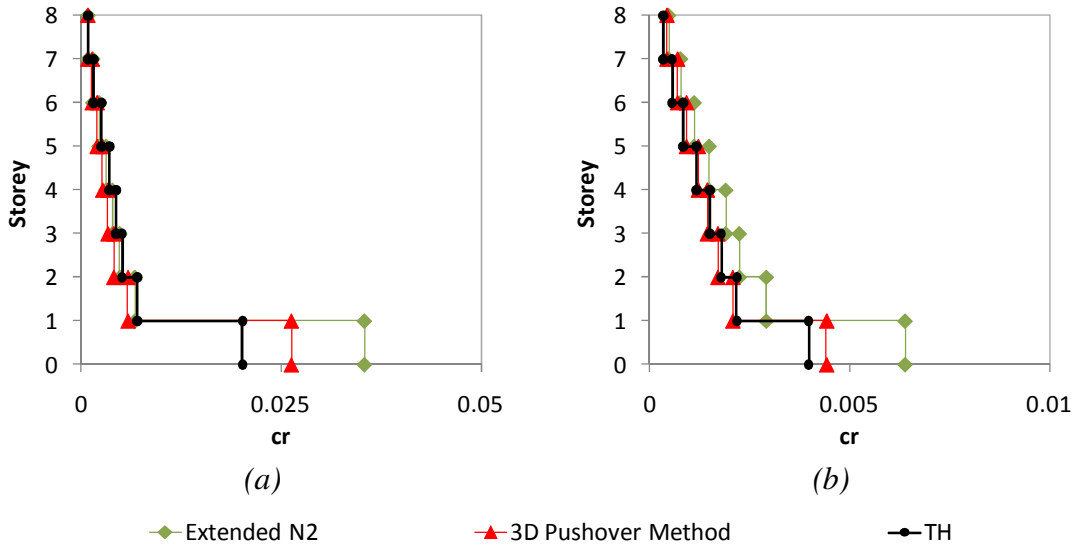

Figure A. 180 – Chord rotations profiles, eight storey building: a) column S72, X direction, 0.4g; b) column S23, X direction, 0.1g.

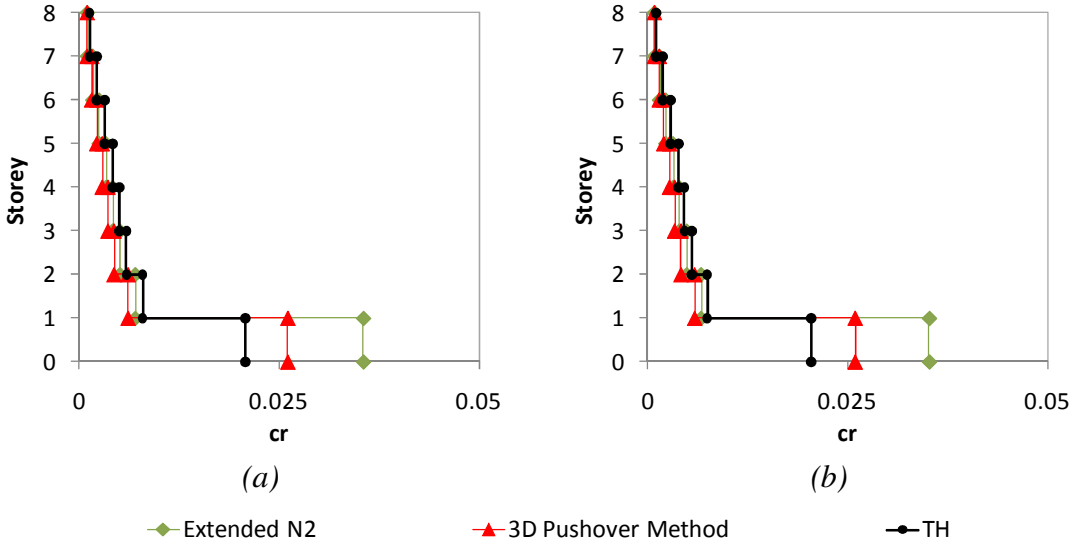

Figure A. 181 – Chord rotations profiles, eight storey building: a) column S23, X direction, 0.4g; b) column S52, X direction, 0.4g.

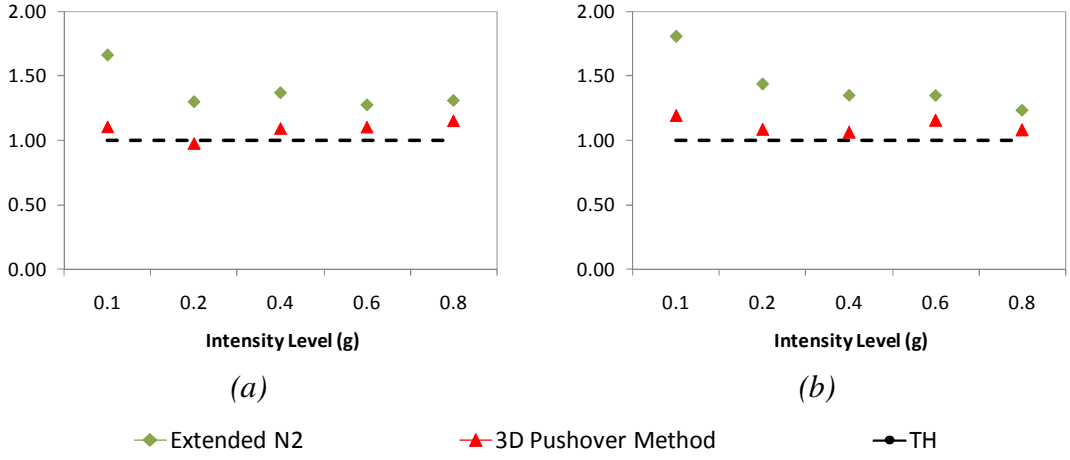

Figure A. 182 – Top displacements ratios five storey building, X direction: a) column S1; b) column S23.

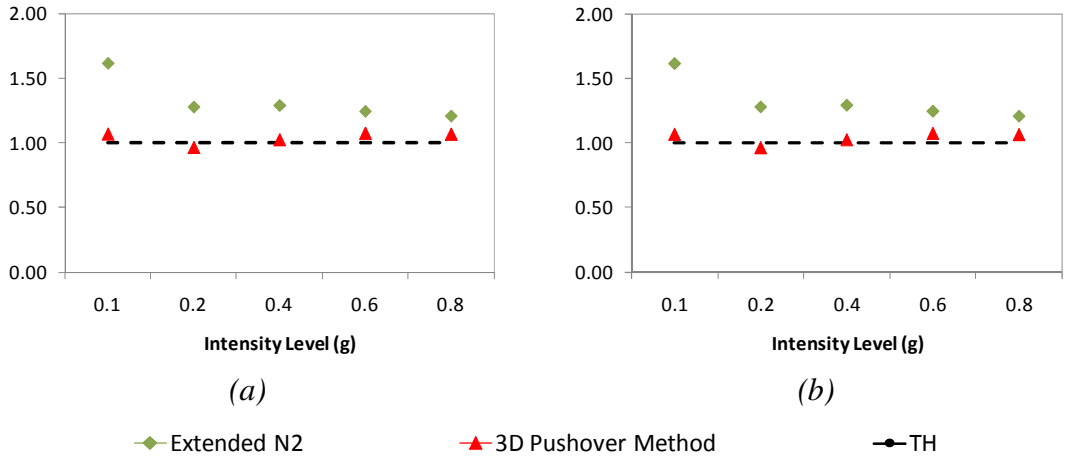

Figure A. 183 – Top displacements ratios, five storey building, X direction: a) column S13; b) column S14.

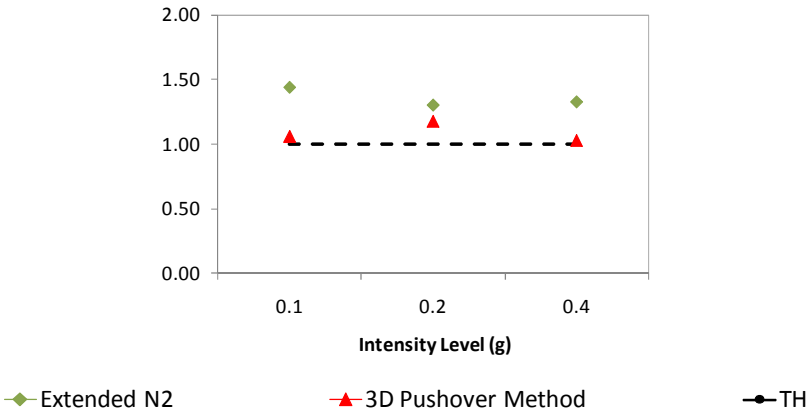

Figure A. 184 – Top displacements ratios eight storey building, X direction, CM.

A18. 3D Pushover procedure *vs.* MPA

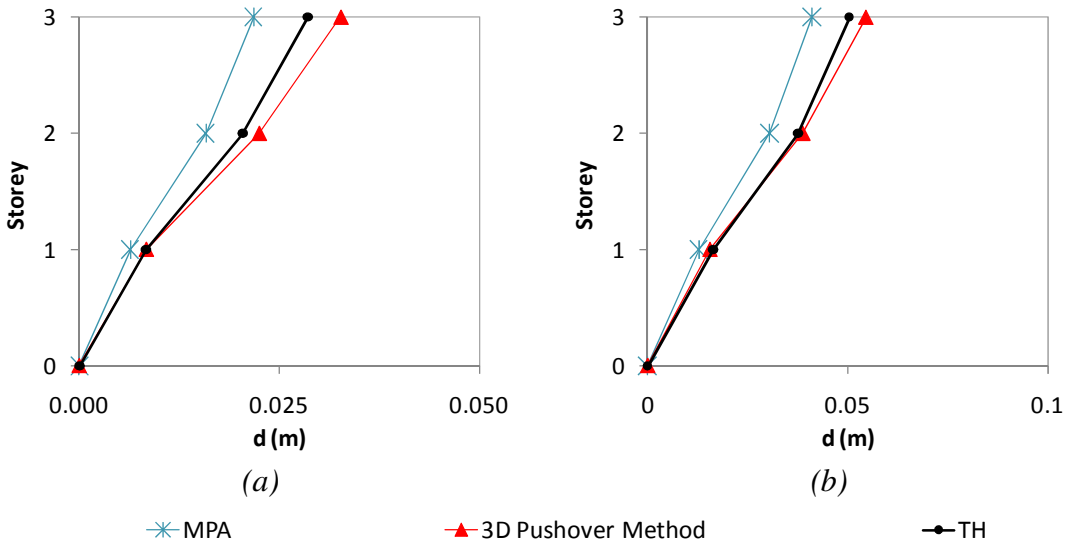

Figure A. 185 – Lateral displacement profiles, three storey building: a) column C2, X direction 0.05g; b) column C8, X direction 0.1g.

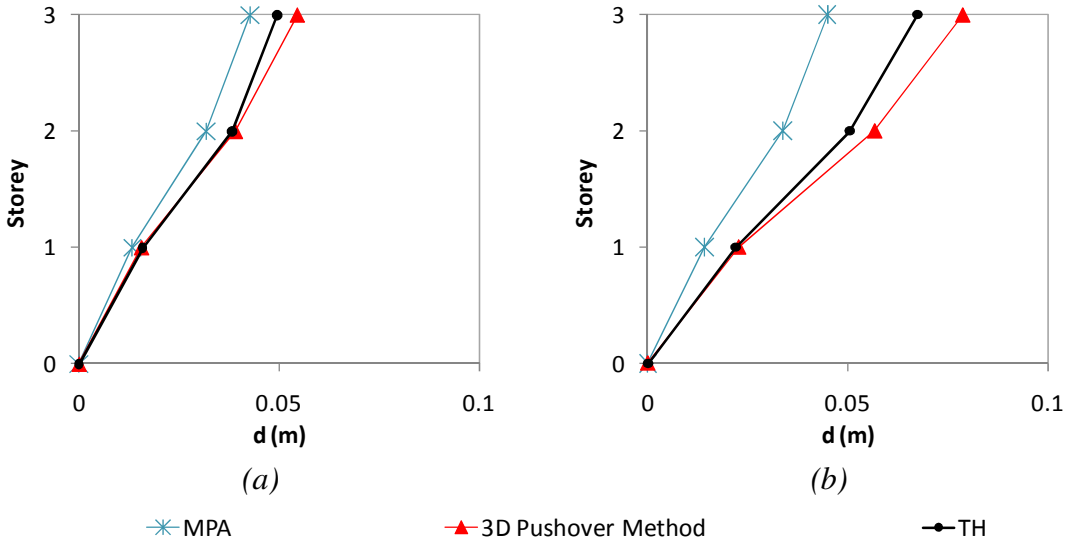

Figure A. 186 – Lateral displacement profiles, three storey building: a) column C3, X direction 0.1g; b) column C2, X direction 0.1g.

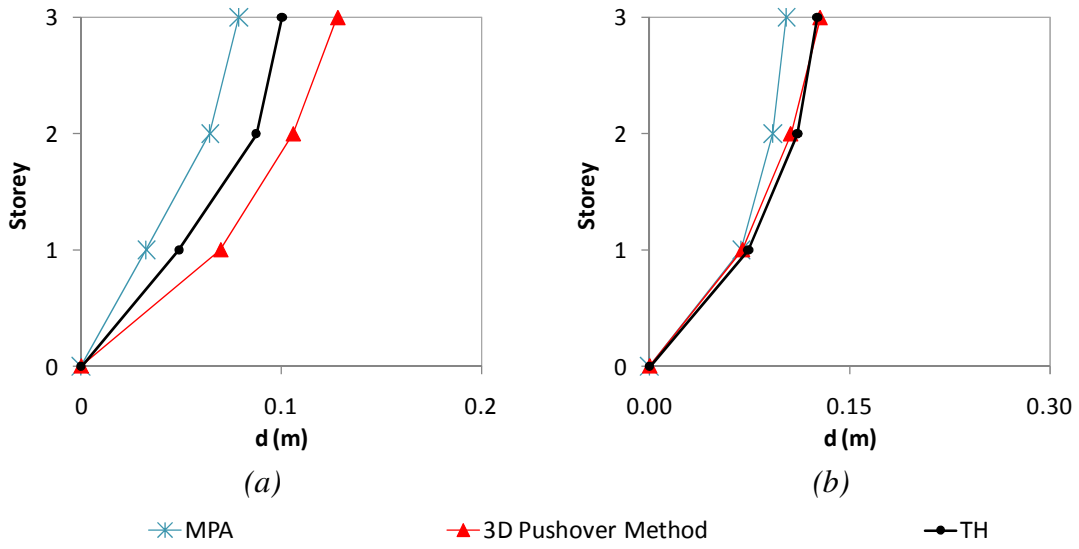

Figure A. 187 – Lateral displacement profiles, three storey building: a) column C8, X direction 0.2g; b) column C8, X direction 0.3g.

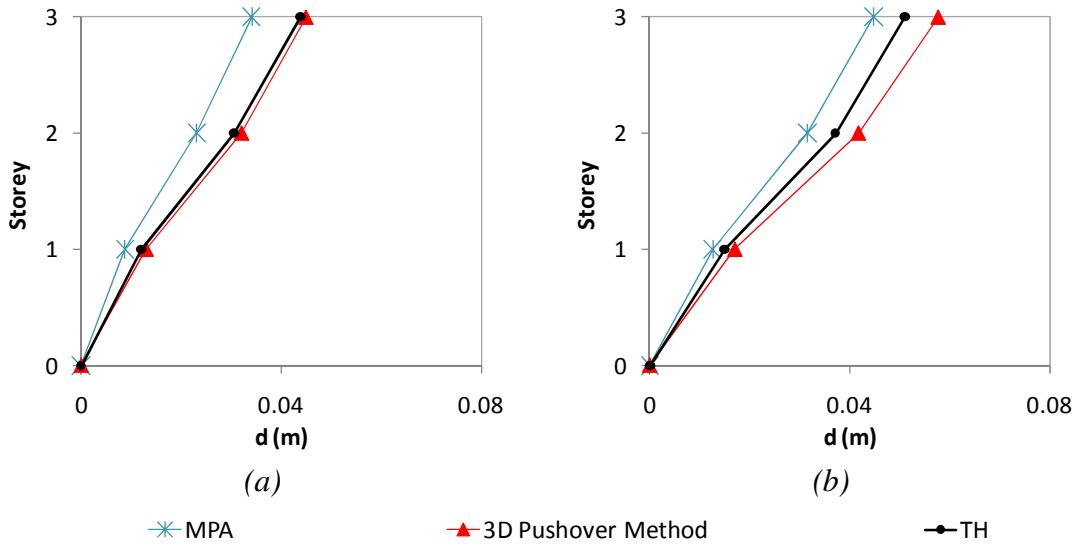

Figure A. 188 – Lateral displacement profiles, three storey building: a) column C8, Y direction 0.1g; b) column C2, Y direction 0.1g.

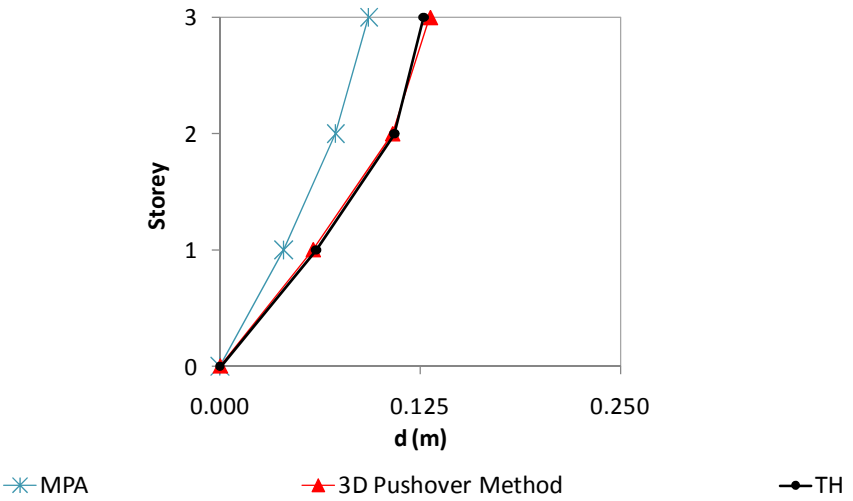

Figure A. 189 – Lateral displacement profiles, three storey building, column C8, Y direction 0.3g.

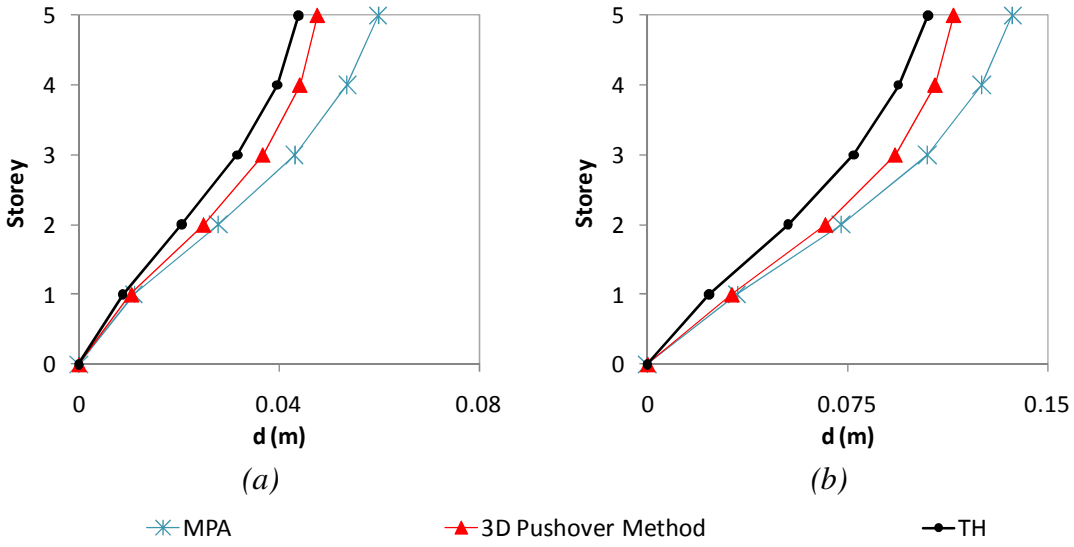

Figure A. 190 – Lateral displacement profiles, five storey building: a) column S23, X direction 0.2g; b) column S1, X direction 0.4g.

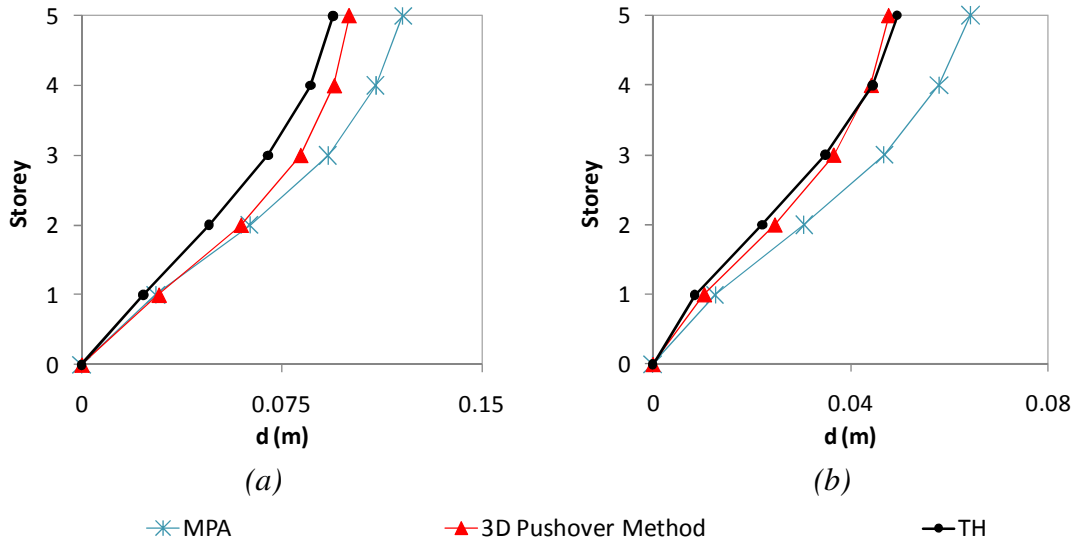

Figure A. 191 – Lateral displacement profiles, five storey building: a) column S23, X direction 0.4g; b) column S13, X direction 0.2g.

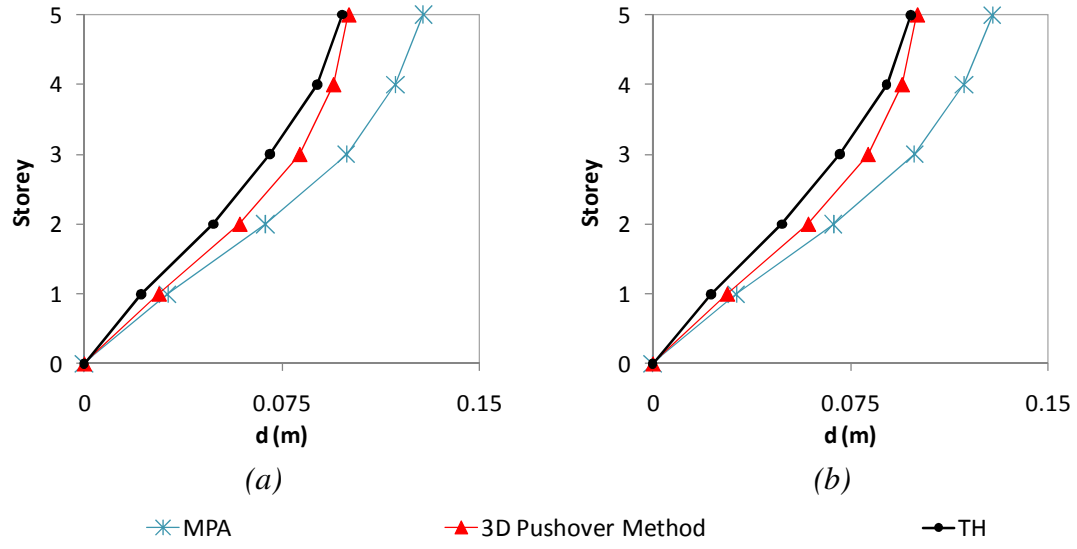

Figure A. 192 – Lateral displacement profiles, five storey building: a) column S13, X direction 0.4g; b) column S14, X direction 0.4g.

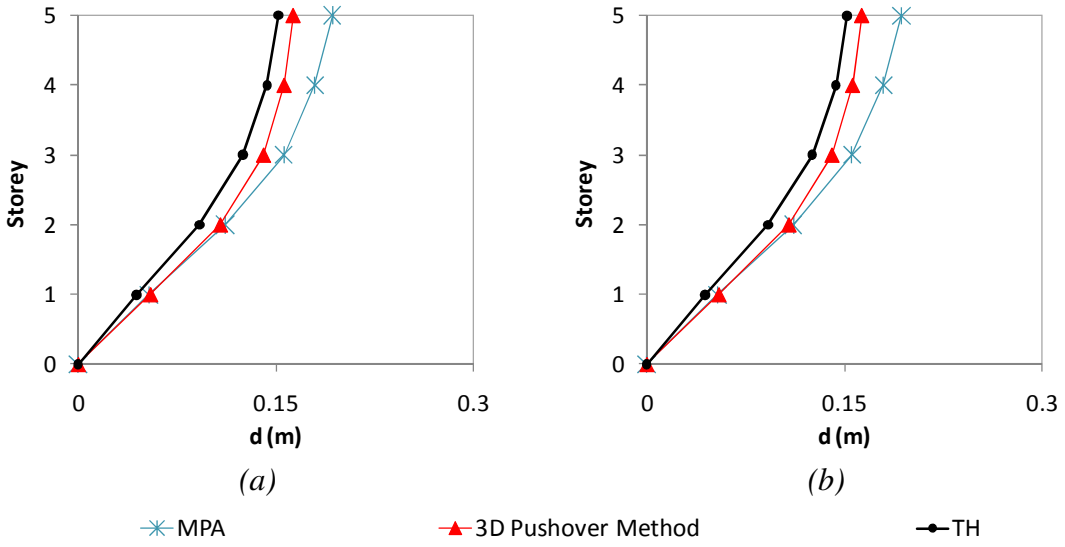

Figure A. 193 – Lateral displacement profiles, five storey building: a) column S13, X direction 0.6g; b) column S14, X direction 0.6g.

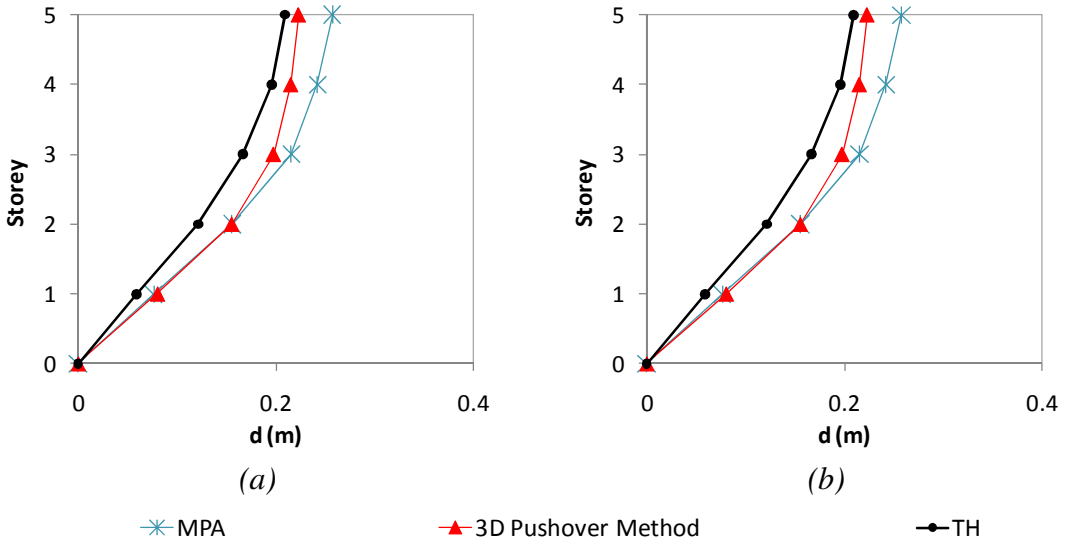

Figure A. 194 – Lateral displacement profiles, five storey building: a) column S13, X direction 0.8g; b) column S14, X direction 0.8g.

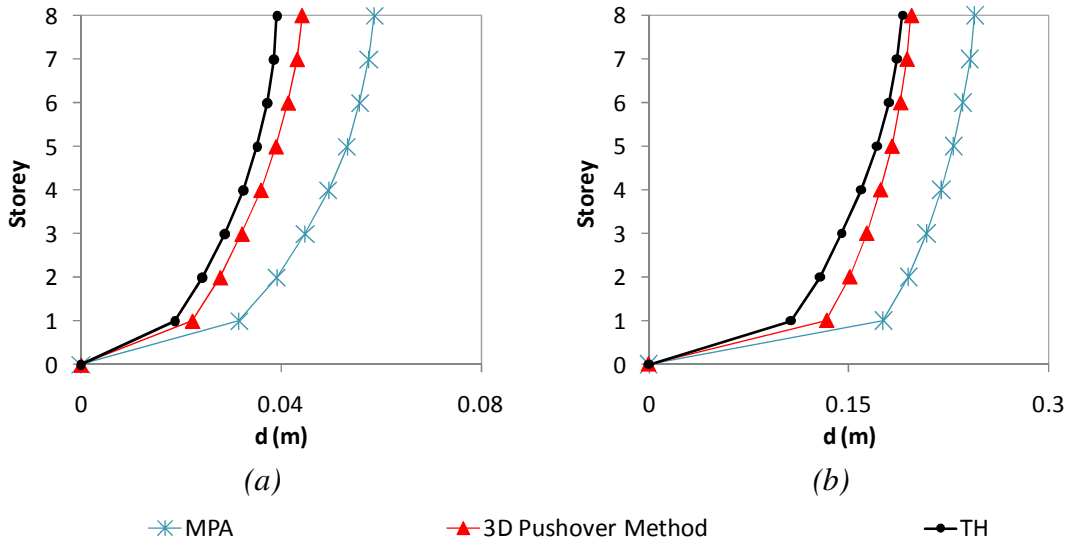

Figure A. 195 – Lateral displacement profiles, eight storey building: a) column S69, X direction 0.1g; b) column S9, X direction 0.4g.

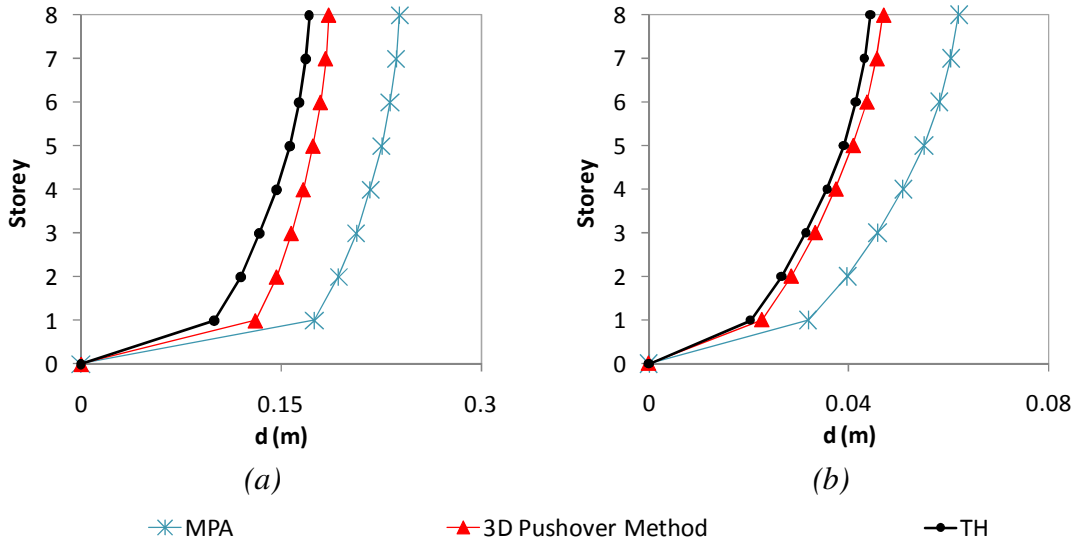

Figure A. 196 – Lateral displacement profiles, eight storey building: a) column S69, X direction 0.4g; b) column 15, X direction 0.1g.

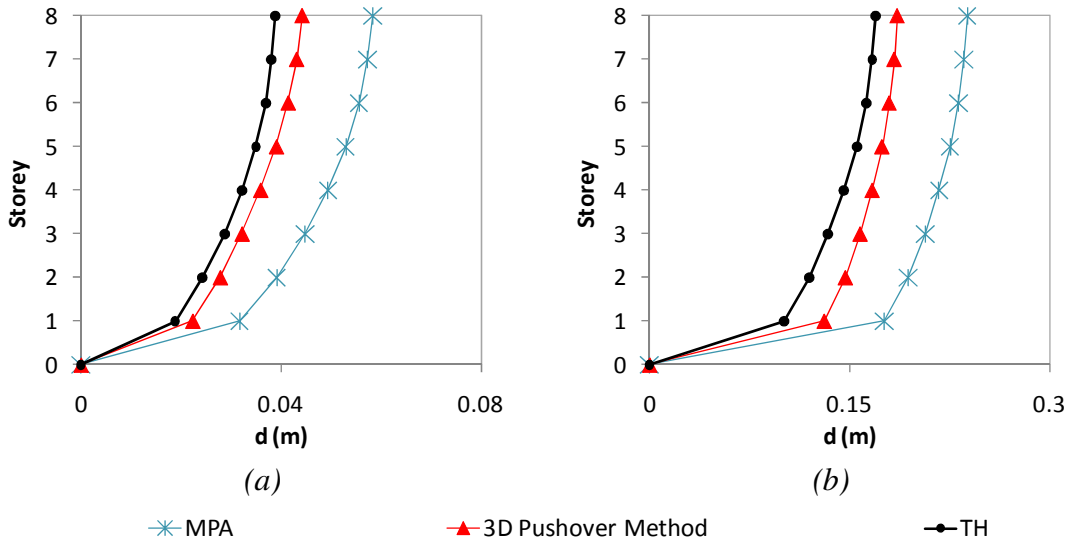

Figure A. 197 – Lateral displacement profiles, eight storey building: a) column S72, X direction 0.1g; b) column S72, X direction 0.4g.

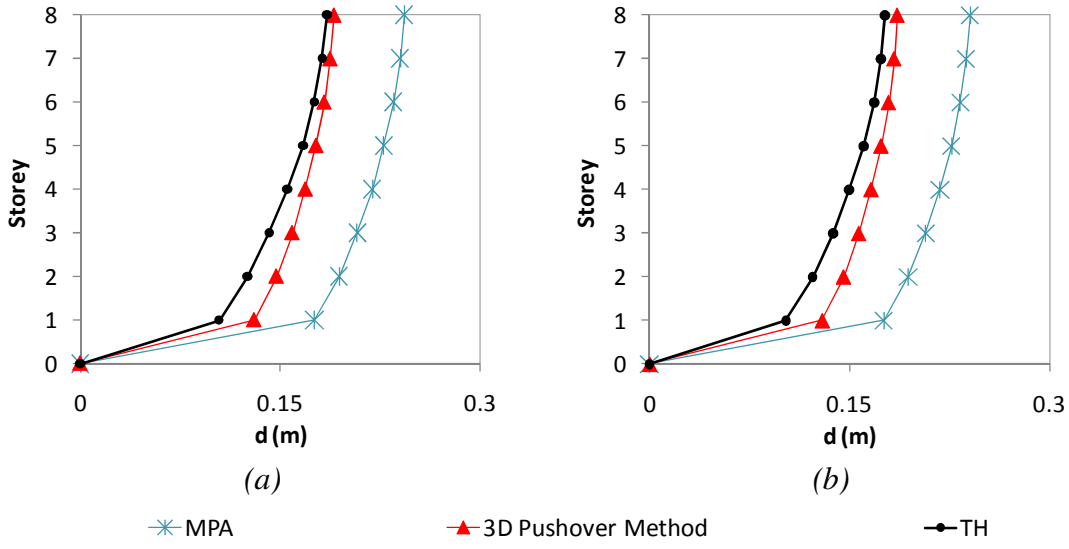

Figure A. 198 – Lateral displacement profiles, eight storey building: a) column S23, X direction 0.4g; b) column S52, X direction 0.4g.

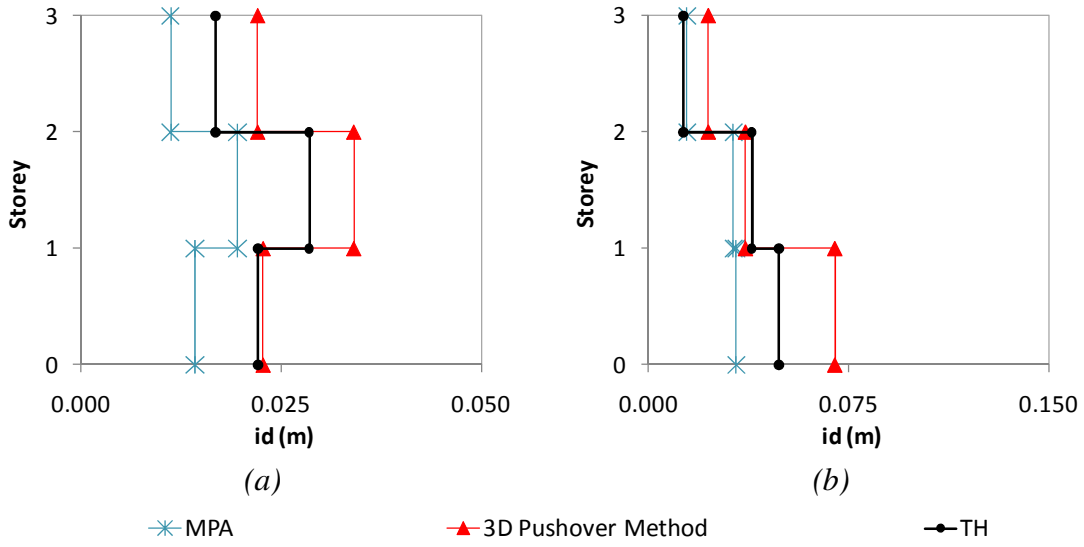

Figure A. 199 – Interstorey drifts profiles, three storey building: a) column C2, X direction, 0.1g; b) column C8, X direction, 0.2g.

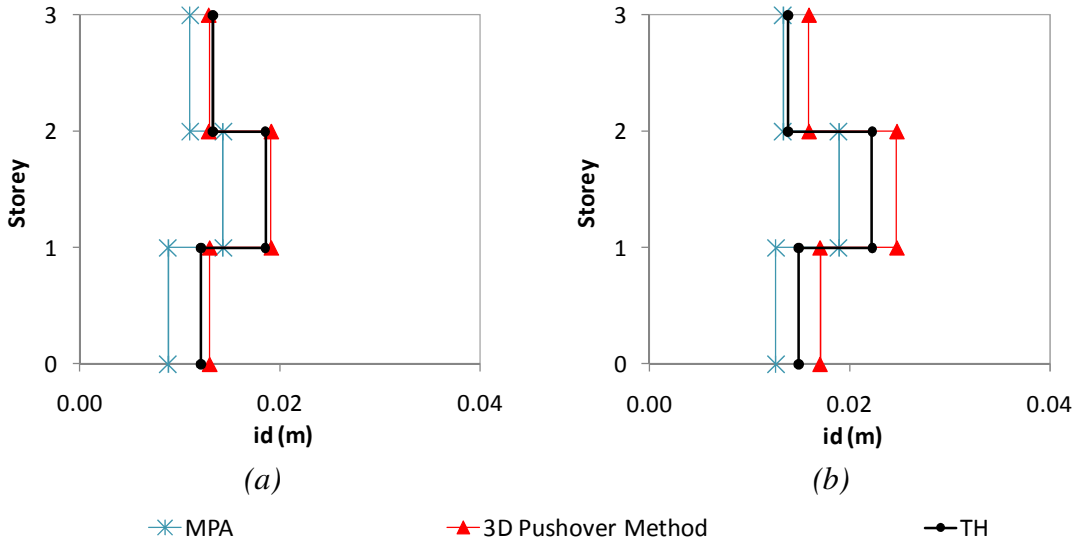

Figure A. 200 – Interstorey drifts profiles, three storey building: a) column C8, Y direction, 0.1g; b) column C2, Y direction, 0.1g.

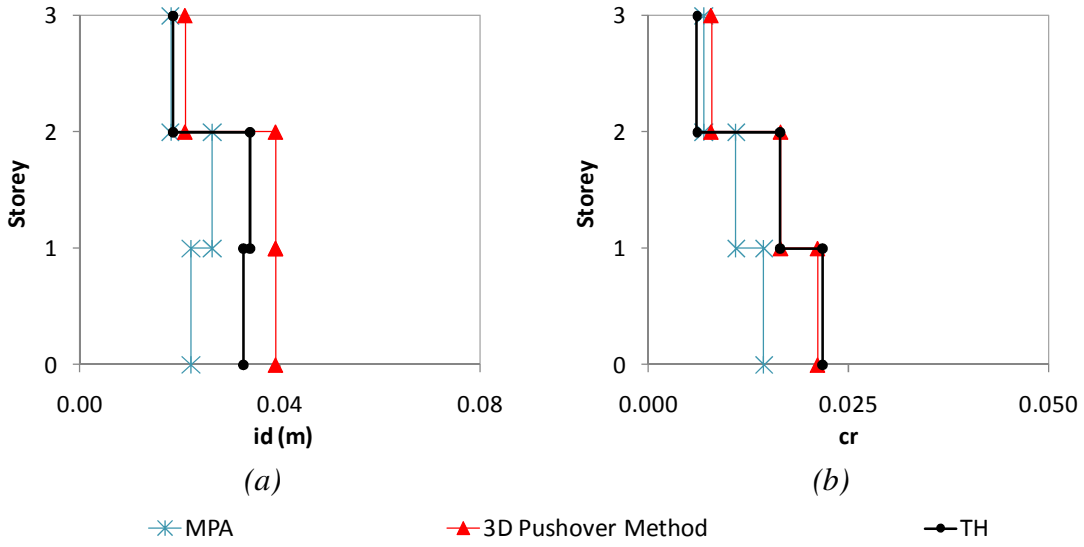

Figure A. 201 – Interstorey drifts profiles, three storey building: a) column C8, Y direction, 0.2g; b) column C8, Y direction, 0.3g.

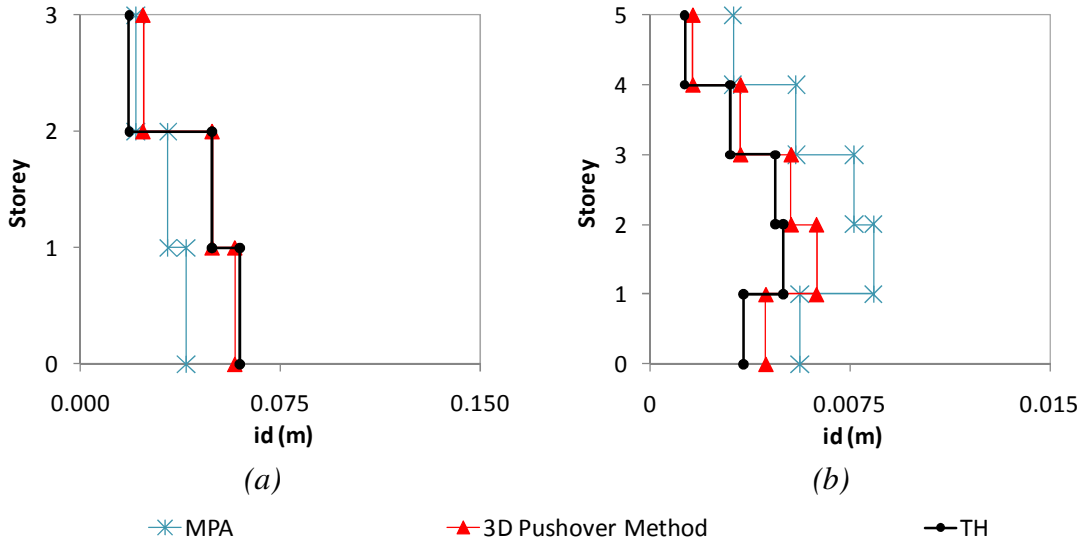

Figure A. 202 – Interstorey drifts profiles: a) three storey building, column C8, Y direction, 0.3g; b) five storey building, column S23, X direction, 0.1g.

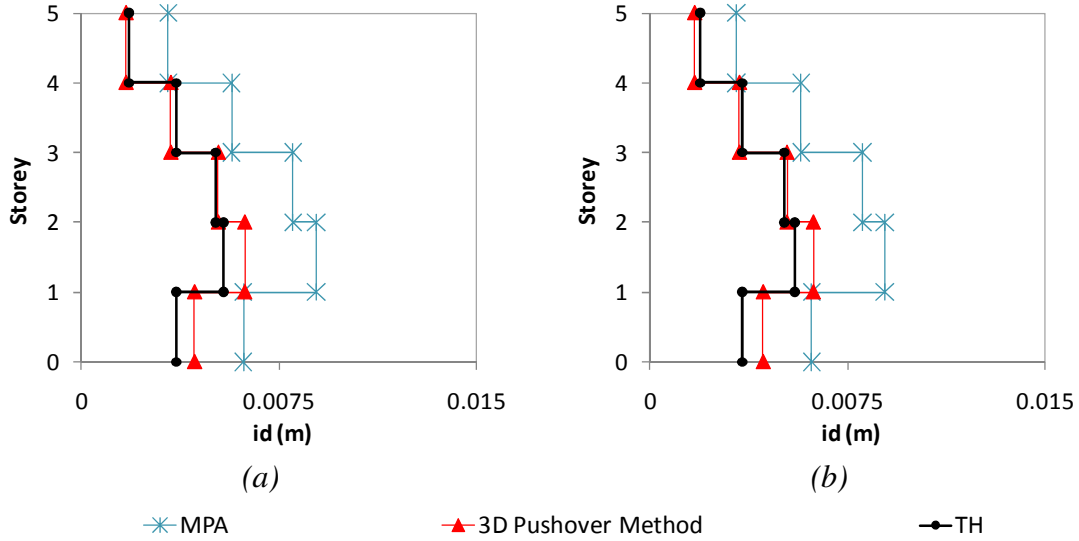

Figure A. 203 – Interstorey drifts profiles, five storey building: a) column S13, X direction, 0.1g; b) column S14, X direction, 0.1g.

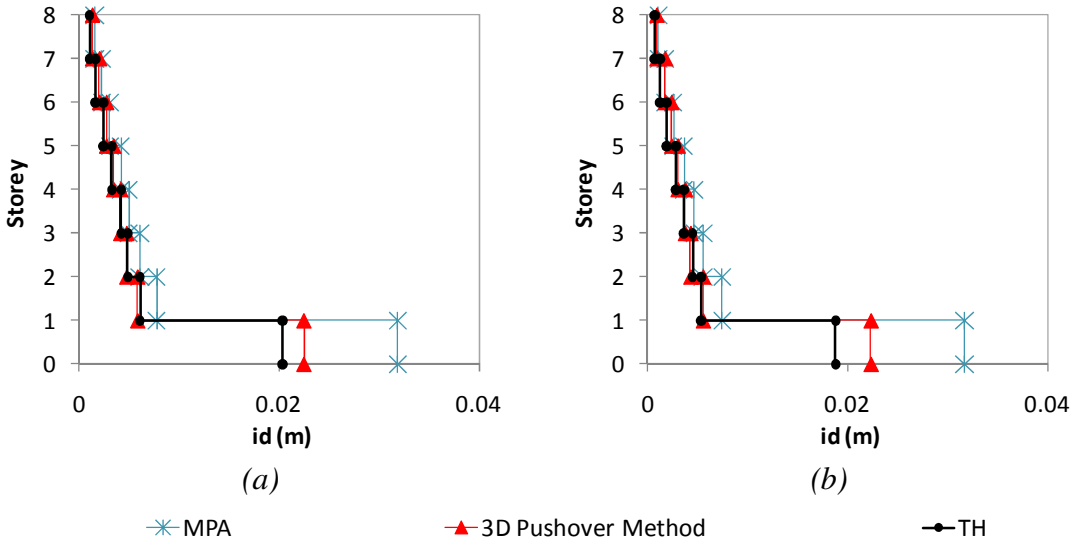

Figure A. 204 – Interstorey drifts profiles, eight storey building: a) column S9, X direction, 0.1g; b) column S69, X direction, 0.1g.

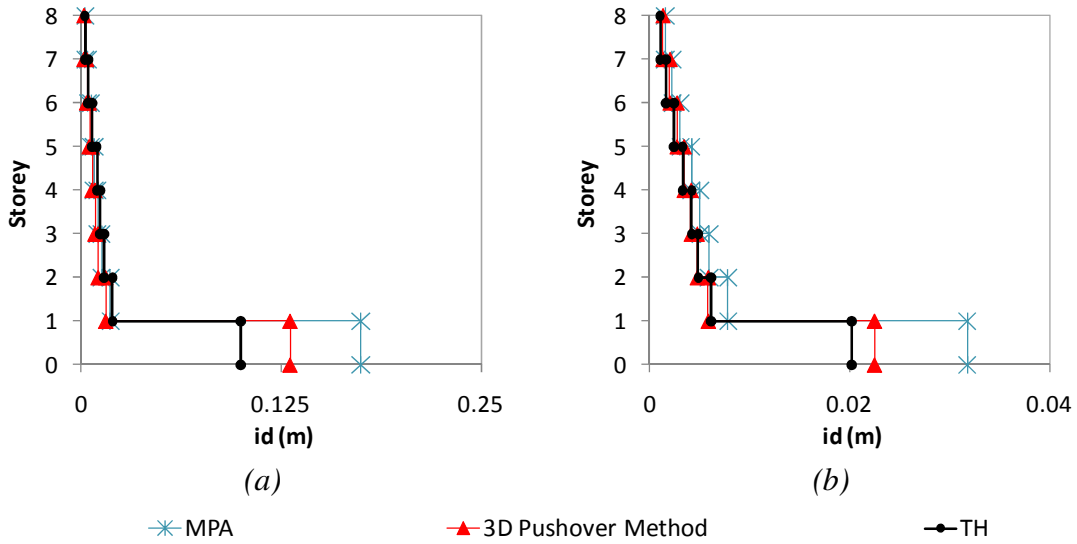

Figure A. 205 – Interstorey drifts profiles, eight storey building: a) column S69, X direction, 0.4g; b) column S15, X direction, 0.1g.

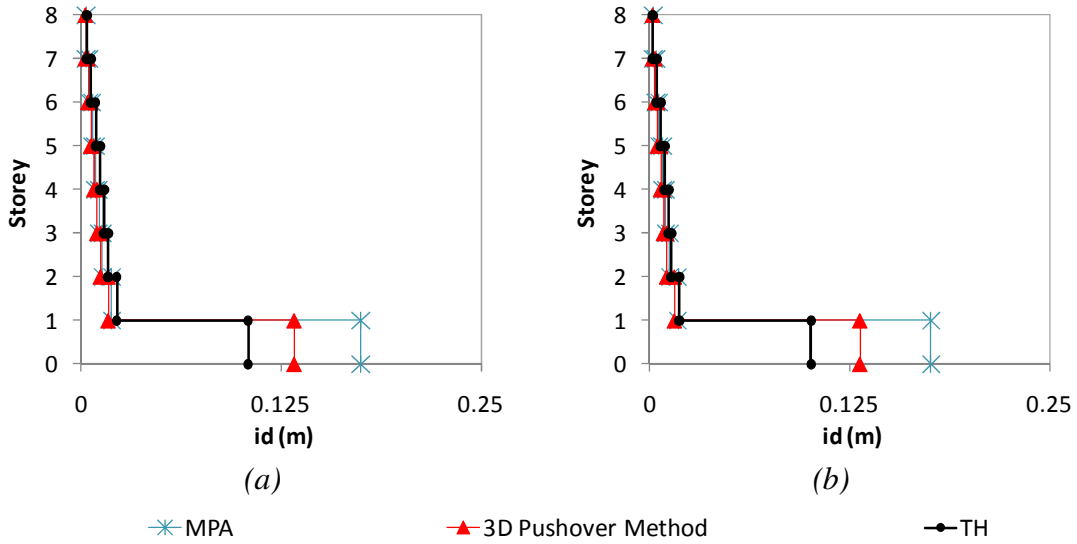

Figure A. 206 – Interstorey drifts profiles, eight storey building: a) column S15, X direction, 0.4g; b) column S72, X direction, 0.4g.

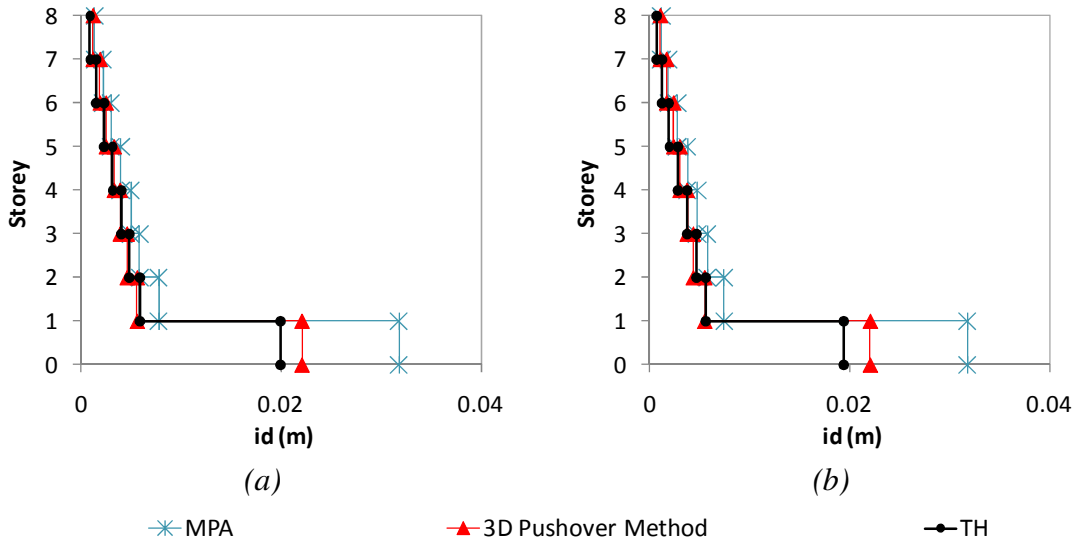

Figure A. 207 – Interstorey drifts profiles, eight storey building: a) column S23, X direction, 0.1g; b) column S52, X direction, 0.1g.

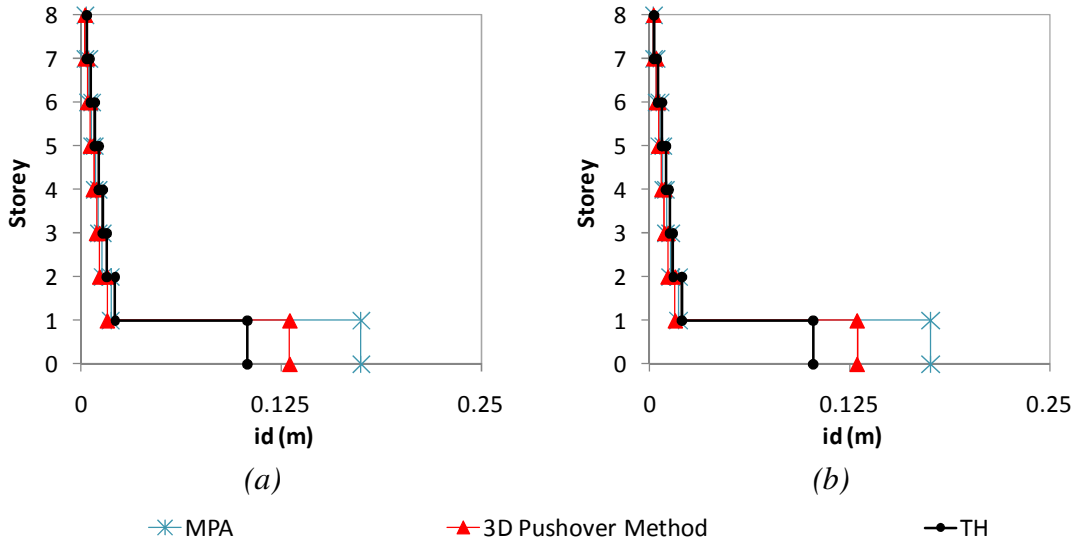

Figure A. 208 – Interstorey drifts profiles, eight storey building: a) column S23, X direction, 0.4g; b) column S52, X direction, 0.4g.

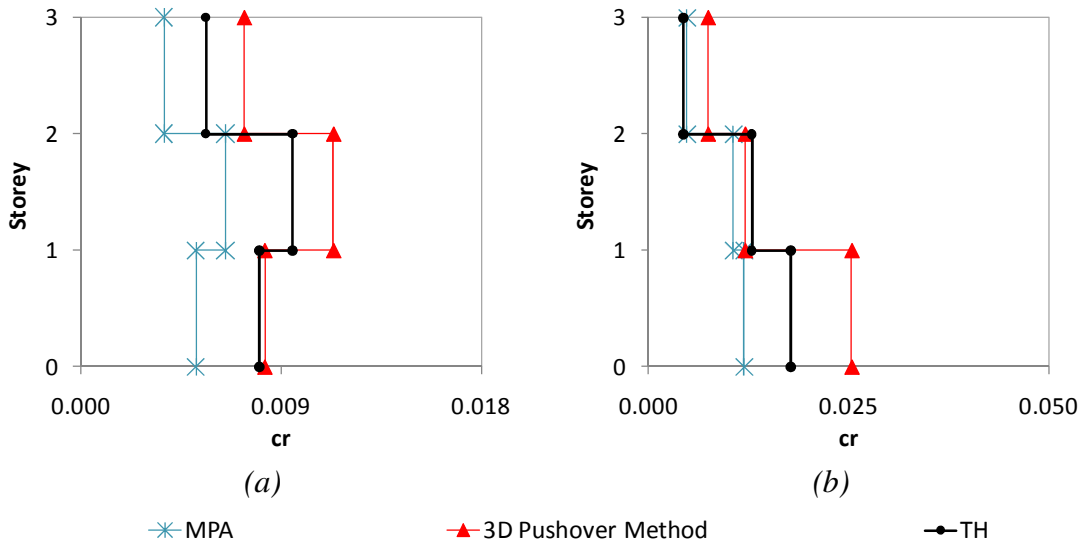

Figure A. 209 – Chord rotations profiles, three storey building: a) column C2, X direction, 0.1g; b) column C8, X direction, 0.2g.

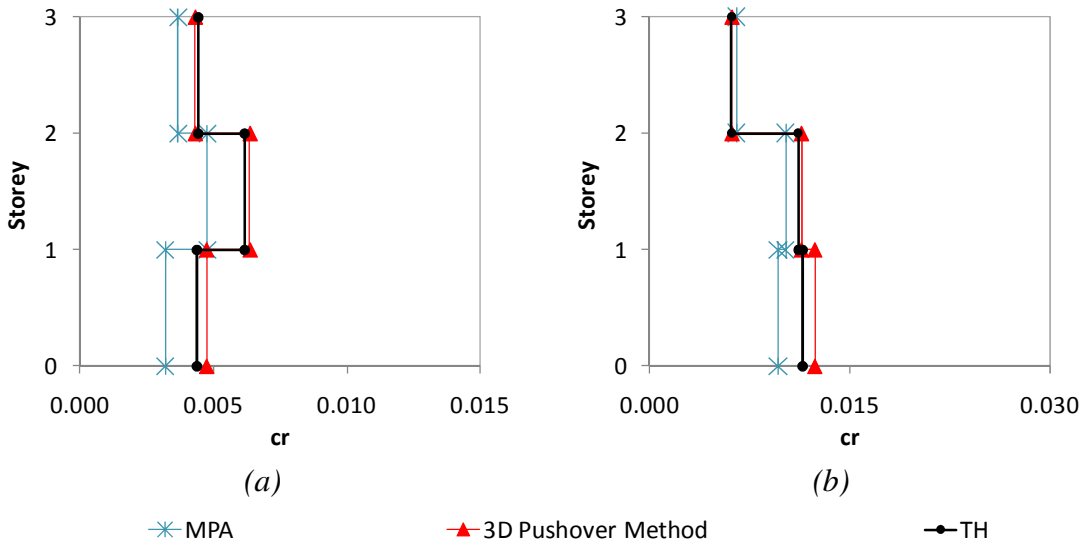

Figure A. 210 – Chord rotations profiles, three storey building: a) column C8, Y direction, 0.1g; b) column C3, Y direction, 0.2g.

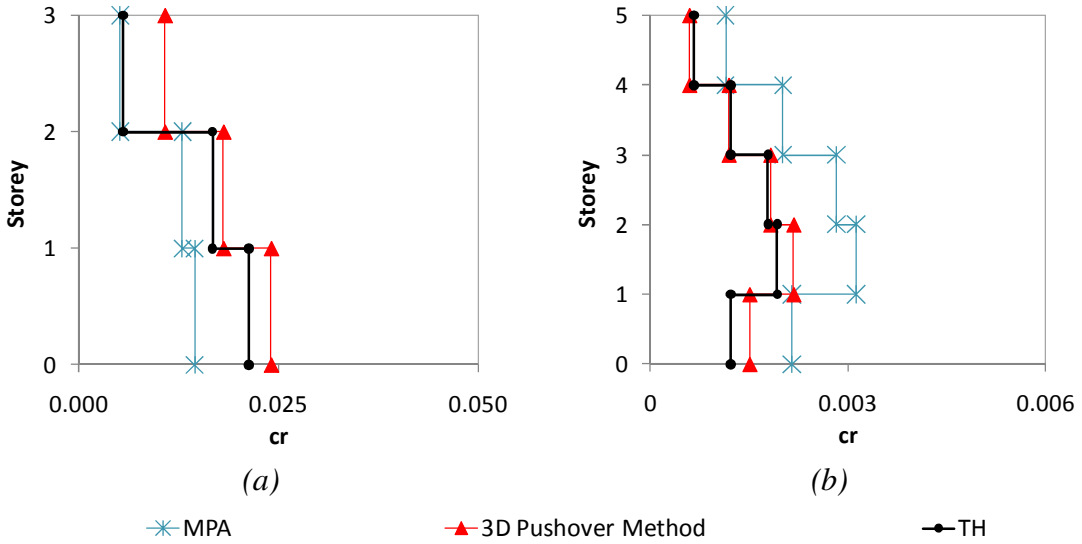

Figure A. 211 – Chord rotations profiles: a) three storey building, column C2, X direction, 0.2g; b) five storey building, column S14, X direction, 0.1g.

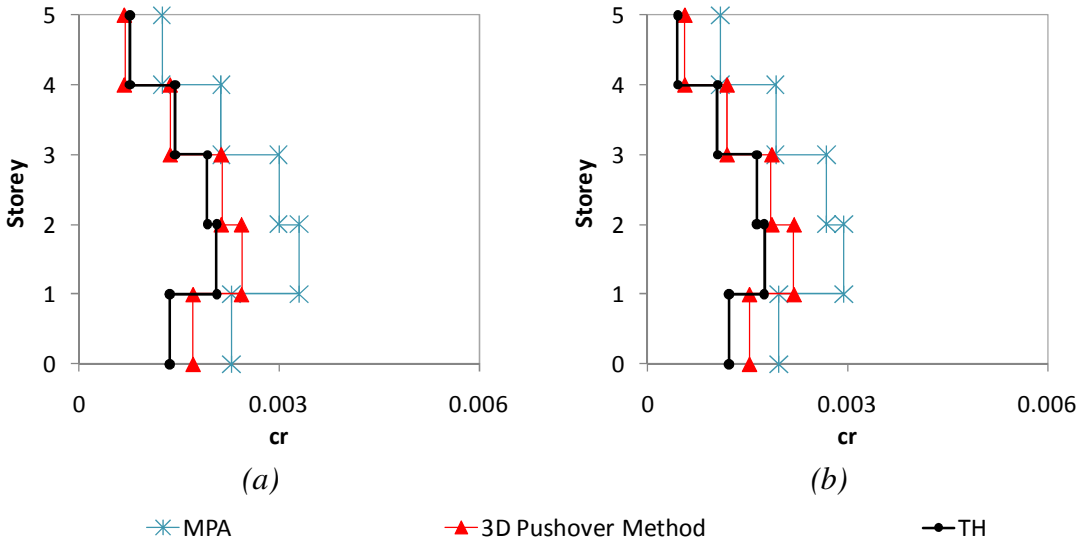

Figure A. 212 – Chord rotations profiles, five storey building: a) column S18, X direction, 0.1g; b) column S23, X direction, 0.1g.

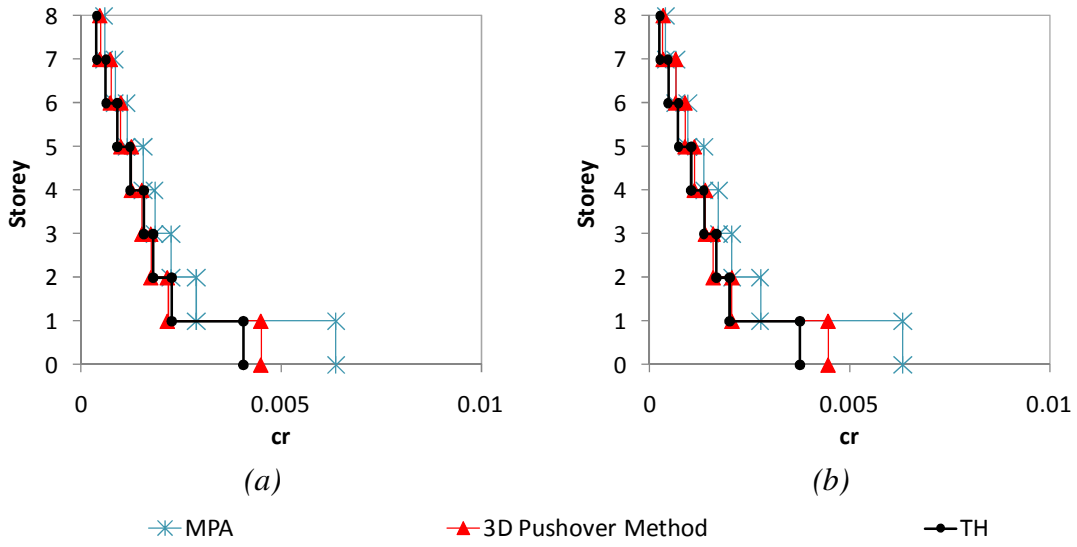

Figure A. 213 – Chord rotations profiles, eight storey building: a) column S9, X direction, 0.1g; b) column S69, X direction, 0.1g.

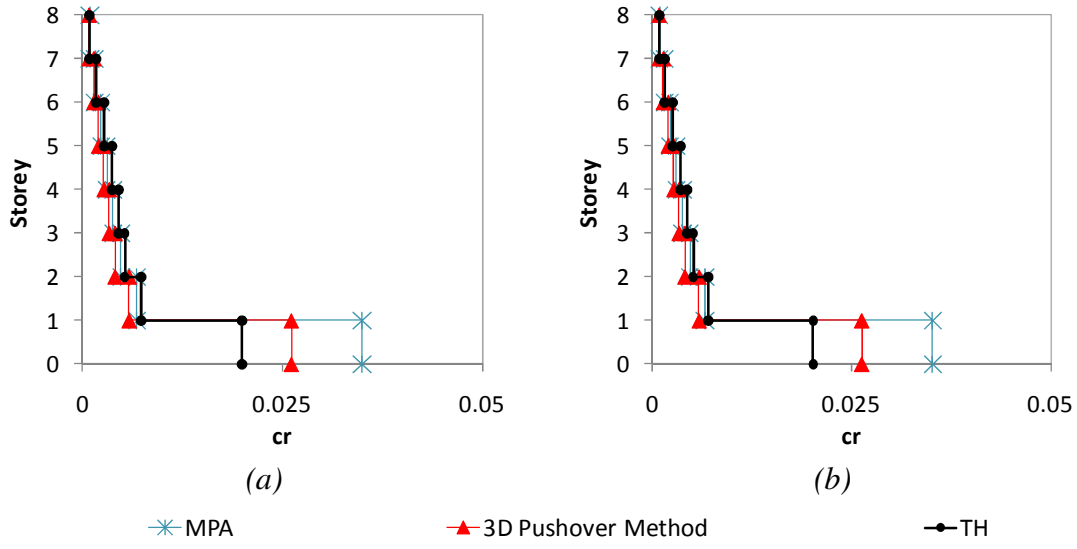

Figure A. 214 – Chord rotations profiles, eight storey building: a) column S69, X direction, 0.1g; b) column S72, X direction, 0.4g.

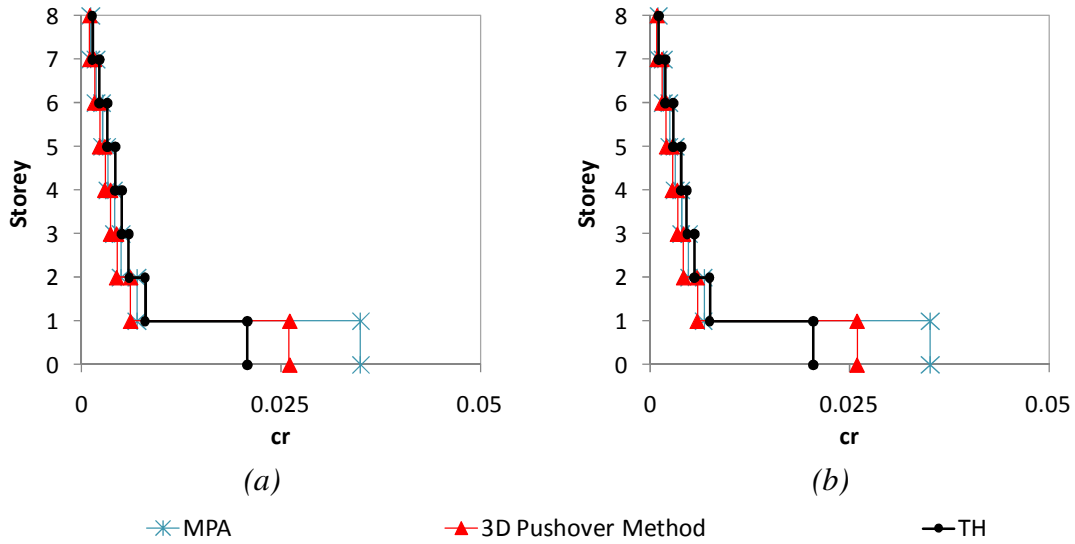

Figure A. 215 – Chord rotations profiles, eight storey building: a) column S23, X direction, 0.4g; b) column S52, X direction, 0.4g.

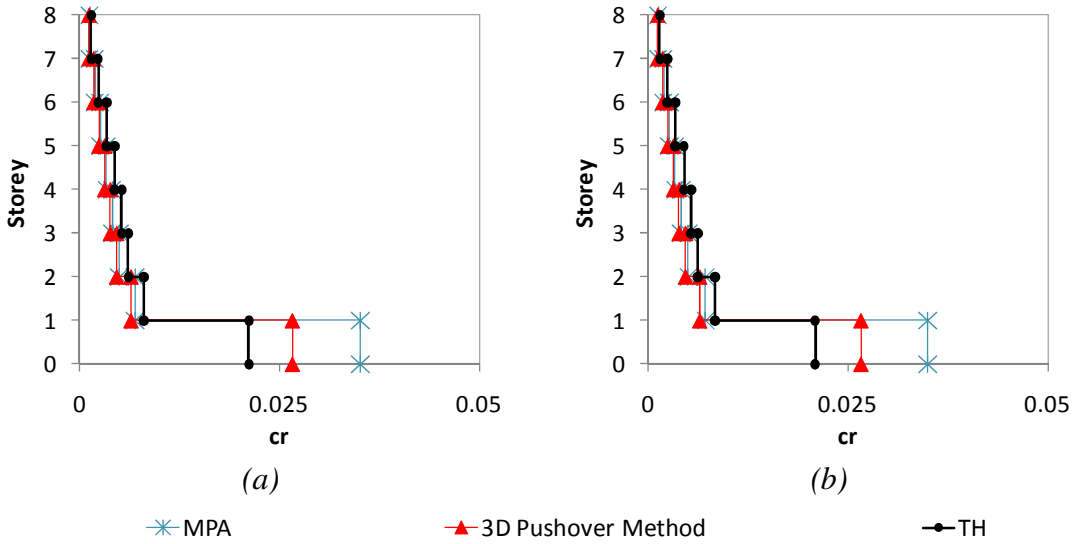

Figure A. 216 – Chord rotations profiles, eight storey building: a) column S9, X direction 0.4g; b) column S15, X direction 0.4g.

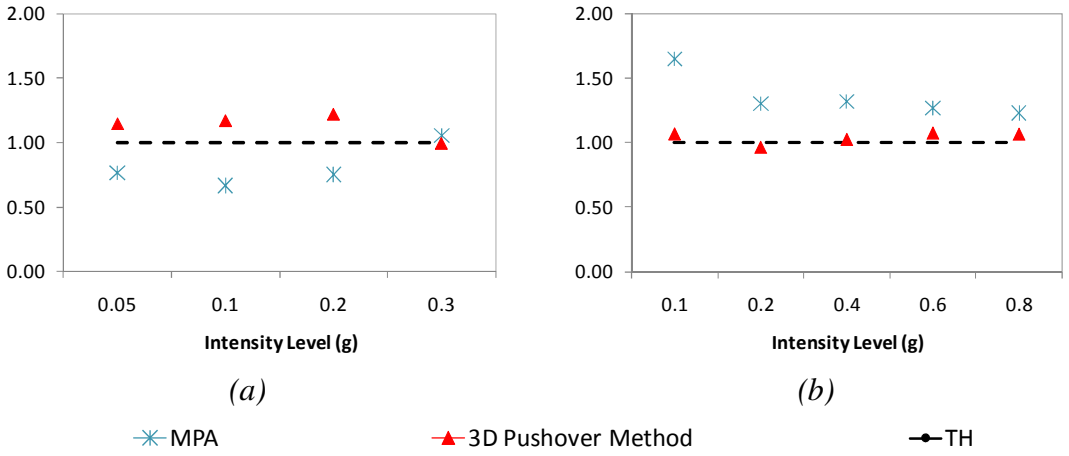

Figure A. 217 – Top displacement ratios, X direction: a) three storey building, column C2; b) five storey building, column S14.

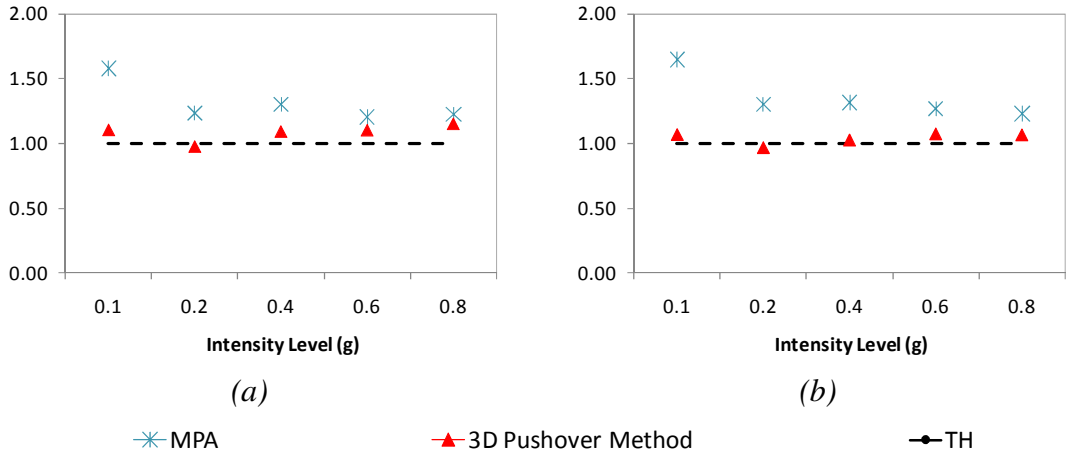

Figure A. 218 – Top displacement ratios, five storey building: a) column S1, X direction; b) CM, X direction.

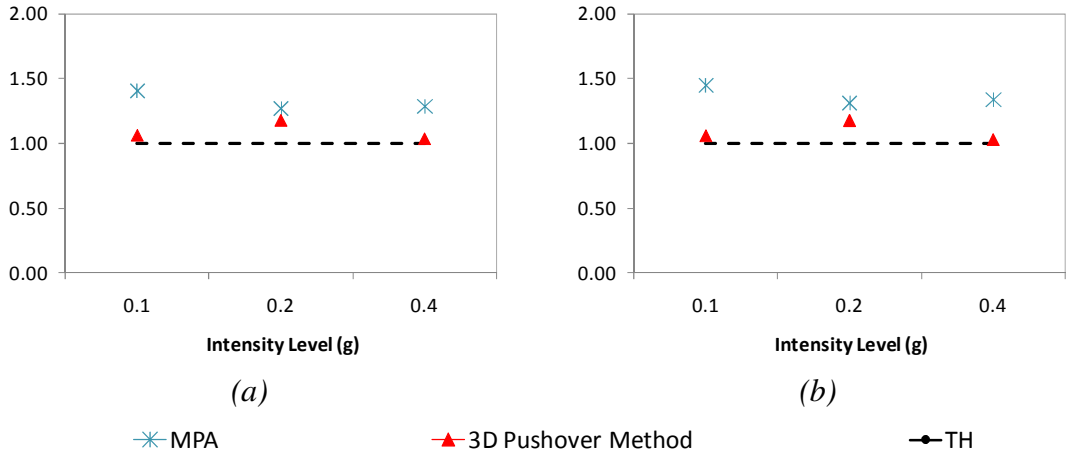

Figure A. 219 – Top displacement ratios, eight storey building: a) column S15, X direction; b) CM, X direction.

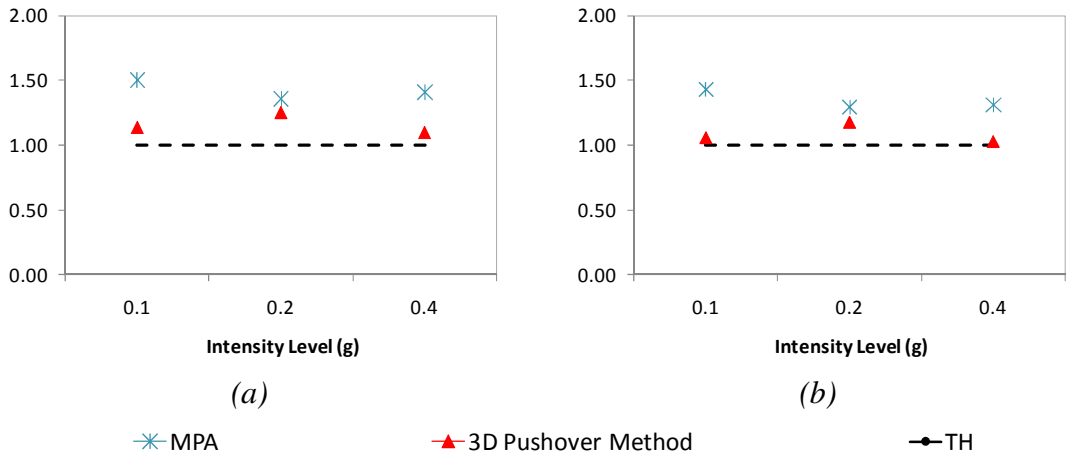

Figure A. 220 – Top displacement ratios, eight storey building: a) column S72, X direction; b) column S23, X direction.

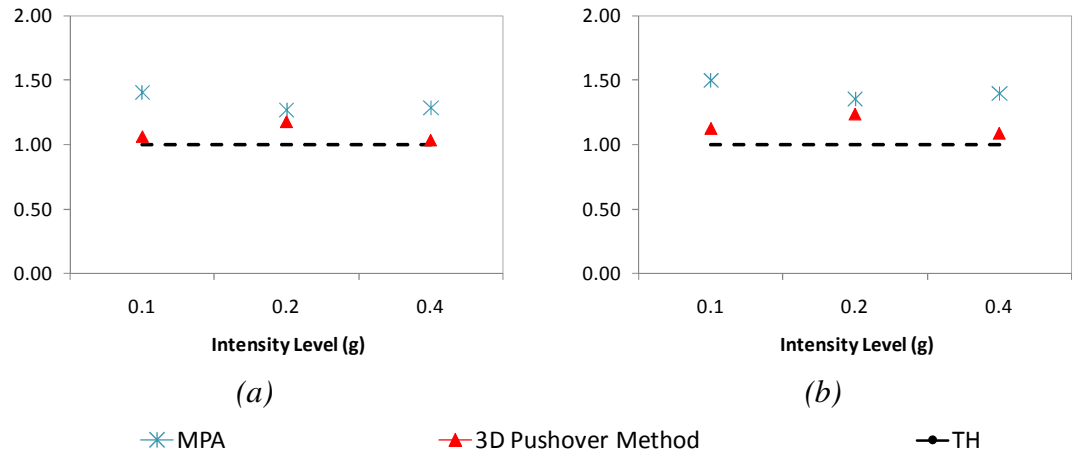

Figure A. 221 – Top displacement ratios, eight storey building: a) column S9 X direction; b) column S69 X direction.

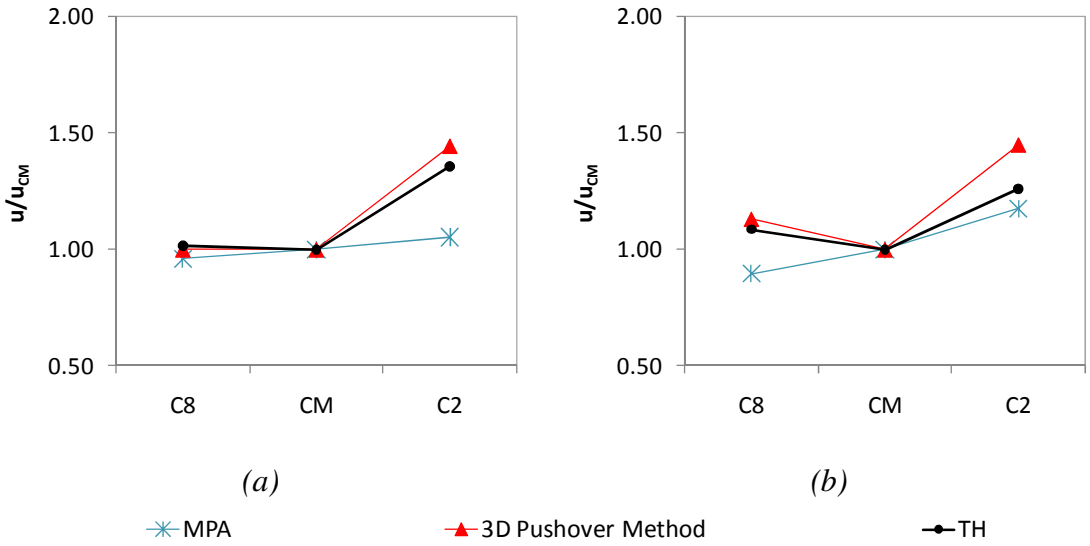

Figure A. 222 – Normalized top displacements three storey building: a) X direction 0.1g; b) Y direction 0.1g.

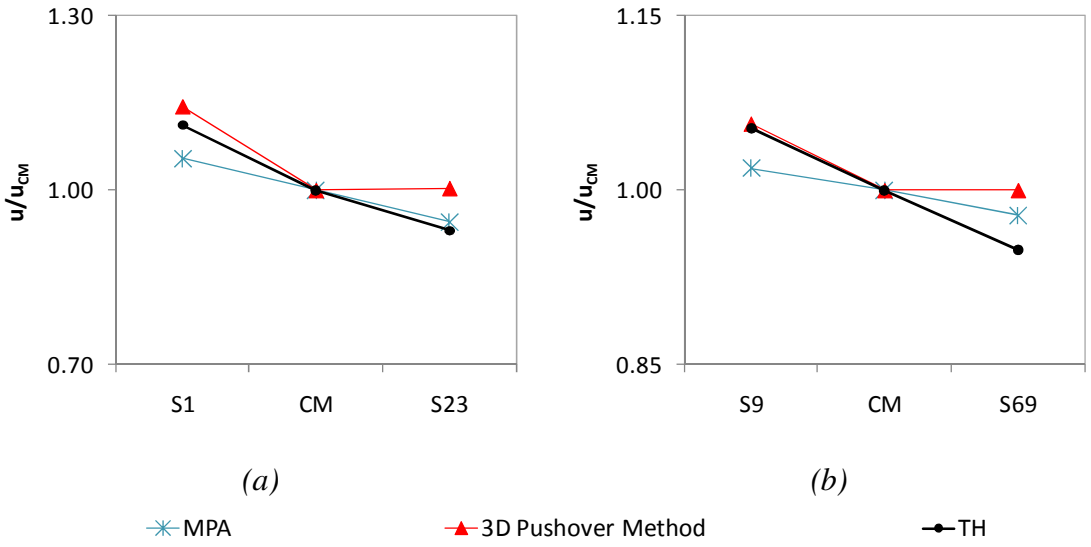

Figure A. 223 – Normalized top displacements, X direction: a) five storey building, 0.6g; b) eight storey building, 0.2g.

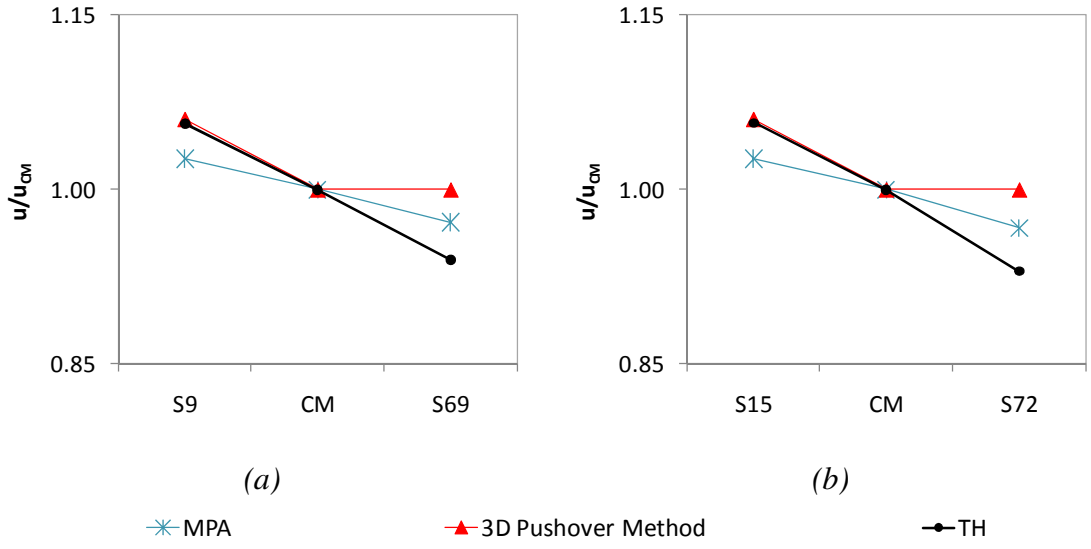

Figure A. 224 – Normalized top displacements eight storey building, X direction, 0.1g.

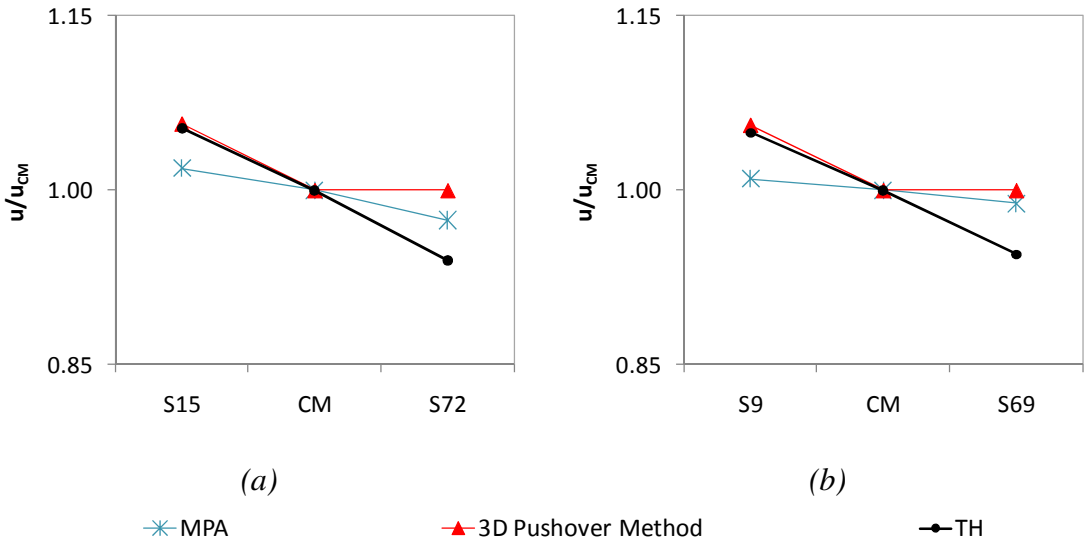

Figure A. 225 – Normalized top displacements, X direction: a) eight storey building 0.2g; b) eight storey building, 0.4g.